NASA CR 72702

FINAL REPORT

INVESTIGATION OF EFFECTS OF ABLATIVE DISCREPANCIES ON NOZZLE PERFORMANCE RELIABILITY

Prepared by:

Aerojet Solid Propulsion Company
Advanced Technology
Sacramento, California

Author: J. J. Warga

National Aeronautics and Space Administration
Lewis Research Center
Cleveland, Ohio

Technical Management
J. J. Notardonato, Project Manager

aerojet solid propulsion company
A DIVISION OF AEROJET-GENERAL

FINAL REPORT

INVESTIGATION OF EFFECTS OF ABLATIVE DISCREPANCIES ON NOZZLE PERFORMANCE RELIABILITY

Prepared by:

Aerojet Solid Propulsion Company
Advanced Technology
Sacramento, California

Author: J. J. Warga

January 1970

Contract NAS3-12008

Prepared for:

National Aeronautics and Space Administration
Lewis Research Center
Cleveland, Ohio

Technical Management
J. J. Notardonato, Project Manager

aerojet solid propulsion company

A DIVISION OF AEROJET-GENERAL

ABSTRACT

Carbon and silica fabric reinforced ablative plastic nozzle components were fabricated with discrepancies introduced during the wrapping and curing cycles. The ablative performance of the components was evaluated after static test firing; the mechanical and physical properties of duplicate flame liners were determined at room and elevated temperatures. Structural and ablative performance predictions based on the measured properties were compared to the actual results and accept/reject criteria for the introduced discrepancies derived.

TABLE OF CONTENTS

TABLE OF CONTENTS (cont)

LIST OF TABLES

LIST OF TABLES (cont)

LIST OF TABLES (cont)

FIGURE LIST

FIGURE LIST (cont)

FIGURE LIST (cont)

FIGURE LIST (cont)

FIGURE LIST (cont)

FIGURE LIST (cont)

APPENDIX

FOREWORD

The research and development work described herein was conducted by the Space Booster Department of the Aerojet-General Corporation under NASA Contract NAS3-12008. The work was done under the direction of J. J. Notardonato, Project Manager for the NASA Lewis Research Center.

This program was conducted under the management of J. J. Warga, who also served as project engineer. Principal investigators were R. L. Knapp in the area of heat transfer analysis; H. Efron in structural analysis; D. B. Syrek for statistical analyses; J. M. Amaral for evaluation and analysis of nondestructive testing techniques; and E. Wong for development of accept/reject criteria.

I. INTRODUCTION

In scaling up the fabrication of reinforced ablative plastic nozzle components to the sizes required for use in the 260-in.-dia motor feasibility demonstration program, it was found that deviations from the materials and processing requirements frequently occurred. This introduced delays in the manufacturing schedule while the effects of the deviations were evaluated. Because of the large, few-of-a-kind components that were being fabricated, the accept-reject criteria tended to be either arbitrary or excessively conservative. The former were based on prior experience with much smaller nozzle components; the latter consisted of submitting all manufacturing and material test data to a critical engineering review. While the conservative approach had the advantage of minimum risk, the adverse effects on costs and schedules would outweigh this advantage in repetitive manufacture. It became apparent that the use of some predetermined standards of acceptance were necessary basing these standards on the knowledge of the effects of the deviations upon the ablative component performance. Essentially, it would be advantageous, in reducing costs to: (1) consider the use of ablative nozzle components that contained discrepancies of a nature, size, and frequency that would not compromise reliable performance, but that heretofore had been considered rejectable; (2) develop repair techniques that would cause rejectable discrepancies to become ineffective in producing failures in full-size components.

Accordingly, this program was initiated with the objective of developing accept-reject criteria for discrepancies in reinforced ablative plastic nozzle components fabricated by tape-wrapping. This objective was to be achieved by:

A. Designing and fabricating reinforced ablative plastic nozzle components incorporating material and processing discrepancies at predetermined levels of severity.

I. Introduction (cont)

B. Evaluating the physical and mechanical properties of the defect containing components and conducting ablative and structural analyses to determine the most probable origins and locations of failures within the components.

C. Assessing the capabilities of NDT techniques to locate discrepancies at the levels introducted in the nozzle components.

D. Conducting static test firings to verify the ablative and structural performance of the discrepant nozzle components.

E. Developing techniques to repair discrepant nozzle components and conducting static test firings to verify the efficacy of such repair techniques.

II. SUMMARY

A subscale ablative nozzle assembly with a throat diameter of 3.50 in (8.89 cm) was designed to be fabricated by tape-wrapping and hydroclave-curing techniques. Discrepancies were introduced at three levels of severity into each of three nozzle components: entrance cap, throat insert, and exit cone. Twenty sets of nozzle components and twenty duplicate sets of flame liners were fabricated from carbon fabric reinforced phenolic (MX-4926) and silica fabric reinforced phenolic (MX-2600) prepreg tapes. Two of each of these sets were fabricated without deliberately introduced discrepancies; the remaining eighteen sets of components and duplicate flame liners contained:

Delaminations

Wrinkles

Resin-segregated areas

Density variations

Volatile content variations

Cure cycle variations

The duplicate sets of flame liners were used for the preparation of specimens for measurement of mechanical and physical property reductions associated with the discrepancies. Compressive properties of the carbon and silica fabric reinforced components were determined in directions radial, axial, and tangential to the nozzle centerline and at room and elevated temperatures up to 3000°F (1649°C); tensile properties were determined only at room temperature. The density of the virgin composite was determined at room temperature; specific heat and thermal conductivities were determined up to 1600°F (871°C); and the thermal dilation up to 1000°F (538°C). Except for density variations there was no correlation of properties to discrepancy levels.

II. Summary (cont)

The nozzle components were inspected by radiographic and pulse ultrasonic techniques to determine the location and extent of each discrepancy. Then selected components were examined by techniques new to the 260-in. motor program (infrared thermography, eddy-current and resonant frequency ultrasonic techniques) for comparison to the radiographs and ultrasonic scans. In general, discrete flaws were accurately described by pulse ultrasonics and radiography. The effects of material variations such as high volatile content and cure cycle variations could not be detected but rather had to be inferred from the presence of discrete flaws. While the "new" NDT techniques were rated good or excellent in many instances, they received such high ratings only in instances where radiography and ultrasonics were also high-rated. The use of the "new" methods would thus be indicated only for reasons of economy or for convenience.

Assembly of the ablative components into the steel nozzle shell was accomplished by adhesive bonding. Of the 20 discrepant nozzle assemblies, six were assembled with areas free of adhesive varying from 20 to 60 percent. The unbonded regions were detected and defined by the use of a contact, ultrasonic technique operating in the pulse-echo mode.

The twenty discrepant nozzle assemblies were test fired in the nozzle-up position during the period January to May 1969. The baseline (defect-free nozzles) motors operated at an average pressure of 600 psia (4.1 MN/M^2) for an average time of 26.4 sec, using an aluminum loaded propellant with a flame temperature of 5800°F (3477°K) — well within the program requirements. After test, the nozzles were disassembled and examined to determine the material regression and depth of char produced by the discrepancies. The flame surfaces were examined for evidences of material failures and specimens were removed for determination of the char density. During the course of the testing, it was determined that structural failures in the exit cone could not result with the original design configuration. Accordingly, the silica

II. Summary (cont)

aft-exit section was machined to a wall thickness of 0.250 in. (0.635 cm). Additionally, the steel nozzle shell was removed behind this reduced section thickness. This led to the failure of an exit cone by burnthrough at an area of delamination, subsequent unravelling of the plies of material around the delaminations and ejection of the exit cone aft of the introduced discrepancy.

Analysis of the performance of the ablative nozzles was performed by heat transfer and thermoelastic techniques. A charring-ablation computer program, which combined the inputs of the heat transfer analysis with the corrosion kinetics, resin pyrolysis and thermophysical properties of the virgin and charred ablative composites was used to predict the material regression during test firing. A finite element computer program, which combined the inputs of the temperature profile with the elevated temperature mechanical properties and thermal expansions of the composites was used to predict the structural performance. It was found that the effects of discrepancies which directly affected the char density, such as resin segregation, could be predicted with a fair degree of accuracy. It was also found that the finite element computer program indicated that discrepancies of the type and severity under study would not themselves initiate a structural failure, but would propagate a failure initiated by some other cause, such as a localized burnthrough.

Eight additional ablative nozzle assemblies containing introduced discrepancies were fabricated and tested to evaluate the worth of resin filling techniques for repairing the discrepancies. Two types of room-temperature-curing resins (epoxy and furane) were used. Neither type was successful in improving the ablative performance of the discrepant areas. From the results, it was concluded that a phenolic resin base, which would have a higher char yield would be more successful. Additional work was recommended.

II. Summary (cont)

Combining the ablative and structural analysis techniques with a statistical analysis of variance it was possible to establish accept/reject criteria for defect levels in ablative nozzle components fabricated from carbonaceous and silica reinforced tape prepregs. The accept/reject criteria are listed with regard to the effect of the discrepancies in the inlet, throat and exit sections of the nozzle and recommendations are made to revise NDT specifications for large nozzle components to include the acceptance levels resulting from this program.

III. MOTOR AND NOZZLE DESIGN

A. PROGRAM REQUIREMENTS

1. Design

The following motor ballistic and nozzle design requirements* were specified for this program:

Throat diameter, in. (cm)	3.5 (8.9) approximately
Expansion ratio	6:1
Chamber pressure, psia (MN/m^2)	600 ± 50 (4.14)
Firing duration, sec	25 minimum
Propellant aluminum content, %	15 ± 1 by weight
Propellant combustion temperature, °F	5800 ± 200
Propellant type	PBD

In addition, ablative required in the throat and near-throat regions were carbon fabric reinforced phenolic prepreg (MX-4926 or equivalent) and other regions of the nozzle were silica fabrics (MX-2600 or equivalent) that was fabricated into the required nozzle components by the use of wrapping and hydroclave cure techniques. Also, it was specified that the maximum strain in the silica material used for overwrap insulation be no greater than 0.15 percent (0.0015 in./in.).

B. TEST MOTOR

1. Description

The solid rocket motor used in this program was a test-weight design, insulated to provide for multiple use without the need for rehabilitation

*Ref: Contract NAS3-12008.

III.B. Test Motor (cont)

between firings. The motor assembly is shown in Figure III-1. Essentially, the motor consists of two parts, a chamber with attached fore-end plate closure and a conical aft closure. Both parts were designed to withstand internal pressures up to 3000 psi (20.7 MN/m^2) at a safety factor of 1.25.

The chamber barrel section, the fore-end plate, and the aft closure are all insulated with uncured V-44 rubber (Specification AGC-34161) vulcanized in place. The forward end of the chamber is potted with SD-810 elastomeric compound (Specification AGC-36468) to reduce the chamber volume and provide support for the propellant cartridge.

Attachment of the aft closure to the chamber is provided by three circular hardened steel retainer segments, visible in Figure III-2. These retainers fit into a groove in the chamber flange, moving into position along the slots at each end of the segment. Each segment is locked in place with three high-strength steel internal wrenching bolts threaded into the closure. Propellant gas leakage between the chamber and closure is prevented by an O-ring seal located in a groove machined on the O.D. of the closure.

2. Motor Ballistics

ANB-3066 propellant was selected for use in the motor. To meet the program requirements for motor operation, size of the propellant cartridge was established to be 28.20 in. (71.6 cm) O.D. by 10.20 in. (25.9 cm) I.D. by 30.70-in. (78.0 cm) long for a total weight of 1065 $\pm$ 5 lb (484 $\pm$ 2.6 kgm). For the 3.5 in. (8.89 cm) nozzle throat diameter, the motor was calculated to have a web action time of 25.78 sec with an average pressure of 603 psia (4.15 MN/m^2). The predicted pressure-time curve is shown in Figure III-3.

III. Motor and Nozzle Design (cont)

C. NOZZLE DESIGN

1. Configuration

The basic nozzle design is shown in Figure III-4. It is a four-piece assembly consisting of a convergent entrance cap, a throat insert, and a divergent exit cone, all contained in a steel nozzle shell. The throat and aft portion of the entrance cap are contoured to a radius of 3.5 in. (8.9 cm) and the exit cone has a half-angle of 17.5 degrees.

a. Ablative Parts

The entrance cap, Figure III-5, consists of a forward flame liner of silica phenolic and an aft liner of carbon phenolic, with the fabric plies oriented 80 degrees to the nozzle centerline. The flame liners are overwrapped with silica phenolic oriented parallel to the outer surface of the flame liners.

The throat insert, Figure III-6, is carbon phenolic with fabric plies oriented 45 degrees to the nozzle centerline, overlaid with silica phenolic wrapped parallel to the outer surface.

The exit cone, Figure III-7, consists of a forward flame liner of carbon phenolic and an aft liner of silica phenolic, with the plies oriented parallel to the nozzle centerline. The flame liners are overwrapped with silica phenolic oriented parallel to the outer surface of the flame liners.

b. Nozzle Shell

The ablative nozzle components were supported by a hardened steel shell designed to withstand a maximum pressure of 750 psia

III.C. Nozzle Design (cont)

(5.16 MN/m^2). Attachment of the nozzle shell to the aft closure is effected by flat spiral rings (Spiralox RRT-950). Propellant gas leakage between the nozzle shell and chamber aft closure is prevented by an O-ring seal located forward of the spiral locking groove in the closure.

c. Nozzle Assembly

The nozzle test components are dry-fitted prior to bonding into the nozzle shell. Bonding is accomplished with a room-temperature curing epoxy adhesive. All joints between ablative components are filled with a room-temperature vulcanizing rubber.

2. Nozzle Design Justification

The following paragraphs summarize the results of analyses conducted to verify the ablative and structural adequacy of the basic nozzle design. The analytical techniques are described in detail in Section VI, "Failure Analysis."

a. Ablative Analysis

The local convective heat transfer coefficients along the nozzle contour are shown in Figure III-8. The data were generated by the boundary layer growth method (Aerojet Computer Program E-25202) for ANB-3066 propellant and an arbitrarily selected chamber pressure of 500 psia (4.44 MN/m^2). The maximum heat transfer coefficient occurred slightly upstream of the throat ($\varepsilon = 1.025$) and was 1715 Btu/ft^2-hr-°F. At the geometric throat, the local value was 1650 Btu/ft^2-hr-°F. Since the predicted value varies during the firing in accordance with Figure III-3, the data of Figure III-8 were corrected to account for this variation according to the following schedule:

III.C. Nozzle Design (cont)

Time	Chamber Pressure, psia (MN/m^2)	Heat Transfer Factor*
0	550 (3.79)	1.08
5	605 (4.17)	1.16
10	625 (4.30)	1.19
15	120 (4.27)	1.18
20	590 (4.06)	1.14
25.5	525 (3.62)	1.04
26.2	ambient	--

*Ratio of heat transfer coefficient at given chamber pressure to value at 500 psia (3.45 MN/m^2)

For the above conditions, five separate stations were investigated to evaluate the extent of surface regression, char depth formation, and heat penetration within the nozzle, using a charring-ablation program (AGC-8096). The results of the thermal response calculations for the five selected stations are shown in Table III-1 and Figure III-9. The greatest regression occurred upstream of the throat and was predicted to be 0.398 in.(1.01 cm), an average rate of 15.6 mils/sec. The throat regression was predicted to be 0.275 in. (0.070 cm) or 10.7 mils/sec and the char depth subsequent to heat soak was estimated to be an additional 0.285 in. (0.072 cm) for a total depth of 0.560 in. (1.42 cm) from the original contour. Figure III-10 shows the predicted regression and char depths at the throat. The results indicate that the basic design is thermally adequate and that all interfaces between flame liners and overwrap insulation will remain virgin composite.

b. Stress Analysis

Strain in the flame liners and insulation overwraps was analyzed by finite element techniques, using the temperature distributions

III.C. Nozzle Design (cont)

developed in the thermal analysis. Structural analysis was performed using Aerojet-General Corporation Computer Program E-11405, an elastic analysis that is applicable to thin walled structures. Computer runs were made for the conditions 0, 1, 12 and 25 sec after fireswitch. The results, shown in Table III-2, indicate that maximum strains occurred at 25 sec after fireswitch and were less than half the required maximum strain of 0.0015 in./in.

D. TEST MATRIX

Identification of the discrepancies which cause failures in reinforced ablative plastic nozzle components is largely a matter of historical observation. One of the most recent complete records was assembled during fabrication of the 260-in.-dia motor nozzles (References 1 through 3). Discrepancies observed in these nozzles, as well as in other programs (References 4 through 10) are listed in Table III-3 in their relative order of importance in initiating ablative and structural failures. The listed discrepancies were incorporated in a test matrix of 20 nozzle assemblies as summarized in Table III-4. The bases for selection are described in the following paragraphs.

1. Baseline Nozzle

Flame liners and overwrap insulation for two baseline nozzles were programed to be fabricated by tape-wrapping techniques, followed by hydroclave curing at a pressure of 1000 $\pm$ 50 psig (6.89 $\pm$ 0.30 MN/m^2) to yield a maximum volatile content of 3 percent and a minimum density in the carbon composite of 87.4 lb/cu ft (1.40 gm/cc), and in the silica composite of 107.3 lb/cu ft (1.72 gm/cc).

III.D. Test Matrix (cont)

2. Density Variations

The effects of density variations on the regression rates of ablative plastics have been widely recognized and composite and char densities are important inputs to the analytical ablation program. Structural properties are also affected by density variations. Accordingly, three levels of density were selected for evaluation in order of increasing severity as follows:

a. 100 percent (baseline)
b. 80 to 90 percent
c. 70 to 80 percent

3. Resin Content Variations

Variations in resin content caused by resin-rich and resin-starved areas in the composite produce changes in the regression and char rates. The total effect on performance depends on the surface area that is affected. Accordingly, four levels of resin content variation were selected for evaluation:

a. None (baseline)
b. Resin-rich (10 plies)
c. Resin-rich (20 plies)
d. Resin-starved (10 plies)

4. Volatile Content Variations

The effects of volatile content variations are not well documented. Excessive volatile content has been suspected of contributing to surface spalling and chunking and volatile limits for large ablative nozzle

III.D. Test Matrix (cont)

components have been arbitrarily set at 3 percent maximum to avoid such effects. Three levels of increasing volatile content were programed for evaluation:

a. 3 percent (baseline)
b. 6 percent
c. 9 percent

5. Processing Cycle Variations

Variations in processing of ablative nozzles have occurred primarily during the cure cycle, as a result of equipment or pressure bag malfunctions. Three cycle variations were programed:

a. Loss of temperature during debulk phase of final cure.
b. Bag leakage during debulk cycle.
c. Bag leakage during final cure cycle.

In addition, because of the need to verify the effects of reduced cure pressures, the following were programed for evaluation:

a. Vacuum cure (27 in. Hg) (68.6 cm Hg)
b. Autoclave cure (125 psig) (0.86 MN/m^2)

6. Delaminations

The available data on delaminations (separations between plies) indicated that while there was an effect on both the thermal stress distribution and the regression rate, it was a critical discrepancy only when a free-standing flame liner was used. In general, overwrap insulations

III.D. Test Matrix (cont)

prevented failure of the assembly. Since the primary effect was a reduction of structural capability, delaminations were evaluated by varying the total extent:

a. 7 plies
b. 14 plies
c. 28 plies

7. Wrinkles

Localized departures of the fabric plies from the desired orientation as evidenced by wrinkled or folded plies influence both the ablative and structural performance because of the effect on the thermal conductivity and thermal stress distribution. Wrinkles were programed for evaluation at three levels of increasing severity.

a. 0.125-in. high x 1-in. amplitude
b. 0.25-in. high x 1.5-in. amplitude
c. 0.375-in. high x 1.5-in. amplitude

8. Bondline Discrepancies

Incomplete bonding between the ablative nozzle components and the structural shell exerts a structural effect because of abnormal pressure loadings or burnthrough of the shell. In this program, bondline separations were introduced in amounts varying from 0 to 60 percent of the bonding area.

9. Location of Ablative Discrepancies

Density, volatile content and processing cycle variations affected the entire component. Resin content variations, delaminations, and

III.D. Test Matrix (cont)

wrinkles were introduced locally in the nozzle flame liners as shown in Figure III-11. Using this placement, the performance at each of the locations could be evaluated without interference from the upstream discrepancies.

Table III-1

Regression and Char Depths in Basic Nozzle

Station No.	Local Radius		Heat Transfer Coefficient at 500 lbf/in.^{2} abs	(3447 n/mm^2 abs)	Regression Depth		Char Depth*	
	in.	(cm)	Btu/ft^{2}hr °F	(w/m^{2}k)	in.	(mm)	in.	(mm)
1	3.25	8.26	720	4082	0.171	4.34	0.460	11.68
2	2.30	5.84	1200	6804	0.266	6.76	0.538	13.66
3	1.81	4.60	1715	9724	0.398	10.11	0.597	15.16
4	1.75	4.44	1650	9356	0.275	6.98	0.560	14.22
5	1.93	4.90	1085	6152	0.118	3.00	0.462	11.73

* Measured from original surface 40 sec after fire switch.

Table III-2

Hoop Strain in Silica Overwraps of Basic Nozzle

Time After Fire Switch, sec	Hoop Strain, in./in. (m/m)		
	Entrance Cap	Throat	Exit Cone
0	0.0004	0.00032	0.00012
1	0.00055	0.00045	0.00025
12	0.00065	0.00055	0.00033
25	0.0007	0.0007	0.00037

TABLE III-3

RELATIVE ORDER OF IMPORTANCE OF
ABLATIVE NOZZLE DISCREPANCIES

Ablation	Structurally
Density	Delaminations
Resin Content	Wrinkles
Volatile Content	Density
Processing Cycle Variations	Processing Cycle Variations
Delaminations	Volatile Content
	Bond Line Discrepancies

TABLE III-4

MATRIX OF DISCREPANT NOZZLES

Discrepancy	Level or Description
None	Baseline
	Baseline
Density	80 to 90 percent
	70 to 80 percent
Volatile Content	6 percent
	9 percent
Processing Cycle	Temperature loss, debulk phase of cure
	Bag leakage, debulk cycle
	Bag leakage, final cure
	Vacuum bag cure
	Autoclave cure
Resin Content	Resin-rich, 10 plies
	Resin-rich, 20 plies
	Resin-starved, 10 plies
Delaminations	7 plies
	14 plies
	28 plies
Wrinkles	0.125 in. high by 1.0 in. spacing
	0.25 in. high by 1.5 in. spacing
	0.375 in. high by 1.5 in. spacing

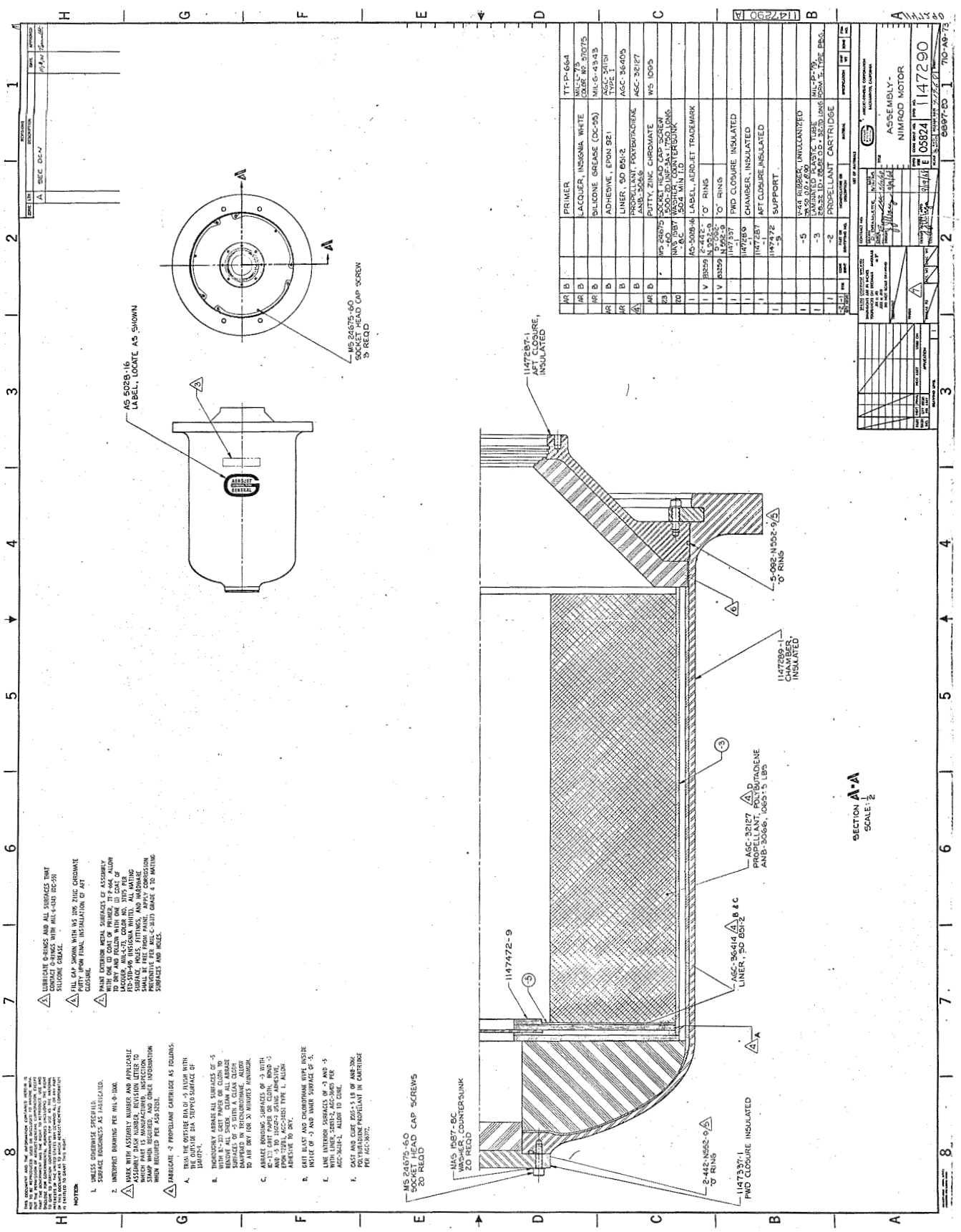

Figure III-1

Test Motor for Evaluation Firings

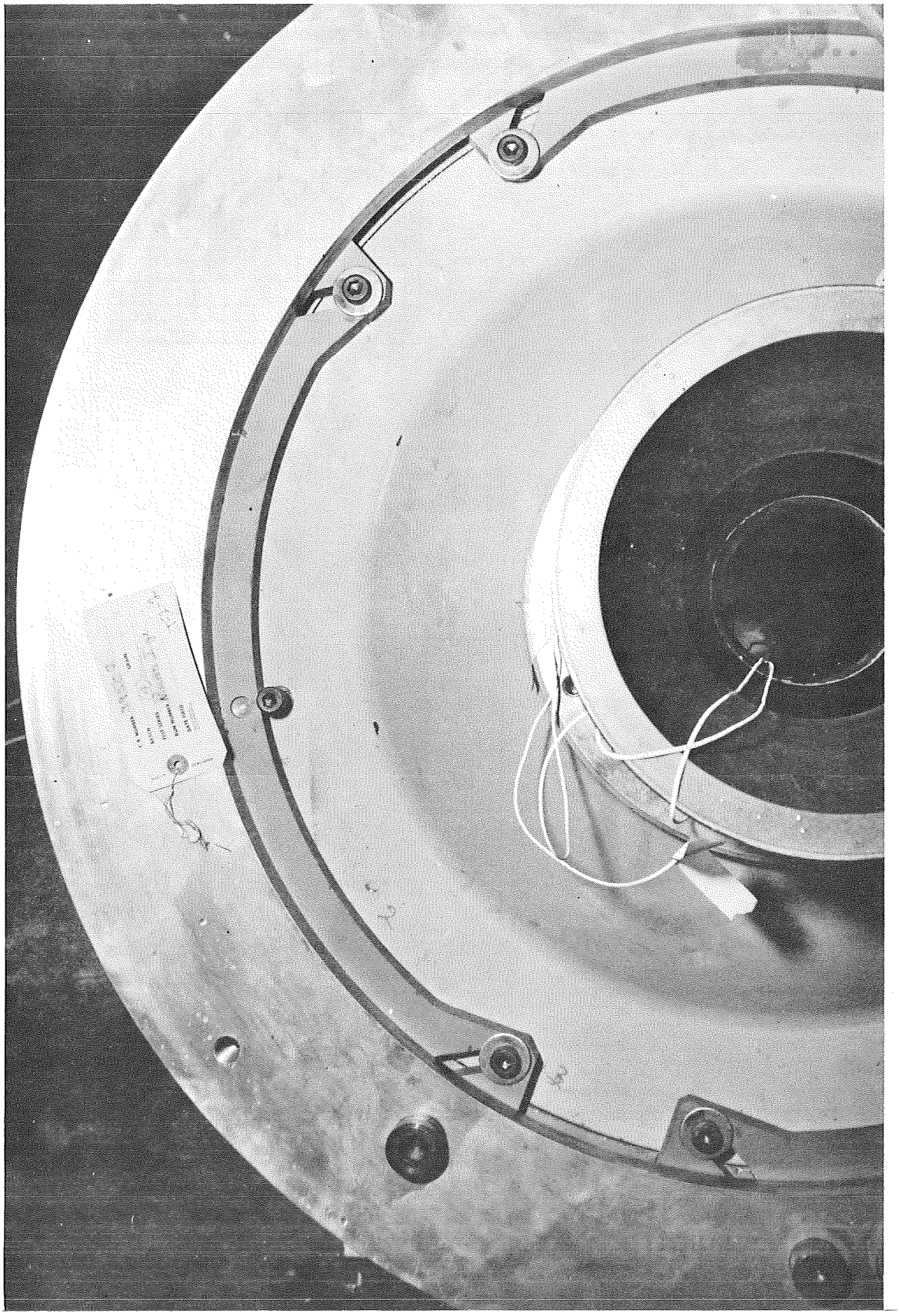

Aft End of NIMROD Motor, Showing Retainers in Closed Position

Figure III-2

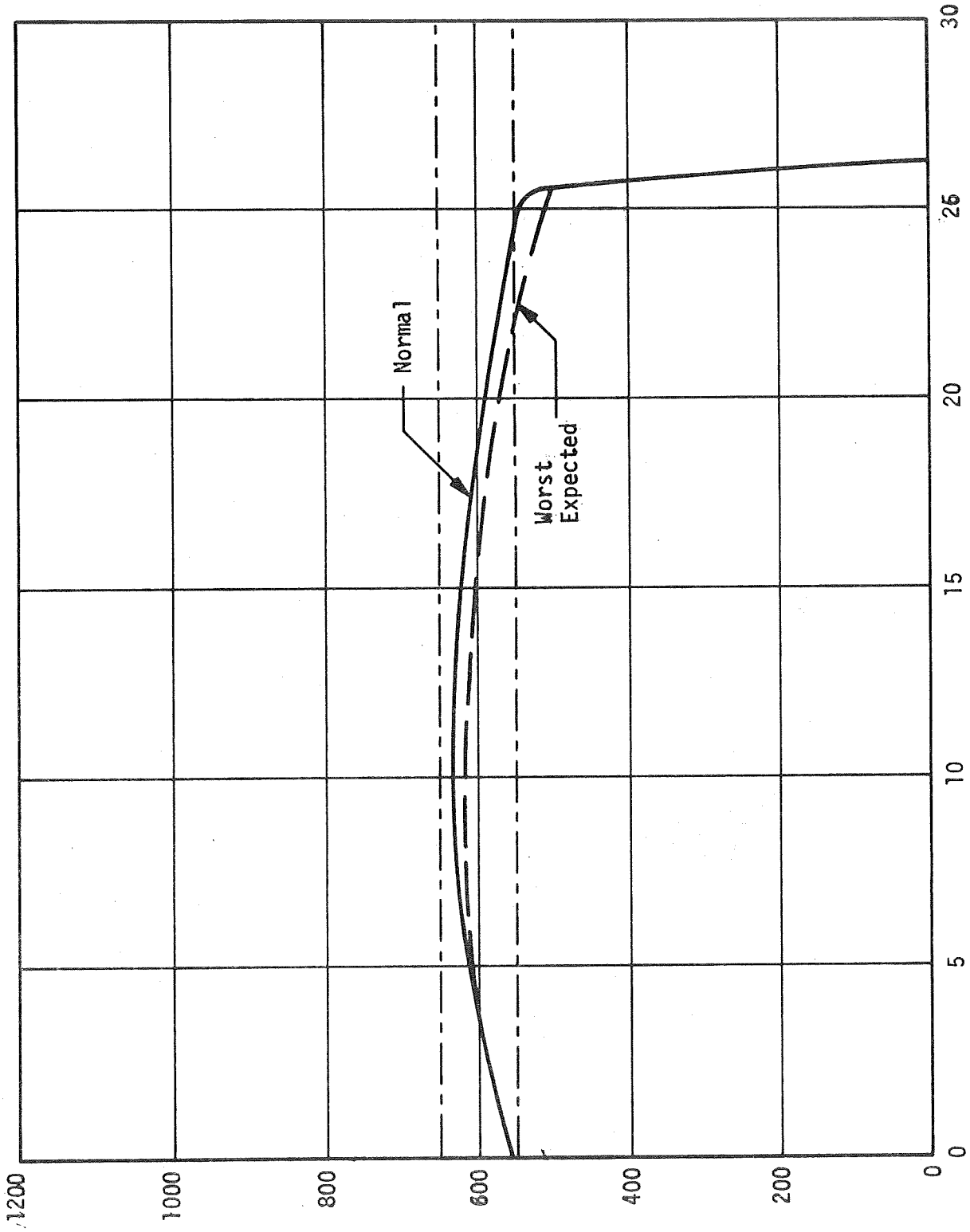

Predicted Pressure-Time Curve of Test Motor

Figure III-3

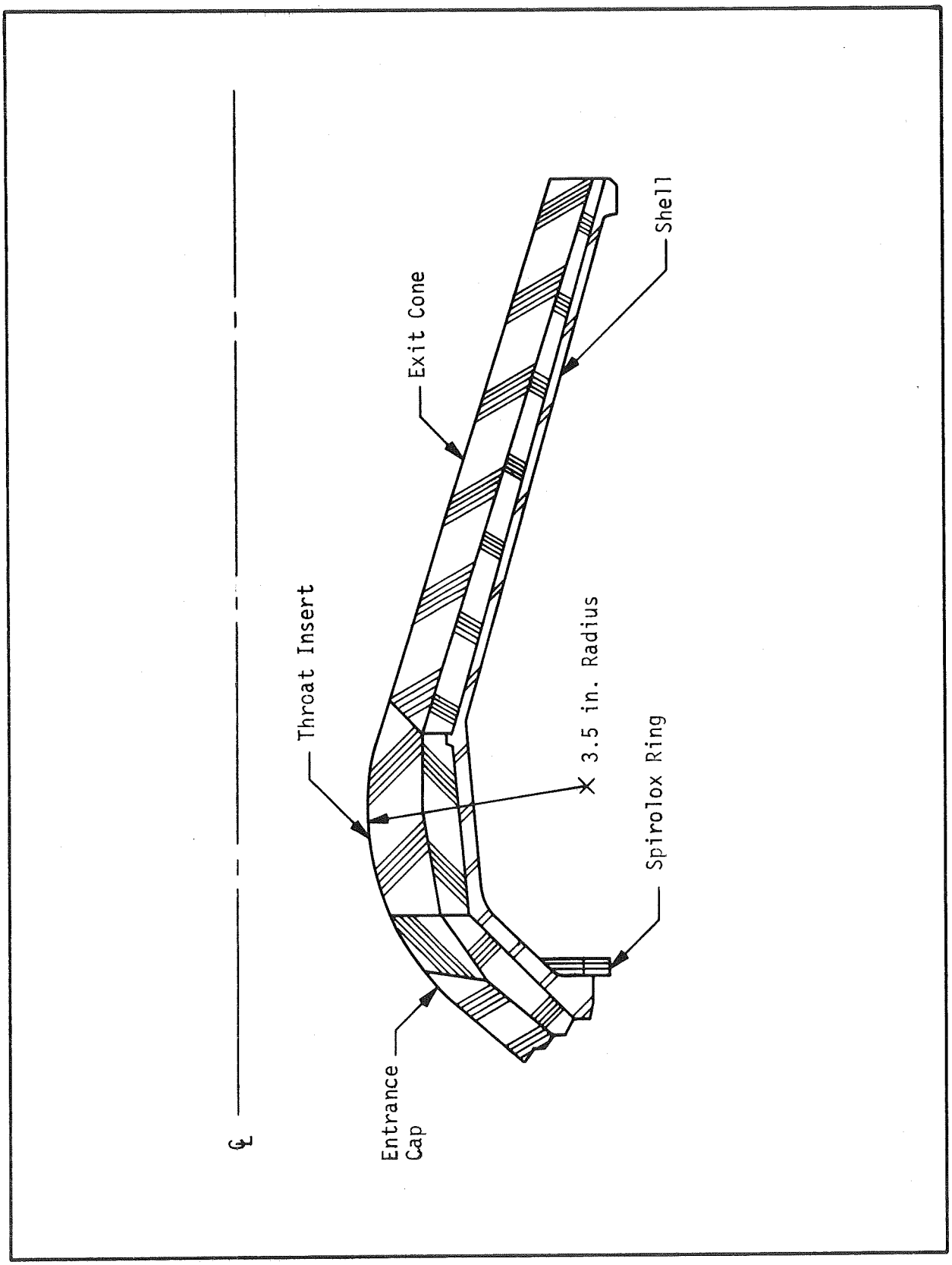

Test Nozzle Configuration

Figure III-4

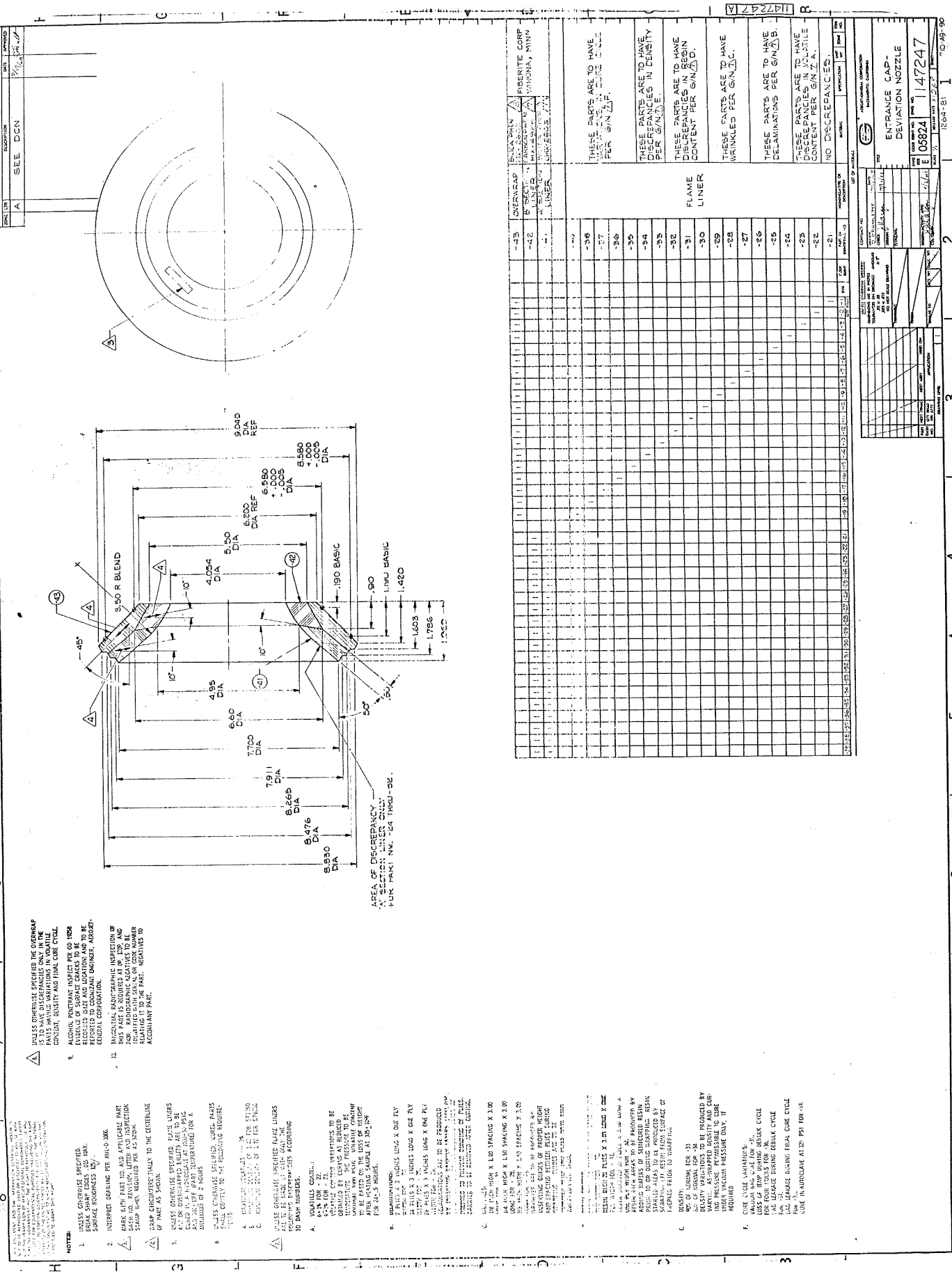

Figure III-5

Entrance Cap, Deviation Nozzle

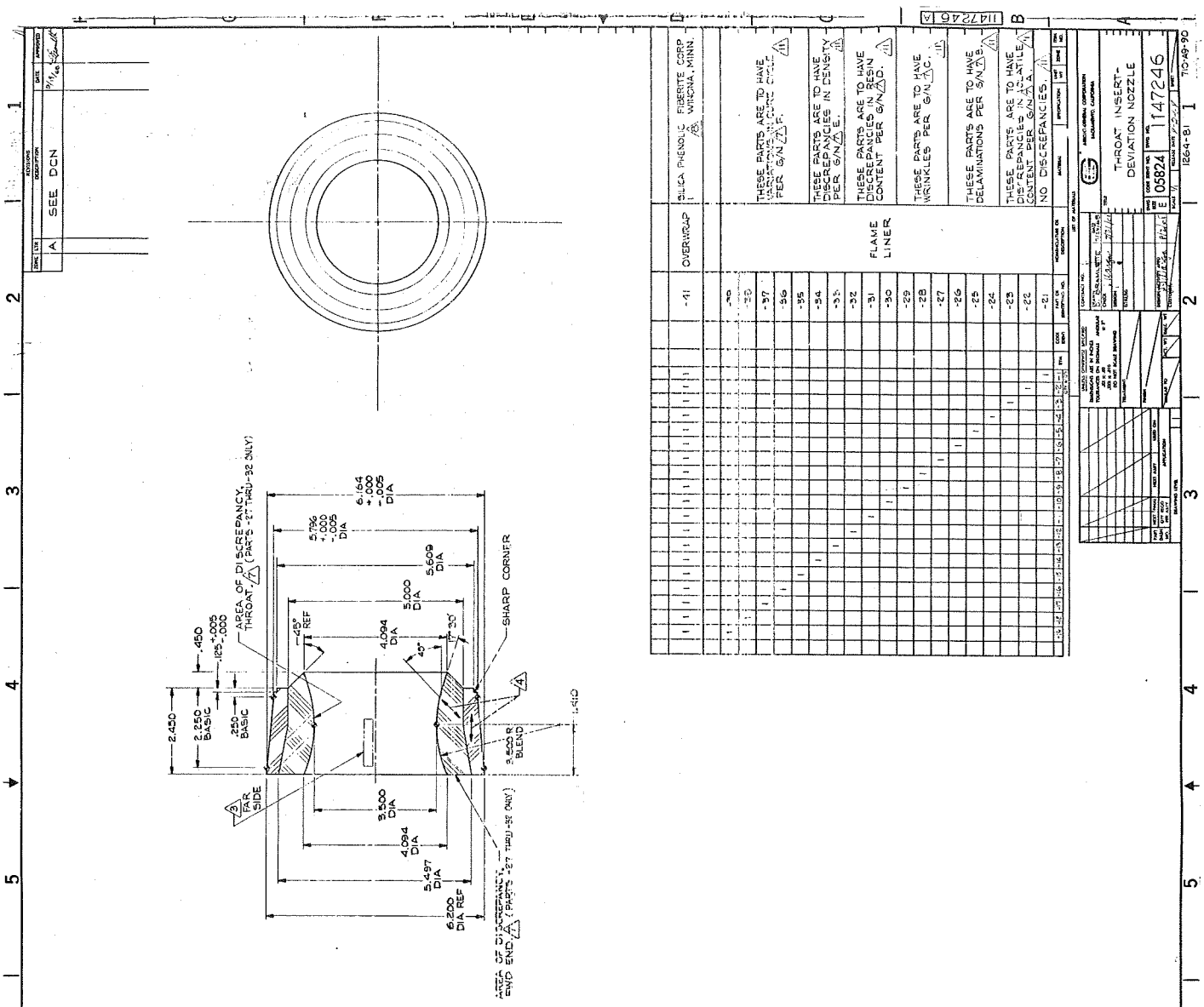

Figure III-6

Throat Insert, Deviation Nozzle

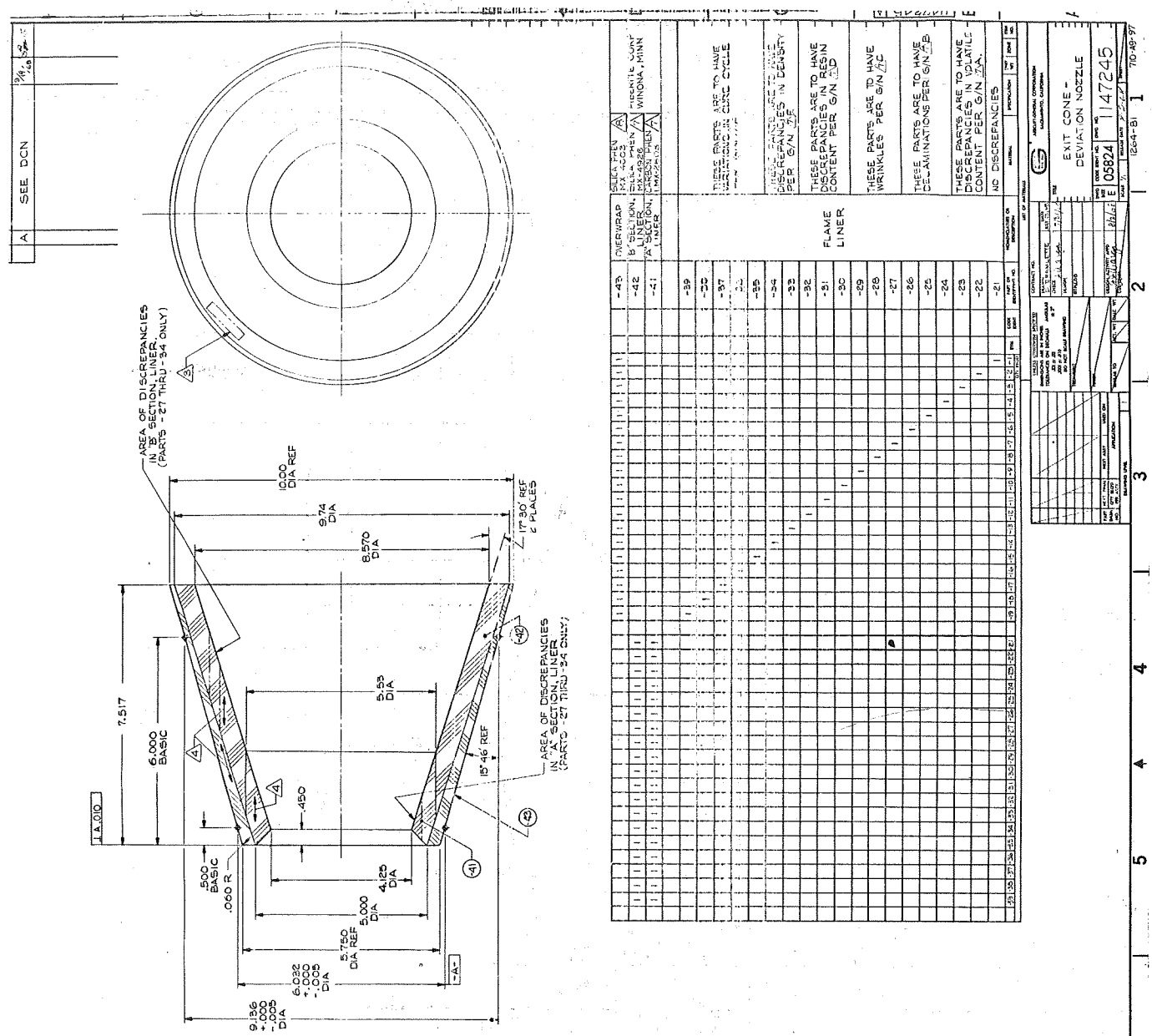

Figure III-7

Exit Cone, Deviation Nozzle

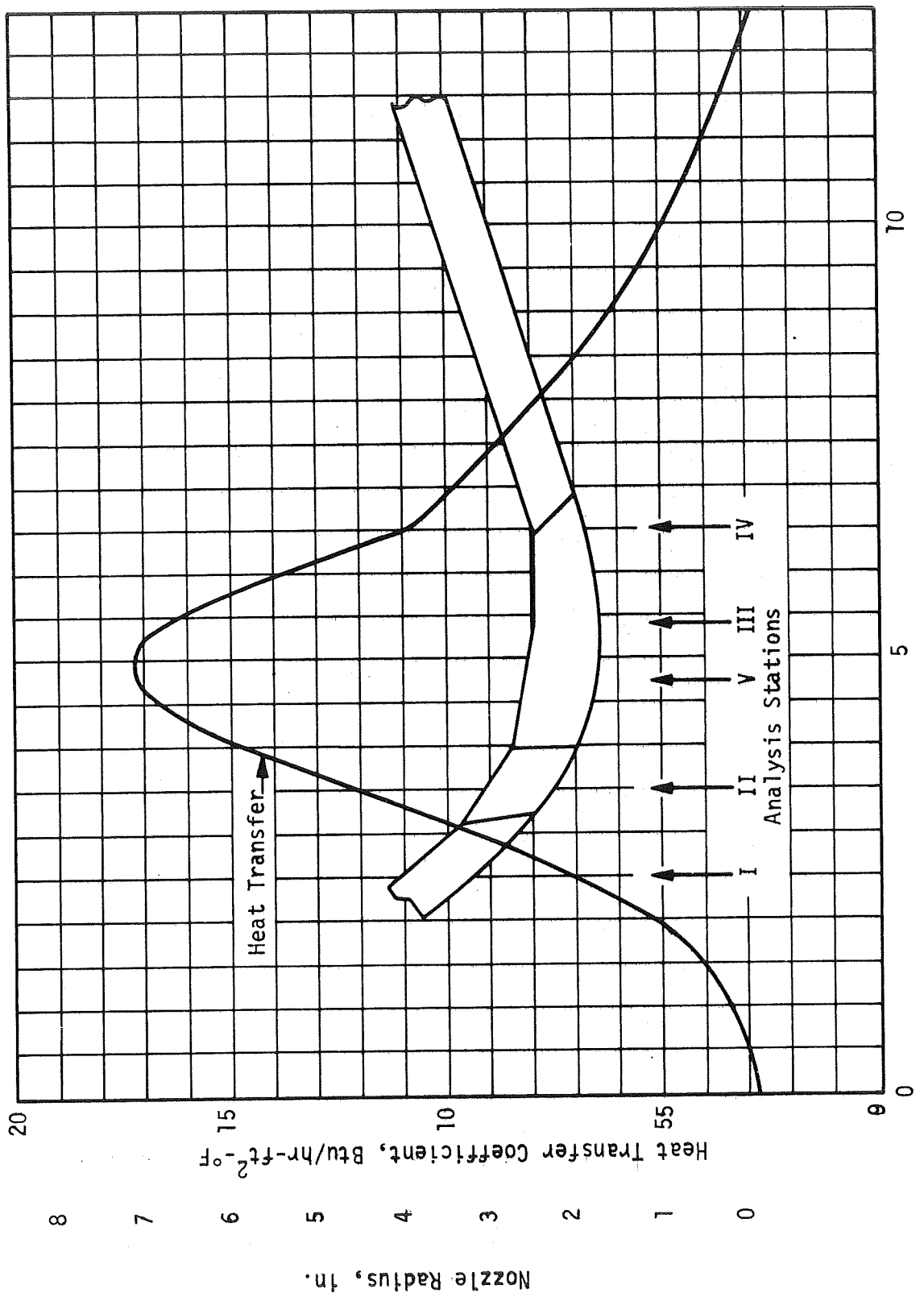

Heat Transfer Coefficient in Throat Region of Deviation Nozzle, P_c = 500 psia

Figure III-8

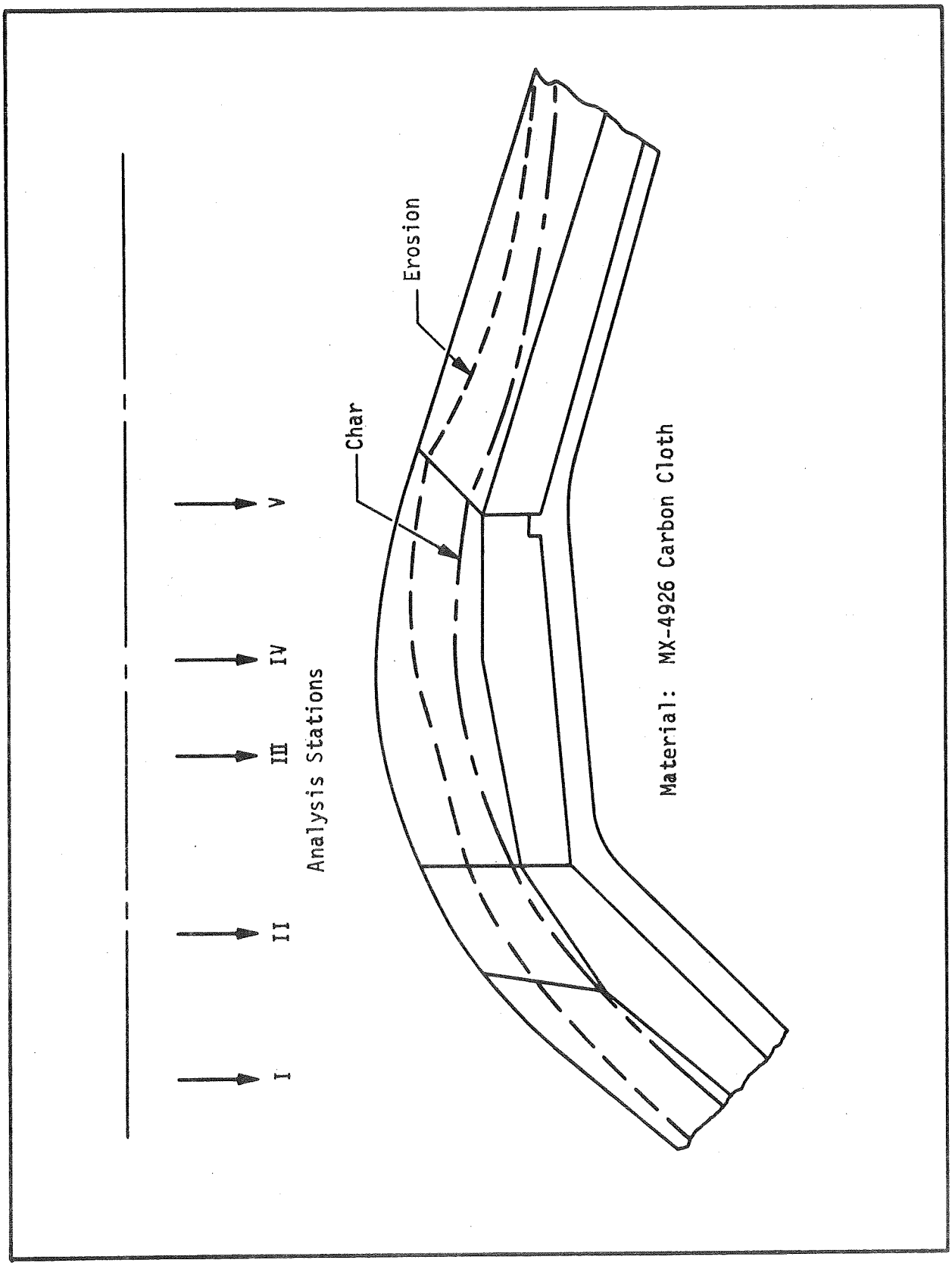

Preliminary Estimate of Erosion and Char in Throat Region of Deviation Nozzle

Figure III-9

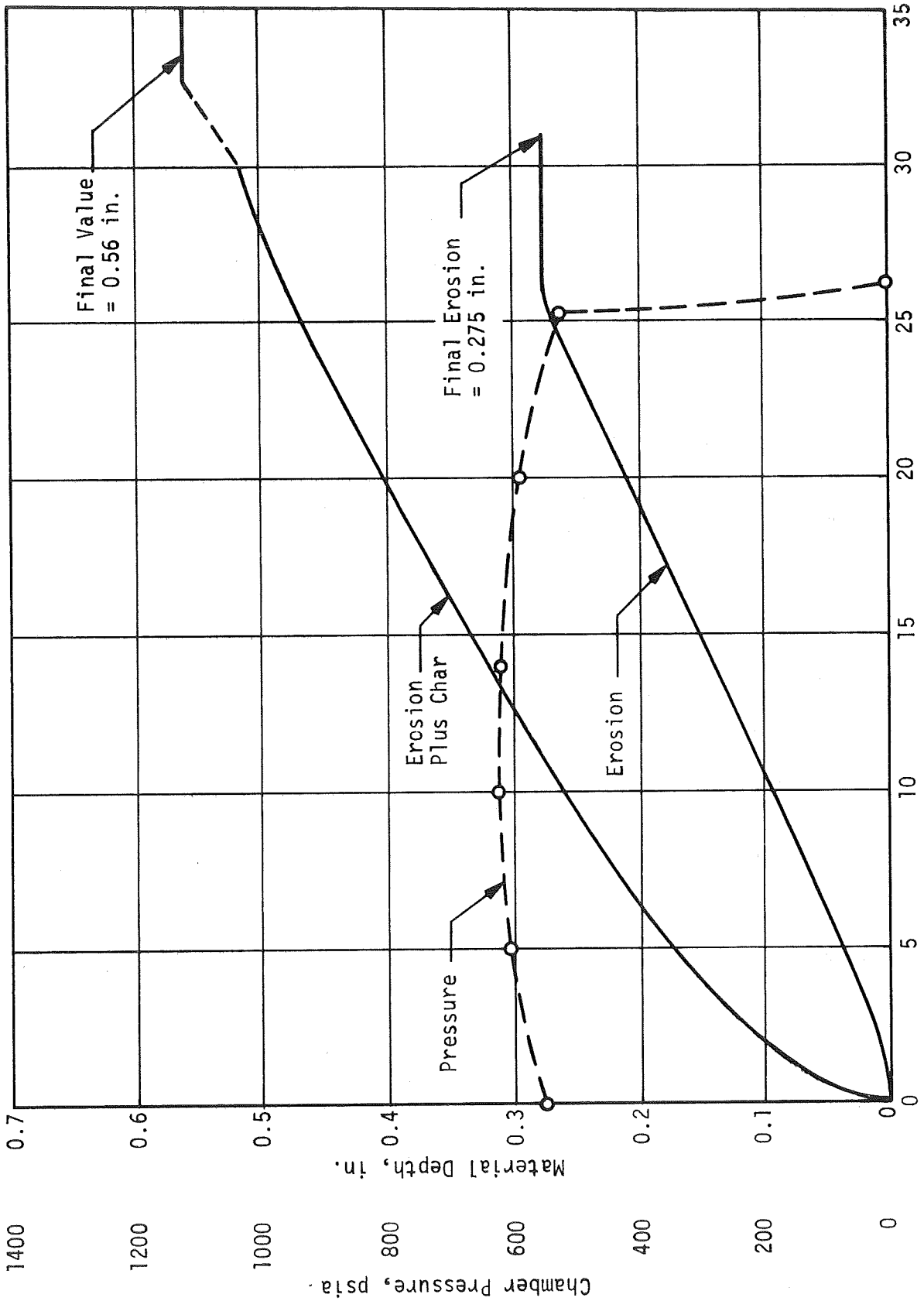

Erosion and Char Growth at Throat of Deviation Nozzle
(Material - MX 4926)

Figure III-10

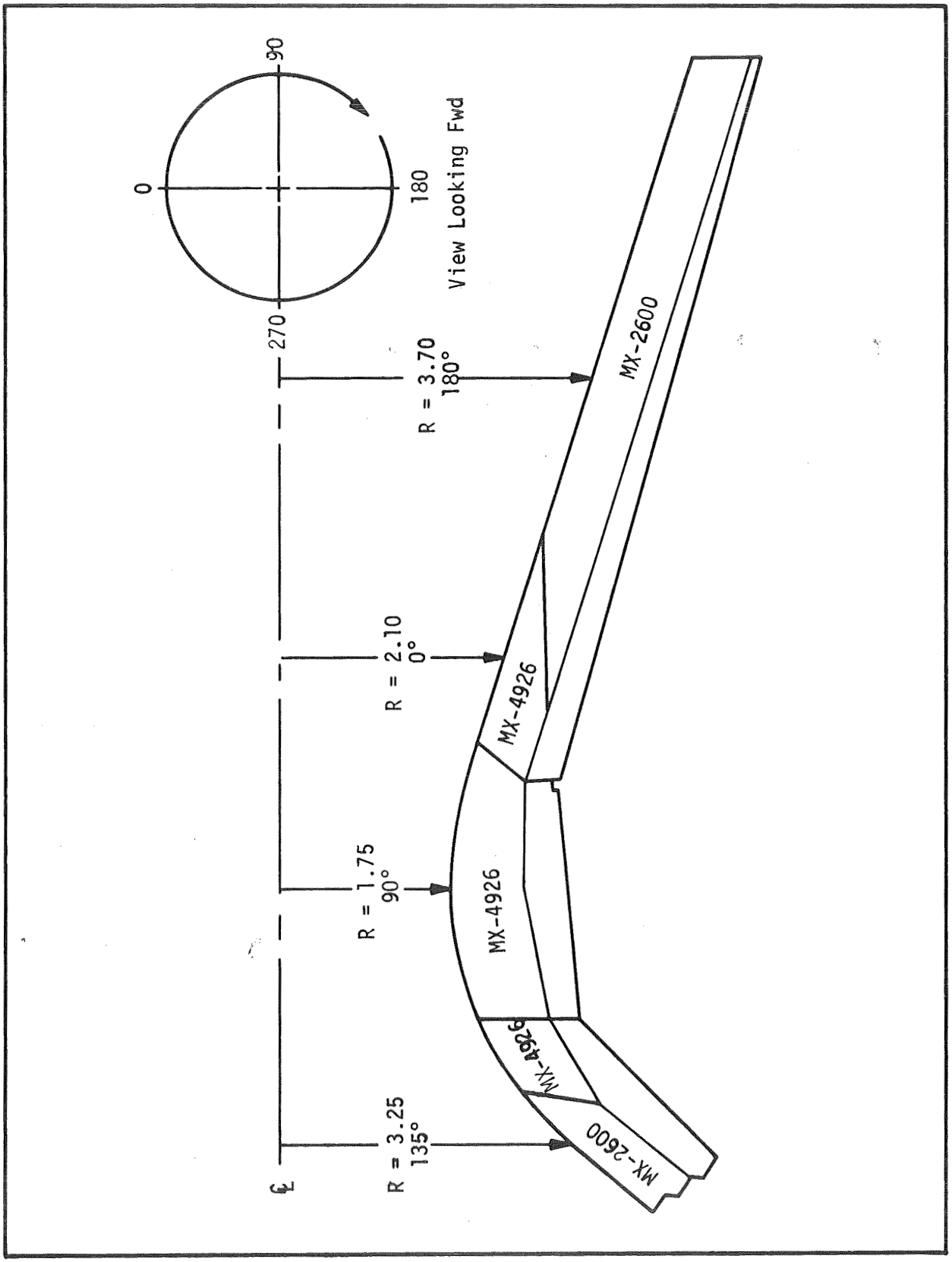

Placement of Localized Discrepancies in Nozzle Flame Liners

Figure III-11

IV. DISCREPANT NOZZLES

A. FABRICATION

The molding tape used in the fabrication of ablative nozzle components is manufactured by impregnating a fabric or mat with a selected plastic resin that has been diluted with a compatible solvent. Powdered fillers such as carbon or silica or hollow spheres (microballoons) of silica or resin may be added to the resin mix. The impregnated fabric or mat is then passed through temperature-controlled towers to remove the solvent and to polymerize the resin to some intermediate stage of advancement suitable for handling any further fabrication. The material — now called prepreg — is then slit into broadgoods and tapes and shipped to the component fabricator.

Fabrication of high performance nozzle components is generally accomplished by wrapping the prepreg tapes on a metal mandrel with the fabric plies oriented at some desired angle to the flame surface of the part. To improve the thermal properties and decrease axial and tangential thermal stresses, it would be desirable to orient the plies of flame liners parallel to the flame surfaces or as close thereto as possible. In actual application, a compromise ply orientation is selected for mechanical retention of each ply and for simplicity in fabrication. Wrapped nozzle components in the entrance and throat sections have ply orientations generally close to 45 degrees to the flame surface, while components in the exit section have the plies aligned parallel to the nozzle centerline. The highly oriented wraps require the use of a bias-fabric tape to produce the required deformation and compaction during wrapping; the parallel wraps have straight tapes.

Wrapping may be performed in either the horizontal or vertical positions. During wrapping, which is illustrated schematically in Figure IV-1, the prepreg tape is heated prior to lay-up, using hot air jets or radiant heaters. This softens the resin to provide for interply bonding and makes the

IV.A. Fabrication (cont)

prepreg more formable under the pressure rollers. The tape temperature, roller pressure and mandrel rotation during wrapping are controlled within narrow limits and the temperature of the wrapped preform is also controlled.

After the nozzle preform has been wrapped, it is covered with a porous fabric ("bleeder cloth"), enveloped in an impervious bag (usually butyl rubber) and cured by one of two alternative procedures. If the flame liner is to be overwrapped with another prepreg material of higher thermal insulating value, the preform is debulked (partially cured at full pressure and temperature between 165 and 180°F) so that a regular surface may be machined to accept the overwrap. If the flame liner is not to be overwrapped, the preform is fully cured at full pressure and the required resin polymerization temperature. During debulking and curing, a vacuum is maintained in the enveloping bag and the polymerization reaction products are drawn off through the bleeder cloth.

Pressurization may be applied during debulking and curing by one of several methods. Hydroclaves, using water pressures of up to 1000 psi; autoclaves, using gas pressures of up to 350 psi (2.41 MN/m^2); and nylon shrink tapes exerting hoop tensions between 75 (0.516) and 150 psi (1.03 MN/m^2) have all been used. Vacuum bag pressurization has also been used.

1. Materials for Test Nozzles

MX-4926 and MX-2600 prepreg materials, supplied by the Fiberite Corporation (Winona, Minn.) were used to fabricate the test nozzle components. MX-4926 is a carbon fabric impregnated with SC-1008 phenolic resin (Monsanto) filled with carbon powder. MX-2600 is a C-100-48 silica fabric impregnated with SC-1008 resin filled with silica powder. The properties of the prepreg materials used in fabricating the test nozzles are shown in Table IV-1, as reported by Fiberite.

IV.A. Fabrication (cont)

2. Processing of Test Nozzles

In general, the wrapping, debulking, and curing procedures used to fabricate the test nozzle components were as noted in Table IV-2. Departures from the general procedure were made to introduce individual discrepancies. Methods of introducing discrepancies and departures from the general procedure are described below:

a. Baseline

No discrepancies were introduced during fabrication and no departures from the general procedures occurred.

b. Density Variations

Density variations were produced by reducing the cure pressures and/or roller pressures during wrapping. The 80 to 90 percent dense components were wrapped at full roller pressures and cured under a vacuum pressure of 26 in. Hg (61 cm Hg); the 70 to 80 percent dense components were wrapped at one-half the basic roller pressures and cured under a vacuum pressure of 26 in. Hg (61 cm Hg).

c. Resin Content Variations

Wafers of semicured (190°F, 60 min.) resin 3-in.(7.62 cm)-long by one ply width weighing approximately one gram were introduced between the plies of the carbon and silica prepregs to produce the resin-rich discrepancies. The resin-starved discrepancy was produced by introducing pieces of carbon or silica prepreg 3-in.(7.62 cm)-long by one ply width from which the resin had been removed by immersion in acetone. All wrapping, debulking, and curing procedures conformed to the general procedures.

IV.A. Fabrication (cont)

d. Volatile Content Variations

Volatile content variations were produced by exposing the prepregs in covered containers containing isopropanol. The prepregs for the 6 percent volatile content parts were exposed for 20 hours; those for the 9 percent volatile content parts were exposed for 46 hours. In addition, the tape temperature during wrapping was reduced to 150°F, the flame liners were not debulked prior to the final cure, no vacuum was drawn during cure, and the cure temperature was reduced to 280 to 300°F.

e. Processing Cycle Variations

(1) Temperature Loss During Debulk Phase of Curing

To simulate equipment malfunction during hydroclave curing, the debulk phase was suspended after the part temperature had reached 175°F and the hydroclave pressure 200 psig (1.38 MN/m^2). After a four-hour hold (to replace heating elements) during which time the part temperature dropped to 160°F and vacuum pressure was maintained at 27 in. (68.6 cm), the cure cycle was continued in accordance with the general procedure.

(2) Bag Leakage During Debulk Cycle

Bag leakage was simulated by introducing a water line into the bagged part. After the part temperature had reached 175°F and the hydroclave pressure 1000 (6.89 MN/m^2) psig, water was introduced into the bag. Debulking was continued while the water was introduced. The flame liner was then overwrapped and cured in accordance with the general procedure.

IV.A. Fabrication (cont)

(3) Bag Leakage During Final Cure Cycle

In this variation, the flame liners were wrapped and debulked in accordance with the general procedures. The overwrap was applied and the part enveloped in a rubber bag. Water was introduced into the bag at the full hydroclave pressure of 1000 psig (6.89 MN/m^2) after the part temperature had reached 300°F. Curing was completed in the water-filled bag.

(4) Vacuum Cure

In this variation, the flame liners and overwraps were fabricated using normal wrapping procedures. During debulking and final curing, however, a maximum vacuum pressure of 27 in. (68.6 cm) Hg was applied.

(5) Autoclave Cure

The flame liners and overwraps were fabricated using normal wrapping procedures. During debulking and final curing a maximum pressure of 120 to 135 psig (0.826 to 0.93 MN/m^2) was applied.

f. Delaminations

Ply separations were introduced by placing wafers of Teflon 3-in.(7.62 cm)-long by one ply width by 0.005-in.(0.013 cm)-thick between the plies of the carbon and silica prepreg during wrapping of the flame liners. The Teflon wafers were left in the test nozzle components.

IV.A. Fabrication (cont)

g. Wrinkles

Wrinkles were introduced by placing carbon or silica composite rods of the required diameter and spacing between the plies of prepreg during wrapping. The rods were cured in place and left in the test nozzle components.

h. Bond Line Discrepancies

Bond line separations were introduced only between the nozzle support shell and the exit cone. Small discontinuous voids were produced by inserting Teflon patches; large, continuous areas of unbonding were produced by applying adhesive only to certain areas of the shell and exit cone. Figure IV-2 illustrates the procedures.

B. PROPERTIES

Since the introduced discrepancies were expected to influence the structural and ablative performances of the nozzle components, both mechanical and physical properties were determined. To permit the properties to reflect as closely as possible the actual effects of the discrepancies, duplicate sets of flame liners were fabricated concurrently with the test nozzle components. Specimens were machined from these duplicate flame liners at the discrepancy locations (with the exception that no specimens could be machined from the delaminated areas) and tested in accordance with the following procedures.

1. Density

Density was determined using the weight-volume procedure of Federal Test Method Standard (FTMS) 406, Method 5012. The results are shown

IV.B. Properties (cont)

in Table IV-3. In general, the hydroclave-cured components had a density of 89.9 lb/cu ft (1.44 gm/cc) for the MX-4926 composites and 109.8 lb/cu ft (1.76 gm/cc) for the MX-2600. Minor differences from these values were observed in specimens taken from the silica flame liners of high volatile content and one of those with resin-rich areas (105.5 to 106.1 lb/cu ft or 1.69 to 1.702 gm/cc). Major differences were observed in specimens taken from the carbon and silica flame liners cured by vacuum pressurization (MX-4926 = 65.6 to 84.3 lb/cu ft (1.05 to 1.35 gm/cc) and MX-2600 = 87.4 to 104.7 lb/cu ft (1.4 to 1.68 gm/cc). The flame liners cured by autoclave pressurization had densities equal to those of the hydroclave cured liners, indicating that the critical cure pressure to attain full density was less than 125 psig (0.86 MN/m^2).

2. Volatile Content

Volatile content was determined by measuring the weight loss of specimens of the virgin composite exposed in an air-recirculating oven at 325 $\pm$ 5°F (162.8 $\pm$ 2.7C) for 4 hours. The results are shown in Table IV-4. Generally, the volatile contents were well below 3 percent. Of particular interest are the results obtained with specimens from the components fabricated with deliberately introduced high volatile content. The final product did not meet the aim points of 6 and 9 percent; the maximum attained was 4.55 percent in the throat liner fabricated to an aim point of 6 percent.

The highest volatile content (4.62 percent) of any specimen was recorded for the throat liner fabricated with bag leakage during the debulk cycle.

3. Resin Content

The resin contents of the as-cured MX-2600 components were determined by the burn-off method, in which samples of the cured composite are

IV.B. Properties (cont)

heated in a muffle furnace at 1550 ± 50°F (815.6 ± 26.7°C) until a constant residue weight is reached. The method yielded reproducible results. Two methods of determining the resin content of the as-cured MX-4926 were tried — vacuum pyrolysis and nitric acid digestion; neither yielded reproducible results. Accordingly, the resin content of the MX-4926 flame liners was estimated from the initial resin content of the prepreg and the relationship observed in the MX-2600 material. Table IV-5 shows the measured resin contents of the MX-2600 and estimated resin contents of the MX-4926 components.

4. Compressive Properties

Compressive strength and modulus were determined at room and elevated temperatures in accordance with the procedures of FTMS-406, Method 1021. Prismatic specimens of square cross-section were machined from the flame liners with the long (loading) axis aligned parallel to the radial, axial, and tangential directions of the liners. These directions are illustrated in Figure IV-3. Consequently, the fabric plies, except in the cases of the radial and axial specimens taken from the exit cone, were aligned at some acute angle to the direction of loading. Table IV-6 shows the relationship between the specimen loading and the fabric ply orientation.

a. Room Temperature Results

Tables IV-7 and IV-8 show the average compressive strengths and moduli of specimens taken from the flame liners and tested at 75°F (23.9°C). If one examines the results obtained for the baseline specimens, they are representative of the results for MX-4926 and MX-2600 composites of comparable ply orientations (Reference 11), specifically with regard to the cross-ply (exit cone, radial) and parallel-to-ply (exit cone, axial) orientations. In examining the data on compressive properties, the following conclusions may be drawn:

IV.B. Properties (cont)

(1) The compressive strength and modulus decreased as the density decreased. Figure IV-4 shows the change in compressive properties of radial throat (MX-4926, 45-degree-to-ply) specimens as a function of density, using the values obtained from flame liners produced with density variations only. The increased spread in strength values at the low densities is associated with non-uniform porosity. The same relationship is indicated for the specimens of MX-4926 and MX-2600 materials taken from the other components, but the number of specimens was insufficient to establish range limits.

(2) There were no significant trends that could be established between compressive properties and severity of the remainder of the introduced discrepancies, although in the case of resin content, variations in the properties peaked at intermediate levels of resin content (Figures IV-5 and IV-6).

b. Elevated Temperature Results

Selected specimens of MX-4926 and MX-2600 were tested to determine the decrease in compressive properties that resulted from exposure to elevated temperatures. Tables IV-9 and IV-10 show the results that were obtained at a test temperature of 3000°F (1922K) for MX-4926 and at 2500°F (1644K) for MX-2600.

The specimens were charred at the temperature of testing in an argon atmosphere and machined square prior to test. Testing was conducted in a graphite furnace, using graphite anvils and push rods to apply the load. An argon atmosphere was maintained during testing.

IV.B. Properties (cont)

Two conclusions may be drawn from the data:

(1) The charred composites, particularly the MX-4926, retain a significant portion of their compressive properties at elevated temperatures.

(2) The compressive properties at elevated temperature vary directly with the density of the char.

5. Tensile Properties

The tensile strengths and moduli of specimens from selected flame liners were determined to verify the trends observed during compression testing. Tensile testing was performed at room temperature in accordance with the procedures of FTMS 406, Method 1011, using the specimen configuration of Figure IV-7.

The results, shown in Tables IV-11 and IV-12, indicate that the tensile properties decrease as the density decreases.

There was no available data regarding the tensile strength of carbon or silica reinforced composites in the cross-ply direction. Accordingly, tensile tests were conducted with specimens from the MX-4926 throat liners in which the tensile loading was applied normal to the lay of the fabric. The results are shown in Table IV-13. Comparing the cross-ply strength to that of the throat specimens tested in the transverse orientation (Table IV-11), in which the testing direction is substantially parallel to the plies, it appears that at full density, the cross-ply strength is 10% that of the with-ply value. At the lower density, the ratio of cross-ply to with-ply strength rises to approximately 25%.

IV.B. Properties (cont)

6. Specific Heat

The specific heats of specimens from the flame liners were determined by the standard drop-method technique using water as the heat-transfer medium. The calorimeter consisted of a Dewar flask equipped with a calibrated mercury thermometer and a fitted aluminum receiving cup. An electric multiple tube furnace was used to heat the specimens to the desired test temperatures. A single specimen from each flame liner was used for each series of determinations, the specimen being heated successively to the temperatures of measurement. The calculated specific heats are shown in Table IV-14.

7. Thermal Conductivity

Thermal conductivities of the flame liners were calculated from measured values of specific heat, density and thermal diffusivity by means of the following relationship:

$$K = \alpha \rho C_p \qquad \text{(Equation 1)}$$

a. Thermal Diffusivity

The thermal diffusivities of the flame liners were determined by the flash method described in Reference 12. The apparatus is shown schematically in Figure IV-8. The specimen used was a 0.750-in.(1.9 cm) dia wafer, 0.040 in.(1.01 mm)-thick, with the ply orientation aligned to the energy source in the same direction as it occurred in the nozzle component. As with the specific heat specimens, the same sample was used at all test temperatures. The results are shown in Table IV-15. The postscripts (c), (t), and (e) following the material designation refer to entrance cap, throat and exit cone, respectively. In most cases, it was possible to machine specimens from all

IV.B. Properties (cont)

components; where the values are missing, the amount of defective material was not sufficient to provide the required specimens.

b. Thermal Conductivity

The values of thermal conductivity calculated from the measured heat capacities, densities and thermal diffusivities are shown in Table IV-16. Except for the density variations there were no definite trends that could be established. Decreases in density decreased the thermal conductivity.

8. Thermal Expansion

Thermal expansion of specimens from the flame liners was determined in accordance with the procedures of ASTM Standard D696-44 using a quartz dilatometer. The specimens were machined to cylindrical configuration 0.125-in. (0.3175 cm) dia by 0.394 in.(1.0 cm) long and were tested over the range between 73°F (22.8°C) and 1000°F (537.8°C). The heating rate was maintained at 15°F (8.33°C) per minute and changes in length were measured optically at intervals of 50°F (27.7°C). An argon atmosphere was maintained around the specimens during test.

The unit dimensional changes with temperature and the range between maximum unit expansion and maximum unit shrinkage for each of the specimens tested are shown in Tables IV-17, IV-18, and IV-19, arranged in order of decreasing shrinkage. In general, dimensional changes were affected most by density changes, and changes in resin content. Two notable exceptions to the general rule were observed, both in the MX-2600 silica fabric reinforced material. In the entrance section tests (Table IV-19), the high expansion and shrinkage of the specimens in which temperature loss occurred during debulk

IV.B. Properties (cont)

were traced to the presence of improper ply orientation (approximately 50 degrees). On the exit-section tests (Table IV-18), no explanation could be found for the high expansion and shrinkage of the 9% volatile content specimens, since the actual volatile content was only 1.90% (see Table IV-4).

TABLE IV-1

PROPERTIES OF PREPREG MATERIALS USED IN DISCREPANT NOZZLE COMPONENTS

	MX-4926				MX-2600			
Lot	E-545	E-545	E-545	E-545	E-543	E-543	E-543	E-543
Roll	2	3	4	1	1A	1B	2A	2B
Resin Solids, %	37.0	36.0	37.6	35.2	31.0	31.4	31.1	30.6
Volatile Content, %	5.0	4.9	4.9	4.8	4.5	4.3	4.1	3.9
Laminate Flow, % at 150 psi	18.0	20.5	17.9	13.3				
% at 500 psi	--	--	--	--	13.2	10.1	10.0	8.8

General Fabrication Procedures

Nozzle Component	Wrapping					Debulk					Cure				
	Roller Pressure		Tape Temperature		As-wrapped Density, %	Temperature		Pressure, Gage		Time, min	Temperature		Pressure, Gage		Time, min
	lbf/in.	(N/cm)	°F	(K)		°F	(K)	lbf/in.^{2}	(N/mm^2)		°F	(K)	lbf/in.^{2}	(N/mm^2)	
Entrance Cap															
Carbon Liner	150	263	180-195	355-364	95-98	175-185	353-358	220-225	1517-1551	50-60	300-320	422-433	1000	6895	150-180
Silica Liner	185	324	190-195	361-364	90-98										
Overwrap	250	434	190-195	361-364	85-90	- -		- -		- -					
Throat															
Carbon Liner	150	263	190-195	361-364	90-95	175-185	353-358	220-225	1517-1551	45-60	300-320	422-433	1000	6895	140-170
Overwrap	350	613	185-195	358-364	90-95	- -		- -		- -					
Exit Cone															
Carbon Liner	150	263	190-195	361-364	97-99	175-185	353-358	200-225	1379-1551	50-60	300-320	422-433	1000	6895	130-170
Silica Liner	100	175	190-95	361-364	94-98										
Overwrap	175	306	190-195	361-364	90-95	- -		- -		- -					

Table IV-2

TABLE IV-3

DENSITIES OF NOZZLE COMPONENTS

Discrepancy	Material	Location	Density, lb/cu ft	Density, gm/cc
None (Baseline)	MX-4926	All	89.9	1.44
	MX-2600	All	109.8	1.76
Vacuum Bag, 25 in. Hg	MX-4926	Throat	65.5	1.05
		Exit	78.6	1.26
	MX-2600	Entrance	94.2	1.51
		Exit	104.7	1.65
Autoclave, 125 psig	MX-4926	All	89.9	1.44
	MX-2600	Entrance	108.6	1.74
		Exit	109.3	1.75
Bag Leak, Debulk	MX-4926	All	90.5	1.45
	MX-2600	All	109.8	1.76
Bag Leak, Final Cure	MX-4926	All	90.5	1.45
	MX-2600	All	109.8	1.76
Temp., Loss, Debulk	MX-4926	All	89.9	1.44
	MX-2600	All	109.8	1.76
70 to 80% Density	MX-4926	Throat	65.6	1.05
		Exit	78.6	1.26
	MX-2600	Entrance	87.4	1.40
		Exit	102.4	1.64
80 to 90% Density	MX-4926	Entrance	67.4	1.08
		Throat	66.2	1.06
		Exit	84.3	1.35
	MX-2600	Entrance	96.1	1.54
		Exit	101.1	1.62
6% Volatiles	MX-4926	Throat	88.7	1.42
		Exit	89.2	1.43
	MX-2600	Entrance	108.6	1.74
		Exit	105.5	1.69
9% Volatiles	MX-4926	All	89.9	1.44
	MX-2600	Entrance	107.3	1.72
		Exit	106.1	1.70
Wrinkles, 0.125 in.	MX-4926	All	90.5	1.45
	MX-2600	All	110.5	1.77
Wrinkles, 0.25 in.	MX-4926	All	89.9	1.44
	MX-2600	All	109.8	1.76
Wrinkles, 0.375 in.	MX-4926	All	89.9	1.44
	MX-2600	All	105.5	1.69
Resin Rich, 10 plies	MX-4926	All	89.9	1.44
	MX-2600	All	110.5	1.77
Resin Rich, 20 plies	MX-4926	All	89.3	1.43
	MX-2600	All	105.5	1.69
Resin Starved, 10 plies	MX-4926	All	89.9	1.44
	MX-2600	All	109.8	1.76

TABLE IV-4

VOLATILE CONTENTS OF NOZZLE COMPONENTS

Discrepancy	Material	Location	Volatile Content, percent
None (Baseline)	MX-4926	Throat	2.68
		Entrance	2.40
	MX-2600	Exit	1.40
		Entrance	1.35
Vacuum Bag, 25 in. Hg	MX-4926	Throat	1.6
	MX-2600	Exit	1.71
Autoclave, 125 psig	MX-4926	Throat	2.8
	MX-2600	Exit	1.88
Bag Leak, Debulk	MX-4926	Throat	4.62
	MX-2600	Exit	1.52
Bag Leak, Final Cure	MX-4926	Throat	2.83
	MX-2600	Exit	1.72
Temperature Loss, Debulk	MX-4926	Throat	2.24
	MX-2600	Exit	2.08
70 to 80% Density	MX-4926	Throat	1.81
		Exit	2.47
	MX-2600	Exit	2.25
80 to 90% Density	MX-4926	Throat	2.88
		Exit	3.37
		Entrance	2.47
	MX-2600	Exit	3.98
		Entrance	2.50
6% Volatiles	MX-4926	Throat	3.56
		Exit	4.55
	MX-2600	Exit	2.62
9% Volatiles	MX-4926	Throat	4.06
	MX-2600	Exit	1.90
Wrinkles, 0.125 x 1	MX-4926	Throat	2.28
	MX-2600	Exit	1.45
Wrinkles, 0.25 x 1.5	MX-4926	Throat	2.37
	MX-2600	Exit	1.75
Wrinkles, 0.375 x 1.5	MX-4926	Throat	2.61
	MX-2600	Exit	2.11
Resin Rich, 10 plies	MX-4926	Throat	3.23
	MX-2600	Exit	1.55
Resin Rich, 20 plies	MX-4926	Throat	2.99
	MX-2600	Exit	2.13
Resin Starved, 10 plies	MX-4926	Throat	2.76
	MX-2600	Exit	1.53

TABLE IV-5

RESIN CONTENTS OF FLAME LINERS

Discrepancy	Material	Resin Content, %	Method
Baseline	MX-2600	32.6	Burn-Off
Resin-Rich, 10 plies	MX-2600	36.5	
Resin-Rich, 20 plies	MX-2600	45.3	
Resin-Starved, 10 plies	MX-2600	23.1	Burn-Off
Baseline	MX-4926	37.5	Estimated
Resin-Rich, 10 plies	MX-4926	41.0	
Resin-Rich, 20 plies	MX-4926	53.0	
Resin-Starved, 10 plies	MX-4926	26.0	Estimated

TABLE IV-6

RELATIONSHIP BETWEEN SPECIMEN LOADING AND PLY ORIENTATION

Component	Specimen Loading		Ply Orientation
Entrance	Radial	(R)	80 Degrees
	Axial	(A)	10 Degrees
	Tangential	(T)	90 Degrees (curved)
Throat	Radial	(R)	45 Degrees
	Axial	(A)	45 Degrees
	Tangential	(T)	90 Degrees (curved)
Exit Cone	Radial	(R)	Normal-to-Ply
	Axial	(A)	Parallel-to-Ply
	Tangential	(T)	90 Degrees (curved)

TABLE IV-7

COMPRESSIVE PROPERTIES OF MX-4926 COMPONENTS AT 75°F (297K)

Discrepancy	Location		Density, gm/cc	Strength, Ksi	Strength, MN/m^2	Modulus, psi x 10^6	Modulus, GN/m^2
None (Baseline)	Entrance	(R)	1.44	32.0	220.6	2.87	19.8
		(A)		N.T.	---	N.T.	---
		(T)		29.2	201.3	3.15	21.7
	Throat	(R)	1.44	34.4	237.2	2.74	18.9
		(A)		31.6	217.9	3.12	21.5
		(T)		29.3	202.0	3.27	22.5
	Exit	(R)	1.44	75.4	519.9	2.43	16.8
		(A)		36.4	251.0	3.37	23.2
		(T)		28.7	197.9	3.39	23.4
Vacuum Bag 25 in. Hg	Throat	(R)	1.05	14.6	100.7	1.44	9.9
		(A)		13.4	92.4	1.64	11.3
		(T)		12.4	85.5	1.72	11.9
Autoclave, 125 psig	Throat	(R)	1.44	33.6	231.7	3.41	23.5
		(A)		30.9	213.1	3.88	26.8
		(T)		28.7	197.9	4.07	28.1
Bag Leak, Debulk	Throat	(R)	1.45	35.0	241.3	2.48	17.1
		(A)		32.2	222.0	2.93	20.2
		(T)		29.9	206.1	3.07	21.2
Bag Leak, Final Cure	Throat	(R)	1.45	31.7	218.6	2.82	19.4
		(A)		29.1	200.6	3.21	22.1
		(T)		27.0	186.2	3.36	23.2
Temperature Loss, Debulk	Exit	(R)	1.44	72.2	497.8	3.27	22.5
		(A)		37.7	259.9	3.9	26.9
		(T)		29.7	204.8	3.92	27.0
70 to 80% Density	Throat	(R)	1.05	6.09	42.0	0.88	6.1
		(A)		6.13	42.3	0.91	6.3
		(T)		5.75	39.6	0.86	5.9
	Exit	(R)	1.26	24.7	170.3	2.26	15.6
		(A)		14.4	99.3	2.46	17.0
		(T)		11.1	76.5	2.81	19.4

TABLE IV-7

COMPRESSIVE PROPERTIES OF MX-4926 COMPONENTS AT 75°F (297K)

Discrepancy	Location		Density, gm/cc	Strength, Ksi	Strength, MN/m^2	Modulus, psi x 10^6	Modulus, GN/m^2
80 to 90% Density	Entrance	(R)	1.08	7.3	50.3	1.44	9.9
		(A)		8.5	58.6	1.45	10.0
		(T)		18.8	129.6	2.66	18.3
	Throat	(R)	1.06	8.8	60.7	1.47	10.1
		(A)		11.1	76.5	1.39	9.6
		(T)		18.5	127.6	2.65	18.3
80 to 90% Density	Exit	(R)	1.35	44.1	304.1	2.51	17.3
		(A)		16.9	116.5	3.1	21.4
		(T)		35.8	246.8	3.6	24.8
6% Volatiles	Throat	(R)	1.42	26.2	180.6	2.53	17.4
		(A)		26.3	181.3	2.6	17.9
		(T)		24.4	168.2	2.47	17.0
	Exit	(R)	1.43	48.5	334.4	2.89	19.9
		(A)		27.7	91.0	3.16	21.8
		(T)		21.4	147.6	3.6	24.8
9% Volatiles	Throat	(R)	1.44	28.3	195.1	3.32	22.9
		(A)		26.0	179.3	3.78	26.1
		(T)		24.0	165.5	3.96	27.3
Wrinkles, 0.125 x 1	Exit	(A)	1.45	28.4	195.8	3.49	24.1
Wrinkles, 0.25 x 1.5	Exit	(A)	1.44	27.2	187.5	3.69	25.4
Wrinkles, 0.375 x 1.5	Throat	(A)	1.44	29.1	200.6	4.32	29.8
Resin Rich, 10 plies	Exit	(A)	1.44	35.2	242.7	3.58	24.7
Resin Rich, 20 plies	Exit	(A)	1.43	31.8	219.3	3.74	25.8
Resin Starved, 10 plies	Exit	(A)	1.44	21.2	146.2	4.22	29.1

TABLE IV-8

COMPRESSIVE PROPERTIES OF MX-2600 COMPONENTS AT 75°F (297K)

Discrepancy	Location		Density, gm/cc	Strength		Modulus	
				Ksi	MN/m^2	psi x 10^6	GN/m^2
None (Baseline)	Entrance	(R)	1.76	47.6	328.2	3.11	21.4
		(A)		36.4	251.0	3.48	24.0
		(T)		28.7	197.9	3.97	27.4
	Exit	(R)	1.76	63.4	437.1	3.07	21.2
		(A)		54.5	375.8	4.87	33.6
		(T)		63.6	438.5	4.85	33.4
Vacuum, Bag, 25 in. Hg	Exit	(R)	1.65	49.3	339.9	2.17	15.0
		(A)		42.4	292.3	4.27	29.5
		(T)		49.5	341.3	4.26	29.4
Autoclave, 125 psig	Exit	(R)	1.75	65.0	448.2	3.28	22.6
		(A)		55.8	384.7	5.21	35.9
		(T)		65.2	449.6	5.19	35.8
Bag Leak, Debulk	Exit	(R)	1.76	62.0	427.5	2.91	20.1
		(A)		53.3	367.5	4.61	31.8
		(T)		62.2	428.9	4.6	31.7
Bag Leak, Final Cure	Exit	(R)	1.76	65.6	452.3	2.93	20.2
		(A)		56.5	389.6	4.65	32.1
		(T)		65.8	453.7	4.63	31.9
Temperature Loss, Debulk	Exit	(R)	1.76	59.7	411.6	3.63	25.0
		(A)		49.8	343.4	4.52	31.2
		(T)		58.1	400.6	4.5	31.0
70 to 80% Density	Exit	(R)	1.64	43.0	296.5	3.3	22.8
		(A)		42.9	295.8	3.82	26.3
		(T)		39.1	269.6	2.96	20.4
80 to 90% Density	Entrance	(R)	1.54	17.9	123.4	2.04	14.1
		(A)		18.5	127.6	2.40	16.5
		(T)		21.7	149.6	2.84	19.6
	Exit	(R)	1.62	36.8	253.7	2.54	17.5
		(A)		36.9	254.4	4.01	27.6
		(T)		44.7	308.2	4.19	28.9

TABLE IV-8

COMPRESSIVE PROPERTIES OF MX-2600 COMPONENTS AT 75°F (297K)

Discrepancy	Location		Density, gm/cc	Strength		Modulus	
				Ksi	MN/m^2	psi x 10^6	GN/m^2
6% Volatiles	Exit	(R)	1.69	55.7	384.1	3.78	26.1
		(A)		55.5	382.7	4.38	30.2
		(T)		50.6	348.9	3.4	23.4
9% Volatiles	Exit	(R)	1.70	65.3	450.2	2.93	20.2
		(A)		56.1	386.8	4.65	32.1
		(T)		65.5	451.6	4.6	31.7
Wrinkles, 0.125 x 1	Exit	(A)	1.77	51.2	353.0	4.25	29.3
Wrinkles, 0.25 x 1.5	Exit	(A)	1.76	50.0	344.8	3.5	24.1
Wrinkles, 0.375 x 1.5	Exit	(A)	1.69	54.8	377.8	5.8	40.0
Resin Rich, 10 plies	Exit	(A)	1.77	57.3	395.1	3.8	26.2
Resin Rich, 20 plies	Exit	(A)	1.69	46.0	317.2	2.92	20.1
Resin Starved, 10 plies	Exit	(A)	1.76	52.0	358.5	5.48	37.8

TABLE IV-9

COMPRESSIVE PROPERTIES OF MX-4926 COMPONENTS AT 3000°F (1922K)

Discrepancy	Location		Density, lb/cu ft	Density, gm/cc	Strength, ksi	Strength, MN/m^2	Modulus, psi x 10^6	Modulus, GN/m^2
None (Baseline)	Entrance	(R)	68.6	1.10	7.9	54.5	0.41	2.8
		(T)	68.6	1.10	7.2	49.6	0.75	5.2
	Throat	(R)	69.9	1.12	7.2	49.6	0.71	4.9
		(A)	69.9	1.12	9.1	62.7	0.81	5.6
		(T)	69.9	1.12	6.0	41.4	0.85	5.9
	Exit	(A)	71.1	1.14	12.1	83.4	0.92	6.3
		(T)	71.1	1.14	9.5	65.5	0.95	6.6
Vacuum Bag, 25 in. Hg	Throat	(R)	56.2	0.90	3.1	21.4	0.37	2.6
		(A)	56.2	0.90	2.8	19.3	0.42	2.9
		(T)	56.2	0.90	2.6	17.9	0.45	3.1
Autoclave, 125 psig	Throat	(R)	70.5	1.13	7.1	49.0	0.88	6.1
		(A)	70.5	1.13	6.5	44.8	1.02	7.0
70 to 80% Density	Throat	(R)	56.2	0.90	2.8	19.3	0.35	2.4
80 to 90% Density	Throat	(R)	56.2	0.90	2.5	17.2	0.35	2.4

TABLE IV-10

COMPRESSIVE PROPERTIES OF MX-2600 COMPONENTS AT 2500°F (1644K)

Discrepancy	Location		lb/cu ft	gm/cc	Strength ksi	Strength MN/m^2	Modulus psi x 10^6	Modulus GN/m^2
None (Baseline)	Entrance	(R)	88.7	1.42	2.72	18.8	0.055	0.38
		(A)	88.7	1.42	2.26	15.6	0.061	0.42
		(T)	88.7	1.42	2.51	17.3	0.070	0.48
	Exit	(R)	90.5	1.45	3.55	24.5	0.054	0.37
		(A)	90.5	1.45	3.05	21.0	0.086	0.59
		(T)	90.5	1.45	3.56	24.5	0.086	0.59
80 to 90% Density	Entrance	(R)	71.8	1.15	0.9	6.2	0.016	0.11
		(A)	71.8	1.15	0.74	5.1	0.027	0.19
		(T)	71.8	1.15	0.82	5.7	0.023	0.16
	Exit	(A)	84.3	1.35	2.65	18.3	0.072	0.5

TABLE IV-11

TENSILE PROPERTIES OF MX-4926 COMPONENTS AT 75°F (297K)

Discrepancy	Location		Density, gm/cc	Strength		Modulus	
				Ksi	MN/m^2	psi x 10^6	GN/m^2
None (Baseline)	Throat	(A)	1.44	2.7	18.6	1.97	13.6
		(T)	1.44	11.8	81.4	3.1	21.4
	Exit	(T)	1.44	9.65	66.5	2.7	18.6
Vacuum Bag, 25 in. Hg	Throat	(A)	1.05	1.15	7.9	0.6	4.1
		(T)	1.05	4.2	29.0	1.65	11.4
Autoclave, 125 psig	Throat	(A)	1.44	2.7	18.6	2.0	13.8
		(T)	1.44	11.6	80.0	3.1	21.4
	Exit	(T)	1.44	9.5	65.5	2.65	18.3
70 to 80% Density	Throat	(A)	1.05	1.2	8.3	0.83	5.7
80 to 90% Density	Throat	(A)	1.06	1.4	9.7	0.92	6.3

TABLE IV-12

TENSILE PROPERTIES OF MX-2600 COMPONENTS AT 75°F (297K)

Discrepancy	Location	Density, gm/cc	Strength		Modulus	
			Ksi	MN/m^2	psi x 10^6	GN/m^2
None (Baseline)	Exit (17.5°)	1.76	7.2	49.6	2.4	16.5
	(T)	1.76	10.8	74.5	2.7	18.6
Vacuum Bag, 25 in. Hg	Exit (17.5°)	1.65	6.0	41.4	2.2	15.2
	(T)	1.65	8.5	58.6	2.4	16.5
Autoclave, 125 psig	Exit (17.5°)	1.75	7.0	48.3	2.5	17.2
	(T)	1.75	11.1	76.5	2.9	20.0
80 to 90% Density	Exit (17.5°)	1.62	5.4	37.2	1.69	11.7

TABLE IV-13

CROSS-PLY TENSILE PROPERTIES OF MX-4926 COMPONENTS AT 75°F (297K)

Discrepancy	Location	Density, gm/cc	Strength, ksi	Strength, MN/m^2	Modulus, psi x 10^6	Modulus, GN/m^2
None (Baseline)	Throat	1.44	1.5	10.3	0.85	5.9
70 to 80% Density	Throat	1.05	0.83	5.7	0.90	6.2
80 to 90% Density	Throat	1.06	0.97	6.7	0.99	6.8
6% Volatiles	Throat	1.42	1.4	9.7	1.2	8.3
9% Volatiles	Throat	1.44	1.8	12.4	1.18	8.1

TABLE IV-14

SPECIFIC HEATS OF TEST MATERIALS, cal/g-°C

Discrepancy	Material	212°F (100°C)	392°F (200°C)	500°F (260°C)	700°F (371°C)	1040°F (560°C)	1600°F (871°C
None (Baseline)	MX-4926	0.2845	0.2919	0.2998	0.3240	0.3439	0.3617
	MX-2603	0.2387	0.2519	0.2606	0.2733	0.2878	0.2630
Vacuum Bag, 25 in. Hg	MX-4926	0.2435	0.2881	0.3095	0.3229	0.3515	0.3615
	MX-2603	0.2182	0.2533	0.2774	0.2690	0.2935	0.2837
Autoclave, 125 psig	MX-4926	0.2513	0.3109	0.3200	0.3232	0.3538	0.3618
	MX-2603	0.2447	0.2620	0.2743	0.2768	0.2873	0.2736
Bag Leakage, Debulk	MX-4926	0.2921	0.3113	0.3241	0.3236	0.3440	0.3644
	MX-2603	0.2307	0.2551	0.2641	0.2742	0.2891	0.2826
Bag Leakage, Final Cure	MX-4926	0.2459	0.3101	0.3277	0.3232	0.3475	0.3610
	MX-2603	0.2397	0.2599	0.2710	0.2833	0.2870	0.2717
Temperature Loss, Debulk	MX-4926	0.2836	0.2983	0.3127	0.3307	0.3625	0.3660
	MX-2603	0.2323	0.2872	0.2860	0.2953	0.2992	0.2765
70 to 80% Density	MX-4926	0.2459	0.2985	0.3026	0.3398	0.3520	0.3534
	MX-2603	0.2693	0.3016	0.2779	0.2900	0.3050	0.2888
80 to 90% Density	MX-4926	0.2435	0.2881	0.3095	0.3229	0.3515	0.3615
	MX-2603	0.2182	0.2533	2.774	0.2690	0.2935	0.2837
6% Volatiles	MX-4926	0.3279	0.3417	0.3109	0.3364	0.3600	0.3839
	MX-2603	0.2641	0.3004	0.2805	0.2919	0.3019	0.2797
9% Volatiles	MX-4926	0.2492	0.3204	0.3048	0.3365	0.3588	0.3662
	MX-2603	0.2379	0.2788	0.2817	0.2967	0.3003	0.2782

TABLE IV-14

SPECIFIC HEATS OF TEST MATERIALS, cal/g-°C

Discrepancy	Material	212°F (100°C)	392°F (200°C)	500°F (260°C)	700°F (371°C)	1040°F (560°C)	1600°F (871°C)
Wrinkles, 0.125 x 1 x 3	MX-4926	0.2553	0.3147	0.3239	0.3345	0.3626	0.3676
	MX-2603	0.2479	0.2752	0.2817	0.2935	0.2955	0.2843
Wrinkles, 0.25 x 1.5 x 3	MX-4926	0.2797	0.3187	0.3217	0.3308	0.3601	0.3652
	MX-2603	0.2497	0.2767	0.2757	0.2902	0.2987	0.2865
Wrinkles, 0.375 x 1.5 x 3	MX-4926	0.2628	0.3020	0.3226	0.3349	0.3616	0.3637
	MX-2603	0.2371	0.2807	0.2721	0.2858	0.2951	0.2852
Resin Rich, 10 plies	MX-4926	0.2644	0.3179	0.3299	0.3308	0.3600	0.3560
	MX-2603	0.2272	0.2859	0.2795	0.2922	0.2980	0.2744
Resin Rich, 20 plies	MX-4926	0.2982	0.3306	0.3223	0.3344	0.3608	0.3673
	MX-2603	0.2462	0.2742	0.2939	0.3004	0.3047	0.2854
Resin Starved, 10 plies	MX-4926	0.2722	0.3027	0.3189	0.3344	0.3608	0.3673
	MX-2603	0.2292	0.2658	0.2694	0.2838	0.2862	0.2798

TABLE IV-15

THERMAL DIFFUSIVITIES OF TEST MATERIALS, cm^2/sec

Discrepancy	Material	75°F (23.9°C)	212°F (100°C)	392°F (200°C)	500°F (260°C)	700°F (371°C)	950°F (510°C)	1200°F (649°C)	1600°F (871°C)
None (Baseline	MX-2603 (C)	2.52	2.31	2.64	2.74	3.83	3.51	4.10	4.55
	MX-4926 (T)	3.45	4.24	4.47	4.36	8.72	8.91	7.2	9.37
	MX-2603 (E)	2.48	2.49	2.59	2.53	4.59	3.47	4.06	4.55
Vacuum Bag, 25 in. Hg	MX-2603 (C)	2.38	1.89	2.52	2.91	3.24	3.53	3.81	4.95
	MX-4926 (T)	4.04	3.92	5.39	6.15	9.74	8.28	10.35	10.57
	MX-2603 (E)	2.24	2.04	2.49	2.69	3.88	3.49	3.77	4.90
Autoclave, 125 psig	MX-2603 (C)	2.64	2.00	2.83	2.63	3.01	3.64	2.98	3.67
	MX-4926 (T)	3.71	3.39	4.61	4.87	7.63	7.39	6.83	8.33
	MX-2603 (E)	2.60	2.16	2.78	2.43	3.60	3.60	2.94	3.61
Bag Leakage, Debulk	MX-2603 (C)	2.18	2.14	2.63	2.78	3.12	3.44	3.66	4.05
	MX-4926 (T)	3.95	4.33	4.48	4.89	8.81	9.95	7.16	7.40
	MX-2603 (E)	2.15	2.31	2.58	2.56	3.74	3.40	3.62	4.00
Bag Leakage, Final Cure	MX-2603 (C)	2.57	2.18	2.80	2.98	3.28	2.80	3.08	3.33
	MX-4926 (T)	4.44	3.65	4.14	4.60	6.63	5.39	4.79	6.13
	MX-2603 (E)	2.53	2.35	2.75	2.75	3.93	2.77	3.05	3.29
Temperature Loss, Debulk	MX-4926 (T)		3.755	4.065	4.29	4.315	4.17	4.44	8.35
70 to 80%, Density	MX-2603 (C)		2.06	2.17	2.23	2.37	2.43	3.68	4.60
	MX-4926 (T)		3.69	3.70	4.03	4.03	3.80	4.97	8.13
80 to 90%, Density	MX-2603 (C)	1.84	2.06	2.165	2.225	2.37	2.46	3.72	4.60
	MX-4926 (T)		4.14	4.60	4.515	4.515	4.69	5.84	9.06

TABLE IV-15

THERMAL DIFFUSIVITIES OF TEST MATERIALS, cm^2/sec

Discrepancy	Material	75°F (23.9°C)	212°F (100°C)	392°F (200°C)	500°F (260°C)	700°F (371°C)	950°F (510°C)	1200°F (649°C)	1600°F (871°C)
6% Volatiles	MX-4926 (T)		3.39	3.92	4.06	4.07	3.975	5.36	8.76
9% Volatiles	MX-4926 (T)		3.34	4.07	3.95	3.83	4.01	5.72	7.64
Wrinkles,	MX-2603 (C)	2.41	2.41	2.44	2.26	3.63	3.24	3.54	4.02
0.125 x 1	MX-4926 (T)	4.22	4.08	4.28	4.51	7.6	6.98	6.81	7.35
x 3	MX-2603 (E)	2.37	2.59	2.39	2.09	4.35	3.2	3.51	4.12
Wrinkles,	MX-2603 (C)	2.34	2.55	2.64	2.79	3.56	3.56	3.65	3.81
0.25 x 1.5	MX-4926 (T)	3.86	3.04	3.78	3.96	8.62	8.77	9.08	9.57
x 3	MX-2603 (E)	2.30	2.74	2.59	2.58	4.27	3.52	3.62	3.91
Resin Rich,	MX-2603 (C)	2.54	2.84	2.74	2.68	3.59	3.35	3.43	4.13
10 x 3 in.	MX-4926 (T)	2.86	3.22	4.71	4.55	6.81	6.81	6.81	8.33
	MX-2603 (E)	2.5	3.05	2.69	2.47	4.31	3.31	3.4	4.23
Resin Rich,	MX-2603 (C)	2.36	2.5	2.46	2.38	3.85	4.0	3.95	4.0
20 x 3 in.	MX-4926 (T)	3.00	2.69	3.48	3.48	7.9	8.14	7.9	8.95
	MX-2603 (E)	2.32	2.69	2.42	2.20	3.62	3.96	3.92	4.10

TABLE IV-16

THERMAL CONDUCTIVITIES OF TEST MATERIALS

Discrepancy	Material	K in Btu-in./ft^2 - hr - °F (watt/cm/cm^2-°K) 212°F	(100°C)	392°F	(200°C)	500°F	(260°C)	700°F	(371°C)	1600°F	(871°C)
None (Baseline)	MX-2603 (C)	2.8	(0.58)	3.39	(0.7)	3.64	(0.76)	5.08	(1.05)	4.89	(1.02)
	MX-4926 (T)	5.04	(1.05)	5.45	(1.13)	5.45	(1.13)	11.47	(2.38)	10.32	(2.14)
	MX-2603 (E)	3.03	(0.63)	3.33	(0.69)	3.37	(0.7)	6.09	(1.26)	5.00	(1.04)
Vacuum Bag, 25 in. Hg	MX-2603 (C)	1.67	(6.35)	2.59	(6.54)	3.28	(0.68)	3.24	(0.67)	4.4	(0.91)
	MX-4926 (T)	2.91	(0.60)	4.73	(0.98)	5.8	(1.20)	9.26	(1.92)	9.42	(1.96)
	MX-2603 (E)	2.76	(0.57)	3.02	(0.63)	3.57	(0.74)	4.57	(0.95)	4.6	(0.95)
Autoclave, 125 psig	MX-2603 (C)	2.48	(0.52)	3.76	(0.78)	2.66	(0.76)	4.06	(0.84)	4.1	(0.85)
	MX-4926 (T)	3.56	(0.74)	5.99	(1.24)	6.51	(1.35)	10.01	(2.1)	9.44	(1.96)
	MX-2603 (E)	2.68	(0.56)	3.7	(0.77)	3.38	(0.70)	4.85	(1.00)	4.04	(0.84)
Bag Leakage, Debulk	MX-2603 (C)	2.52	(0.52)	3.42	(0.71)	3.75	(0.78)	4.6	(0.95)	4.7	(0.98)
	MX-4926 (T)	5.27	(1.09)	5.82	(1.21)	6.18	(1.28)	11.75	(2.40)	8.76	(1.82)
	MX-2603 (E)	2.72	(0.56)	3.36	(0.7)	3.45	(0.72)	5.0	(1.04)	4.66	(0.97)
Bag Leakage, Final Cure	MX-2603 (C)	2.67	(0.55)	3.71	(0.77)	4.56	(0.95)	4.53	(0.94)	3.70	(0.77)
	MX-4926 (T)	3.77	(0.78)	5.44	(1.13)	6.34	(1.32)	8.76	(1.82)	7.57	(1.57)
	MX-2603 (E)	2.88	(0.6)	3.65	(0.76)	3.8	(6.79)	5.42	(1.13)	3.66	(0.76)
Temp. Loss, Debulk	MX-4926 (T)	4.45	(0.92)	5.06	(1.05)	5.6	(1.16)	5.96	(1.24)	9.93	(2.06)
70 to 80% Density	MX-4926 (T)	2.76	(0.57)	3.36	(0.7)	3.71	(0.77)	4.17	(0.87)	6.94	(1.44)
	MX-2603 (E)	2.64	(0.55)	3.11	(0.65)	2.95	(0.61)	3.13	(0.65)	5.36	(1.11)
80 to 90% Density	MX-4926 (T)	3.1	(0.64)	4.1	(0.85)	4.3	(0.89)	4.5	(0.93)	9.9	(2.06)
	MX-2603 (E)	2.1	(0.44)	2.58	(0.54)	2.9	(0.60)	2.81	(0.58)	4.35	(0.90)
6% Volatiles	MX-4926 (T)	4.58	(0.95)	5.52	(1.15)	5.2	(1.08)	5.64	(1.17)	8.87	(1.84)
9% Volatiles	MX-4926 (T)	3.48	(0.72)	5.45	(1.13)	5.03	(1.04)	5.38	(1.12)	8.44	(1.75)

TABLE IV-16

THERMAL CONDUCTIVITIES OF TEST MATERIALS

Discrepancy	Material	K in Btu-in./ft^2 - hr - °F (watt/cm/cm^2-°K) 212°F (100°C)	392°F (200°C)	500°F (260°C)	700°F (371°C)	1600°F (871°C)
Wrinkles, 0.125 x 1	MX-2603 (C)	3.07 (0.64)	3.45 (0.72)	3.27 (0.68)	4.91 (1.02)	4.67 (0.97)
	MX-4926 (T)	4.38 (0.91)	5.66 (1.18)	6.14 (1.27)	10.47 (2.17)	9.72 (2.02)
	MX-2603 (E)	3.30 (0.69)	3.38 (0.70)	3.02 (0.63)	5.89 (1.22)	4.79 (0.99)
Wrinkles, 0.25 x 1.5	MX-2603 (C)	3.25 (0.67)	3.73 (0.77)	3.93 (0.82)	5.03 (1.04)	4.34 (0.90)
	MX-4926 (T)	3.55 (0.74)	5.03 (1.04)	5.32 (1.10)	11.66 (2.42)	11.55 (2.4)
	MX-2603 (E)	3.49 (0.72)	3.66 (0.76)	3.63 (0.75)	6.04 (1.25)	4.45 (0.82)
Resin Rich 10 x 3 in.	MX-2603 (C)	3.31 (0.69)	4.02 (0.84)	3.85 (0.8)	5.08 (1.05)	4.2 (0.87)
	MX-4926 (T)	3.56 (0.74)	6.25 (1.3)	6.14 (1.27)	7.57 (1.57)	10.41 (2.16)
	MX-2603 (E)	3.56 (0.74)	3.96 (0.82)	3.54 (0.73)	6.10 (1.27)	4.3 (0.89)
Resin Rich 20 x 3 in.	MX-2603 (C)	3.02 (0.63)	3.31 (0.69)	3.43 (0.71)	5.43 (1.13)	4.54 (0.94)
	MX-4926 (T)	3.33 (0.69)	4.77 (0.99)	4.65 (0.97)	10.73 (2.23)	10.77 (2.24)
	MX-2603 (E)	3.25 (0.67)	3.25 (0.67)	3.17 (0.66)	5.11 (1.06)	4.65 (0.97)

Table IV-17

Thermal Dilation of MX-4926 Throat Specimens
in Axial (45-Degree-to-Ply) Orientation

Discrepancy	ΔL/L, Milli-in./in. (mm/m) 100°F (311°K)	200°F (366°K)	300°F (422°K)	400°F (477°K)	500°F (533°K)	600°F (589°K)	700°F (644°K)	800°F (700°K)	900°F (755°K)	1000°F (811°K)	Range
None (Baseline)	0.21	0.91	1.77	2.55	2.7	1.7	-0.86	-1.07	-5.63	-13.2	15.9
Vacuum Bag	0.13	0.9	1.4	1.05	2.05	2.4	2.9	1.8	-9.1	-32.1	35.0
Autoclave	0.0	0.76	1.5	3.7	3.3	2.5	1.9	1.4	-3.8	-11.4	15.1
70 to 80% Density	0.129	0.64	0.90	1.0	0.0	0.26	-0.65	-4.25	-13.3	-24.6	25.6
80 to 90% Density	0.13	0.76	1.14	0.76	0.51	0.89	1.01	-1.64	-10.6	-22.8	23.94
Bag Leak, Debulk	0.13	0.64	0.76	-0.39	-1.65	-2.4	-1.8	-1.9	-7.2	-16.3	17.06
Bag Leak, Final Cure	0.13	0.66	1.4	2.6	2.5	2.0	2.0	1.7	-1.45	-5.9	8.5
Temperature Loss, Debulk	0.13	0.78	1.69	3.38	1.95	1.3	2.08	0.52	-8.33	-19.8	24.18
6% Volatiles	0.255	2.42	8.05	7.55	2.42	-0.12	-1.41	-1.41	-9.05	-18.3	26.35
9% Volatiles	0.0	1.54	4.99	9.21	4.48	0.77	-1.54	-2.68	-8.05	-14.5	23.71
Wrinkles, 0.125 in. (0.3175 cm)	0.25	0.9	1.9	3.55	3.8	3.7	3.55	2.4	-5.6	-17.0	20.8
Wrinkles, 0.250 in. (0.6350 cm)	0.13	0.77	1.65	3.2	3.2	2.6	2.55	1.9	-3.6	-17.2	20.4
Wrinkles, 0.375 in. (0.9525 cm)	0.38	0.13	0.89	2.92	2.54	1.91	1.77	1.14	-6.35	-19.0	21.92
Resin-Rich, 10 plies	0.25	1.0	3.5	4.7	5.2	3.0	-1.5	-2.0	-11.0	-27.5	32.5
Resin-Rich, 20 plies	0.27	1.5	3.0	4.3	5.0	3.0	-1.0	-1.6	-9.5	-28.0	33.0
Resin-Starved, 10 plies	0.0	0.0	-0.28	-0.84	-2.66	-2.8	-4.35	-7.72	-13.6	-17.9	17.9

Table IV-18

Thermal Dilation of MX-2600 Exit Specimens in Radial (Normal-to-Ply) Orientation

Discrepancy	ΔL/L, Milli-in./in. (mm/m) 100°F (311°K)	200°F (366°K)	300°F (422°K)	400°F (477°K)	500°F (533°K)	600°F (589°K)	700°F (644°K)	800°F (700°K)	900°F (755°K)	1000°F (811°K)	Range
None (Baseline)	0.25	1.65	3.3	9.5	17.8	10.75	10.1	9.5	6.1	-9.4	27.2
Vacuum Bag	0.13	1.4	2.9	6.19	10.5	7.1	6.6	8.5	6.0	-13.7	24.2
Autoclave	0.39	1.9	4.3	11.8	19.0	10.8	9.95	8.55	4.35	-12.4	31.4
80 to 90% Density	0.26	1.91	3.96	9.12	17.45	11.6	10.8	11.45	7.79	-13.6	31.05
Bag Leak, Debulk	0.25	1.9	4.45	12.1	19.5	12.3	11.8	11.8	8.5	-8.8	28.3
Bag Leak, Final Cure	0.13	1.8	3.8	10.8	19.4	12.1	11.2	11.5	8.3	-10.0	29.4
9% Volatiles	0.27	2.72	6.13	17.12	20.8	14.55	12.5	10.2	-3.94	-24.86	45.66
Wrinkles, 0.375 in. (0.9525 cm)	0.13	1.77	3.68	11.25	20.47	16.8	16.43	17.43	15.17	-10.61	31.07

Table IV-19

Thermal Dilation of MK-2600 Entrance Specimens in Radial (80-Degree-to-Ply) Orientation

Discrepancy	ΔL/L, Milli-in./in. (mm/m) 100°F (311°K)	200°F (366°K)	300°F (422°K)	400°F (477°K)	500°F (533°K)	600°F (589°K)	700°F (644°K)	800°F (700°K)	900°F (755°K)	1000°F (811°K)	Range
None (Baseline)	0.14	1.13	2.13	3.4	4.25	2.55	2.27	2.27	1.27	-2.7	6.95
70 to 80% Density	0.129	0.65	1.29	1.6	1.41	1.03	0.77	0.39	-0.13	-0.65	2.25
80 to 90% Density	0.13	0.89	1.65	2.16	2.16	1.65	1.65	1.27	-0.13	-4.58	6.74
Temperature Loss, Debulk	0.38	1.92	3.96	10.1	16.0	9.05	8.69	8.3	5.24	-10.85	26.85
6% Volatiles	0.127	0.76	1.78	2.03	2.03	1.27	1.14	1.01	0.76	0.0	2.03
Wrinkles, 0.125 in. (0.3175 cm)	0.13	0.9	1.65	1.9	1.4	1.15	1.15	0.9	0.4	-0.65	2.55
Wrinkles, 0.250 in. (0.6350 cm)	0.13	1.0	1.9	2.7	2.7	1.15	1.0	0.76	-0.26	-3.2	5.9
Resin-Rich, 10 plies	0.25	1.4	2.4	2.1	1.0	1.0	0.51	-0.14	-1.8	-4.25	6.65
Resin-Rich, 20 plies	0.26	1.15	2.2	2.8	1.4	1.3	1.15	0.67	-1.3	-3.6	6.4
Resin-Starved, 10 plies	0.13	0.76	1.65	3.18	5.71	4.44	4.95	5.59	3.68	-3.81	6.99

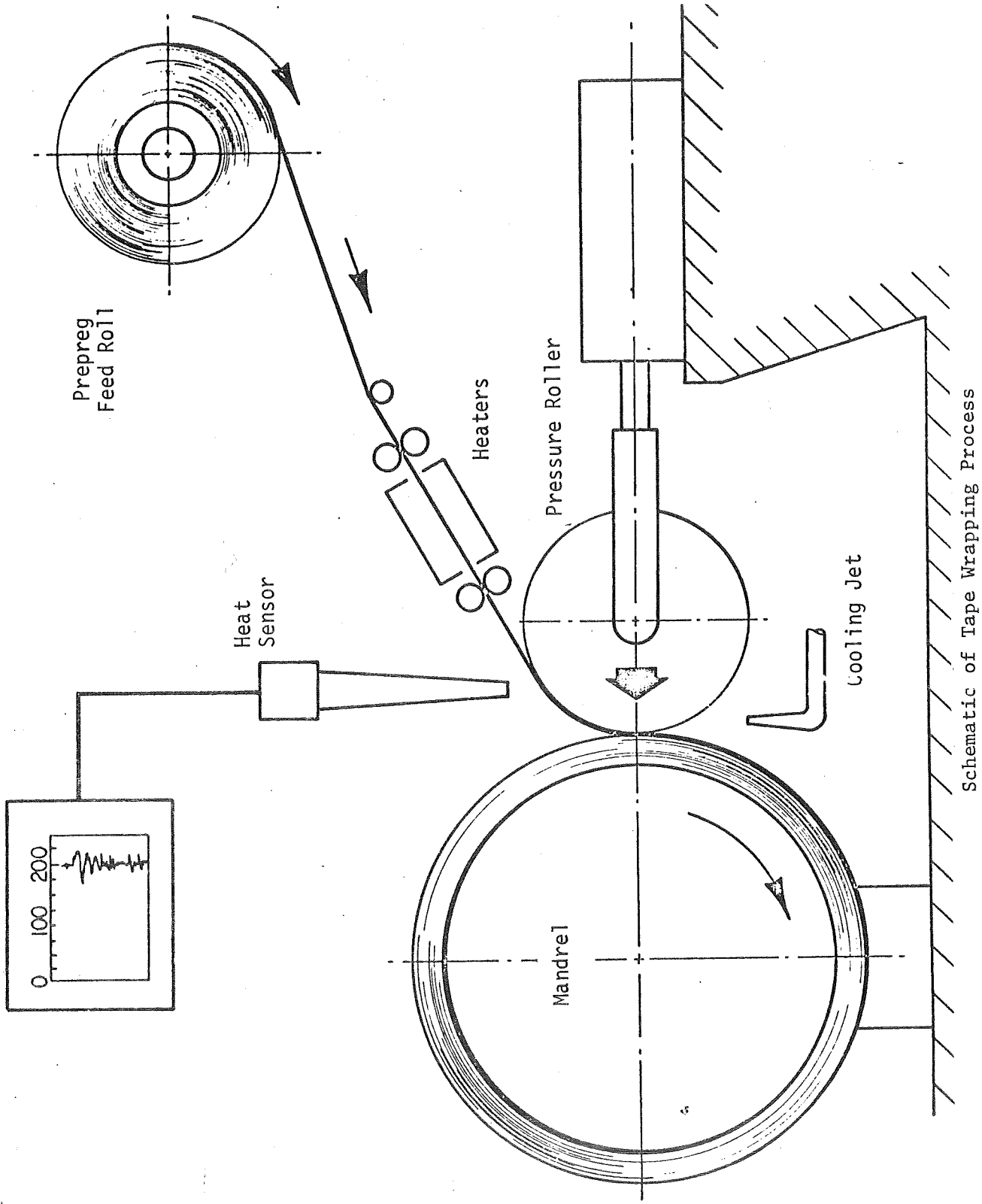
Prepreg
Feed Roll
Heaters
Pressure Roller
Heat
Sensor
Cooling Jet
Mandrel
0
100
200
Schematic of Tape Wrapping Process

Figure IV-1

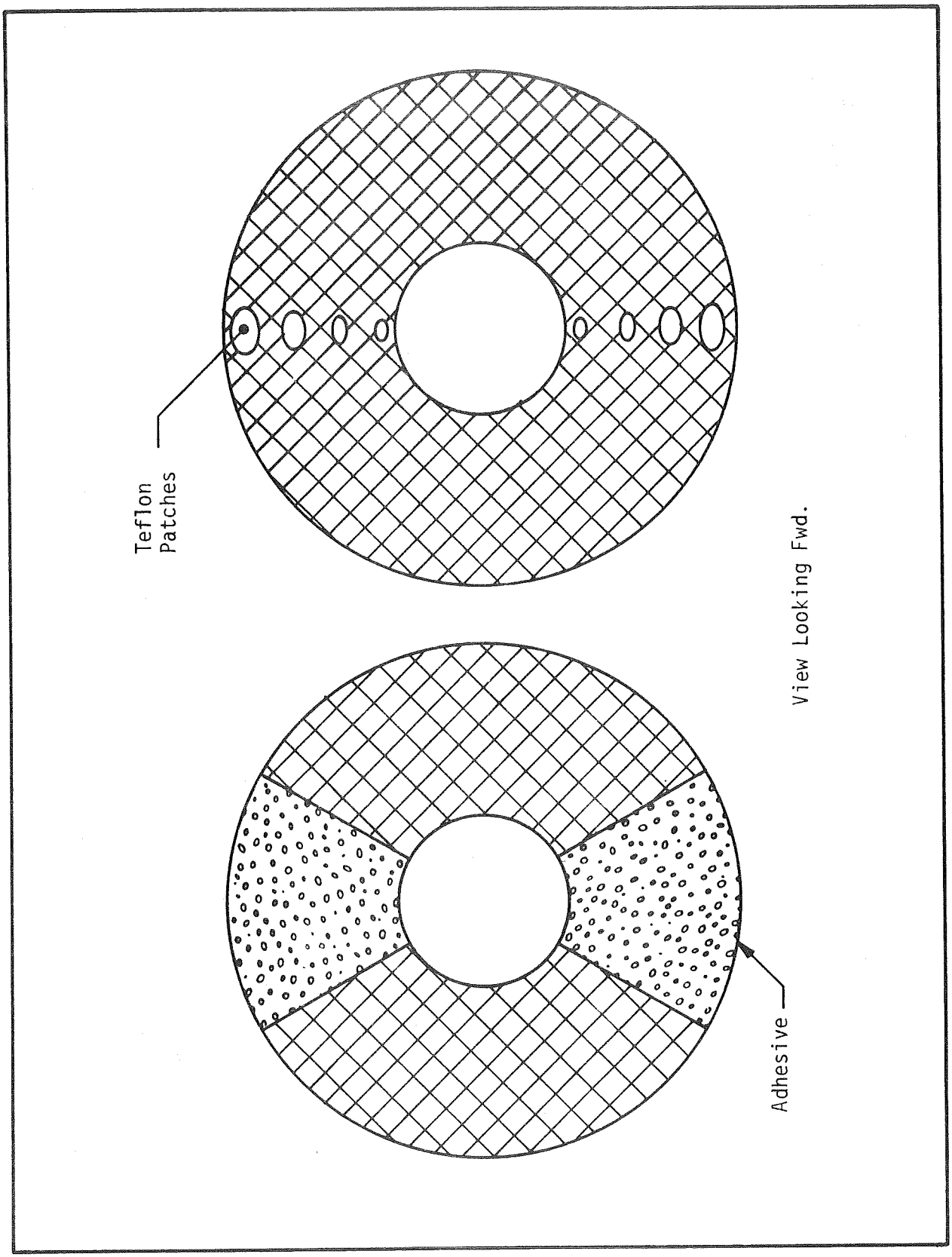

Procedures for Producing Bond Line Separations

Figure IV-2

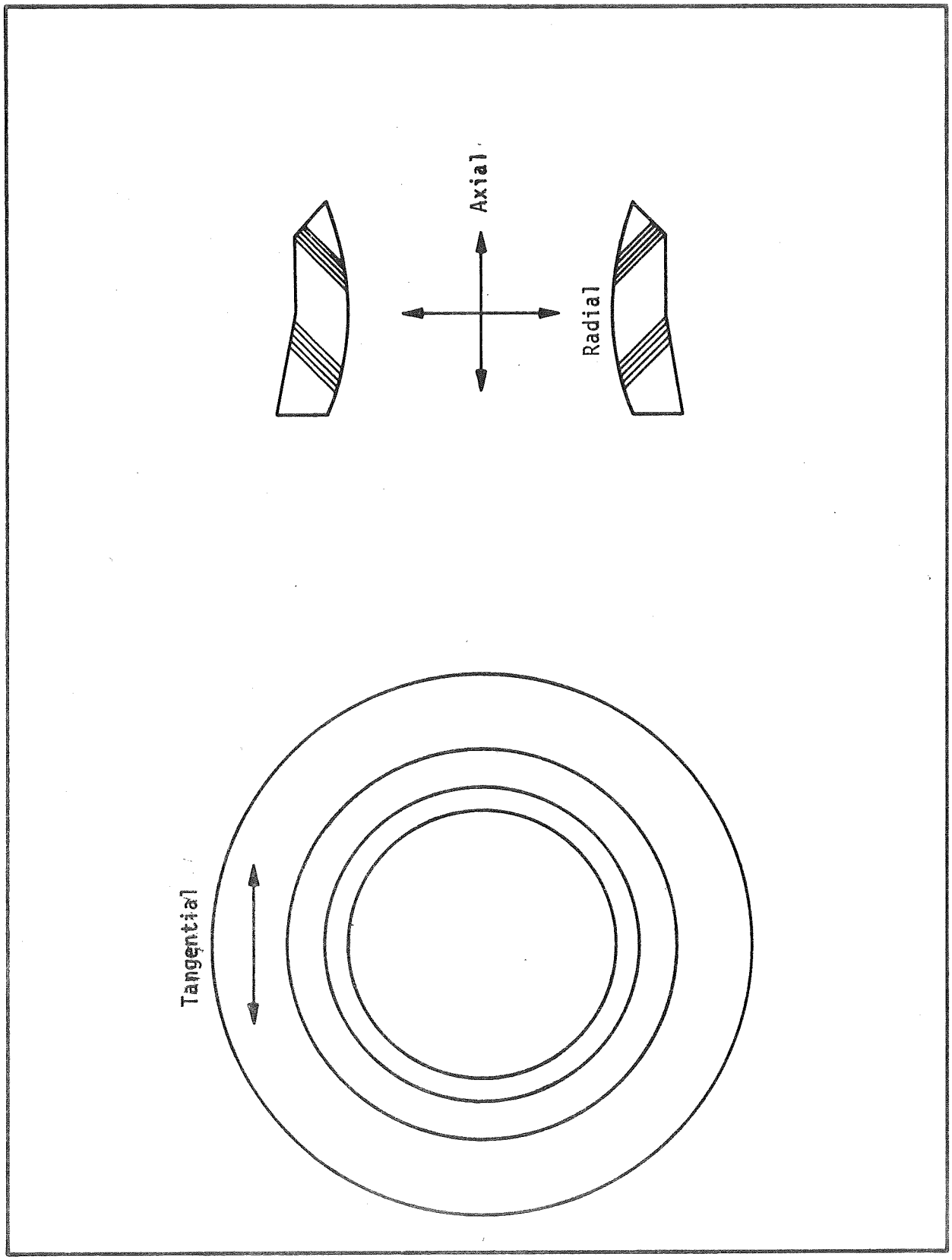

Orientation of Test Specimens in Throat Flame Liner

Figure IV-3

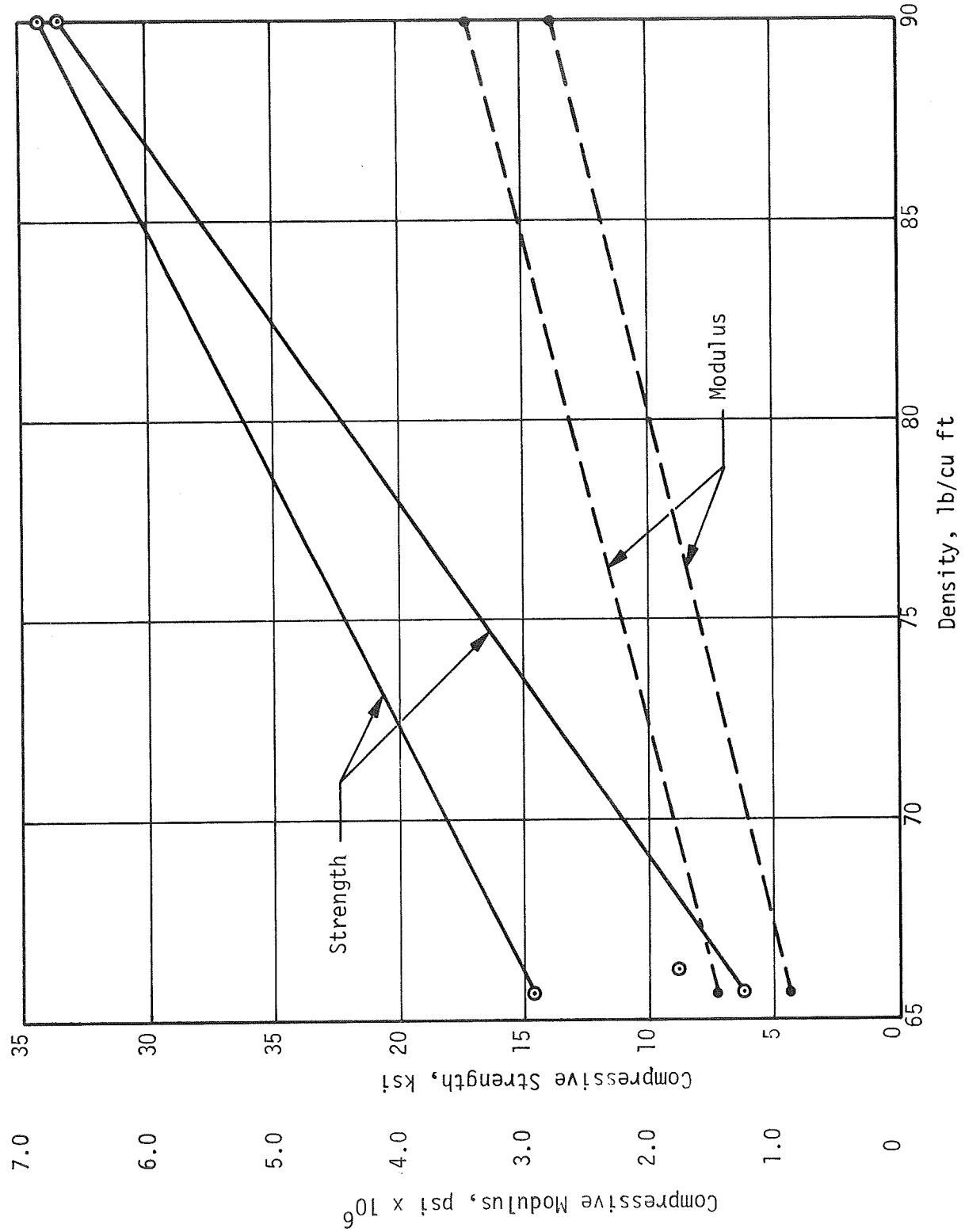

Relationship Between Density and Compressive Properties for MX-4926 Throat Specimens Tested in Radial Direction

Figure IV-4

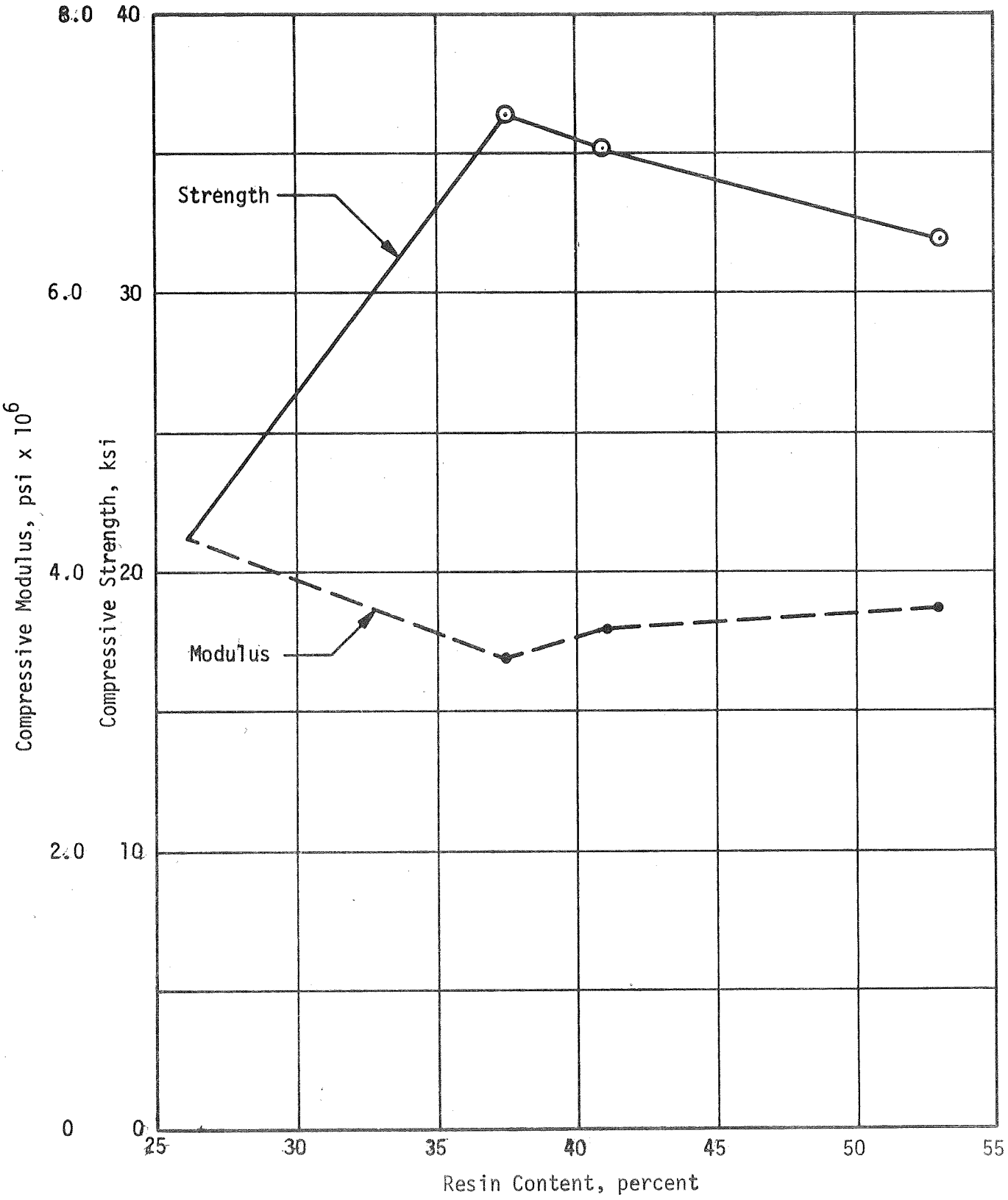

Estimated Relationship Between Resin Content and Compressive Properties of MX-4926 Exit Cone Specimens Tested in Axial Direction

Figure IV-5

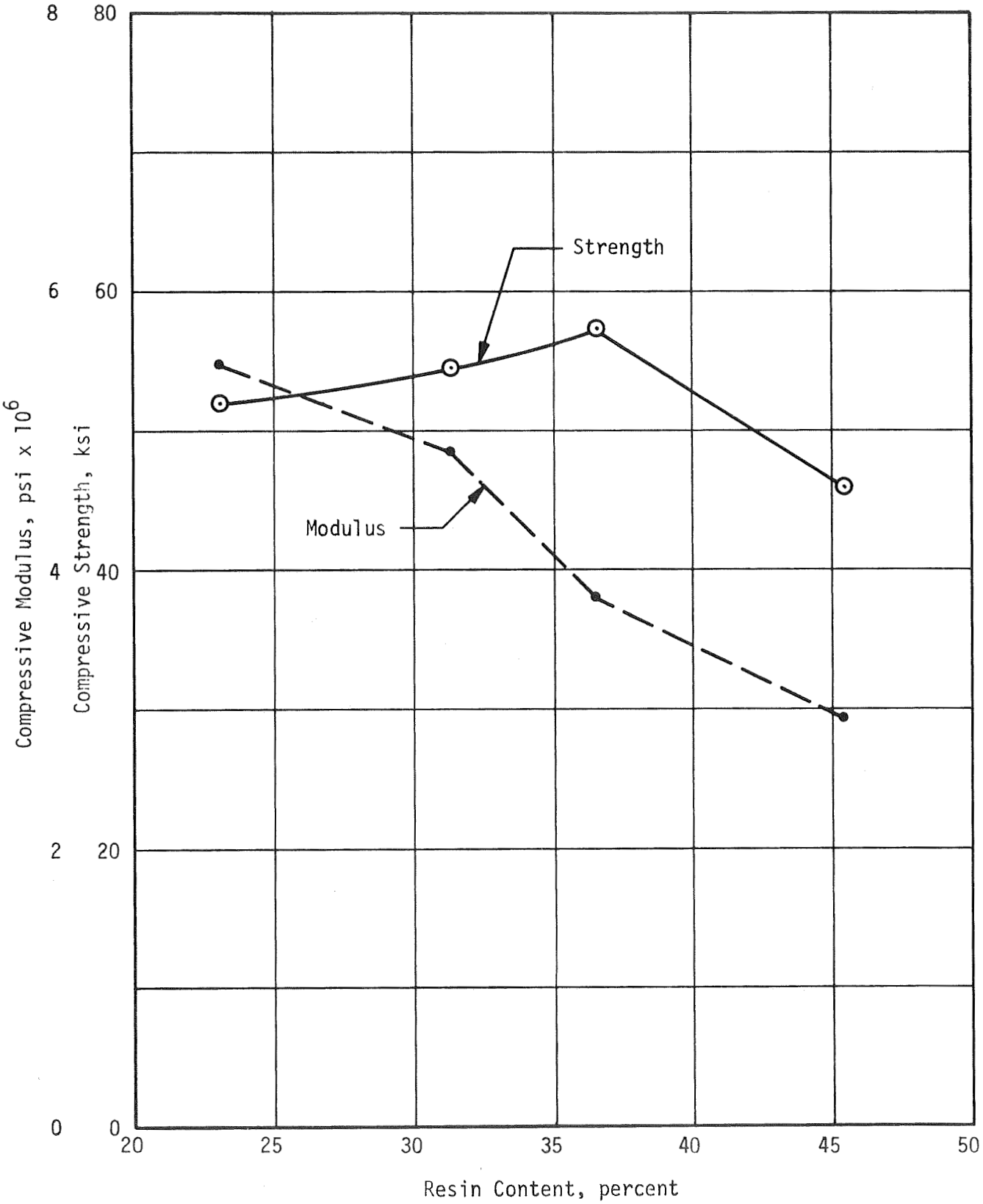

Relationship Between Resin Content and Compressive Properties of MX-2600 Exit Cone Specimens Tested in Axial Direction

Figure IV-6

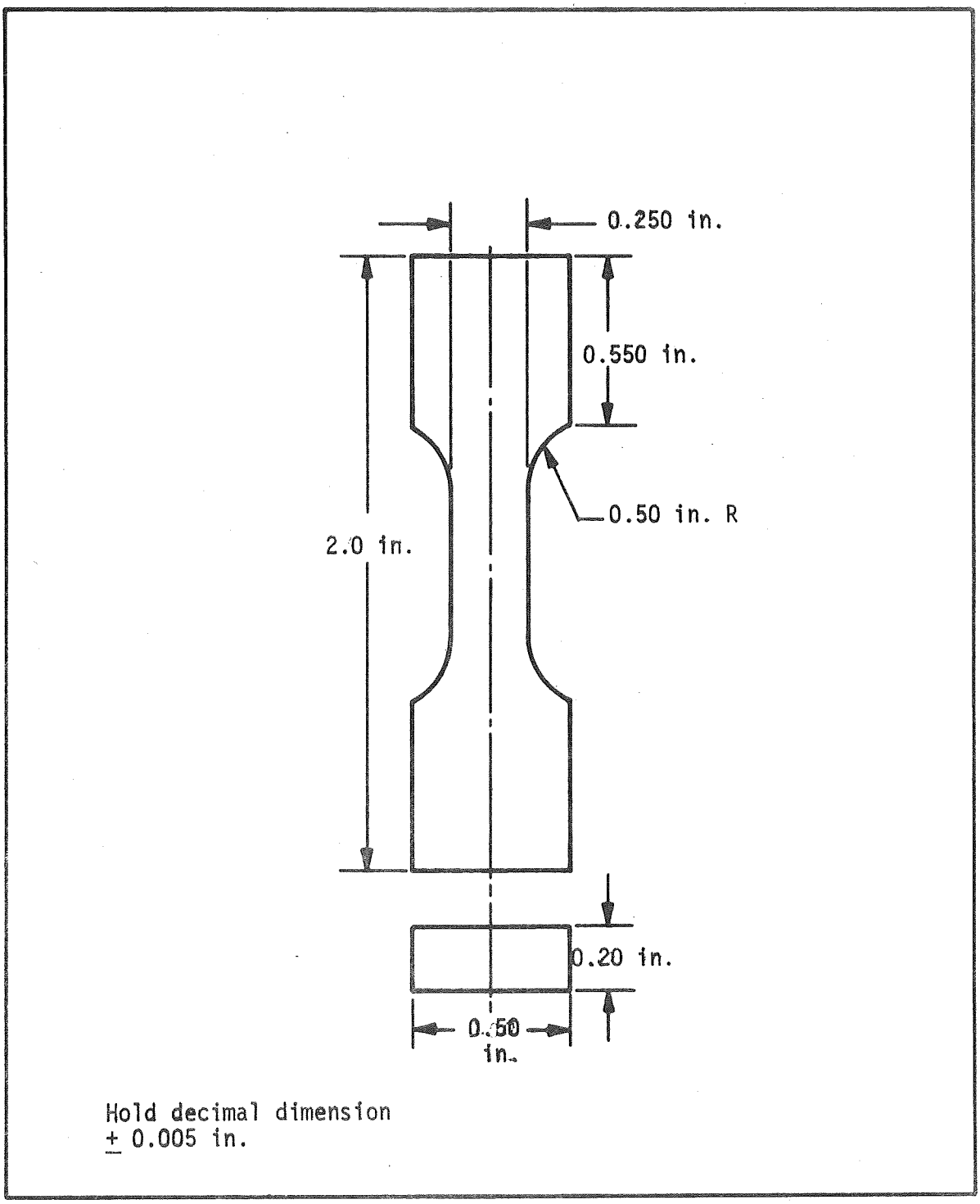

Flat Tensile Specimen

Figure IV-7

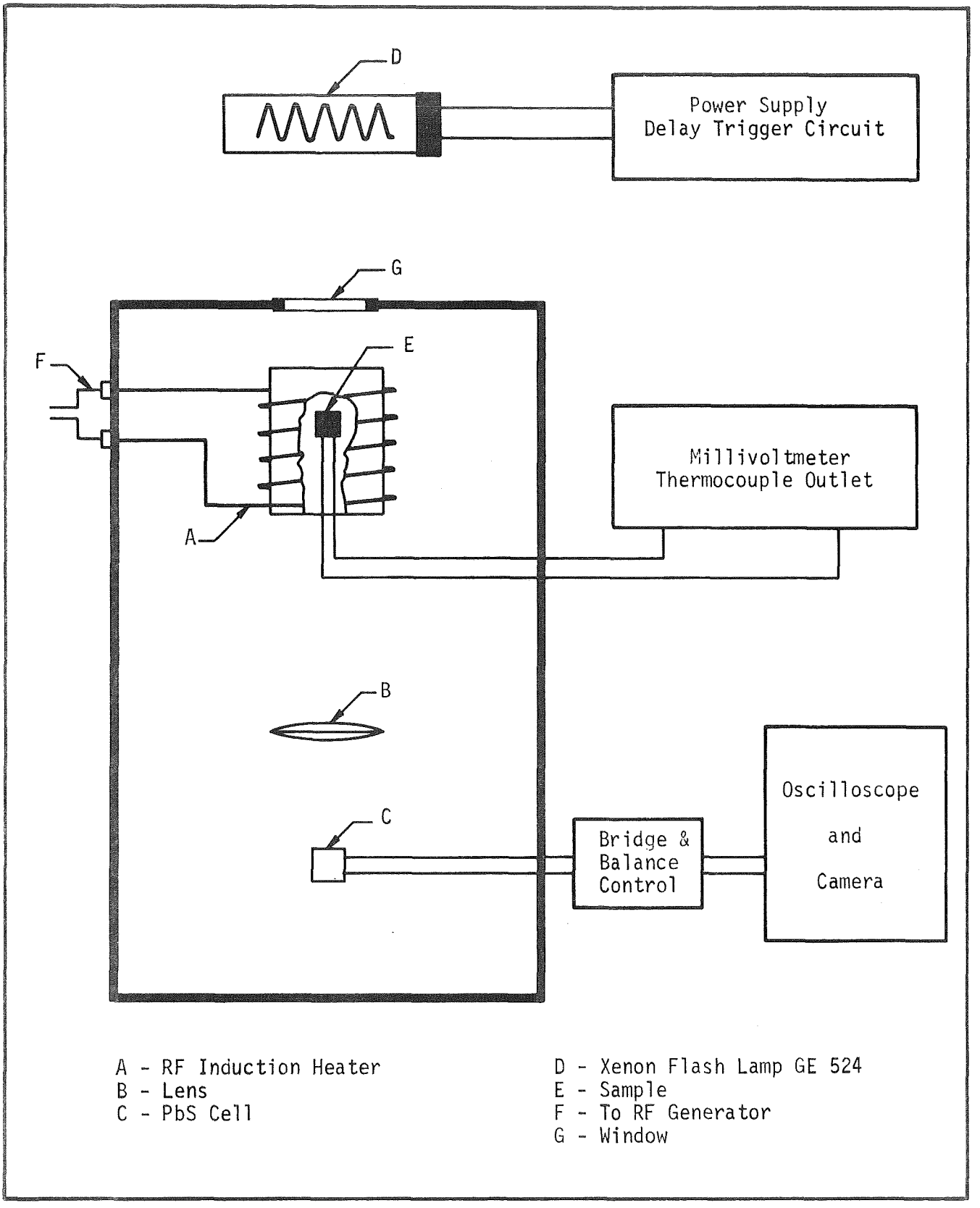

Schematic Diagram of Diffusivity Apparatus

Figure IV-8

V. EVALUATION OF NONDESTRUCTIVE TESTING TECHNIQUES

A. SUMMARY

An associated task of this program consisted of an evaluation of five techniques for detecting discrepancies in ablative nozzles, and their component parts. Two established techniques of inspection were evaluated along with three others which required varying degrees of development before an evaluation could be made. Six general groups of flaws were considered: (1) variations in volatile contents; (2) delaminations; (3) wrinkles; (4) resin content variations; (5) density variations; and (6) cure cycle discrepancies. The NDT techniques evaluated included: radiography and pulse ultrasonic (established techniques); infrared thermography; special eddy current techniques; and CW- and resonant frequency ultrasonics.

The nozzle components inspected were of carbon fabric and silica fabric reinforced resin composites. These materials had similar flaws, and were both of tape wrapped construction although the silica parts were, of course, not conductive and hence unsuitable for eddy current. Otherwise the techniques were applicable to both materials.

The routine pulse ultrasonic and radiographic inspections were performed using production facilities, and the inspections performed were well within the routine capabilities of an established aerospace inspection facility. The infrared thermography inspections, and the CW ultrasonic techniques considered are not routinely used methods, and hence required survey of available equipment, and some development of technique before evaluation. The use of eddy currents is commonly used for inspection of metal parts, but it is a rather special technique when applied to non-metallics, and required considerable experimentation. The effects of scale-up of the new techniques to the 260-in. dia motor could not be defined within the scope of this contract.

V.A. Summary (cont)

For the established methods there was enough experience to make good estimates. The preparation of specimens in the form of sections of a full-scale nozzle part would be of no use because with tape-wrap construction one must make the entire part to be remotely realistic, and this was not feasible.

In general, all discrete flaws are covered by pulse ultrasonics and radiography. The effects of material variations such as high volatile content and cure cycle discrepancies are not so easily detected. While the new techniques were rated good or excellent in seven instances, they did not receive such high ratings in any case in which neither radiography or pulsed ultrasonics were so rated. It can be concluded that the new techniques are not required for adequate results. The use of the new methods would thus be indicated only for reasons of economy or convenience. Such considerations are premature at this time. Evaluations are summarized at the end of this section.

A problem which does merit immediate consideration is that of NDT methods for detecting volatile content and the effects of the various cure cycle discrepancies. Generalized studies of NDT methods usually develop a bias in favor of discrete flaws at the expense of bulk material properties, almost unavoidably since most NDT techniques excel at detecting discrete flaws. Furthermore, analysis of samples is the traditional method of dealing with process discrepancies and NDT techniques have traditionally not been directed at problems of this nature. The detection of processing discrepancies should be investigated as a separate project if NDT techniques are to be applied in this area.

V. Evaluation of Nondestructive Testing Techniques (cont)

B. TEST PROCEDURES AND RESULTS

1. Radiography, Normal Exposure

The ablative components were radiographically inspected at the suppliers' facilities. These radiographs and the discrepancies specified by the supplier were reviewed at Aerojet. The radiographs were through exposures of the entire part, which combined normal and tangential views. These radiographs were found to be of excellent quality, and no discrepancies were noted in the analysis furnished with the film.

Delaminations were clearly shown, and high- and low-density regions were identifiable. Wrinkles and resin/fiber ratio variations were also shown but less clearly than the delaminations, as would be expected since such flaws do not usually have well defined boundaries. The known density variations (80% and 90% of normal) were marked by a porous condition throughout the part, with small voids in the silica regions.

The process discrepancies presented a special problem in that a specific defect was not being produced, but rather a process change was made which is likely to cause several types of defect. No general statements can be made concerning the use of X-rays to verify that the process discrepancies occurred, but some results of these discrepancies were detected. Without prior knowledge of the processing, the defect cause could not be established from X-ray data. The autoclave cure at 125 psi produced very little deviation from normal as seen on the radiographs. Other variations tended to produce low-density bands, with the carbon being more affected than the silica. Occasional surface delaminations were observed.

V.B. Test Procedures and Results (cont)

High volatile content in the resin appeared to produce porosity in the carbon composite, wrinkles in the silica composite, delaminations at the carbon/silica interface, and some delaminations within the carbon.

These radiographs showed a complete cross section, being made with film and source on opposite sides, both outside the part. Thus both normal and tangential views are included. Because of the low energy X-rays, however, the portion of the film showing a tangential view was of limited value, so that these radiographs are considered to be normal radiographs, and do not duplicate the tangential radiographs described in the following paragraph.

2. Radiography, Tangential

Both the Linac and VandeGraaff machines at Aerojet produce X-rays of adequate energy to penetrate the maximum chord for tangential shots of the test nozzle assembly. Nozzle assemblies, SN 001 and 002, were radiographed using the Varian 10 mev Linac. No unbonds could be detected, although unbonds were known to be present (they were found by ultrasonic inspection). Assemblies SN 003 and 004, also known to have unbonds were radiographed with the High Voltage Engineering 2 mev VandeGraaf Generator. These radiographs were superior in quality to the ones made with the Linac, and gave an excellent picture of ply alignment, but no evidence of the ultrasonically located unbonds could be found. The conclusion is that there is unbond, or very weak bond, but with little or no separation. The superior results with the VandeGraaf would be expected since the Linac is a high-output machine in which high output is obtained at some sacrifice in resolution. These small parts do not require either the 10 mev energy or the high roentgen output of the Linac, even though the complete assembly is in a steel shell.

V.B. Test Procedures and Results (cont)

3. Ultrasonic Inspection, Immersion Through-Transmission (Component Parts Only)

The parts were placed in a water tank after being coated to protect them from water damage with a mixture of 50% LOTOL and 50% BUTUARC. This produced a strippable latex coating with good sound coupling properties. With the part immersed, scanning was quite simple since the water is a very effective couplant. The equipment included an Automation Industries Immersion Test Unit with 3-in. Transigraph and Transigate to Model EM550, and a Sperry Reflectoscope Model UM700. The part was mounted on a turntable equipped for Z axis scanning as well as rotation. An Alfax 1047, 18-in. recorder was used to produce C-Scans, and the ultrasonic frequency used was 2.25 MH_Z. The equipment is shown in Figures V-1 and V-2.

The results of this inspection are shown in Figures V-3, V-4, and V-5, which are the C-Scans of parts with delaminations. The flaws are well mapped.

4. Ultrasonic Inspection, Contact Pulse-Echo

The nozzle assembly was inspected with a contact coupled, pulse echo technique for the purpose of detecting unbond between the steel shell and the sections of the liner. There was an epoxy bond between silica and steel, with a good possibility of epoxy on both surfaces even in an unbonded region, a condition which makes pulse echo inspection difficult. The presence of adhesive on an unbonded surface produces a condition intermediate between a good bond and an unbond with no adhesive on the surface.

V.B. Test Procedures and Results (cont)

This method requires a couplant film between the single transducer and the part. Waterless hand cleaner, an emulsion, was employed in this case, and proved satisfactory. The Sperry UM700 in the pulse echo mode of operation was used with a frequency of 2.25 MH_z. The inspection was performed by plotting the strength of the echo from the steel-to-liner interface. Because the echo is far from constant under any circumstances, a defect must be recognized as an anomalous region by comparison with its immediate surroundings rather than by the absolute strength of the echo, thus recognition of an unbonded region requires reasonably well defined boundaries. Nevertheless it was possible to locate unbonded regions on the nozzle assemblies examined. Although there was no confirmation of these unbonds by other methods, the unbonds did correspond to the location of deliberate unglued areas. The epoxy would tend to flow somewhat as the liner sections were seated in the shell during assembly. Thus the actual unbond would not be exactly the same as the area left unglued. Nevertheless, the correspondence was good enough to establish that contact ultrasonics could locate unbonds.

There is another ultrasonic technique which combines contact and immersion features and which would be most satisfactory for the full-scale nozzle assembly and for its parts. This method was used by Rohr Corporation in inspecting the nozzle for Motor 260-SL-3. It cannot be used for parts as small as the subscale nozzle, however. For this inspection the nozzle is placed vertically on a turntable. A carriage is provided which moves two transducers vertically, one inside and one outside of the nozzle, and keeps them aligned. The transducers are mounted in wheels (Figure V-6). These wheels are water-filled rubber tires turning on a fixed axle. A transducer is mounted on the axle, inside the tire. The tire is placed against the nozzle, and can roll along with the transducer pointed at the surface. The water in the tire acts as a couplant, and sliding friction is eliminated.

V.B. Test Procedures and Results (cont)

Liquid coupling is required between tire and nozzle, but since there is no sliding friction, the couplant need not be a lubricant. A spray of alcohol directed at the nozzle just ahead of the wheel is sufficient, and the alcohol evaporates quickly with negligible surface contamination. Rohr obtained results on the nozzle components for Motor 260-SL-3, which compared favorably with the results of an immersion inspection. The immersion inspection of the very large, full-scale nozzle components would pose problems, and the Sperry wheel method is a logical substitute.

5. Infrared Thermography

The major portion of the infrared thermography study was performed by Automation Industries (Boulder, Colorado) and their report is included as Appendix A. The study was somewhat more generalized than others in this program, since there is less information available on the application of infrared thermography to parts of this kind. Some representative samples of carbon and silica-phenolic parts were supplied to Automation Industries. A ply separation and machined holes were included. Among the more significant results reported was the fact that defects must have a diameter at least equal to twice their depth, and that flaws as small as 0.125-in. dia can be detected Also noted was the requirement that some of the brighter surfaces be given dull coatings.

The infrared thermography study did not reach the stage of actual evaluation as did the radiographic and ultrasonic programs. The technique is certainly applicable to parts of the general type under consideration here. It is not, however, sufficiently well developed to permit accurate estimates of how desirable it would prove in practice. In particular, the technique is not sufficiently developed to allow good extrapolation to a full-scale nozzle.

V.B. Test Procedures and Results (cont)

Although attention should be paid to any future developments in the field of infrared thermography NDT, it cannot be regarded as an immediate candidate for use in inspection of 260-in.-dia motor nozzles. The infrared method is potentially useful, but there are many practical problems to be worked out. These were beyond the scope of this study.

A demonstration of the Bofors Model T101 infrared camera was arranged at Aerojet. There was not sufficient time to arrange anything resembling an evaluation of inspection capability, as this depends more on temperature conditioning of the part than on the camera. The demonstration did, however, give an indication of the resolution and sensitivity possible with the equipment.

6. Special Eddy Current Techniques

The use of eddy currents for inspecting metal parts is well known. Non-metallic parts may also be inspected for thickness if they have a conductive backing, since the usual eddy current instrument may be adjusted to give an indication of distance from probe to a conductor of constant conductivity as well as to variations in the conductivity of a part in contact with the probe. In the case of carbon fabric composites there is enough conductivity to allow some inspection for flaws. Because the conductivity of carbon fabric composites is quite low compared with that of metals, sensitivity to fine cracks is not nearly so great, although the carbon composite may be penetrated to much greater depths than metals. The usual eddy current probe has a coil axis that is perpendicular to the surface of the specimen so that the eddy current loops in the specimen are symmetric about the coil axis.

V.B. Test Procedures and Results (cont)

Such a probe is not sensitive to anisotropic conductivity. The probes made for the present project were wound so that their axes were parallel to the surface of the specimen. In this way, the eddy current loops within the specimen were made to lie almost exclusively in planes perpendicular to the surface, and parallel to each other, thus the current pattern was not symmetrical. If there were a direction of higher conductivity, it could be found by placing the probe on the surface and rotating it. Since the carbon parts involved in this program had a definite fiber structure, it was to be expected that there would be directions of higher conductivity. Figure V-7 shows a specimen of the material. Figure V-8 shows two of the probes tested. The different faces of the test block did show different conductivities, and the direction of the majority of the fibers could be determined by rotating the probe. Such a technique has been used with some success for testing Polaris motor nozzle exit cones. Figure V-9 shows the arrangement for automatic scanning. The Magnaflux ED500 has been modified to accept the special probes and a recorder output provided (these are minor modifications). Figure V-10 shows the records of the inspection.

Contrary to expectations, it was not possible to reliably detect wrinkles in the carbon composite. This was probably a result of the relative irregularity of the carbon parts. They always had some wrinkling, and wrinkling serious enough to constitute a defect did not cause a conspicuous change in the conductivity. The traces did indicate defects, but these were gross surface cracks which are easily found with penetrants or in some cases by visual inspection. The eddy current inspection did not contribute anything to the evaluation of these parts. Such data as it yielded could be obtained from other inspections which would have been required in any case. The full-scale nozzle might be more suitable for inspection by this method, since the greater diameter may make the fiber orientation more regular.

V.B. Test Procedures and Results (cont)

Should this be the case eddy current inspection can be re-evaluated at very little expense. Hence, it does not appear worthwhile to pursue the subject any further at this time. For planning purposes it should be assumed that there is only a very slight probability that eddy current inspection will be useful for carbon parts of the 260-in.-dia motor nozzle.

7. CW - Ultrasonics

The familiar ultrasonic testers use a short pulse in order that the time required for the signal to travel through the part can be determined. This is most useful information, but it means that transient effects predominate. Another approach is possible. Continuous (CW) signals can be used. In this case, the steady state is reached, and the part is made to vibrate in a stable mode, with resonances being observable. It is thus possible to observe the resonant frequency spectrum, and to measure the acoustic impedance represented by the specimen which becomes the load on the transducer. There are a number of things which can be measured, and at least two ways of getting sound into the specimen, giving rise to three different instruments, the North American Sonic Resonator, the Automation Industries Eddy-Sonic System, and the Aerojet Acoustic Impedance Bridge. The Sonic Resonator and Acoustic Impedance Bridge both use contact coupled transducers and are similar in operation, differing in transducer design and in the precise method of measuring the response of the part. The Eddy-Sonic System has an unusual transducer. Coupling is by means of a magnetic field. This field is the magnetic component of the non-radiative field from a coil whose dimensions are small compared to the wavelength of the signals. This is the same field used in eddy current testing, from which the name is derived. The field is used to generate sound in the part, which must be metallic. This system has the advantage of not requiring contact.

V.B. Test Procedures and Results (cont)

The Rohr Corporation performed tests with the Eddy-Sonic System on the nozzle assembly for Motor 260-SL-3, and reported good results in mapping separations between the steel shell and the liner. Rohr engineers considered the system fast and reliable, but somewhat deficient in resolution. Rohr also tested the North American Sonic Resonator, and found it superior in resolution, but slower to use, and recommended its use for accurately mapping flaws located with the Eddy-Sonic System.

The Aerojet Acoustic Impedance Bridge was tested only on the smaller subscale assemblies of this program. Results were unsatisfactory because adequate coupling could not be obtained on the sharply curved surfaces. The larger radius of the full-scale nozzle should eliminate this problem. The Acoustic Impedance Bridge has shown resolution superior to that of the Sonic Resonator in tests on flat aluminum honeycomb panel, and should be evaluated on a full-scale nozzle.

C. RATING SYSTEM AND RESULTS

A rating system was devised to present the evaluation of various techniques in numerical form. These ratings are somewhat subjective because the tests were mostly conducted with subscale parts, and the effect of the increase in size to a nozzle for the 260-in. dia motor had to be estimated. The ratings are shown in Table V-1.

Numbers from 1 through 5 were assigned, 1 indicating an excellent chance of locating a defect, 5 indicating a negligible chance of locating one. The standard for a rating of 1 was a good quality radiograph of a defect for which radiography is the customary method. In the charts which follow, the entry "Negative" indicates that no evidence of defects or discrepancy was found, and that the inspection operation appeared satisfactory. "No test" indicates that no conclusive test was made on a particular part. U indicates that preliminary tests showed that the method would not work.

V.C. Rating System and Results (cont)

Excluded from the chart are the CW ultrasonic methods, which could not be adequately evaluated on subscale parts, and contact ultrasonics, through-ultrasonics, and tangential radiography which were used only for the inspection of the ablative liner bonds to steel shell. Results for these methods are:

Tangential Radiography	3
Through-ultrasound with wheels	1*
Contact ultrasonic pulse echo	3
CW-ultrasonic	2*

*Based on previous tests with a full-scale nozzle

TABLE V-I

RATING OF NDT TECHNIQUES FOR DETECTING ABLATIVE DISCREPANCIES

Defects	Normal X-ray	Through Ultrasonic	Eddy Current	Infrared
Volatile Components 6%	3,5,3	U	U	N.T.
9%	3,5,3	U	U	
Delamination 7 ply	1,1,1	1,1,1	N.T.,3,4	N.T.,N.T.,1
14 ply	1,1,1	1,1,1	N.T.	N.T.
28 ply	1,1,1	N.T.	N.T.	N.T.
Wrinkle 0.125 x 1 x 3 in.	2,5,3	4,3,3	U	N.T.,U.,N.T.
0.25 x 1 x 3 in.	2,5,3	4,3,5	U	N.T.
0.125 x 1.5 x 3 in.	2,5,5	N.T.	U	N.T.
Resin-Rich 10 ply	1,1,1	1,4,4	1,1,N.T.	3,N.T.,N.T.
20 ply	1,1,1	3,2,2	N.T.	N.T.
Resin-Starved 10 ply	1,1,1	N.T.	2,1,4	N.T.
Density 90% normal	2,2,3	N.T.	U	N.T.
80% normal	2,2,3	N.T.	U	N.T.
Process Discrepancies				
Cure with low bag vacuum	1,2,2	4,4,4	N.T.	N.T.
Cure with low temperature	2,1,2		2,2	N.T.
Cure with bag leak in debulk	4,2,5	4,4,4	N.T.	N.T.
Cure with bag leak final cure	4,2,3	4,3,3	N.T.	N.T.
Cure with autoclave pressure low (125 psi)	4,4,4	4,4,4	N.T.	N.T.
Control Specimen	Negative	Negative	N.T.	N.T.
Control Specimen	Negative	Negative	N.T.	N.T.

Ratings are for exit cure, throat and entrance cap, in that order

1 = Excellent 5 = Hopeless N.T. = No Test
U = Method rejected on basis of preliminary tests

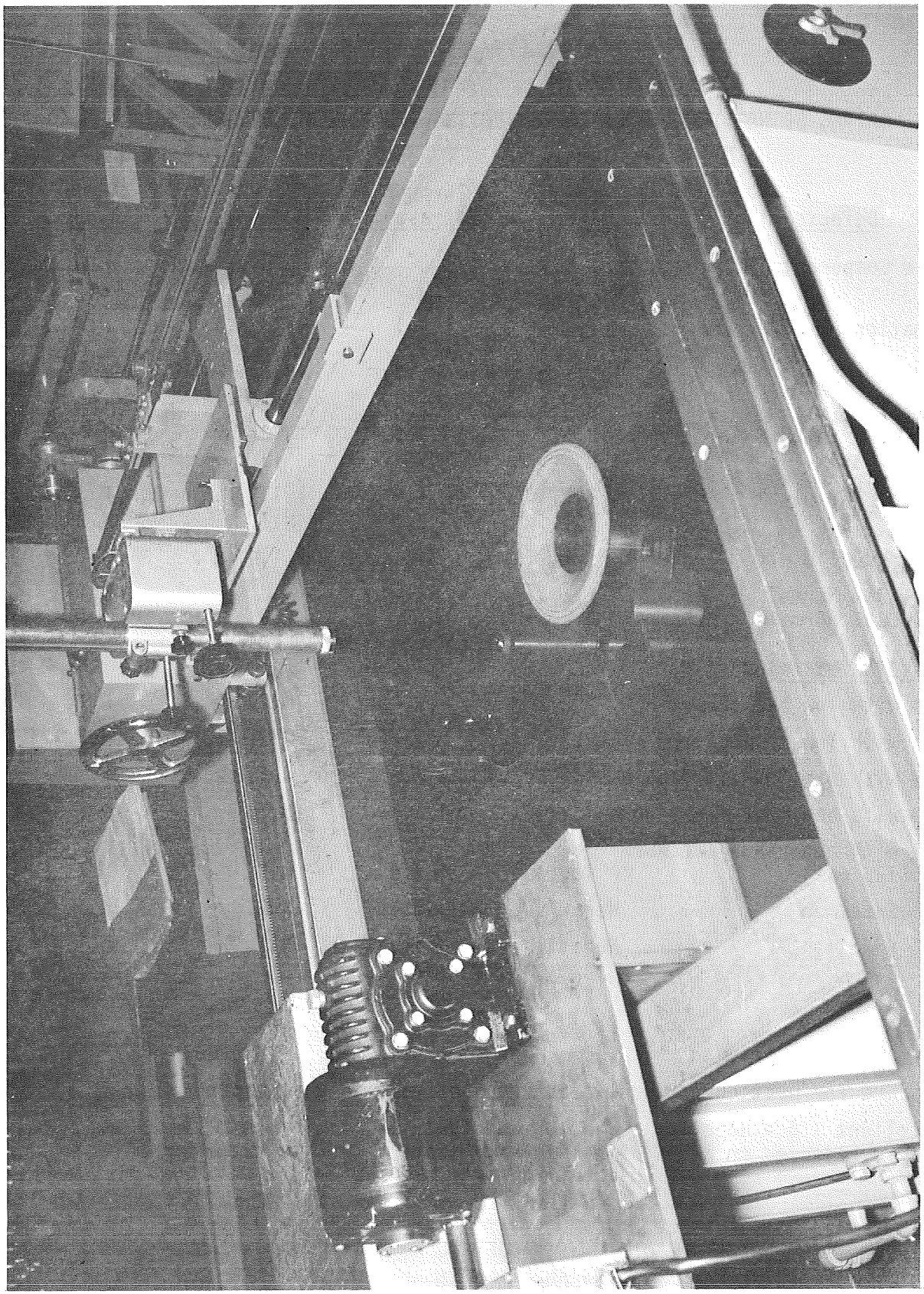

Immersion Ultrasonic Test Unit

Figure V-1

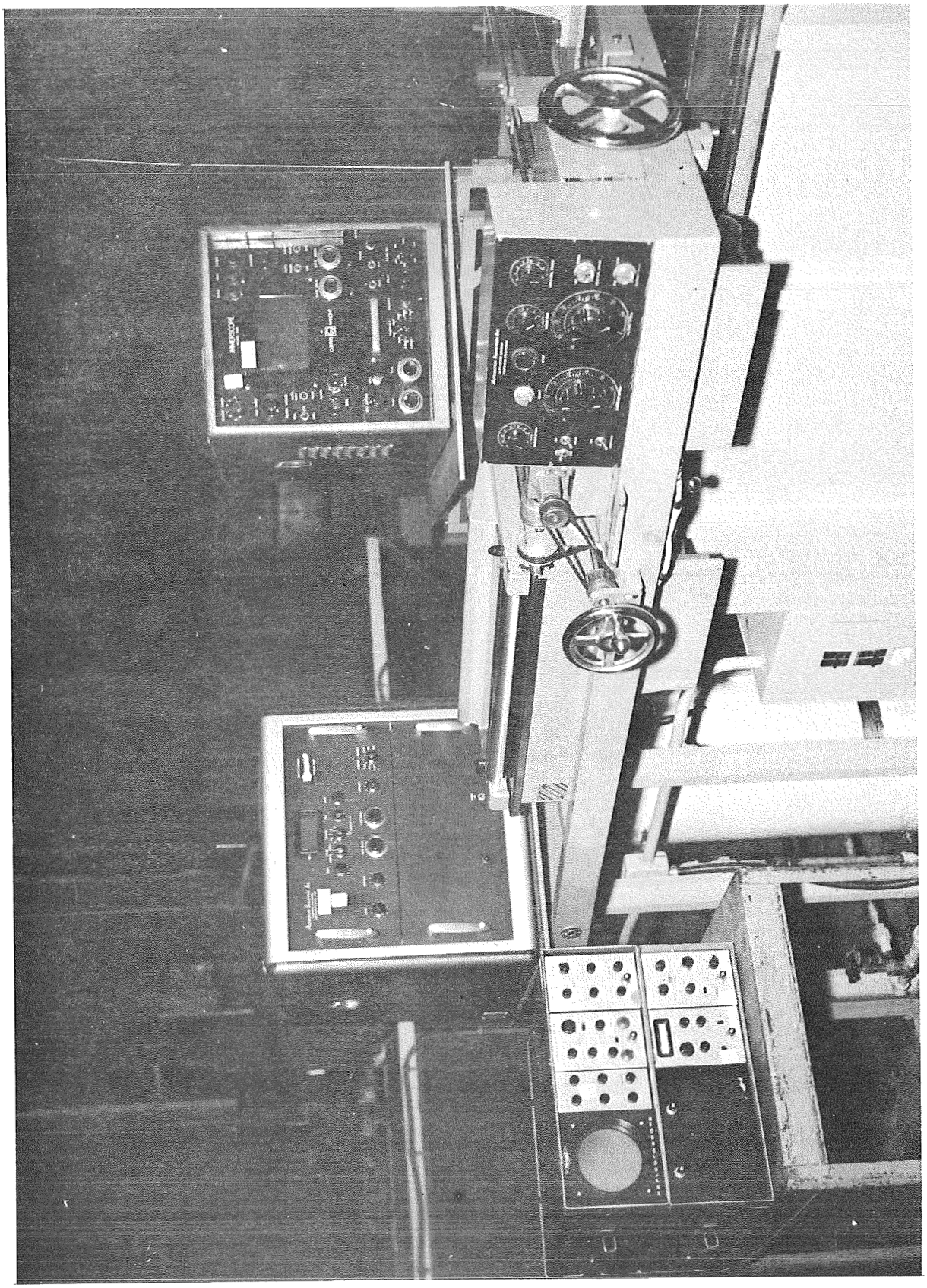

Immersion Ultrasonic Test Unit Readout-Panel

Figure V-2

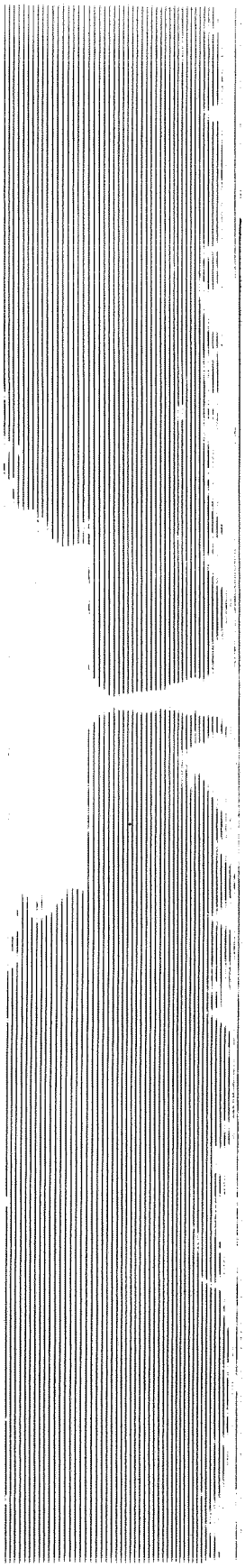

C-Scan of Throat S/N 009, Delaminated 7 Plies

Figure V-3

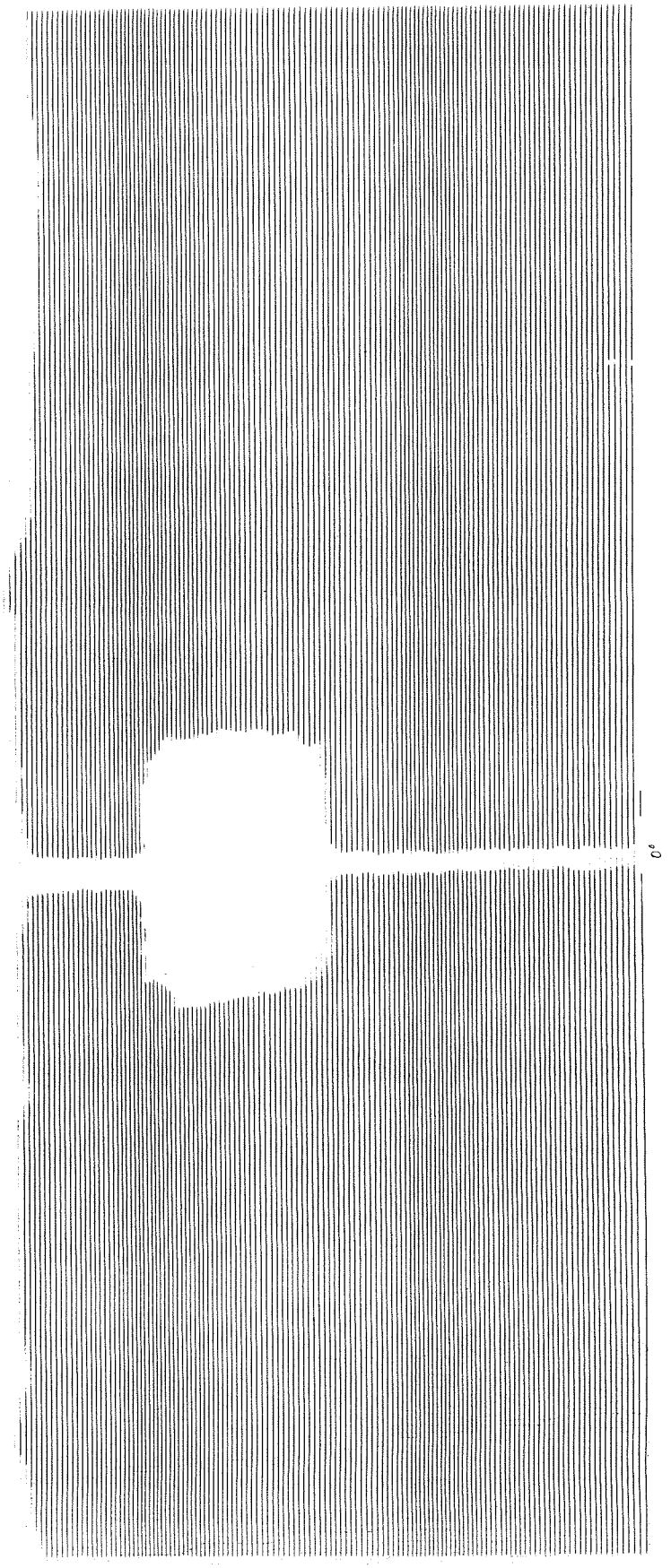

C-Scan of Exit Cone S/N 009, Delaminated 7 Plies

Figure V-4

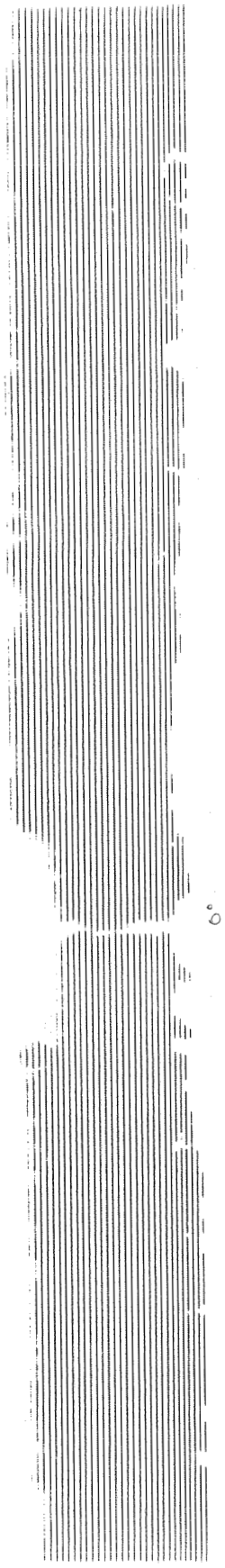

C-Scan of Entrance Cap S/N 009, Delaminated 7 Plies

Figure V-5

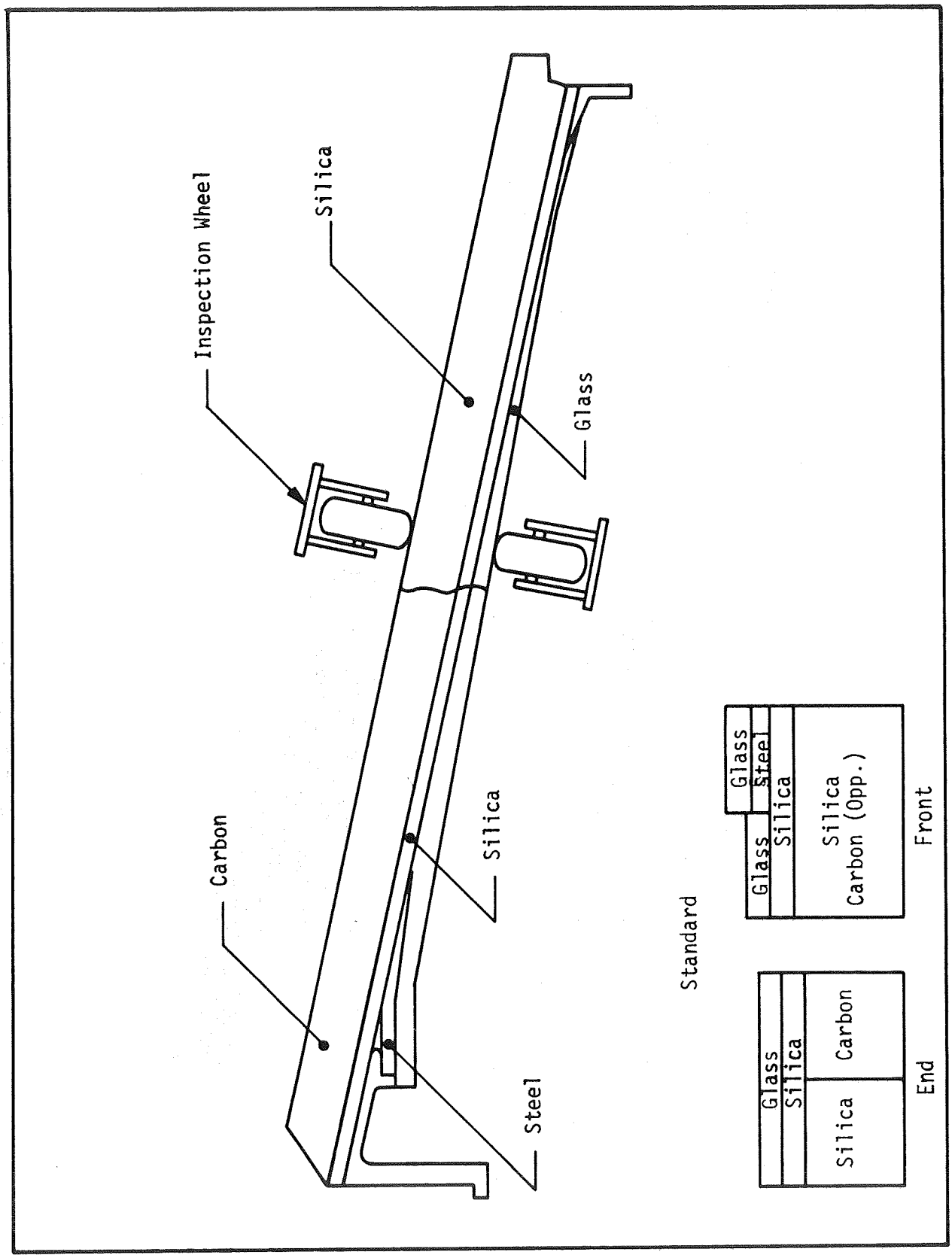

Ultrasonic Technique for Full-Scale Nozzle Assembly

Figure V-6

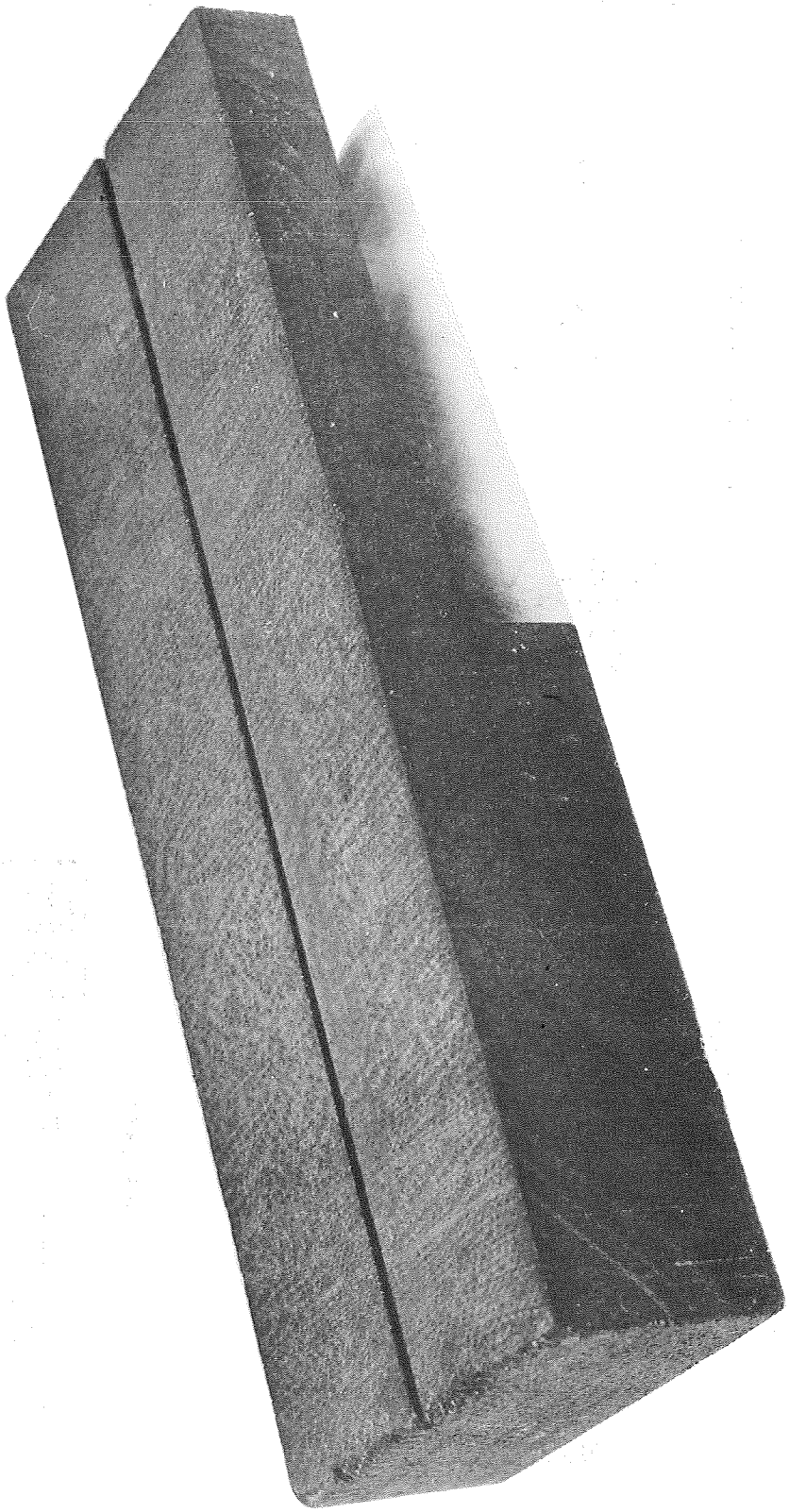

Specimen of Carbon Composite for Evaluation of Eddy Current Techniques

Figure V-7

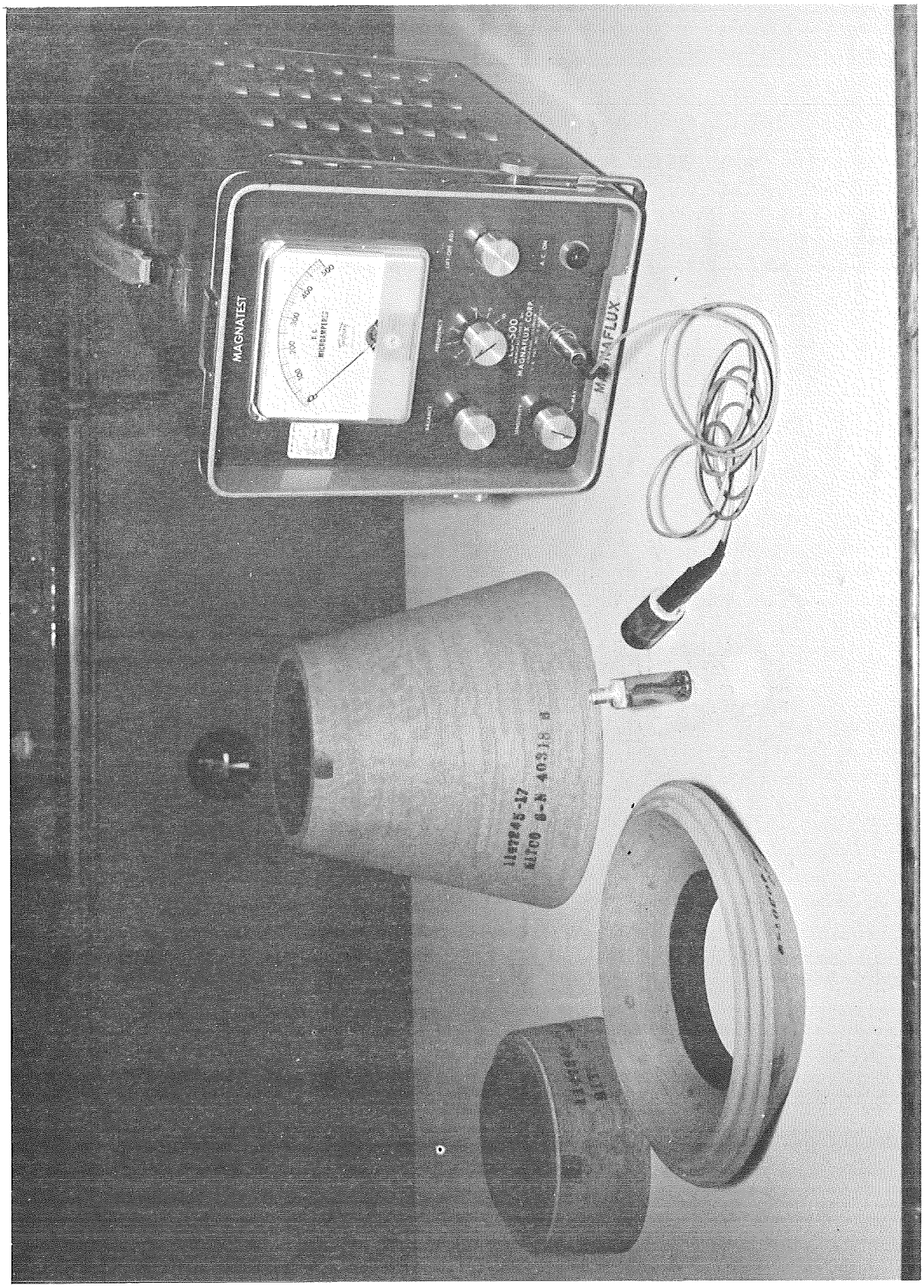

Figure V-8

Eddy Current Probes and Discrepant Nozzle Parts Evaluated

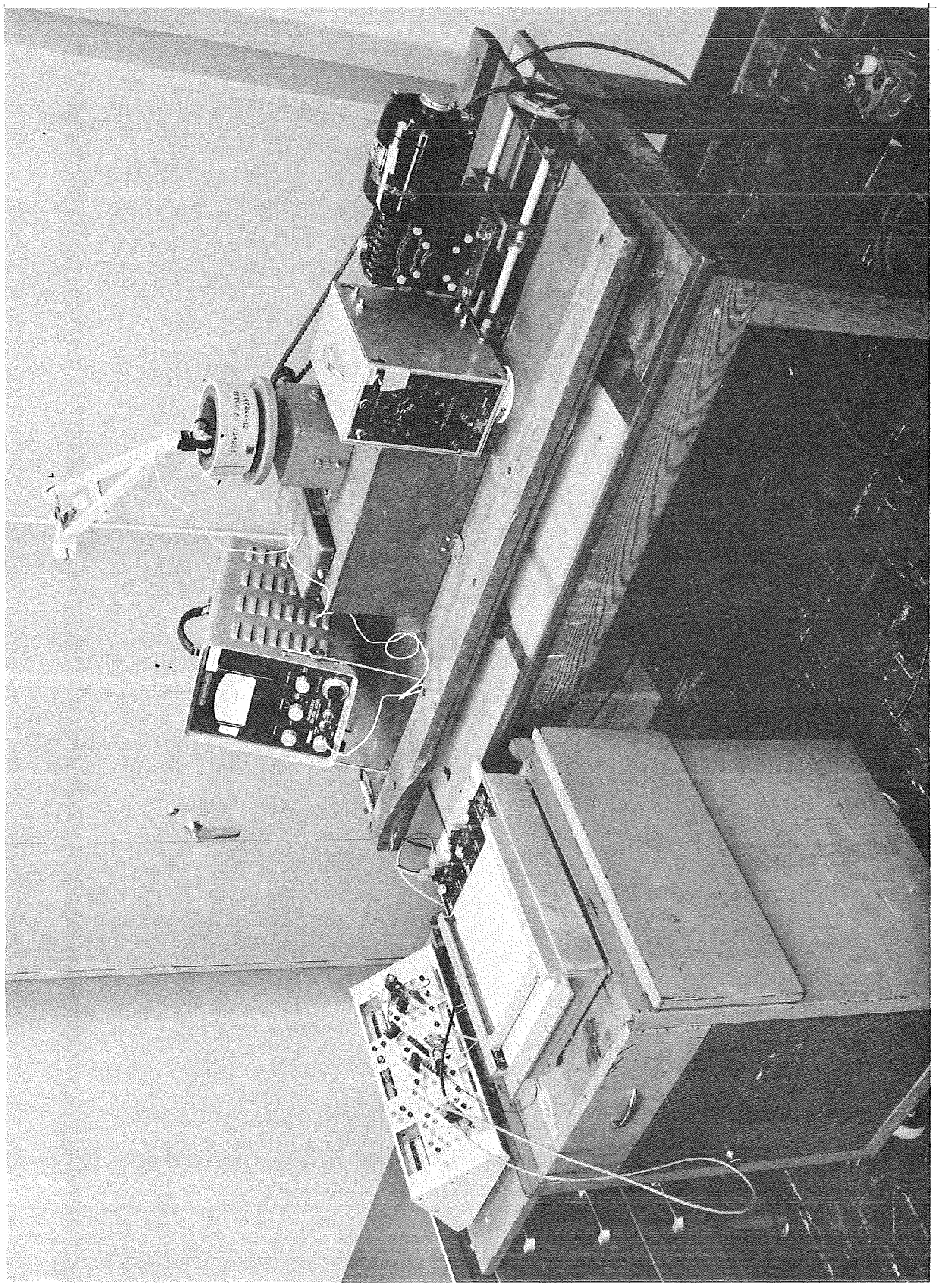

Arrangement for Automatic Eddy Current Scanning
with Throat Insert in Position

Figure V-9

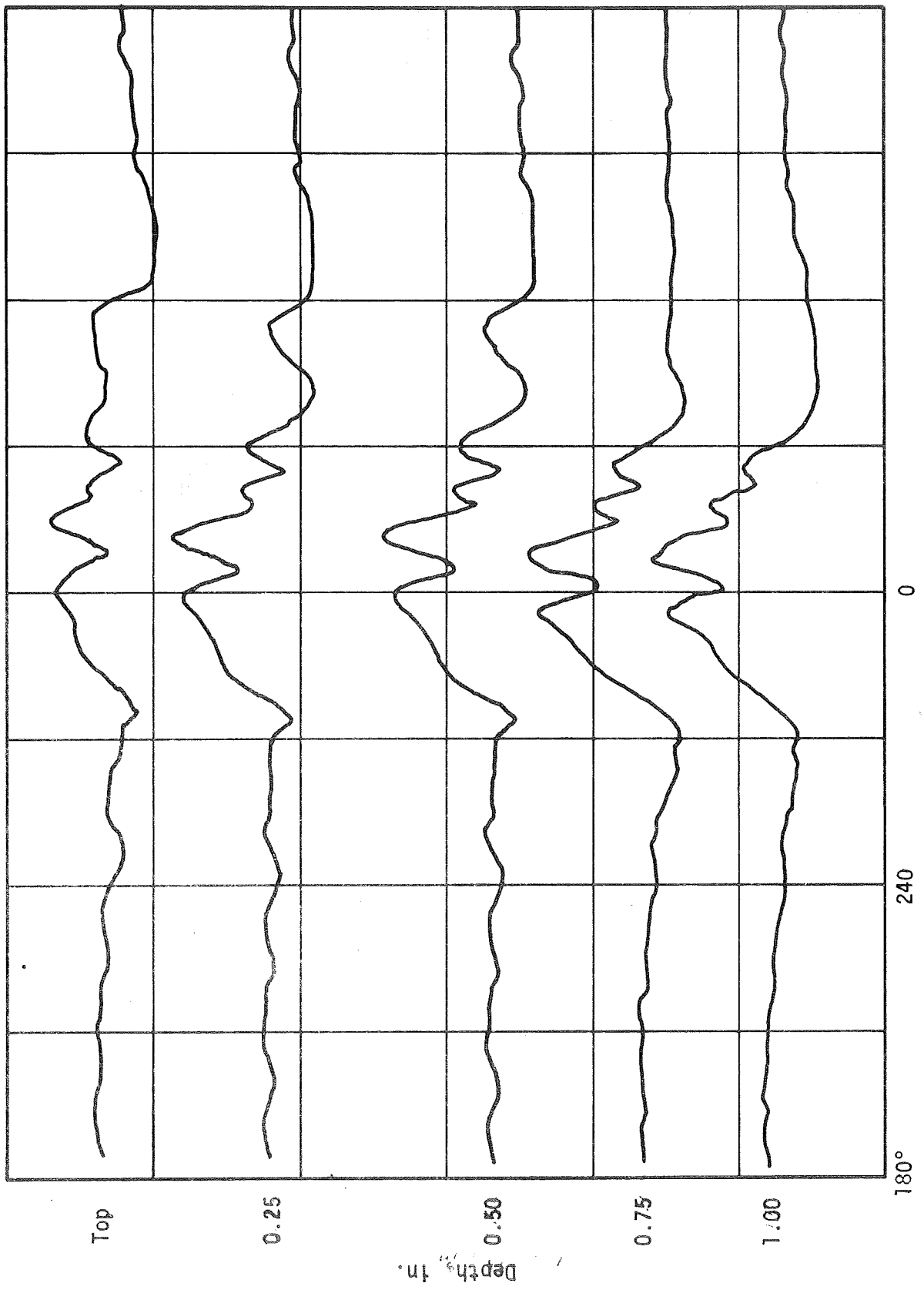

Eddy Current Inspection Traces of Throat SN 007, Resin-Rich 10 Plies

Figure V-10, Sheet 1 of 2

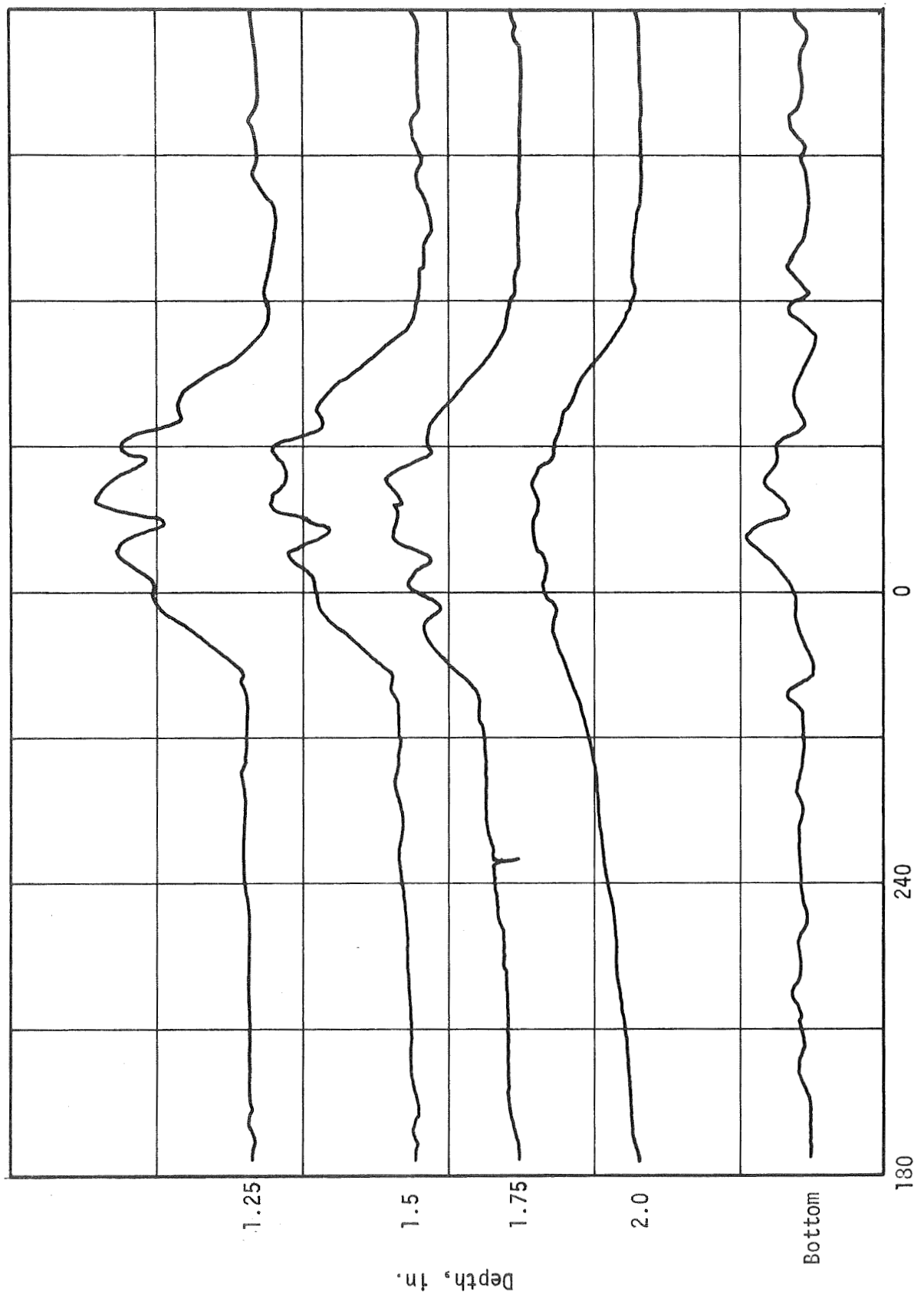

Eddy Current Inspection Traces of Throat SN 007, Resin-Rich 10 Plies

Figure V-10, Sheet 2 of 2

VI. VERIFICATION FIRINGS

A. STATIC TEST

1. Procedure

Twenty test motors with attached nozzle assemblies containing ablative components with introduced discrepancies were statically test fired in the nozzle-up condition during the period January to May 1969. Measurements were made of chamber pressure only.

To facilitate motor handling, a test fixture was fabricated from flanged steel pipe welded to a steel base plate fitted with slots to accept the two forks of a lift truck. The insulated chamber was inserted into the test fixture and the aft flange of the chamber was bolted to the upper flange of the test fixture, as shown in Figure VI-1.

To prepare a motor for firing, the propellant cartridge, consisting of a PBD type propellant previously cast in a paper-phenolic sleeve and stored in a conditioning cell at 75 $\pm$ 10°F, was loaded into the chamber (Figure VI-1). The motor aft closure with attached nozzle assembly was then fitted to the chamber (Figure VI-2) and the retainers (Figure III-2) locked in position. The assembled motor on the test fixture (Figure VI-3) was placed in the conditioning cell, a packaged igniter taped to the closure (Figure VI-4) and stored until the test bay was free.

In the test bay, pressure transducers were attached to the fore end as shown in Figure VI-5 and checked out. The igniter was then lowered into the motor through the nozzle throat opening (Figure VI-6) and the lead wires taped to the nozzle shell. Figure VI-7 shows the motor in the test bay, ready for test.

VI.A. Static Test (cont)

After each test firing, the motor was disassembled and the chamber and closure examined to determine the effect of the test on the inert parts insulation. Figure VI-8 shows the aft closure after two firings. It was found that generally there was only a slight removal of insulation except at the nozzle opening; this area was patched with V-61 potting compound between firings. The chamber insulation was virtually unaffected by firing because of the protection afforded by the paper-phenolic sleeve around the propellant. Figure VI-9 is a photograph of the motor after test, showing the charring of the sleeve and propellant base.

2. Test Results

Figures VI-10 through VI-29 are the pressure-time curves of the twenty verification firings plotted from digital readouts. Maximum and average chamber pressures were calculated from the readouts; burn time* was determined from the curves. A summary of the verification firings is shown in Table VI-1.

Test Numbers 2 and 3, which were conducted with baseline nozzle assemblies, indicate that the basic motor and nozzle designs were acceptable, since the chamber pressures and burn times meet the program requirements (Section III, A) and were within 3 percent of the predicted values of 603 psia (4.15 MN/m^2) average, and 25.78 sec.

B. PERFORMANCE

After static test, the nozzle components were removed from the steel

* Burn Time - The interval measured from 75% of maximum pressure during rise to the point the pressure-time curve which lies on a line bisecting the angle formed by the tangents to the curve prior to and immediately after the beginning of tail-off. Construction lines are shown in the figures.

VI.B. Performance (cont)

shell and examined visually. Figures VI-30 through VI-36 are photographs of some discrepant nozzle components after firing.

In general, the forward (silica) portion of the nozzle entrance cap exhibited severe attack. Figures VI-30 and VI-31 show the appearance of the low-density entrance caps. The 70 to 80% dense component (Figure VI-30) exhibited preferential resin removal between plies of the silica reinforcement and cracking, particularly at the silica-carbon interface. Local attack (pinholes) were observed in the carbon portion. The 80 to 90% dense component (Figure VI-31) exhibited the same features, but to a lesser degree. The more dense components were not subject to cracking or pinholing and the erosion tended to be localized at the introduced discrepancies, as indicated in Figures VI-32 and VI-33.

Material removal in the nozzle throats was greater at the defect locations, but no cracking was observed. Figure VI-34 shows the outlines of a baseline throat (a) and of four others with low density (b), resin-rich area (c), delaminations (d) and wrinkles (e), and illustrates the non-uniformity of erosion associated with the local defects.

In the exit cone material removal was also greater at the defect locations, and except in two instances no cracking was observed. In the instances where cracking occurred, the exit cone configuration was thin-walled. (refer to Section VI, B, 2 "Structural Performance"). Figure VI-35 shows the failure experienced with the exit cone fabricated with 28 plies of delaminations. Figure VI-36 shows a crack formed in the exit cone fabricated with 0.125-in. (0.317cm) wrinkles.

Following the visual examination, the components were sectioned at five radial locations - zero, 90, 135, 180 and 270 degrees. Measurements of

VI.B. Performance (cont)

regression and char depth were made axially along each of the sections. These were plotted and are shown in Figures VI-37 through VI-56.

After measurements of regression and char depth had been completed, samples of the char were removed from the throat insert and from the silica portion of the exit cone, at the locations of the introduced discrepancies, and the densities were determined by weight-volume measurements. The char densities are reported in Table VI-2.

1. Ablative Performance

The regression and char depths were adjusted to a common basis of 600 psia (4.14 MN/m^2) chamber pressure by multiplying the measured values by a factor calculated from the following relationship:

$$\frac{A600}{A_o} = \left(\frac{600}{P_o}\right)^{0.8} \qquad \text{(Equation 2)}$$

where the subscript (o) refers to the measured regression, char depth and chamber pressure for each of the individual firings. Tables VI-3 through VI-6 show the corrected regression and char depths at the axial locations at which the discrepancies were present. Also shown are the regression and charring rates, calculated by dividing the total depths by the respective motor burn times.

In the MX-2600 entrance section (see Table VI-3) the regression rate was found to be dependent upon the relative number or severity of the introduced discrepancy. The maximum regression rate (20.03 mils/sec = 0.51 mm/sec) was experienced in the resin starved material, followed by the 70 to 80% dense component (17.39 mils/sec = 0.44 mm/sec). Cure cycle variations involving equipment malfunction had no effect on regression. The two baseline components exhibited an average regression rate of 10.24 mils/sec (0.26 mm/sec) and a charring rate of 13.84 mils/sec (0.35 mm/sec).

VI.B. Performance (cont)

At the minimum throat diameter (Table VI-4), the maximum regression rate of 12.98 mils/sec (0.33 mm/sec) occurred in the MX-4926 component fabricated to a density of 70 to 80 percent of normal. The regression rate of the throat containing 28 delaminated plies was almost as high—12.90 mils/sec (0.33 mm/sec). Resin starvation and cure cycle variables due to equipment malfunctions had no appreciable effect. In the two baseline throats average regression rate was 7.425 mils/sec (0.185 mm/sec) and charring rate was 14.05 mils/sec (0.36 mm/sec).

The maximum regression rate in the MX-4926 exit cone forward section (from Table VI-5) was 11.89 mils/sec (0.30 mm/sec), in the 10-ply resin-rich material. This rate was almost twice as high as that observed in components containing 0.375-in. wrinkles (6.50 mils/sec = 0.17 mm/sec) and 80 to 90 percent density (6.35 mils/sec = 0.16 mm/sec). Equipment malfunctions had no effect on regression. The average regression rate of the two baseline components was 2.08 mils/sec (0.055 mm/sec) and the average charring rate was 11 mils/sec (0.28 mm/sec).

The maximum regression rate in the MX-2600 exit cone aft section (Table VI-6) was experienced in the resin-starved material (3.85 mils/sec = 0.098 mm/sec). Cure cycle variations caused by equipment malfunctions had no observable effect. The average regression rate of the baseline components was 1.71 mils/sec (0.045 mm/sec) and the average charring rate was 7.02 mils/sec (0.178 mm/sec).

2. Structural Performance

As the mechanical and physical properties of the discrepant components were determined, it became apparent that there was little likelihood that structural failures would occur in the nozzle assembly as originally

VI.B. Performance (cont)

designed. To increase the probability of structural failure, the ablative exit section and steel support shell were modified, as shown in Figure VI-57.

The removal of the overwrap insulation was instrumental in producing the failure noted in Figure VI-35, in which 28 delaminated plies were introduced into the nozzle components. Examination of the failure indicated that burnthrough occurred at and aft of the delaminated section, after which the exit cone unwound circumferentially and ejected. A close-up of the failure origin is shown in Figure VI-58. When one end of the delaminated plies is sealed, burnthrough and subsequent failure cannot occur as indicated by the absence of burnthrough and failure in the entrance cap, throat insert, and forward exit sections of this same nozzle. All of these contained 28 delaminated plies covered by insulation overwraps. This is further confirmed by the absence of failure in the aft exit section containing seven delaminated plies, all of which were sealed at the O.D. surface. Figure VI-59 shows this exit section after static test.

Gross ply separation and cracking occurred in three nozzle components—the aft exit section containing 0.125-in. wrinkles and the entrance caps fabricated to 70 to 80 percent density. Figure VI-60 shows the exit section, with a crack extending for 120 degrees; Figures VI-61 and VI-62 show cracks at and near the carbon-silica interface of the 70 to 80 percent density entrance cap. Further examination of all low density entrance caps leads to the conclusion that the cracking was associated with wrinkles (see Figures VI-30 and VI-31). No wrinkles nor cracking were observed in the vacuum bagged entrance cap, which had been fabricated to a high as-wrapped density.

TABLE VI-1

SUMMARY OF VERIFICATION FIRINGS

Test No.	Discrepancy	Chamber Pressure, psia (MN/m^2) Maximum	Average	Burn Time, sec
1	Autoclave, 125 psig	635.5 (4.38)	577 (3.98)	26.45
2	None (Baseline)	642.5 (4.43)	590 (4.07)	26.6
3	None (Baseline)	670.5 (4.62)	610 (4.21)	26.1
4	Vacuum Bag, 25 in. Hg	638.0 (4.4)	573 (3.95)	27.0
5	Bag Leak, Debulk	665.0 (4.59	606 (4.18)	26.15
6	Bag Leak, Final Cure	657.0 (4.53)	604 (4.16)	26.3
7	Resin-Rich, 20 plies	680.0 (4.69)	615 (4.24)	26.0
8	Delams, 14 plies	654.0 (4.51)	597 (4.12)	26.3
9	Wrinkles, 0.25-in.	659.0 (4.54)	595 (4.10)	26.15
10	Resin-Starved, 10 plies	646.5 (4.46)	585 (4.03)	26.5
11	Temperature Loss, Debulk	658.0 (4.54)	598 (4.12)	26.4
12	9% Volatiles	651.0 (4.49)	588 (4.05)	26.9
13	Delams, 28 plies	632.5 (4.36)	572 (3.94)	27.05
14	6% Volatiles	635.0 (4.38)	574.5 (3.96)	26.75
15	Wrinkles, 0.375-in.	633.0 (4.36)	570.0 (3.93)	27.25
16	70 to 80% Density	557.0 (3.84)	503 (3.47)	29.1
17	Resin-Rich, 10 plies	610.5 (4.21)	554 (3.82)	27.8
18	Delams, 7 plies	632.5 (4.36)	576 (3.97)	26.75
19	Wrinkles, 0.125-in.	626.0 (4.32)	572 (3.94)	26.95
20	80 to 90% Density	600.5 (4.14)	537 (3.70)	27.55

TABLE VI-2

DENSITIES OF CHARRED NOZZLE COMPONENTS

Discrepancy	Material	Location	Density, lb/cu ft	Density, gm/cc
None (Baseline)	MX-4926	Throat	68.0	1.09
			67.4	1.08
	MX-2600	Exit	87.4	1.40
			88.0	1.41
Vacuum Bag, 25 in. Hg	MX-4926	Throat	53.1	0.85
	MX-2600	Exit	84.3	1.35
Autoclave, 125 psig	MX-4926	Throat	67.4	1.08
	MX-2600	Exit	88.0	1.41
Bag Leak, Debulk	MX-4926	Throat	67.4	1.08
	MX-2600	Exit	88.7	1.42
Bag Leak, Debulk	MX-4926	Throat	73.7	1.18
	MX-2600	Exit	88.0	1.41
Temperature Loss,	MX-4926	Throat	69.9	1.12
Debulk	MX-2600	Exit	79.3	1.27
70 to 80% Density	MX-4926	Throat	54.3	0.87
	MX-2600	Exit	86.8	1.39
80 to 90% Density	MX-4926	Throat	54.9	0.88
	MX-2600	Exit	71.8	1.15
6% Volatiles	MX-4926	Throat	56.8	0.91
	MX-2600	Exit	84.9	1.36
9% Volatiles	MX-4926	Throat	64.9	1.04
	MX-2600	Exit	81.2	1.30
Wrinkles, 0.125-in.	MX-4926	Throat	77.4	1.24
	MX-2600	Exit	-	-
Wrinkles, 0.25-in.	MX-4926	Throat	71.2	1.14
	MX-2600	Exit	85.5	1.37
Wrinkles, 0.375-in.	MX-4926	Throat	73.7	1.18
	MX-2600	Exit	85.5	1.37
Resin-Rich, 10 plies	MX-4926	Throat	75.5	1.21
	MX-2600	Exit	79.9	1.28
Resin-Rich, 20 plies	MX-4926	Throat	70.5	1.13
	MX-2600	Exit	85.5	1.37
Resin-Starved, 10 plies	MX-4926	Throat	70.5	1.13
	MX-2600	Exit	80.5	1.29
Delaminations, 7 plies	MX-4926	Throat	73.7	1.18
	MX-2600	Exit	90.5	1.45
Delaminations, 14 plies	MX-4926	Throat	69.9	1.12
	MX-2600	Exit	89.3	1.43
Delaminations, 28 plies	MX-4926	Throat	65.6	1.05
	MX-2600	Exit	88.7	1.42

TABLE VI-3

CORRECTED* REGRESSION AND CHAR DEPTH OF MX-2600 IN ENTRANCE CAP AT AREA RATIO 3.5 (3.25 in. rad.)

	Regression				Char Depth			
	Total		Rate		Total		Rate	
Discrepancy	in.	cm	mil/sec	cm/sec	in.	cm	mil/sec	cm/sec
Baseline	0.29	0.737	10.96	0.028	0.39	0.991	14.73	0.037
	0.25	0.635	9.52	0.024	0.34	0.864	12.95	0.033
Vacuum Bag	0.23	0.584	8.83	0.022	0.30	0.762	11.52	0.029
Autoclave	0.16	0.406	6.23	0.016	0.26	0.660	10.12	0.026
70 to 80% Density	0.44	1.118	17.39	0.044	0.53	1.346	20.95	0.053
80 to 90% Density	0.24	0.61	9.52	0.024	0.36	0.914	14.28	0.036
Bag Leak, Debulk	0.26	0.660	9.86	0.025	0.37	0.94	14.04	0.036
Bag Leak, Final Cure	0.20	0.508	7.56	0.019	0.30	0.762	11.34	0.029
Temperature Loss	0.24	0.61	9.11	0.023	0.36	0.914	13.66	0.035
6% Volatiles	0.24	0.61	9.27	0.024	0.34	0.864	13.13	0.033
9% Volatiles	0.383	0.973	14.47	0.037	0.45	1.143	17.0	0.043
Wrinkles, 0.125 x 1	0.34	0.864	13.11	0.033	0.41	1.041	15.81	0.040
(Defect free areas)	0.30	0.762	11.57	0.029	0.375	0.953	14.46	0.037
Wrinkles, 0.25 x 1.5	0.41	1.041	15.77	0.040	0.47	1.194	18.08	0.046
(Defect free areas)	0.285	0.724	10.96	0.028	0.345	0.876	13.27	0.034
Wrinkles, 0.375 x 1.5	0.46	1.168	17.59	0.045	0.52	1.321	19.88	0.050
(Defect free areas)	0.335	0.851	12.81	0.033	0.415	1.054	15.87	0.040
Resin Rich, 10 plies	0.27	0.686	10.35	0.026	0.36	0.914	13.80	0.035
(Defect free areas)	0.255	0.648	9.78	0.025	0.34	0.865	13.04	0.033
Resin Rich, 20 plies	0.34	0.864	12.80	0.033	0.43	1.092	16.19	0.041
(Defect free areas)	0.26	0.660	9.79	0.025	0.34	0.864	12.80	0.033
Resin Starved, 10 plies	0.52	1.321	20.03	0.051	0.60	1.524	23.12	0.059
(Defect free areas)	0.30	0.762	11.56	0.029	0.37	0.94	14.26	0.036
Delaminations, 7 plies	0.37	0.94	14.29	0.036	0.45	1.143	17.38	0.044
(Defect free areas)	0.195	0.495	7.53	0.019	0.265	0.673	10.23	0.026
Delaminations, 14 plies	0.40	1.016	15.27	0.039	0.49	1.245	18.71	0.048
(Defect free areas)	0.25	0.635	9.54	0.024	0.335	0.851	12.79	0.032
Delaminations, 28 plies	0.45	1.143	17.28	0.044	0.53	1.346	20.36	0.052
(Defect free areas)	0.29	0.737	11.14	0.028	0.40	1.016	15.36	0.039

*Corrected to 600 psia (4.14 MN/m^2) chamber pressure

TABLE VI-4

CORRECTED* REGRESSION AND CHAR DEPTH OF MX-4926 AT MINIMUM THROAT DIAMETER (1.75 in. rad.)

	Regression				Char Depth			
	Total		Rate		Total		Rate	
Discrepancy	in.	cm	mil/sec	cm/sec	in.	cm	mil/sec	cm/sec
Baseline	0.168	0.427	6.44	0.016	0.355	0.902	13.6	0.035
	0.223	0.566	8.41	0.021	0.386	0.980	14.5	0.037
Vacuum Bag	0.286	0.726	10.6	0.027	0.473	1.201	17.51	0.044
Autoclave	0.171	0.434	6.46	0.016	0.357	0.907	13.5	0.034
70 to 80% Density	0.378	0.960	12.98	0.033	0.551	1.4	18.93	0.048
80 to 90% Density	0.285	0.724	10.34	0.026	0.449	1.140	16.3	0.041
Bag Leak, Debulk	0.194	0.493	7.41	0.019	0.382	0.970	14.61	0.037
Bag Leak, Final Cure	0.205	0.521	7.8	0.02	0.385	0.98	14.62	0.037
Temperature Loss	0.172	0.437	6.54	0.017	0.342	0.869	12.98	0.033
6% Volatiles	0.237	0.602	8.85	0.022	0.422	1.072	15.77	0.040
9% Volatiles	0.216	0.549	8.03	0.020	0.38	0.965	14.12	0.036
Wrinkles, 0.125 x 1	0.208	0.528	7.72	0.02	0.374	0.95	13.88	0.035
(Defect free areas)	0.203	0.516	7.52	0.019	0.364	0.925	13.5	0.034
Wrinkles, 0.25 x 1.5	0.216	0.549	8.29	0.021	0.358	0.909	13.69	0.035
(Defect free areas)	0.216	0.659	8.29	0.021	0.357	0.907	13.65	0.035
Wrinkles, 0.375 x 1.5	0.205	0.521	7.52	0.019	0.361	0.917	13.24	0.034
(Defect free areas)	0.183	0.465	6.73	0.017	0.355	0.902	13.04	0.033
Resin Rich, 10 plies	0.252	0.640	9.06	0.023	0.427	1.085	15.36	0.039
(Defect free areas)	0.174	0.442	6.27	0.016	0.377	0.958	13.55	0.034
Resin Rich, 20 plies	0.231	0.587	8.9	0.023	0.402	1.021	15.66	0.040
(Defect free areas)	0.171	0.434	6.59	0.017	0.348	0.884	13.37	0.034
Resin Starved, 10 plies	0.204	0.518	7.71	0.02	0.367	0.932	13.86	0.035
(Defect free areas)	0.184	0.467	6.94	0.018	0.332	0.843	12.52	0.032
Delaminations, 7 plies	0.237	0.602	8.85	0.023	0.407	1.034	15.21	0.039
(Defect free areas)	0.181	0.46	6.76	0.017	0.351	0.892	13.13	0.033
Delaminations, 14 plies	0.211	0.536	8.03	0.020	0.412	1.046	15.65	0.040
(Defect free areas)	0.186	0.472	7.06	0.018	0.366	0.93	13.93	0.035
Delaminations, 28 plies	0.349	0.886	12.90	0.033	0.439	1.115	16.22	0.041
(Defect free areas)	0.204	0.518	7.55	0.019	0.39	0.991	14.4	0.037

*Corrected to 600 psia (4.14 MN/m^2) chamber pressure

TABLE VI-5

CORRECTED* REGRESSION AND CHAR DEPTH OF MX-4926
IN EXIT CONE AT AREA RATIO 1.44 (2.1 in. rad.)

	Regression				Char Depth			
	Total		Rate		Total		Rate	
Discrepancy	in.	cm	mil/sec	cm/sec	in.	cm	mil/sec	cm/sec
Baseline	0.07	0.178	2.64	0.007	0.31	0.787	11.71	0.03
	0.04	0.102	1.52	0.004	0.27	0.685	10.28	0.026
Vacuum Bag	0.08	0.203	3.07	0.008	0.29	0.737	11.14	0.028
Autoclave	0.05	0.127	1.95	0.005	0.27	0.685	10.51	0.027
70 to 80% Density	0.11	0.279	4.35	0.011	0.37	0.94	14.62	0.037
80 to 90% Density	0.016	0.406	6.35	0.016	0.37	0.94	14.68	0.037
Bag Leak, Debulk	0.10	0.254	3.79	0.01	0.34	0.864	12.9	0.033
Bag Leak, Final Cure	0.043	0.109	1.63	0.004	0.307	0.78	11.6	0.029
Temperature Loss	0.09	0.229	3.42	0.009	0.29	0.737	11.01	0.028
6% Volatiles	0.08	0.203	3.09	0.008	0.31	0.787	11.97	0.030
9% Volatiles	0.12	0.305	4.53	0.012	0.33	0.838	12.46	0.032
Wrinkles, 0.125 x 1	0.11	0.279	4.24	0.011	0.29	0.737	11.18	0.028
(Defect free areas)	0.05	0.127	1.93	0.005	0.32	0.813	12.34	0.031
Wrinkles, 0.25 x 1.5	0.08	0.203	3.08	0.008	0.29	0.737	11.16	0.028
(Defect free areas)	0.07	0.178	2.69	0.007	0.28	0.711	10.77	0.027
Wrinkles, 0.375 x 1.5	0.17	0.432	6.50	0.017	0.31	0.787	11.85	0.030
(Defect free areas)	0.07	0.178	2.68	0.007	0.30	0.762	11.47	0.029
Resin Rich, 10 plies	0.31	0.787	11.89	0.030	0.42	1.067	16.11	0.041
(Defect free areas)	0.075	0.191	2.88	0.007	0.30	0.762	11.5	0.029
Resin Rich, 20 plies	0.14	0.356	5.27	0.013	0.39	0.991	14.69	0.037
(Defect free areas)	0.06	0.152	2.26	0.006	0.30	0.762	11.3	0.029
Resin Starved, 10 plies	0.07	0.178	2.70	0.007	0.32	0.813	12.33	0.031
(Defect free areas)	0.055	0.14	2.12	0.005	0.265	0.673	10.21	0.026
Delaminations, 7 plies	0.07	0.178	2.70	0.007	0.24	0.61	9.27	0.024
(Defect free areas)	0.05	0.127	1.93	0.005	0.305	0.775	11.78	0.03
Delaminations, 14 plies	0.13	0.330	4.96	0.013	0.41	1.041	15.65	0.04
(Defect free areas)	0.055	0.14	2.1	0.005	0.255	0.648	9.73	0.025
Delaminations, 28 plies	0.14	0.356	5.38	0.014	0.34	0.864	13.06	0.033
(Defect free areas)	0.05	0.127	1.92	0.005	0.245	0.622	9.41	0.024

*Corrected to 600 psia (4.14 MN/m^2) chamber pressure

TABLE VI-6

CORRECTED* REGRESSION AND CHAR DEPTH OF MX-2600
IN EXIT CONE AT AREA RATIO 4.5 (3.7 in. rad.)

	Regression				Char Depth			
	Total		Rate		Total		Rate	
Discrepancy	in.	cm	mil/sec	cm/sec	in.	cm	mil/sec	cm/sec
Baseline	0.05	0.127	1.89	0.005	0.19	0.483	7.18	0.018
	0.04	0.102	1.52	0.004	0.18	0.457	6.85	0.017
Vacuum Bag	0.05	0.127	1.92	0.005	0.18	0.457	6.91	0.018
Autoclave	0.02	0.051	0.78	0.002	0.13	0.330	5.12	0.013
70 to 80% Density	0.03	0.076	1.19	0.003	0.20	0.508	7.90	0.020
80 to 90% Density	0.04	0.102	1.59	0.004	0.18	0.457	7.14	0.018
Bag Leak, Debulk	0.03	0.076	1.14	0.003	0.18	0.457	6.83	0.017
Bag Leak, Final Cure	0.03	0.076	1.13	0.003	0.18	0.457	6.8	0.017
Temperature Loss	0.04	0.102	1.52	0.004	0.18	0.457	6.83	0.017
6% Volatiles	0.04	0.102	1.54	0.004	0.18	0.457	6.95	0.018
9% Volatiles	0.06	0.152	2.27	0.006	0.19	0.483	7.18	0.018
Wrinkles, 0.125 x 1	0.06	0.152	2.31	0.006	100%	-	-	-
(Defect free areas)	-	-	-	-	-	-	-	-
Wrinkles, 0.25 x 1.5	0.05	0.127	1.92	0.005	0.19	0.483	7.31	0.019
(Defect free areas)	0.04	0.102	1.54	0.004	0.185	0.47	7.12	0.018
Wrinkles, 0.375 x 1.5	0.06	0.152	2.29	0.006	100%	-	-	-
(Defect free areas)	0.05	0.127	1.91	0.005	100%	-	-	-
Resin Rich, 10 plies	0.03	0.076	1.15	0.003	0.20	0.508	7.67	0.019
(Defect free areas)	0.03	0.076	1.15	0.003	0.17	0.432	6.52	0.017
Resin Rich, 20 plies	0.04	0.102	1.51	0.004	0.19	0.483	7.15	0.018
(Defect free areas)	0.03	0.076	1.13	0.003	0.175	0.445	6.59	0.017
Resin Starved, 10 plies	0.10	0.254	3.85	0.0098	0.23	0.584	8.86	0.023
(Defect free areas)	0.04	0.102	1.54	0.004	0.195	0.495	7.51	0.019
Delaminations, 7 plies	0.04	0.102	1.54	0.004	100%	-	-	-
(Defect free areas)	0.03	0.076	1.16	0.003	100%	-	-	-
Delaminations, 14 plies	0.03	0.076	1.15	0.003	0.19	0.483	7.25	0.018
(Defect free areas)	0.015	0.038	0.57	0.001	0.165	0.419	6.3	0.016
Delaminations, 28 plies	Ejected		Ejected		Ejected		Ejected	
(Defect free areas)	-	-	-	-	-	-	-	-

*Corrected to 600 psia (4.14 MN/m^2) chamber pressure

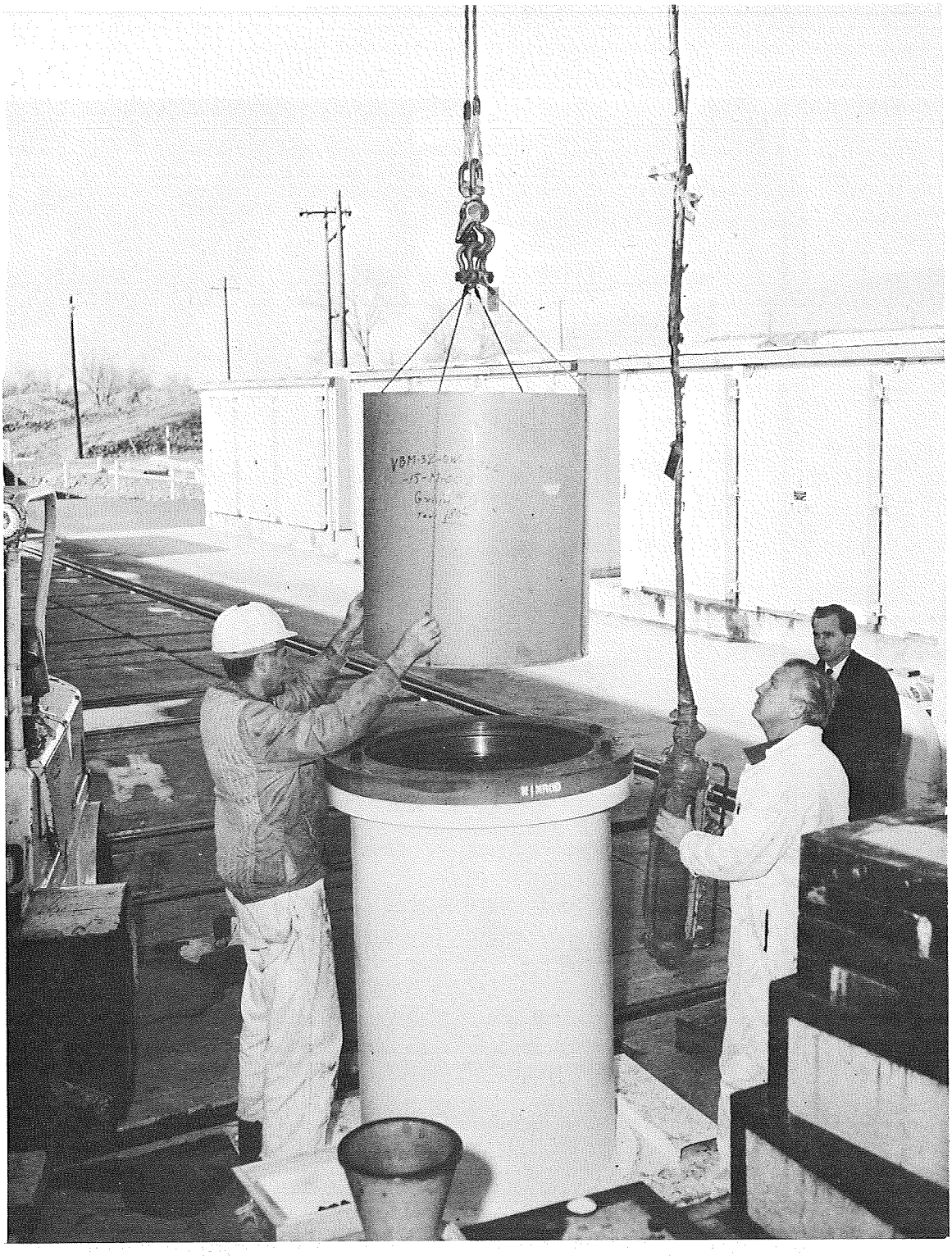

Loading Propellant Cartridge Into Motor

Figure VI-1

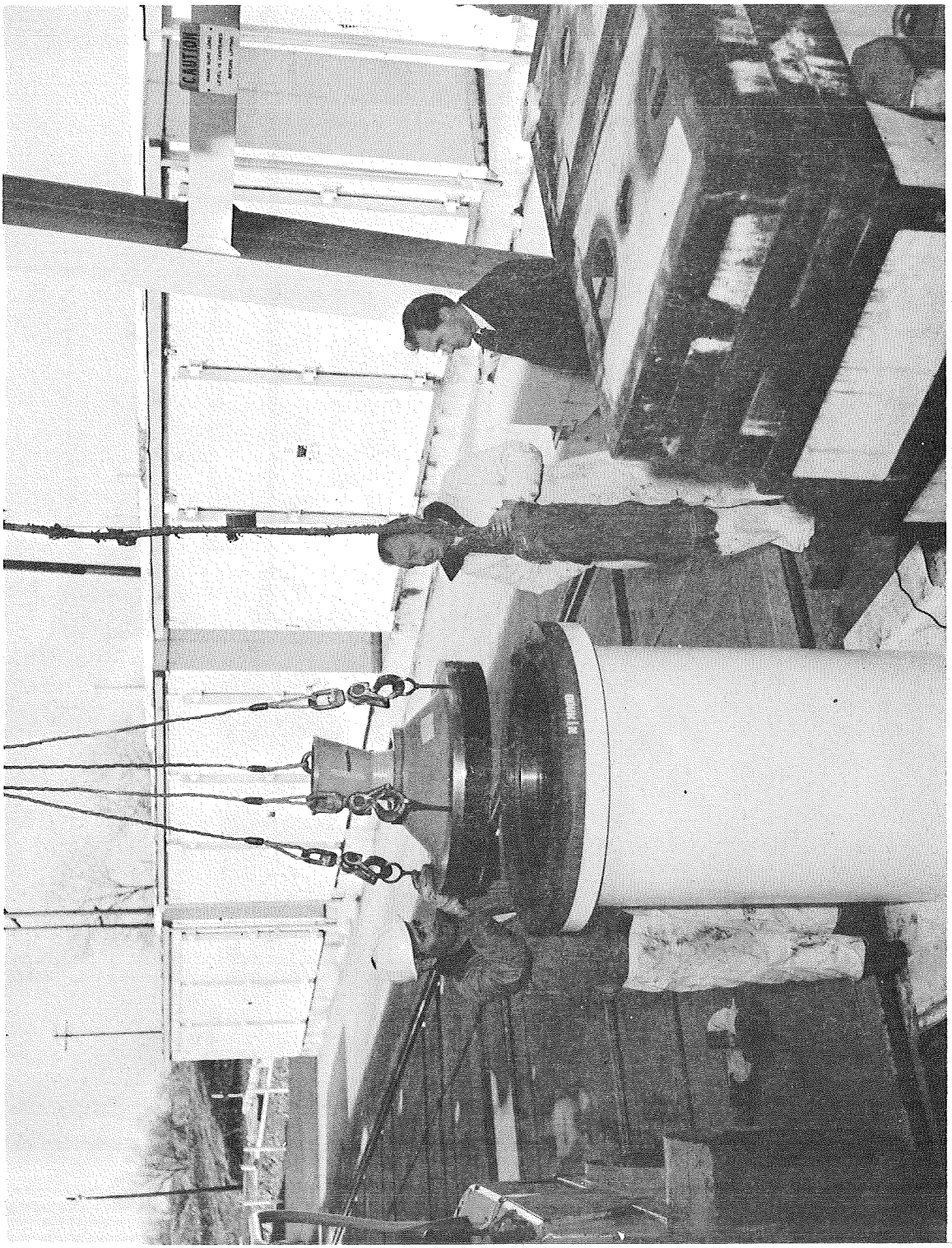

Installation of Aft Closure and Attached Nozzle Shell

Figure VI-2

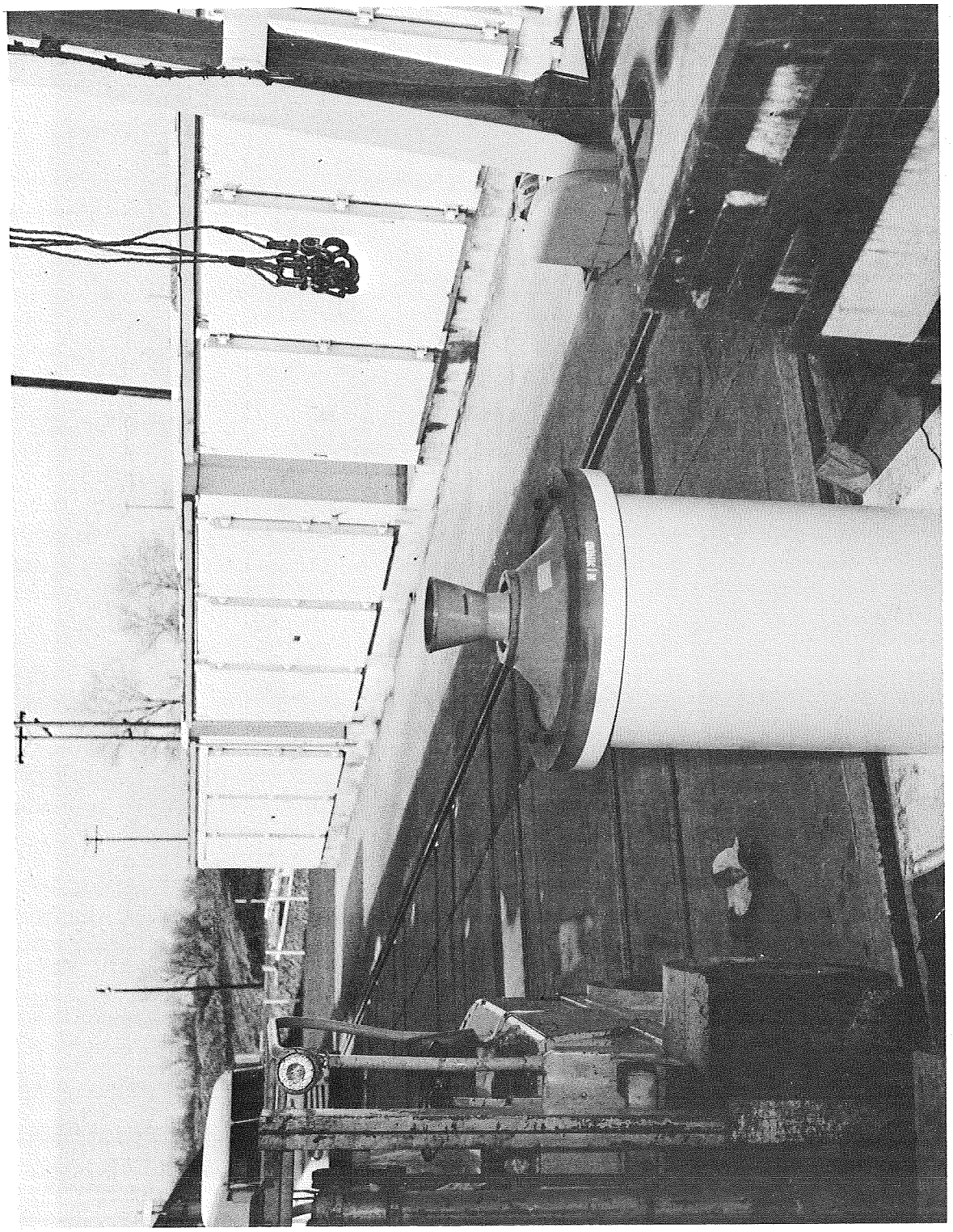

Assembled NIMROD Motor in Test Fixture

Figure VI-3

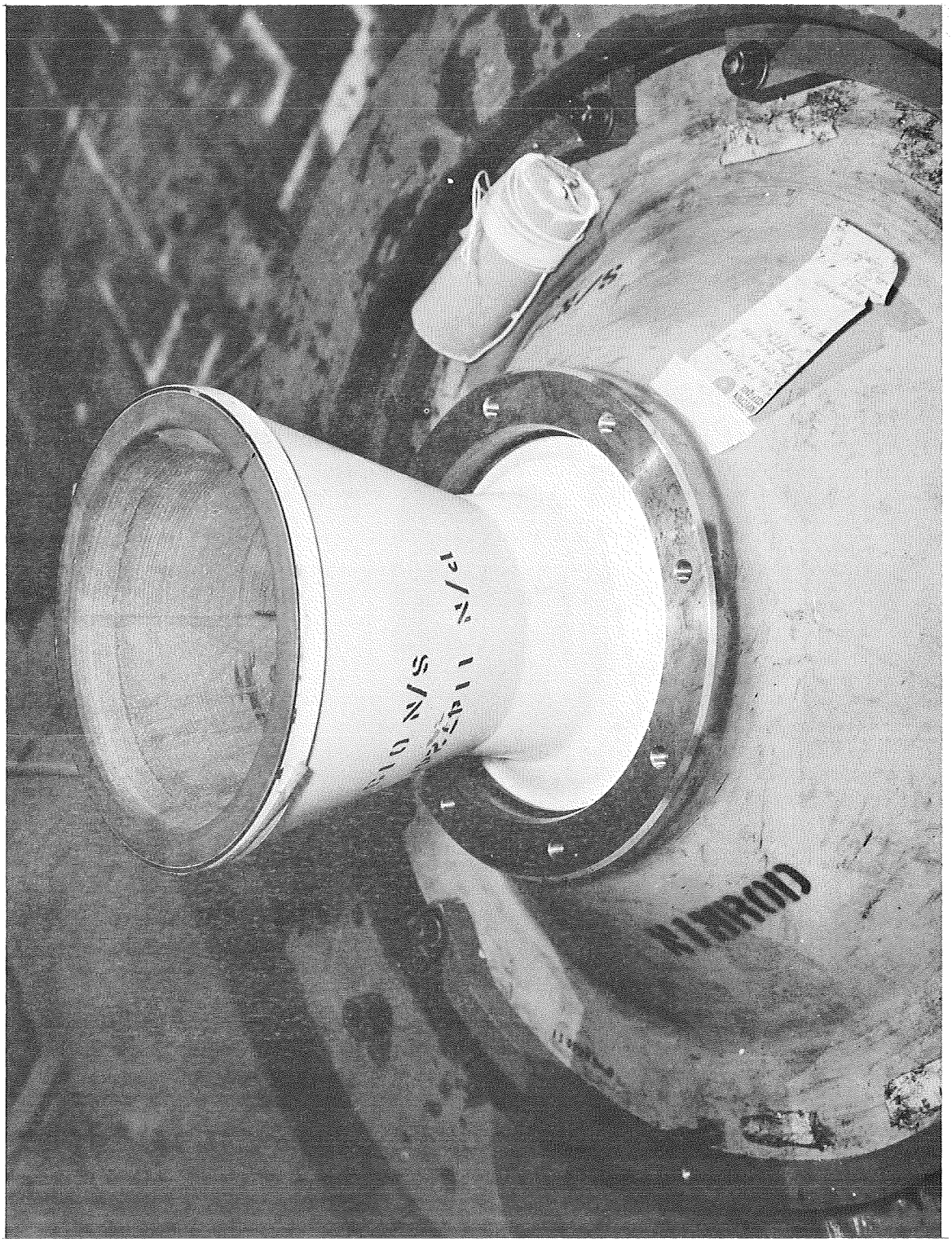

Nozzle Assembly

Figure VI-4

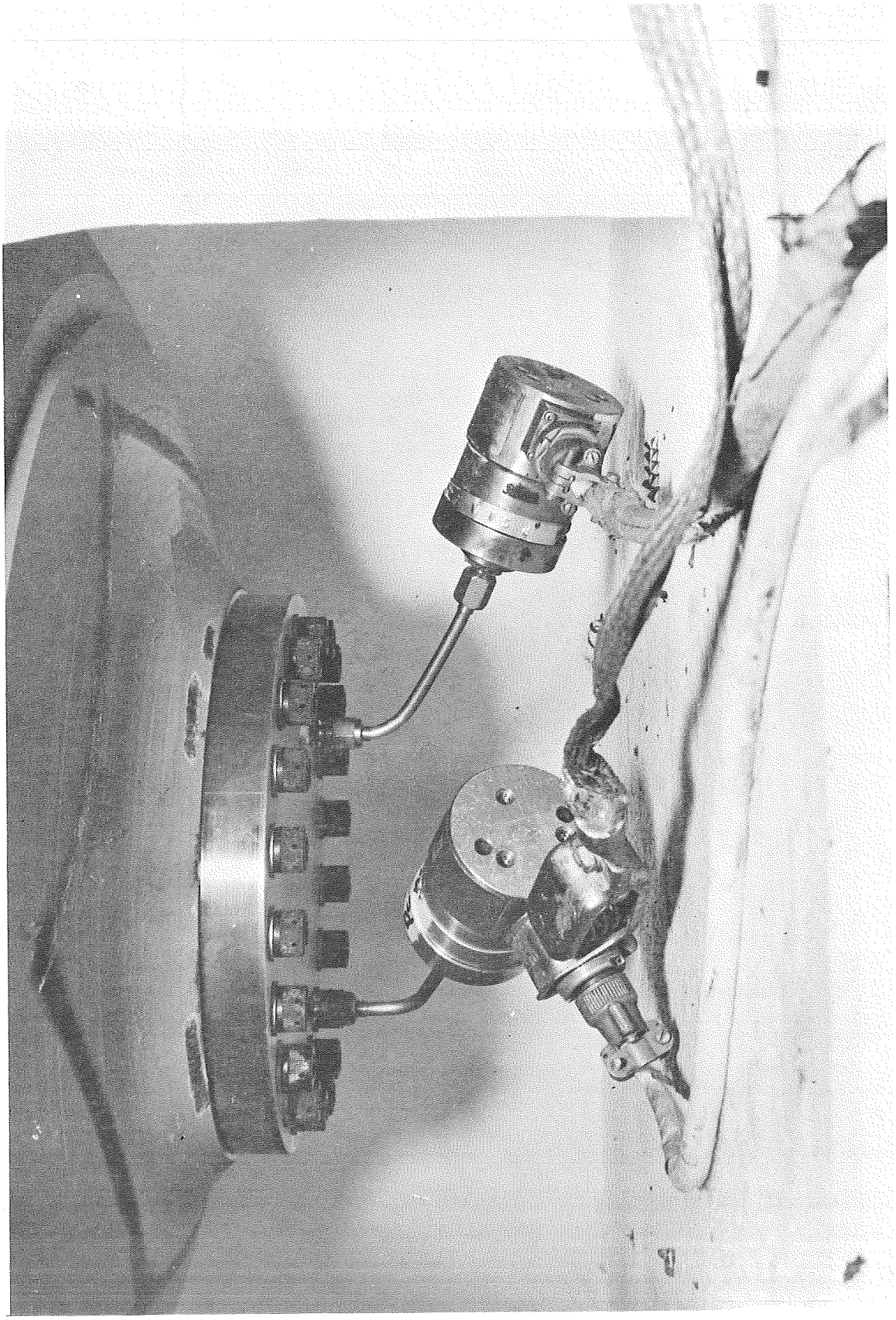

Pressure Transducers

Figure VI-5

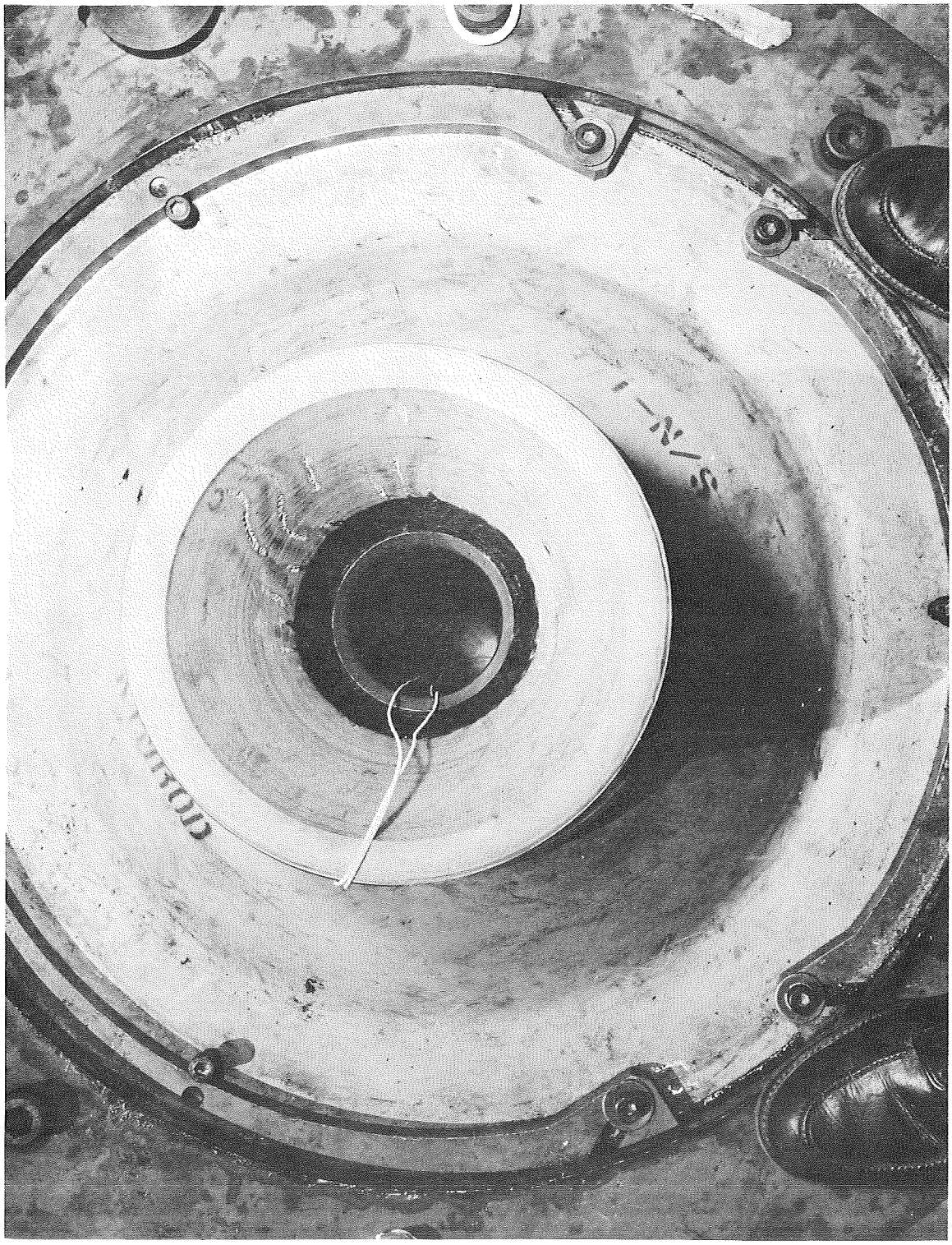

Retainers in Locked Position

Figure VI-6

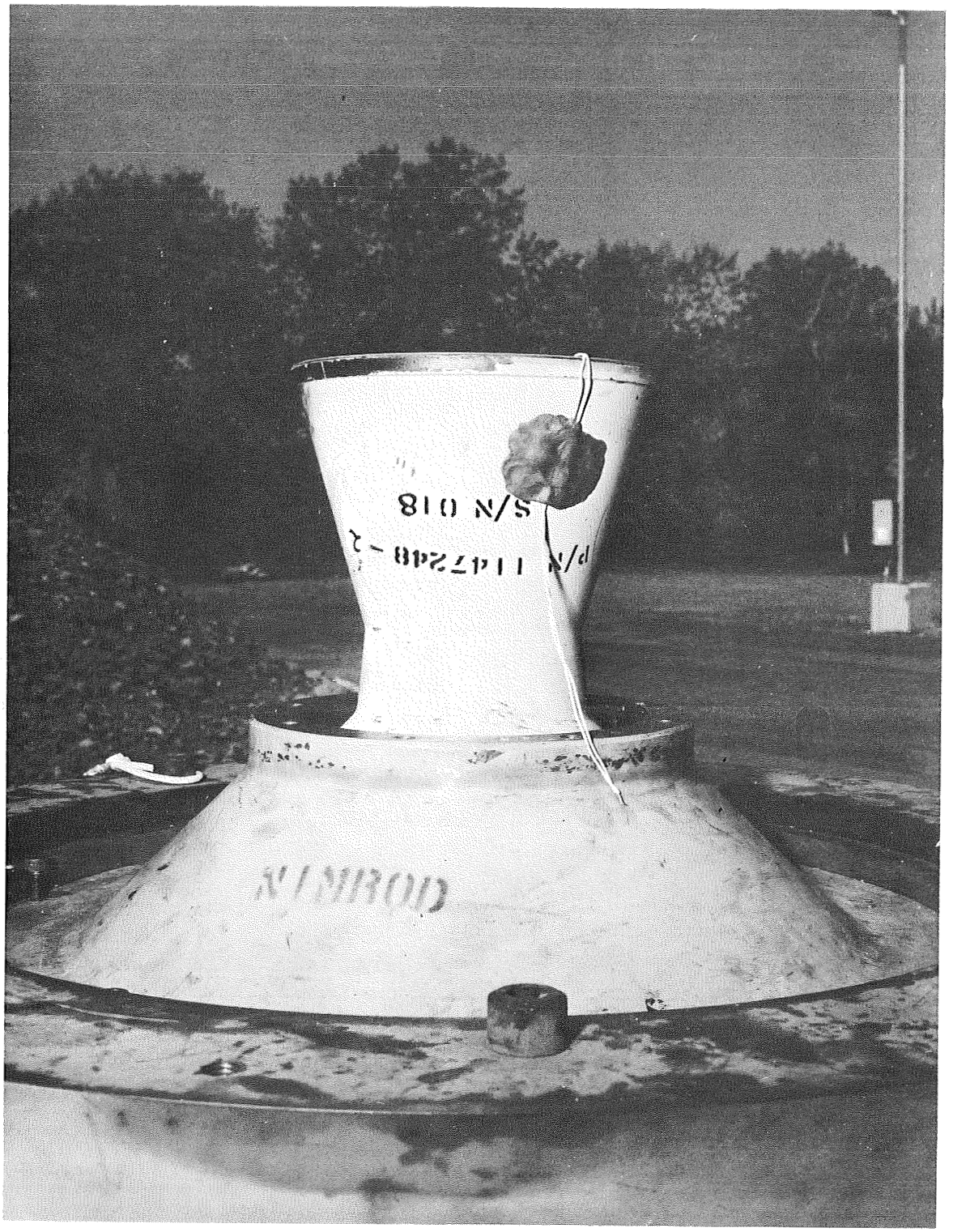

Motor in Test Bay Ready for Test

Figure VI-7

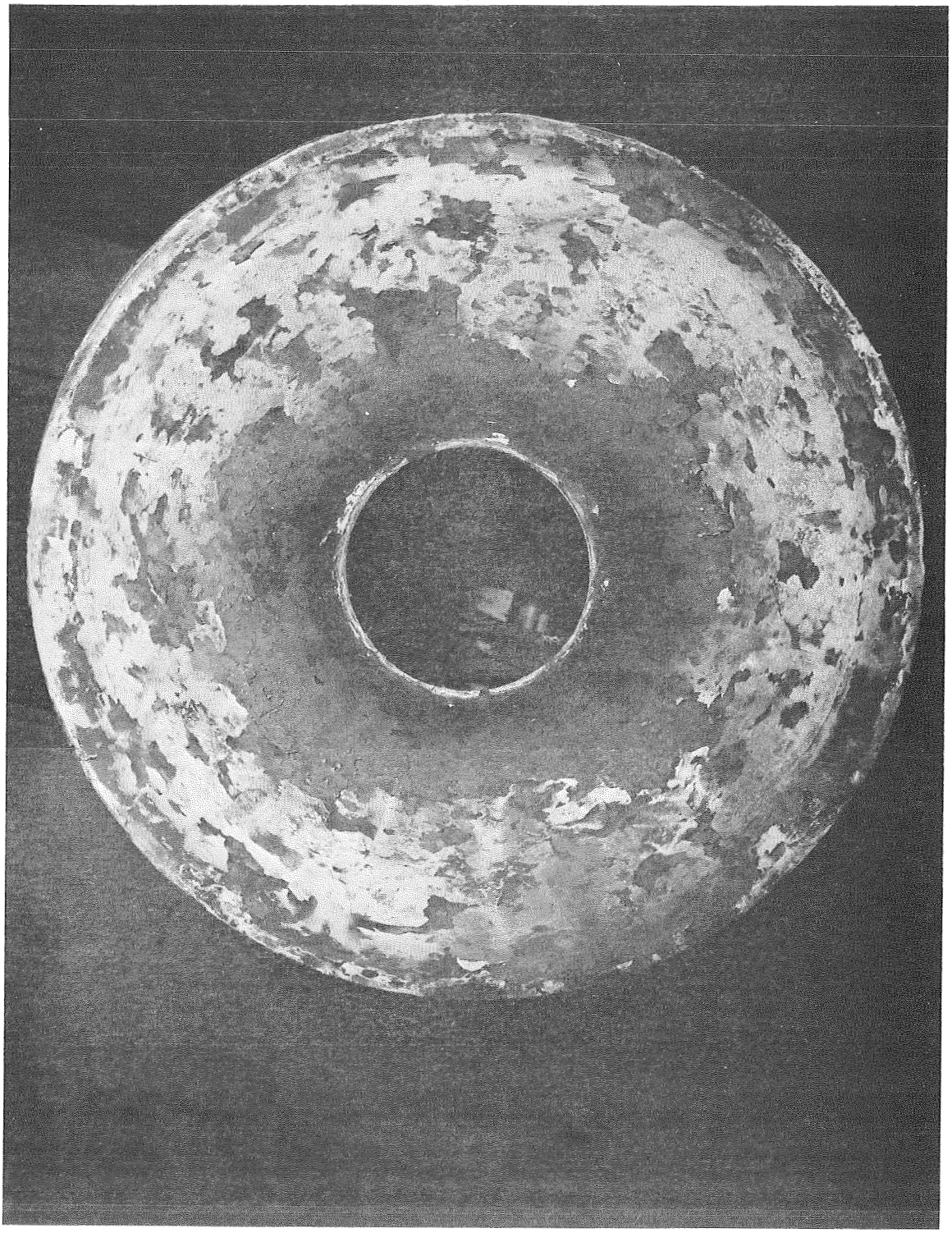

Aft Closure after Two Firings

Figure VI-8

Cartridge Sleeve and Base after F iring

Figure VI-9

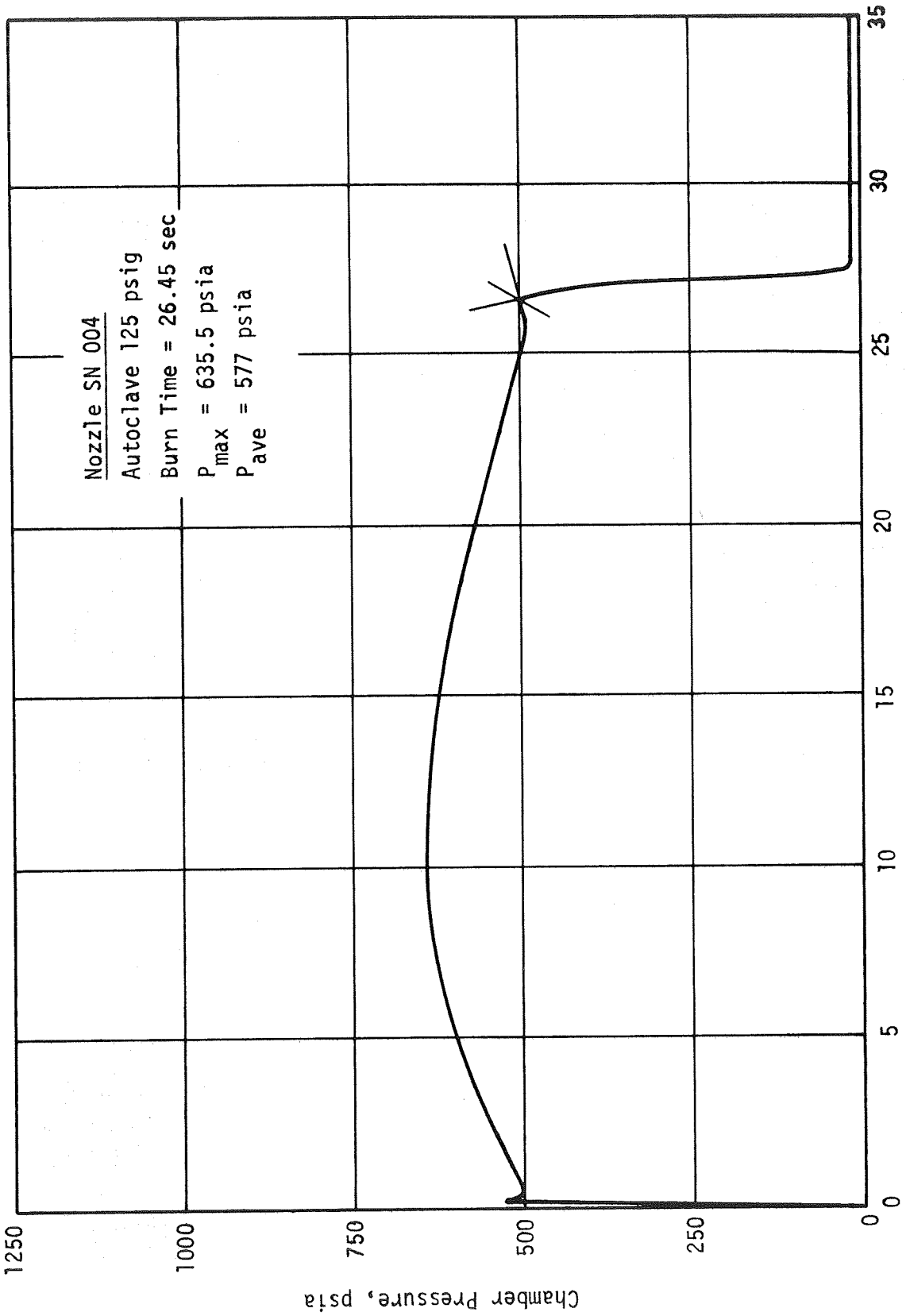

Pressure-Time Curve of Autoclaved Nozzle

Figure VI-10

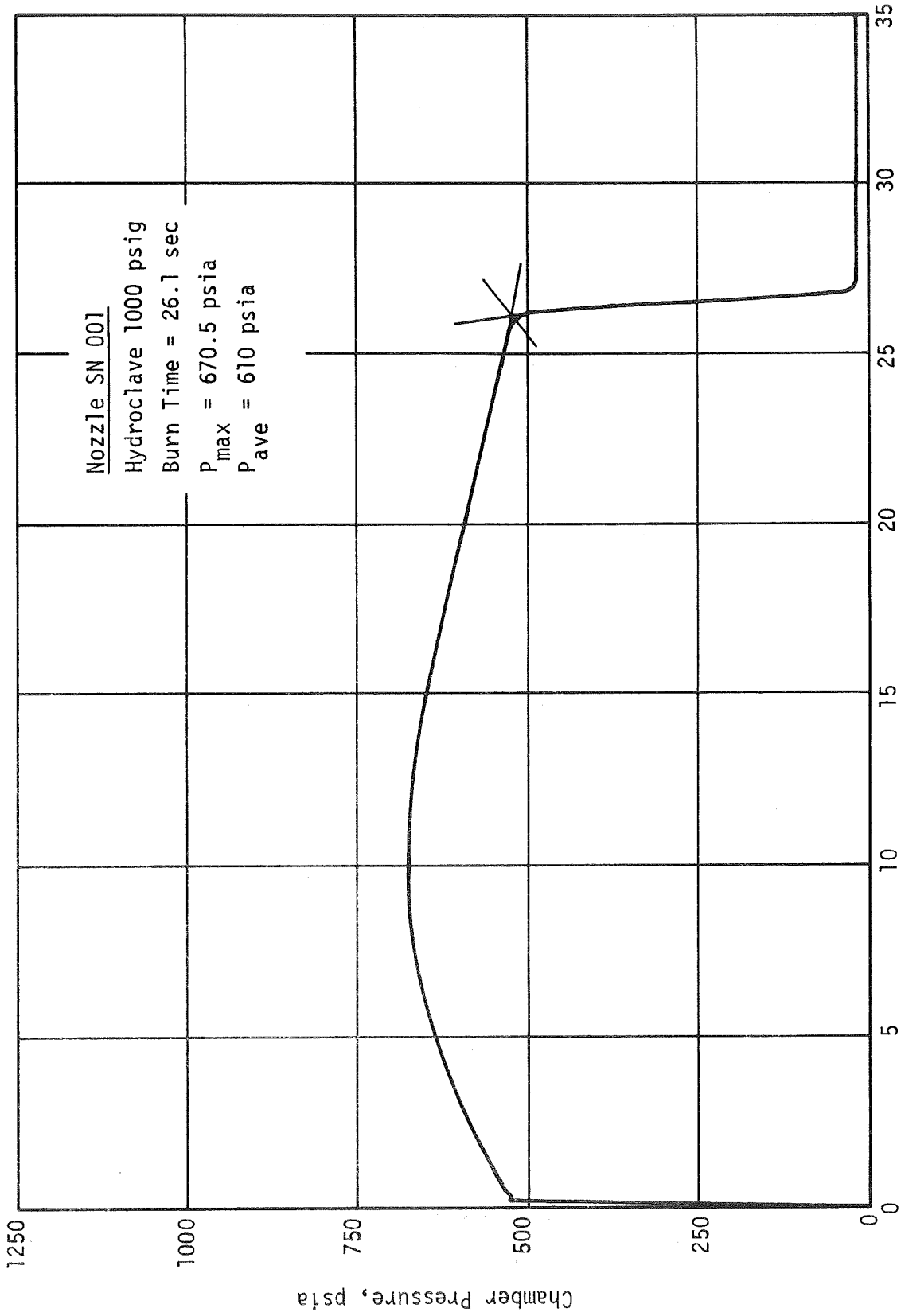

Pressure-Time Curve of Baseline Nozzle

Figure VI-11

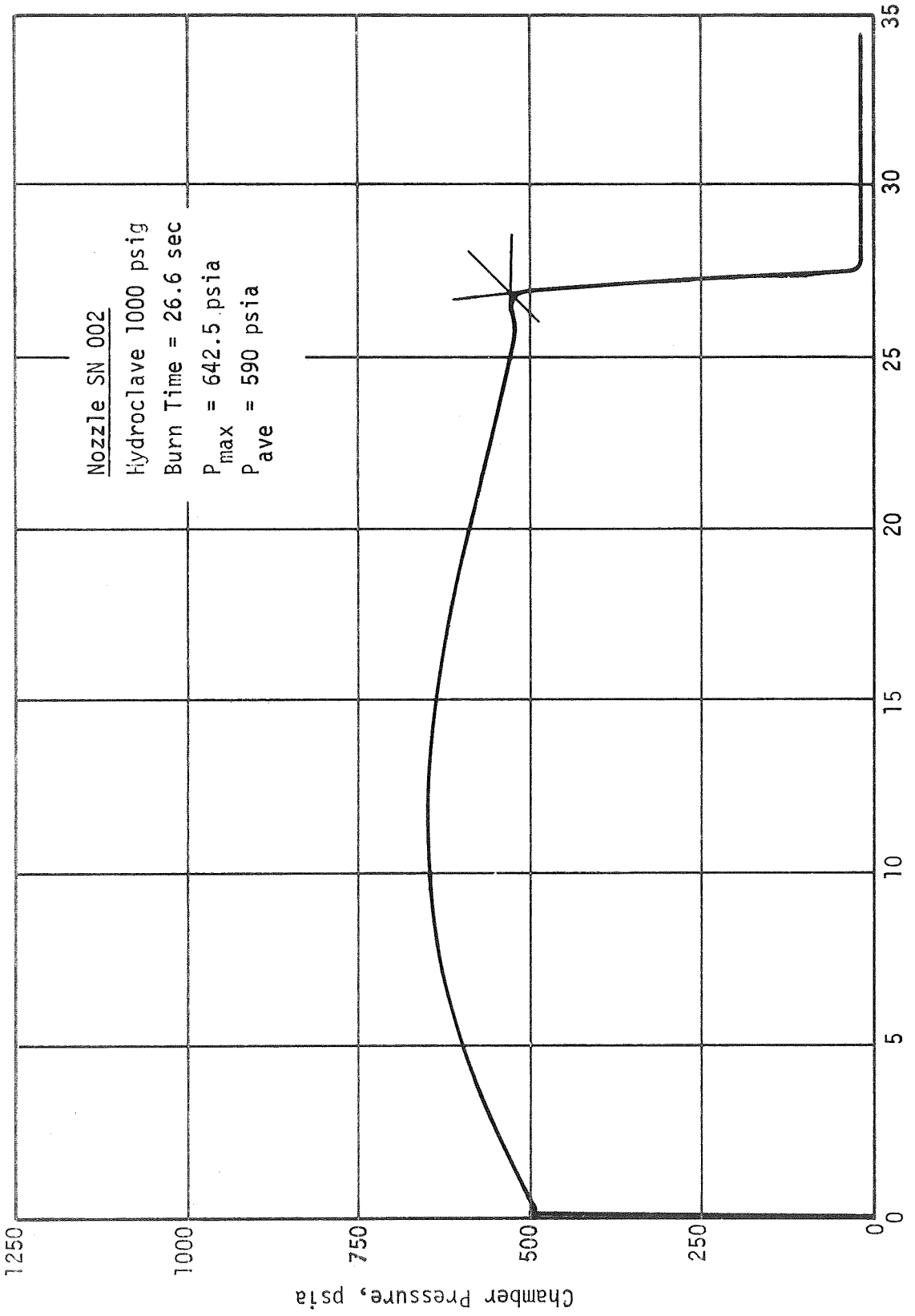

Pressure-Time Curve of Baseline Nozzle

Figure VI-12

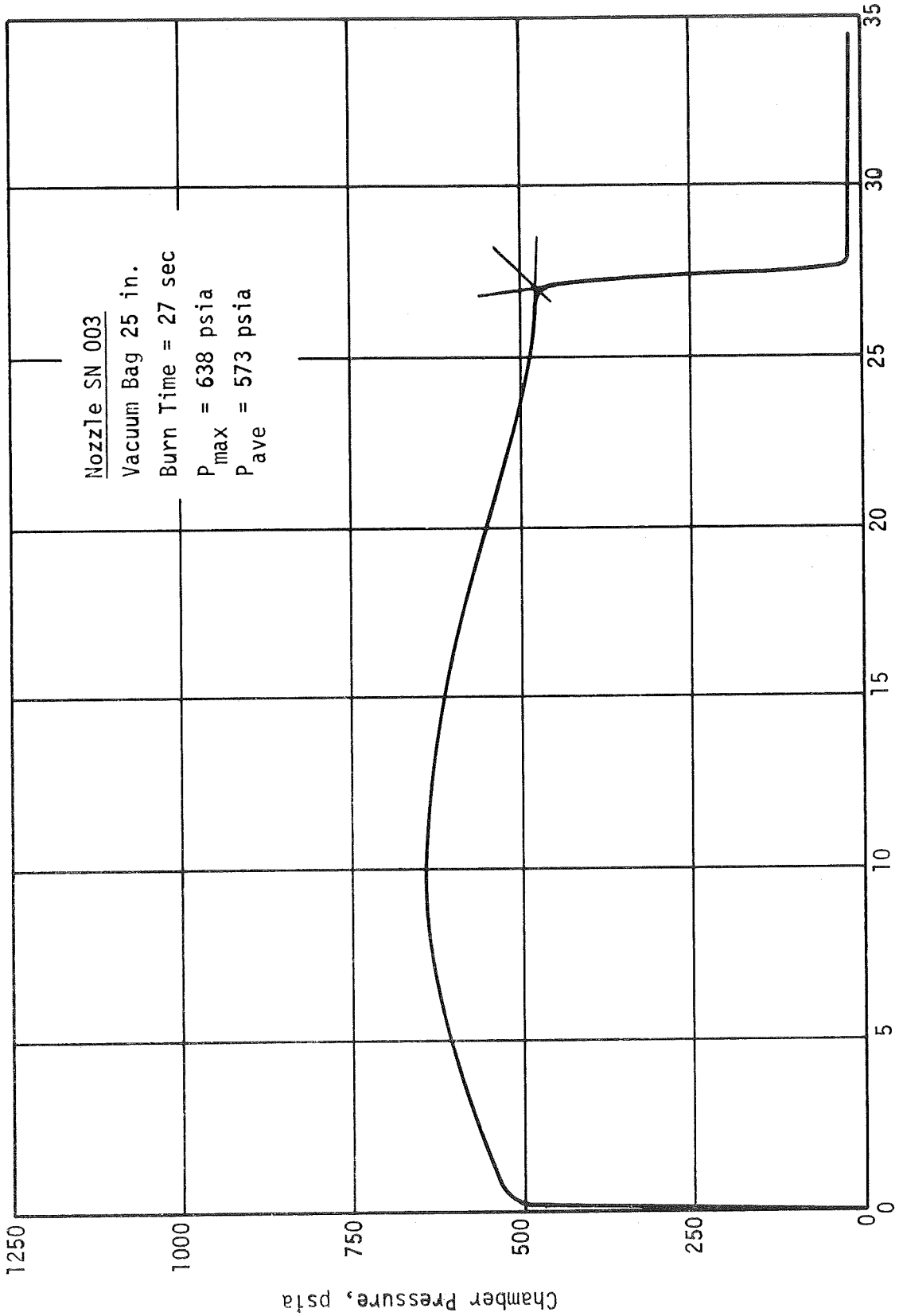

Pressure-Time Curve of Vacuum Bagged Nozzle

Figure VI-13

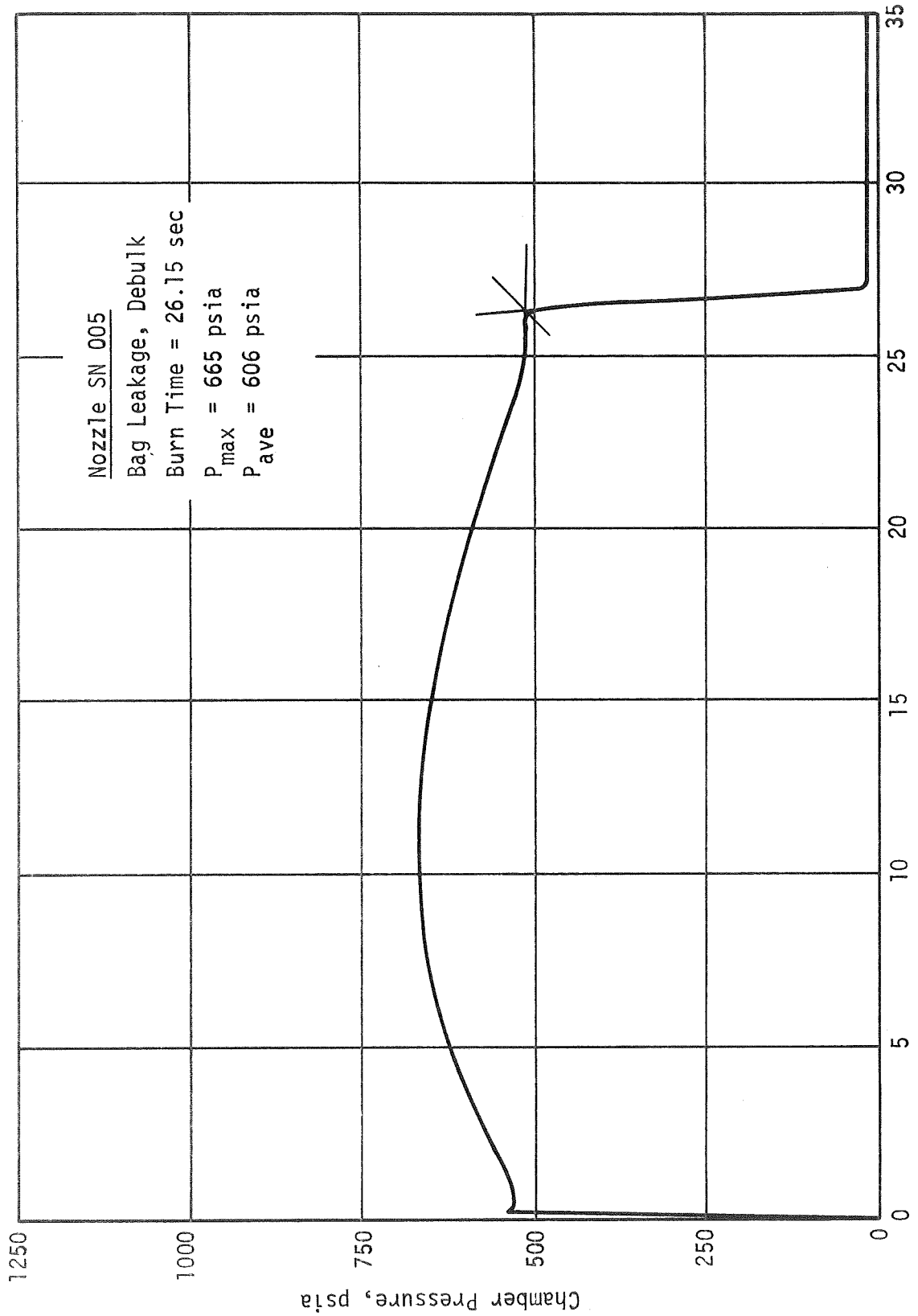

Pressure-Time Curve of Bag Leak Debulk Nozzle

Figure VI-14

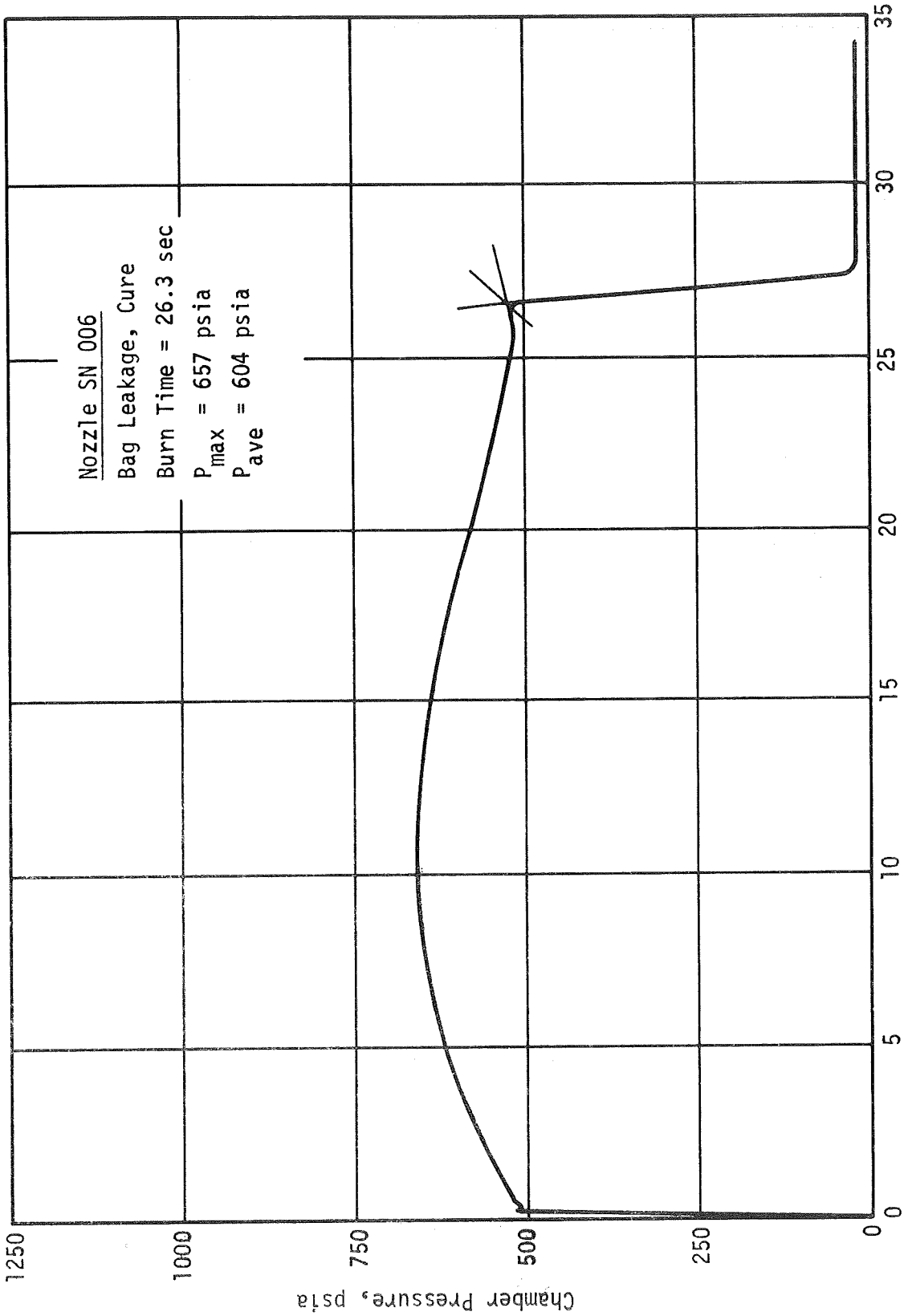

Pressure-Time Curve of Bag Leak Final Cure Nozzle

Figure VI-15

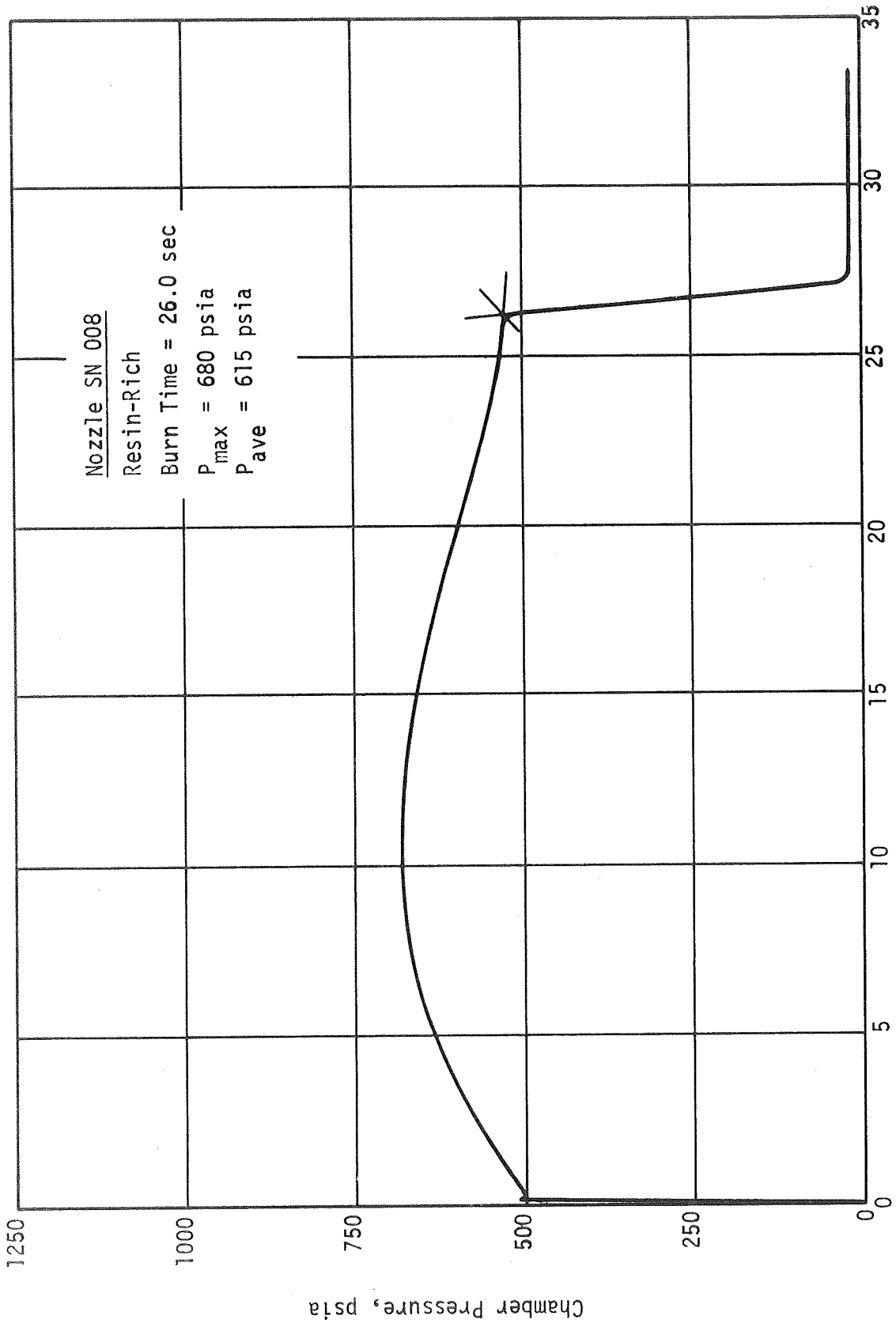

Pressure-Time Curve of Resin-Rich 20 Ply Nozzle

Figure VI-16

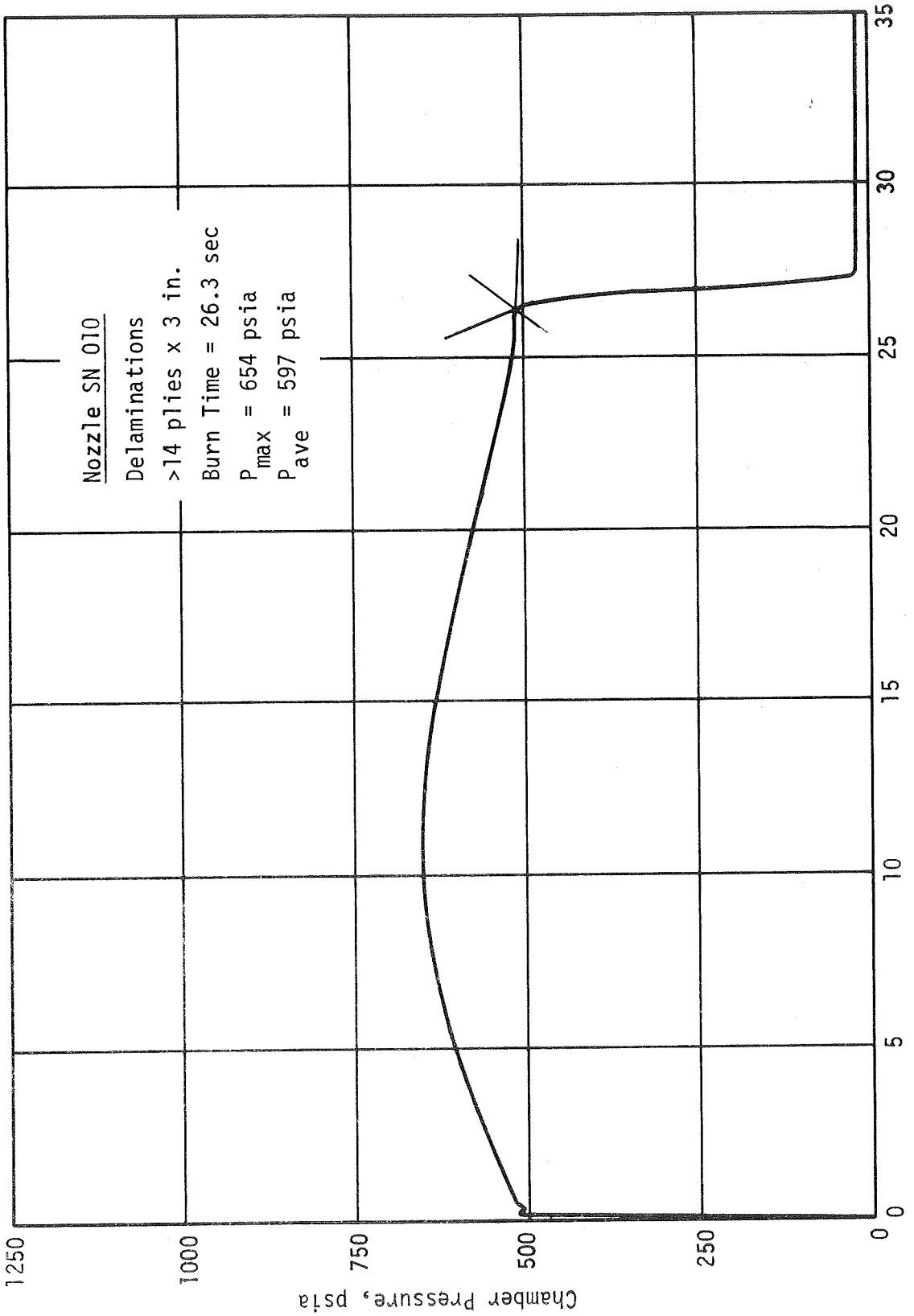

Pressure-Time Curve of Delaminated 14 Ply Nozzle

Figure VI-17

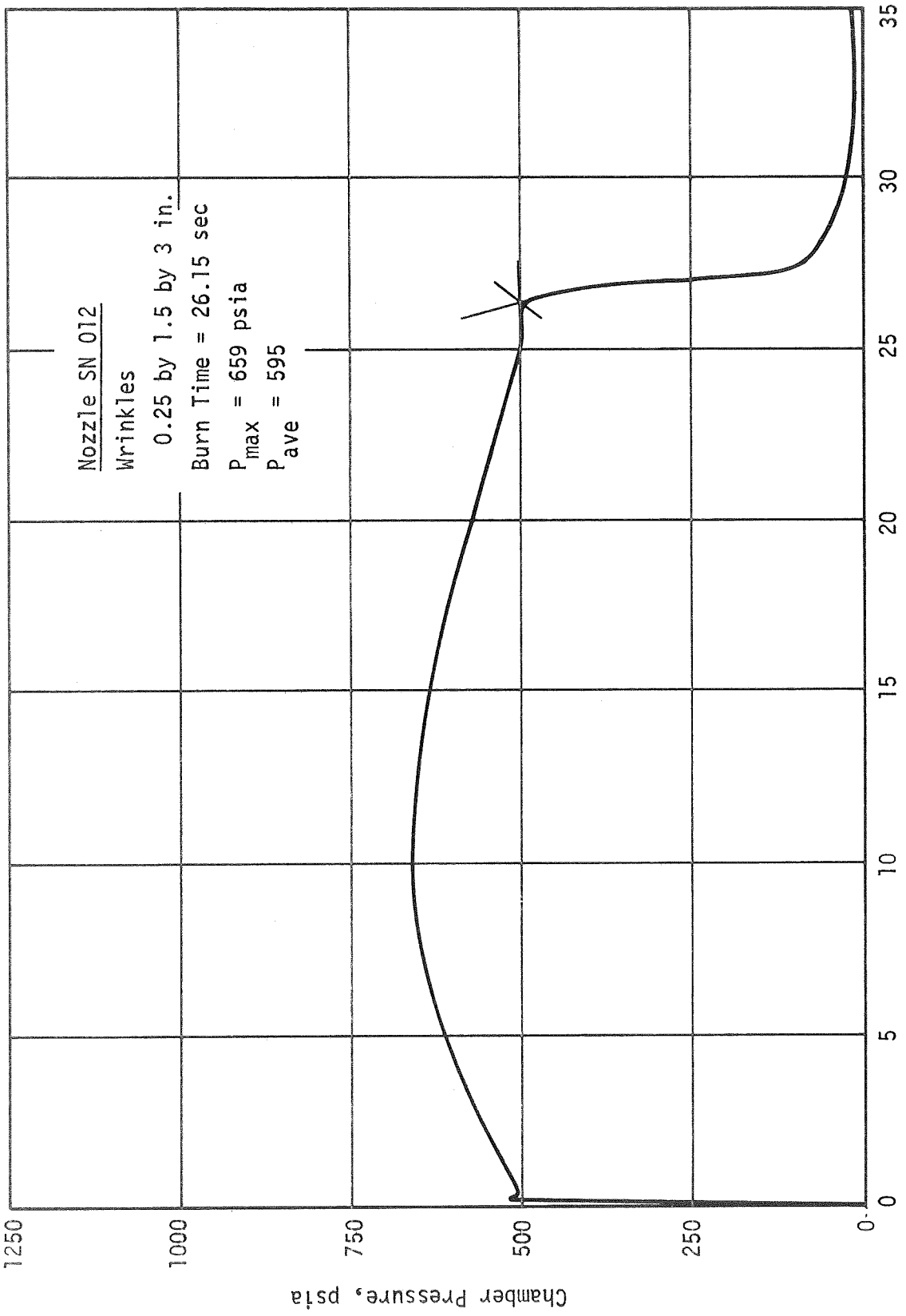

Pressure-Time Curve of 0.25 in. Wrinkle Nozzle

Figure VI-18

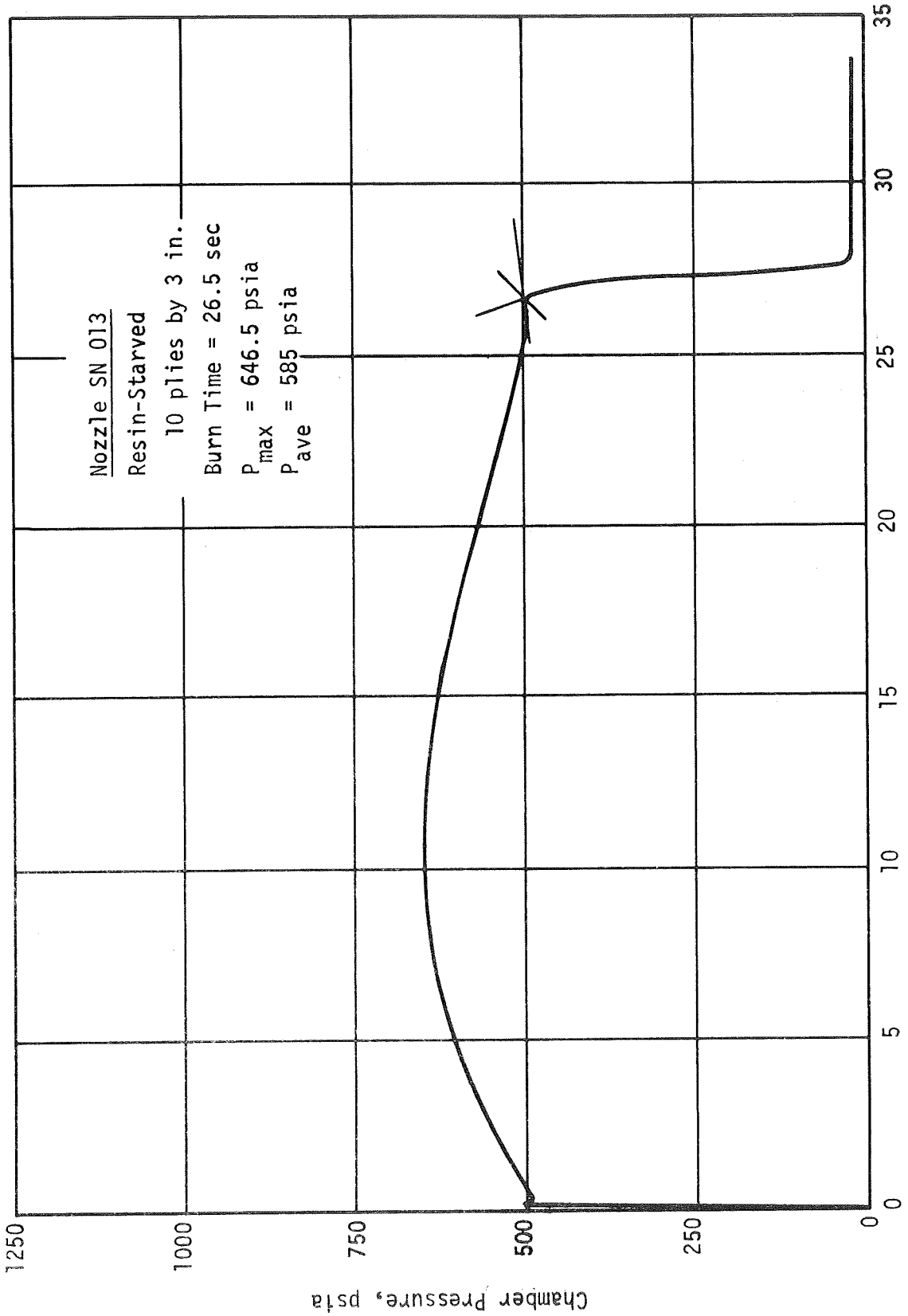

Pressure-Time Curve of Resin-Starved Nozzle

Figure VI-19

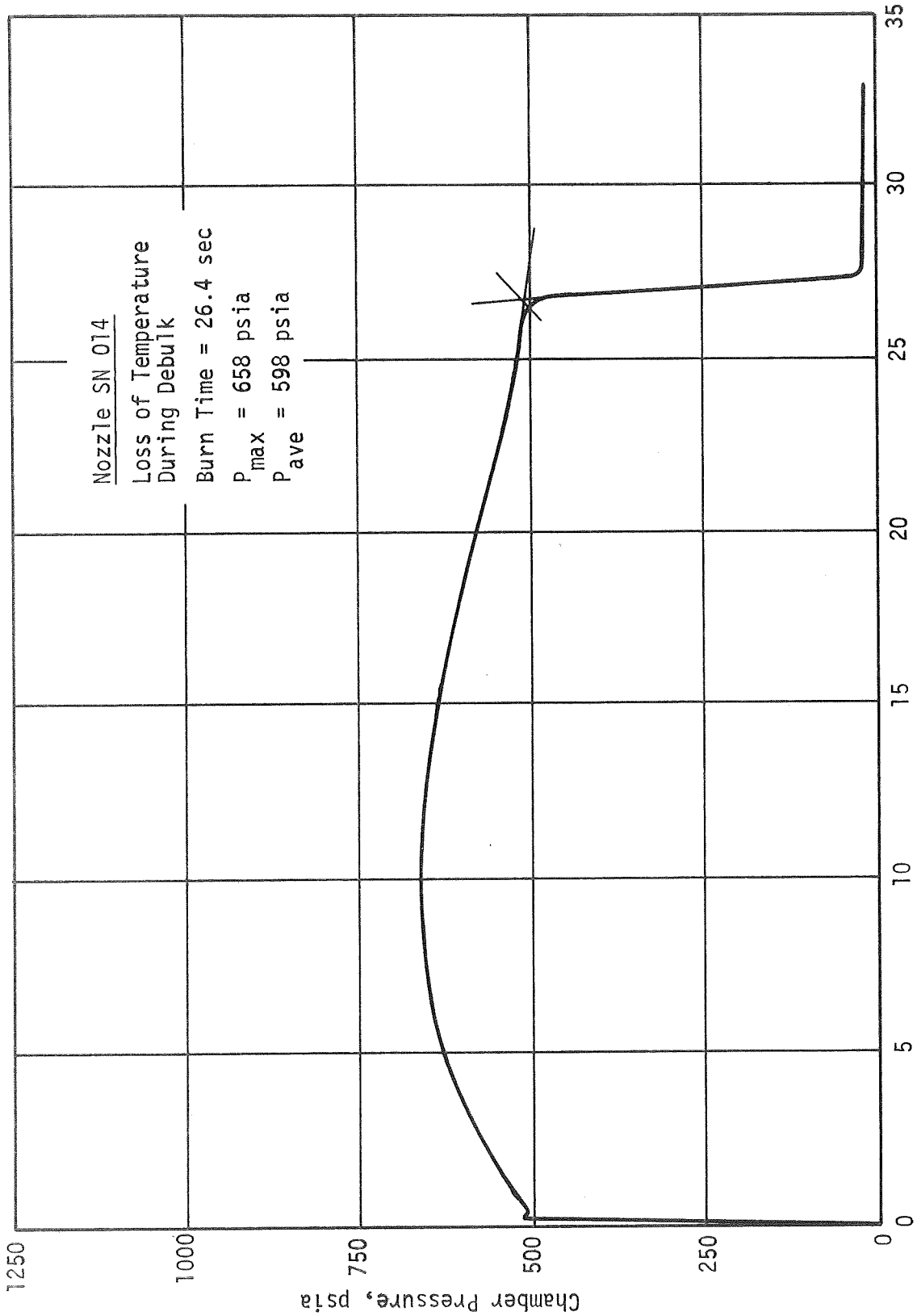

Pressure-Time Curve of Temperature Loss Nozzle

Figure VI-20

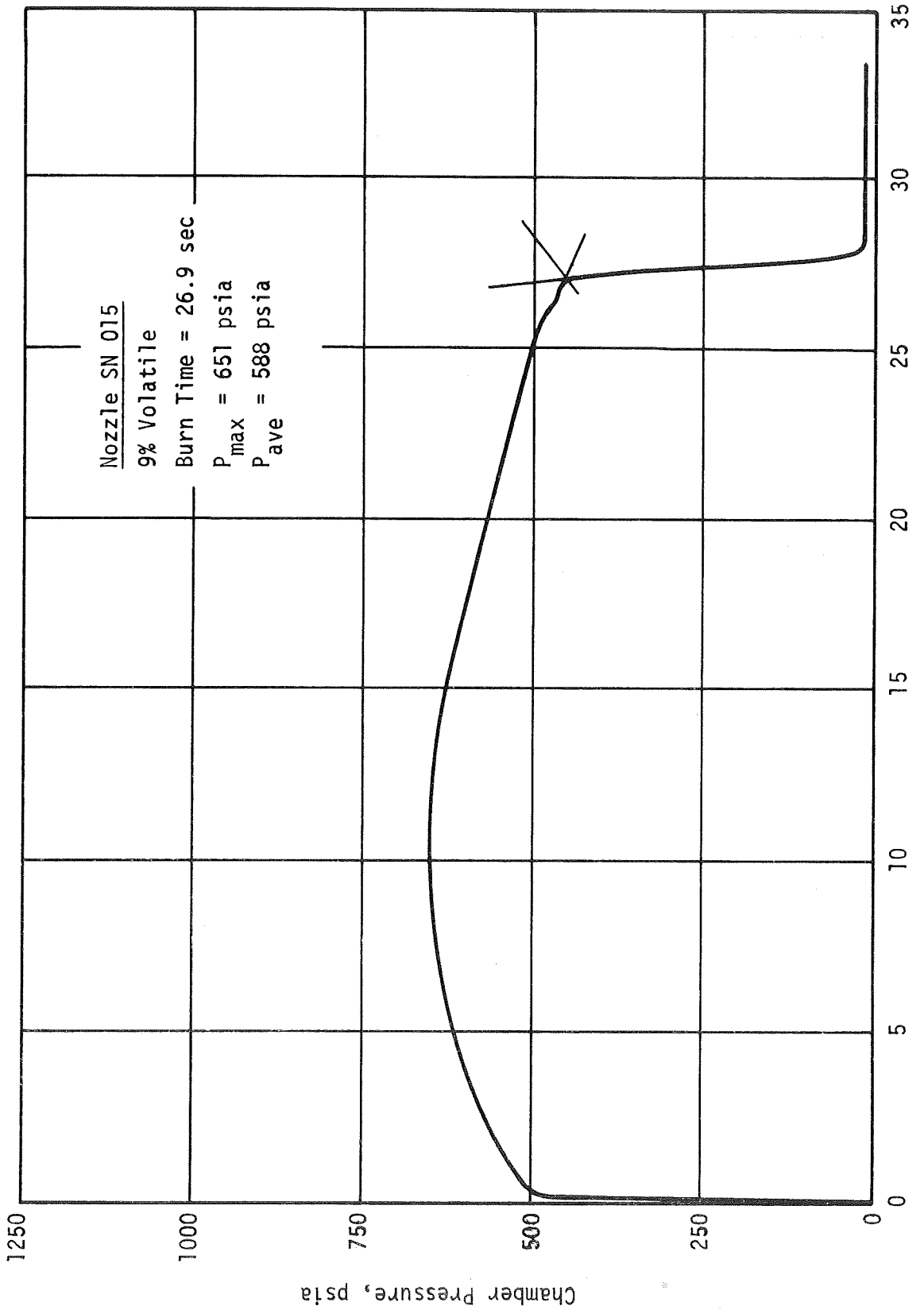

Pressure-Time Curve of 9 Percent Volatile Content Nozzle

Figure VI-21

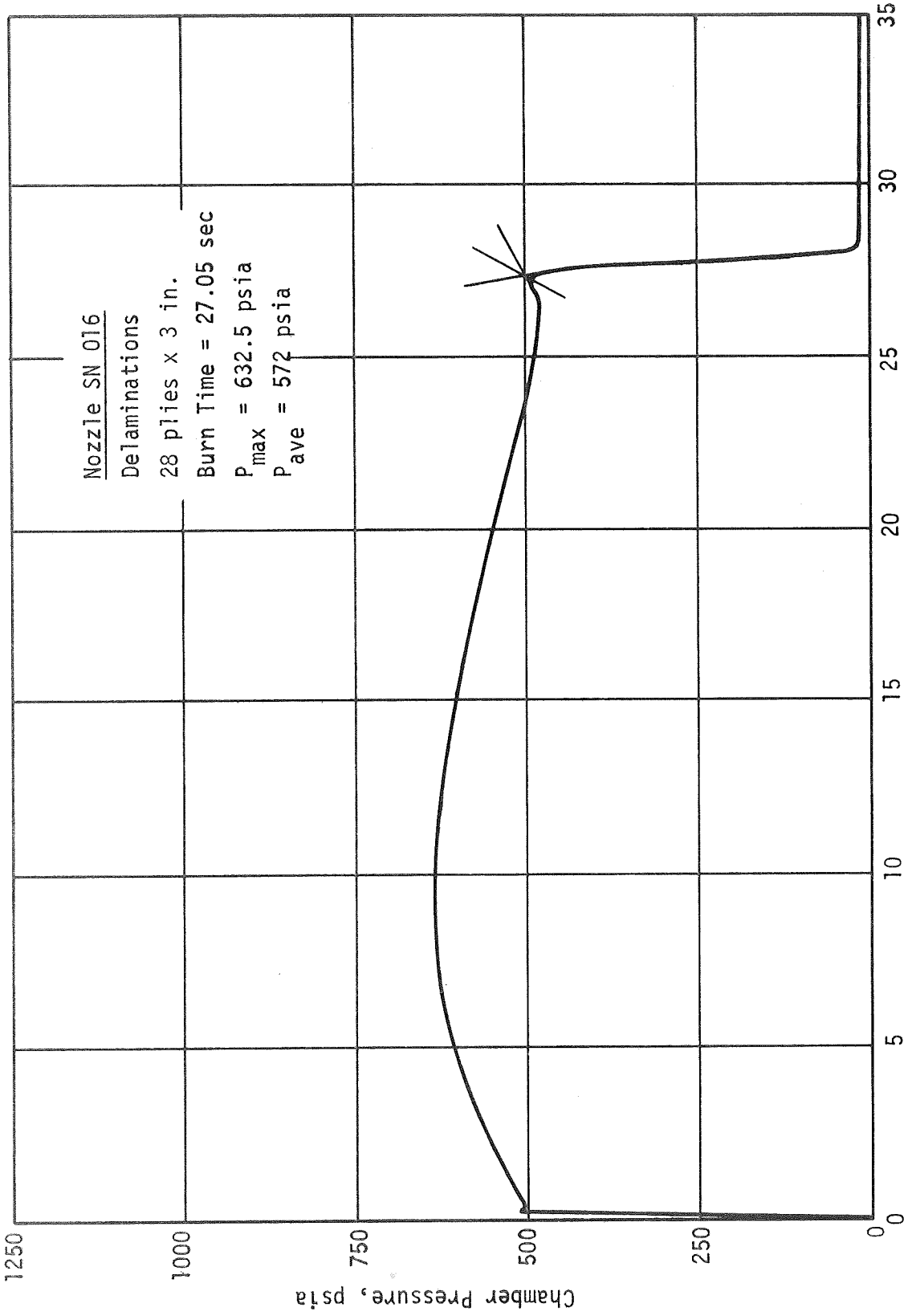

Pressure-Time Curve of Delaminated 28 Ply Nozzle

Figure VI-22

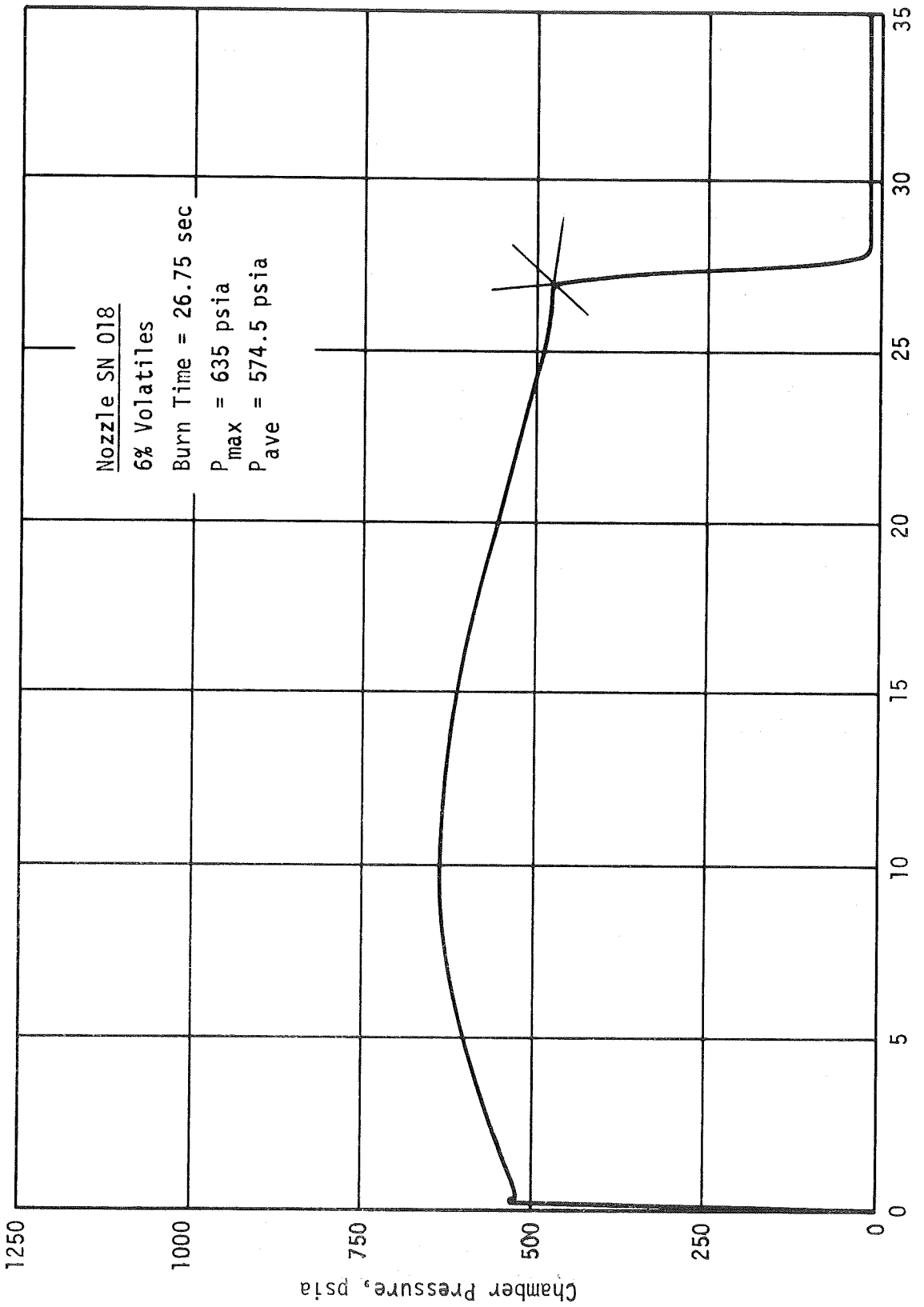

Pressure-Time Curve of 6 Percent Volatile Content Nozzle

Figure VI-23

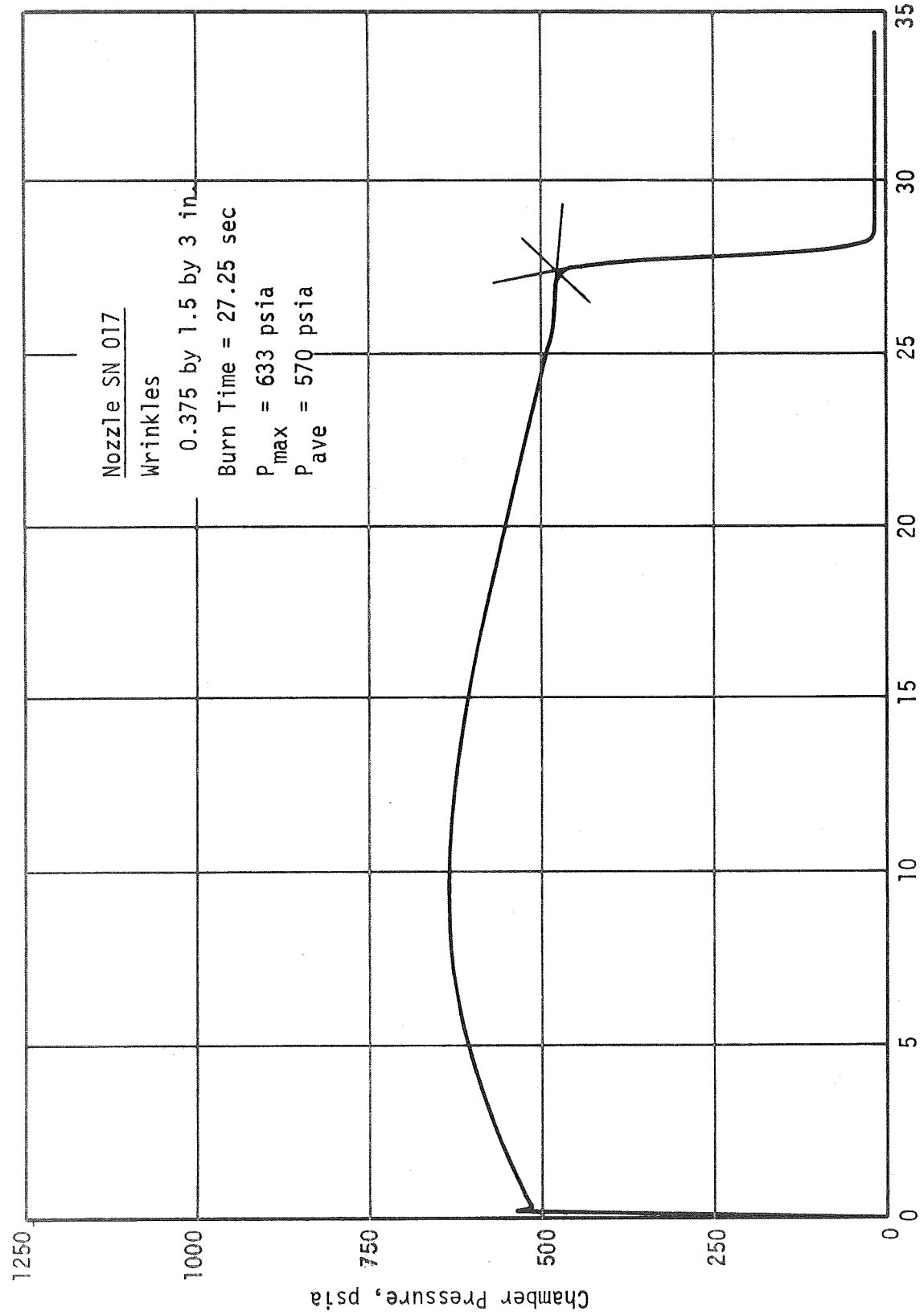

Pressure-Time Curve of 0.375 in. Wrinkle Nozzle

Figure VI-24

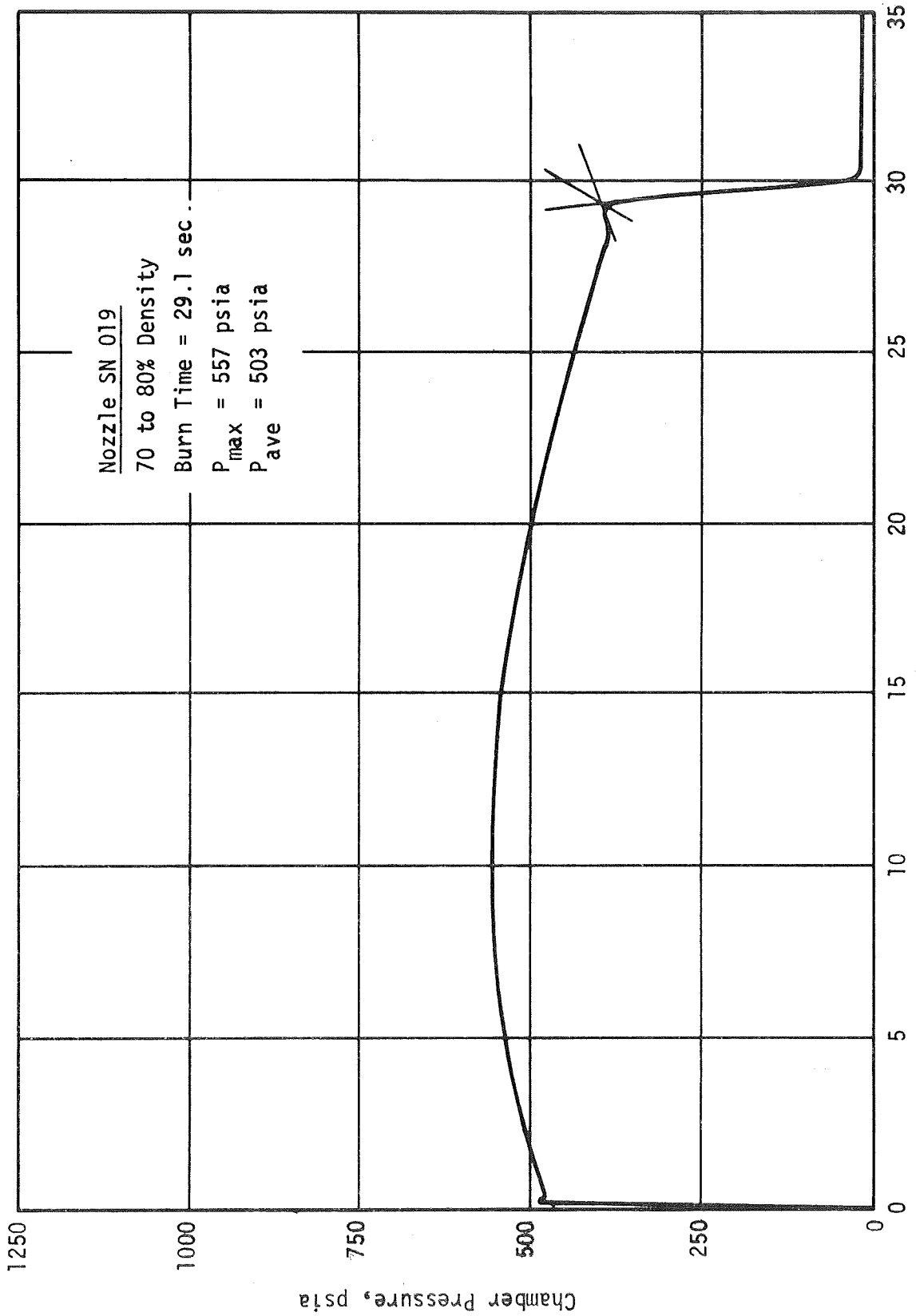

Pressure-Time Curve of 70 to 80 Percent Density Nozzle

Figure VI-25

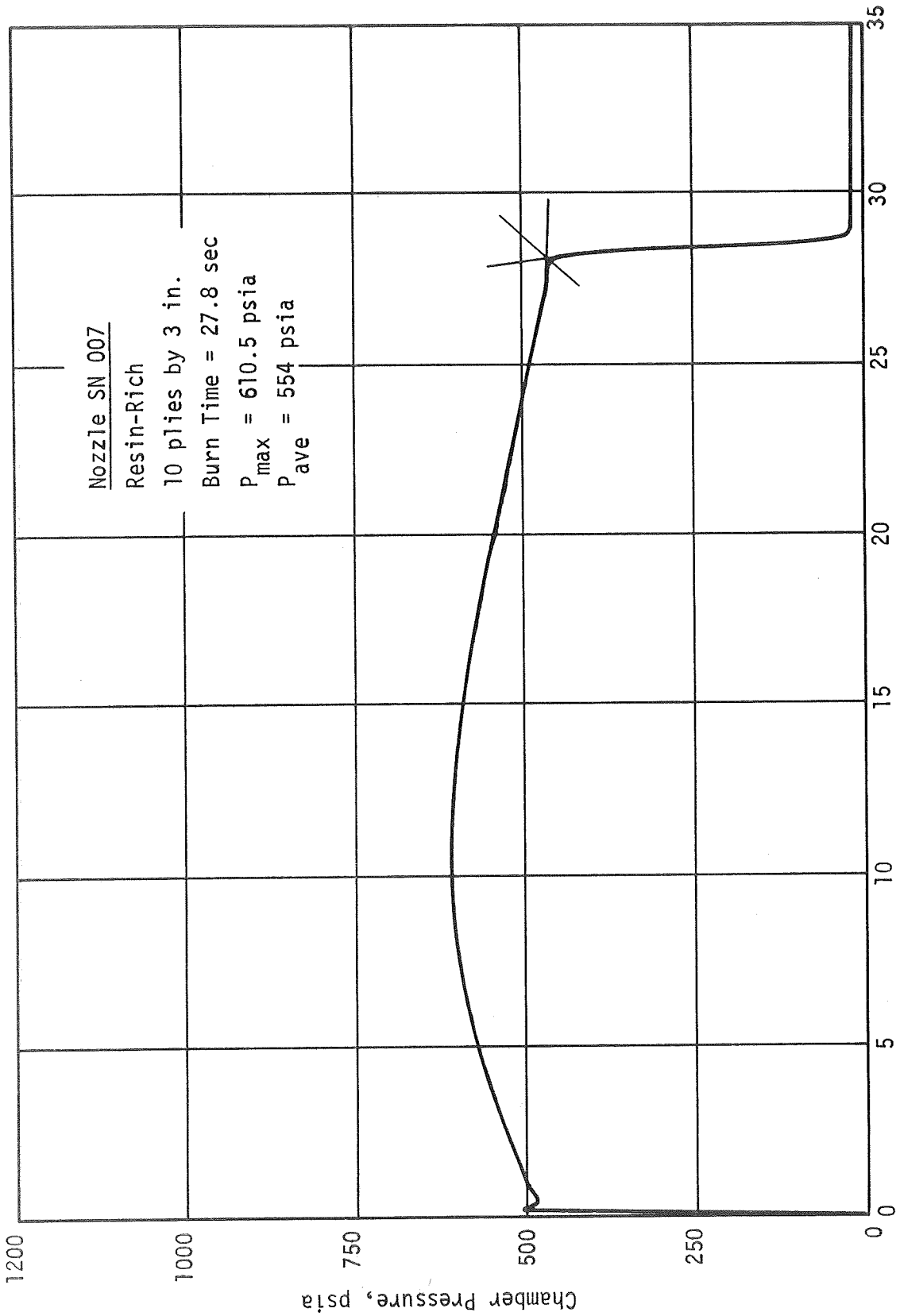

Pressure-Time Curve of Resin-Rich 10 Ply Nozzle

Figure VI-26

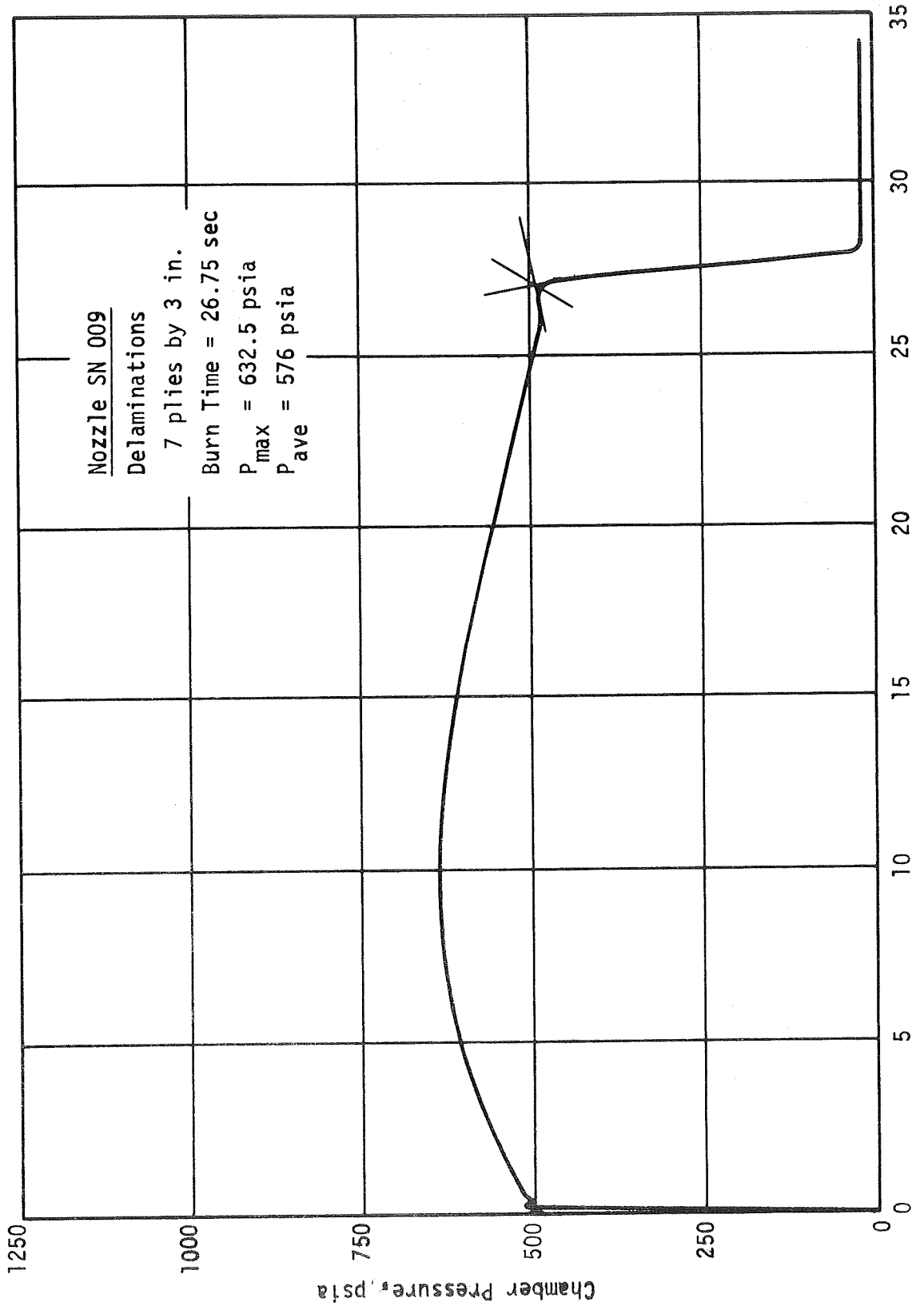

Pressure-Time Curve of Delaminated 7 Ply Nozzle

Figure VI-27

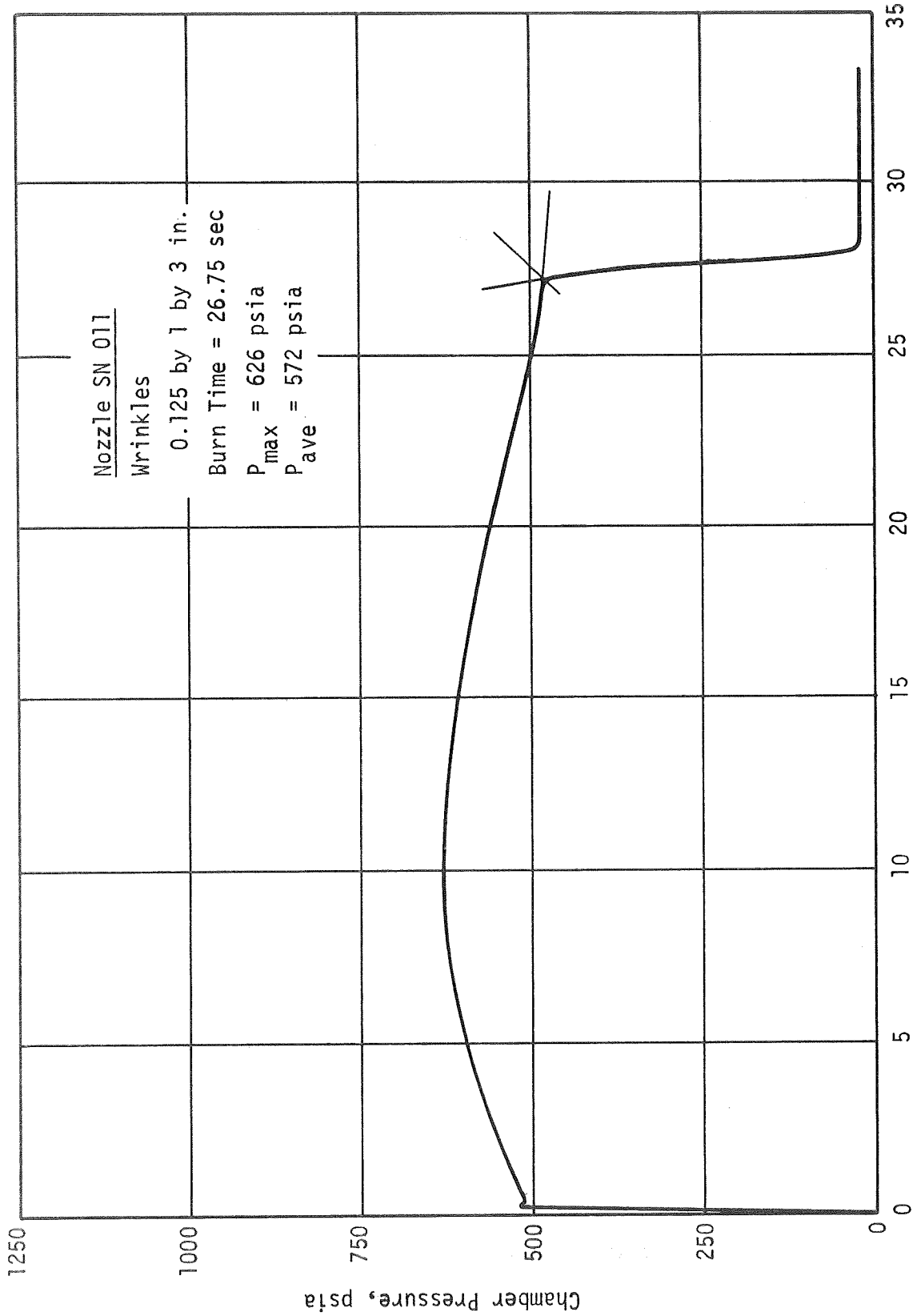

Pressure-Time Curve of 0.125 in. Wrinkle Nozzle

Figure VI-28

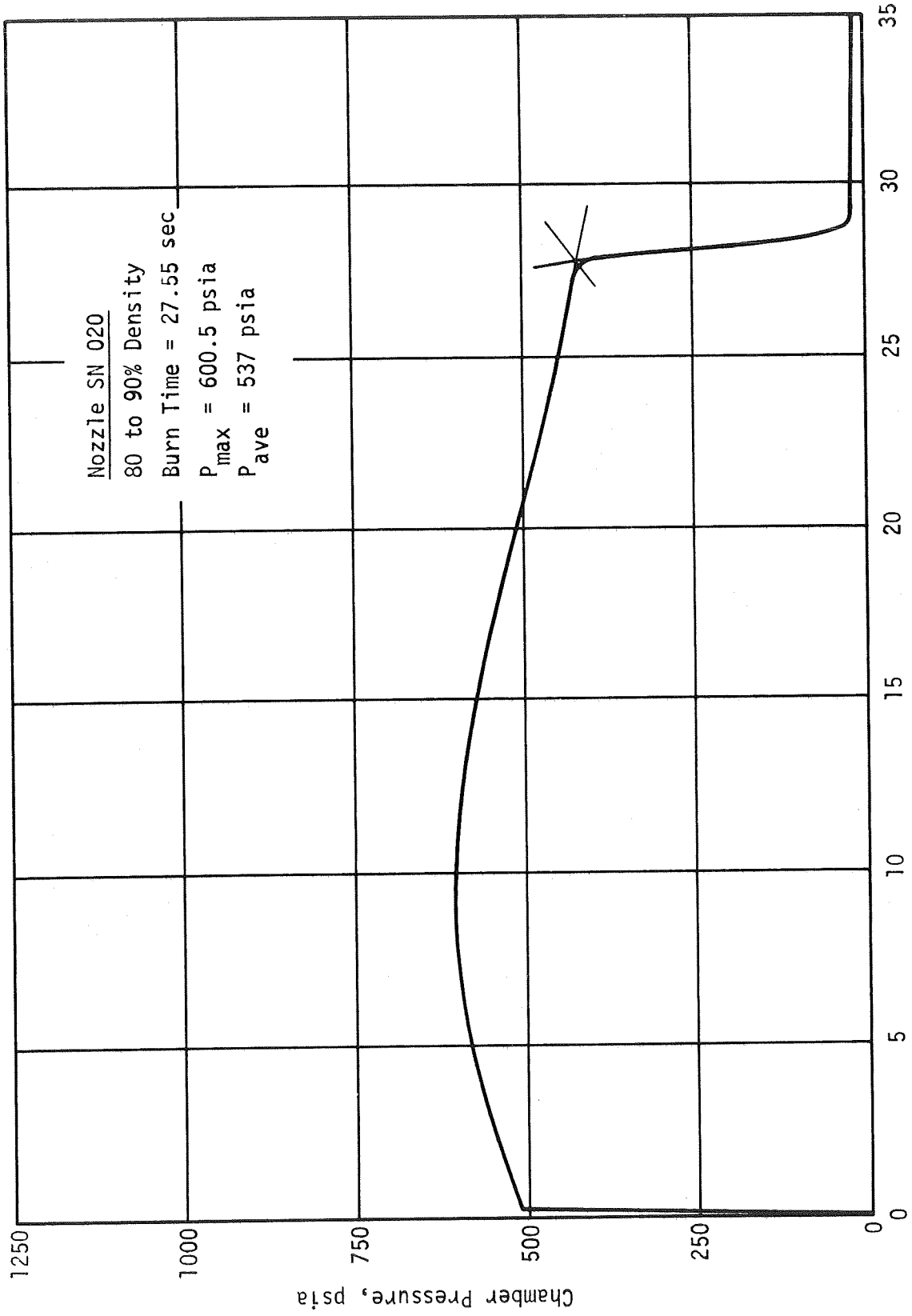

Pressure-Time Curve of 80 to 90 Percent Dense Nozzle

Figure VI-29

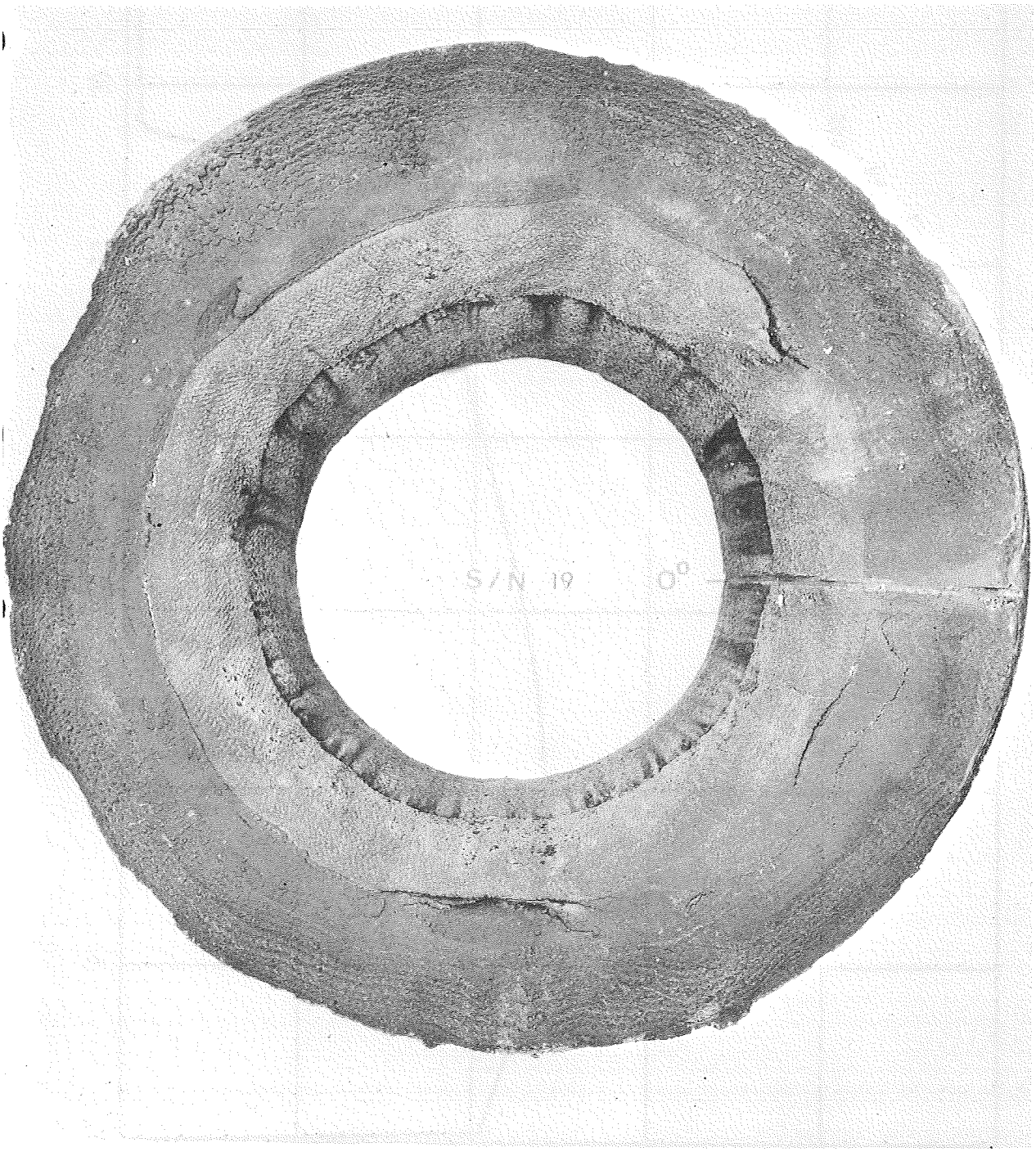

70 to 80 Percent Dense Entrance Cap

Figure VI-30

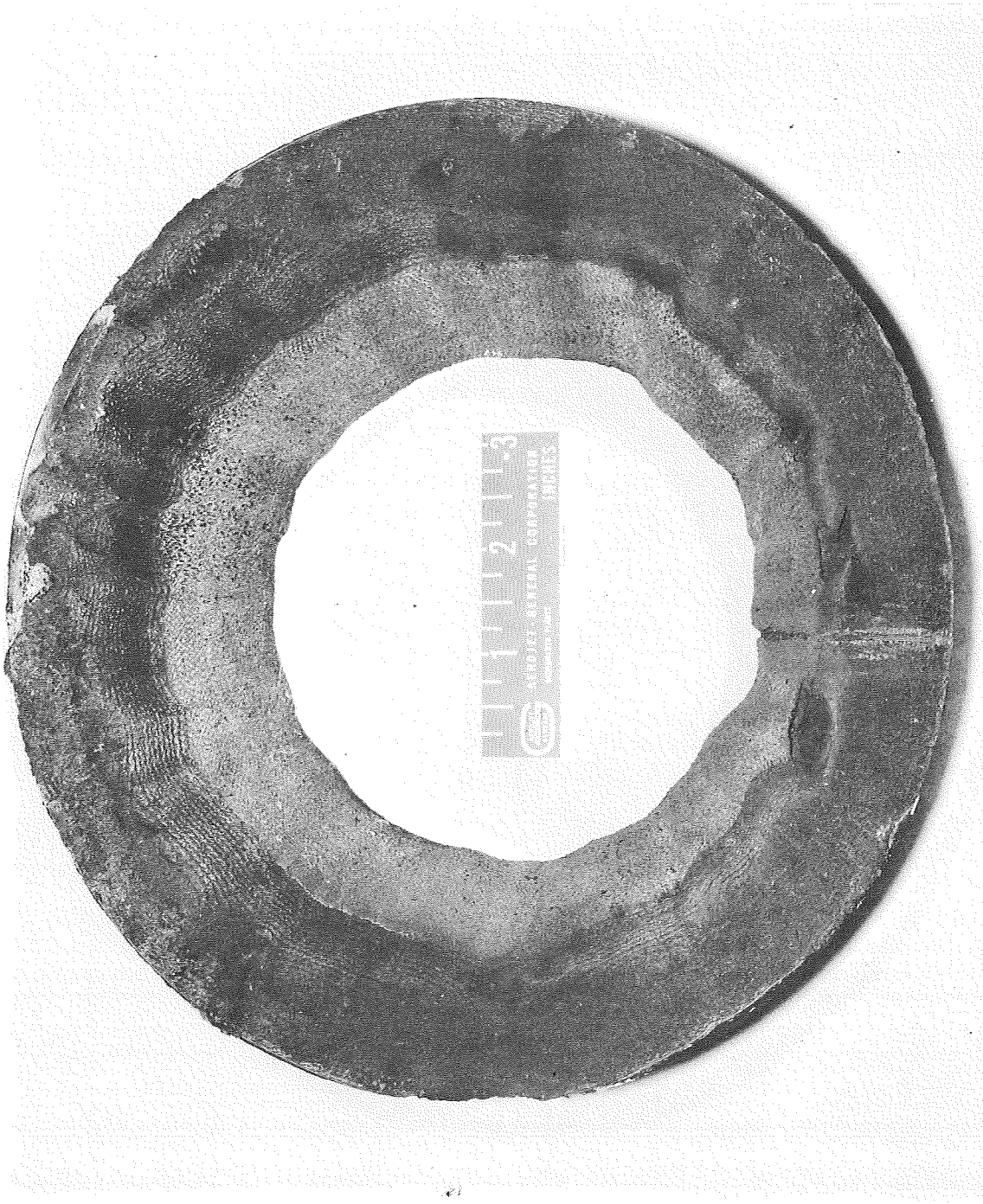

80 to 90 Percent Dense Entrance Cap

Figure VI-31

Resin-Rich (10-Ply) Entrance Cap

Figure VI-32

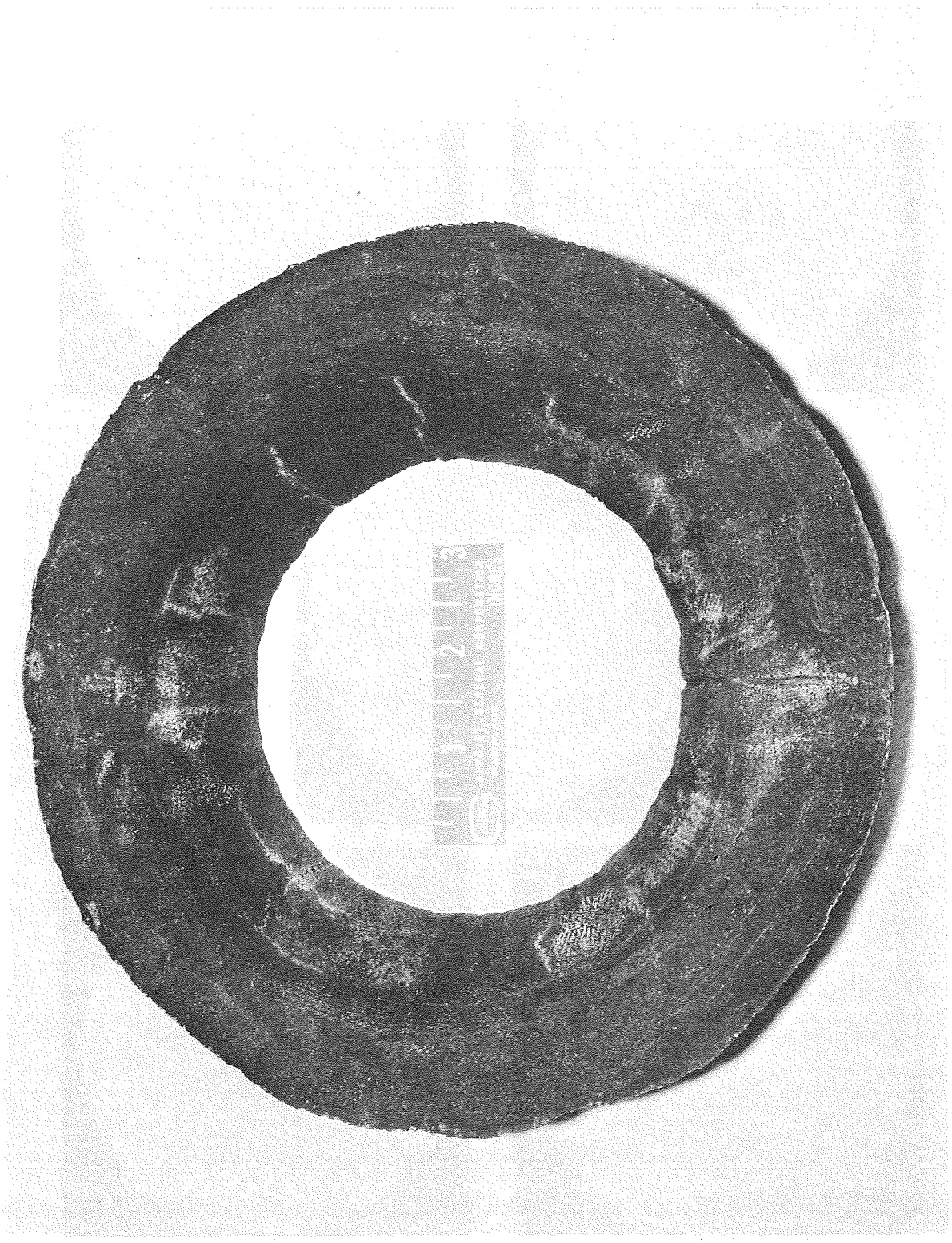

Delaminated (7-Ply) Entrance Cap

Figure VI-33

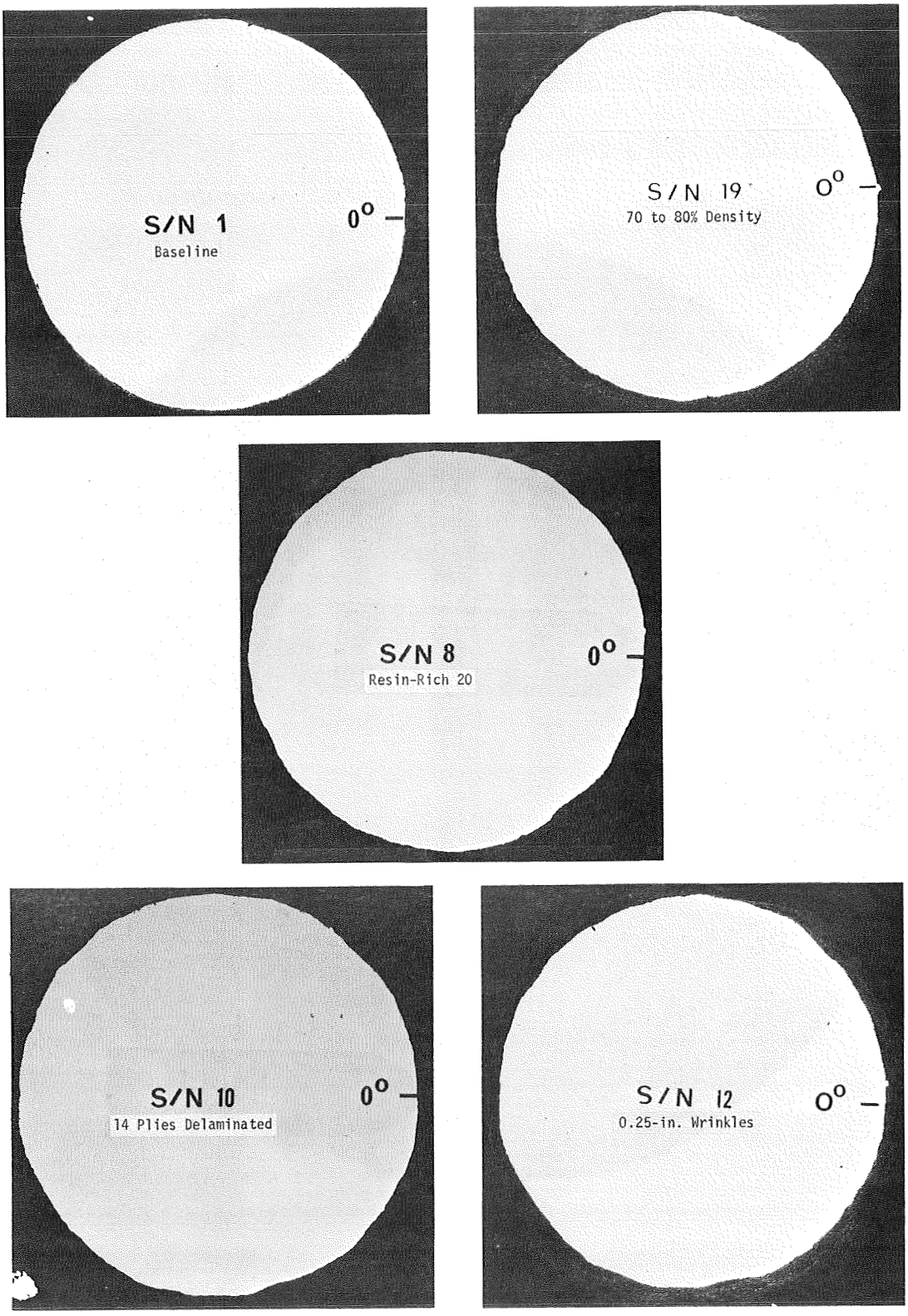

Shadowgraph of (a) Baseline Throat (b) Low-Density (c) Resin-Rich (d) Delaminations and (e) Wrinkles

Figure VI-34

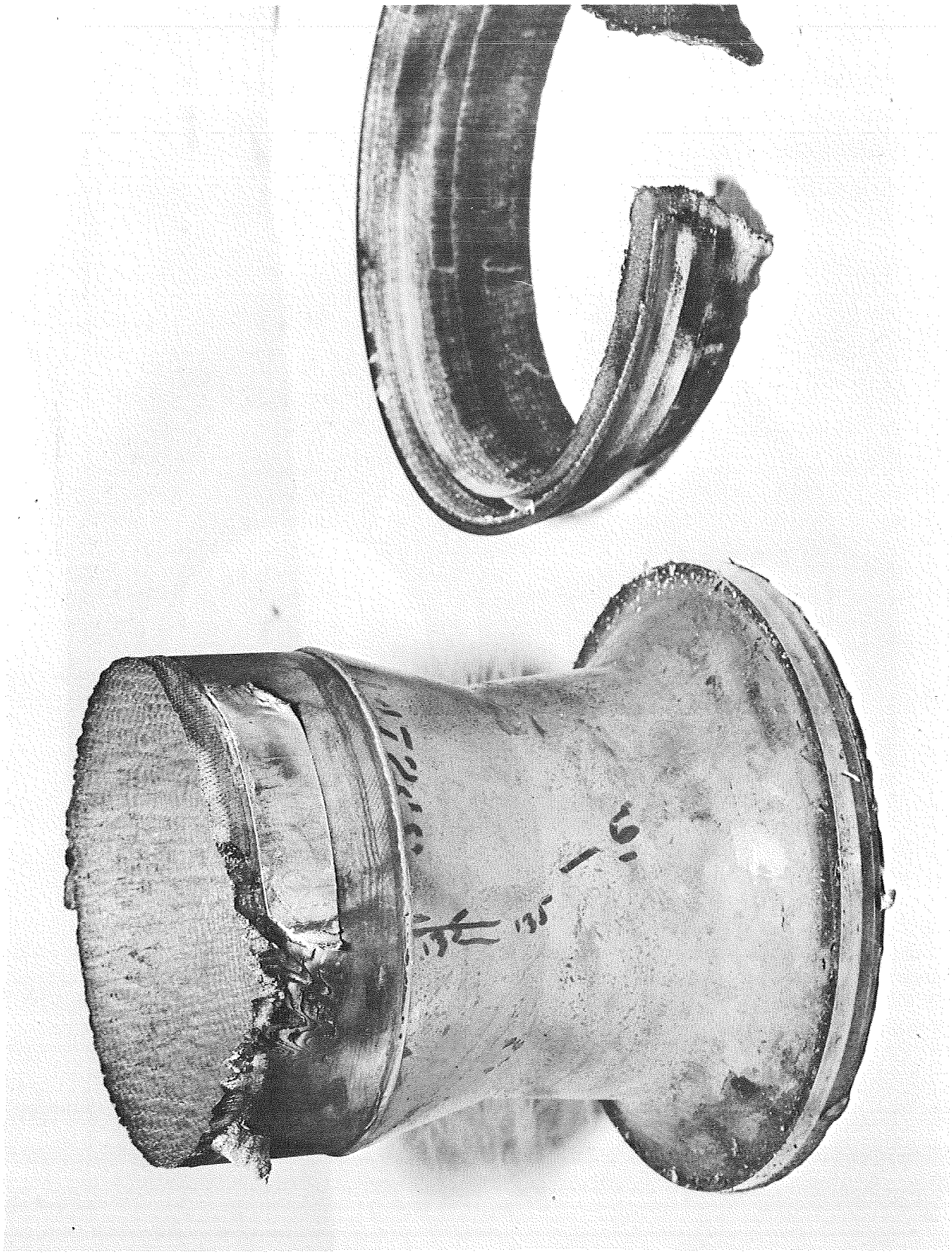

Delaminated (28-Ply) Exit Cone

Figure VI-35

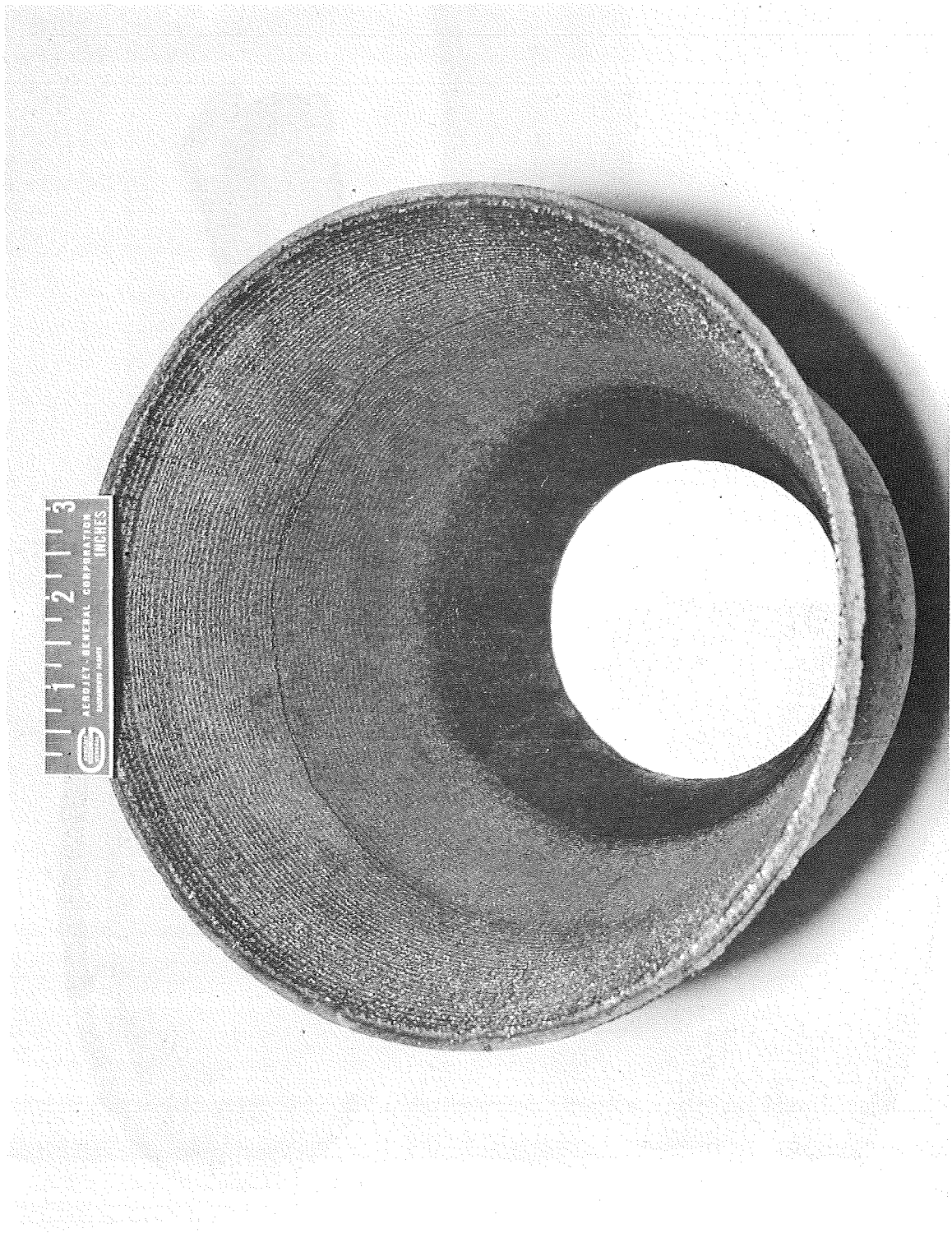

1/8-in. Wrinkle Exit Cone

Figure VI-36

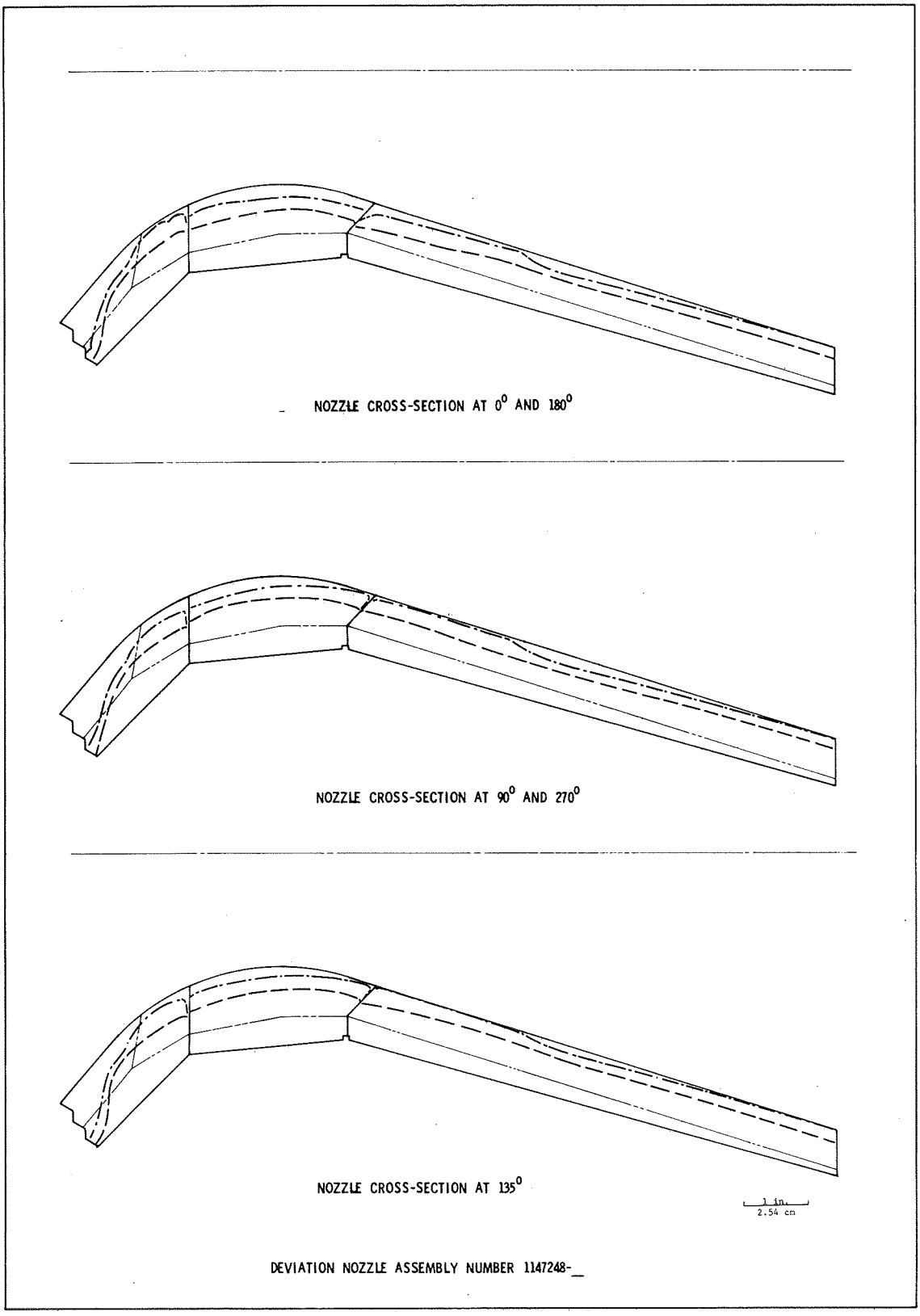

Regression and Char Depth in Nozzle S/N 001

Figure VI-37

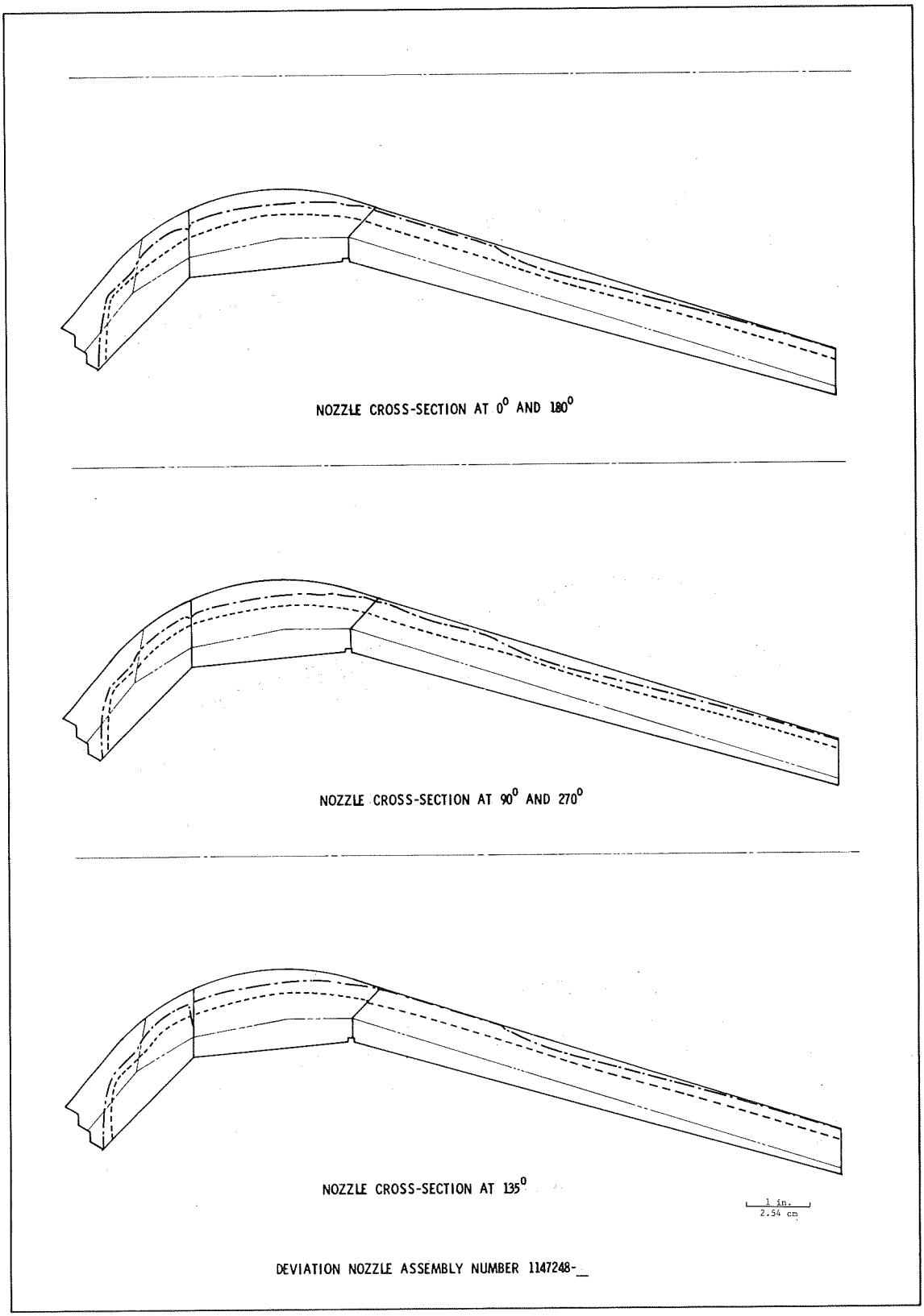

Regression and Char Depth in Nozzle S/N 002

Figure VI-38

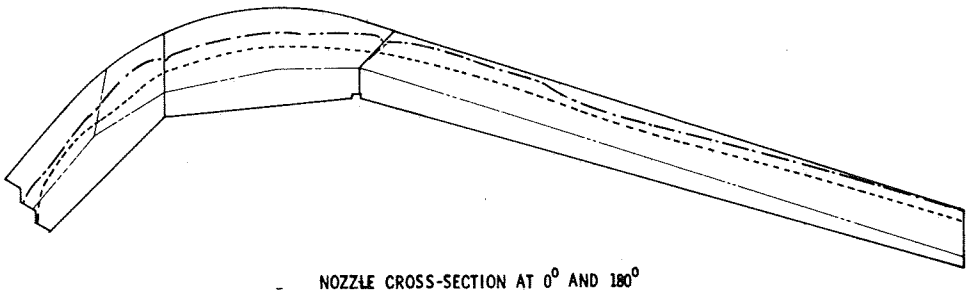

NOZZLE CROSS-SECTION AT 0^{0} AND 180^{0}

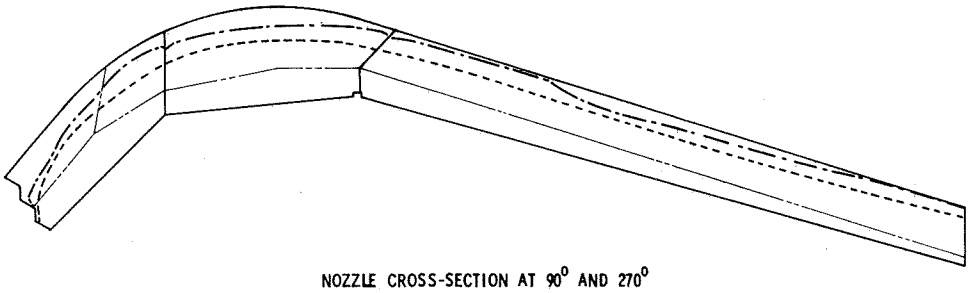

NOZZLE CROSS-SECTION AT 90^{0} AND 270^{0}

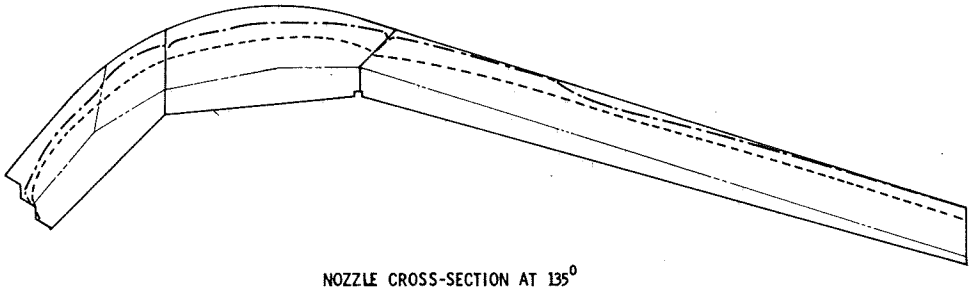

NOZZLE CROSS-SECTION AT 135^{0}

1 in.
2.54 cm

DEVIATION NOZZLE ASSEMBLY NUMBER 1147248-_

Regression and Char Depth in Nozzle S/N 003

Figure VI-39

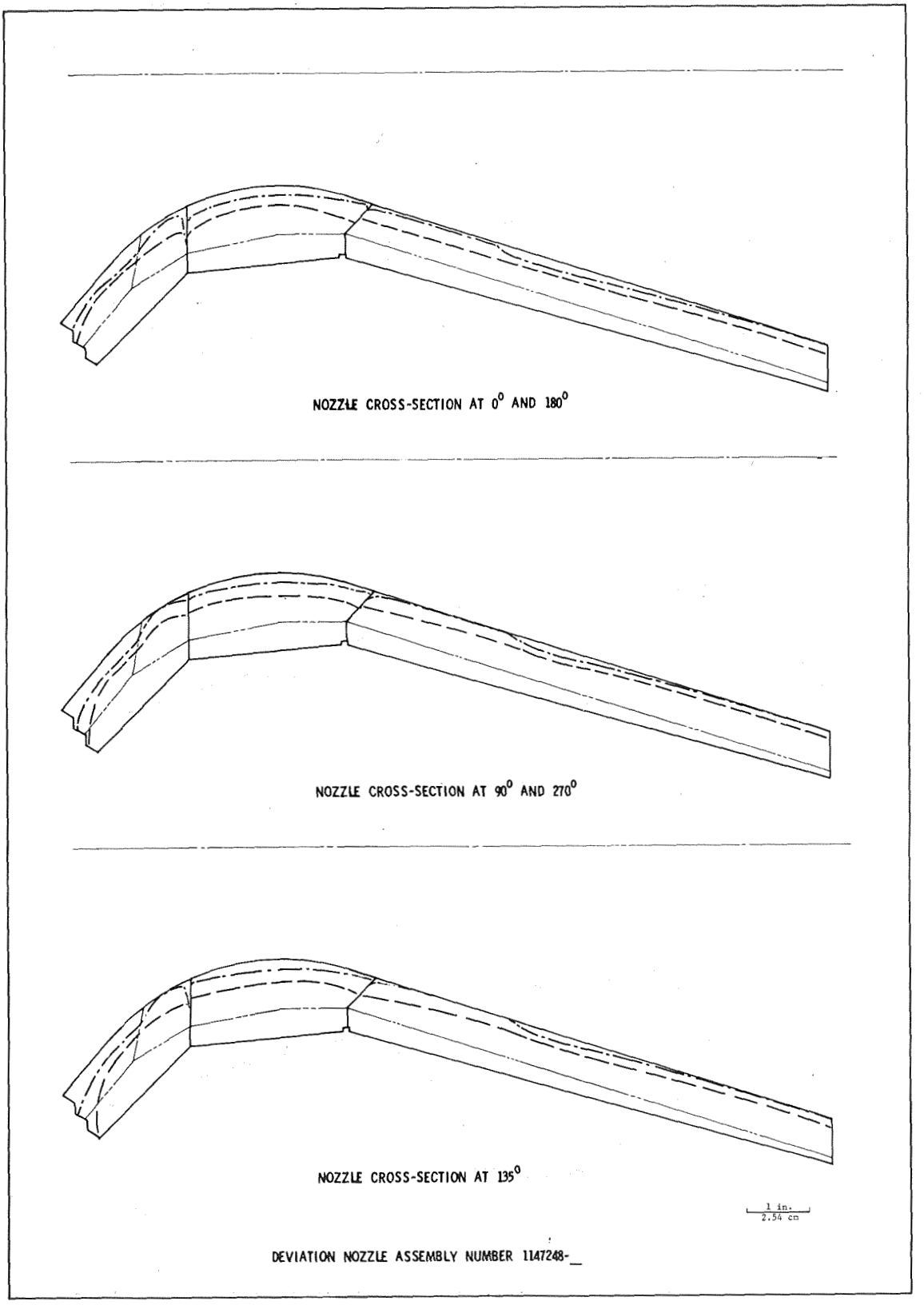

Regression and Char Depth in Nozzle S/N 004

Figure VI-40

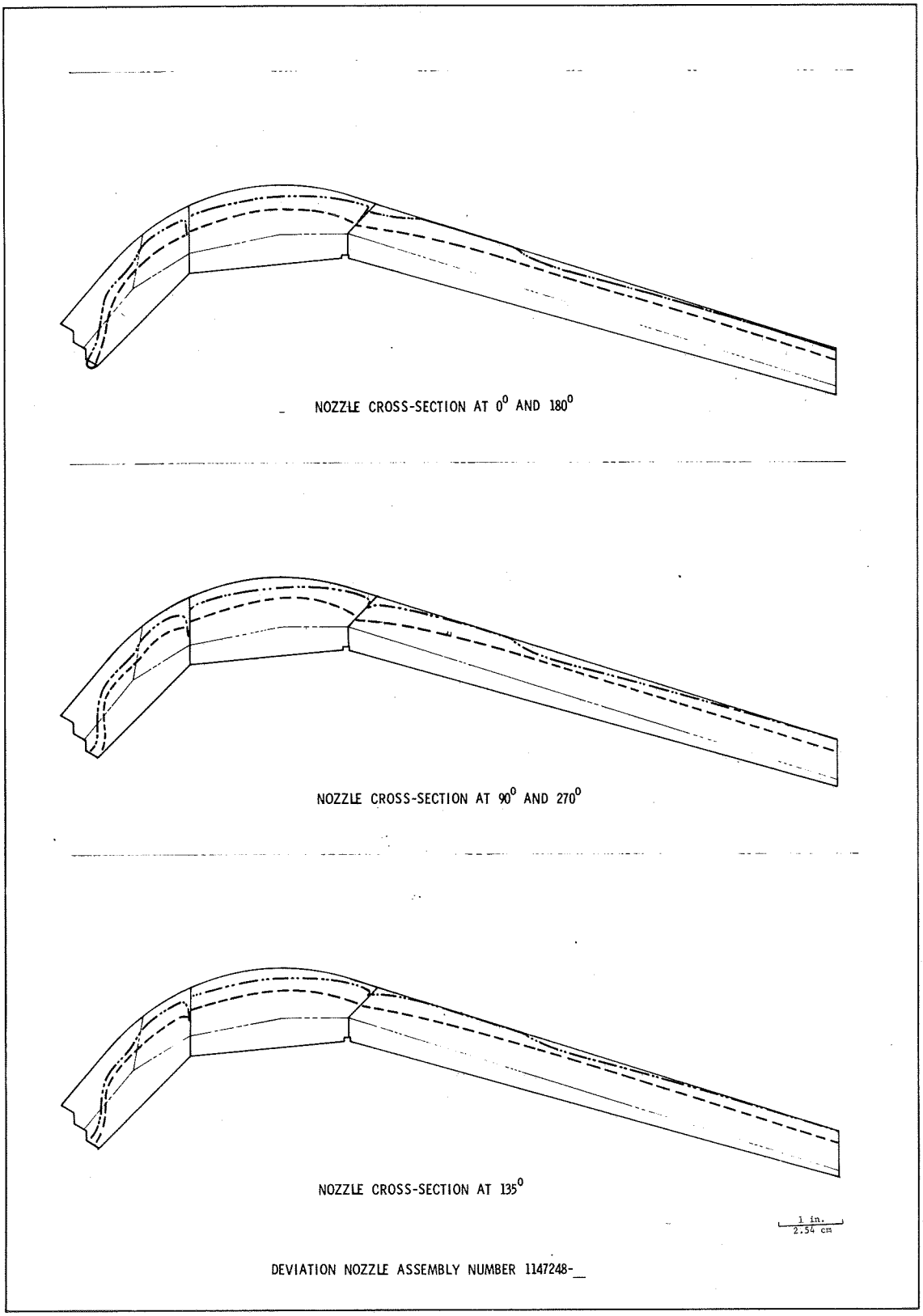

Regression and Char Depth in Nozzle S/N 005

Figure VI-41

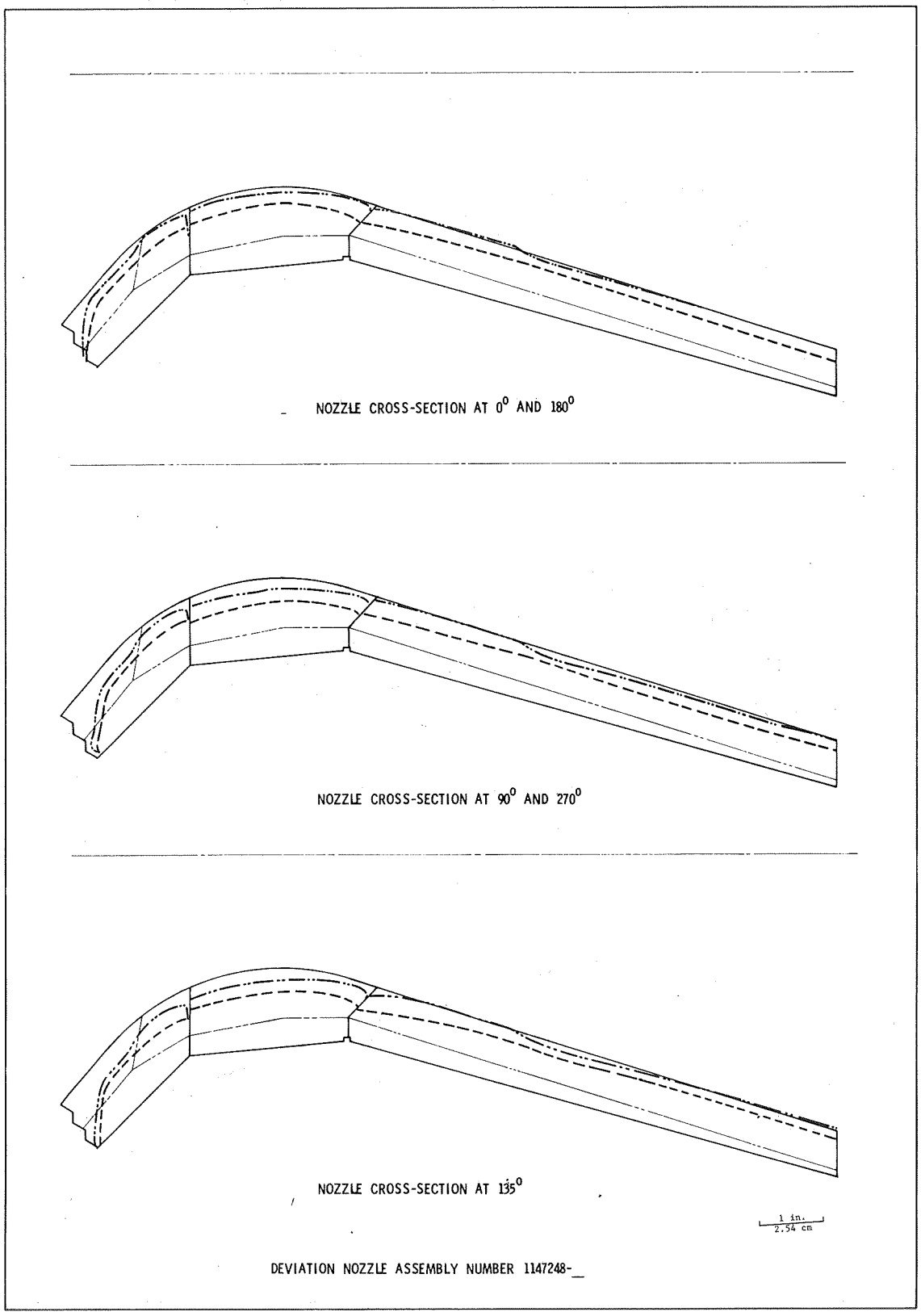

Regression and Char Depth in Nozzle S/N 006

Figure VI-42

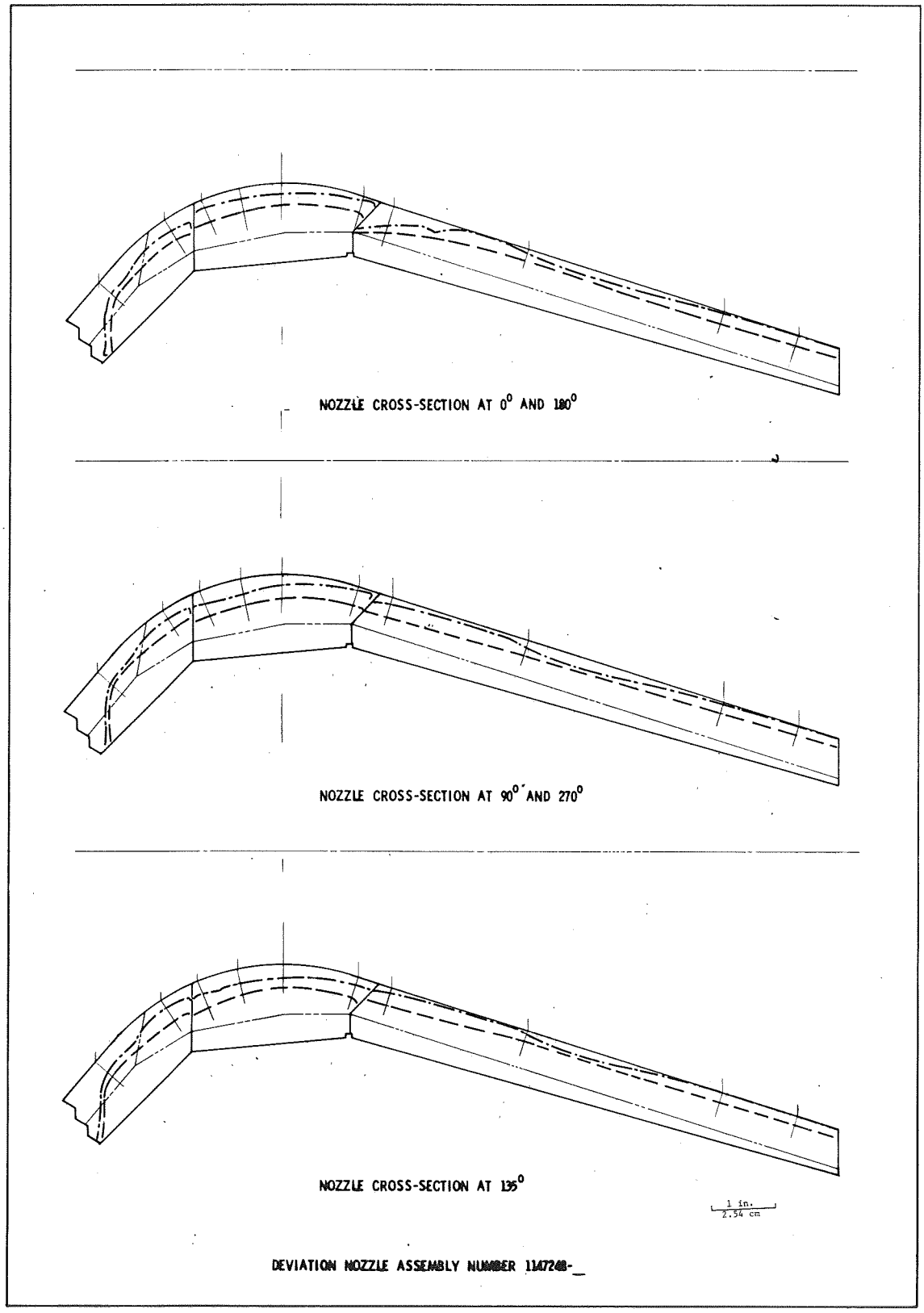

Regression and Char Depth in Nozzle S/N 007

Figure VI-43

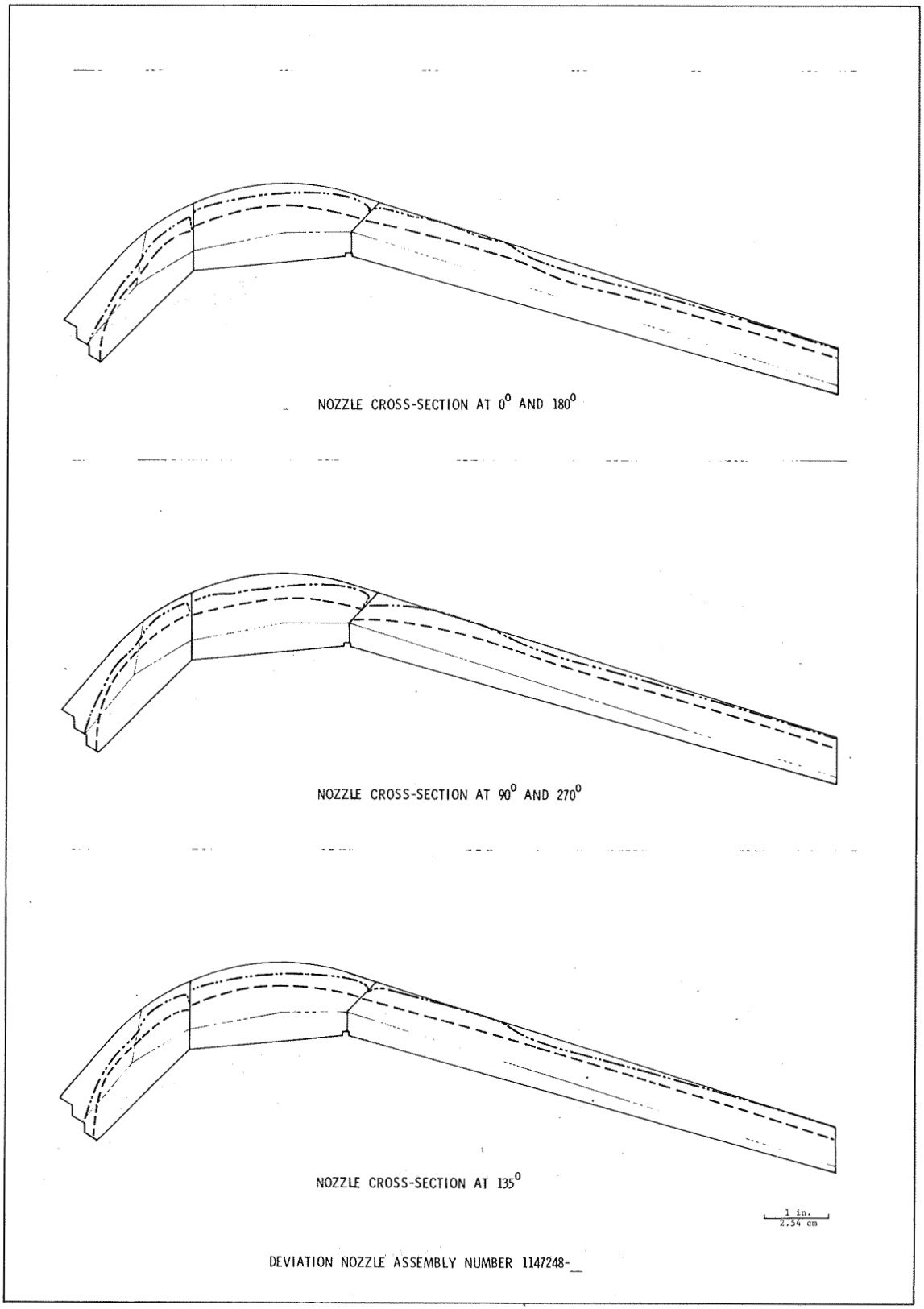

Regression and Char Depth in Nozzle S/N 008

Figure VI-44

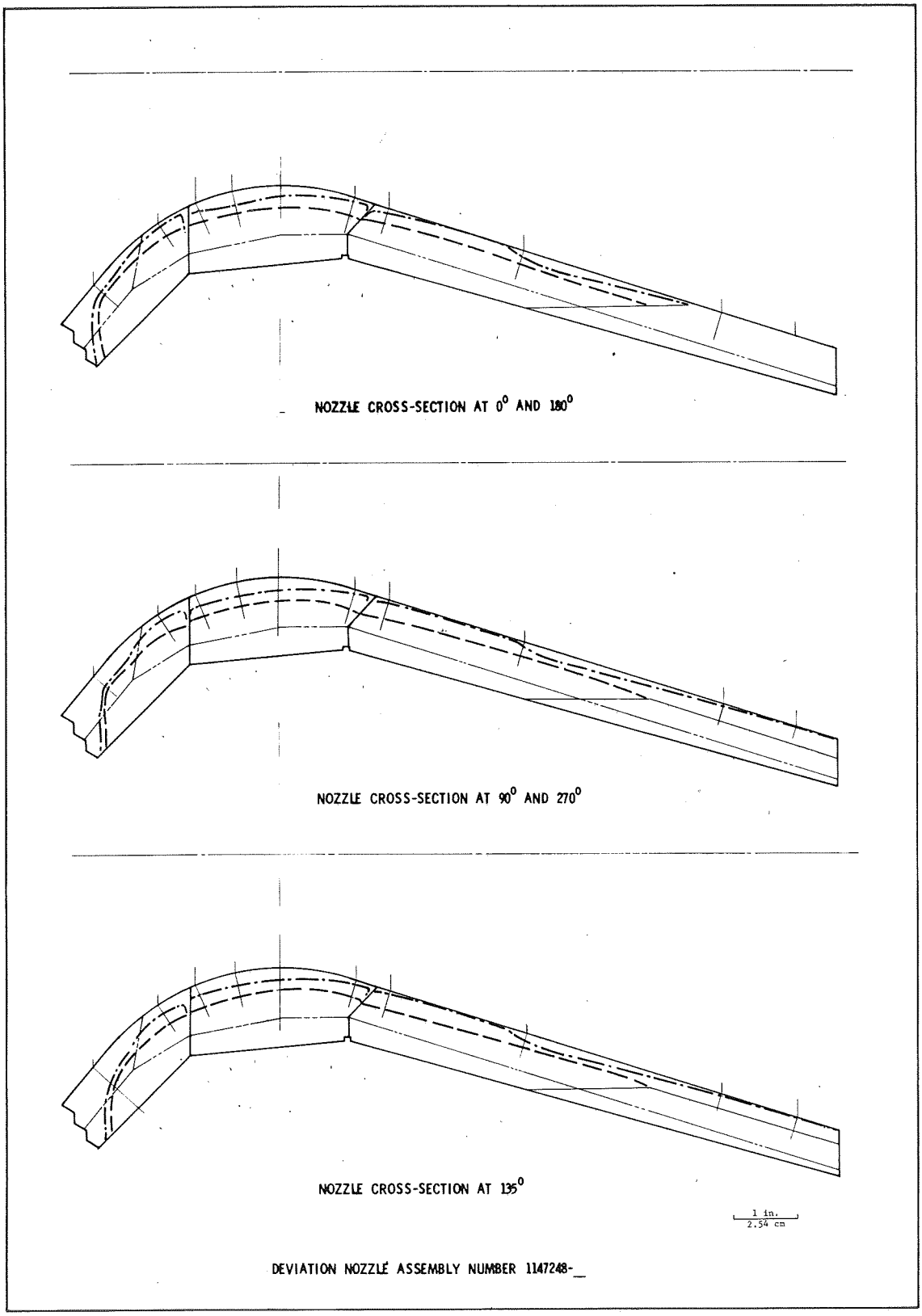

Regression and Char Depth in Nozzle S/N 009

Figure VI-45

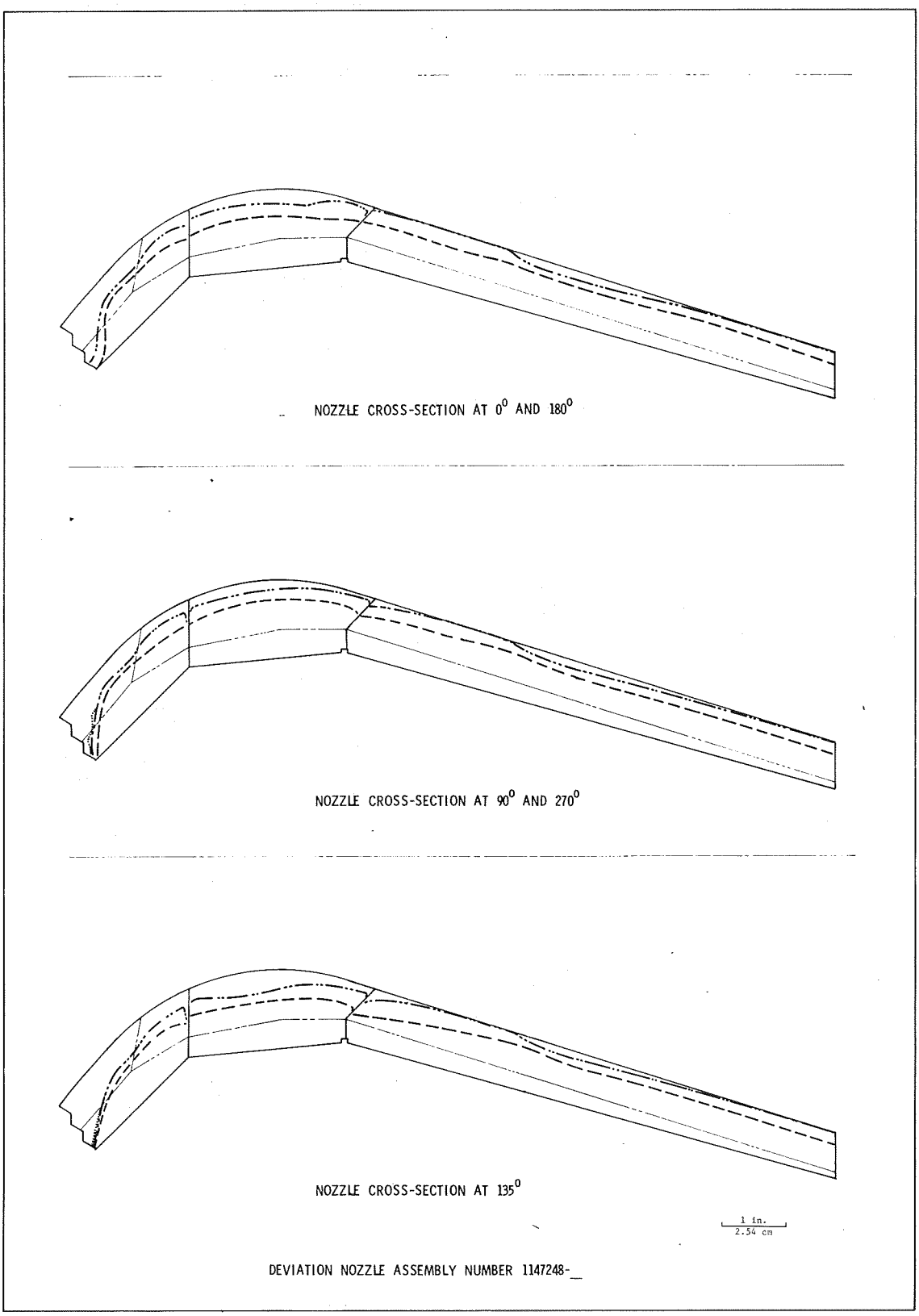

Regression and Char Depth in Nozzle S/N 010

Figure VI-46

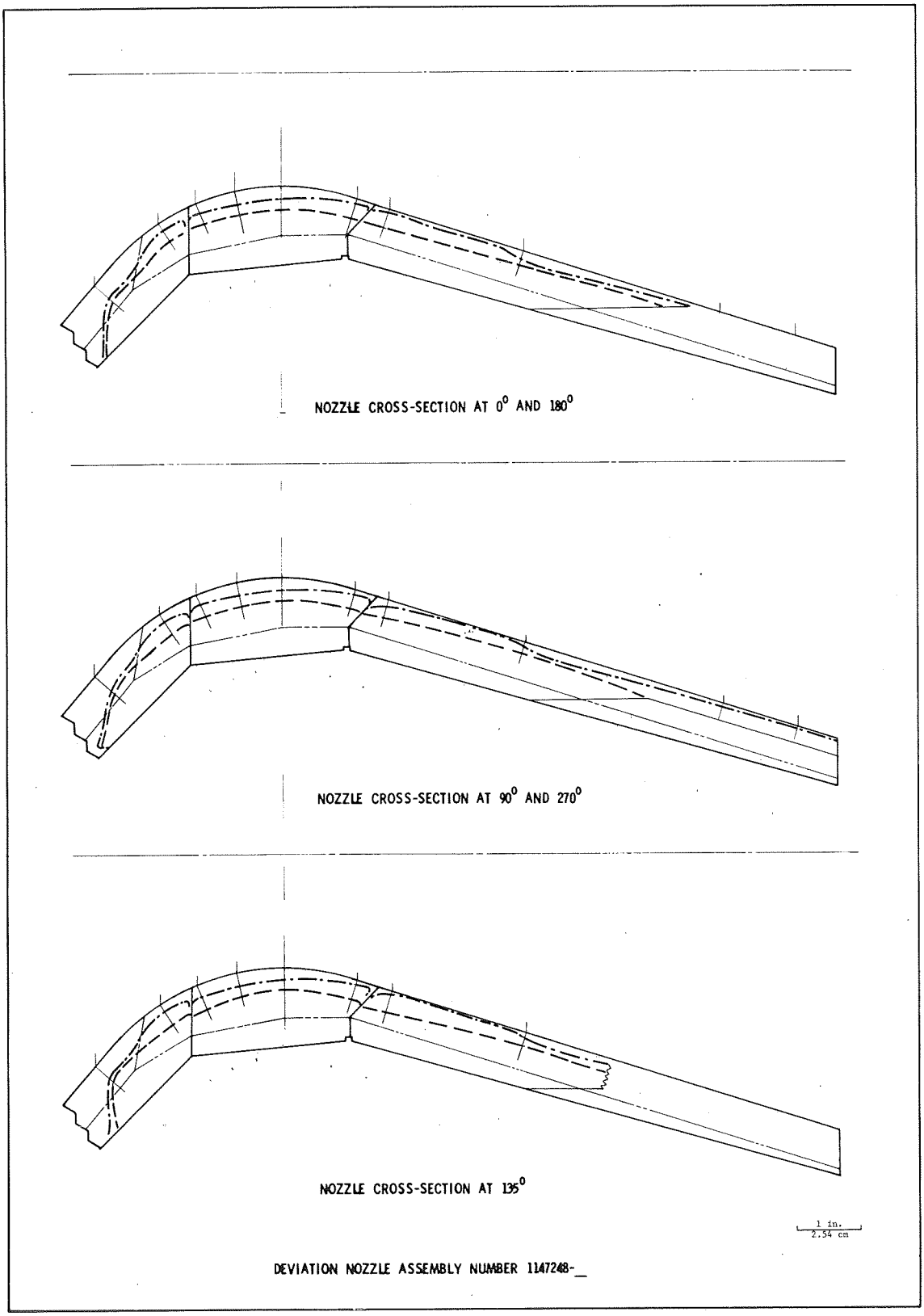

Regression and Char Depth in Nozzle S/N 011

Figure VI-47

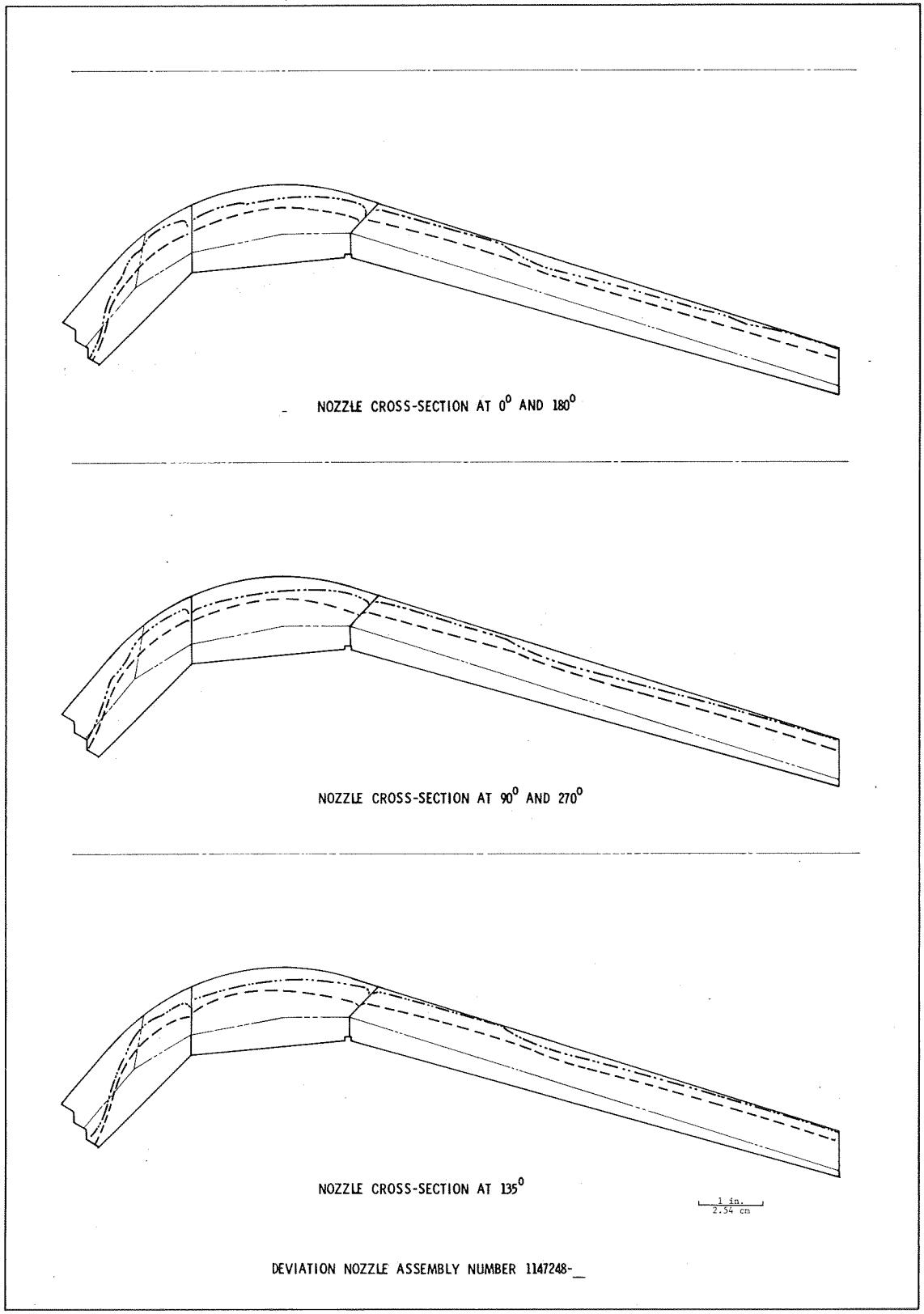

Regression and Char Depth in Nozzle S/N 012

Figure VI-48

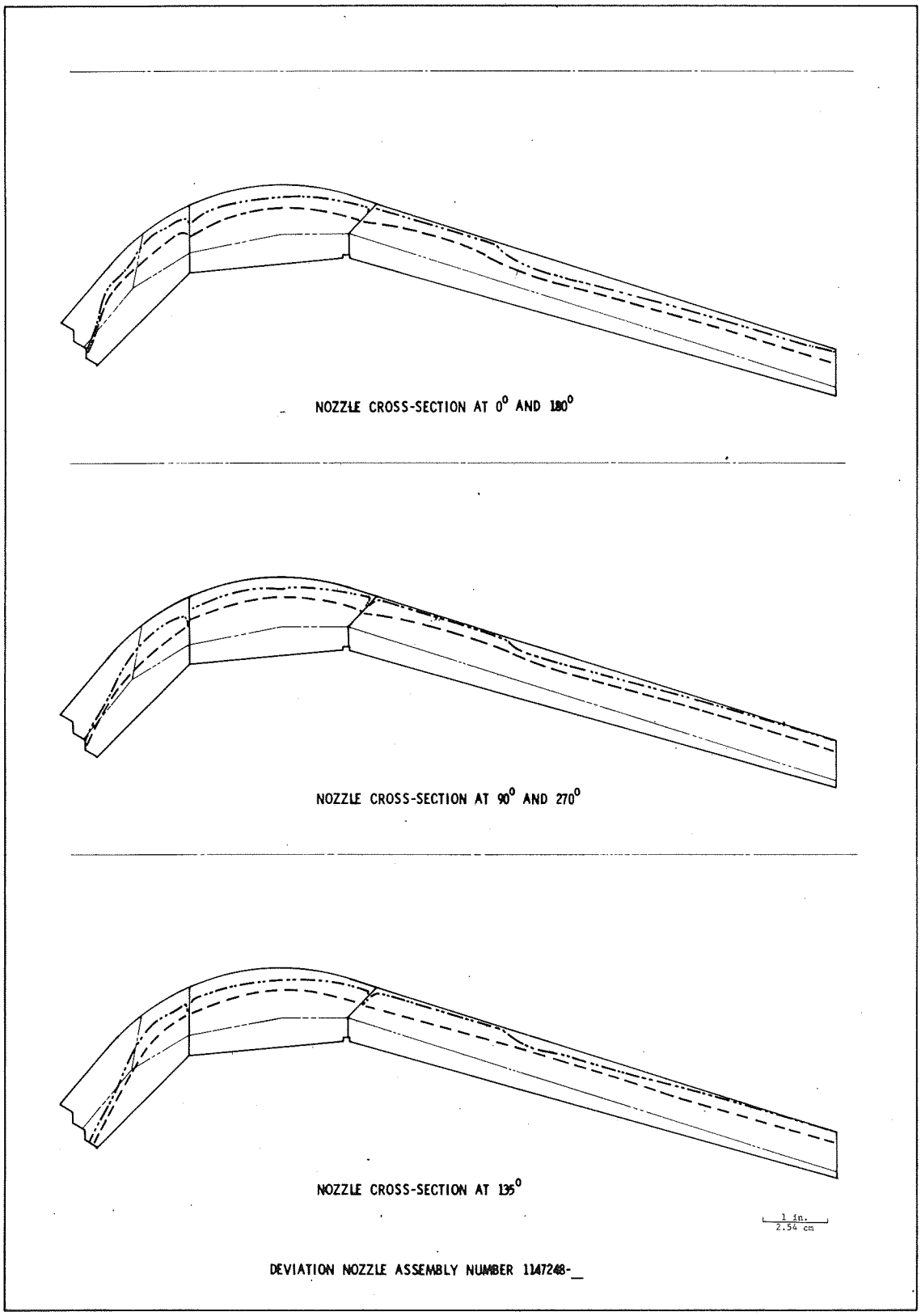

Regression and Char Depth in Nozzle S/N 013

Figure VI-49

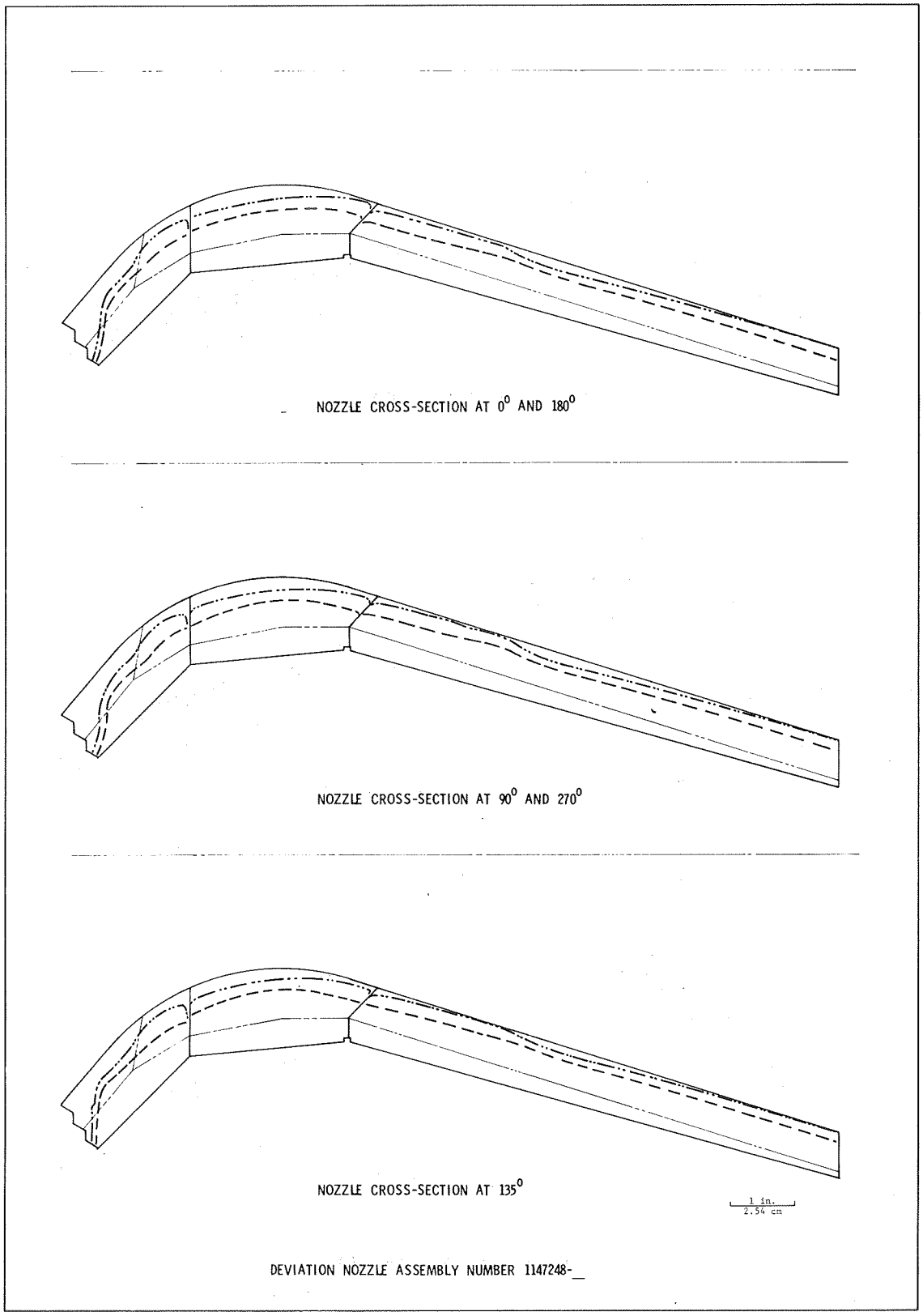

Regression and Char Depth in Nozzle S/N 014

Figure VI-50

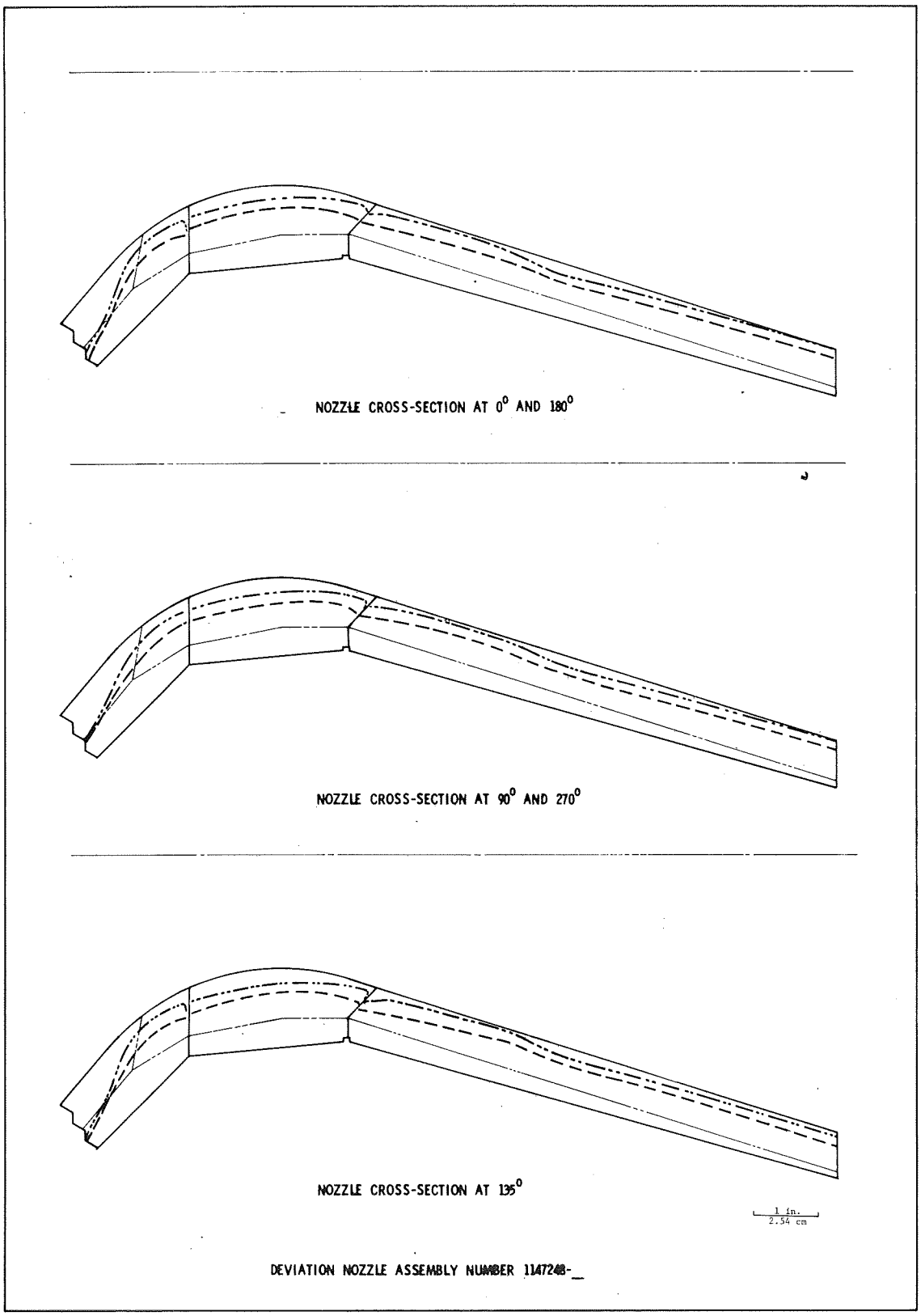

Regression and Char Depth in Nozzle S/N 015

Figure VI-51

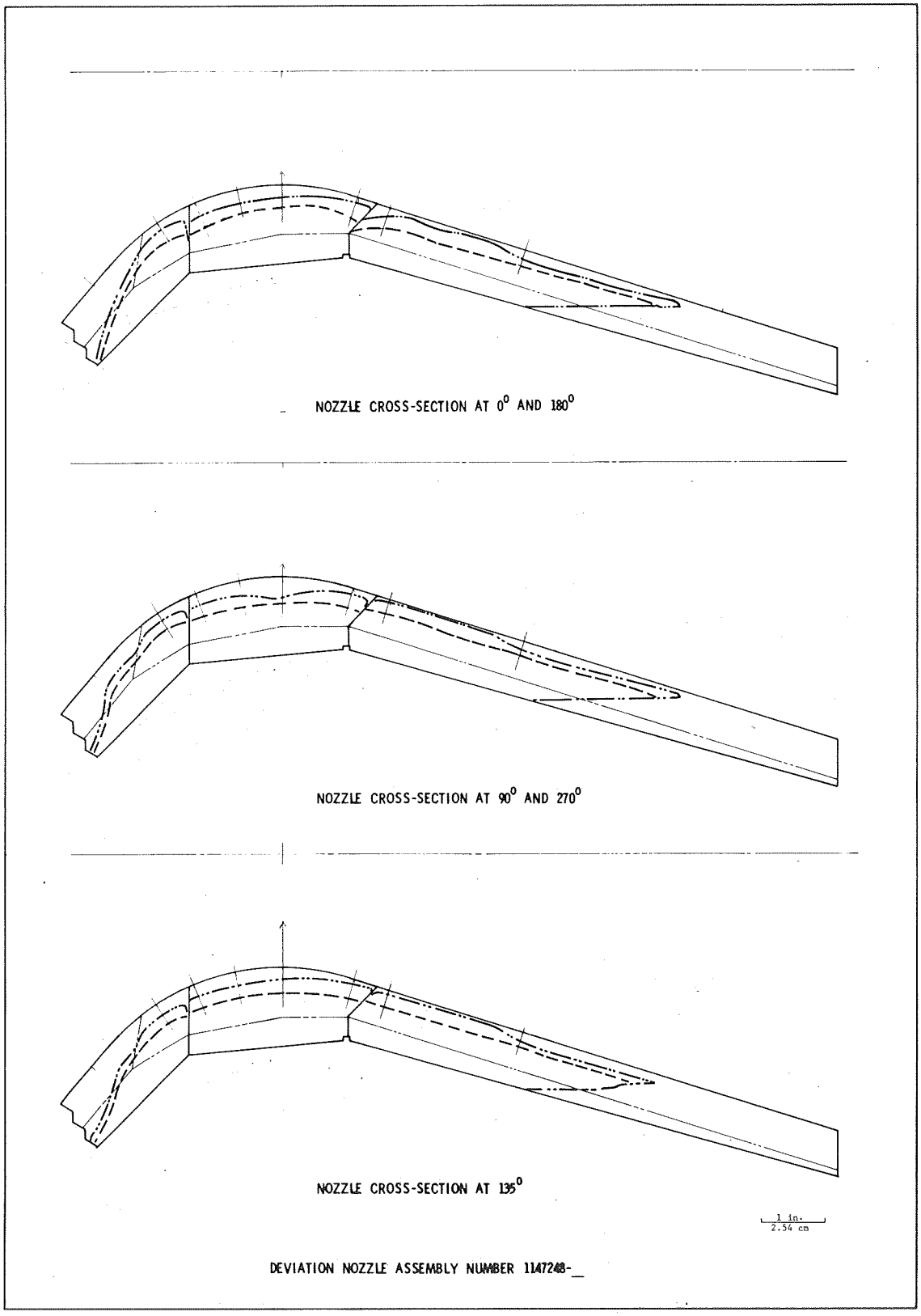

Regression and Char Depth in Nozzle S/N 016

Figure VI-52

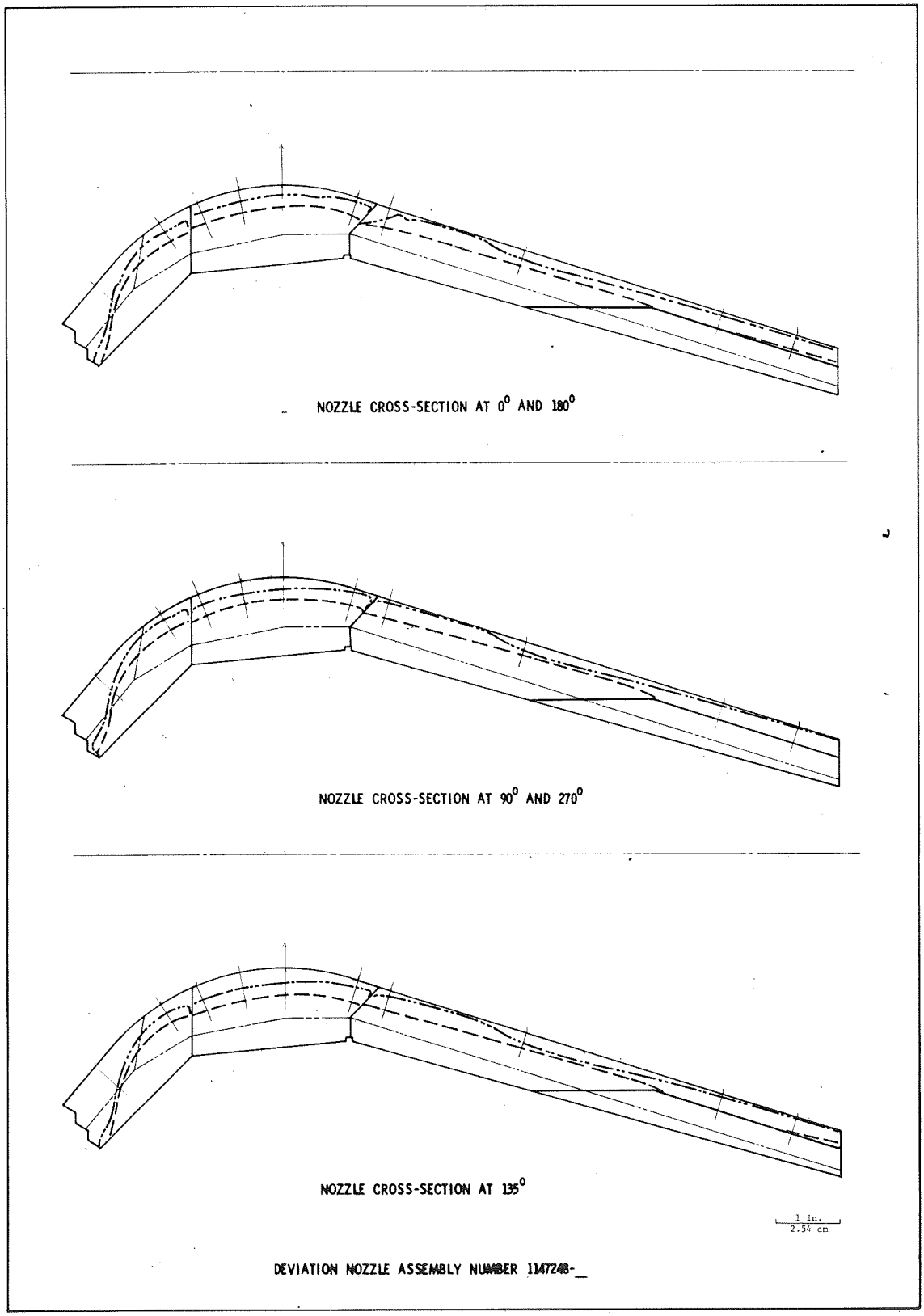

Regression and Char Depth in Nozzle S/N 017

Figure VI-53

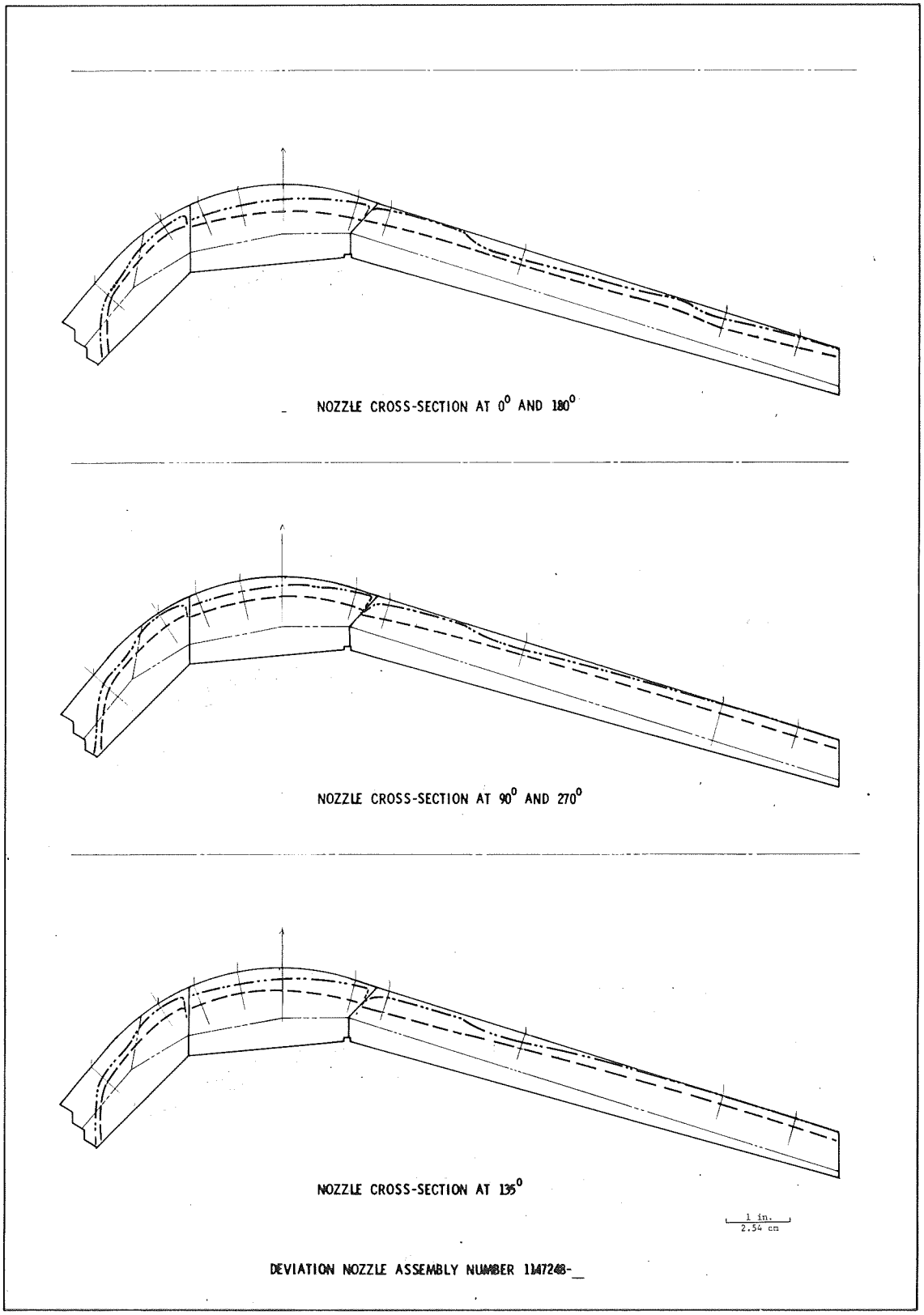

Regression and Char Depth in Nozzle S/N 018

Figure VI-54

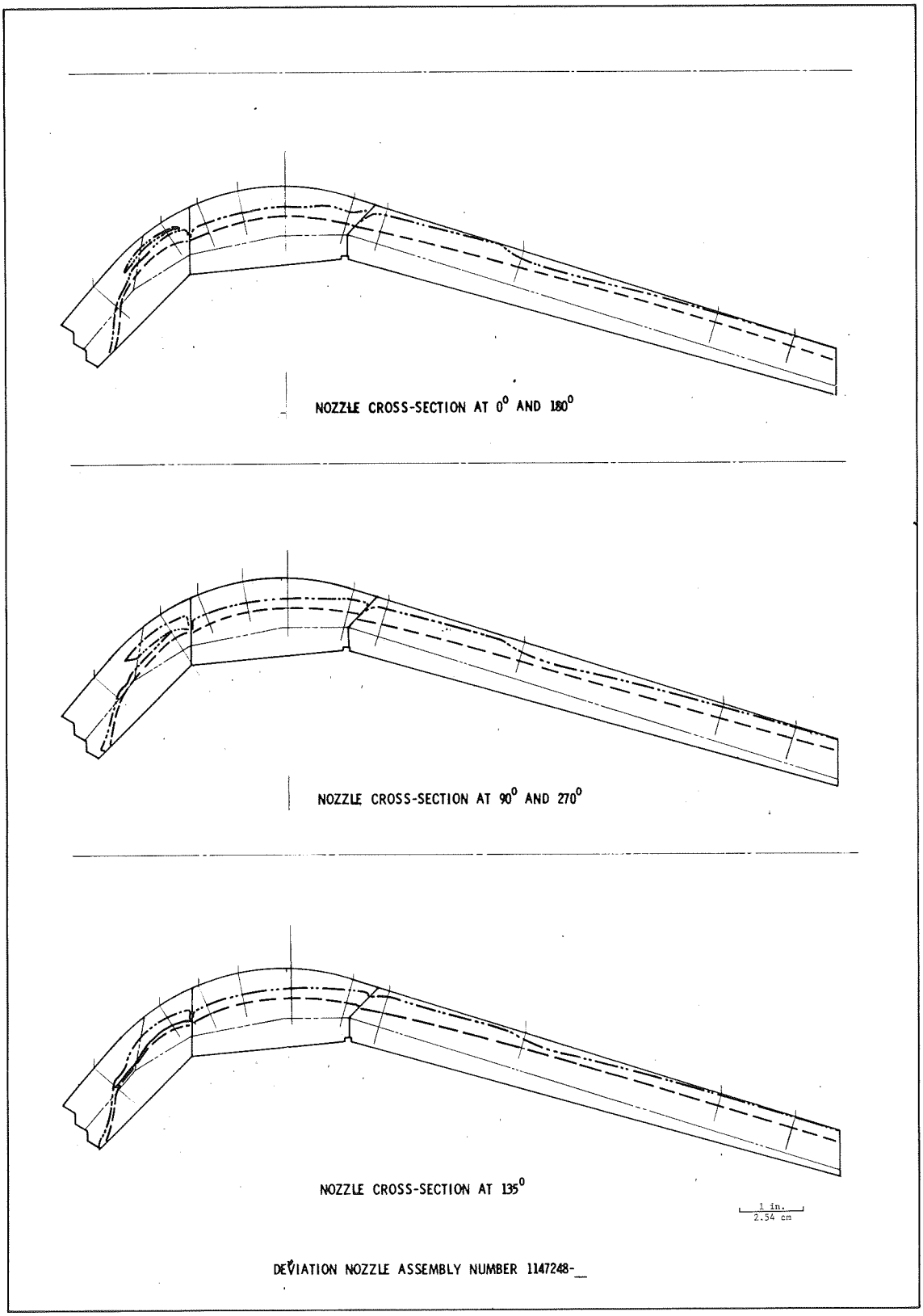

Regression and Char Depth in Nozzle S/N 019

Figure VI-55

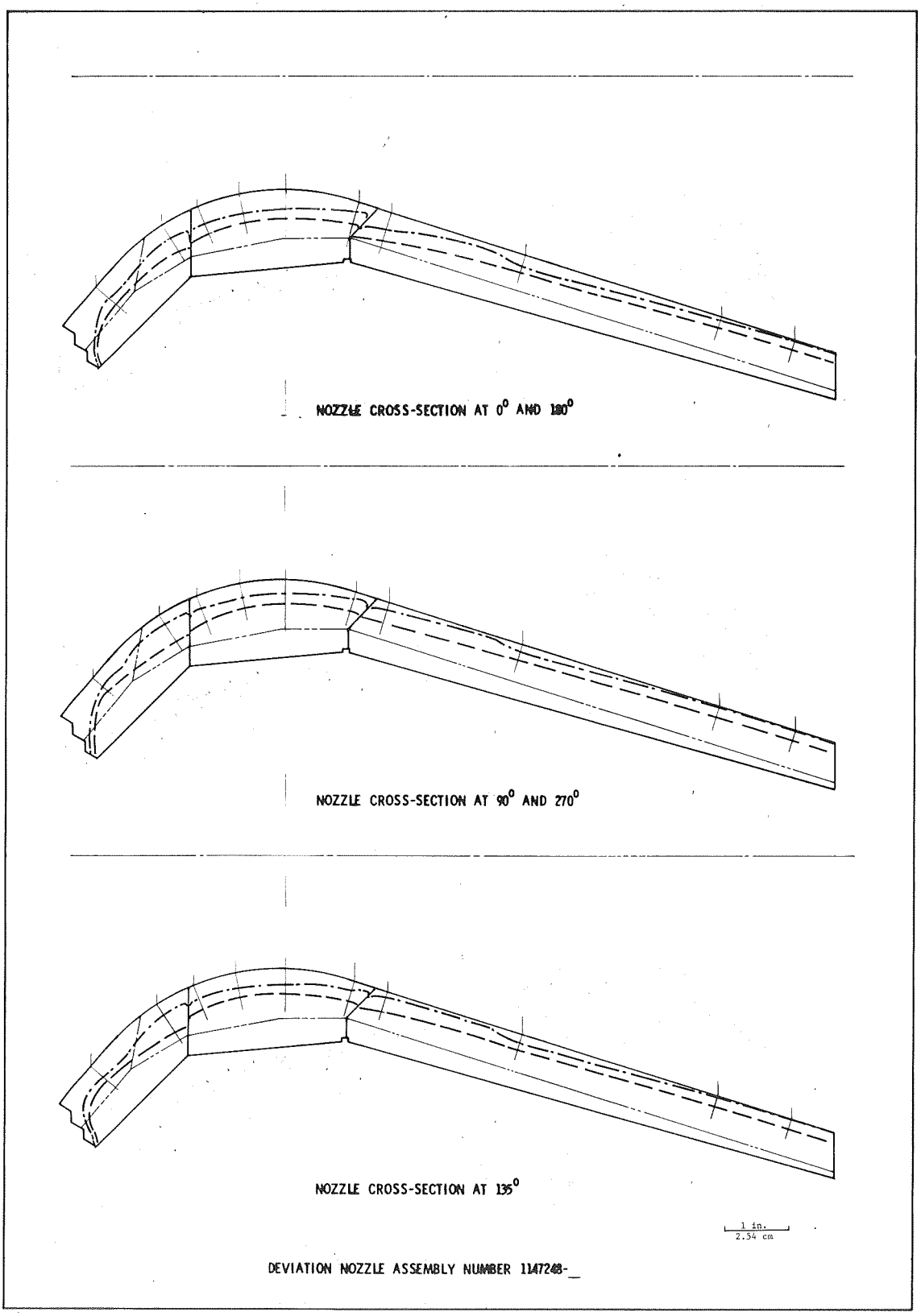

Regression and Char Depth in Nozzle S/N 020

Figure VI-56

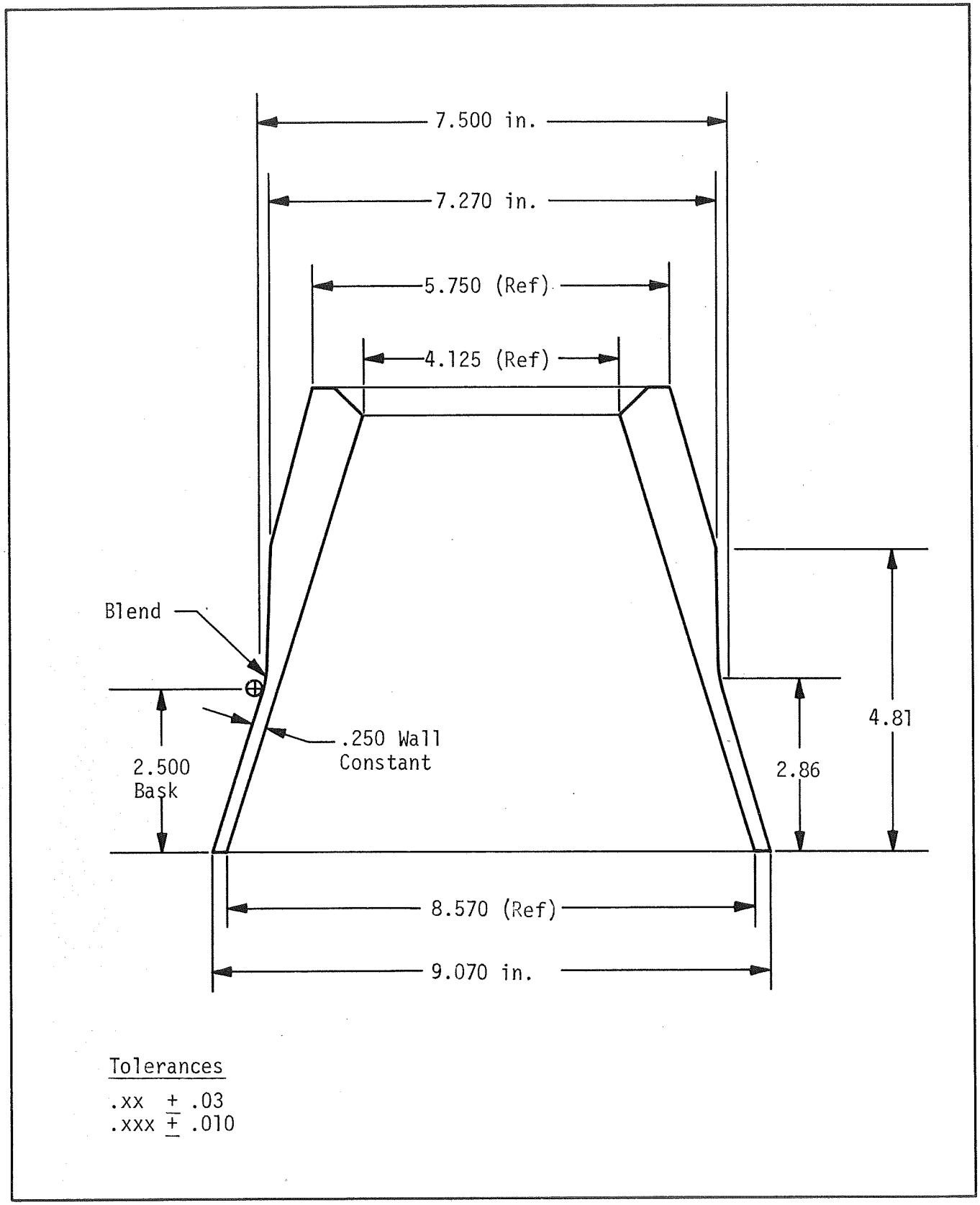

Modified, Thin-Wall Exit Cone

Figure VI-57

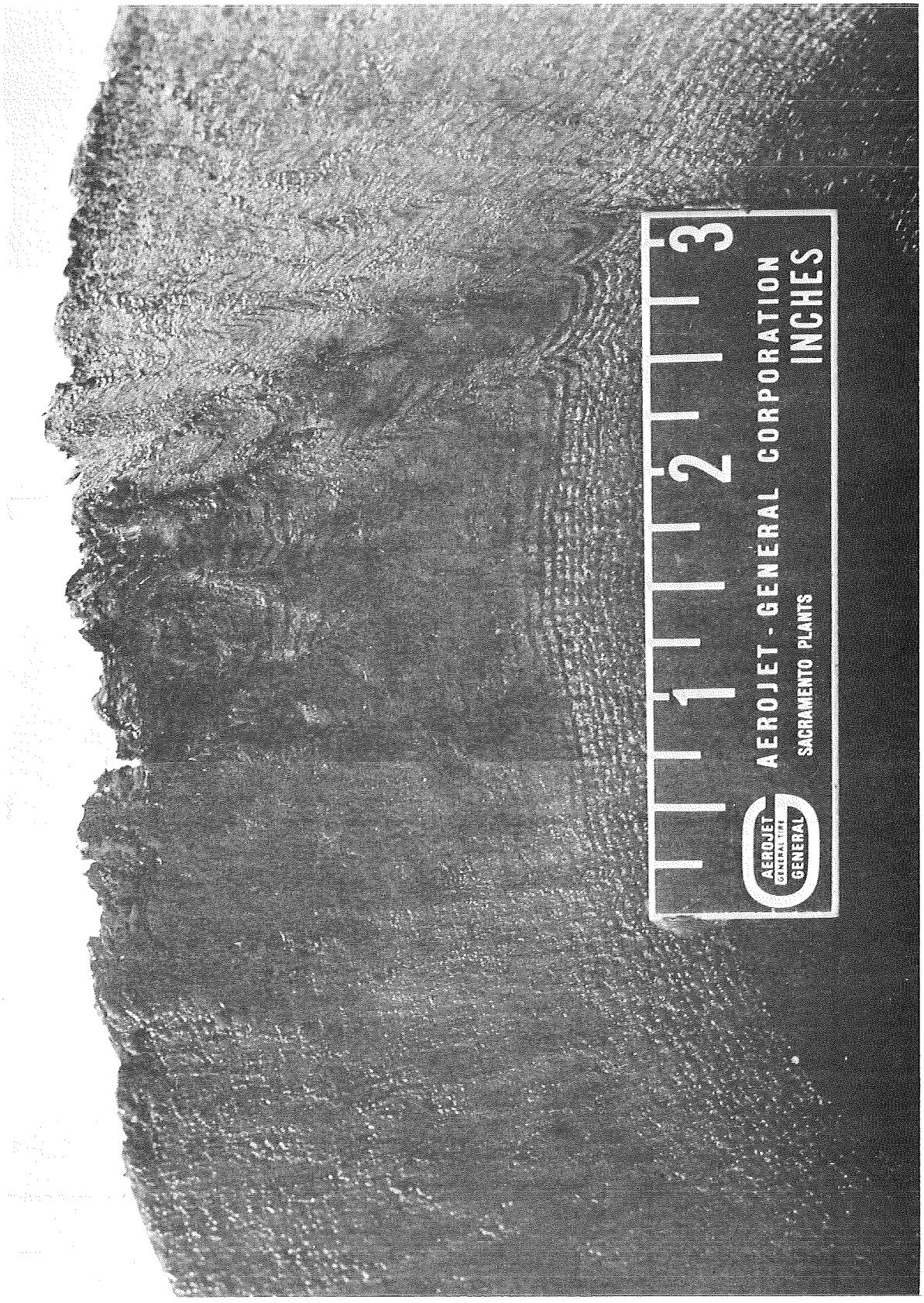

Origin of Failure in Exit Cone Section with 28 Delaminated Plies

Figure VI-58

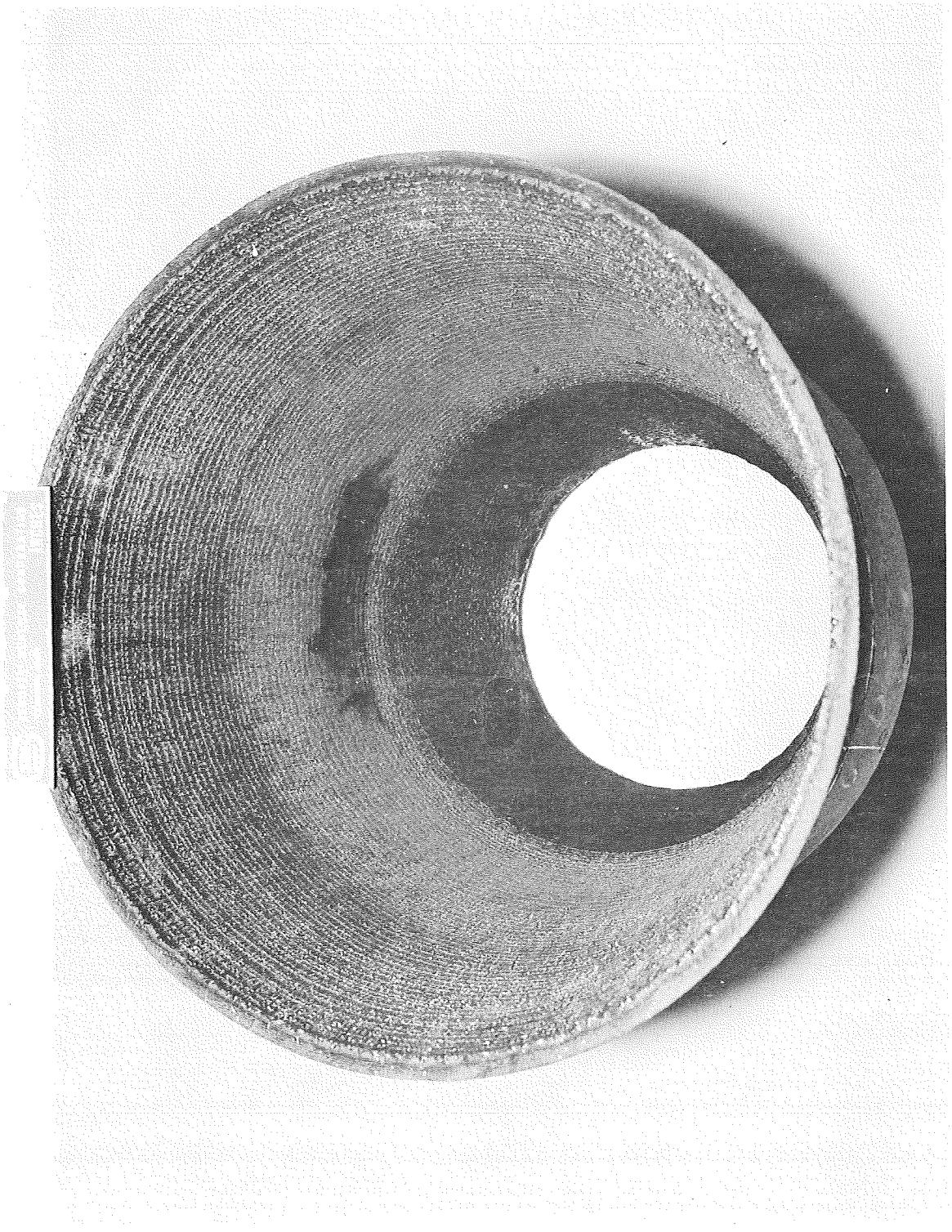

Exit Cone Section with 7 Delaminated Plies,
after Static Test Firing

Figure VI-59

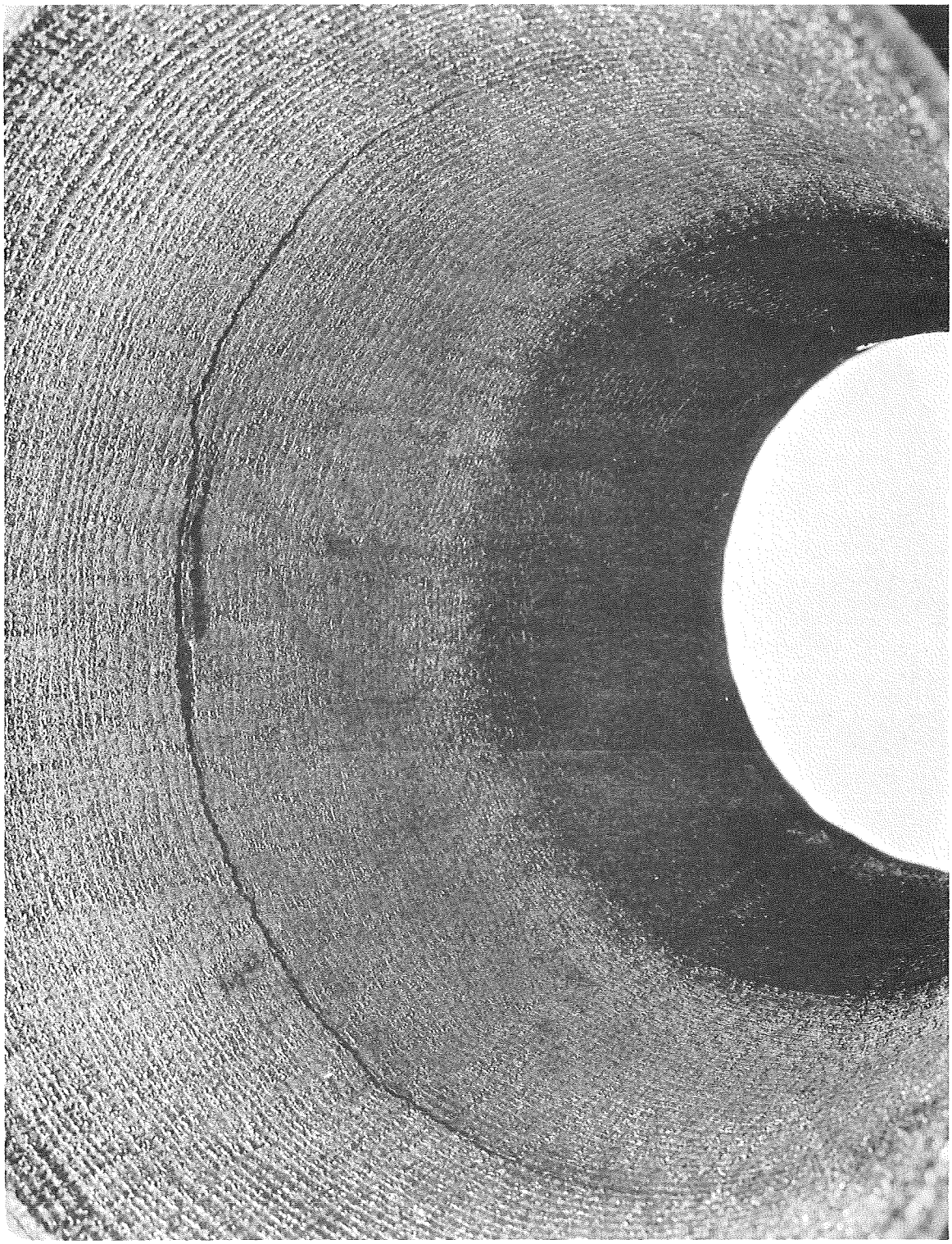

Crack Extending for 120 Degrees in Aft Exit Section with 1/8-in. Wrinkle

Figure VI-60

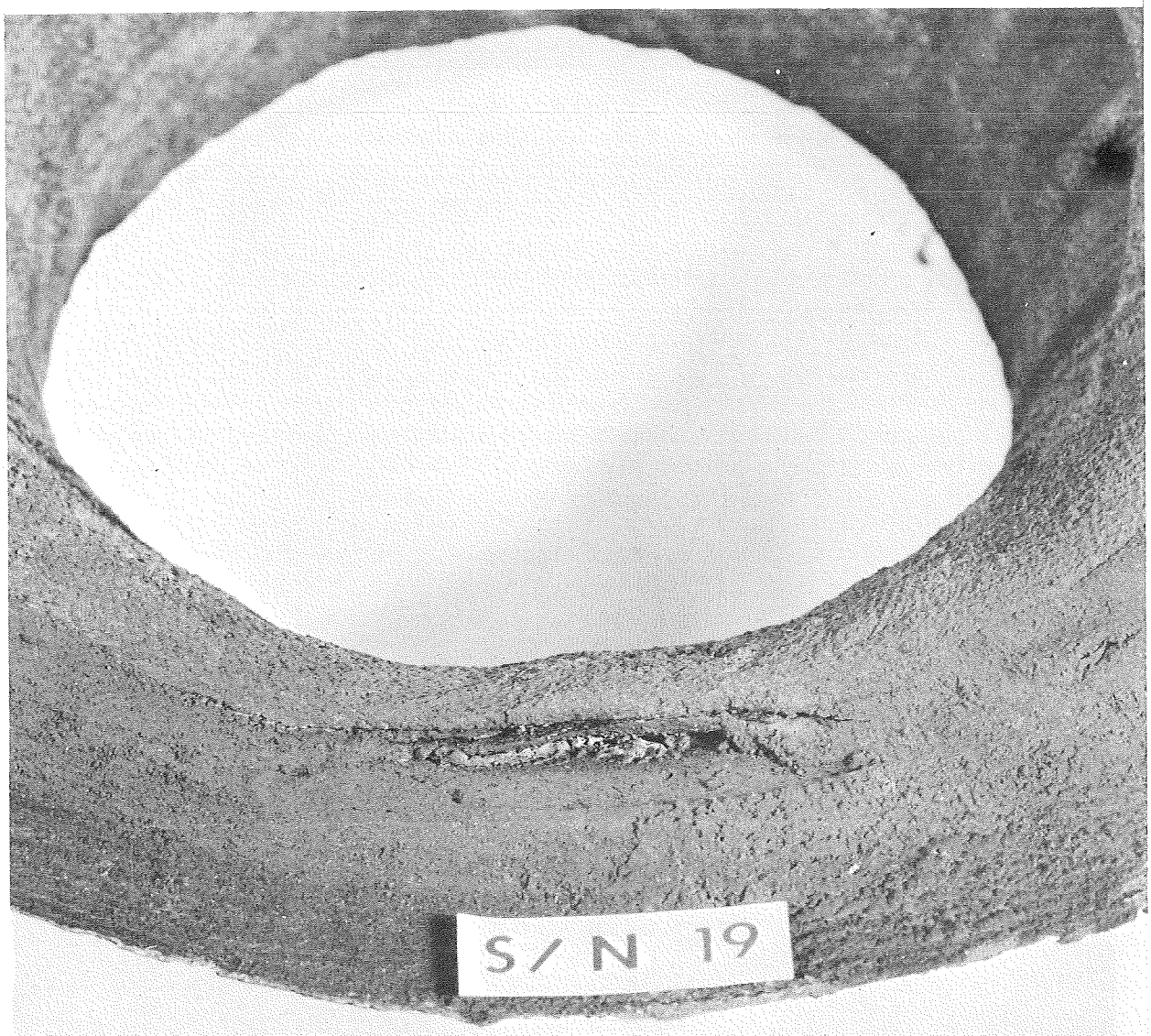

Separation Between Carbon and Silica Plies of
70 to 80 Percent Dense Entrance Cap

Figure VI-61

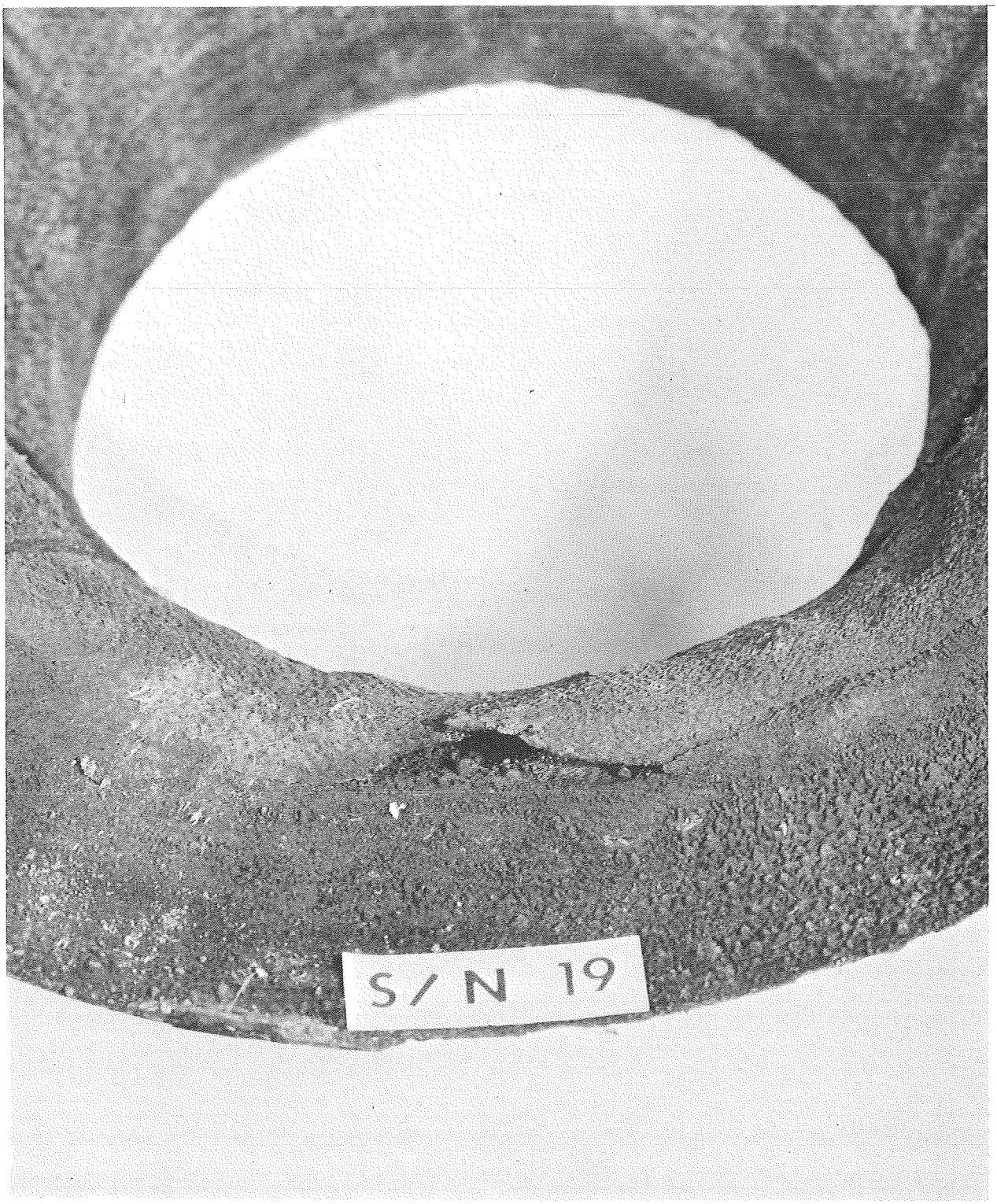

Crack at Carbon-Silica Interface of 70 to 80 Percent
Dense Entrance Cap

Figure VI-62

VII. ANALYTICAL PREDICTION TECHNIQUES

Any rocket motor nozzle design represents an engineering solution to the problem of containing and directing a corrosive propellant exhaust at pressures and temperatures higher than ambient. For an uncooled nozzle fabricated from a reinforced ablative composite, the solution consists of, first, defining the local thermal environment at the exposed surfaces; second, estimating the ablative response of the exposed material to the propellant exhaust products; and third, computing the transient response of a composite material that reacts at the hot surface, decomposes in depth, and is subjected to mechanical strains generated by pressure loads and modified by thermal expansion. A nozzle design is thus a performance prediction, and the suitability of the design can be judged by the accuracy of the prediction techniques.

The following section describes the analytical techniques used to verify the ablative and structural suitability of the basic nozzle design, modifications of the techniques to set baseline conditions, and the establishment of prediction techniques for nozzles containing ablative and structural discrepancies.

A. HEAT TRANSFER ANALYSIS

1. Verification of Basic Nozzle Design

The need for a rigorous, realistic thermal analysis technique requires techniques that encompass all modes of heat and mass transfer, including convection, radiation, conduction, and corrosion-erosion.

a. Exhaust Gas Composition and Transport Properties

The local thermal environment must be evaluated independently and used as input to the charring-ablation computer program. To establish

VII.A. Heat Transfer Analysis (cont)

the required parameters, certain data pertaining to the properties of the heat transfer media must be available. This includes the propellant combustion product composition for any region of interest, thermal properties (specific heats, thermal conductivity), transport properties (viscosity, diffusion coefficients and Prandtl number). For the propellant used in this program, a list of the moles of each chemical specie per 100 grams of propellant are shown in Table VII-1. The data, which were obtained by analytical methods, together with the local pressure and temperature, are subsequently used to obtain theoretical values of the thermal and transport properties. For chamber pressures of 500 and 1000 psia the following were obtained:

	500 psia	1000 psia
Chamber Temperature, °F	5719	5836
Specific Heat, Btu/lb-°F	0.494	0.496
Prandtl Number	0.490	0.493
Viscosity, lbf/sec	6.28×10^{-5}	6.36×10^{-5}
Mass Flow Coefficient	0.0063	0.0063
Thermal Conductivity Btu/hr-ft-°F	0.227	0.230

The particular method of obtaining these properties represents a rigorous development of the kinetic theory of monatomic molecules (Reference 13). The properties of each individual specie are first computed at the specified conditions. Subsequently, these results are modified by two factors. The first, which is again derived from kinetic theory, uses combining laws to obtain properties of multi-component gas mixtures. The second factor, often referred to as the "Eucken" correction, is applied to gas molecules which possess internal degrees of freedom. Since the internal structure influences the transport of energy, this correction will have a primary effect on the value of thermal conductivity.

VII.A. Heat Transfer Analysis (cont)

In the calculation of heat transfer coefficients viscosity is assumed to vary as the 0.65 power of temperature. The remainder of the listed properties are assumed to be independent of the temperature.

b. Flow Field Analysis

Since the local convective heat transfer is dependent, not only on the local flow conditions, but also on the upstream development of the boundary layer, the product of local density and the velocity component parallel to the wall is required to facilitate heat flux calculations. Three separate methods were applied at various regions to calculate the local surface mass fluxes within the nozzle.

Since the test motor was designed to incorporate a core (internal) burning grain, flow concentrations due to grain design are eliminated and the initial flow streamlines are uniform and axisymmetric. Thus, the use of one-dimensional isentropic flow relationships is considered applicable in high subsonic area ratio regions of the nozzle. This method, in addition to its obvious ease of calculation, provides reasonable estimates over more rigorous methods such as potential flow theory in areas where the wall curvature is not excessive.

The entrance of the test nozzle is in the same category (45 degree half-angle convergent section), consequently the assumption is made that the velocity and other properties vary along and not across streamlines. Using the mass continuity relationship and the fact that the maximum mass flow is dependent only on the upstream pressure, the local mass flux becomes a function of area ratio only.

VII.A. Heat Transfer Analysis (cont)

Thus $$(\rho V)_{local} = \frac{A_t}{A_{local}} (\rho V)_{max} \qquad \text{(Equation 3)}$$

and, $$(\rho V)_{max} = C_o P_c$$

therefore; $$(\rho V)_{local} = C_w P_c A_t / A_{local}$$

This one-dimensional approximation is considered valid for predicting the flow along the chamber side wall and the conical convergent section. However, in the subsonic region near the geometric throat, the influences of wall curvature, pressure gradients and the boundary layer accelerates the flow to slightly higher Mach number than predicted by Equation 3. Thus, the use of cold-flow model pressure measurements was used to predict local surface mass flux in this area. The internal contour of the test nozzle is formed by a constant 3.5 in. (7.26 cm) radius circular arc (radius ratio 2:1) which is tangent to a 45 and 17.5 degree half-angle entrance and exit cone, respectively. This particular configuration has been tested and the local surface Mach numbers up to and including the throat station have been measured by the above noted cold-flow technique. In the supersonic region, the flow field was obtained by the "Method of Characteristics" using an effective isentropic exponent ($\gamma = 1.2$).

The three separate methods describe the entire flow field as depicted in Figure VII-1. Here the local surface Mach number is plotted as a function of axial station. As noted, the actual Mach number at the geometric throat is approximately 1.14 while the sonic point, which coincides with the peak heat flux, occurs slightly upstream.

VII.A. Heat Transfer Analysis (cont)

c. Heat Transfer Criteria

Having discussed the preliminary data requirements, i.e., the exhaust gas composition transport properties and the local flow field, there remains the problem of establishing the net heat flux from the two-phase, high temperature exhaust gas to the exposed surface of the nozzle. The basic mechanisms which govern this energy transfer can be placed in three categories:

- convection from the gases
- radiation from metal oxides (particles)
- energy due to particle impingement

The methods used during this program to evaluate each mode of heat transfer are discussed in the following paragraphs.

(1) Convection

The rate of heat transfer between any high-velocity fluid and its bonding surfaces can be expressed by an equation of the form:

$$\dot{q}_c = h_c \, (T_{BL} - T_w) \qquad \text{(Equation 4)}$$

Thus, to predict convection heat fluxes, the driving temperature, T_{BL}, and the appropriate coefficient, h_c, represent the unknowns that must be evaluated. The instantaneous, local wall temperature, T_w, usually is known or can be computed as part of a transient thermal analysis.

VII.A. Heat Transfer Analysis (cont)

A standard approach has been adopted to evaluate the driving temperature. From the well established boundary layer concept, where the flow velocity is retarded as the wall is approached, an energy balance or an adiabatic surface indicates the maximum temperature the surface could attain to be slightly less than the total temperature of the surrounding fluid.

The driving temperature can then be expressed in terms of an isentropic exponent and the local Mach number by the expression:

$$\frac{T_{BL}}{T_o} \text{ or } \frac{i_{BL}}{i_o} \quad \frac{2 + (\gamma - 1)\, r\, M^2}{2 + (\gamma - 1)\, M^2} \qquad \text{(Equation 5)}$$

In this expression, the recovery factor denoted by "r" is related to the Prandtl number, evaluated by the method outlined in the previous section, by the relation which is appropriate for turbulent flow:

$$r = (Pr)^{1/3} \qquad \text{(Equation 6)}$$

The method used for evaluating the heat transfer coefficients is essentially the integral boundary layer growth method derived by Elliott, Bartz, and Silver (Reference 14). This procedure is directed toward axisymmetric nozzle flow, and considers the effect of pressure gradient on the simultaneous solution of the momentum and energy equations. The boundary layer shape parameters are approximated using a one-seventh power profile of velocity and stagnation temperature, while skin friction and Stanton nmmbers are evaluated as a function of the boundary layer thickness by use of Von Karman's form of the Reynolds' analogy. The local heat transfer coefficient (h_c) is related to the Stanton number (C_h) and the surface mass fluxes by the expression:

$$h_c \sqrt{C_p} = C_h (\rho V) = h_c' \qquad \text{(Equation 7)}$$

The boundary layer analysis is used to calculate Stanton number as a function of nozzle location.

VII.A. Heat Transfer Analysis (cont)

(2) Radiation

In analyzing the erosion and/or temperature predictions, the thermal radiation between the exhaust products and the exposed wall can be neglected. This conclusion has been substantiated by development of an analytical technique for calculation of particle radiation effects. The significant assumptions incorporated in this model are as follows: The solution considers the radiant heat transfer between a bounding surface and participating medium. Within the medium (an anisotropically scattering, absorbing, and emitting cloud) convective heat transfer between the particles and the gas, between the turbulent boundary layer and the plate, and the energy balance which relates the temperature gradient parallel to the plate with the heat flux normal to the plate is included. The resulting technique which represents an analytical estimate of the net absorption, emission, and thermal scattering of the individual particles within the cloud indicate that the radiation heat flux to the wall is typically less than 5% of the isothermal blackbody calculation. Since the added complexity of estimating the effective emittance for each analysis station is not warranted because of the small predicted contribution it is considered valid to ignore the radiation contribution in analyzing the heat flux to the exposed surfaces during a firing.

(3) Particle Impingement

The analytical method that has contributed to the understanding of the impingement problem is the determination of particle trajectories from a knowledge of the gas flow field. The usual procedure is to first approximate the gas-flow field by any of the previously discussed methods (potential flow, cold flow). Then, using the second law of motion and an appropriate drag law for various sized particles, the velocity and direction of each individual particle can be traced through the chamber to predict local areas of impingement. Previous application of this technique has revealed that

VII.A. Heat Transfer Analysis (cont)

entrance regions could be designed to minimize the effects of particle impacts. For example, if the wall curvature is gradual the particle impaction can then be ignored. Also, grain design has an important influence on impaction. It has been found, for example, that cylindrical ports or end-burning grains are desirable in reducing particle effects. Since the test motor was designed as an end-burner, the role of particle impingement is believed to be much less important than either the radiation or convection contribution.

In summary, for the thermal analysis of the basic nozzle, the net heat flux to the nozzle surfaces can be considered to be governed solely by Equation . The local heat transfer coefficient, h_c, evaluated using a boundary layer growth solution, is shown as a function of nozzle axial length in Figure VII-1. Also presented in this figure is the Mach number distribution, which together with an isentropic exponent (γ - 1.2) characterizes the flow field. Each of these curves represents values for the original non-eroded contour. The eight analysis stations within the nozzle are defined in Table VII-2. The heat transfer coefficients are noted to vary within the analysis regions between values of 249 (1412) to 1535 Btu/hr/ft^2-°F (8703 W/m^{2}k).

In addition, since the grain design is not neutral and throat area is changing, it is necessary to adjust the above heat transfer coefficients to compensate for variations in chamber pressure. It is to be noted that the heat transfer coefficients given in Figures VII-1 and Table VII-2 represent values at a chamber pressure of 500 psia. For any specified pressure they were varied according to the following expression.

$$(HTC)_{P_c} = h_{(P_c = 500)} \times (P_c/500)^{.8} \quad \text{(Equation 8)}$$

VII.A. Heat Transfer Analysis (cont)

d. Thermal Behavior of a Plastic Ablator

Typical insulation materials for large booster application are composites that consist of a resin system and inorganic fillers. In the analytical treatment of such a composite, the resin component is considered to have a fraction that decomposes when it is heated and a residual (char) that remains after decomposition. In discussing the role of the various components, it is convenient to divide the material into three distinct zones: the virgin material, the decomposition zone, and the fully charred zone.

In the virgin layer, the thermal transport phenomena are relatively simple. Since temperatures are relatively low, there are negligible changes in material properties and the thermal response is defined by simple conduction and absorption of sensible energy.

Within the decomposition zone, the material response becomes considerably more complex. The resin material decomposes by a kinetically controlled process that is observed to be time- and temperature-dependent. As the temperature increases, the decomposition also increases and produces a substantial weight loss. The weight loss represents the pyrolysis gas rate. The rate of change of the density of the solid phase is obtained from equations that describe the decomposition rates of the solid phase components. These relations may be written in the form:

$$\frac{\alpha \rho i}{\alpha \Theta} = -B_i \quad \rho o_i \left(\frac{\rho i - \rho r_i}{\rho i} \right)^{\psi_i} \quad \text{EXP } [-\Delta E/RT]_i \qquad \text{(Equation 9)}$$

As decomposition begins, two energy transfer modes are present. In addition to the usual conduction, energies transported by the decomposition gases that transpire toward the heated surface. It is assumed that these pyrolysis gases are

VII.A. Heat Transfer Analysis (cont)

in local thermal equilibrium with the char. Thus, the magnitude of the energy associated with the internal ablation process is a heat of decomposition and a sensible enthalpy increase of the gases.

In the third, or char zone, characteristics similar to those in the decomposition zone can be expected. As a result of very high temperatures, continued decomposition of organic components will occur and in some cases, there will be a decomposition of inorganic components (such as the loss of occluded water in asbestos fillers). The final product after complete decomposition will consist of a lower density char layer made up of carbanaceous residue and any remaining filler material. The modes of energy transfer and absorption will be similar to those that occur in the decomposition zone.

e. Surface Regression

Thus far, the discussion has pertained to the response that occurs in the internal structure of a typical insulation material when it is exposed to solid propellant exhaust products. As exposure continues, surface material is lost by erosion. The relative performance therefore becomes a measure of how well a particular material can resist chemical corrosion and/or mechanical removal. Aerojet has adopted the term "surface regression" to describe the various modes of surface loss. These could include surface chemical reactions (oxidation of carbon residue) with the propellant exhaust products, erosion from pressure and shear forces acting on the low density char layer, structural failure of the char as the result of thermal stresses, spallation resulting from pressure buildup within the decomposition zone, and combinations of chemical and mechanical modes acting on the exposed surface (i.e., particle impacts).

VII.A. Heat Transfer Analysis (cont)

The particular type of computer program which has been successfully used for evaluating nozzle erosion is basically the program described in Reference 15. This particular program is available to industry contractors and has been widely used for analyzing ablative nozzles for solid propellant boosters. A modified version is presently being used by Aerojet to predict the rate of surface regression, internal degradation rate (charring), and the transient temperature distributions in ablative insulations. The analytical treatment of these quantities requires first that the local environment be evaluated at the exposed surfaces (as discussed previously). Subsequently, these data are used as the boundary conditions to solve the one-dimensional transient heat conduction equation. The solution of this relationship defines the temperature distribution within a nonreacting body. For ablative materials that decompose in depth, additional equations must be considered to account for the decomposition reactions and the transpiration of the gas-phase decomposition products. The energy equations and the corresponding mass balance relations are therefore solved simultaneously by the above program. A complete derivation of the appropriate equations have been reported by several sources and will not be repeated here (References 15 and 16).

The particular form of the energy equation which contains the ratio of the mass transfer coefficient to the convective heat transfer coefficient (equivalent to Lewis Number to the 2/3 power), allows by proper choice of Lewis Number a relationship between heat and mass transfer. If it is assumed that the surface material is removed solely by a reaction characterized by a diffusion-limited process, and the Lewis Number is taken as unity, then the mass transfer and convective heat transfer coefficients are exactly equal. The resulting erosion rate then becomes proportional to the magnitude of the local heat transfer coefficient. The importance and usefulness of this assumption will be discussed further.

VII.A. Heat Transfer Analysis (cont)

(1) Analytical Approach - Erosion-Corrosion

As noted in the previous section, the analytical ablation model considers the surface removal to be controlled by chemical or mechanical interaction between the exhaust gases and the surface material. The procedure used to predict ablative performance depends on the type or class of material being considered, i.e., carbonaceous or silica type materials.

In carbon composites, the surface regression is considered to be controlled by oxidation reactions between the water, carbon dioxide and lesser amounts of other oxygen bearing species in the exhaust products. To estimate the chemical response in terms of a dimensionless mass removal rate of carbon, two different methods are available. The first assumes that thermo-chemical equilibrium exists and thus computes the equilibrium composition of gas and carbon adjacent to the wall. The second method performs essentially the same calculation; however, instead of the equilibrium assumption, separate reactions which control the carbon removal are considered to be kinetically controlling. In the second method, which is used in this analysis, the carbon char erosion becomes strongly dependent on the surface temperature.

Below a value of 3000°F (1667K) no surface removal will occur since the reaction rates are extremely low, yielding results that are in agreement with experimental data for both graphite and carbon composite throats. (The equilibrium assumption typically overpredicts the instantaneous erosion for a particular nozzle operating condition by a factor of two or three). The assumption of kinetic reaction rates was felt to be the more realistic and was adopted for this program.

VII.A. Heat Transfer Analysis (cont)

The propellant used in this Deviation Nozzle Program, ANB-3066, has a fairly high oxidation potential. This is made evident by comparing the important oxidizing species of the propellants used in the Low Cost Nozzle Program (Reference 8) with ANB-3066.

Propellant	H_2O*	CO_2*
ANP-2862	0.5557 moles/100 gm	0.056
ANP-2864	0.5278 moles/100 gm	0.0529
ANB-3066	0.7146 moles/100 gm	0.0779

The difference in oxidation potential between the two is estimated to be 25 percent. For the ANB-3066 propellant, the resulting erosion prediction data for MX-4926 carbon composite are summarized in Figure VII-2. This figure shows the dimensionless mass removal rate of carbon char ($\dot{m}_c/C_M$) as a function of reaction temperature (or surface temperature) for the four analysis stations in the throat region. The difference noted between mass removal rate at the four stations (solid lines) is attributed to variation in the ratio (C_m/P) at each position. The dashed curve in Figure VII-2 shows the influence of dimensionless pyrolysis gas injection rate on the mass removal at the throat station. At the typical surface temperature which occurs during a firing, approximately 5100°F, the correction due to a dimensionless pyrolysis gas injection rate of 0.03 is noted to be about 25 percent. For other gas rates, the correction which is similarly applied at all stations is assumed to vary linearly between the two calculated values.

*At chamber pressure - 500 psia

VII.A. Heat Transfer Analysis (cont)

Analytical-empirical procedures developed to predict the performance of carbon fabric composites such as those discussed above have been used in a wide variety of development programs. It is to be noted that existing analysis procedures are continually being revised on the basis of their ability to predict, within acceptable limits, the performance characteristics of such materials. The charring-ablation program with experimentally adjusted input parameters has proven to be a realistic approach to defining the mechanism of degradation that occurs in carbon-base materials.

(2) Silica Cloth Material

To apply the above charring-ablation model to a silica cloth material, it is again first assumed that the surface material is removed solely by a mechanism which is characterized by a diffusion-limited process. The mass transfer is then calculated assuming a unity mixture Lewis number, thereby making the mass transfer and convective heat transfer coefficients equal. The resulting erosion rate then becomes proportional to the magnitude of the local heat transfer coefficient. By plotting the experimental surface mass regression rate as a function of local convective heat transfer coefficient, the resulting slope then becomes the scaling parameter $(\dot{m}_{ch}/C_m)^*$ required as input to the charring-ablation program. With this parameter, it is possible to predict erosion in any motor in which the local value of heat transfer coefficient is accurately known. Based on the results of numerous nozzle firings using silica fabric composites, the dimensionless char removal

---

*Scaling parameter $= \dot{m}_{CH}/C_m = \dfrac{\dot{a}\,\rho_c}{h_c/\bar{C}_p}$

Where: $\dot{a}$ = erosion rate, ρ_c = char density, $\bar{C}_p$ = specific heat of exhaust gas and h_c = convective heat transfer coefficient

VII.A. Heat Transfer Analysis (cont)

rate which best fits the data is depicted in Figure VII-3. The particular functional relationship with surface temperature is again adjusted on the basis of experimental evidence. Below 3960°F (2200°K) the erosion of silica is found to be negligible, while between 4000 and 5000°F the temperature controls the removal rate. Above 5000°F (2778°K), the erosion becomes independent of surface temperature and is controlled by the local heat transfer coefficient.

(3) Summary of Thermal Behavior Model

The prediction of ablative material performance in the Deviation Nozzle Program was accomplished by using a charring-ablation computer program which solves the energy transport processes that occur in the virgin, decomposition zone, and char layer. The treatment of surface regression depended on the type of material. For carbon cloth, a kinetically controlled oxidation reaction rate technique was used for defining the char removal rate as a function of surface temperature. In lieu of a more rigorous model for surface regression of silica cloth, a provisional model was used. Treatment of the surface regression for silica essentially combines all modes of regression (i.e., surface melting, mechanical erosion, etc.) into an effective removal rate which is obtained from previous motor firing experience.

f. Experimental Data Requirements

To predict the thermal response of a given ablative material in a particular nozzle environment by the analytical methods discussed above it is necessary to have available the thermal conductivity, specific heat, density, decomposition rates, and weight ratio of resin in a particular component. The first three are typical thermal properties which are required to solve the transient conduction equation. All values are directly measurable and are shown for a significant number of material samples in Section IV.B. of this report.

VII.A. Heat Transfer Analysis (cont)

Typical values which were ultimately used in the charring-ablation program are presented in Figures VII-4 and VII-5. In these figures, the thermal diffusivity and specific heat for a particular carbon cloth and silica cloth component, respectively, are given as a function of temperature. Values at the lower temperatures are based on a density equal to the measured value for the virgin sample. Above 2000°F (1093°C) where the particular material is considered completely charred, the appropriate char density is used. In the temperature range between the initial resin decomposition and final char formation, the charring ablation program automatically interpolates linearly between the two curves using the instantaneous density as a parameter.

The temperature dependent rate of decomposition of the resin system considered in this effort is expressed in the form of an Arrhenius relation as given previously by Equation 9. Determination of the constants B, ψ, and ΔE is accomplished by curve fitting experimental thermogravimetric analysis data for a particular resin at a constant heating rate. It is to be noted that several techniques exist for evaluating the constants as well as for determining appropriate values for phenolic resin (Reference 17). The values which are considered appropriate for both the material systems considered herein are presented in the following table (Reference 18).

Decomposition Rate Constants
for Phenolic Resin

Reaction	Frequency Factor - B	Order Reaction - ψ	Activation Energy - E'
A	1.4×10^4 1/sec	3.0	15400°R
B	4.48×10^9	3.0	36800

VII.A. Heat Transfer Analysis (cont)

The constants in the above table define the rates at which the phenolic resin decomposes. To relate this with the actual density variation of the respective ablative component, knowledge of the resin weight or volume fraction is required. In general, the weight fraction is the logical parameter to measure or predict. Knowing the virgin density, phenolic resin density and the weight fraction of resin, the volume fraction is given in the following expression:

$$\Gamma = f \frac{\rho_r}{\rho} \qquad \text{(Equation 10)}$$

From which the density of the particular ablative sample can be evaluated from its component parts, namely resin and filler, from the expression:

$$\rho_v = \Gamma\rho_r + (1-\Gamma)\,\rho_c \qquad \text{(Equation 11)}$$

Likewise, the char density can be evaluated in terms of the volume fraction of resin, carbon residual after decomposition and virgin density by:

$$\rho_{CH} = \rho_v - (\rho_r - \rho_{rf}) \qquad \text{(Equation 12)}$$

The carbon residual fraction, which represents the amount of carbon yield subsequent to complete decomposition of the resin, is given in Reference 18 as 40 percent. Based on char and virgin density measurements made during this present program a value of 33 percent best represents the data and was therefore used.

Equations 9, 10, 11, and 12 define the density variations between virgin and fully charred material that can occur for a given weight fraction of resin. Thus, each individual analysis of a particular defect required appropriate adjusting of the resin volume fraction and filler density to properly account for the total weight loss during decomposition.

VII.A. Heat Transfer Analysis (cont)

2. Modification of Thermal Response Analysis

The first series of analyses were performed on the nozzle design defined in Aerojet Drawing 1147248, (Figure III-4). These predictions were performed early in the program to verify design of the so-called "base case" in which a common material, MX-4926 carbon cloth, was investigated under environmental conditions which simulated the anticipated actual firing conditions. The preliminary results indicated that the design was thermally adequate since thermal penetration was not considered excessive. All bond lines between the various flame inserts and the backup insulators remained essentially virgin material. Temperatures within the steel housing remained at ambient (initial) values.

The results of this preliminary investigation were presented in Section III.C. Figure III-10 represents the predicted regression and char growth as a function of time. Total throat erosion amounted to 0.275 in. (10.7 mils/sec) and the char depth (defined as the 750°F isotherm) subsequent to complete heat soak was estimated to be an additional 0.285 in. (0.70 cm) for a total depth of 0.56 in. (1.42 cm) from the original contour.

From the results of the early firing, including the two baseline (defect free) nozzles, it was apparent that the preliminary erosion and char estimates were quite conservative. The actual erosion at the throat amounted to 75% of the predicted value while the measured char zone thickness was lower by a factor of 66%. To be capable of predicting small variations in defective parts, it was felt that the analytical model should do a better job on the baseline nozzle. Therefore, the general input data were reviewed for apparent sources of error.

VII.A. Heat Transfer Analysis (cont)

The first and most logical inherent error was the use of an estimated pressure-time curve (see Figure III-3) instead of the actual pressure history of the baseline firings. Secondly, the heat transfer coefficients were re-evaluated to better account for the full growth of boundary layer between the grain surface and the throat. This added approximately 8 inches of flow length and ultimately reduced the throat heat transfer coefficient by about 11 percent. A third correction pertained to the injection of pyrolysis gas into the boundary layer and its influence on the char removal rate. At early times, the rate of decomposition of the resin is quite high and its transpiration through the char tends to delay both the surface temperature rise and the surface chemical reaction rates. Thus, as often occurs in short firings, the surface regression at early times is somewhat lower than later when there seems to be negligible influence from injection of pyrolysis gases. The net effect is a reduced regression rate during the first few seconds followed by an increase to normally predicted values based on surface corrosion and the local heat transfer coefficient.

Applying the above criteria to the baseline nozzle (S/N 002), the revised prediction of the thermal response at the throat (Station 4) is presented in Figure VII-6. Here the thermal gradient (i.e., temperature as a function of depth below the surface) is presented for times of 26 and 40 seconds. At 26 seconds, which represents the end of the firing, the predicted erosion (0.208 in. (0.529 cm)) is now in much better agreement with the range of the measured data from the two baseline firings (0.14 (0.356 cm) to 0.23 in. (0.585 cm)), see cross-hatched zone in Figure VII-6. Although the two baseline nozzles were expected to perform in a like manner, the actual erosion pattern showed considerable variation between firings. For example, at the throat station the actual erosion varied at the measurement locations as follows:

VII.A. Heat Transfer Analysis (cont)

Angular Location, degree	Throat Erosion			
	Baseline SN 001,		Baseline SN 002,	
	in.	cm	in.	cm
0 and 180	0.20	0.51	0.23	0.585
90 and 270	0.16	0.406	0.23	0.585
135	0.14	0.356	0.19	0.484
Average	0.17	0.431	0.22	0.560

The erosion experienced by SN 001 is between 15 and 40 percent lower than the respective values for SN 002. In general, this trend which appears at essentially all measurement stations, is not unique in that such unexplained differences have occurred in previous programs. For example, the average throat erosion for Motors 260-SL-1 and -2 varied by 15 percent. Based on the above comparison and the fact that the predicted erosion was within 8 percent of the average measured value, the analytical technique was considered satisfactory and no further corrections would be required.

In the exit cone, the modified thermal response of silica cloth, again predicted for baseline nozzle SN 002 is presented in Figure VII-7. Temperature gradients are given for 26 and 40 seconds. The predicted erosion is noted to be 0.060 in. (0.152 cm). Based on these results, it is likewise concluded that the analytical technique for predicting silica cloth thermal response is valid and additional attempts to improve the method are not warranted at this time.

Having established a reasonable correlation between the predicted and measured erosion at the throat and in the exit cone, the analytical model was subsequently used to calculate the thermal response at all eight stations along the contour. The resulting erosion, visible char and total char zone depths are summarized in Table VII-3. The erosion predictions have

VII.A. Heat Transfer Analysis (cont)

been discussed previously and no further comments are required except to note that the values presented represent the surface removal in the direction perpendicular to the local surface. With respect to the char depth predictions, the method of defining and comparing the proper value is not as straightforward. This is primarily due to the difficulty in assigning an analytical parameter to help define a depth below the surface which corresponds to a measured char value. For example, the usual practice is to section a fired nozzle component and measure the thickness of heat affected zone. This depth is usually discernible by an abrupt change in color and/or texture of the viewed cross-section, and is thus referred to as the visible char. In addition, close examination reveals a secondary char layer which presumably defines the thickness of the decomposition zone. A typical postfire cross-section in the baseline nozzle is presented in Figure VII-8. Here the erosion, visible char, and secondary char zone require experimental verification or trial and error approximation. Referring back to Figures VII-6 and VII-7 in addition to the temperature profiles, the predicted density distributions within the carbon cloth and silica cloth materials, respectively, are given for times of 26 and 40 seconds. From Figure VII-6, the density of carbon cloth is noted to vary between 90.1 lb/ft^3 (1.44g/cc) for the virgin material to 67.5 lb/ft^3 (1.08g/cc) for the fully charred state, and the depth for any intermediate density is easily obtained. Considering the density variation predicted at 40 seconds, the time required to assure maximum char growth, the density which yields a minimum measured char value of 0.34 in. (0.865 cm) corresponds to a factor 1 percent higher than the fully charred density. In a like manner, the density which corresponds to the average baseline nozzle char depth, 0.373 in. (0.95 cm) is a value 5 percent higher than the fully charred condition.

VII.A. Heat Transfer Analysis (cont)

In addition to using density profiles to define char growth, the local temperature could similarly be considered. From Reference 19, which describes the use of temperature sensors for measuring thermal profiles in ablative nozzles, it is shown by measurement that the maximum soak temperature at the visible char depth varies between 1000 and 1200°F (538 and 649°C). If a nominal value of 1100°F is assumed, then by plotting the envelope of the maximum temperature predicted for an arbitrary depth (as given by the dashed curves in Figures VII-6 and VII-7), the resulting char depth for carbon cloth is noted to be 0.40 in. (1.03 cm). This coincides with the upper limit of the measured data. At the exit cone station, the use of the 1100°F temperature to define the visible char depth is in excellent agreement with the actual data.

In brief, the analytical description of char depth in a fired nozzle must rely on somewhat arbitrary definitions. Density profiles with appropriate factors to describe the different char zones is one method; however, experimental verification of density distributions in ablative materials is scarce and incomplete. Thus, the use of maximum temperature remains the only logical parameter to define visible char depth. In the analysis to be presented for various nozzle defects, the maximum temperature envelope is plotted and the visible char depth defined as the 1100°F (593°C).

A summary of the erosion, visible char and secondary char zone predicted for the eight baseline nozzle analysis stations is presented in tabular form in Table VII-3 and plotted with respect to the original nozzle contour in Figure VII-9. An indication of the ability of the charring-ablation program to predict the thermal response throughout the baseline nozzle is provided in Figure VII-10. Here, the predicted erosion and visible char depth are compared to the combined results of the two baseline firings. The experimental results are presented in terms of both the range of values measured

VII.A. Heat Transfer Analysis (cont)

together with the average of all respective measurement positions. In general, the analytical results are in agreement and show the same trends as the test results. The highest erosion occurs upstream of the throat as the theory predicts, and decreases downstream in the same general manner. Erosion of silica cloth in the exit cone is in fair agreement with the test data; however, the trend is to underpredict by 0.03 in. (0.076 cm) near the carbon-silica transition and over-predict by 0.025 in. (0.0635 cm) near the exit plane. The only region where the analytical model fails is in the nozzle entrance section. Here the erosion depth for silica cloth is 0.10 in. (0.25 cm) less than the measured average. This variation is presumably due to a flow disturbance produced by high regression of the material used in the aft closure.

3. Prediction of Discrepant Material Performance

The analytical model predicts the same type of erosion pattern that occurred in the baseline nozzle. Since the measured data contains considerable scatter between maximum and minimum, exact correlation is impossible and improvements in the technique are not deemed necessary for predicting the performance trend of various ablative defects. As noted in Section III,A, the defect areas were placed in the entrance region, throat insert, and exit cone. Since the thermal model under-predicts the erosion in the entrance region, no further calculations were attempted. Thus, the analysis of defects in the throat (Station 4) and the exit cone (Station 7) only were considered.

Using the technique described above for the baseline nozzle, seven different ablative component discrepancies were analyzed. The particular nozzles selected for analysis represented all the types of possible anomalies considered in this program which can be predicted by the thermal model. These include; cure cycles, such as autoclave or vacuum bag; inconsistent resin-rich or -starved areas; and low apparent densities. The results of these calculations are discussed in the following paragraphs.

VII.A. Heat Transfer Analysis (cont)

Figures VII-11 through VII-19 represent the thermal profiles at burnout for the throat and exit cone station of each respective nozzle analyzed. Also noted in each figure is the maximum temperature envelope which is used to define the predicted visible char zone thickness. A summary of the thermal analysis results is presented in Table VII-4.

a. Baseline Nozzle

The thermal gradients for each baseline nozzle are again presented in Figures VII-11 and VII-12. These data have previously been discussed in detail and are provided only for the purpose of comparing the discrepant components with a defect-free nozzle.

b. Cure Cycles

The influence of cure cycle on ablative performance is depicted in Figures VII-13 and VII-14. Of the two cure cycles analyzed, vacuum bag and autoclave, the autoclave cycle compared favorably with the baseline erosion data, while the vacuum bag components result in a 42 percent higher prediction at the throat. Comparing these values with the actual firings indicates the autoclave parts perform somewhat better than baseline, 0.16 in. (0.406 cm) compared to 0.192 in. (0.489 cm) average, while the vacuum bag throat insert showed a 0.27 in. (0.686 cm) average erosion which is as predicted, 40 percent higher than the baseline.

In the exit cone, the predicted erosion differed by only 4.5 mils (0.0637 to 0.0683), while the measured values varied in the same manner between 0.02 in. (0.050 cm) for the autoclave cure and 0.05 in. (0.127 cm) for the lower density vacuum bag. The rather large variance in measured data for a given nozzle (up to four to one) make any conclusion regarding the analytical model somewhat difficult to reach.

VII.A. Heat Transfer Analysis (cont)

c. Resin Variation

The predicted thermal performances of nozzle components which reflect various resin-rich or -starved areas are presented in Figures VII-15, VII-16 and VII-17. The first two figures represent the resin-rich condition wherein the analytical model predicted 0.210 (0.534 cm) and 0.234 in. (0.595 cm), respectively, or a difference of 24 mils. Actual firing data is somewhat lower, being 0.178 (0.452 cm) and 0.193 in. (0.49 cm) average at the throat of each nozzle.

For the condition of resin starvation, the predicted erosion from Figure VII-17 is noted to be 0.207 in. (0.526 cm) which compares favorably with the measured value of 0.200 in. (0.50 cm). From the three sets of data, the analytical model will predict favorable performance as the resin content is reduced. However, this trend is not apparent from the firing data, since the resin-starved component is noted to have performed the worst and the 10-ply resin-rich insert the best. It is possible that normal variations, such as occurred between the two baseline nozzles, masked the small differences actually predicted (0.207 (0.526 cm) to 0.234 in. (0.595 cm) 27 mils total).

In the exit cone, the variation in predicted erosion is noted to be quite small. The highest predicted erosion is again a function of highest resin content or from Figure VII-16, 0.070 in. (1.78 cm). In contrast, the highest measured values occur in resin-starved areas. The reason for this anomaly is not readily apparent from the results of one firing. Additional data are required to verify the probable mode of failure for resin-starved silica components.

VIIA. Heat Transfer Analysis (cont)

d. Low Density

The remaining two nozzles analyzed reflect the performance induced by a low density component. Thermal profiles for these parts are noted in Figures VII-18 and VII-19, where the predicted erosion at the throat is 0.292 (0.742 cm) and 0.282 in. (0.717 cm), respectively. This compares to the firing results which are, 0.313 (0.795 cm) and 0.261 in. (0.662 cm) average. As noted, the influence of density for the throat insert is obviously treated in a reasonable manner by the thermal model.

In the exit cone, the influence of density again is not apparent due to the data scatter. The predicted erosion shows little effect by reduction in density. Conversely, the average measured erosion depth shows a lower value for a lower density part; however, the data scatter may again mask the actual trend.

A tabulation of all predicted erosion and char depths together with analogous measured values for each respective nozzle analyzed is presented in Table VII-4.

B. STRUCTURAL ANALYSIS

1. Method

The structural analyses of the basic (Figure III-4) and revised (Figure VI-37) nozzle designs were based on finite element techniques. In this approach, the continuous structure of the composite is broken up into quadrilateral elements as shown in Figure VII-20. These are interconnected at

VII.B. Structural Analysis (cont)

their mutual corners (called nodal points). The model used in this program is shown in Figure VII-21. Three planes of reference were used: the axial, which is parallel to the nozzle centerline; the radial, which is normal to the nozzle centerline; and the hoop which lies in a circular arc around the nozzle centerline.

To analyze the capability of the structure the properties of the material used are input into the computer program, along with the variation of the properties as a function of temperature. Also input into the program are the pressure distribution along the gas flow surface and the temperature at the nodal points, both of which are obtained from the heat transfer analysis. The output of the computer program are stresses and strains for each element.

2. Verification of Basic Design

The properties of tape reinforced composites used for ablative nozzles are strongly anisotropic with respect to the lay of the fabric reinforcement. Consequently in the analysis of the basic design, the input properties were those of a composite whose ply orientation matched those of the specific nozzle component being analyzed with respect to the centerline.

The results of the analysis of the strains in the insulation overwrap of the exit cone 25 sec after fireswitch are plotted in Figure VII-22. Maximum strain was 0.00037 in./in. at the inside fiber of element 357. Similarly plots of the strain in the throat and entrance overwraps yielded the values shown in Table III-2.

VII.B. Structural Analysis (cont)

3. Analysis of Discrepant Nozzles

Material properties were determined using specimens cut from duplicate nozzle components, and whose loading axes were aligned radially, axially and tangentially with respect to the nozzle centerline (see Section IV.B.).

These measured properties were input into the computer programs for each of the flame liners to check for the liklihood of failure. Evaluation of the plotted output indicated that, with a steel nozzle shell no structural failure could be induced by any of the discrepancies. It was indicated that the rigid steel shell placed the plastic components in compression.

To revise the stress field in the nozzle assembly, computer runs were made using the original program, but reducing the thickness (deleting some of the elements in the input). In this way, it was indicated as a rough approximation, that the maximum hoop strain in the outside of the MX-2600 exit cone flame liner shown in Figure VI-37 would be 0.00196 in./in. at 12 sec after fireswitch and 0.0032 in./in. at 25 sec when fabricated without discrepancies. Since the original program used the temperature profile of the thick exit cone, the strains in the thinner exit cone would be somewhat lower due to a higher back-side temperature. A state of incipient structural failure was indicated, however, and any decrease in the material properties could lead to failure.

Table VII-1

Theoretical Equilibrium Gas Composition, moles/100 g

	P_c/P_e = 1000/14.7		P_c/P_e = 500/14.7	
Product	Chamber at 5836°F	Exhaust at 3434°F	Chamber at 5719°F	Exhaust at 3715°F
MCl	0.5000	0.6167	0.4959	0.6102
N_2	0.3103	0.3123	0.3100	0.3123
H_2O	0.7275	0.6913	0.7146	0.6974
N_2	0.8784	0.9368	0.8762	0.9278
O_2	0.0013	-	0.0019	-
O	0.0043	-	0.0061	-
OH	0.0444	0.0007	0.0513	0.0021
Cl	0.0477	0.0039	0.0580	0.0090
NO	0.0041	-	0.0046	0.0001
Cl_2	0.0001	-	0.0001	-
H	0.1255	0.0082	0.1531	0.0191
CO	0.7863	0.7599	0.7867	0.7664
CO_2	0.0783	0.1048	0.0779	0.0983
AlH	0.0001	-	0.0001	-
Al	0.0004	-	0.0005	-
AlCl	0.0128	-	0.0144	0.0001
$AlCl_2$	0.0291	0.0003	0.0256	0.0009
$AlCl_3$	0.0007	-	0.0005	-
AlO	0.0003	-	0.0004	-
Al_2O	0.0001	-	0.0001	-
AlOCl	0.0001	-	0.0001	-
Al_2O_3	0.2563(l)	0.2779(s)	0.2572(l)	0.2775(a)
Moles of gas / 100g propellant	3.5520	3.4350	3.5781	3.4438

Table VII-2

Revised Thermal Input Data

Station No.	Local Radius		Area Ratio, A/A_t	Axial Length		Heat Transfer Coefficient at 500 lbf/in.^{2} abs (3447 /mm^2 abs)		Adiabatic Wall Temperature, Taw	
	in.	(cm)		in.	(cm)	Btu/ft^{2}hr °F	(W/m^{2}K)	°F	(K)
1	3.25	8.26	3.45	7.75	19.68	591	3351	5716	3431
2	2.30	5.84	1.72	8.725	22.16	1010	5727	5700	3422
3	1.81	4.60	1.07	10.0	25.40	1535	8703	5632	3384
4	1.75	4.44	1.00	10.652	27.06	1490	8448	5564	3346
5	1.926	4.89	1.21	11.75	29.84	995	5642	5416	3264
6	2.95	7.49	2.84	15.0	38.10	498	2824	5256	3175
7	3.66	9.30	4.34	17.25	43.82	313	1775	5181	3134
8	4.055	10.30	5.40	18.5	46.99	249	1412	5132	3106

Table VII-3

Summary of Baseline Nozzle Predictions

Station No.	Material	Regression		Char (Includes Regression)							
				Case 1		Case 2		Case 3		Case 4	
		in.	(mm)	in.	(mm)	in.	(mm)	in.	(mm)	in.	(mm)
1	MX-2600	0.172	4.37	0.242	6.15	0.264	6.71	0.277	7.04	0.336	8.53
2	MX-4926	0.201	5.10	0.328	8.33	0.365	9.27	0.391	9.93	0.508	12.90
3	MX-4926	0.255	6.48	0.370	9.40	0.406	10.31	0.429	10.90	0.555	14.10
4	MX-4926	0.208	5.28	0.346	8.79	0.382	9.70	0.400	10.16	0.526	13.36
5	MX-4926	0.080	2.03	0.260	6.60	0.300	7.62	0.328	8.33	0.455	11.56
6	MX-2600	0.126	3.20	0.198	50.03	0.221	5.61	0.235	5.97	0.281	7.14
7	MX-2600	0.063	1.60	0.150	3.81	0.173	4.39	0.187	4.75	0.260	6.60
8	MX-2600	0.045	1.14	0.140	3.56	0.163	4.14	0.178	4.52	0.225	5.72

Case 1 corresponds to density 1% higher than fully charred density.

Case 2 corresponds to density 5% higher than fully charred density.

Case 3 - 1100°F (866 k) isotherm.

Case 4 corresponds to density 1% lower than virgin density.

Table VII-4

Results of Deviation Nozzle Thermal Analyses

Test No.	Nozzle Type	Nozzle SN	Carbon Erosion						Carbon Char				Silica Erosion						Silica Char			
			Predicted		Actual Max/Min		Actual Average		Predicted		Actual Average		Predicted		Actual Max/Min		Actual Average		Predicted		Actual Average	
			in.	(mm)	in.	(mm)	in.	(mm)	in.	(mm)	in.	(mm)	in.	(mm)	in.	(mm)	in.	(mm)	in.	(mm)	in.	(mm)
1	Autoclave	004	0.208	5.28	0.17/0.15	4.3/3.8	0.160	4.06	0.411	10.44	0.340	8.64	0.0637	1.618	0.04/0.01	1.0/0.3	0.02	0.5	0.190	4.83	0.130	3.30
2	Baseline	002	0.208	5.28	0.23/0.19	5.8/4.8	0.220	5.59	0.400	10.16	0.380	9.65	0.0633	1.608	0.06/0.03	1.5/0.8	0.04	1.0	0.186	4.72	0.180	4.57
3	Baseline	001	0.209	5.31	0.20/0.14	5.1/3.6	0.170	4.32	0.403	10.24	0.360	9.14	0.0638	1.620	0.06/0.03	1.5/0.8	0.05	1.27	0.187	4.75	0.190	4.83
4	Vacuum Bag	003	0.296	7.52	0.32/0.23	8.1/5.8	0.270	6.86	0.522	13.26	0.450	11.43	0.0683	1.735	0.07/0.02	1.8/0.5	0.005	1.27	0.201	5.10	0.180	4.57
7	Resin Rich, 20 plies	008	0.234	5.94	0.23/0.23	5.8/5.8	0.230	5.84	0.424	10.77	0.41	10.41	0.0704	1.788	0.04/0.03	1.0/0.8	0.033	0.84	0.192	4.88	0.200	5.08
10	Resin Starved, 10 plies	013	0.207	5.26	0.20/0.20	5.1/5.1	0.20	5.59	0.426	10.82	0.360	9.14	0.0636	1.615	0.10/0.10	2.5/2.5	0.100	2.54	0.196	4.98	0.230	5.84
16	70-80% Density	019	0.292	7.42	0.32/0.31	8.1/7.9	0.313	7.95	0.530	13.46	0.460	11.68	0.064	1.62	0.05/0.02	1.3/0.5	0.030	0.76	0.202	5.13	0.200	5.08
17	Resin Rich, 10 plies	007	0.210	5.33	0.21/0.21	5.3/5.3	0.214	5.44	0.421	10.69	0.370	9.40	0.0614	1.560	0.03/0.0	0.8/0.0	0.020	0.51	0.190	4.83	0.200	5.08
20	80-90% Density	020	0.282	7.16	0.30/0.22	7.6/5.6	0.261	6.63	0.511	12.98	0.417	10.59	0.0646	1.641	0.06/0.02	1.5/0.5	0.040	1.02	0.199	5.05	0.180	4.57

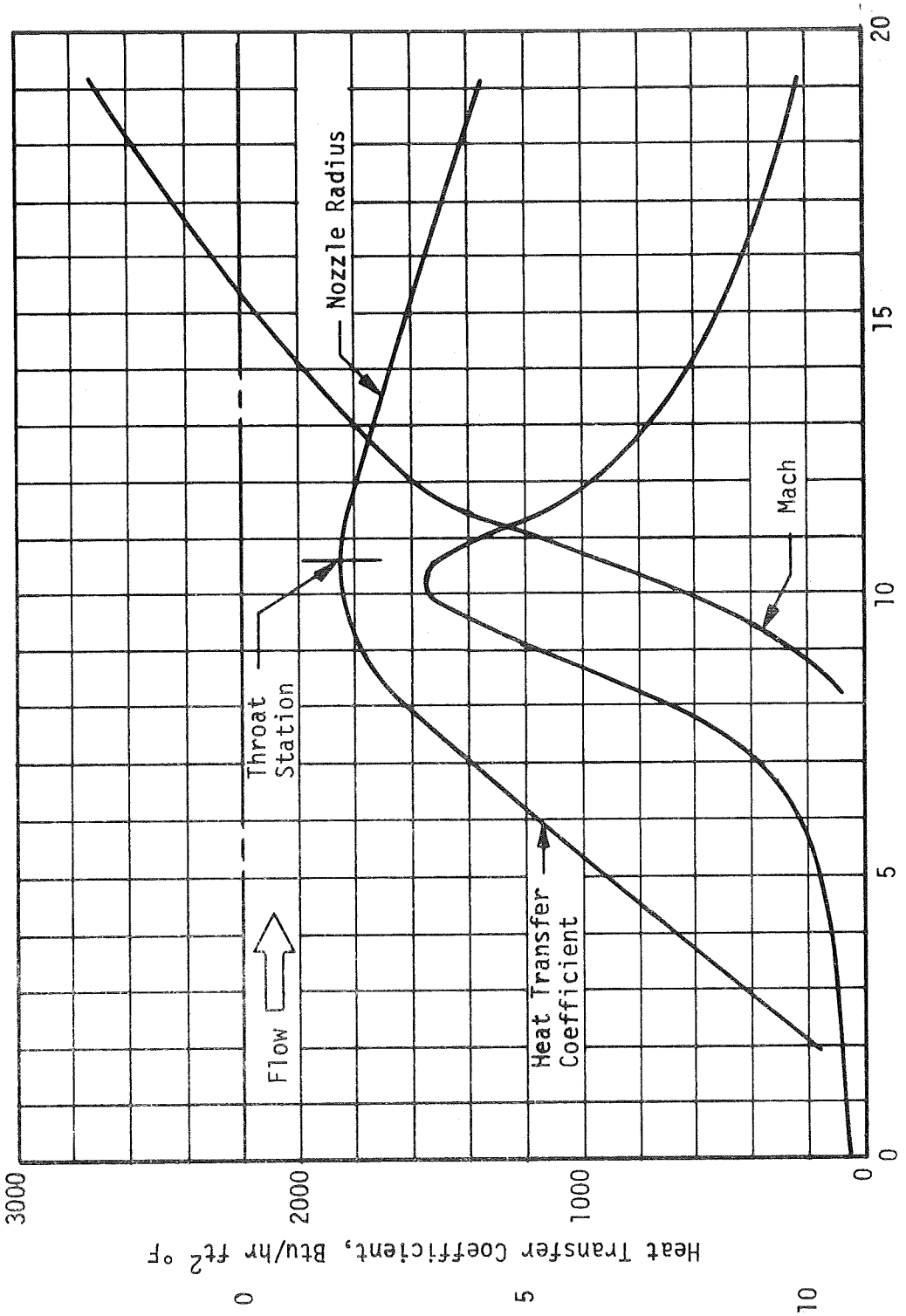

Deviation Nozzle Contour, Flow Field and Thermal Environment
(P_c, 500 psia)

Figure VII-1

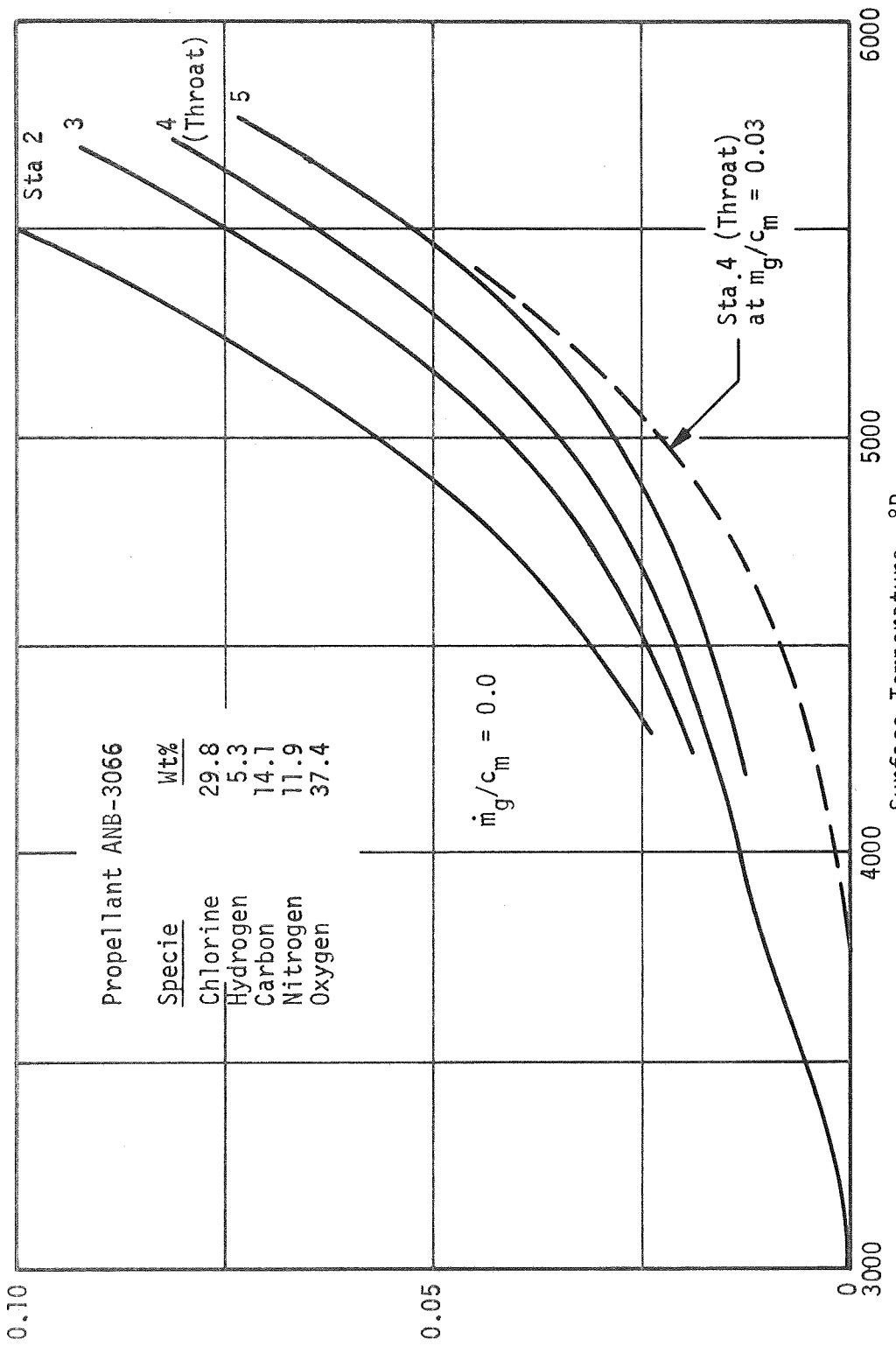

Dimensionless Char Removal Rate as a Function of Surface Temperature
(Carbon Cloth - MX 4926)

Figure VII-2

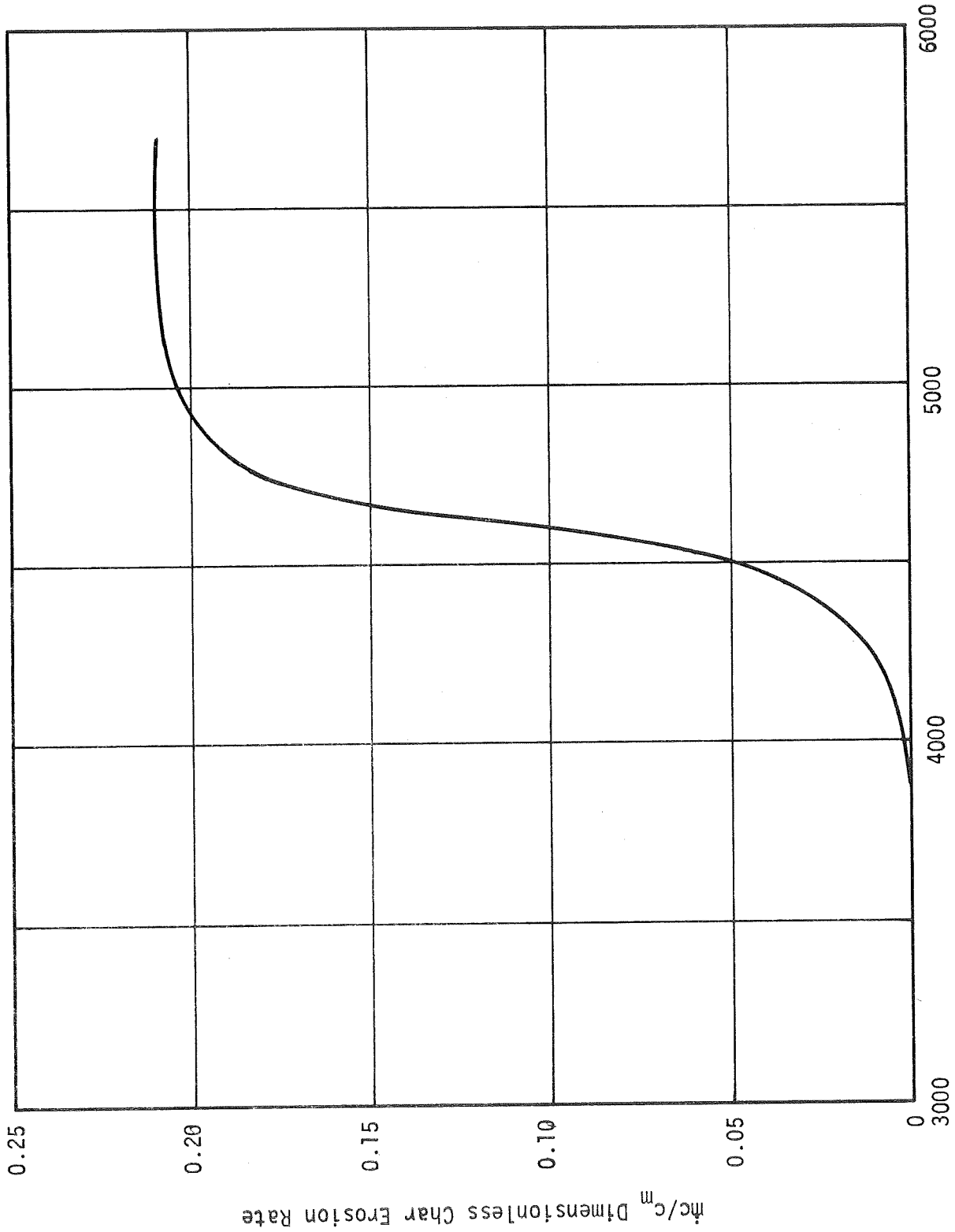

Dimensionless Char Removal Rate as a Function of Surface Temperature
(Silica Cloth)

Figure VII-3

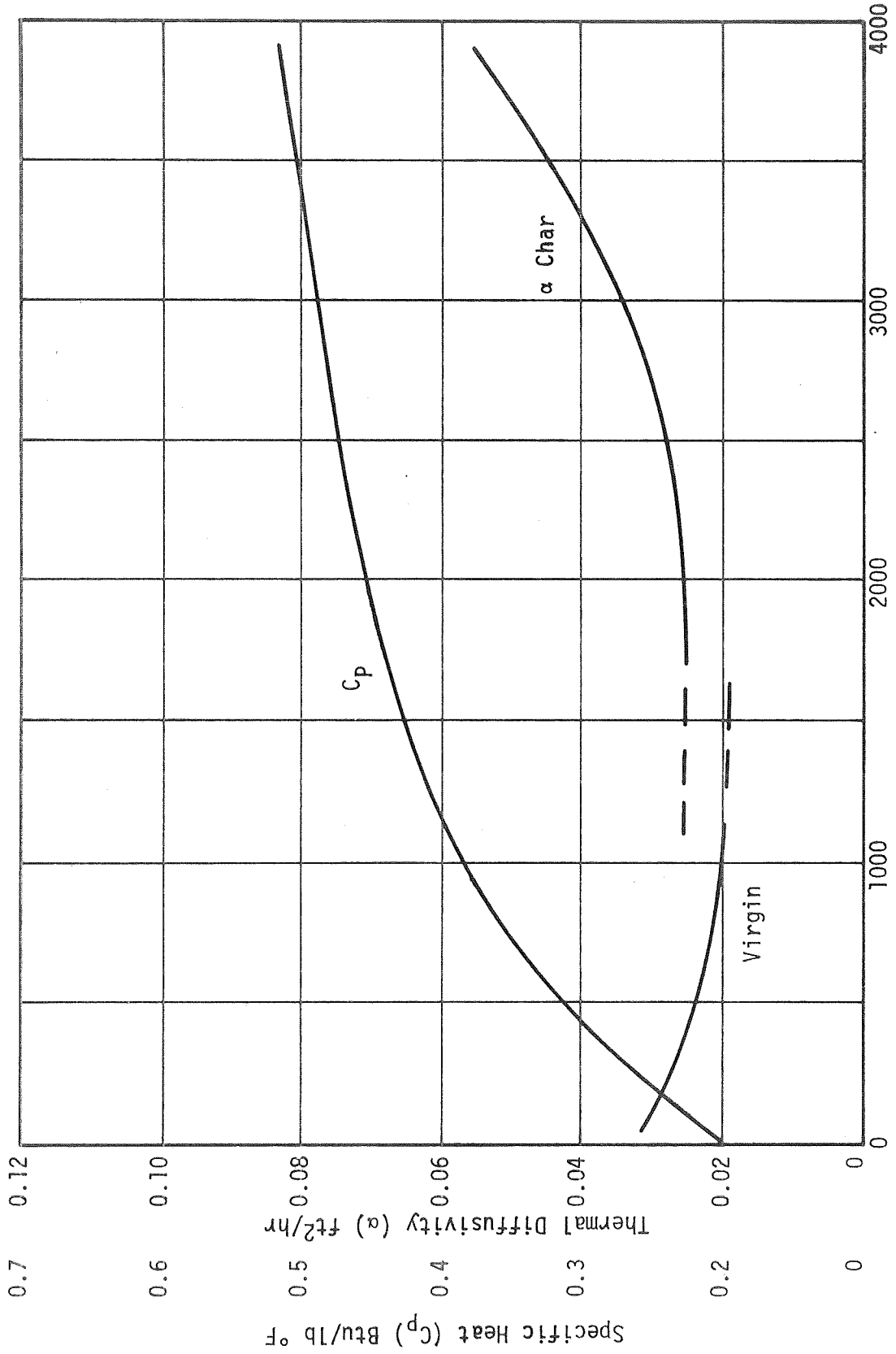

Thermal Properties for Carbon Cloth Phenolic

Figure VII-4

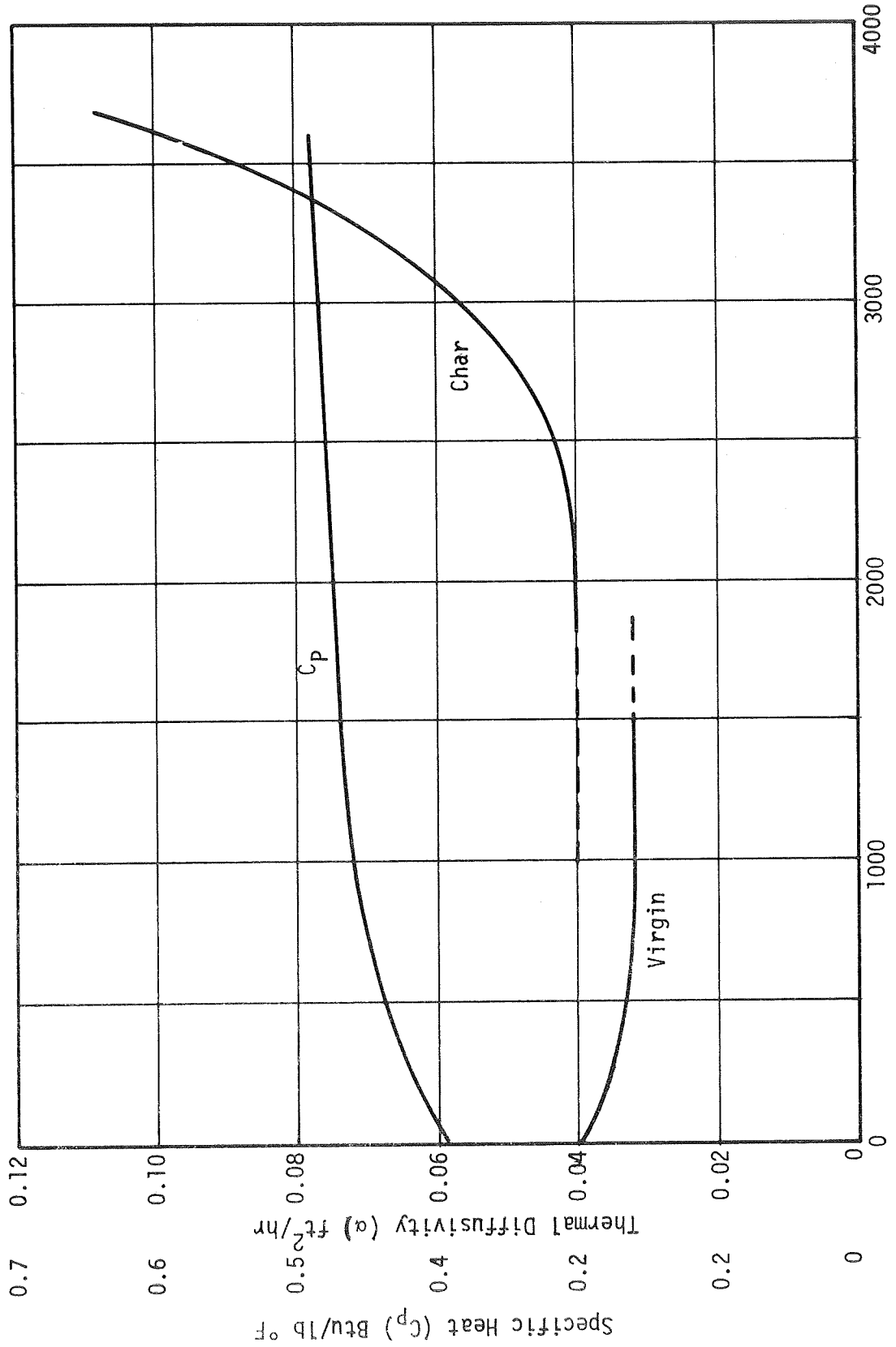

Thermal Properties for Silica Cloth Phenolic

Figure VII-5

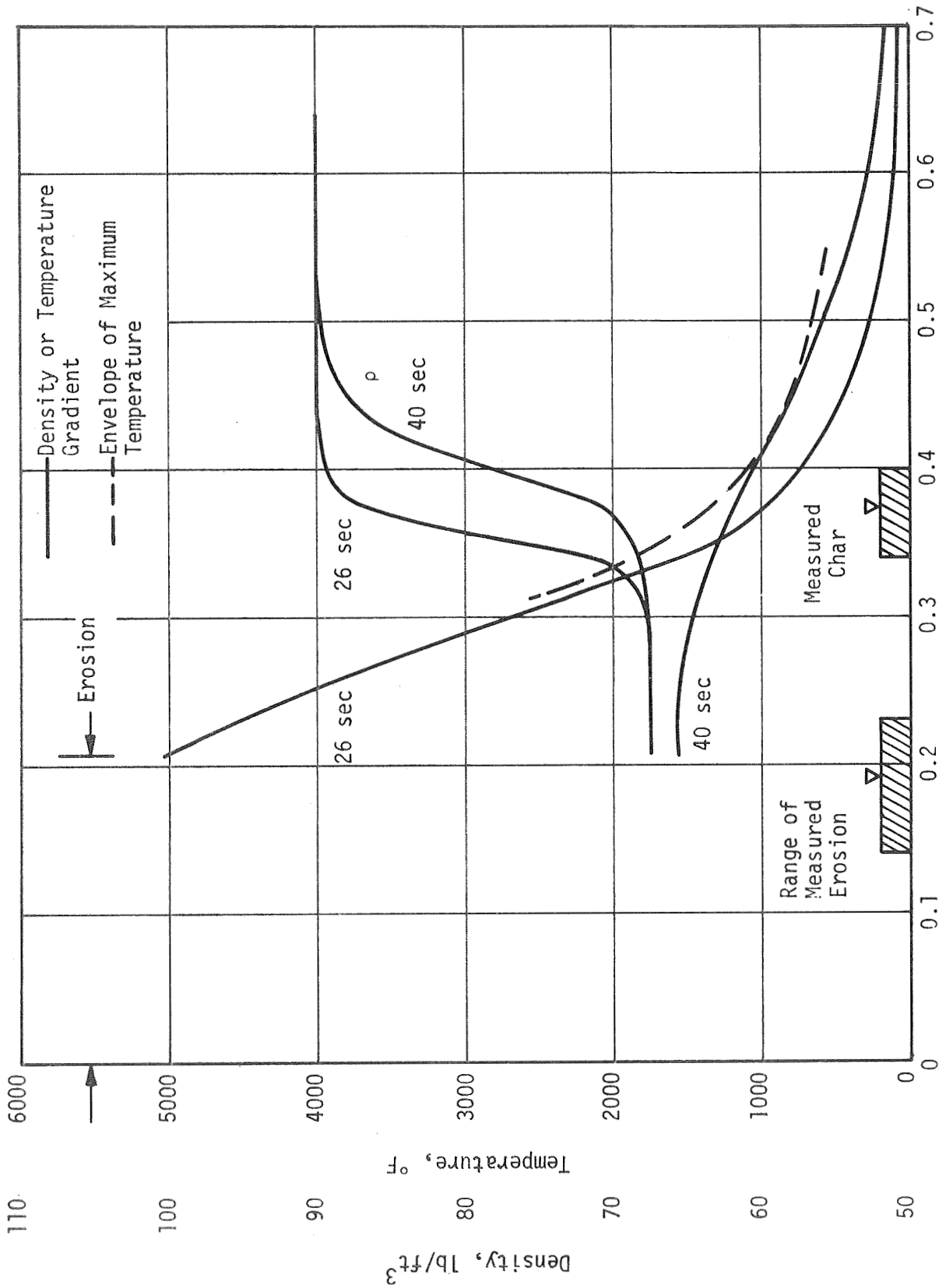

Thermal Response of MX 4926 Carbon Cloth at Throat of Deviation Nozzle (Baseline)

Figure VII-6

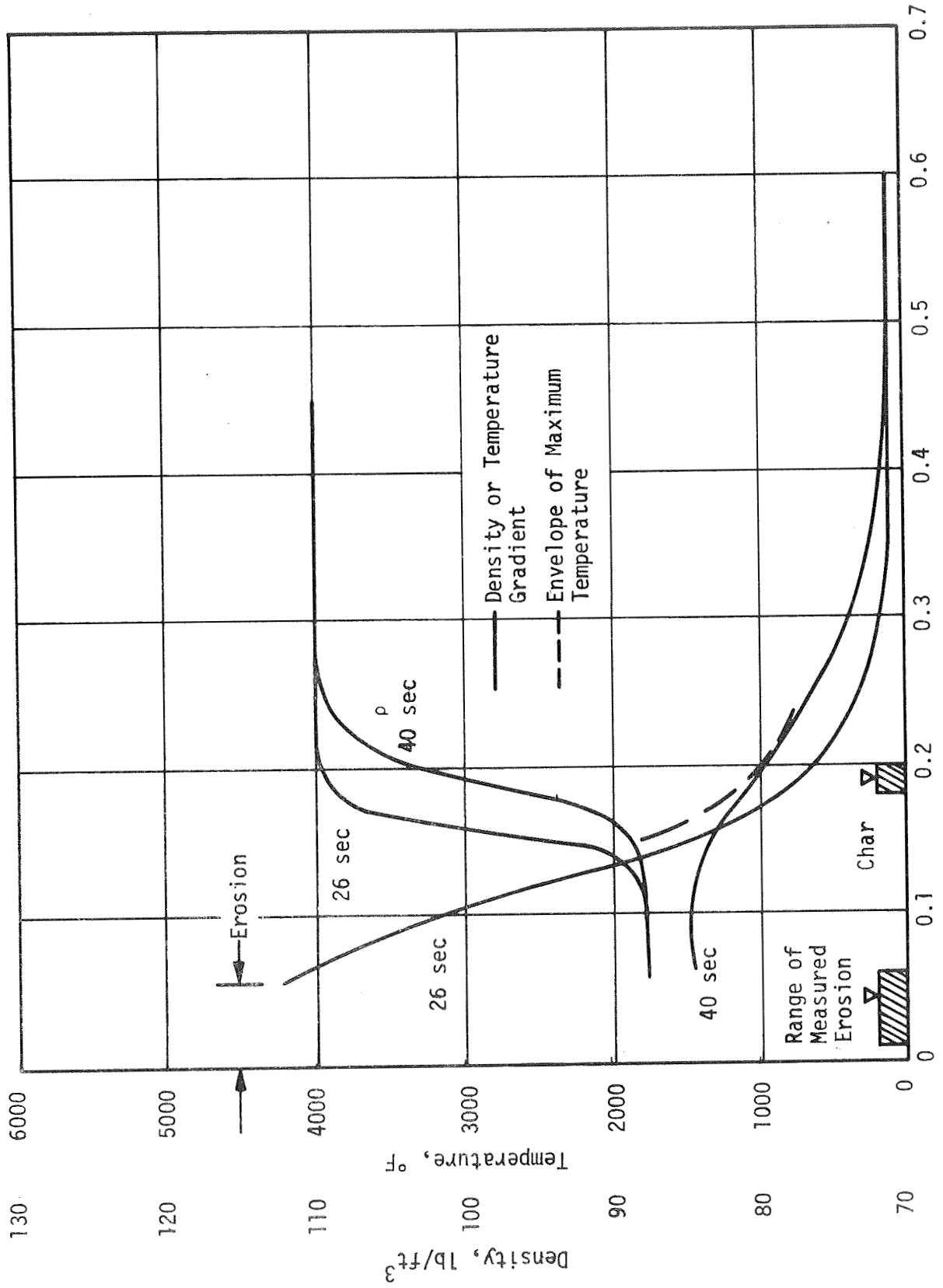

Thermal Response of Silica Cloth in Exit Cone of Deviation Nozzle (Baseline)

Figure VII-7

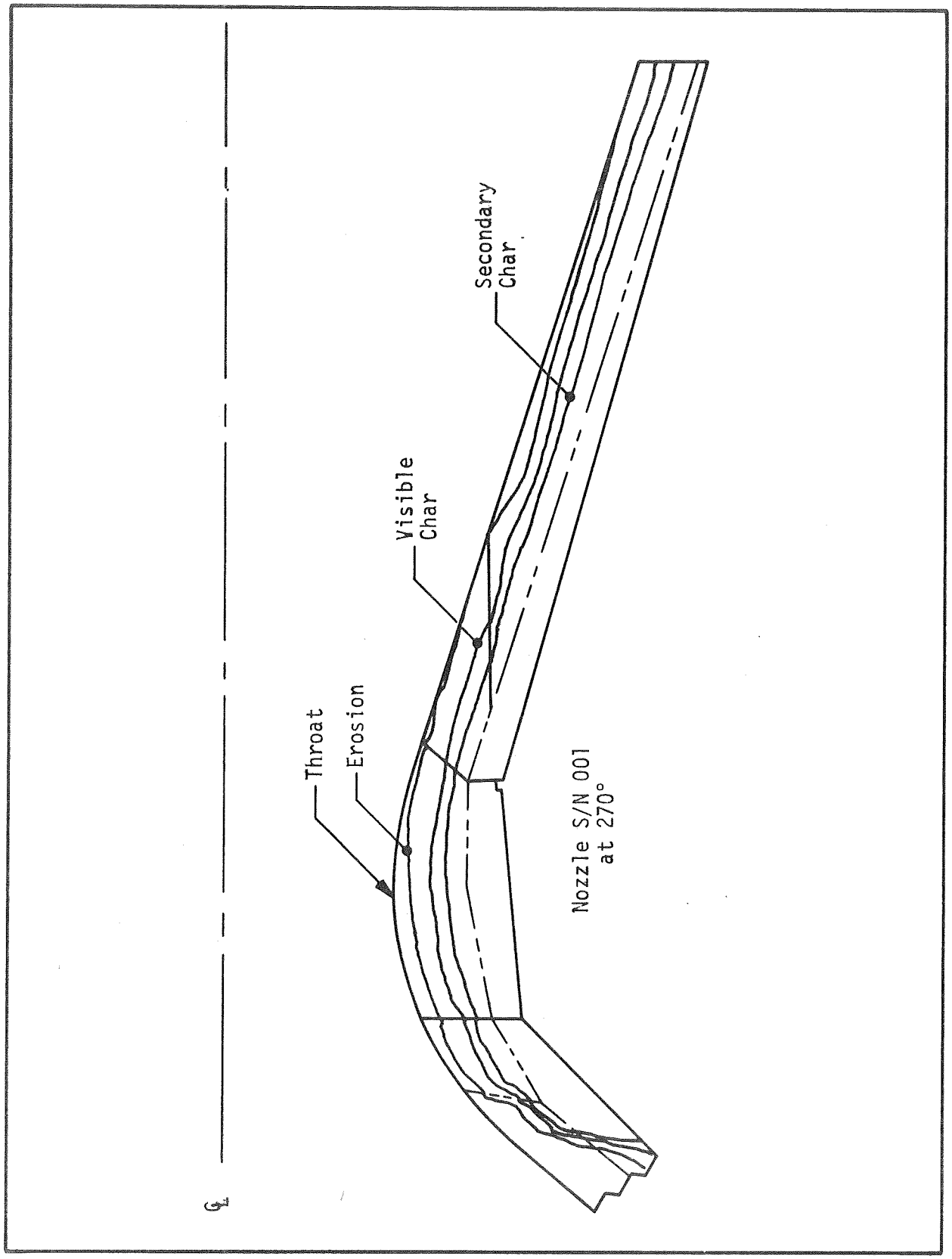

Nozzle Cross-Section

Figure VII-8

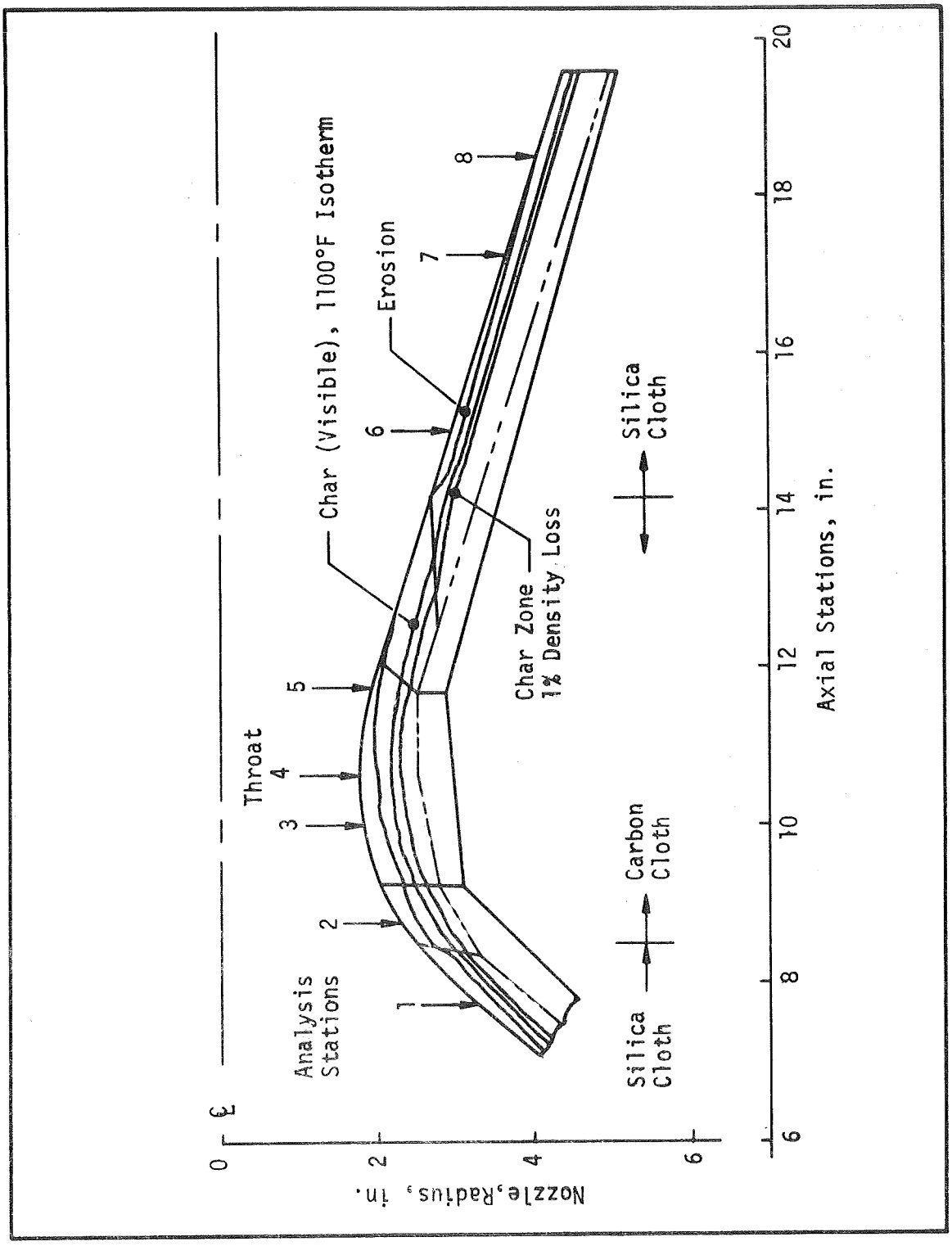

Predicted Erosion and Char Profiles in Baseline Deviation Nozzle

Figure VII-9

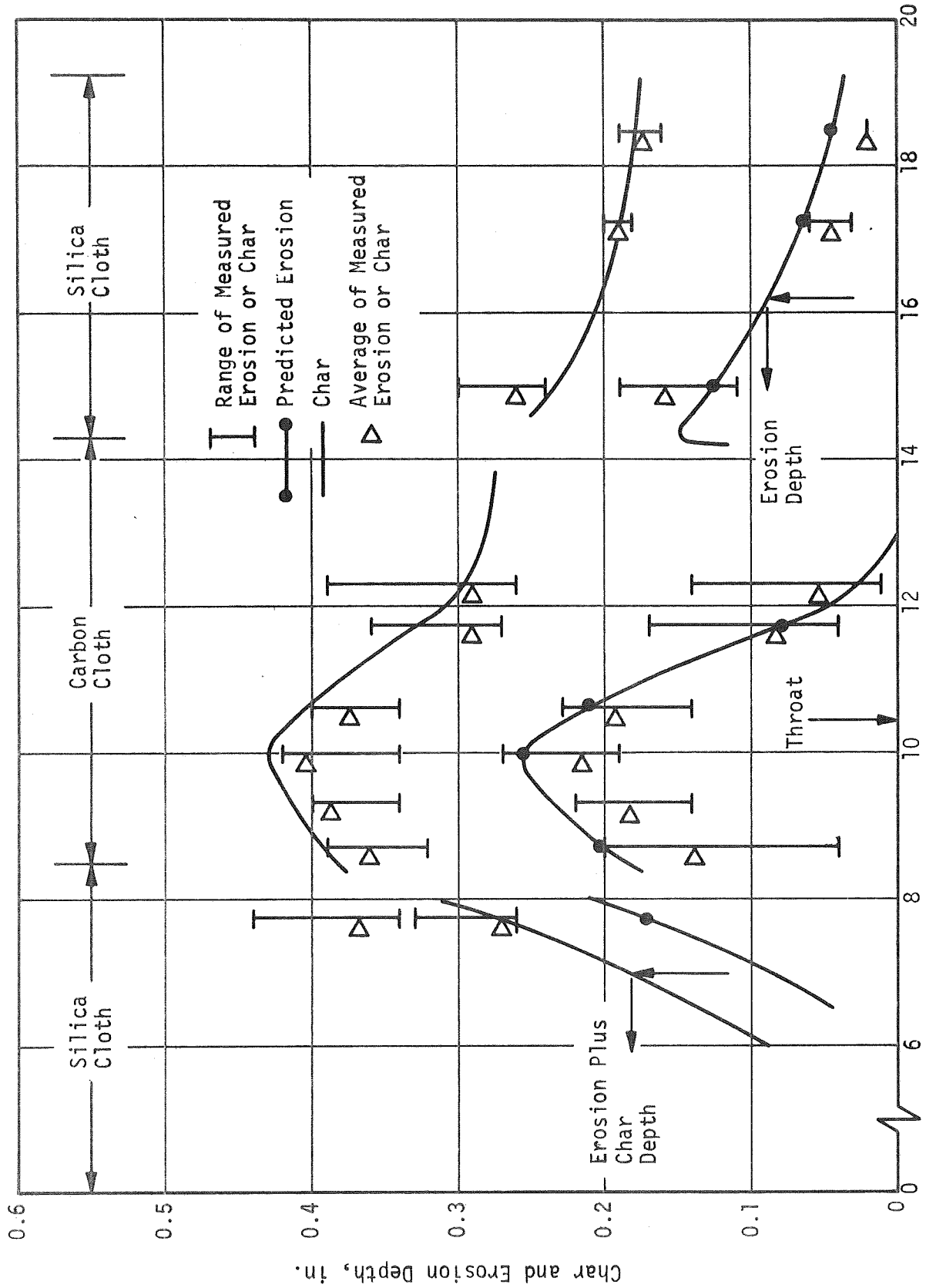

Comparison of Measured and Predicted Erosion and Char in Baseline Deviation Nozzle

Figure VII-10

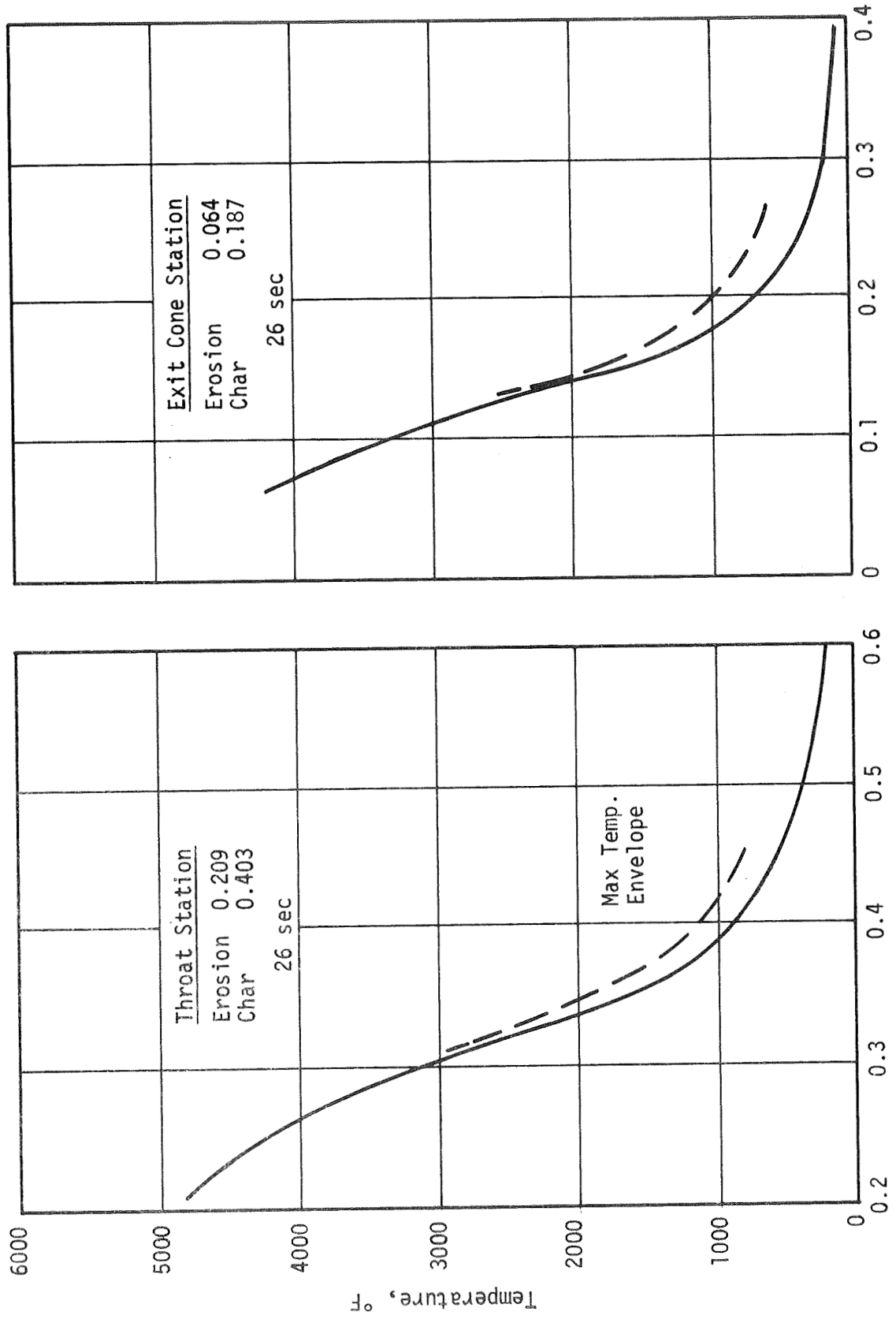

Temperature Gradients in Deviation Nozzle SN 001 (Baseline)

Figure VII-11

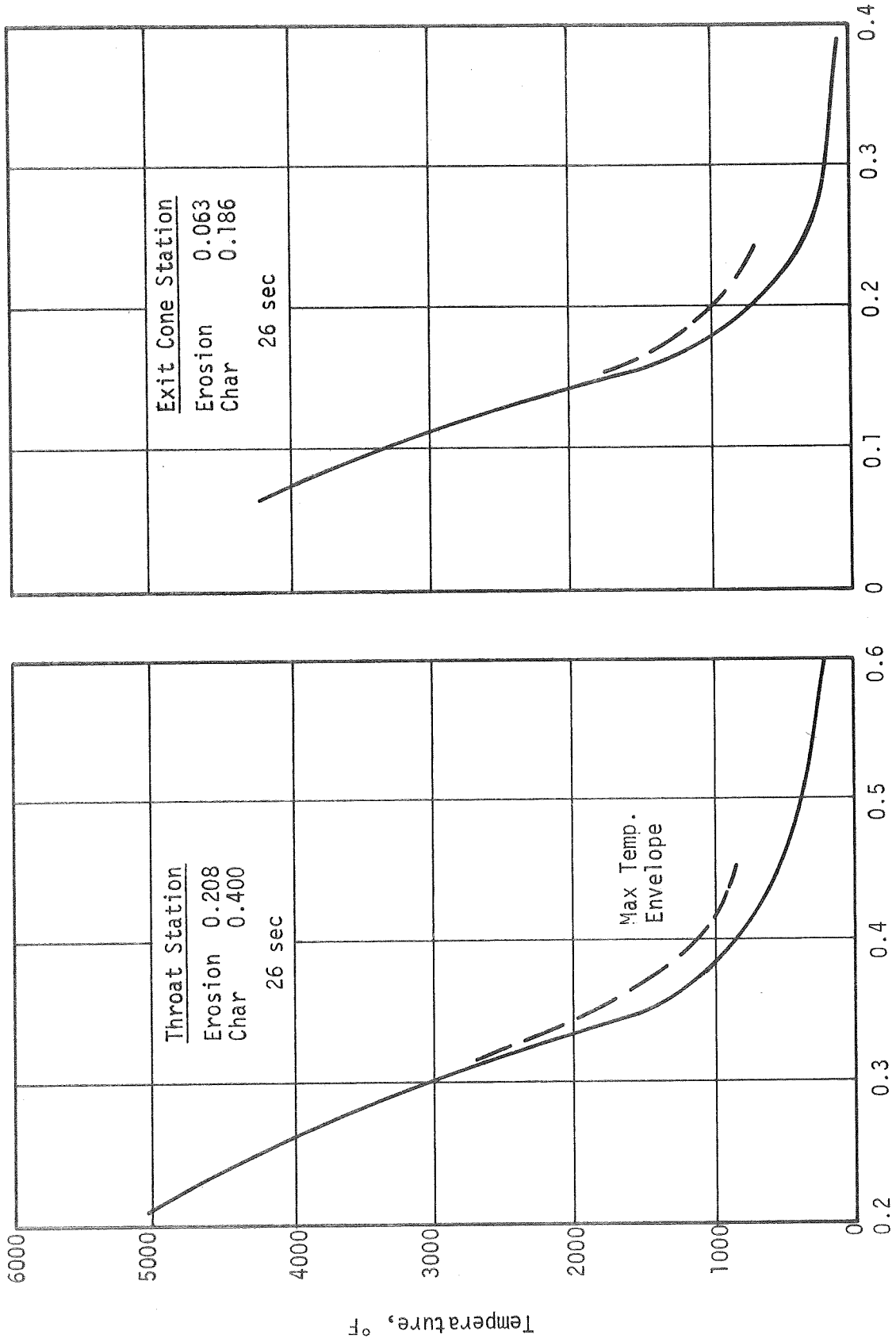

Temperature Gradients in Deviation Nozzle SN 002 (Baseline)

Figure VII-12

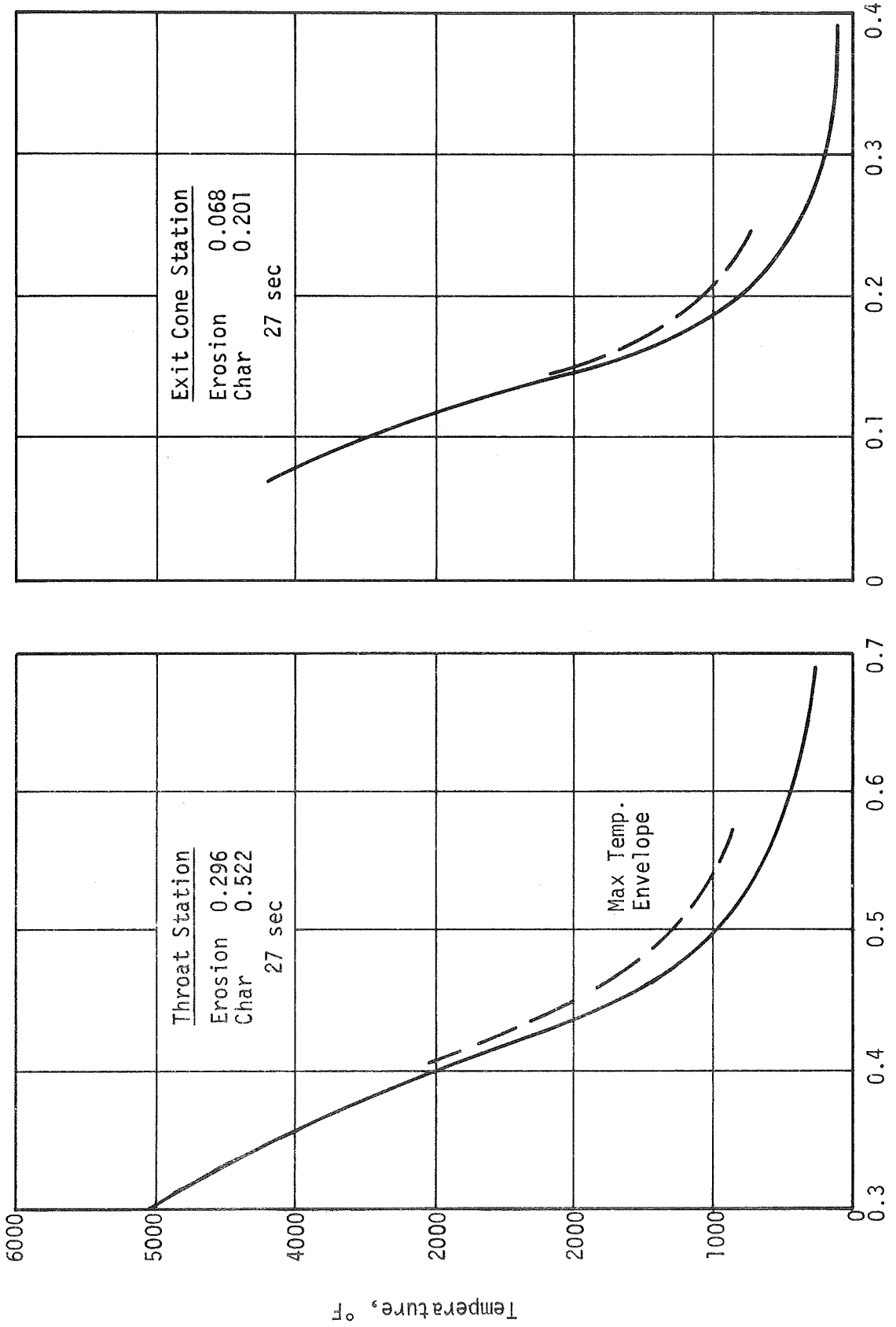

Temperature Gradients in Deviation Nozzle SN 003 (Vacuum Bag)

Figure VII-13

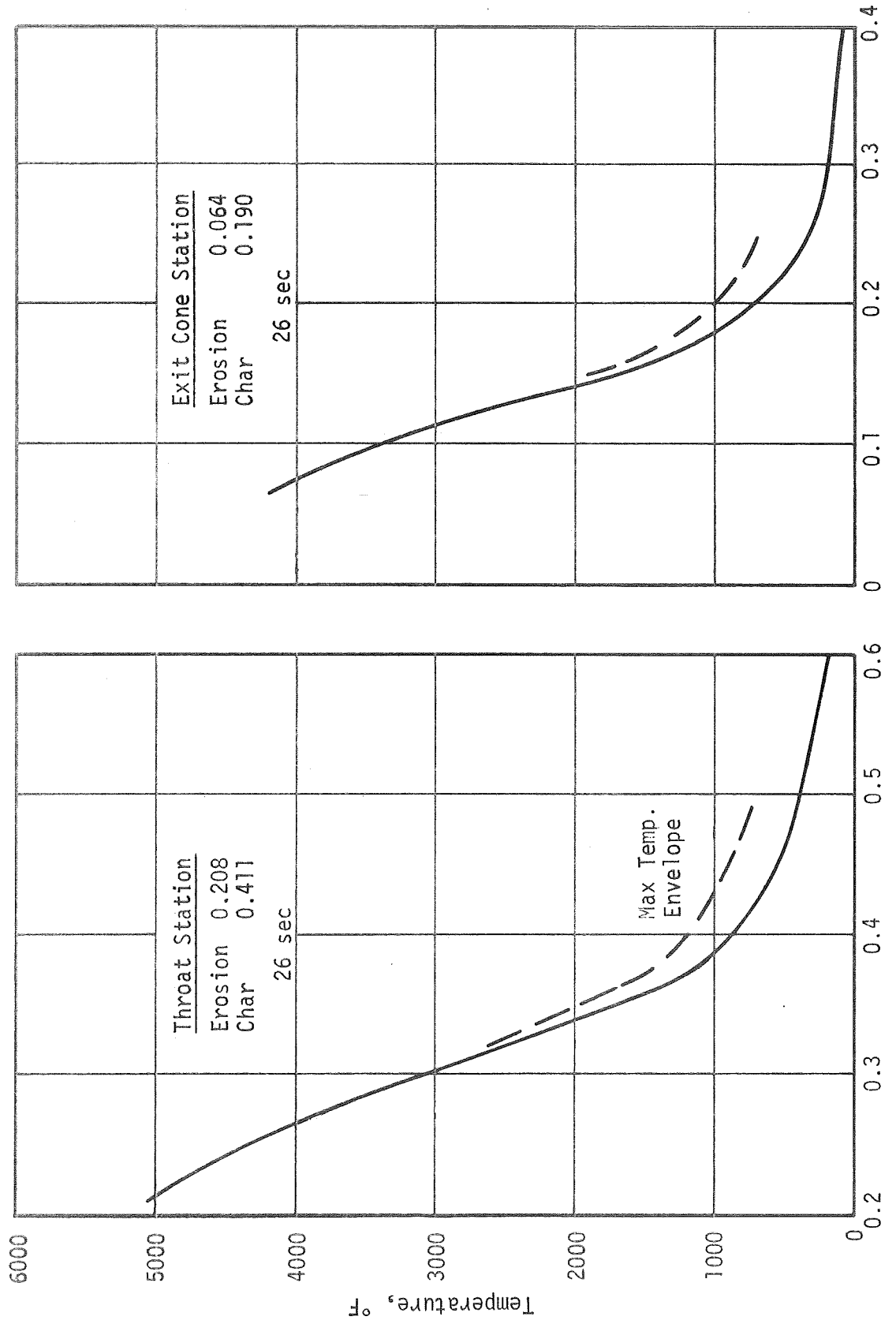

Temperature Gradients in Deviation Nozzle SN 004 (Autoclave)

Figure VII-14

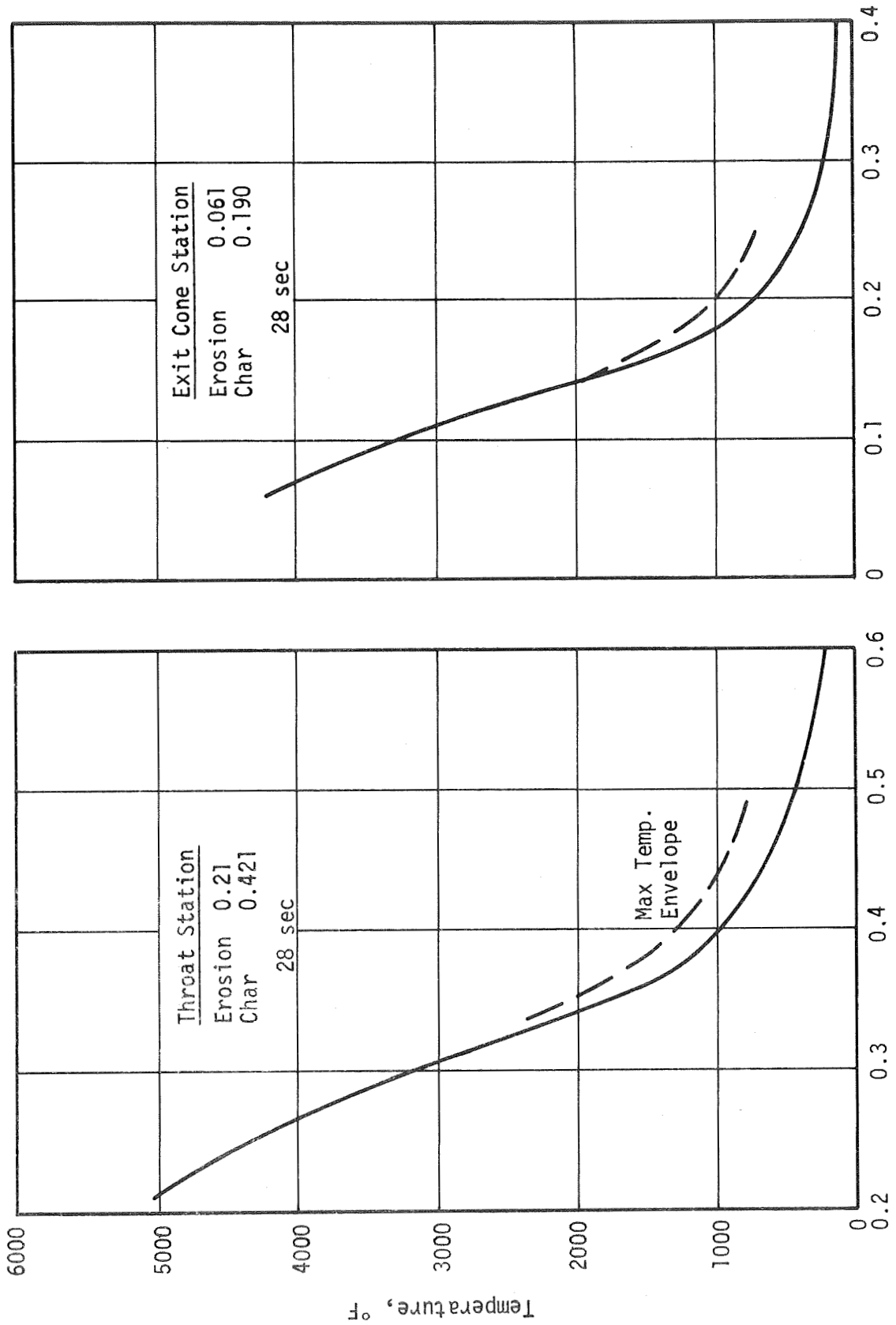

Temperature Gradients in Deviation Nozzle SN 007 (Resin-Rich)

Figure VII-15

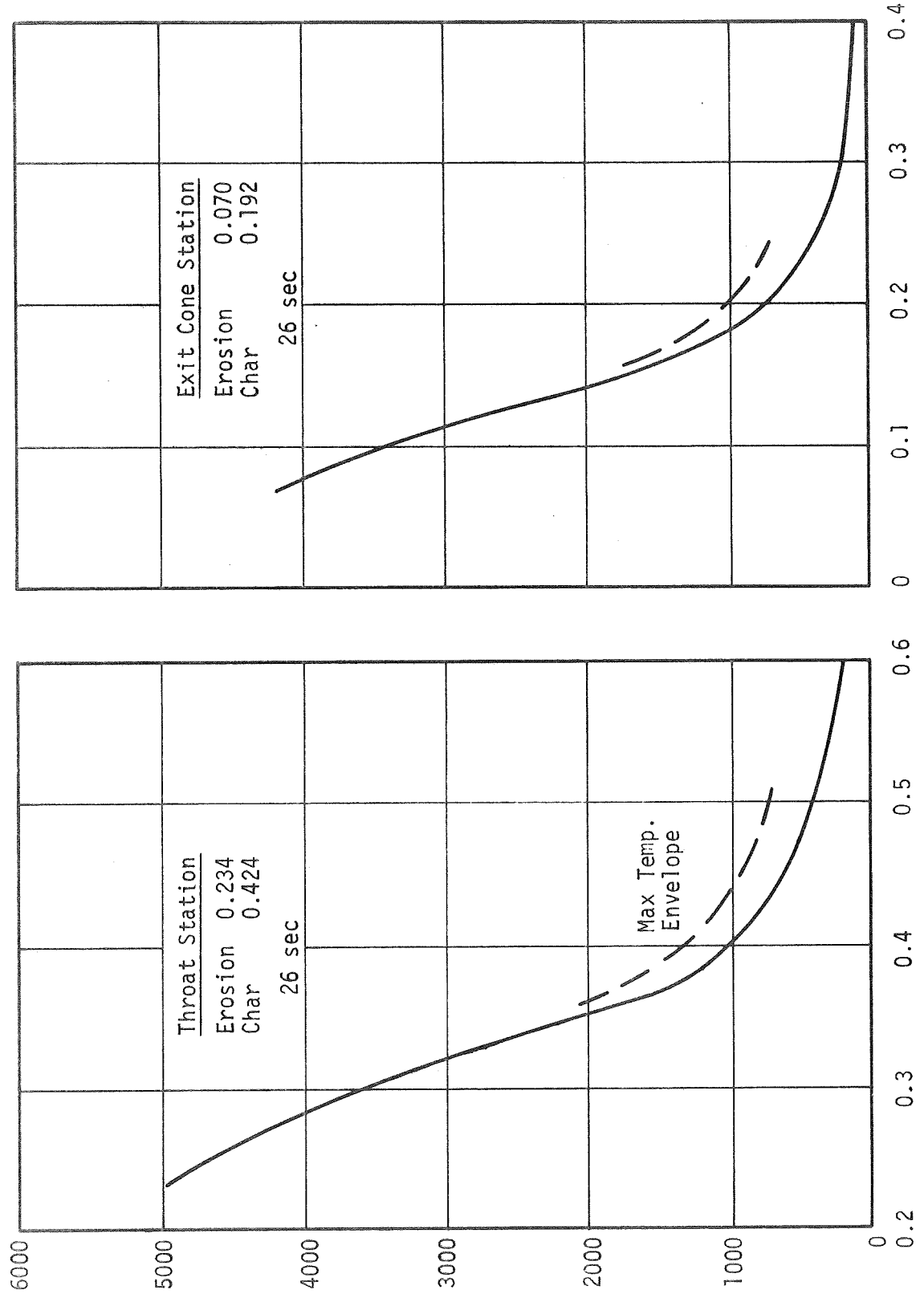

Temperature Gradients in Deviation Nozzle SN 008 (Resin-Rich)

Figure VII-16

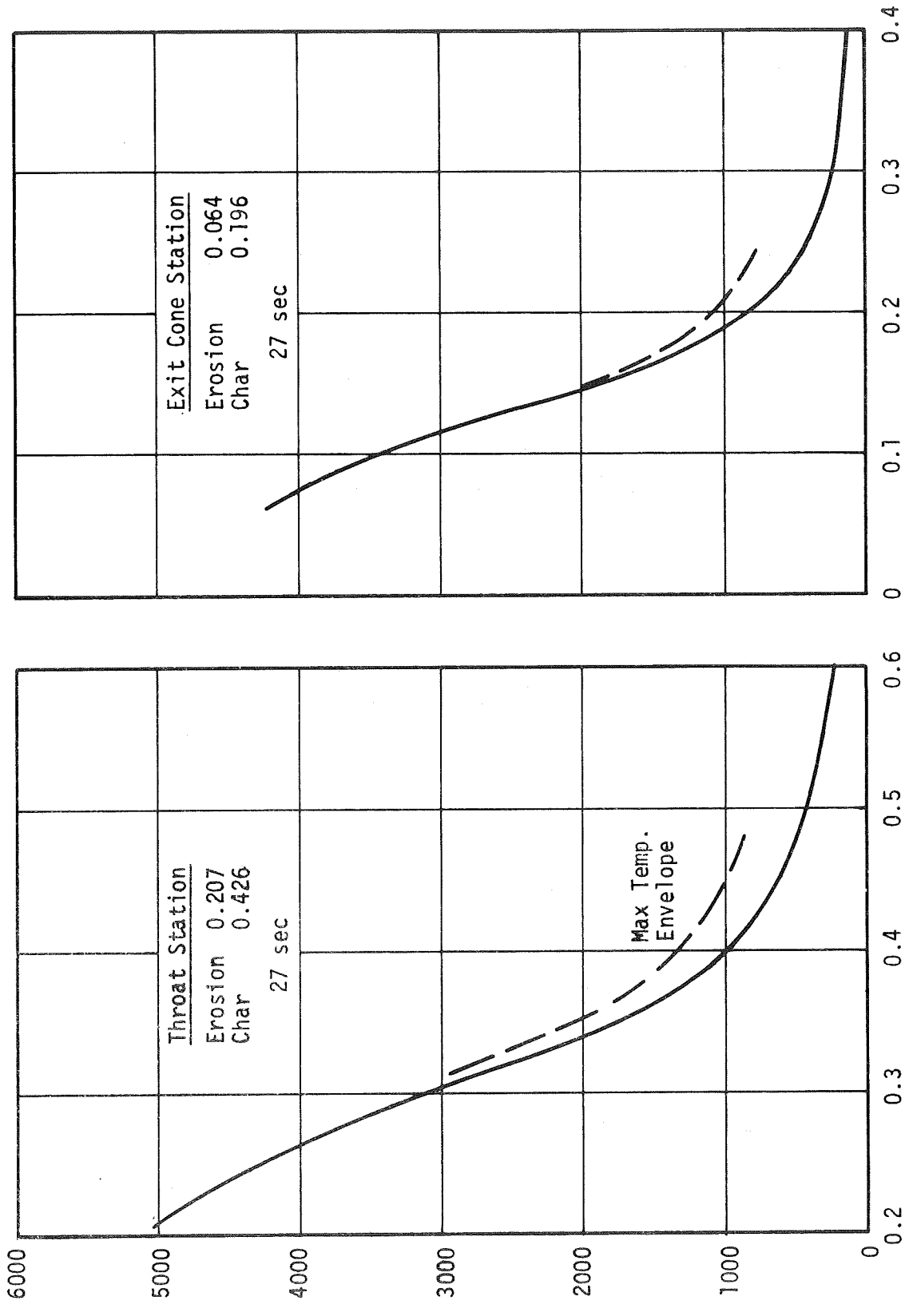

Temperature Gradients in Deviation Nozzle SN 013 (Resin Starved)

Figure VII-17

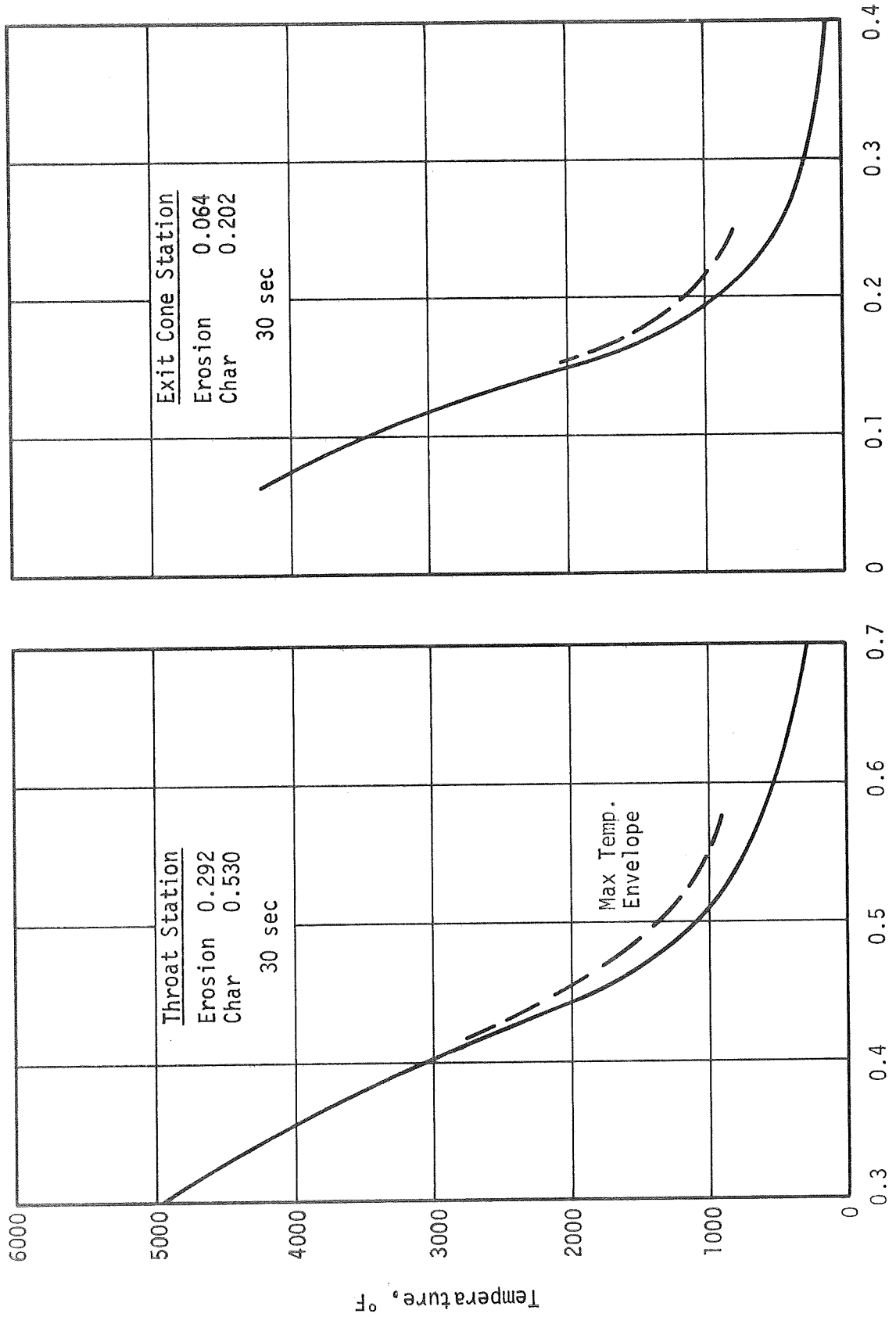

Temperature Gradients in Deviation Nozzle SN 019 (70 to 80% Density)

Figure VII-18

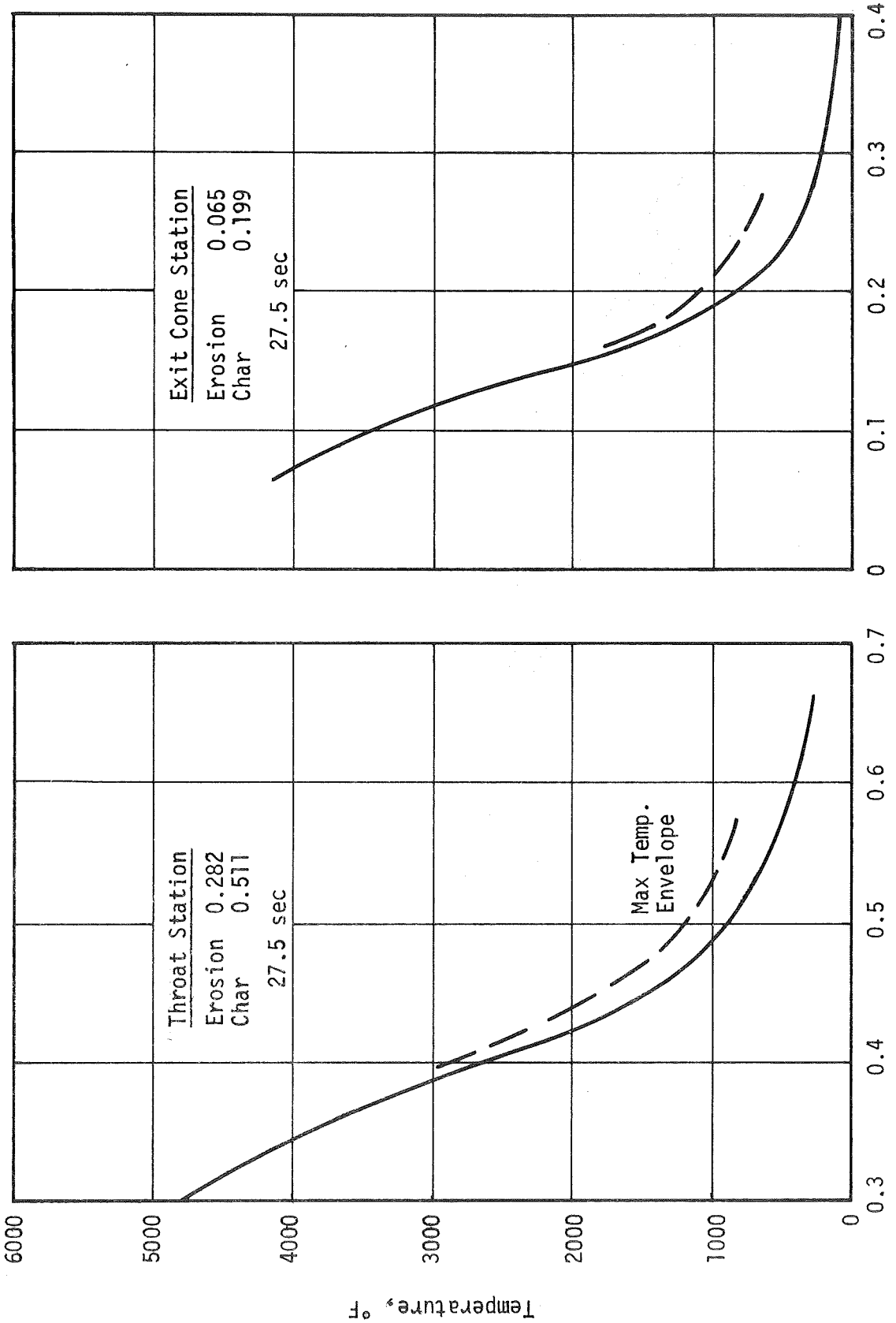

Temperature Gradients in Deviation Nozzle SN 020 (80 to 90% Density)

Figure VII-19

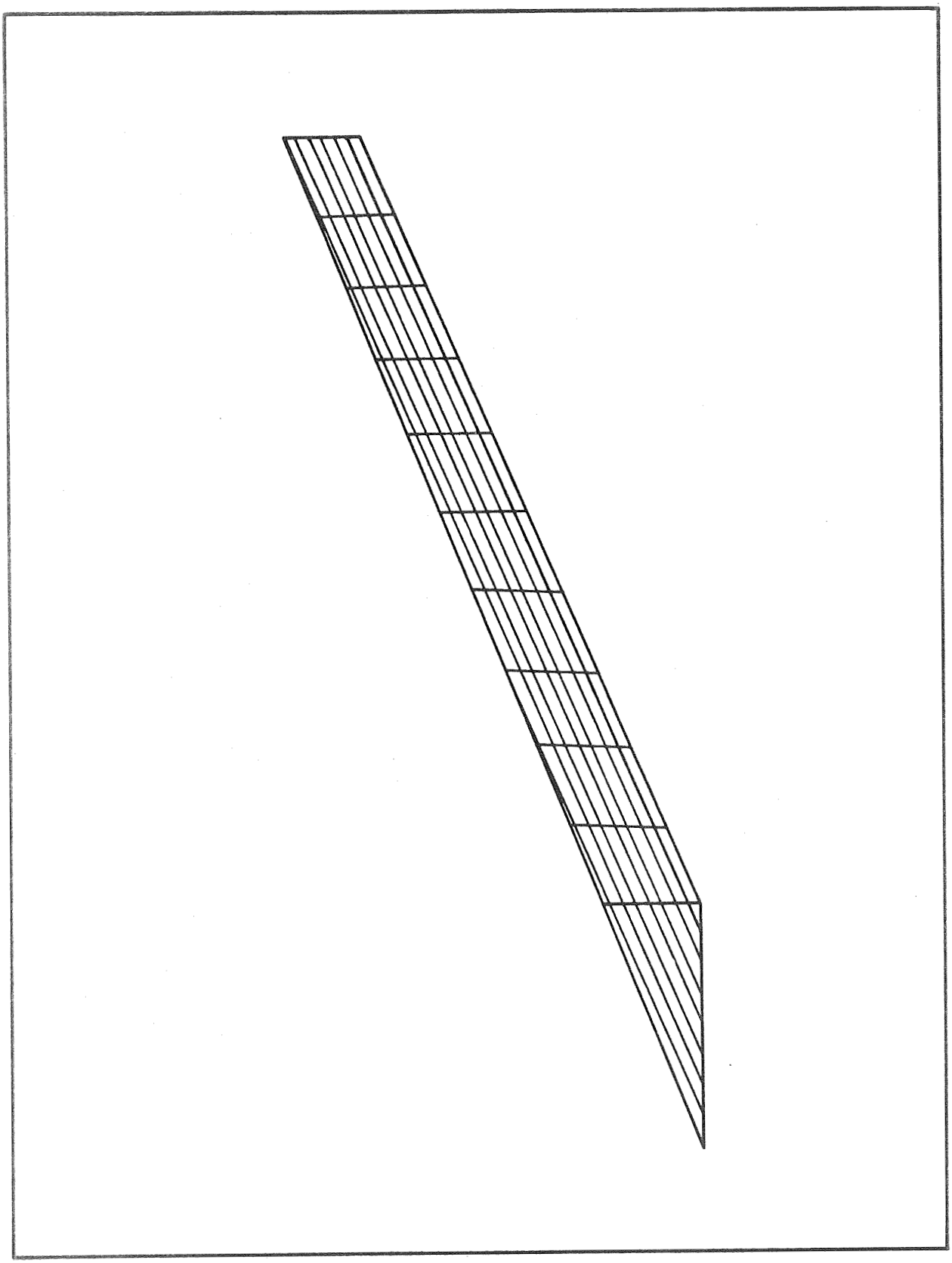

Structural Elements in Exit Cone Aft Section

Figure VII-20

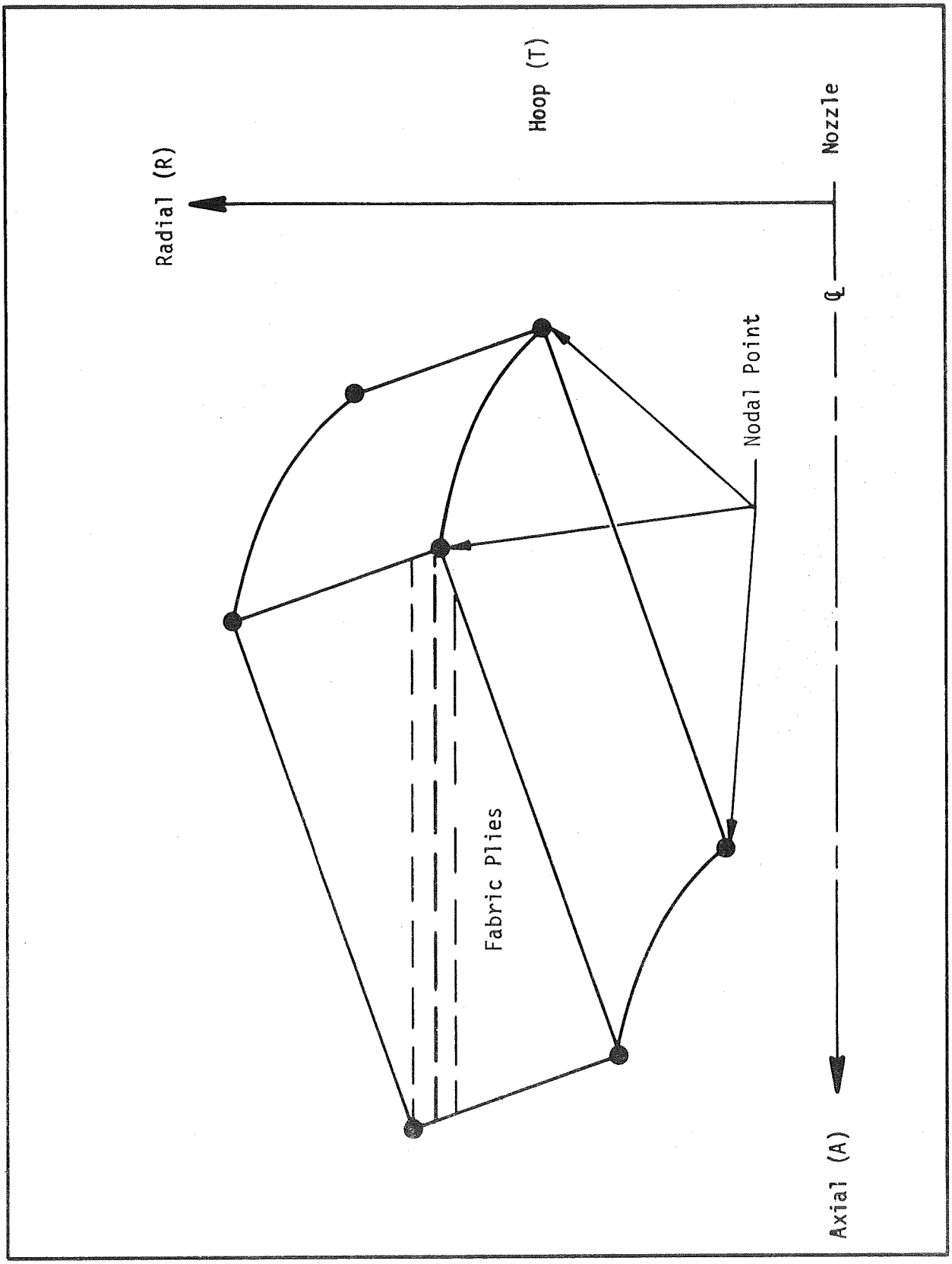

Finite Element Model for Program

Figure VII-21

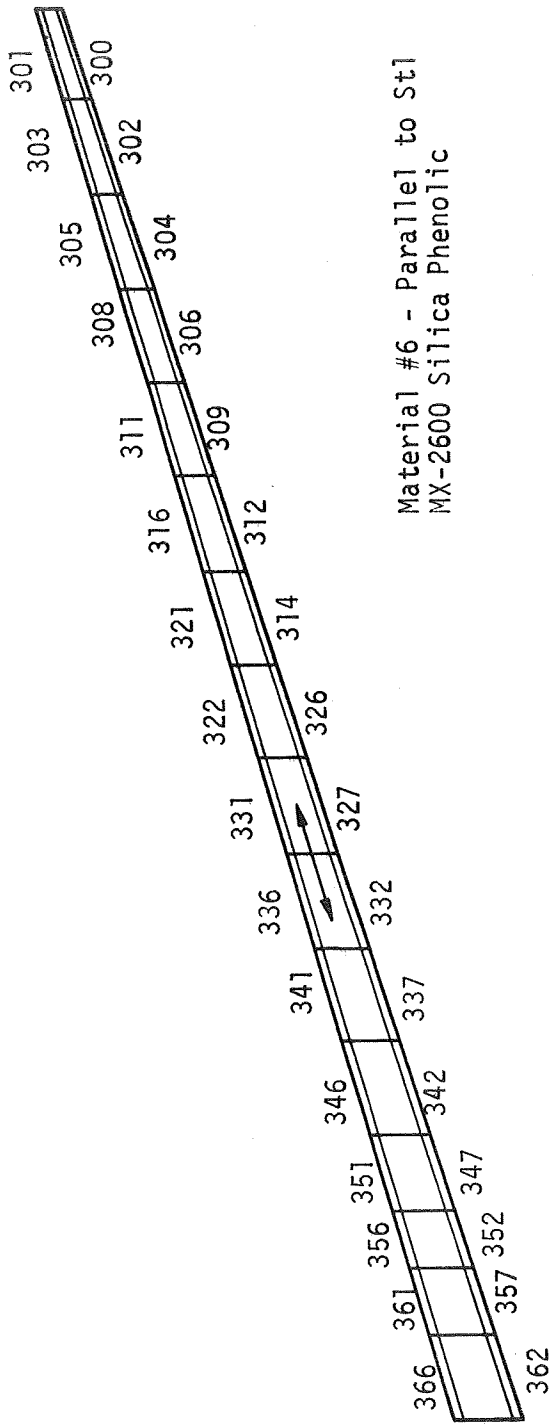

Material #6 - Parallel to Stl
MX-2600 Silica Phenolic

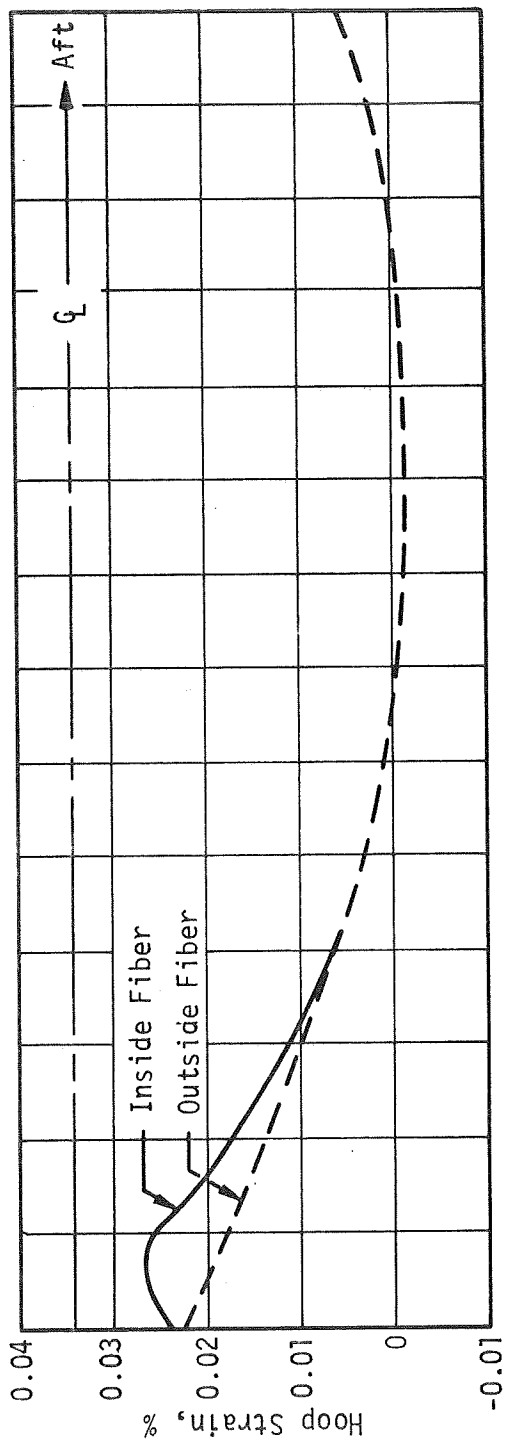

Thermal Stress Analysis Results for Exit Cone Overwrap, t = 25 sec

Figure VII-22

VIII. EVALUATION OF REPAIR TECHNIQUES

A. TEST MATRIX

The verification firings (Section VI) confirmed that significant changes in ablative performance could result from gross density and resin content variations and from delaminations and wrinkles within the ablative plastic nozzle component. Furthermore, the presence of either of the latter two discrepancies increased the probability of mechanical failure.

Volatile content up to 4.5 percent, water from bag leakage (up to 4.6 percent) and other cure cycle malfunctions had no significant effects on the performance of the discrepant nozzle components and were eliminated from further consideration of repair.

A total of eight nozzle assemblies were assigned for use in this task. In selecting the repair techniques to be evaluated, primary consideration was given to repairs that could be made without removing and replacing discrepant areas; as a result of previous work (References 1, 2, 3, and 10) this type of repair was considered to be satisfactory without the need of further corroboration.

1. Delaminations

Repair procedures were investigated that filled or sealed the separations between the plies of throat and exit inserts. The delaminated components for the verification firings were fabricated by introducing teflon wafers between the plies of the prepreg material at certain locations in known sizes and amounts for control purposes. The teflon wafers, however, could not be removed after insertion. For the present series of tests, the objective was to duplicate naturally occurring delaminations and then repair them. Four separate assemblies, as noted in Table VIII-1, were assigned to evaluate

VIII.A. Test Matrix (cont)

repair procedures for delaminations. One assembly was used to measure the performance of the delaminated parts; the other three evaluated repairs made by resin impregnation and by tape overwrapping.

2. Wrinkles

Two separate assemblies to evaluated repair procedures for wrinkles. One assembly was used to measure the performance of parts with naturally occurring wrinkles; the other evaluated the use of resin impregnation.

3. Low Density

Two assemblies were assigned to confirm further the relationship between density and surface regression. The throat inserts of both assemblies were used for confirmation; the exit inserts were used to evaluate the use of resin impregnation for repair.

B. FABRICATION

1. Materials

MX-4926 carbon fabric reinforced phenolic and MX-2600 silica fabric reinforced phenolic prepregs were used to fabricate the repair nozzle assemblies. The properties of the prepreg tapes are shown in Table VIII-2. Although from different lots than those used in the discrepant nozzle (Table IV-1), the properties are similar.

Two types of resin impregnants were used to repair the selected nozzle assemblies. One type was a two-part room temperature curing epoxy (Epon 919, lot number 5LAB901, manufactured 5/69); the other was a two-part room temperature curing furfural (Furane X-2, batch B-3962, manufactured 4/69).

VIII.B. Fabrication (cont)

2. Fabrication

a. Introduction of Defects

The discrepant nozzles containing delaminations had been fabricated by inserting teflon shims between the plies of prepreg tape (Section III,D,5). Although this was an excellent means of setting the bounds of the defect, it had the disadvantage that the shims could not be removed. While this did not affect the ablative or structural behavior of the composite, since the teflon vaporized during the static test firing, the teflon shims prevented repairing the delaminations by resin impregnation. Accordingly, the procedure for introducing delaminations was revised. Delaminations in nozzle assemblies 21 through 24 were introduced by using overadvanced prepreg.

Wrinkles were introduced by reducing the roller pressure and tape tension at preselected points during wrapping of the throat and exit liners so that the material bunched slightly during curing. Low density was introduced by maintaining the roller pressure at lower than normal values during wrapping.

All components except the low density throats and exit sections were cured in an autoclave at 125 psig (0.86 MN/m^2). The low density parts were cured at a vacuum of 26 in. Hg. All parts were cured at 310 $\pm$ 10°F.

Density and volatile content measurements were made after curing. The results are shown in Table VIII-3. Volatile contents were all well below 3 percent; density measurements indicated that, except for two instances, the planned densities were achieved. In the first instance, the MX-4926 portion of exit section 22 was found to be 80.5 lb/cu ft (1.29 gm/cc), which is lower than normal. In the second instance, the density of throat

VIII.B. Fabrication (cont)

insert 27 was found to be 89.2 lb/cu ft (1.43 gm/cc), much higher than the desired density of 78.0 lb/cu ft (1.25 gm/cc).

b. Resin Impregnation

All parts to be repaired by resin impregnation were cleaned by wiping with methyl ethyl ketone and were dried under ambient conditions for 30 minutes prior to insertion in the impregnating vessel. After insertion in the vessel, the part was maintained under a vacuum of 25 in. Hg for 4 hours. The resin impregnant (Epon 919 or Furane X-2) was metered into the chamber in a quantity sufficient to submerge the part being treated. Liquid submersion of the part was maintained for 1 hour minimum, after which the vacuum was released and the part was removed to drain off the excess resin. Resin curing was effected by maintaining the impregnated part at room temperature for 8 hours minimum.

C. STATIC TEST

The static test firings of the repaired nozzle assemblies were conducted in accordance with the procedures described in Section VII,A,1. The pressure-time curves are reproduced in Figures VIII-1 through VIII-8. The pressures and burn times are listed in Table VIII-4. There do not appear to be any anomalies in the motor performance.

D. PERFORMANCE ANALYSIS

After static test, the nozzle components were removed from the steel shell and examined visually. The nozzle entrance inserts, all of which were fabricated without introduced discrepancies, were examined to determine whether the material removal was localized or whether cracks had occurred.

VIII.D. Performance Analysis (cont)

Neither of these conditions were observed. The throat and exit inserts, in which discrepancies were introduced, were examined in more detail.

Following the visual examination, the nozzle components were sectioned at five angular locations as before, and measurements of regression and char depth were made. Samples of the char were then removed from the throat and forward and aft exit inserts to determine their densities. The regression and char profiles are shown in Figures VIII-9 through VIII-16. The regression and char rates at specific locations are shown in Tables VIII-5 through VIII-8.

1. Entrance Inserts

The regression and char depths of the MX-2600 entrance sections are shown in Table VIII-5. As a group, the performance of these entrance sections was not as good as those of the previous twenty nozzles. The average regression rate was 11.80 mils/sec and the char rate was 15.21 mils/sec, compared to the previously observed 9.85 and 13.35 mils/sec, respectively. It is tempting to speculate that this lowered performance is a consequence of the decreased density of this group compared to the first (107.3 vs 109.8 lb/ft^3). Other differences also contributed, however, such as the differences between prepreg lots, the differences between fabricator techniques and procedures, and the use of different test motors.

2. Delaminations

a. Throat Inserts

The visual appearances of the throat inserts fabricated with introduced delaminations are shown in Figure VIII-17. The delaminated and unrepaired insert (21) had wider and deeper surface separations than those in the resin impregnated inserts (22 and 23). The nondiscrepant insert (24) had only a few shallow separations after firing.

VIII.D. Performance Analysis (cont)

Filling the spaces between delaminated plies with resin did not improve the ablative performance. There was an observed improvement in the epoxy-filled throat insert (22) (see Table VIII-6), in which the regression rate at the 1.81-in. radius at which the delamination occurred was measured to be 5.35 mils/sec compared to an average of 5.74 mils/sec for defect-free areas of the same throat insert. However, if one examines the regression rates of the three unfilled throat inserts (21, 24, and 25) in defect-free areas at 1.81-in. radius, it will be noted that there was a low of 4.64 mils/sec (21) to a high of 6.03 mils/sec (24) and the average was 5.55 mils/sec. Since the measured regression rates of the epoxy-filled insert fall within these limits, there is no apparent significance to the improved rate at the epoxy-filled delaminations. The regression rate at the 1.78-in. radius at which the delamination occurred was measured to be 7.03 mils/sec compared to 5.76 mils/sec for the defect-free areas of the same insert and an average of 4.69 mils/sec for the three unfilled throat inserts

b. Exit Sections

Visually, there were few differences among the four exit sections fabricated with introduced delaminations (Figure VIII-18). The delaminated areas in the MX-4926 forward exit sections were severely attacked during firing, and pieces separated along the delaminated plies during the sectioning operations preparatory to the measurement of char depths. Material removal was not so great in the MX-2600 aft exit sections, but because the thin sections were completely charred after static test, ply separation occurred during sectioning.

It was found that resin fill was ineffective in improving the ablative performance of the delaminated portions of the MX-4926 forward exit sections. The corrected regression data (Table VIII-7) show that, at best, the repaired area filled with Furane resin had twice the rate of regression that was observed in its defect-free counterpart.

VIII.D. Performance Analysis (cont)

In the aft exit section, comprised of MX-2600, the same lack of improvement was recorded (see Table VIII-8), although the filled defective areas had regression rates no higher than the defect-free areas.

3. Wrinkles

a. Throat Inserts

Figure VIII-19 shows that the wrinkled and repaired throat insert (26) was more pitted and separated than the unrepaired insert (25). Comparison of the regression rates of defective and defect-free areas of the inserts (Table VIII-6) shows that resin filling did not improve the ablative performance.

b. Exit Sections

Both the visual appearance (Figure VIII-20) and the regression data (Table VIII-7) show that resin fill was of no value for the MX-4926 forward exit sections. Since the MX-2600 aft exit sections were fabricated without wrinkles, observations were made of the performance of exit insert 25, which was not resin filled. It may be inferred, however, from the results of the delaminated and filled inserts that resin fill would serve no useful purpose in repairing the effects of wrinkles in silica fabric reinforced ablative composites.

4. Low Density

a. Throat Inserts

The throat inserts in nozzle assemblies 27 and 28 were tested in the as-fabricated condition, without any repair. After test, while

VIII.D. Performance Analysis (cont)

surface separations were more numerous in the denser of the two inserts (27 in Figure VIII-21) measurements of surface regression (Table VIII-6) show that insert 28 experienced a regression rate 60 percent greater than that of insert 27 and 160 percent greater than the average rate of the defect-free material in inserts 21, 24, and 25.

b. Exit Inserts

The exit inserts in nozzle assemblies 27 and 28 were tested in the resin-filled condition. After test there was little visual difference between the two (Figure VIII-22). Measurements of regression and char depths in the MX-4926 (2.1-in. radius of Table VIII-7) and MX-2600 (2.93 and 3.7-in. radii of Table VIII-8) portions of the exit section indicate that resin fill was of no value in overcoming the effect of low density (porosity) in the carbon fabric (MX-4926) portion, but was beneficial in the silica fabric (MX-2600) portion.

TABLE VIII-1

REPAIR NOZZLE MATRIX

Nozzle No.	Throat Insert		Exit Insert	
	Defect	Repair	Defect	Repair
21	Delaminations	None	Delaminations	None
22	Delaminations	Resin impregnation	Delaminations	Resin impregnation
23	Delaminations	Resin impregnation	Delaminations	Resin impregnation
24	None	None	Delaminations	Two-ply overwrap
25	Wrinkles	None	Wrinkles	None
26	Wrinkles	Resin impregnation	Wrinkles	Resin impregnation
27	Low density	None	Low density	Resin impregnation
28	Low density	None	Low density	Resin impregnation

TABLE VIII-2

PROPERTIES OF PREPREG MATERIALS USED IN REPAIR NOZZLE COMPONENTS

	MX-4926		MX-2600	
Lot Number	H-335	H-365	H-372	H-372
Roll Number	3	1	3A	3B
Resin Solids, %	34.8	34.7	33.2	33.0
Volatile Content, %	4.5	4.4	3.9	3.9
Laminate Flow, % at 150 psi	5.0	14.1	-	-
% at 500 psi	-	-	14.0	12.7

TABLE VIII-3

PROPERTIES OF REPAIR NOZZLE COMPONENTS

Nozzle Assembly	Material	Location	Volatile Content, %	Density, lb/cu ft	gm/cc
21	MX-4926	Entrance	2.52	88.0	1.41
		Throat	-	93.6	1.50
		Exit	-	91.7	1.47
	MX-2600	Entrance	0.97	106.7	1.71
		Exit	-	108.0	1.73
22	MX-4926	Entrance	2.05	89.9	1.44
		Throat	-	91.1	1.46
		Exit	-	80.5	1.29
	MX-2600	Entrance	1.12	108.0	1.73
		Exit	-	108.0	1.73
	MX-4926	Entrance	0.89	86.1	1.38
		Throat	-	91.1	1.46
		Exit	-	91.7	1.47
	MX-2600	Entrance	0.64	107.3	1.72
		Exit	-	108.0	1.73
24	MX-4926	Entrance	0.62	89.2	1.43
		Throat	0.65	89.9	1.44
		Exit	-	89.9	1.44
	MX-2600	Entrance	0.79	109.2	1.75
		Exit	-	107.3	1.72
25	MX-4926	Entrance	0.63	89.9	1.44
		Throat	-	92.4	1.48
		Exit	-	-	-
	MX-2600	Entrance	1.07	106.1	1.70
		Exit	-	-	-
26	MX-4925	Entrance	0.92	87.4	1.40
		Throat	-	88.6	1.42
		Exit	-	-	-
	MX-2600	Entrance	1.13	108.0	1.73
		Exit	-	-	-
27	MX-4926	Entrance	0.57	91.7	1.47
		Throat	1.41	89.2	1.43
		Exit	-	78.0	1.25
	MX-2600	Entrance	0.89	106.7	1.71
		Exit	-	96.1	1.54
28	MX-4926	Entrance	0.66	91.7	1.47
		Throat	1.62	71.8	1.15
		Exit	-	77.4	1.24
	MX-2600	Entrance	0.98	107.3	1.72
		Exit	-	96.1	1.54

Table VIII-4

Summary of Repair Nozzle Firings

Test No.	Discrepancy Repair	Chamber Pressure				Burn Time, sec
		Maximum		Average		
		psia	psia	psia	(N/mm^2 abs)	
21	Delaminations/None	667.0	4599	606.0	4178	26.7
22	Delaminations/Epoxy Fill	667.0	4599	599.0	4130	26.15
23	Delaminations/Furane Fill	618.5	4264	560.0	3861	27.0
24	Delaminations/Overwrap	664.5	4581	606.0	4178	26.35
25	Wrinkles/None	675.5	4657	608.5	4195	25.85
26	Wrinkles/Furane Fill	644.0	4440	586.0	4040	26.75
27	Low Density/None	632.5	4361	575.0	3964	26.6
28	Low Density/None	583.5	4023	519.0	3578	27.9

TABLE VIII-5

CORRECTED* REGRESSION AND CHAR DEPTH OF MX-2600
IN ENTRANCE SECTION AT 3.25 in. rad (ε = 3.5)

	Regression				Char Depth			
	Total		Rate		Total		Rate	
Test No.	in.	mm	mils/sec	mm/sec	in.	mm	mils/sec	mm/sec
21	0.248	6.32	9.29	0.236	0.377	9.58	14.12	0.357
22	0.210	5.33	8.03	0.204	0.310	7.87	11.85	0.301
23	0.381	9.68	14.11	0.358	0.476	12.09	17.63	0.448
24	0.278	7.06	10.55	0.268	0.347	8.81	13.17	0.335
25	0.376	9.55	14.55	0.37	0.435	11.05	16.83	0.427
26	0.306	7.77	11.44	0.291	0.397	10.09	14.84	0.377
27	0.393	9.98	14.77	0.375	0.455	11.56	17.11	0.435
28	0.326	8.27	11.68	0.297	0.449	11.40	16.09	0.409

*Corrected to 600 psia chamber pressure

Table VIII-6

Corrected Regression and Char Depth of MX-4926
in Throat Insert

Discrepancy/Repair	Location	Char Density		Regression				Char Depth			
				Total		Rate		Total		Rate	
		lb/cu ft	gm/cc	in.	mm	mil/sec	mm/sec	in.	mm	mil/sec	mm/sec
Delaminations/None	1.81 R (fwd)	-	-	0.179	4.55	6.68	0.17	0.377	9.58	14.12	0.359
(Defect free areas)	1.78 R (fwd)	67.4	1.08	0.124	3.15	4.64	0.118	0.366	9.3	13.71	0.348
(Defect free areas)	1.78 R (fwd)	67.4	1.08	0.119	2.95	4.46	0.113	0.377	9.58	14.12	0.359
Delaminations/Epoxy	1.81 R (Fwd)	-	-	0.14	3.56	5.35	0.136	0.35	8.9	13.38	0.34
(Defect free areas)	1.81 R (fwd)	69.9	1.11	0.15	3.81	5.74	0.146	0.365	0.27	13.95	0.354
Delaminations/Furane	1.78 R (aft)	-	-	0.19	4.83	7.03	0.179	0.412	10.46	15.25	0.387
(Defect free areas)	1.78 R (aft)	68.6	1.10	0.159	4.04	5.76	0.146	0.391	9.93	14.17	0.36
None/None	1.81 R (fwd)	-	-	0.159	4.04	6.03	0.153	0.407	10.37	15.44	0.392
None/None	1.78 R (aft)	71.8	1.15	0.122	3.1	4.63	0.118	0.384	9.75	14.57	0.370
Wrinkles/None	1.81 R (fwd)	-	-	0.173	4.39	6.69	0.17	0.386	9.8	14.97	0.380
(Defect free areas)	1.81 R (fwd)	71.1	1.14	0.138	3.51	5.33	0.135	0.356	9.04	13.77	0.35
(Defect free areas)	1.78 R (aft)	71.1	1.14	0.129	3.28	4.99	0.127	0.381	9.68	14.74	0.374
Wrinkles/Furane	1.81 R (fwd)	-	-	0.168	4.27	6.22	0.158	0.372	9.45	13.85	0.352
(Defect free areas)	1.81 R (fwd)	71.1	1.14	0.127	3.23	4.75	0.121	0.336	8.53	12.56	0.319
Low Density/None	1.81 R (fwd)	66.1	1.06	0.241	6.12	9.06	0.23	0.424	10.77	15.93	0.405
Low Density/None	1.81 R (fwd)	59.8	0.96	0.371	9.42	13.29	0.338	0.618	15.7	22.15	0.563

*Corrected to 600 psia chamber pressure

Table VIII-7

Corrected Regression and Char Depth of MX-4926
in Exit Section

Discrepancy/Repair	Location	Char Density		Regression				Char Depth			
				Total		Rate		Total		Rate	
		lb/cu ft	gm/cc	in.	mm	mil/sec	mm/sec	in.	mm	mil/sec	mm/sec
Delaminations/None	2.3 R	-	-	0.0595	1.51	2.23	0.057	0.288	7.32	10.79	0.274
(Defect free areas)	2.1 R	68.0	1.09	0.051	1.29	1.91	0.049	2.75	6.99	10.37	0.263
	2.2 R	68.0	1.09	0.035	0.88	1.31	0.033	0.268	6.81	10.11	0.257
	2.3 R	68.0	1.09	0.025	0.63	0.94	0.024	0.248	6.3	9.36	0.238
	2.45 R	68.0	1.09	0.015	0.38	0.56	0.014	0.248	6.3	9.36	0.238
Delaminations/Epoxy	2.19 R	-	-	0.13	3.3	4.97	0.126	0.31	7.87	11.85	0.301
(Defect free areas)	2.19 R	69.3	1.11	0.04	1.02	1.53	0.039	0.29	7.37	11.09	0.282
Delaminations/Furane	2.3 R	-	-	0.05	1.27	1.85	0.047	0.25	6.35	9.26	0.235
(Defect free areas)	2.3 R	66.8	1.070	0.025	0.64	0.93	0.024	0.295	7.49	10.93	0.278
Delaminations/Overwrap	2.3 R	-	-	0.139	3.53	5.28	0.134	0.357	9.01	13.55	0.344
(Defect free areas)	2.3 R	68.0	1.09	0.045	1.13	1.69	0.043	0.253	6.43	9.60	0.244
	2.1 R	68.0	1.09	0.0595	1.51	2.26	0.057	0.248	6.3	9.41	0.239
	2.2 R	68.0	1.09	0.055	1.39	2.07	0.053	0.288	7.32	10.93	0.278
	2.45 R	68.0	1.09	0.03	0.88	1.33	0.034	0.232	5.92	8.84	0.225
Wrinkles/None	2.1 R	-	-	0.069	1.75	2.67	0.068	0.287	7.29	11.10	0.282
(Defect free areas)	2.1 R	66.1	1.06	0.059	1.5	2.28	0.058	0.307	7.8	11.88	0.302
(Defect free areas)	2.2 R	66.1	1.06	0.037	0.93	1.43	0.036	0.275	6.99	10.64	0.270
(Defect free areas)	2.3 R	66.1	1.06	0.033	0.83	1.28	0.033	0.267	6.78	10.33	0.262
(Defect free areas)	2.45 R	66.1	1.06	0.03	0.75	1.15	0.029	0.259	6.58	10.02	0.255
Wrinkles/Furane	2.45 R	-	-	0.061	1.55	2.28	0.058	0.224	5.69	8.37	0.213
(Defect free areas)	2.45 R	67.4	1.08	0.049	1.24	1.83	0.046	0.255	4.77	9.53	0.24
Low Density/Furane	2.1 R	61.2	0.98	0.135	3.56	5.26	0.134	0.418	10.62	15.71	0.399
Low Density/Furane	2.1 R	58.7	0.94	0.168	4.8	6.77	0.172	0.487	12.19	17.20	0.437

*Corrected to 600 psia chamber pressure

Table VIII-8

Corrected Regression and Char Depth of MX-2600
in Exit Section

Discrepancy/Repair	Location	Char Density		Regression				Char Depty			
				Total		Rate		Total		Rate	
		lb/cu ft	gm/cc	in.	mm	mil/sec	mm/sec	in.	mm	mil/sec	mm/sec
Delaminations/None	2.93 R	-	-	0.198	5.03	7.4	0.188	0.279	7.09	10.45	0.266
(Defect free areas)	2.93 R	84.9	1.36	0.094	2.39	3.52	0.09	0.208	5.28	7.79	0.198
(Defect free areas)	3.7 R	84.9	1.36	0.0595	1.51	2.83	0.072	0.248	6.3	9.29	0.236
Delaminations/Epoxy	2.93 R	-	-	0.13	3.30	4.97	0.126	0.25	6.35	9.56	0.243
(Defect free areas)	2.93 R	86.7	1.39	0.13	3.30	4.97	0.126	0.24	6.1	9.18	0.233
Delaminations/Furane	2.93 R	-	-	0.169	4.29	6.26	0.159	0.275	6.99	10.19	0.259
(Defect free areas)	2.93 R	86.1	1.38	0.169	4.29	6.26	0.159	0.301	7.65	11.15	0.283
Delaminations/Overwrap	2.93 R	-	-	0.198	5.03	7.51	0.191	0.298	7.57	11.31	0.287
(Defect free areas)	2.93 R	88.0	1.41	0.144	3.66	5.46	0.139	0.268	6.81	10.17	0.258
(Defect free areas)	3.7 R	88.0	1.41	0.089	2.27	3.39	0.086	0.258	6.55	9.79	0.249
Wrinkles/None											
(Defect free areas)	2.93 R	89.2	1.43	0.148	3.76	5.72	0.145	0.247	6.27	9.52	0.242
(Defect free areas)	3.7 R	89.2	1.43	0.079	2.00	3.09	0.078	0.247	6.27	9.52	0.242
Low Density/Furane	2.93 R	84.9	1.36	0.176	4.47	6.62	0.168	0.300	7.62	11.28	0.287
Low Density/Furane	3.7 R	84.9	1.36	0.083	2.11	3.12	0.079	0.248	6.3	9.32	0.237
Low Density/Furane	2.93 R	83.6	1.34	0.18	4.57	6.45	0.164	0.347	8.81	12.44	0.316
Low Density/Furane	3.7 R	83.6	1.34	0.079	2.00	2.83	0.072	0.281	7.14	10.07	0.256

*Corrected to 600 psia chamber pressure

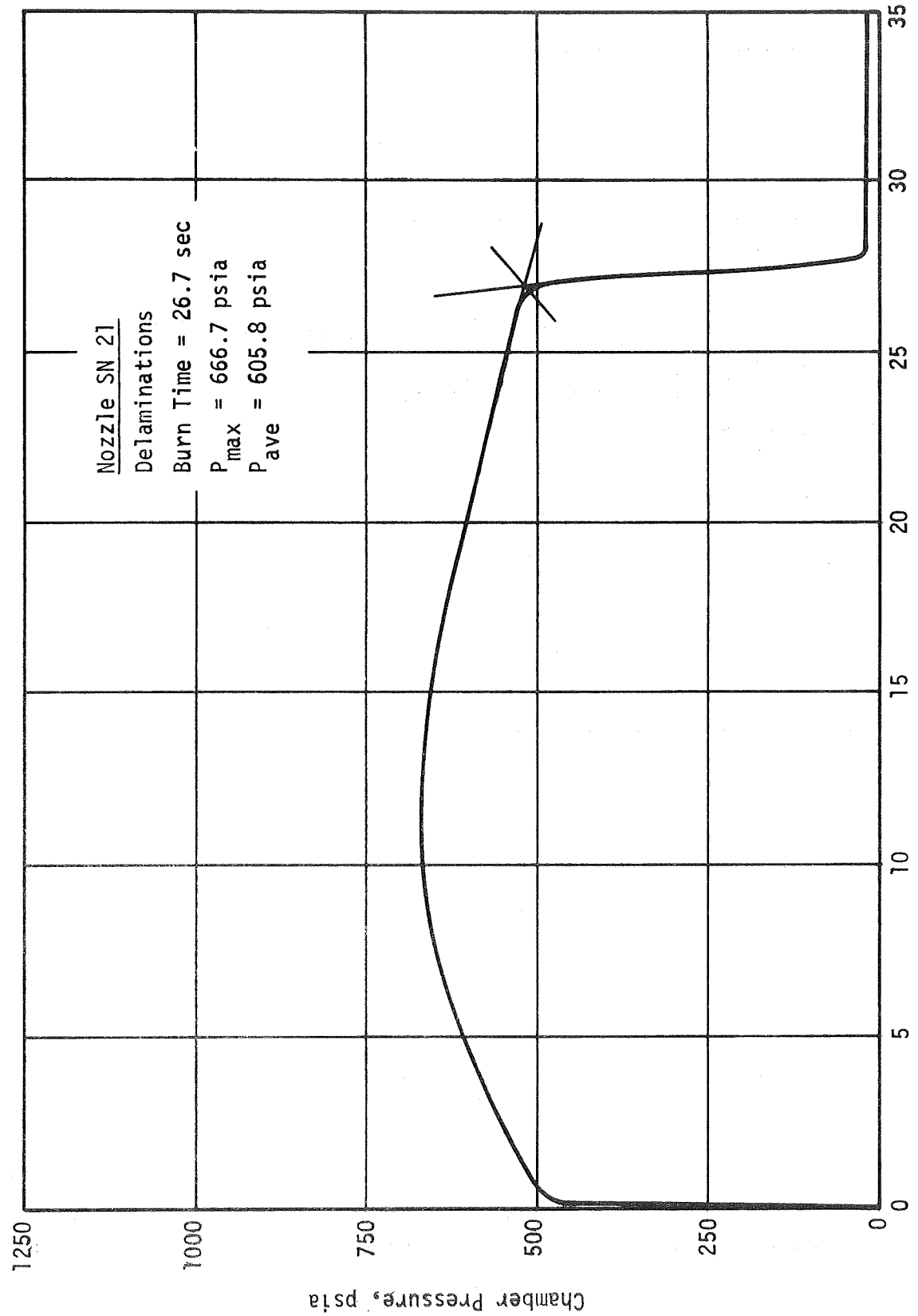

Pressure-Time Curve of Delaminated Nozzle

Figure VIII-1

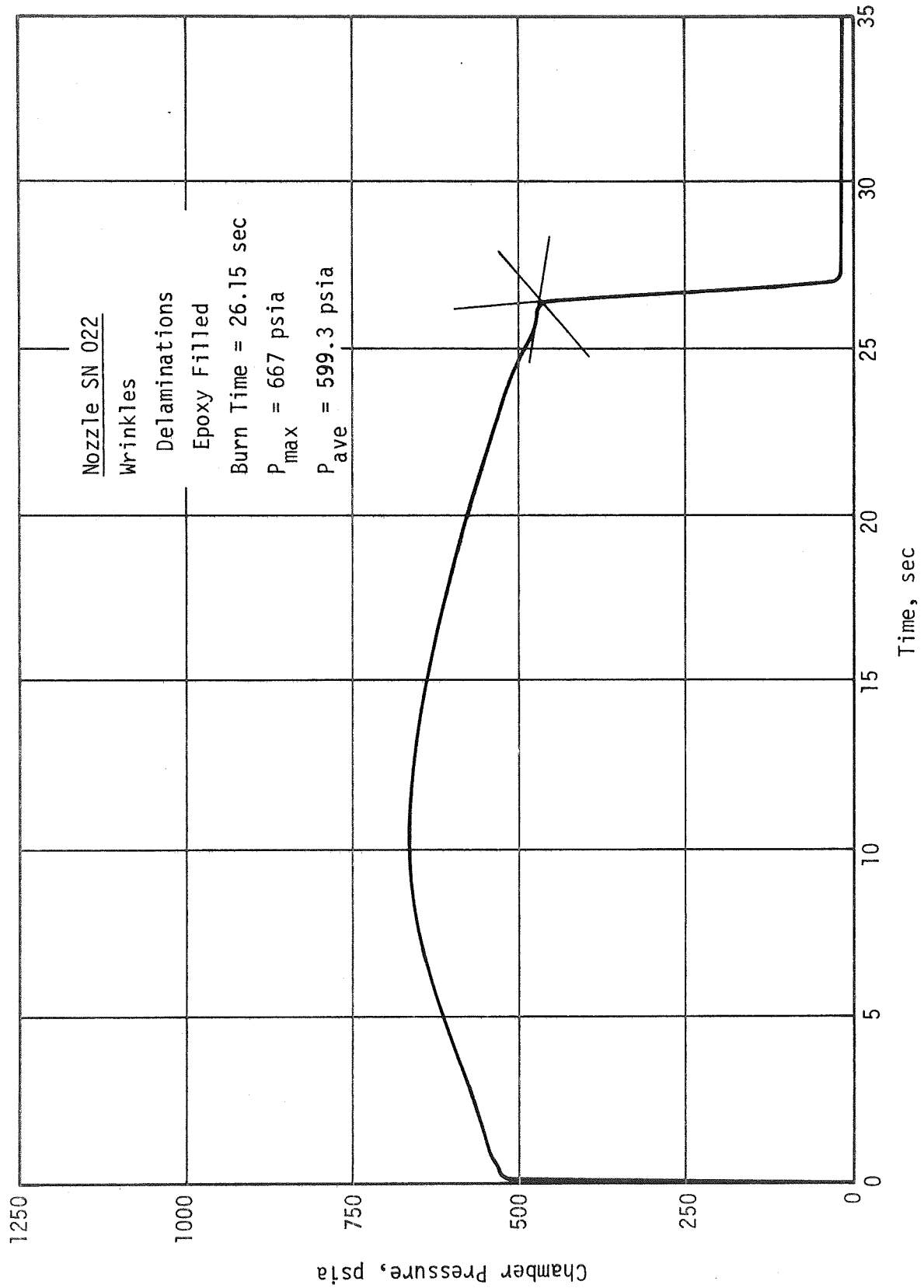

Pressure-Time Curve of Delaminated Nozzle Filled with Epoxy

Figure VIII-2

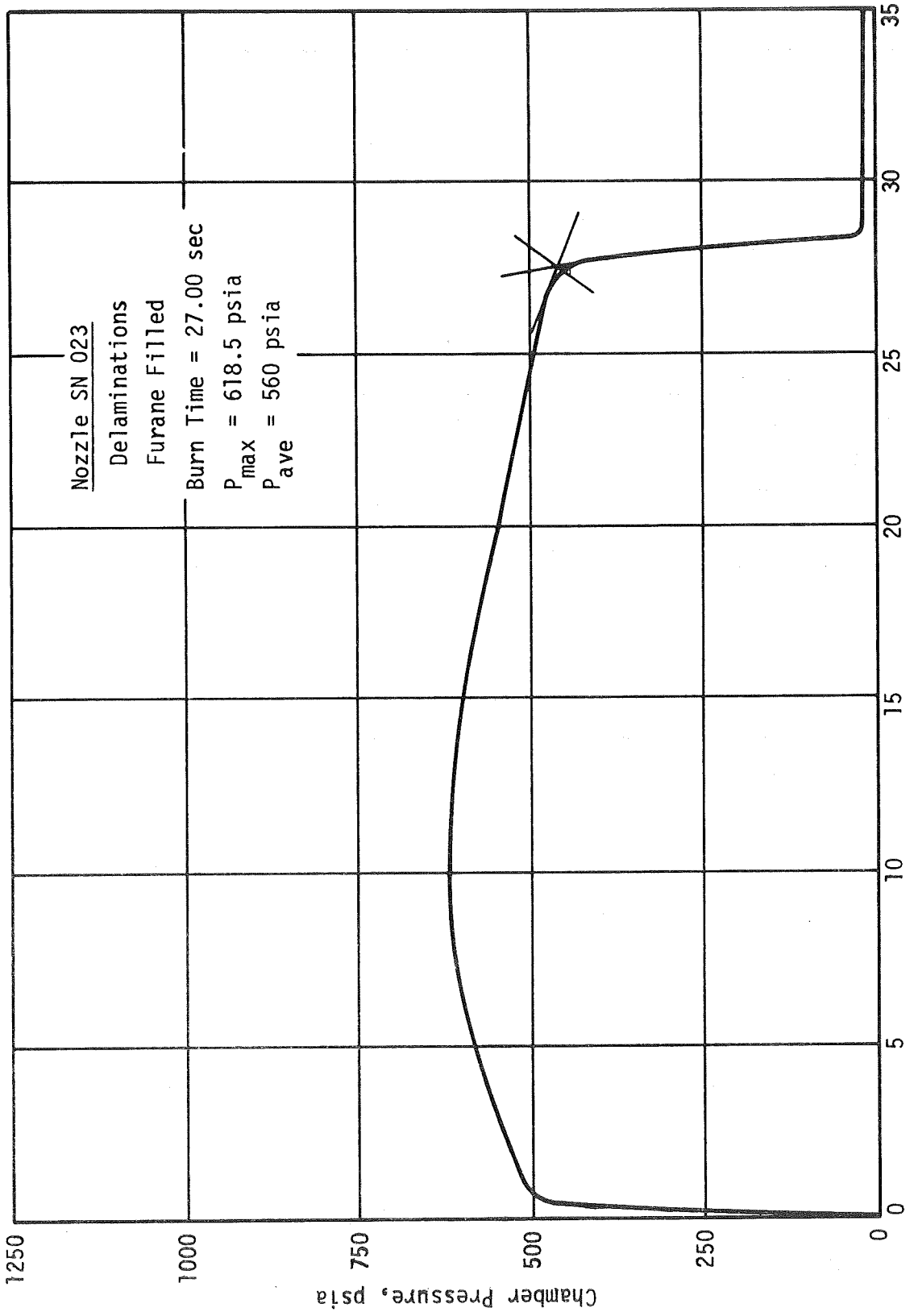

Pressure-Time Curve of Delaminated Nozzle Filled with Furane

Figure VIII-3

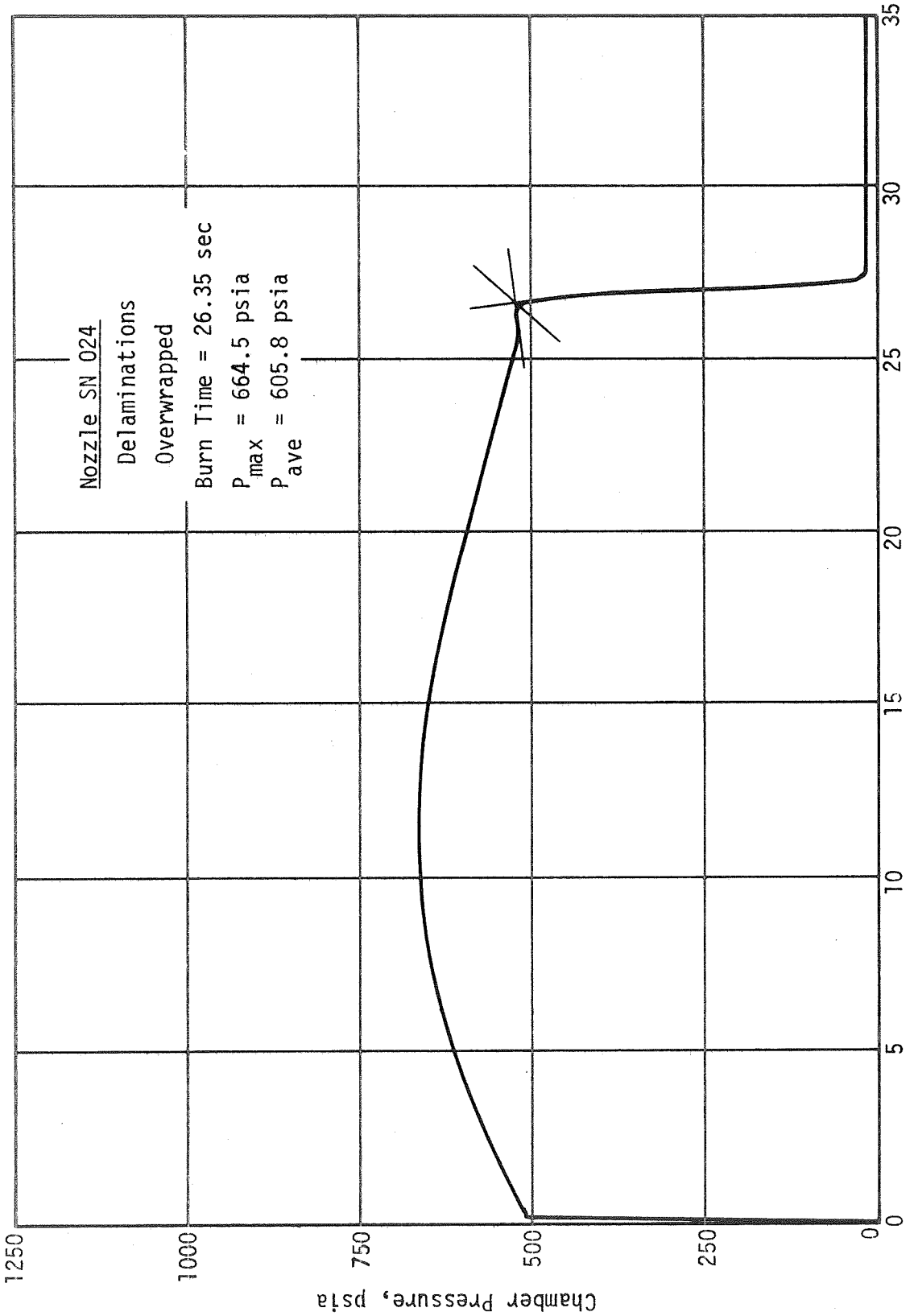

Pressure-Time Curve of Delaminated and Overwrapped Nozzle

Figure VIII-4

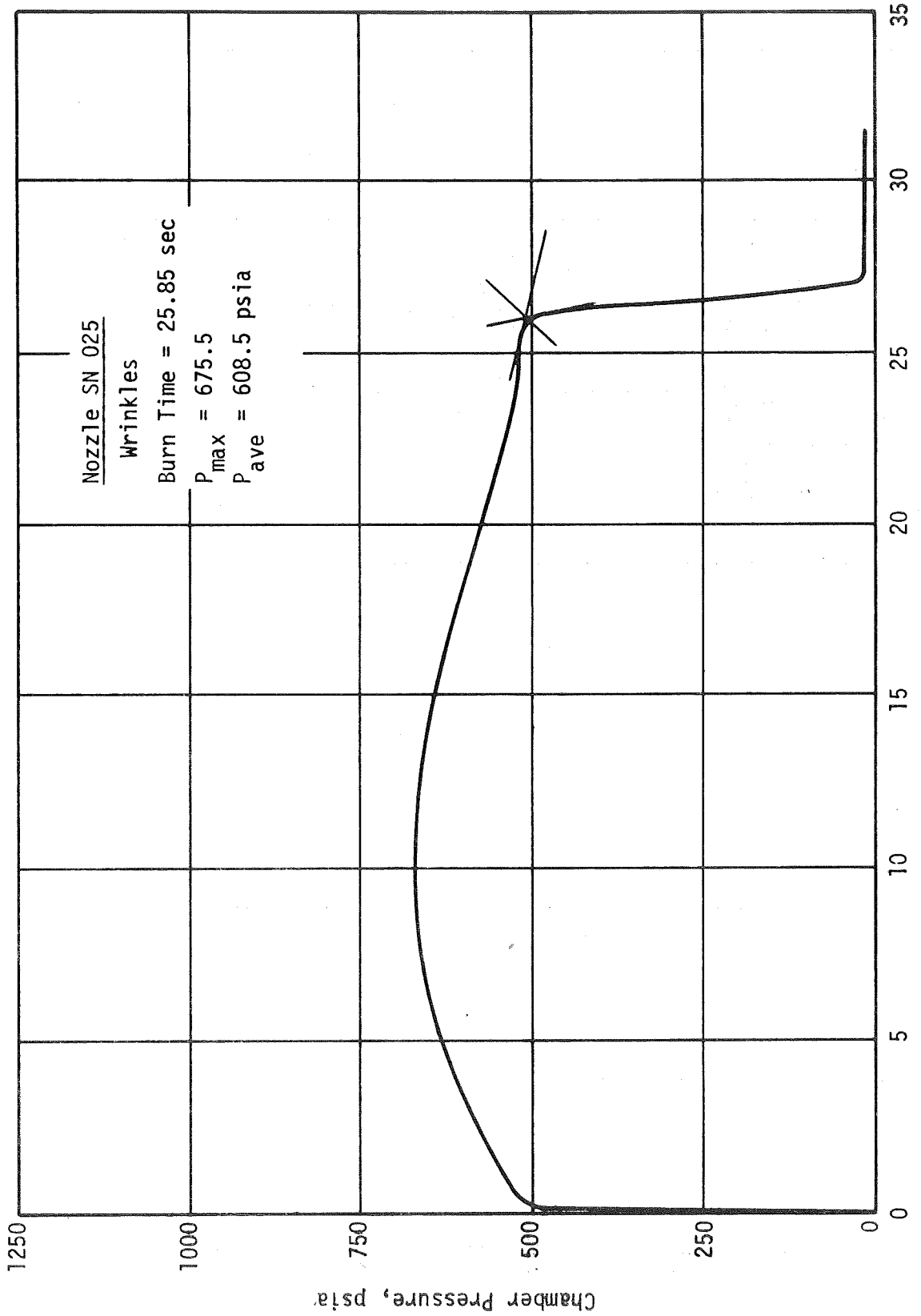

Pressure-Time Curve of Wrinkled Nozzle

Figure VIII-5

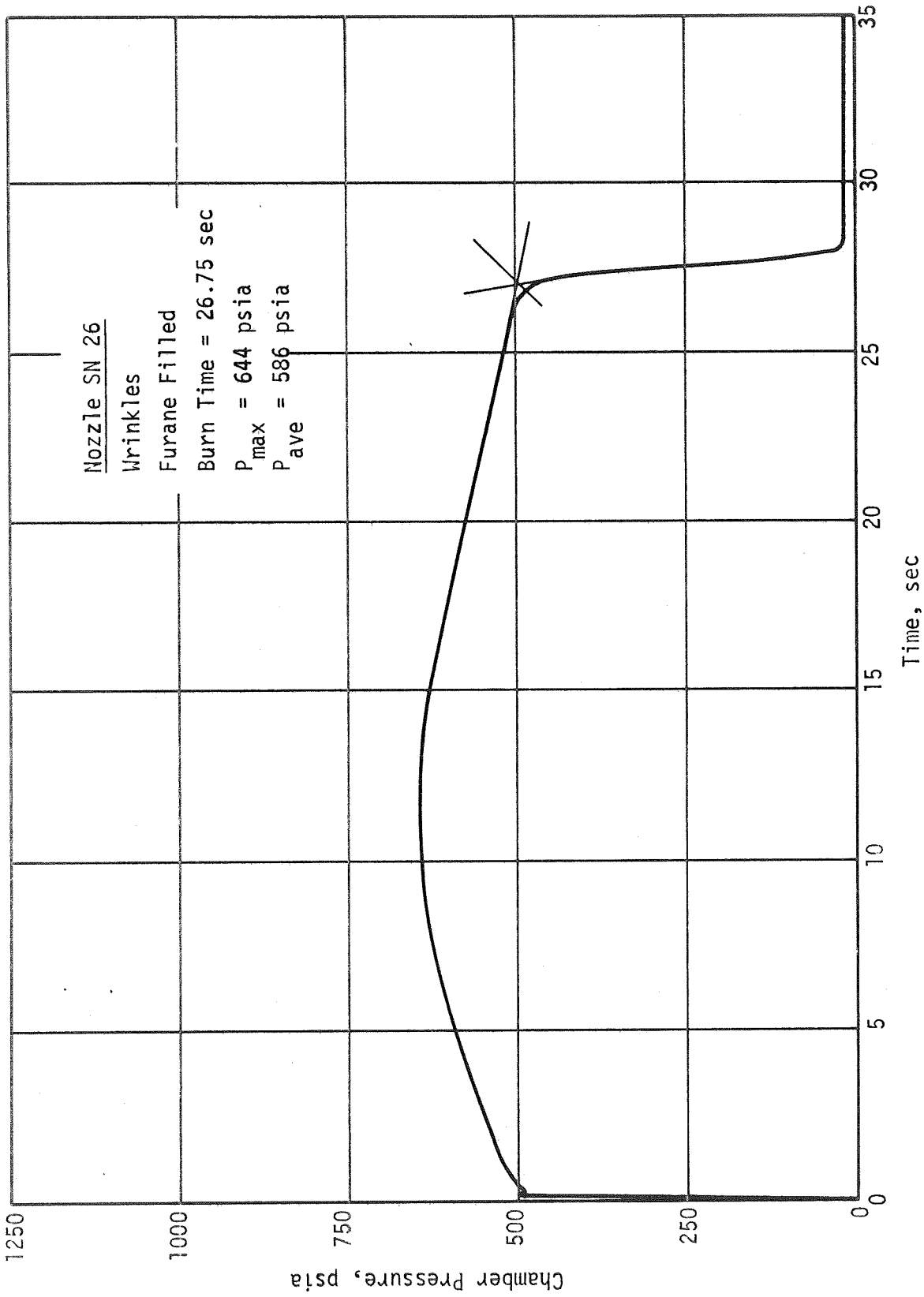

Pressure-Time Curve of Wrinkled Nozzle Filled With Furane

Figure VIII-6

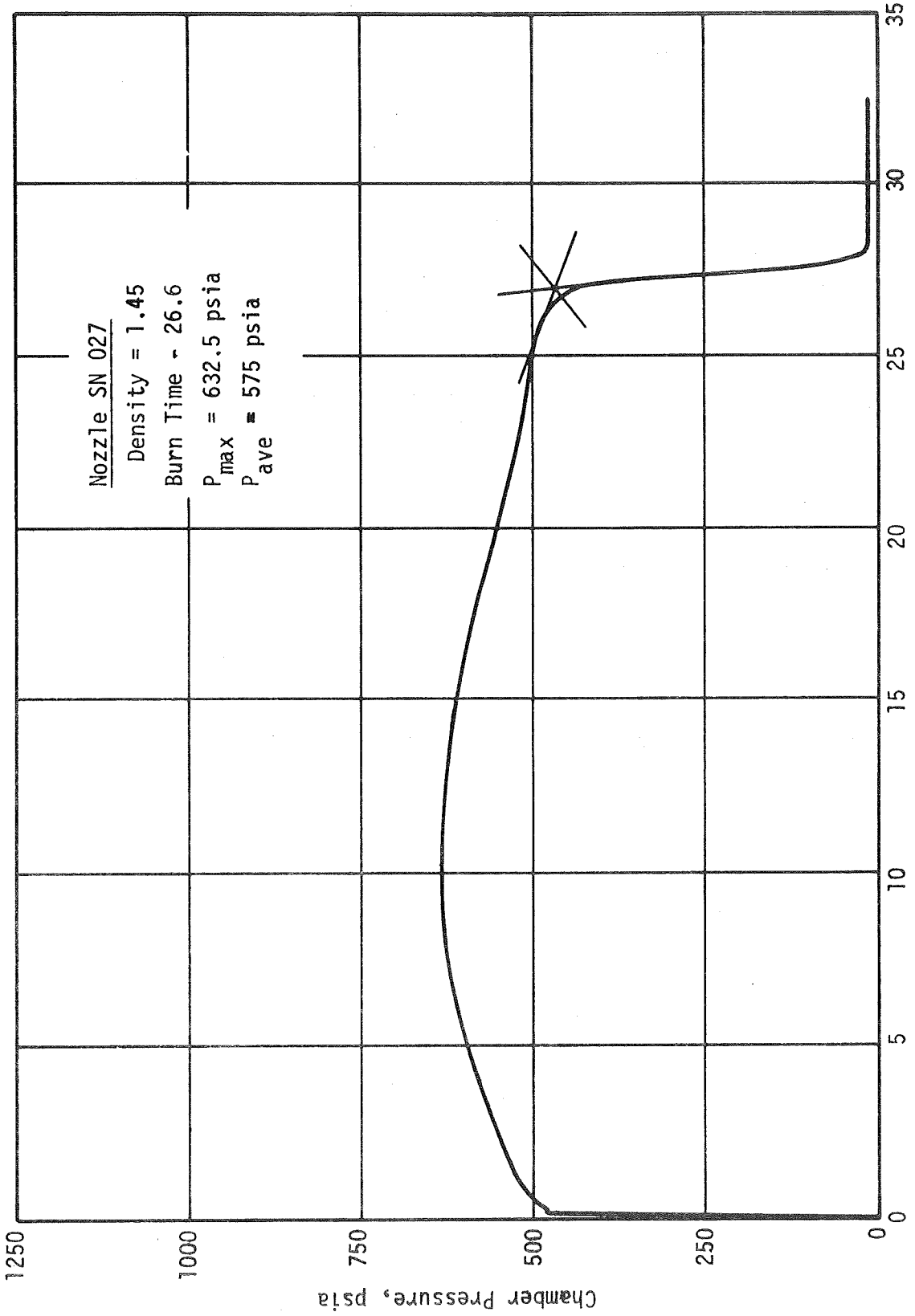

Pressure-Time Curve of Low Density Nozzle

Figure VIII-7

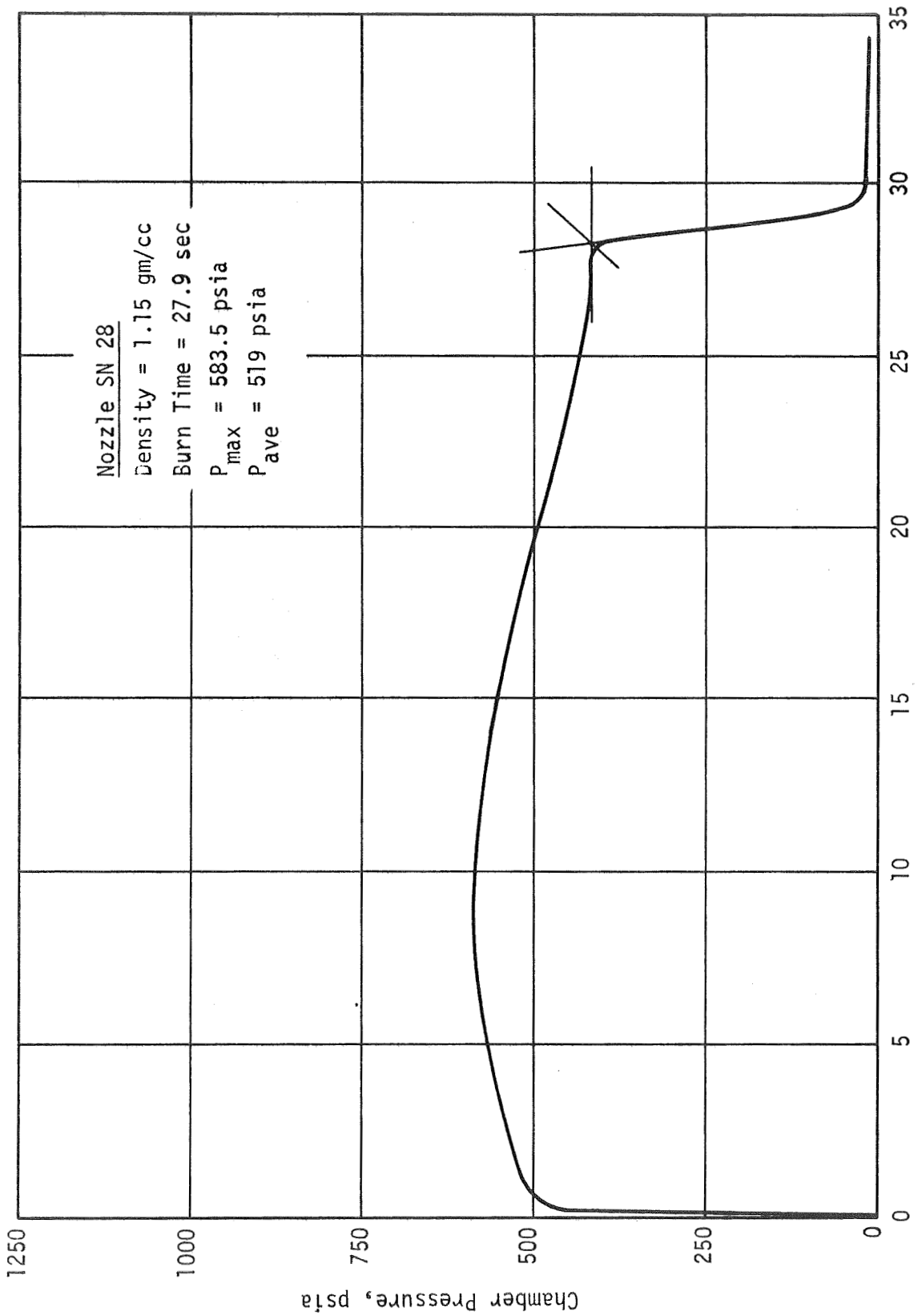

Pressure-Time Curve of Low Density Nozzle

Figure VIII-8

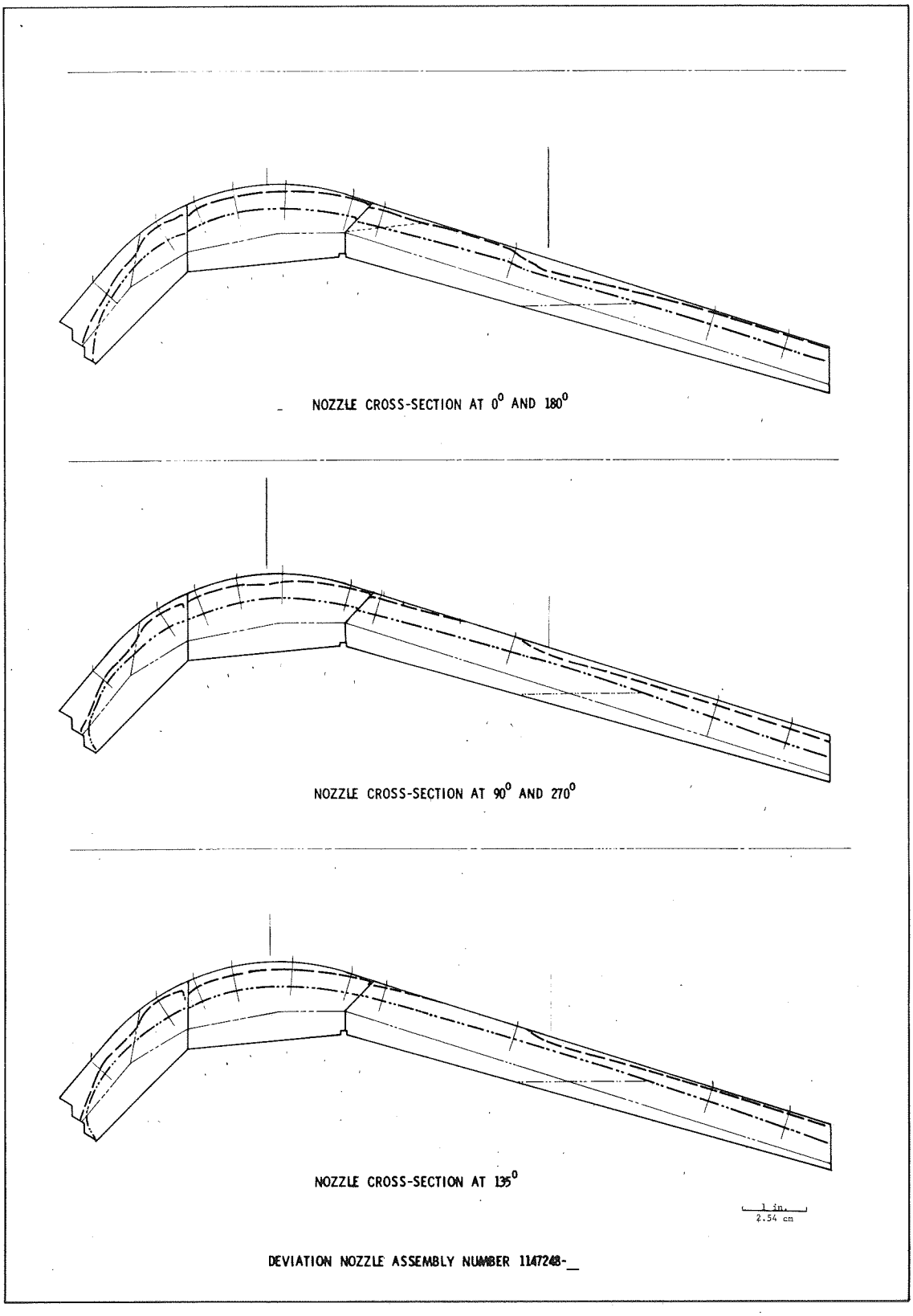

Regression and Char Depth in Nozzle S/N 021

Figure VIII-9

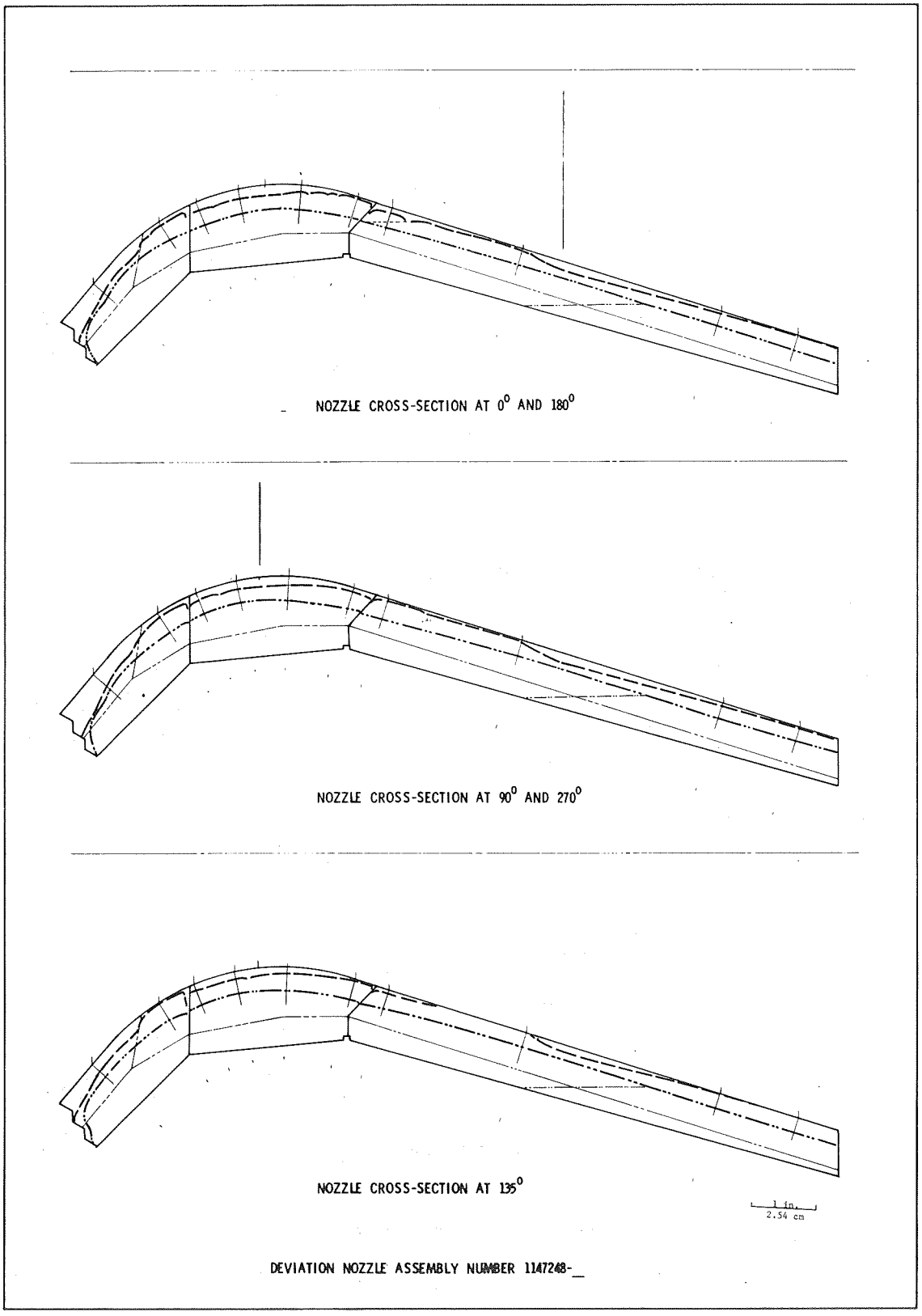

Regression and Char Depth in Nozzle S/N 022

Figure VIII-10

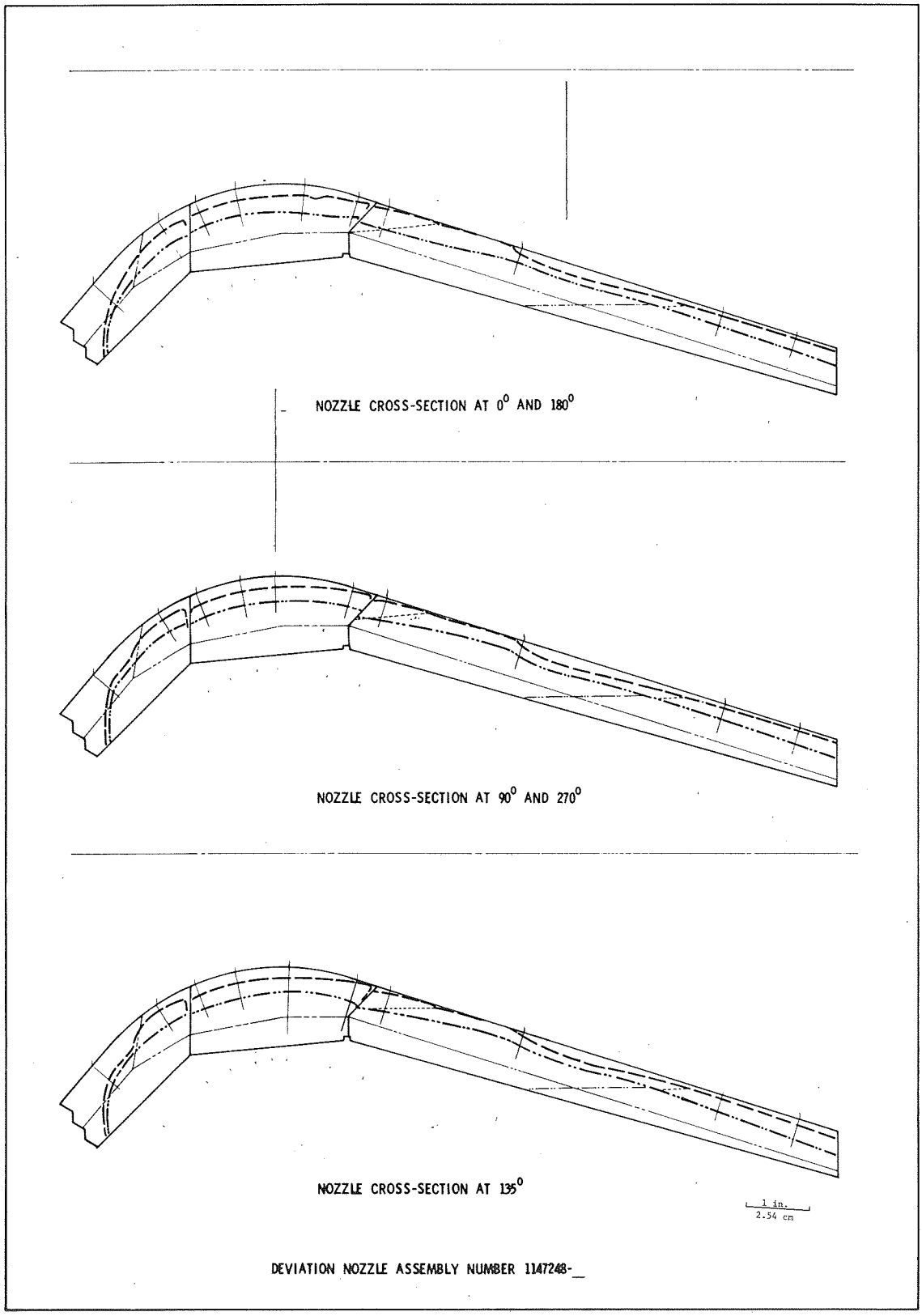

Regression and Char Depth in Nozzle S/N 023

Figure VIII-11

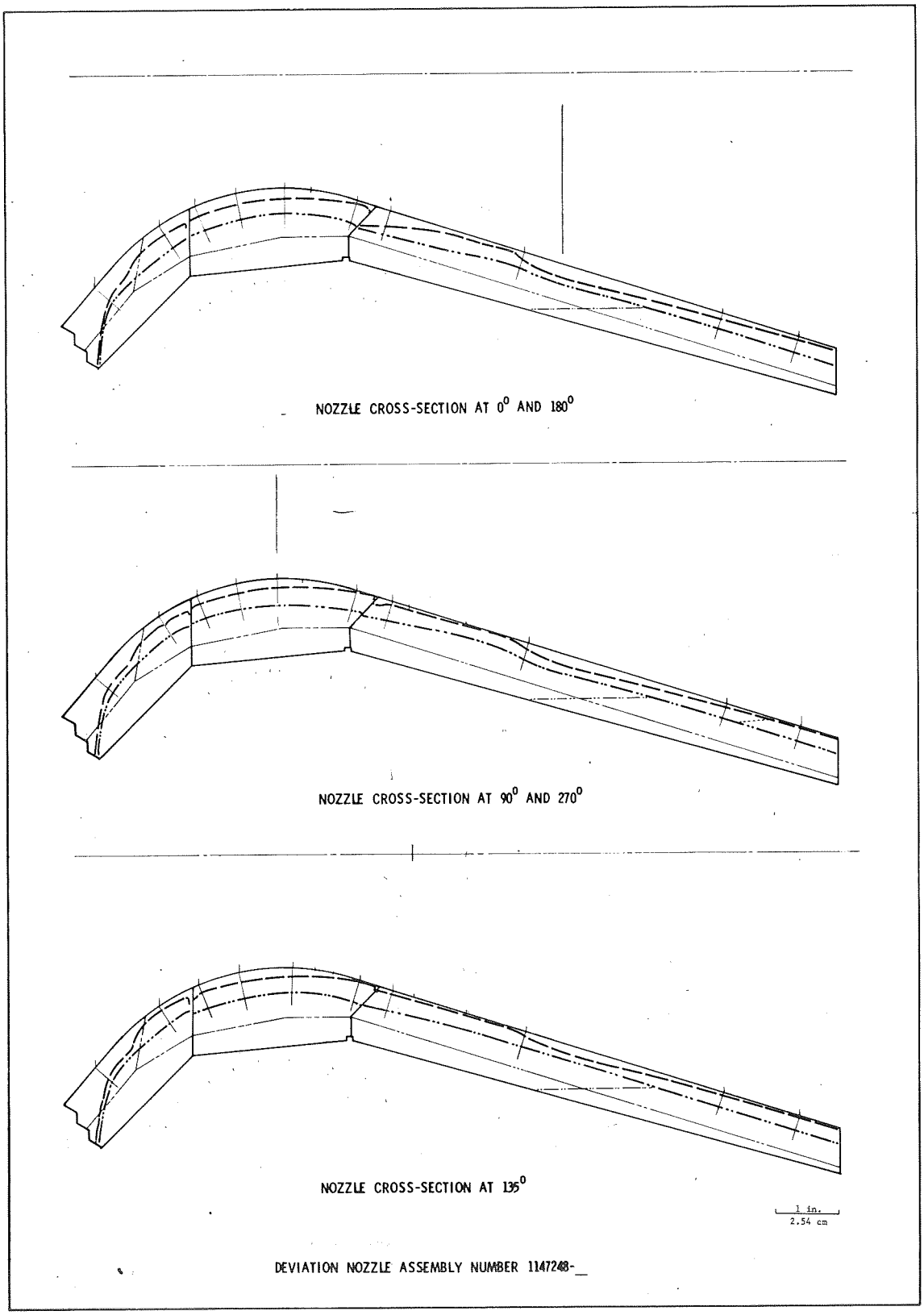

Regression and Char Depth in Nozzle S/N 024

Figure VIII-12

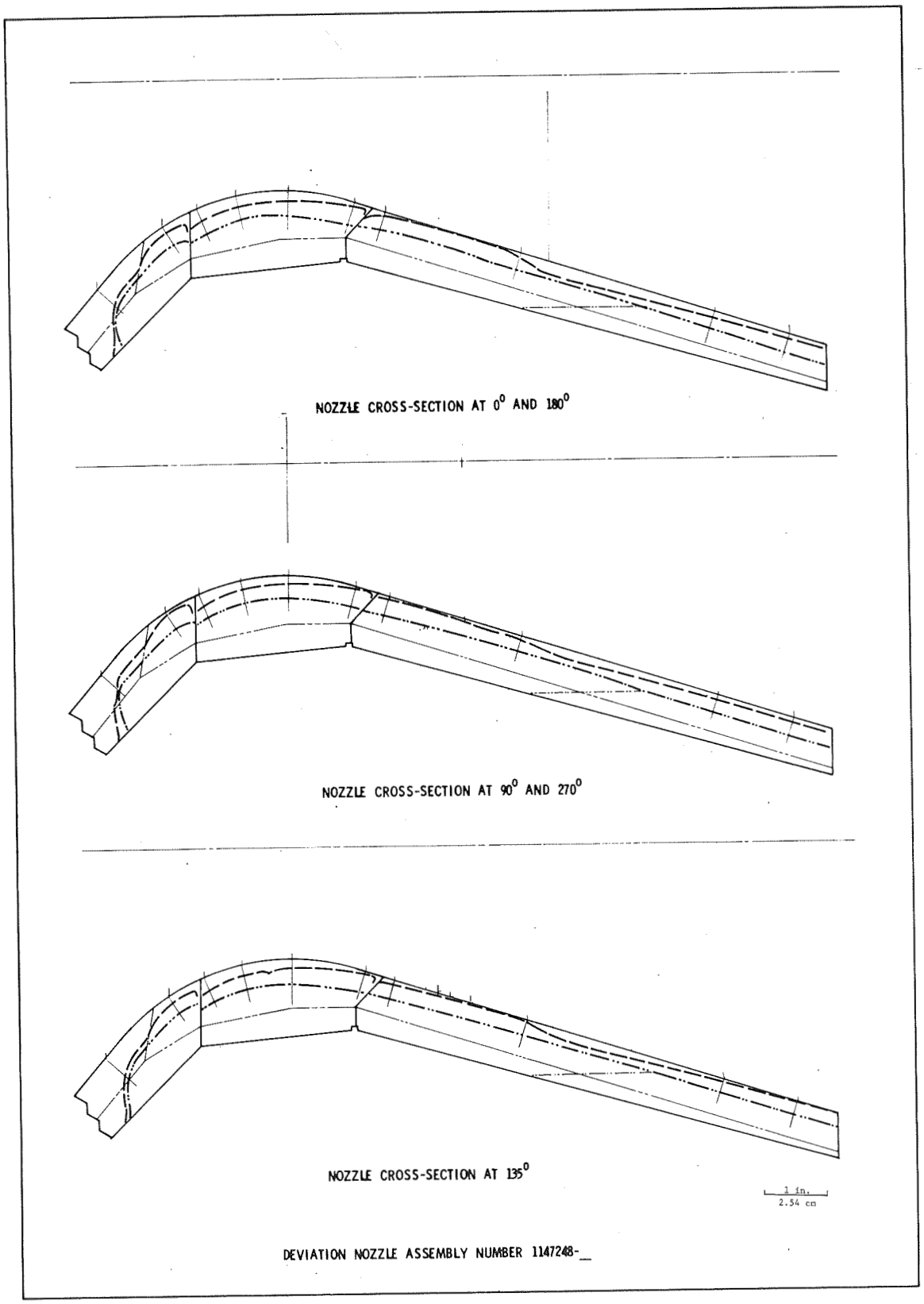

Regression and Char Depth in Nozzle S/N 025

Figure VIII-13

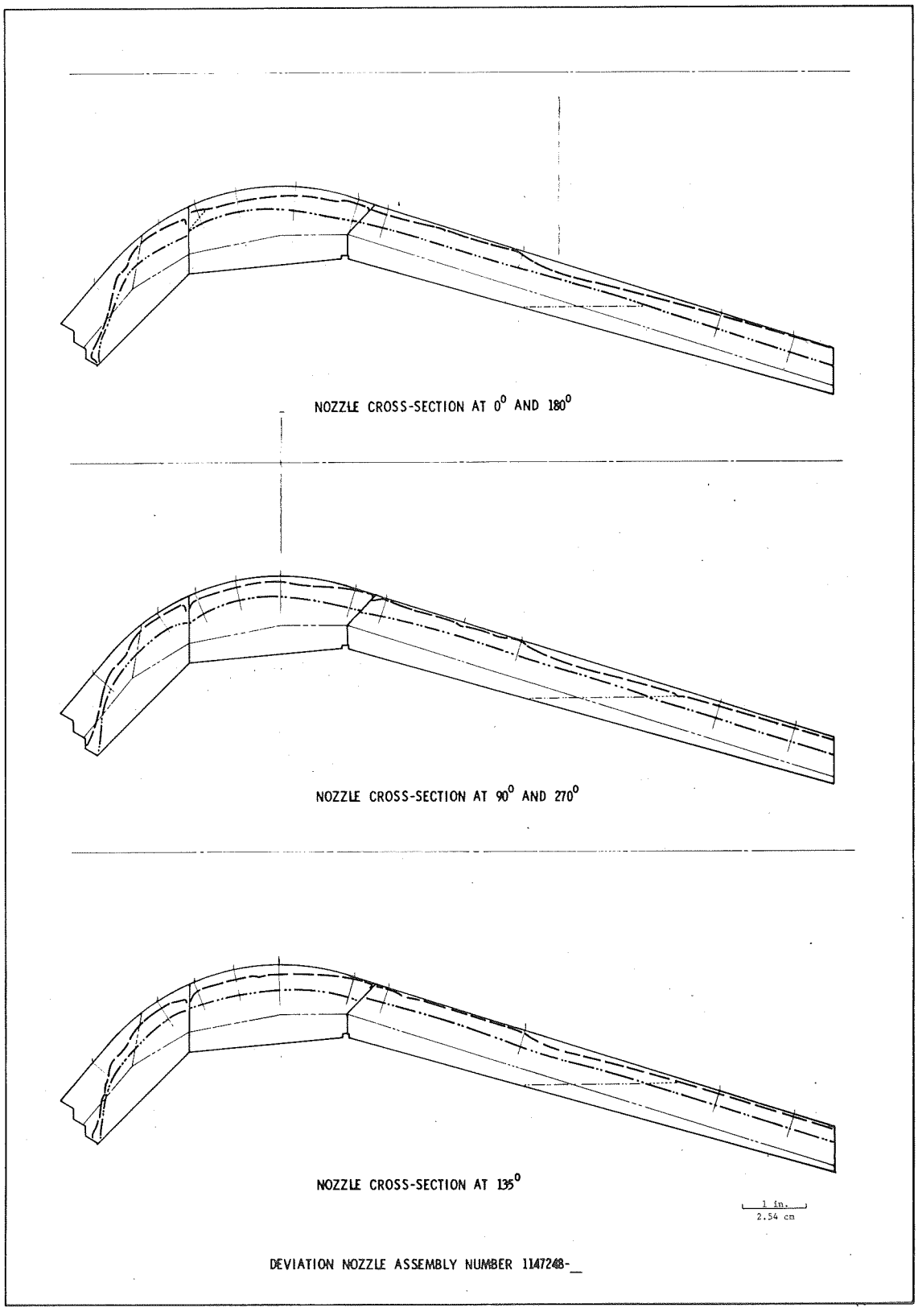

Regression and Char Depth in Nozzle S/N 026

Figure VIII-14

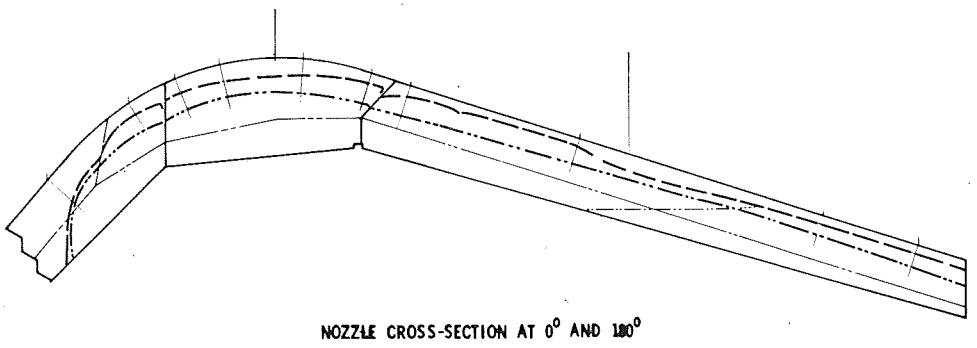

NOZZLE CROSS-SECTION AT 0° AND 180°

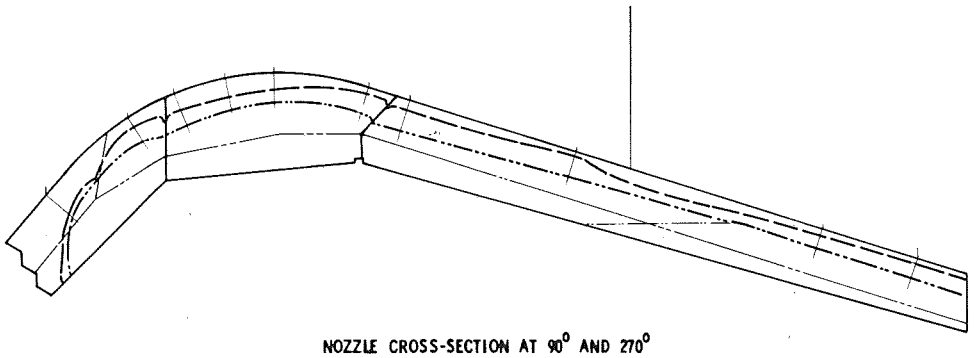

NOZZLE CROSS-SECTION AT 90° AND 270°

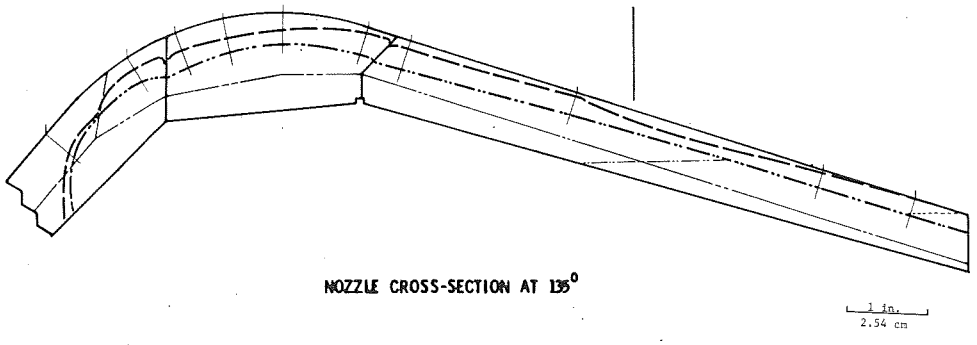

NOZZLE CROSS-SECTION AT 135°

1 in.
2.54 cm

DEVIATION NOZZLE ASSEMBLY NUMBER 1147248-_

Regression and Char Depth in Nozzle S/N 027

Figure VIII-15

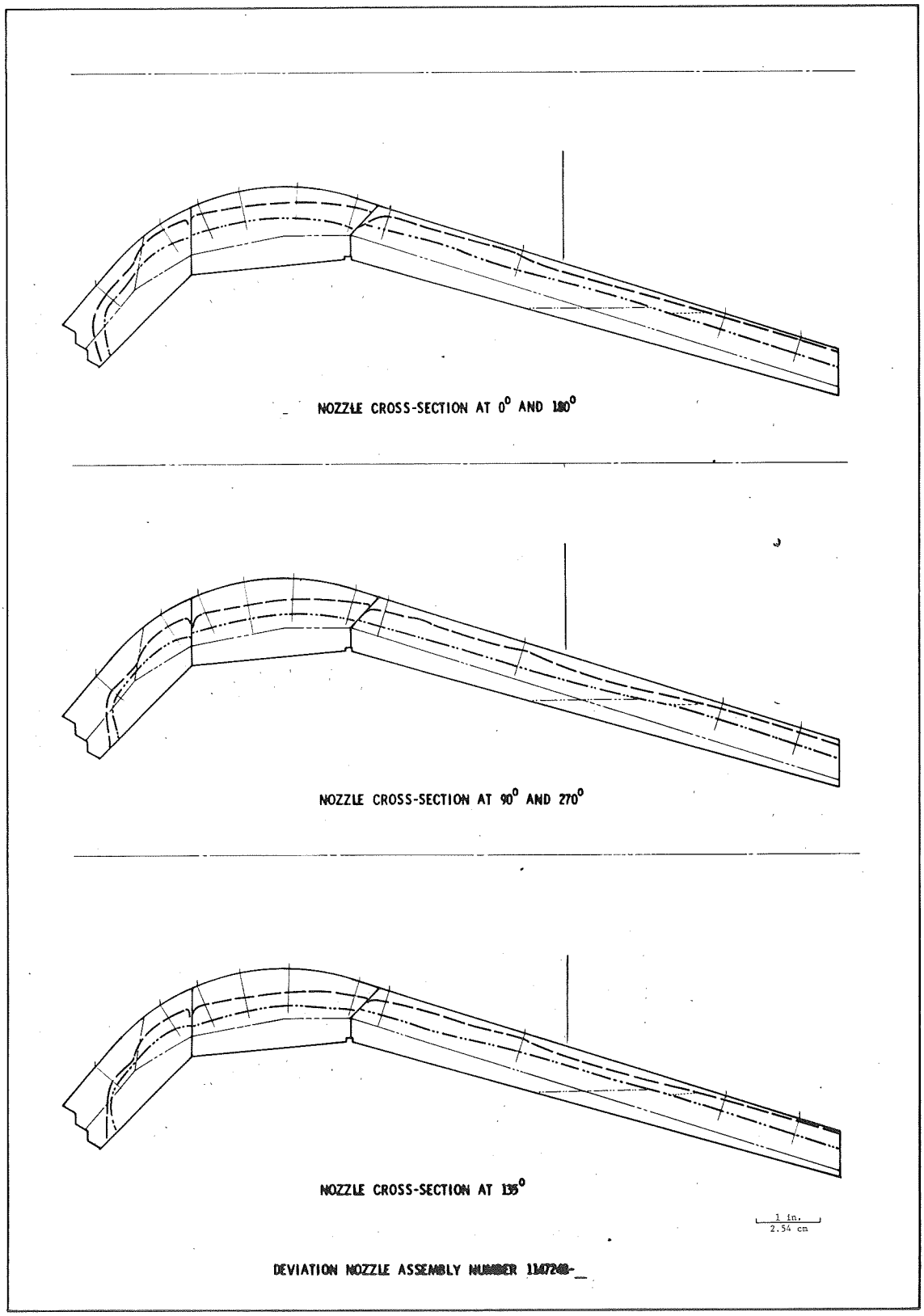

Regression and Char Depth in Nozzle S/N 028

Figure VIII-16

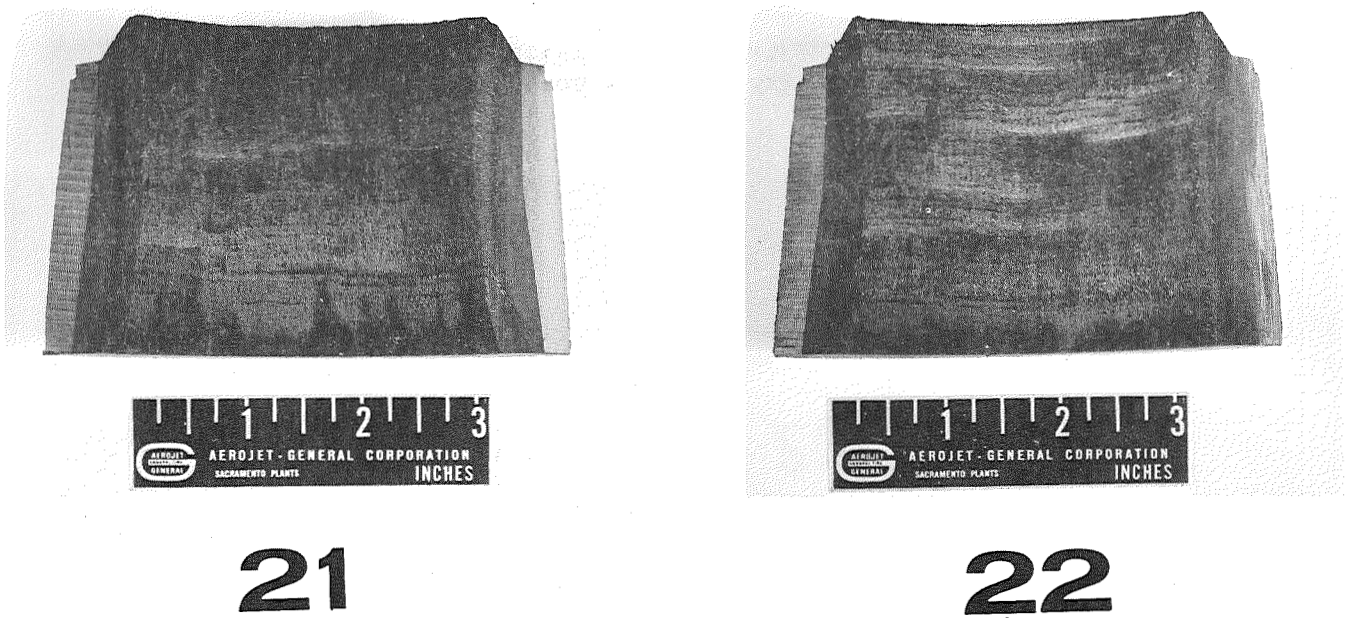

Figure VIII-17

Delaminated and Repaired Throat Inserts After Static Test

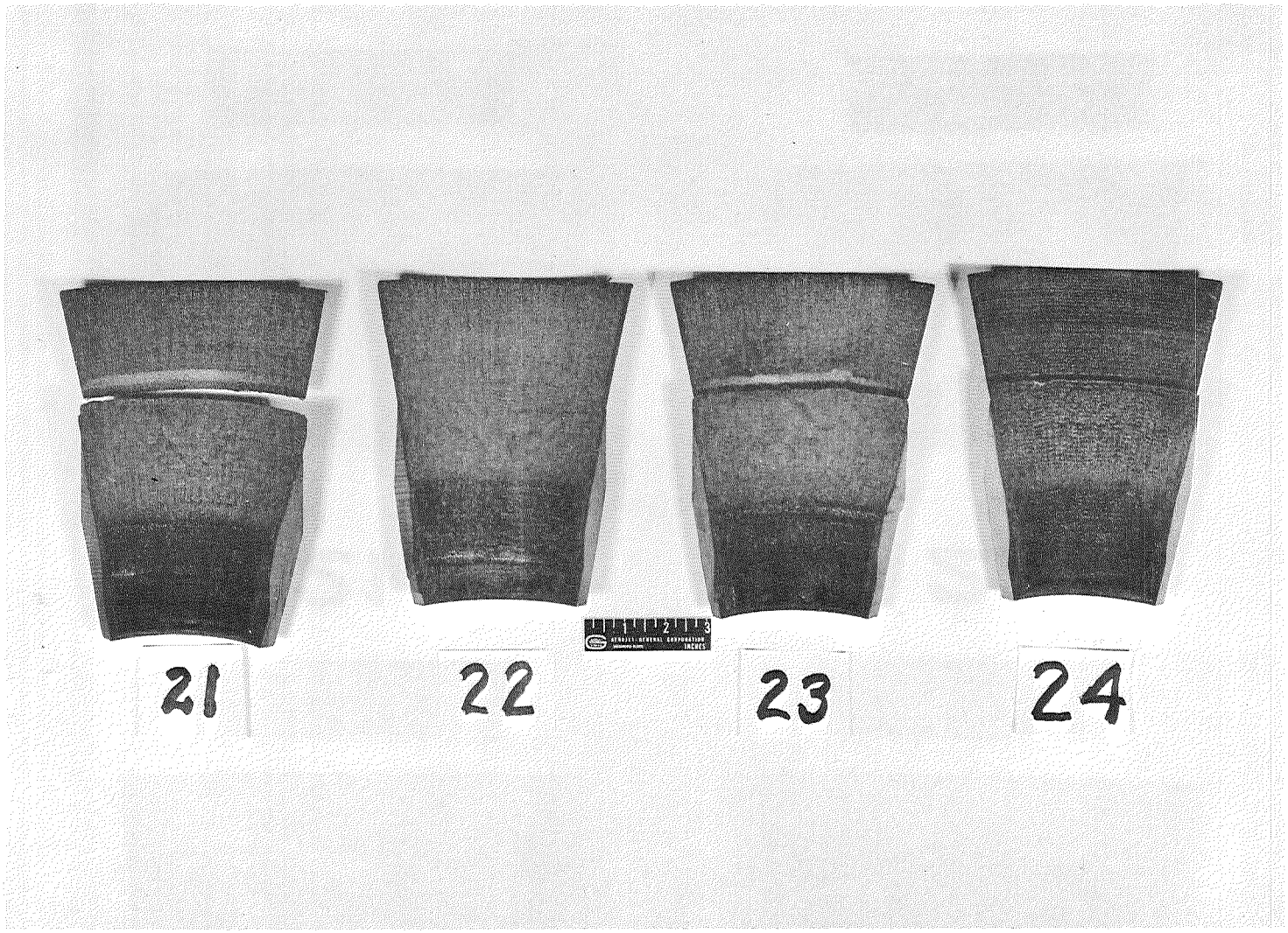

Delaminated and Repaired Exit Sections
after Static Test

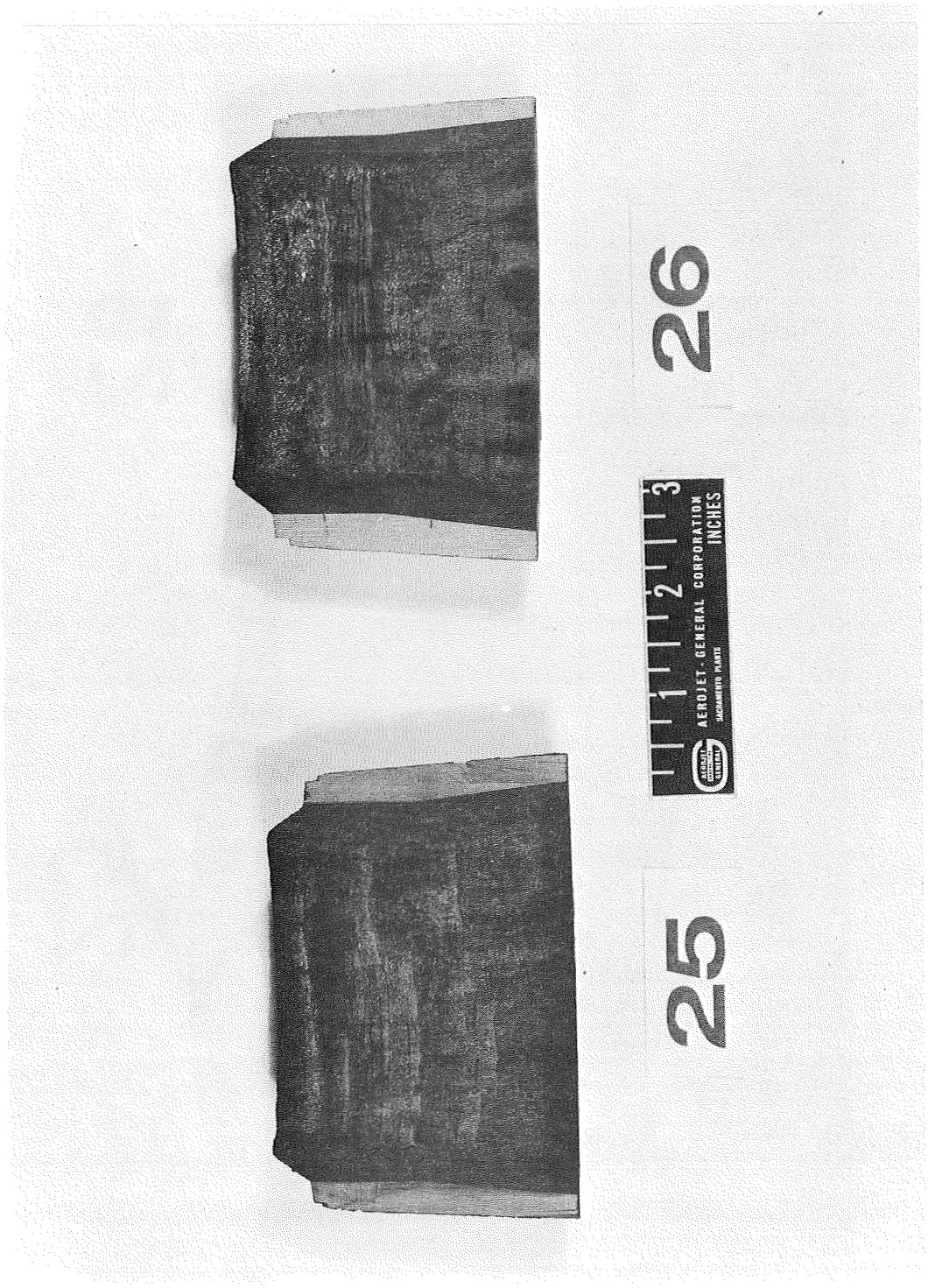

Wrinkled and Repaired Throat Inserts
after Static Test

Figure VIII-19

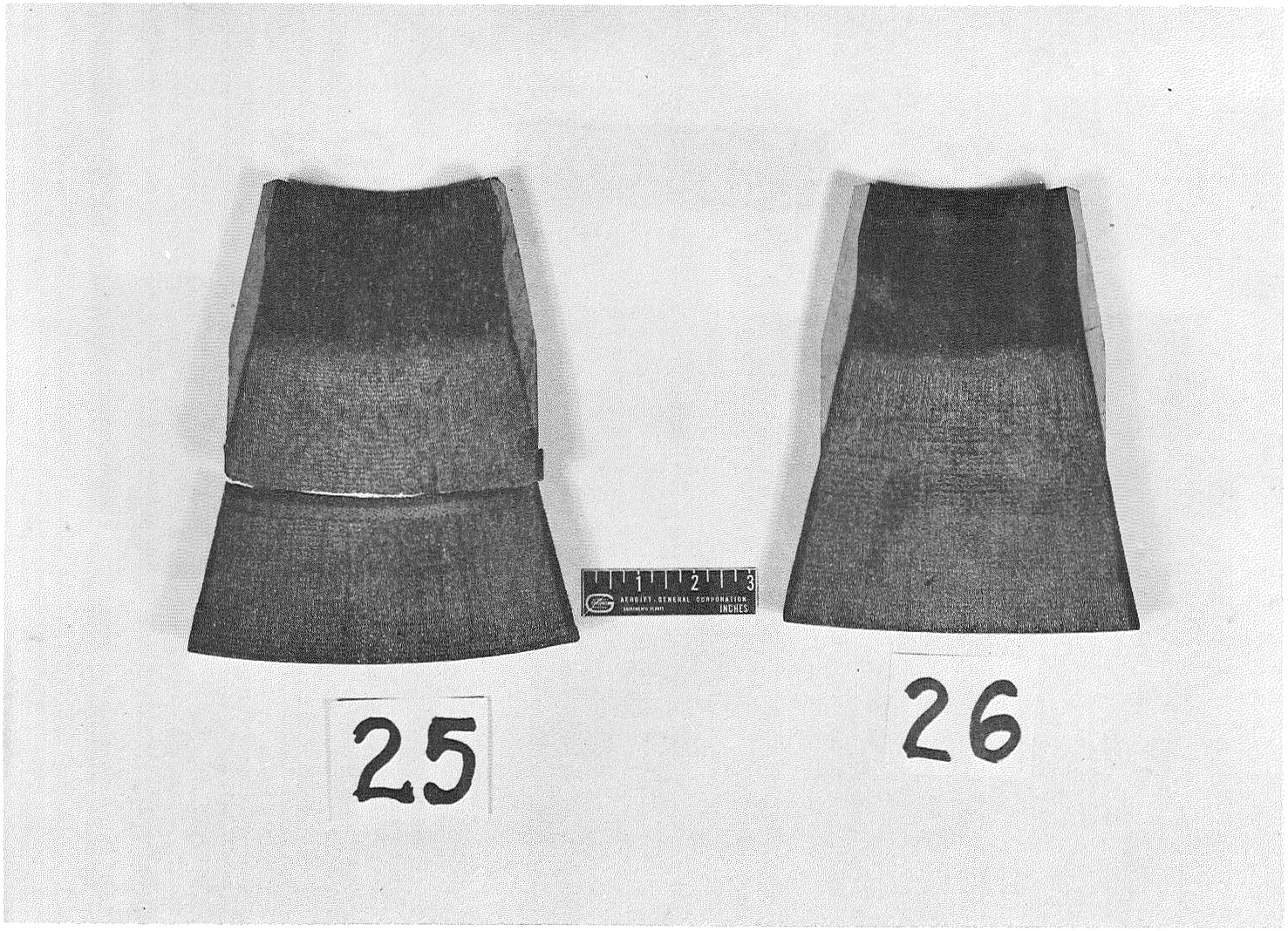

Wrinkled and Repaired Exit Sections
after Static Test

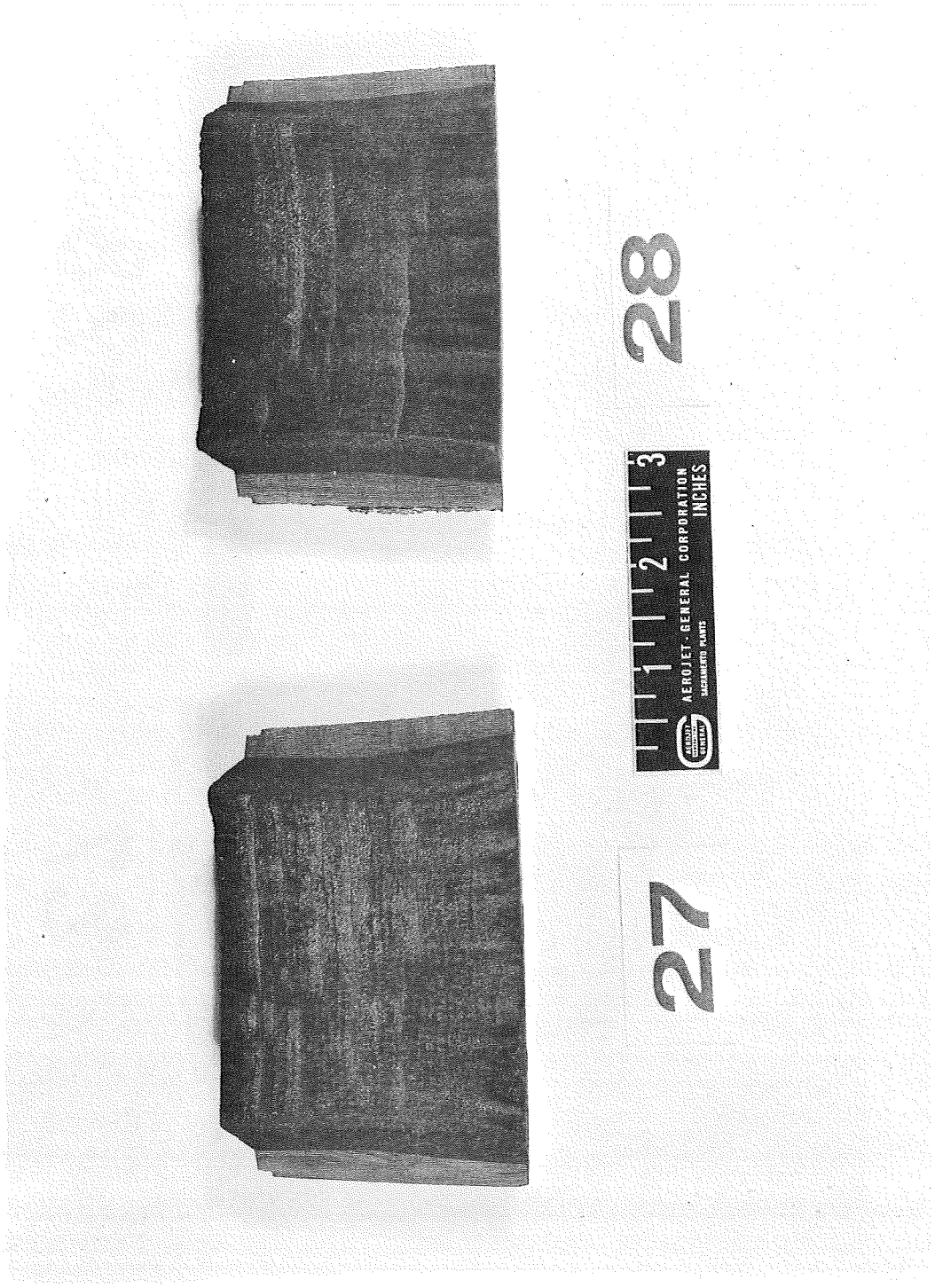

Low Density Throat Inserts after
Static Test

Figure VIII-21

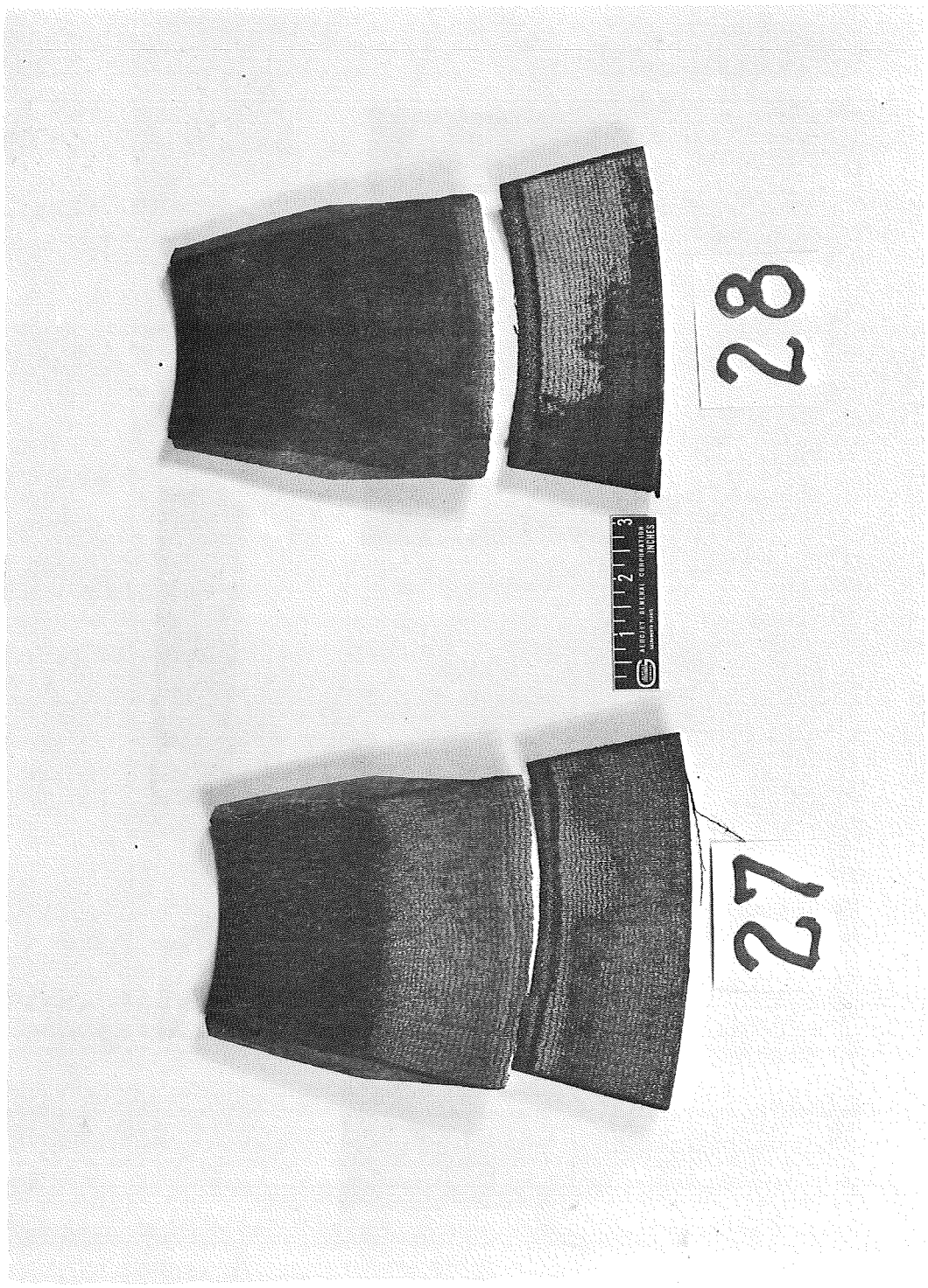

Low Density, Repaired Exit Sections
after Static Test

Figure VIII-22

IX. DISCUSSION OF RESULTS

A. REGRESSION OF DISCREPANT COMPONENTS

1. Analysis of Variance

To evaluate the effects of the introduced discrepancies, regression and char rates were first determined for normal materials. The average rates ($\bar{X}$) shown in Table IX-1 are based on results obtained for the baseline nozzles plus data from the defect-free portions of nozzles with wrinkles, resin-rich, resin-starved, and delaminated areas. The data from bag leakage, temperature loss, and autoclave-cured nozzles were also included in determining the normal regression and char rates, since their rates fell within the range encompassed by the baseline motors. The availability of 10 to 15 samples for each material made possible an estimation of the motor-to-motor standard deviation (σ) for normal materials. These values are also shown in Table IX-1. It was assumed that the averages and standard deviations for the normal materials were population values. Based on the sample size involved, one would expect 90 percent of the measurements of regression and char depth to lie within plus or minus 2.5 standard deviations of the average values. Accordingly, it was assumed that any value for discrepant nozzles greater than 2.5 standard deviations represented a significant departure from the average.

The comparison of regression and charring behavior among the twenty nozzle assemblies is shown in Tables IX-2 through IX-5. The results reveal a mixed pattern of differences between discrepant and normal materials leading to the following observations:

a. Decreases in virgin and charred composite densities significantly increased the regression rates of the MX-4926 material in the throat and tended to increase the regression rate of the MX-2600 material in the exit cone.

IX.A. Regression of Discrepant Components (cont)

b. Cure cycle variations (bag leakages and temperature loss) did not produce significant effects.

c. While most of the tests with volatile content discrepancies showed increases in rates above the average, less than half of the increases were significant. Furthermore, when significant increases in regression occurred there was no correlation to the volatile content.

d. The wrinkled MX-4926 throats showed slight but nonsignificant increases in regression rate. The remainder of the MX-4926 and MX-2600 wrinkled parts showed significant increases in rate. Except for the entrance cap, there was no correlation to increasing severity.

e. Significant increases in rate were observed in the resin-rich areas of MX-4926, although there was no apparent correlation to the resin content. Conversely, significant rate increases were observed in the resin-starved areas of the MX-2600.

f. Parts with delaminations showed generally increasing rates as the number of delaminated plies increased.

2. Thermal Analysis

From the discussion of statiscally significant factors one variable which was noted to have a great influence on throat erosion was the char density. The charring ablation program has inputs of resin content, thus, it could conceivably predict the performance of nozzle parts with resin-rich and resin-starved areas. Table IX-6 shows the values of virgin and fully charred MX-4926 (carbon) and MX-2600 (silica) material densities used in the computer prediction programs. Also shown are the char density values that were

IX.A. Regression of Discrepant Components (cont)

determined during the performance analyses of the test-fired nozzles. In general, the measured and computed values are in close agreement, the major differences occurring with the resin-starved materials.

To indicate more precisely the role of char density, the predicted throat regression of the nine nozzles containing introduced density variations are presented in Figure IX-1 as a function of computed char density. The predicted results are represented by the solid curve, with total regression decreasing as the density increases. The measured regression values are shown as ranges with open triangles denoting the average. Two additional data points, those for the throats of SN 027 and SN 028 are added, since the throats were left in the as-fabricated condition. Although there is some data scatter, the measured averages are very close to the predicted values. It appears, therefore, that a controlled weight loss test could be used to predict performance.

3. Regression and Ablative Composite Properties

The mechanical and physical properties of the reinforced ablative composite test materials changed significantly as the density changed. In an effort to determine whether measurements of virgin composite properties could be used to predict performance, comparisons were made as follows:

Tables IX-7 and IX-8 compare the compressive strength and thermal conductivity of MX-4926 and MX-2600 specimens with the regression rates at the throat and in the exit cone, respectively. There is no correlation of the regression rate to the two designated properties.

IX. Discussion of Results (cont)

B. THERMOELASTIC STRESS ANALYSIS OF NOZZLE SN 016

Figure IX-2 is a plot of the hoop stress and hoop strain in the exit cone that failed. The stress plot shows a waviness of significant amplitude, indicating high discontinuity stresses due to:

1. Delaminations at elements 25, 26 and 27
2. Thickness transitions at elements 44, 53 and 63
3. The steel shell at element 72

Individually and collectively, these stresses would contribute to any failure mode. The possible use of finer grid in this area would have indicated that higher stresses were present than those that were plotted.

The hoop strain distribution shows something that to date is unique in solid rocket exit cone designs. Along the outer fiber there is present a negative hoop strain combined with a positive hoop stress. This is due to the fact that the outer surface of the silica meterial is at 1000°F (538°C). At this temperature, the coefficient of thermal expansion is negative. Thus, a negative total hoop strain occurs because the hotter inner fiber, whose coefficient of thermal expansion has returned to positive, prevents the outer fibers from shrinking. The restraint accounts for the positive hoop tensile stress.

Figure IX-3 shows the erratic axial and shear stresses in the exit cone.

It may be concluded that initial failure was due to local burn-through and propagated between the plies of material because of the high shear and bending stresses.

IX. Discussion of Results (cont)

C. REPAIR PROCEDURES

As discussed in Section VIII, the repair techniques investigated were those that incorporated the use of accelerated plastic resins that could be cured at room temperature. Both an epoxy and a furane base were investigated. Neither improved the ablative performance of delaminated, wrinkled or porous (low density) parts. The answer may lie in the fact that neither resin pyrolyzes to form the amount of char produced by the phenolic resin of the original composite.

It has since been pointed out that there are catalyzed phenolic-base resins commercially available. One material, marketed by Ironsides Resin, Inc. (Columbus, Ohio), under the designation DP5-161, may be cured at temperatures as low as 120°F. The use of such a material for repair purposes would bear investigation.

Because of the lack of improvement imparted by resin-impregnation, it appears that defects of an intolerable size in ablative plastics should continue to be removed, and be replaced by bonded-in sections of acceptable and similar material.

D. ACCEPT/REJECT CRITERIA

The objective of this program was to determine accept-reject criteria for ablative plastics. Accordingly, the effect of each discrepancy on the structural and ablative performance of the test nozzle was analyzed. From the results of the analysis, acceptance limits are proposed for each type of discrepancy that will not result in appreciable reductions in performance when compared to nondiscrepant nozzles. In general, the acceptable limits were established on the basis of ablative performance, since structural failures of a nozzle from the discrepancies tested is unlikely without introducing a gas flow path in the nozzle liner.

IX.D. Accept/Reject Criteria (cont)

Ablative performance is compared on the basis of surface regression and char depth at various stations of the nozzle. The acceptability of each discrepancy beyond the specified limits must consider the effect of the degradation of motor performance resulting from enlargement of the nozzle throat area and increase in the nozzle inert weight.

1. Volatile Content

Volatile contents up to 5% showed no appreciable increase in surface regression and char and this value can be used as the acceptable limit for both silica and carbon phenolic materials. A 9% volatile content resulted in surface regression increases of 30 to 70%. In actual nozzle fabrication, however, volatile contents exceeding 5% will occur only as result of bag leakage and water impregnation in a hydroclave cure process. With the use of either the autoclave or vacuum bag curing processes, a maximum volatile content of 5% can be easily attainable and is recommended as the maximum for large ablative nozzles.

2. Delaminations

The effect of delaminations on surface regression and char depth varied widely dependent upon the location in the nozzle, wrap orientation, and material type. For carbon phenolic materials at the nozzle throat station, seven plies of delaminations resulted in 30% and 16% increase in surface regression and char depth, respectively, compared with a nondiscrepant part. For carbon phenolic at stations downstream from the throat, no appreciable difference in regression or char existed with seven delaminated plies, but a substantial increase in both regression and char was observed with 14 delaminated plies. For silica phenolic material at large area ratio stations downstream from the throat, even 14 plies of delaminations in a parallel-to-centerline wrap orientation had no significant effect on regression and char.

IX.D. Accept/Reject Criteria (cont)

For silica phenolic at stations upstream from the throat, seven plies of delaminations in the high orientation wrap liner resulted in 90% higher regression and 70% higher char depth than a nondiscrepant part. These results indicate that seven plies of delamination is the acceptable limit for the parallel-to-centerline orientation wrap of exit cone stations. Delaminations should not be tolerated at the high wrap orientation angle in the nozzle entrance and throat sections without consideration of an increase in regression and char.

In addition to the number of delaminated plies, the radial length of the delamination must be limited so that structural failure of the nozzle does not occur. In a nozzle liner without a structural outerwrap or shell, the delamination must not extend through the liner to result in a gas flow path and subsequent burnthrough. Sufficient interlaminar strength of the liner must remain to react all the loads acting on the nozzle. This is determined by structural analyses of the discrepant configuration. In a nozzle liner with a structural outerwrap, the delamination can extend to the interface of the outerwrap without inducing structural failure in the nozzle. In this case, the design of the outerwrap must be determined from structural analysis to be adequate to react all the loads.

Delaminations in the nozzle liner may be detected by various inspection techniques. Delaminations that extend to the liner surface can be detected by an alcohol penetrant test. Radiographic inspection in both the radial and tangential directions and infrared techniques were successful in determining the size and location of internal delaminations.

3. Wrinkles

The effect of wrinkles on surface regression and char depth was more significant in the nozzle entrance regions than at stations downstream

IX.D. Accept/Reject Criteria (cont)

from the throat. Wrinkles larger than 0.125-in. (0.3175 cm) amplitude and 1.0-in. (2.54 cm) width resulted in over 20% higher surface regression and char depth for the silica phenolic in the entrance cap. At the throat and downstream stations of the nozzle, even wrinkles with 0.375-in. (0.3175 cm) amplitude and 1.5-in. (3.81 cm) width indicated an insignificant effect on surface regression and char depth. From these results, the size of wrinkles in the nozzle entrance section should be limited to 0.125-in. (0.3175 cm) amplitude and 1.0-in. (2.54 cm) width, whereas wrinkles with 0.25-in. (0.635 cm) amplitude and 1.5-in. (3.81 cm) width are tolerable for the throat and exit cone regions.

Wrinkles generally extend to the surface of the part. In this case, visual inspection and physical measurement provide an indication of the size of the wrinkle. Internal wrinkles can be detected by radiographic inspection, where a difference in density is apparent.

4. Resin Content

The test results indicated that the effect of resin content on surface regression and char depth depends on the material type. Resin-rich areas significantly increased the regression and char depth of carbon phenolic materials, while resin-starved areas increased the regression and char depth of silica phenolic. In the exit cone stations where the wrap orientation of carbon phenolic is parallel-to-centerline, even 10 plies of resin-rich material resulted in more than twice the surface regression compared with a defect-free part and the char depth increased by 30%. In the throat stations where the wrap orientation is 45 degrees, the regression and char increased 30 and 20%, respectively. For silica phenolic, 10 plies of resin-starved material in the parallel-to-centerline wrap orientation of the exit cone resulted in 150 and 70% increase in regression and char depth, respectively. The high-angle-wrap orientation of silica in the entrance cap resulted in 30% increase

IX.D. Accept/Reject Criteria (cont)

in regression and char with 10 plies of resin-starved laminates. These results indicate that for silica phenolic material even 20 plies of resin-rich material are acceptable while resin-starve laminates should not be tolerated. For carbon phenolic material, up to 10 plies of resin-starved laminates are acceptable while resin-rich laminates should not be tolerated.

5. Density

A lower density in a part results in a higher surface regression and char depth. These effects are significant at low area ratio regions near the throat. The test results indicated that parts with 70 to 80% density at the entrance and throat stations increased the surface regression and char depth by more than 50%; whereas parts with 70 to 80% density at an area ratio of 4.5 in the exit cone did not show any significant difference in regression or char depths. The acceptance limits for density of throat and entrance components should be maintained at the level that can be typically achieved by the autoclave curing process. The vacuum bag curing process, therefore, should not be used for the fabrication of the throat and entrance components. In the exit cone regions, 70 to 80% of this density should be the control limit. A vacuum bag curing process has been demonstrated to be adequate to meet this requirement of reduced density.

6. Process Cycle Variations

Parts with discrepancies introduced by water impregnation as a result of bag leakage during the debulk or final cure cycle and by temperature loss during the process cycle did not indicate any difference in surface regression or char depth compared with a nondiscrepant part. Acceptance limits, however, can not be assigned to these discrepancies without including other considerations. In the case of bag leakage, the part must meet the acceptance limits of volatile content and density. The acceptance limits of density and hardness must be used for the acceptance criteria of a discrepant part resulting from temperature loss.

Table IX-1

Averages and Standard Deviations for Regression and Char Rates of Normal Materials

Material	Location	Number of Tests	Regression Rate				Char Rate			
			Average		Standard Deviation		Average		Standard Deviation	
			milli-in./sec	(μm/sec)	milli-in./sec	(μm/sec)	milli-in./sec	(μm/sec)	milli-in./sec	(μm/sec)
MX-4926	Throat	15	7.12	180.0	0.66	16.8	13.61	345.7	0.63	16.0
MX-4926	Exit Cone	15	2.36	59.9	0.68	17.3	11.10	281.9	0.96	24.4
MX-2600	Entrance Cap	13	9.86	250.4	1.34	34.0	13.26	336.8	1.42	36.1
MX-2600	Exit Cone	10	1.32	33.5	0.35	8.9	6.76	171.7	0.34	8.6

Table IX-2

Comparison of Discrepant MX-2600 with Normal in Entrance Cap at Area Ratio 3.5

Discrepancy	Density, Virgin		Regression Rate		Difference, Standard Deviation			Char Rate		Difference, Standard Deviation		
	lbm/ft^3	(kg/m^3)	milli-in./sec	(μm/sec)	milli-in./sec		(μm/sec)	milli-in./sec	(μm/sec)	milli-in.sec		(μm/sec)
None (Baseline)	109.8	1759	10.96	278.4	0.8		20.3	14.73	374.1	1.0		25.4
	109.8	1859	9.52	241.8	-0.3		-7.6	12.95	328.9	-0.3		-7.6
Vacuum Bag	94.2	1509	8.83	224.3	-0.8		-20.3	11.52	292.6	-1.3		-33.0
Autoclave	108.6	1740	6.23	158.2	-2.7	*	-68.6	10.12	257.0	-2.3		-58.4
70 to 80% Density	87.4	1400	17.39	441.7	5.7	*	142.2	20.95	532.1	5.4	*	137.2
80 to 90% Density	96.1	1539	9.52	241.8	-0.3		-7.6	14.28	362.7	0.7		17.8
Bag Leak, Debulk	109.8	1759	9.86	250.4	0		0	14.04	356.6	0.5		12.7
Bag Leak, Final Cure	109.8	1759	7.56	192.0	-1.7		-43.2	11.34	288.0	-1.4		-35.6
Temperature Loss, Debulk	109.8	1759	9.11	231.4	-0.6		-15.2	13.66	347.0	-0.2		-5.1
6% Volatiles	108.6	1740	9.27	235.4	-0.4		-10.2	13.13	333.5	-0.2		-5.1
9% Volatiles	107.3	1719	14.47	367.5	3.5	*	88.9	17.00	431.8	2.6		66.0
Wrinkles, 0.125 in. (0.3175 cm)	110.5	1770	13.11	333.0	1.7		43.2	15.81	401.6	1.7		43.2
Wrinkles, 0.250 in. (0.6350 cm)	109.8	1759	15.77	400.6	4.4	*	111.8	18.08	459.2	3.3	*	83.8
Wrinkles, 0.375 in. (0.9525 cm)	105.5	1690	17.59	446.8	5.8	*	147.3	19.88	505.0	4.6	*	116.8
Resin-Rich, 10 plies	110.5	1770	10.35	262.9	0.4		10.2	13.80	350.5	0.3		7.6
Resin-Rich, 20 plies	105.5	1690	12.80	325.1	2.2		55.9	16.19	411.2	1.9		48.3
Resin-Starved, 10 plies	109.8	1759	20.03	508.8	7.6	*	193.0	23.12	587.2	6.9	*	175.3
Delaminations, 7 plies	-	-	14.29	363.0	3.3	*	83.8	17.38	441.4	2.8	*	71.1
Delaminations, 14 plies	-	-	15.27	387.8	4.0	*	101.6	18.71	475.2	3.8	*	96.5
Delaminations, 28 plies	-	-	17.28	438.9	5.5	*	139.7	20.36	517.1	4.9	*	124.5

Note: *Denotes significant difference.

Table IX-3

Comparison of Discrepant MX-4926 with Normal at Throat

Discrepancy	Density: Virgin lbm/ft^3	Density: Virgin (kg/m^3)	Density: Char lbm/ft^3	Density: Char (kg/m^3)	Regression Rate milli-inch/sec	Regression Rate (μm/sec)	Difference, Standard Deviation milli-inch/sec		Difference, Standard Deviation (μm/sec)	Char milli-inch/sec	Char (m/sec)	Difference, Standard Deviation milli-inch/sec		Difference, Standard Deviation (m/sec)
None (Baseline)	89.9	1440	68.0	1089	6.44	163.6	-1.0		-25.4	13.6	345.5	0		0
	89.9	1440	67.4	1080	8.41	213.6	2.0		50.8	14.5	368.3	1.4		35.6
Vacuum Bag	65.6	1051	53.1	851	10.6	269.2	5.3	*	134.6	17.51	44 .8	6.2	*	157.5
Autoclave	89.9	1440	67.4	1080	6.46	164.1	-1.0		-25.4	13.5	342.9	-0.2		5.1
70 - 80% Density	65.6	1051	54.3	870	12.98	329.7	8.9	*	226.1	18.93	480.8	8.4	*	213.4
80 - 90% Density	66.2	1060	54.9	879	10.34	262.6	4.9	*	124.5	16.3	414.0	4.3	*	109.2
Bag Leak, Debulk	90.5	1450	67.4	1080	7.41	188.2	0.6		15.2	14.61	371.1	1.6		40.6
Bag Leak, Final Cure	90.5	1450	73.7	1181	7.8	198.1	1.0		25.4	14.62	371.3	1.6		40.6
Temperature Loss, Debulk	89.9	1440	69.9	1120	6.54	166.1	-0.9		-22.9	12.98	329.7	-1.0		-25.4
6% Volatiles (3.56)	88.7	1421	56.8	910	8.85	224.8	2.8	*	71.1	15.77	400.6	3.4	*	86.4
9% Volatiles (4.06)	89.9	1440	64.9	1040	8.03	204.0	1.3		33.0	14.12	358.6	0.8		20.3
Wrinkles, 0.125 in. (0.3175 cm)	90.5	1450	77.4	1240	7.72	196.1	0.9		22.9	13.88	352.6	0.4		10.2
Wrinkles, 0.250 in. (0.6350 cm)	89.9	1440	71.2	1140	8.29	210.6	1.9		48.3	13.64	346.4	0.1		2.5
Wrinkles, 0.375 in. (0.9525 cm)	89 9	1440	73.7	1181	7.52	191.0	0.6		15.2	13.24	336.3	-0.6		-15.2
Resin-Rich, 10 plies	89.9	1440	75.5	1209	9.06	230.1	3.0	*	76.2	15.36	390.1	2.8	*	71.1
Resin-Rich, 20 plies	89.3	1430	70.5	1209	8.90	226.1	2.7	*	68.6	15.66	397.8	3.3	*	83.8
Resin-Starved, 10 plies	89.9	1440	70.5	1129	7.71	195.8	0.9		22.9	13.86	352.0	0.4		10.2
Delaminations, 7 plies	-	-	73.7	1181	8.36	225.0	2.6	*	66.0	15.27	387.9	2.6	*	66.0
Delaminations, 14 plies	-	-	69.9	1120	8.03	204.0	1.3		33.0	15.65	397.5	3.2	*	81.3
Delaminations, 28 plies	-	-	65.6	1051	12.90	327.7	8.7	*	221.0	16.22	412.0	4.1	*	104.1

NOTE: *Denotes significant difference.

Table IX-4

Comparison of Discrepant MX-4926 with Normal in Exit Cone at Area Ratio 1.44

Discrepancy	Density Virgin		Regression Rate		Difference, Standard Deviation		Char Rate		Difference, Standard Deviation	
	lbm/ft^3	(kg/m^3)	milli-inch/sec	(μm/sec)	milli-inch/sec	(μm/sec)	milli-inch/sec	(μm/sec)	milli-inch/sec	(μm/sec)
None (Baseline)	89.9	1440	2.64	67.1	0.4	10.2	11.71	297.4	0.6	15.2
	89.9	1440	1.52	38.6	-1.2	-30.5	10.28	261.1	-.09	-22.9
Vacuum Bag	78.6	1259	2.03	51.6	-0.5	-12.7	11.14	283.0	0	0
Autoclave	89.9	1440	1.27	32.2	-1.6	-40.6	10.51	267.0	-0.6	-15.2
70 - 80% Density	78.6	1259	2.79	70.9	0.6	15.2	14.62	371.3	3.7 *	94.0
80 - 90% Density	84.3	1350	4.06	103.1	2.5	63.5	14.68	372.9	3.7 *	94.0
Bag Leak, Debulk	90.5	1450	3.79	96.3	1.1	27.9	12.90	327.7	1.9	48.3
Bag Leak, Final Cure	90.5	1450	1.63	41.4	1.6	40.6	11.60	294.6	0.5	12.7
Temperature Loss, Debulk	89.9	1440	3.42	86.9	2.1	53.3	11.10	281.9	0	0
6% Volatiles (4.55)	89.9	1440	3.09	78.5	1.1	27.9	11.97	304.0	0.9	22.9
9% Volatiles	89.9	1440	4.53	115.1	3.2 *	81.3	12.46	316.5	1.4	35.6
Wrinkles, 0.125 in. (0.3175 cm)	90.5	1550	4.24	107.7	2.8 *	71.8	11.18	284.0		
Wrinkles, 0.250 in. (0.6350 cm)	89.9	1440	3.08	78.2	1.0	25.4	10.16	258.1		
Wrinkles, 0.375 in. (0.9525 cm)	89.9	1440	6.50	165.1	6.1 *	154.9	11.85	301.1	0.8	20.3
Resin-Rich, 10 plies	89.9	1440	11.89	302.0	14.0 *	355.6	16.11	409.2	5.3 *	134.6
Resin-Rich, 20 plies	89.3	1430	5.27	133.9	4.2 *	106.6	14.69	373.1	3.7 *	94.0
Resin-Starved, 10 plies	89.9	1440	2.70	68.6	0.5	12.7	12.33	313.2	1.3	33.0
Delaminations, 7 plies	-	-	2.70	68.6	0.5	12.7	9.27	235.4	-1.9	-48.3
Delaminations, 14 plies	-	-	4.96	126.0	3.8 *	96.5	15.65	397.5	4.7 *	119.4
Delaminations, 28 plies	-	-	5.38	136.6	4.5 *	114.3	13.06	331.7	2.1	53.3

NOTE: *Denotes significant difference.

Table IX-5

Comparison of Discrepant MX-2600 with Normal in Exit Cone at Area Ratio 4.5

Discrepancy	Density: Virgin lbm/ft^3	Density: Virgin (kg/m^3)	Density: Char lbm/ft^3	Density: Char (kg/m^3)	Regression Rate milli-inch/sec	Regression Rate (μm/sec)	Difference, Standard Deviation milli-inch/sec		Difference, Standard Deviation (μm/sec)		Char Rate milli-inch/sec	Char Rate (μm/sec)	Difference, Standard Deviation milli-inch/sec		Difference, Standard Deviation (μm/sec)
None (Baseline)	109.8	1759	87.4	1400	1.89	48.0	1.7		43.2		7.18	182.4	0.9		22.9
	109.8	1759	88.0	1410	1.52	38.6	0.6		15.2		6.85	174.0	0		0
Vacuum Bag	104.7	1677	84.3	1350	1.92	48.8	1.8		45.7		6.91	175.5	0.2		5.1
Autoclave	109.8	1759	88.0	1410	0.78	19.8	-1.5		-38.1		5.12	130.0	-5.1	*	-129.5
70 - 80% Density	102.4	1640	86.8	1390	1.19	30.2	-0.3		-7.6		7.90	200.7	3.1	*	78.7
80 - 90% Density	101.0	1618	71.8	1150	1.59	40.4	0.8		20.3		7.14	181.4	0.8		20.3
Bag Leak, Debulk	109.8	1759	88.7	1421	1.14	29.0	-0.5		-12.7		6.83	173.5	-0.1		-2.5
Bag Leak, Final Cure	109.8	1759	88.0	1410	1.13	28.7	-0.5		-12.7		6.80	172.7	-0.2		-5.1
Temperature Loss, Debulk	109.8	1759	79.3	1270	1.52	38.6	0.6		15.2		6.83	173.5	-0.1		-2.5
6% Volatiles (2.60)	105.5	1690	84.9	1360	1.54	39.1	0.7		17.8		6.95	176.5	0.3		7.6
9% Volatiles (1.90)	106.1	1700	81.2	1301	2.27	57.6	2.8	*	71.1		7.17	182.1	0.9		22.9
Wrinkles, 0.125 in. (0.3175 cm)	110.5	1770	-	-	2.31	58.7	2.9	*	73.7		-	-	-		-
Wrinkles, 0.250 in. (0.6350 cm)	109.8	1759	85.5	1370	1.92	48.8	1.8		45.7		7.31	185.7	1.4		35.6
Wrinkles, 0.375 in. (0.9525 cm)	105.5	1690	85.5	1370	2.29	58.2	2.8	*	71.1		-	-	-		-
Resin-Rich, 10 plies	110.5	1770	79.9	1280	1.15	29.2	-0.4		10.2		7.67	194.8	2.4		61.0
Resin-Rich, 20 plies	105.5	1690	85.5	1370	1.51	38.4	0.6		15.2		7.15	181.6	0.9		22.9
Resin-Starved, 10 plies	109.8	1759	80.5	1290	3.95	100.3	7.3	*	185.4		8.86	225.0	5.9	*	149.9
Delaminations, 7 plies	-	-	90.5	1450	1.54	39.1	0.7		17.8		-	-	-		*
Delaminations, 14 plies	-	-	89.3	1431	1.15	29.2	-0.4		10.2		7.25	184.2	1.1		27.9
Delaminations, 28 plies	-	-	88.7	1421	-	-	-		-		-	-	-		-

NOTE: *Denotes significant difference.

Table IX-6

Virgin and Char Densities of Discrepant Nozzle Materials

Discrepancy	Nozzle S/N	Measured Density								Computed Char Density			
		Virgin				Char							
		Carbon		Silica		Carbon		Silica		Carbon		Silica	
		lbm/ft^3	(kg/m^3)	lbm/ft^3	(kg/m^3)	lbm/ft^3	(kg/m^3)	lbm/ft^3	(kg/m^3)	lbm/ft^3	(kg/m^3)	lbm/ft^3	(kg/m^3)
None (Baseline)	001	89.9	1440	109.8	1759	68.0	1089	88.0	1410	67.60	1083.0	88.30	1414.6
None (Baseline	002	89.9	1440	109.8	1759	67.4	1080	87.4	1400	67.60	1083.0	88.30	1414.6
Vacuum Bag	003	65.4	1048	104.7	1677	53.1	851	84.3	1350	52.93	847.9	84.26	1349.8
Autoclave	004	89.9	1440	109.8	1759	67.4	1080	88.0	1410	67.60	1083.0	88.30	1414.6
70 - 80% Density	019	65.6	1051	102.4	1640	54.3	870	86.8	1390	48.92	783.7	81.35	1303.2
80 - 90% Density	020	66.1	1059	101.0	1618	63.3	1014	71.8	1150	49.56	794.0	80.45	1288.8
Resin-Rich, 10 plies	007	89.9	1440	110.5	1770	75.5	1210	79.9	1280	65.52	1049.6	85.05	1362.5
Resin-Rich, 20 plies	009	89.3	1430	105.5	1690	70.5	1129	85.5	1370	57.77	925.5	75.64	1211.8
Resin-Starved, 10 plies	011	89.8	1438	109.8	1759	70.5	1129	80.5	1290	74.22	1189.0	93.71	1501.2
Low Density	027	89.0	1426	-	-	68.0	1089	-	-				
Low Density	028	71.8	1150	-	-	59.9	960	-	-				

Compressive Strengths and Conductivities of MX-4926 Throat Specimens

Compressive Strength			Thermal Conductivity*						Regression Rate		Discrepancy
			212°F (373°K)		392°F (473°K)		500°F (533°K)				
klbf/in.^{2}		(MN/m^2)	Btu/in./ft^2-hr-°F	(kJ/m-hr-°K)	Btu/in./ft^2-hr-°F	(kJ/m-hr-°K)	Btu/in./ft^2-hr-°F	(kJ/m-hr-°K)	milli-in./sec	(μm/sec)	
34.4	(R)	237.2							6.44	163.6	
31.6	(A)	217.9	5.04	2.62	5.45	2.83	5.45	2.83			None (Baseline)
39.3	(T)	202.0							8.41	213.6	
33.6	(R)	231.7									
30.9	(A)	213.0	3.56	1.85	5.99	3.11	6.51	3.38	6.46	164.1	Autoclave
28.7	(T)	197.9									
14.6	(R)	100.7									
13.4	(A)	93.4	2.91	1.51	4.73	2.45	5.8	3.0	10.6	269.0	Vacuum Bag
12.4	(T)	85.5									
8.8	(R)	60.7									
11.1	(A)	76.5	3.1	1.6	4.1	2.1	4.3	2.2	10.34	262.6	80 to 90% Density
18.5	(T)	127.6									
6.09	(R)	42.0									
6.13	(A)	42.3	2.76	1.43	3.36	1.74	3.71	1.92	12.98	329.7	70 to 80% Density
5.75	(T)	39.6									
35.0	(R)	241.3									
32.2	(A)	222.0	5.27	2.73	5.82	3.02	6.18	3.21	7.41	188.2	Bag Leak, Debulk
29.0	(T)	199.9									
31.7	(R)	218.6									
29.1	(A)	200.6	3.77	1.96	5.44	2.82	6.34	3.29	7.8	198.0	Bag Leak, Final Cure
27.0	(T)	186.2									
28.3	(R)	195.1									
26.0	(A)	179.3	3.48	1.81	5.45	2.83	5.03	2.61	8.03	204.0	9% Volatiles
24.0	(T)	165.5									
26.2	(R)	180.6									
26.3	(A)	181.3	4.58	2.38	5.22	2.71	5.2	2.7	8.85	224.8	6% Volatiles
24.4	(T)	168.2									
-		-	4.38	2.27	5.66	2.94	6.14	3.18	7.73	196.3	Wrinkles, 0.125 in. (0.3175 cm)
-		-	3.55	1.84	5.03	2.61	5.32	2.76	8.29	210.6	Wrinkles, 0.250 in. (0.6350 cm)
29.1	(A)	200.6	-	-	-	-	-	-	6.73	170.9	Wrinkles, 0.375 in. (0.9525 cm)
-		-	3.56	1.85	6.25	3.24	6.14	3.18	10.41	264.4	Resin-Rich, 10 plies
-		-	3.33	1.73	4.77	2.48	4.65	2.41	8.9	226.0	Resin-Rich, 20 plies

Note: *denotes measurements taken perpendicular to original surface.
(R), (A), and (T) denote radial, axial, and tangential measurement, respectively.

Compressive Strengths and Conductivities of MX-2600 Exit Specimens

Compressive Strength			Thermal Conductivity*						Regression Rate		
			212°F (373°K)		392°F (473°K)		500°F (533°K)				
klbf/in.^{2}		(MN/m^2)	Btu/in./ft^2-hr-°F	(kJ/m-hr-°K)	Btu/in./ft^2-hr-°F	(kJ/m-hr-°K)	Btu/in./ft^2-hr-°F	(kJ/m-hr-°K)	milli-in./sec	(μm/sec)	Discrepancy
65.0	(R)	448.2									
55.8	(A)	384.7	2.68	1.39	3.7	1.92	3.38	1.75	0.78	19.81	Autoclave
65.2	(T)	449.5									
63.4	(R)	437.1							1.89	48.01	
54.5		375.8	3.03	1.57	3.33	1.73	3.37	1.75			None (Baseline)
63.6	(T)	438.5							1.52	38.61	
59.7	(R)	411.6									
49.8	(A)	343.4	-	-	-	-	-	-	1.52	38.61	Temperature Loss, Debulk
58.1	(T)	400.6									
49.3	(R)	339.9									
42.4	(A)	292.3	2.76	1.43	3.02	1.57	3.57	1.85	1.92	48.77	Vacuum Bag
49.5	(T)	341.3									
43.0	(R)	296.5									
42.9	(A)	295.8	2.64	1.37	3.11	1.61	2.95	1.53	1.28	32.51	70 to 80% Density
39.1	(T)	269.6									
36.8	(R)	253.7									
36.8	(R)	253.7									
36.9	(A)	254.4	2.1	1.09	2.58	1.34	2.9	1.50	1.59	40.39	80 to 90% Density
44.7	(T)	308.2									
65.5	(R)	452.3									
56.5	(A)	389.6	2.88	1.49	3.65	1.89	3.8	1.97	1.13	28.70	Bag Leak, Final Cure
65.8	(T)	453.7									
62.0	(R)	427.5									
53.3	(A)	367.5	2.72	1.41	3.36	1.74	3.45	1.79	1.14	28.96	Bag Leak, Debulk
62.2	(T)	428.8									
65.3	(R)	450.2									
56.1	(A)	386.8	-	-	-	-	-	-	2.27	57.66	9% Volatiles
65.5	(T)	451.6									
55.7	(R)	384.0									
55.5	(A)	382.6	-	-	-	-	-	-	1.54	39.12	6% Volatiles
50.6	(T)	348.9									
54.8	(A)	377.8	-	-	-	-	-	-	2.29	58.17	Wrinkles, 0.375 in. (0.9525 cm)
51.2	(A)	353.0	3.30	1.71	3.38	1.75	3.02	1.57	2.31	58.67	Wrinkles, 0.125 in. (0.3175 cm)
50.0	(A)	344.7	3.25	1.69	3.73	1.94	3.93	2.04	1.92	48.77	Wrinkles, 0.250 in. (0.6350 cm)
57.3	(A)	395.1	3.31	1.72	4.02	2.08	3.85	2.00	1.15	29.21	Resin-Rich, 10 plies
46.0	(A)	317.2	3.03	1.57	3.31	1.72	3.43	1.78	1.51	38.35	Resin-Rich, 20 plies
52.0	(A)	358.5	-	-	-	-	-	-	3.85	97.79	Resin-Starved, 10 plies

Note: *Denotes measurements taken perpendicular to original surface.
(R), (A), and (T) denote radial, axial, and tangential measurement, respectively.

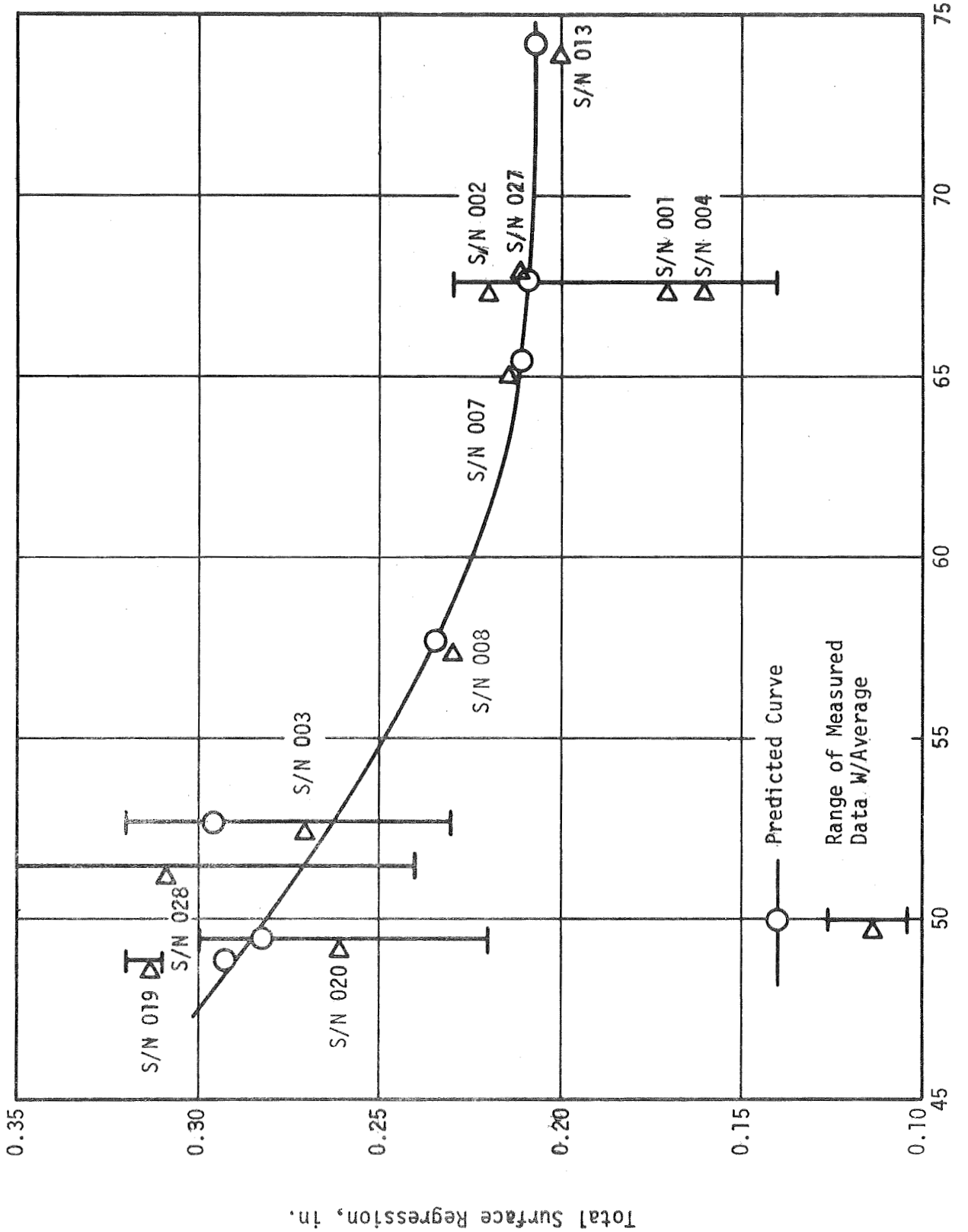

Discrepant Nozzle Throat Regression as a Function of Char Density

Figure IX-1

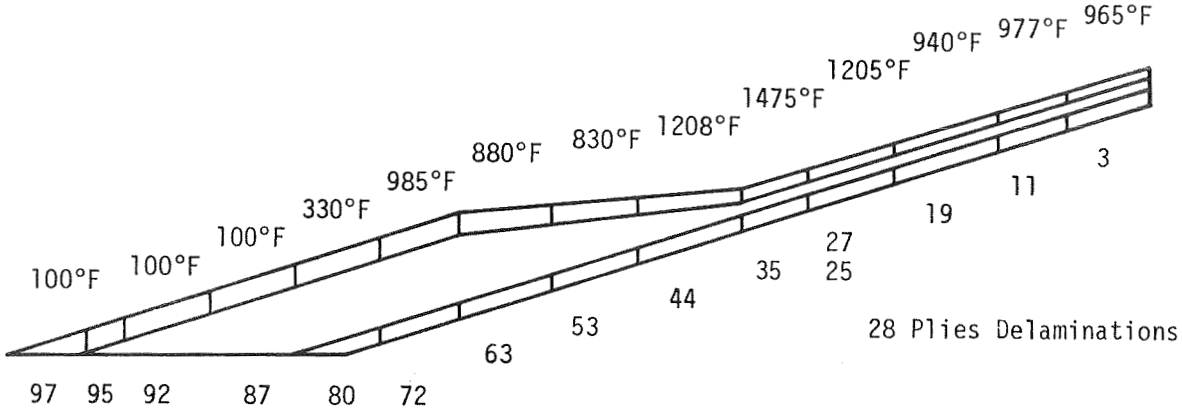

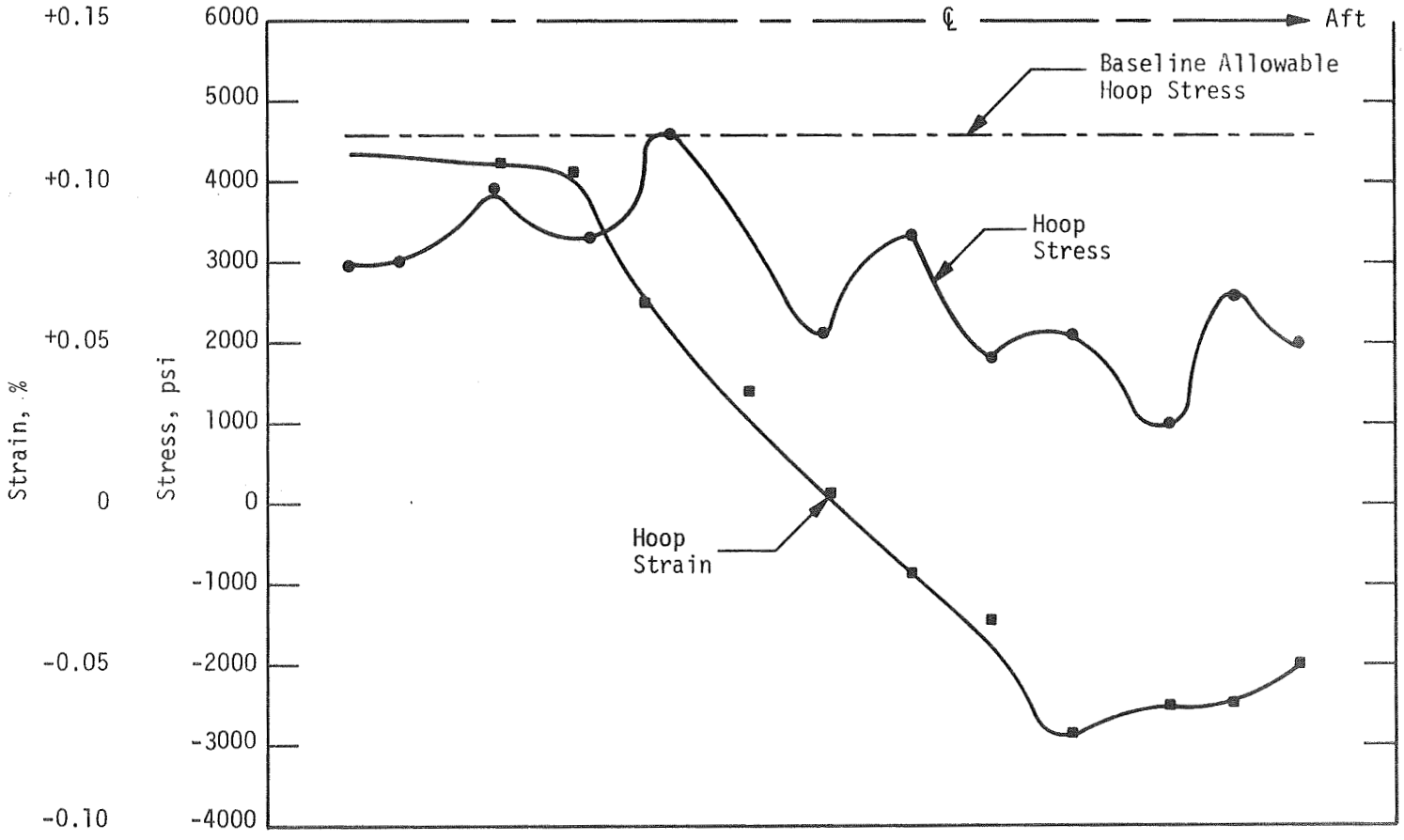

Hoop Stress and Strain at t = 25 sec for MX-2600 Material in Exit Cone S/N 016

Figure IX-2

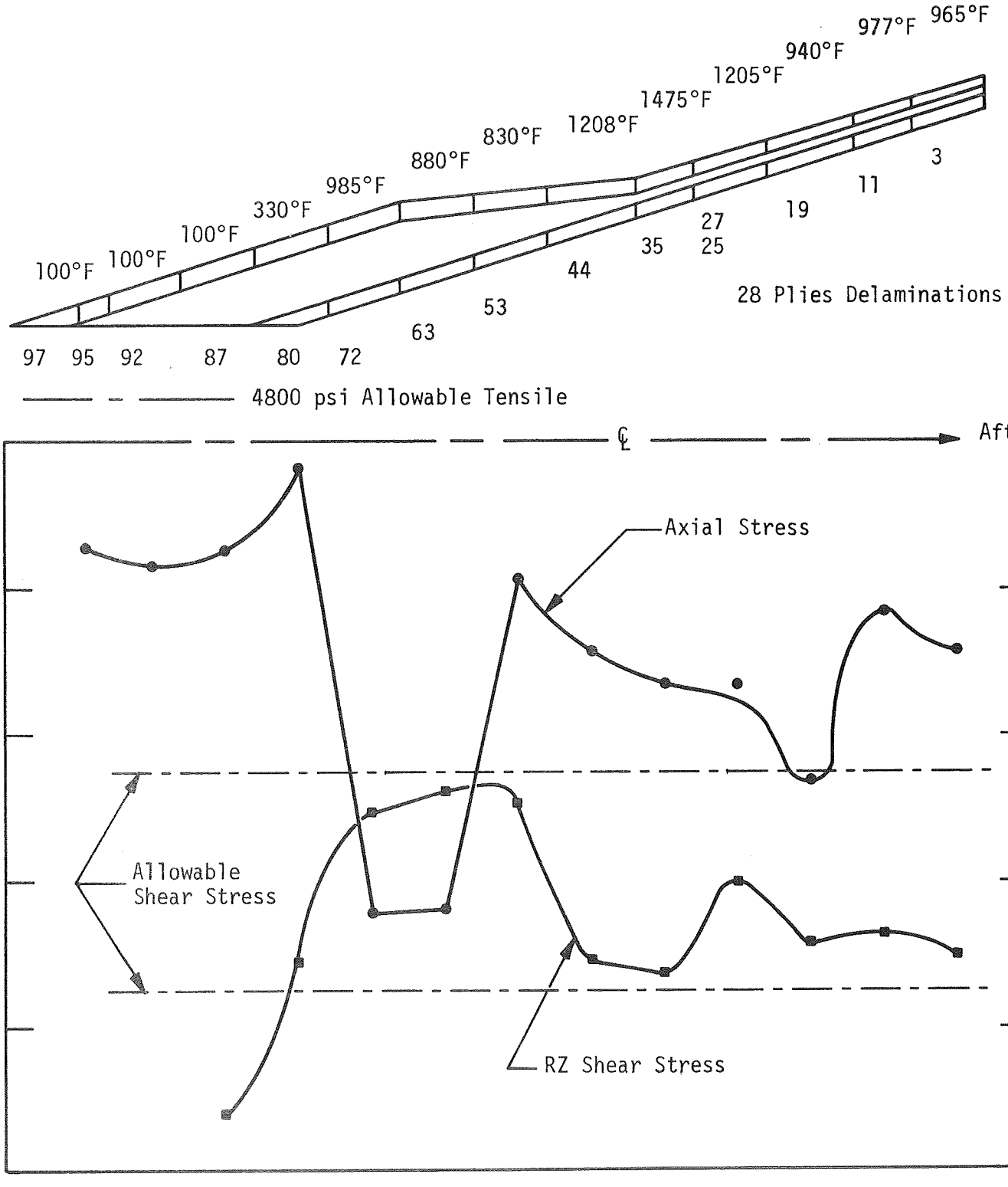

Axial and Shear Stresses in MX-2600 Material in Exit Cone S/N 016

Figure IX-3

X. CONCLUSIONS AND RECOMMENDATIONS

A. CONCLUSIONS

1. Structural failures of large solid rocket motor nozzle components resulting from discrepancies of the type, frequency, and severity evaluated in this program are unlikely unless there is a gas flow path through the liner.

2. Ablative performance of large solid rocket motor nozzle components resulting from discrepancies of the type evaluated in this program will be acceptable at the following limits:

a. Volatile Content - Five percent maximum.

b. Delaminations in parts without surrounding wraps or shells - None.

c. Delaminations in high wrap orientation parts with surrounding wraps or shells - Evaluate effect on ablative performance.

d. Delaminations in parallel-to-centerline wrap parts - Seven plies maximum.

e. Wrinkles in entrance section - 0.125 in. (0.328 cm) high by 1.0 in. (2.54 cm) wide.

f. Wrinkles in throat and exit sections - 0.250 in. (0.655 cm) high by 1.5 in. (3.81 cm) wide.

g. Resin starved carbonaceous composites - 10 plies maximum.

X.A. Conclusions (cont)

h. Resin starved silica composites - None.

i. Resin-rich, carbonaceous composites - None.

j. Resin-rich, silica composites - 20 plies, maximum

k. Density in nozzle entrance and throat - 97.4 lb/cu ft (1.40 gm/cc) minimum for carbonaceous wraps; 106 lb/cu ft (1.70 gm/cc) minimum for silica wraps.

3. Discrepancies beyond the tolerable limits above shall be removed and replaced by acceptable material, except that:

a. Volatile content may be reworked by additional time at cure temperature.

b. Temperature loss during cure may be rectified by curing at full cure cycle of pressure and temperature.

4. Discrepancies up to the limits of acceptability are detectable by pulse echo ultrasonics and tangential radiography.

5. Infrared thermographic techniques are suitable for the detection of delaminations, resin-rich and wrinkled areas; further development is required to scale-up the technique to large nozzle components.

B. RECOMMENDATIONS

1. Specifications for the radiographic and ultrasonic inspection of large ablative nozzle components should be revised to include these new acceptance levels.

X.B. Recommendations (cont)

2. Techniques should be developed that will nondestructively determine the density and resin content of ablative composite in place. This information can be input into the charring ablation program to predict the local ablative performance.

3. A room-temperature-curing phenolic base resin should be evaluated for use in repair of ablative nozzle components.

XI. REFERENCES

1. NASA CR-72125, Vol. I, 260-In. Dia Motor Feasibility Demonstration Program.

2. NASA CR-72125, Vol. II, 260-In. Dia Motor Feasibility Demonstration Program.

3. NASA CR-72283, Vol. III, Final Phase Report, 260-SL-3 Motor Nozzle and Exit Cone Design, Fabrication, and Assembly.

4. Final Report, "Failure Warning System for Large Solid Rockets", (U), Aerojet-General Corporation, April 1962, Report No. 0588-01F (Confidential).

5. Final Report, "Development of Malfunction Detection System Sensors for Large Solid Propellant Rocket Motors" (U), Aerojet-General Corporation, August 1964, Report No. 2904T (Confidential).

6. Determination of Abort System - Mission Effects for Saturn Class Vehicles (U), Aerojet-Genral Corporation, August 1965, Report No. NAS8-11374F (Confidential).

7. Final Report, "Demonstration of a Solid Propellant Motor Malfunction-Detection and Combustion Termination System", Vol. II, Phase II, Combustion Termination, June 1967, Contract NAS8-20219.

8. Warga, J. J., Davis, H. O., DeAcetis, J., and Lampman, J. A.; "Evaluation of Low-Cost Materials and Manufacturing Processes for Large Solid Rocket Nozzles", Aerojet-General Corporation, December 1967, Report AFRPL-TR-67-310.

9. Davis, H. O., and Lampman, J. A.; "Evaluation of Characteristics Affecting Attainment of Optimum Properties of Ablative Nozzle Components", Aerojet-General Corporation, Technical Report AFRPL-TR-66-3, January 1966.

10. Warga, J. J., Lampman, J. A. and Davis, H. O.; "Deviation Nozzle Program", Aerojet-General Corporation, June 1968, Report AFRPL-TR-68-81.

11. Gras, E. G.; "Elevated Temperature Properties of Carbonaceous and Silica Fabric Reinforced Phenolic Composites", Aerojet-General Corporation, Report MF-450, 1 June 1964.

12. Parker, W. J., Jenkins, R. J., Butler, C. P., and Abbott, G. L.; "Flash Method of Determining Thermal Diffusivity, Heat Capacity and Thermal Conductivity", Journal of Applied Physics 32 1679 (1961).

XI. References (cont)

13. Curtis, C. F., Hirschfelder, J. O., Bird, R. B.; "Theories of Gas Transport Properties," Proceedings of the Second Biennial Gas Dynamics Symposium, Northwestern University Press, January 1958, Pages 3-11.

14. Elliot, D. G., Bartz, D. R., and Silver, S.; "Calculation of Turbulent Boundary-Layer Growth and Heat Transfer in Axi-Symmetric Nozzles," Tech. Report 32-387, JPL, California Institute of Technology, February 1963.

15. McCuen, P. A., et al; "A Study of Solid Propellant Rocket Motor Exposed Materials Behavior," Report No. AFRPL-TR-65-33, Vidya Division of Itek Corporation, February 1965.

16. Bradley, W., et al; "Investigation and Evaluation of Motor Insulation for Multiple Restart Application," Tech. Report AFRPL-TR-67-287, November 1967.

17. Nelson, J. B.; "Determination of Kinetic Parameters of Six Ablation Polymers by Thermogravimetric Analysis," NASA TN-D-3919, April 1967.

18. Schaefer, J. W., et al; "Studies of Ablative Material Performance for Solid Rocket Nozzle Application," NASA CR-72429, March 1968.

19. Bradley, W. and Booker P.; "Development of a Temperature-Indicating Sensor for use in Ablative Rocket Nozzles," Technical Report AFRPL-TR-69-172, July 1969.

APPENDIX A
REPORT OF AUTOMATION INDUSTRIES, INC.
ON INFRARED INSPECTION TECHNIQUE

TR 69-20 30 April 1969

Thermal Evaluation of Phenolic Fiberglass Structures

by
J. Hille

INTRODUCTION

A thermal nondestructive application study was performed for Aerojet General Corporation to determine the usefulness of thermal techniques for testing of phenolic fiberglass structures. Particular emphasis was placed on determining the inspection depth, defect size, and test sensitivity. The program was aimed at investigating thermal testing of phenolic and carbon-phenolic structures in general rather than at solving any specific inspection problem.

SAMPLE DESCRIPTION

Test samples with intentional manufactured defects were supplied by Aerojet General Corporation. The general sample configuration and defect locations are shown in Figures 1 through 3. To provide depth and size information, Automation Industries, Inc., machined a set of calibrated reference holes into one of the samples. The sizes and locations of these holes are shown in Figure 4.

TEST EQUIPMENT

The following equipment was used in performing the tests for this study:

Automation Industries' Infrared Radiometer, Model PPL-301
Automation Industries' Turntable, Model 0-60
Hewlett-Packard's X-Y Recorder, Model 2A2D

TEST THEORY

In performing a thermal test the surface temperature of the sample is raised. This is usually done with focused visible radiation. After a short time delay, to allow the heat to penetrate into the sample, the surface temperature is remotely measured with an infrared radiometer. Any subsurface discontinuity obstructs the normal heat diffusion into the sample, and causes a hot spot to develop on the surface. These hot spots are detected by the radiometer and indicate the subsurface defects.

By providing relative motion between the radiometer and heat source, and the sample a single line is tested across the part. The output of the radiometer and the relative motion is used to drive an X-Y recorder. Temperature information is shown on the Y-axis. The X-axis shows distance traveled across the sample.

The three variable test parameters used in thermal testing are as follow:

1. Time-Delay - The time between first application of heat and the surface temperature measurement.
2. Scan-Speed - Speed at which the sample moves past the radiometer and heat source.
3. Heat-Input - Amount of heat energy applied to the test surface.

These test parameters are interacting and can be varied over a wide range to control inspection depth and speed. Of primary importance is time-delay since this parameter regulates test depth. Longer delays before temperature measurement allow the applied heat to diffuse deeper into the part while shorter delays permit only shallow penetration. The thermal conductivity also affects penetration and longer delays are required for slow conducting materials such as nonmetallics.

Time-delay is determined by the distance between the moving heat spot and the trailing radiometer detector spot and the scan speed. To maintain a constant time-delay the distance must be increased as the speed increases.

The Scan-Speed, aside from affecting the time-delay, also affects the heat-input. At a constant heat source setting, less heat is applied to the test surface as the scan speed increases. Therefore, all three parameters affect each other and must be properly adjusted to obtain optimum results.

TEST RESULTS

The test set up used in this study is shown in Figure 5. The relative sample motion is provided by rotating the part.

Initial tests were performed over one of the defects inserted by Aerojet General Corporation personnel. These results, shown in Figures 6 through 8, represent the first tests performed on Sample 1147247-4.

Figures 6 and 7 show tests with increasing time delays. The 1 second scan on Figure 6 shows the normal surface temperature (approximately 15°C above ambient) resulting after 1 second of heating. A slight indication of the defect is evident near the center of the scan. Scans at 2, 3, and 4 seconds delay show the defect in more detail indicating that 1 second does not allow the heat to penetrate to the defect and develop a surface hot spot. A delay of twelve seconds as shown on Figure 7 was sufficient to clearly define the 3 inches unbond in this sample. Figure 8 shows 4 scans taken in 1/4 inch steps crossing the defect. This defect was of constant depth and did not provide a means of comparing the defect indication to the depth or the size of the defect.

After obtaining permission from Aerojet General Corporation, a set of calibrated reference defects were machined into part #1147245-7. The detailed information on these reference defects is shown in Figure 4. The varying depth defects were used to determine the test penetration into the sample.

Tests with varying time delays were performed starting with 1 second and extending out to 120 seconds delay. The results of these tests are shown in Figures 9 through 17.

To more clearly show the relationship of the various test parameters used during these tests, the data from these graphs was compiled in graphical form.

The test sensitivity versus time-delay is shown in the graph of Figure 18. This graph was obtained by calculating the sensitivity of each defect indication as follows:

$$\% \text{ sensitivity} = \frac{\Delta T}{T} \ (100)$$

where ΔT = temperature increase over defect

T = normal sample temperature above ambient.

The sensitivity was then plotted against delay in seconds for each different depth defect. The sensitivity begins at 0% at 0 delay and increases to 35% sensitivity at 120 seconds delay. As shown, the curves for the deeper defects are proportionately lower. Notice that the sensitivity begins to level off and additional delay does not improve the test. In fact the sensitivity reaches an optimum at some given delay and begins to decrease at longer delays.

Figure 19 shows similar results of test sensitivity versus depth for a given delay. Notice that the sensitivity decreases as the defect depth increases. This is as expected since a given delay is optimum for one depth only and must be increased as the defect depth increases to obtain maximum test sensitivity.

The relationship between delay and penetration can be determined by choosing a given sensitivity on Figure 18. These results are shown in Figure 20 and indicate that as the defect extends deeper into the part a longer delay is required to obtain the same sensitivity.

Another important factor to be considered in thermal testing is the minimum size of defect which can be detected. At a constant depth and delay the sensitivity will decrease as the defect size decreases. The thermal recordings in Figures 21 and 22 show the results of tests over a set of decreasing size reference holes at a constant depth. The results are also graphically shown in Figure 23.

Another factor that requires some consideration is the surface condition of the sample. For convenience, visual energy is usually used to establish heat-flow into the sample. Since the amount of heat absorbed by a surface is determined by the surface reflectivity, surface variations can affect the heat absorption. Dark areas absorb more heat than light areas resulting in an erroneous hot spot caused by the surface rather than a defect. If surface variations are present it is necessary to coat the test surface to provide uniform heat absorption.

An example of a nonuniform test surface is shown in Figure 24. This recording shows a test performed over the serial- and part-number of sample 1010062-10. Figures 25 and 26 show how the surface condition can be overcome by applying a uniform coating.

After establishing the proper test parameters over the calibration defects a series of final tests were performed over the defects inserted in the parts by Aerojet General Corporation. The results of these tests are shown in Figures 27 through 30. These recordings represent tests over delaminated and resin rich areas. No thermal test results were obtained on the wrinkled areas contained in the samples. Apparently the wrinkles in the parts do not significantly affect the thermal flow characteristics.

CONCLUSIONS

Use of thermal nondestructive inspection techniques for detection of various defects in phenolic fiberglass structures appears practical from results of this study. Various intentional defects such as delaminations and resin rich areas were detected. A careful study of a series of calibrated reference holes indicated the size and depth limitations of the thermal technique. Defects of 1/2 inch diameter were detected at depths up to .353 inch. Defects as small as 1/8 inch diameter were detected at shallow depths. This study indicates that defect diameter must be at least two times the defect depth to obtain good test sensitivity. This relationship would hold for thicker materials, also.

Inspection speed for the laboratory investigation was quite slow. This was because of the small size of the parts and the limited length of the available heat source. To obtain long delays it was necessary to turn the part very slowly. On larger parts or in a production application this would probably not be a limitation. The important factor is the time the heat is allowed to penetrate. Long heating times could be accomplished with longer heaters or by a preheat process. The inspection could then be performed at a rapid rate.

If large areas are to be tested an area scan system would be advisable. Such a system performs the same type of thermal test as has been described in this study except that a 6 inch wide path is tested in a single pass. Inspection coverages up to 2 to 3 feet^2/minute are then possible.

Some problems were encountered in testing the bright, smooth surface of Sample #1147245-7. This was overcome by applying a darkening coating to the test surface. Coating was not required on the other surfaces tested. This surface problem could probably be eliminated by careful selection and alignment of the heat source. However, a coating might be required for very bright surfaces.

RECOMMENDATIONS

The thermal test results included in this report should be correlated with results from other inspection techniques. Careful consideration should be given to the characteristic test parameter versus defect curves for this material in determining if the thermal test could be used. The advantages of the test such as noncontact and rapid inspection should be evaluated.

If the thermal test appears feasible for phenolic fiberglass material the next logical step would be to investigate actual inspection problems. Details such as inspection speed, optimum test parameters, and data read out should be considered. Alternate methods of performing the test such as oven heating the parts and performing a test as the part cools should also be evaluated.

Automation Industries, Inc., would be happy to supply additional details for such an investigation or for thermal inspection equipment to perform these tests. Please direct any questions regarding this report to Mr. J. A. Robinson, Regional Manager, Automation Industries, Inc., 2995 Corvin Drive, Santa Clara, California, 95050, telephone 408-245-5994, or directly to the Thermal Research Applications Group, Research Division, P. O. Box 950, Boulder, Colorado, 80302, telephone 303-443-6011.

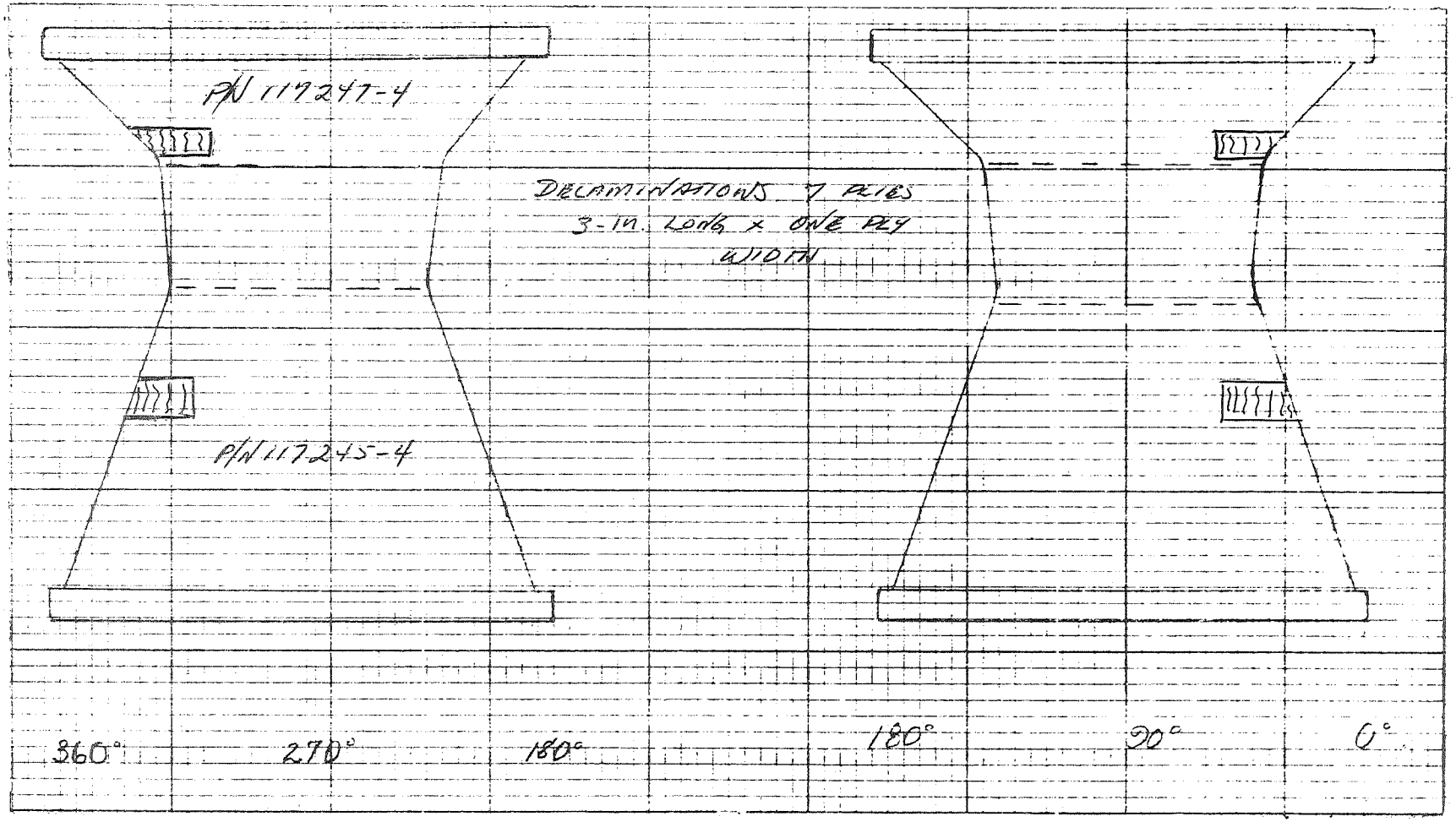

Figures supplied by Aerojet General Corporation

Figure 1. Sample Description

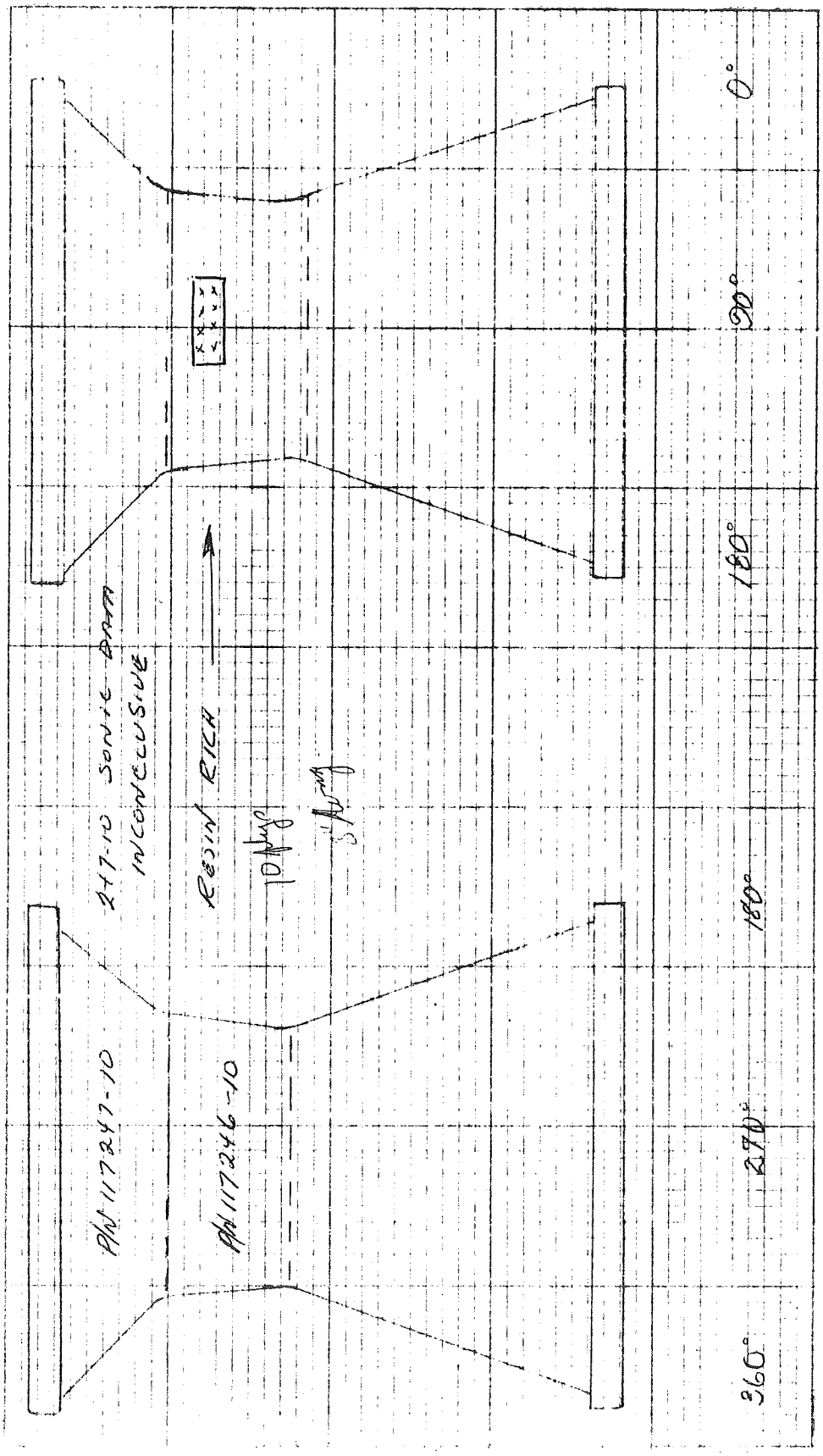

Figures supplied by Aerojet General Corporation

Figure 2. Sample Description

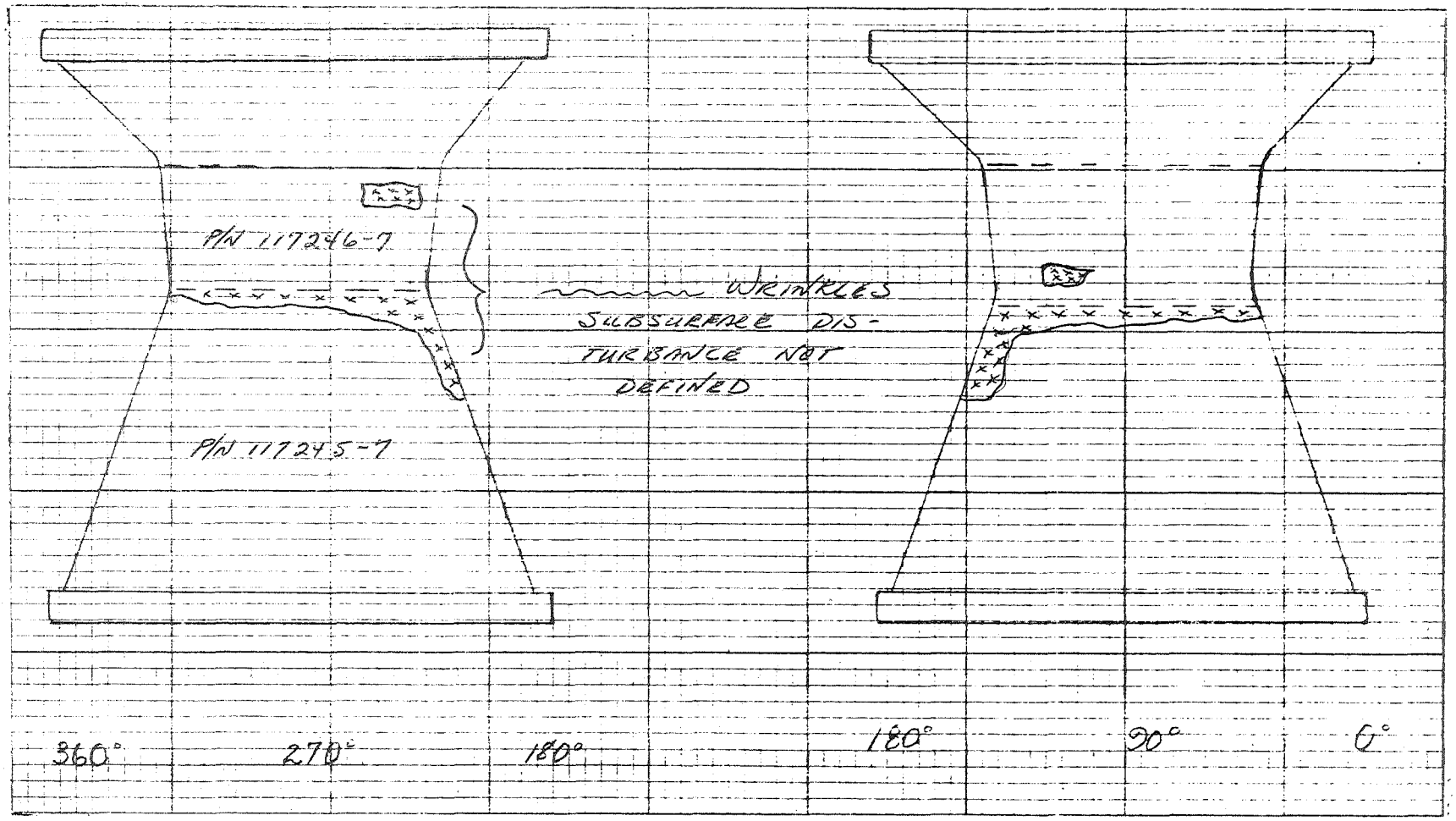

Figures supplied by Aerojet General Corporation

Figure 3. Sample Description

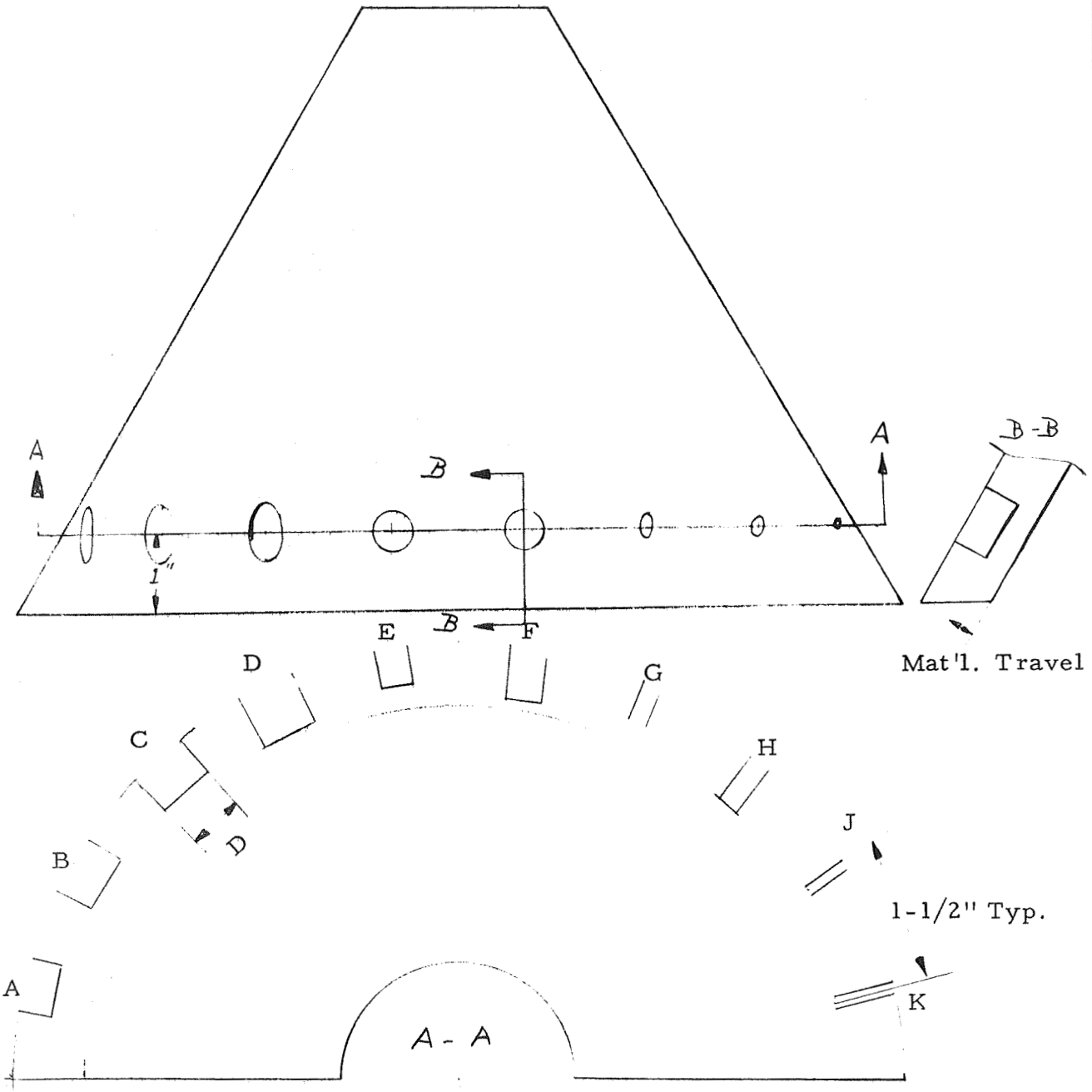

	Diameter	Mat'l. Travel
A	0.500	0.353
B	0.500	0.264
C	0.500	0.176
D	0.500	0.088
E	0.375	0.176
F	0.375	0.088
G	0.250	0.176
H	0.250	0.088
J	0.125	0.176
K	0.125	0.088

Figure 4. Reference Holes

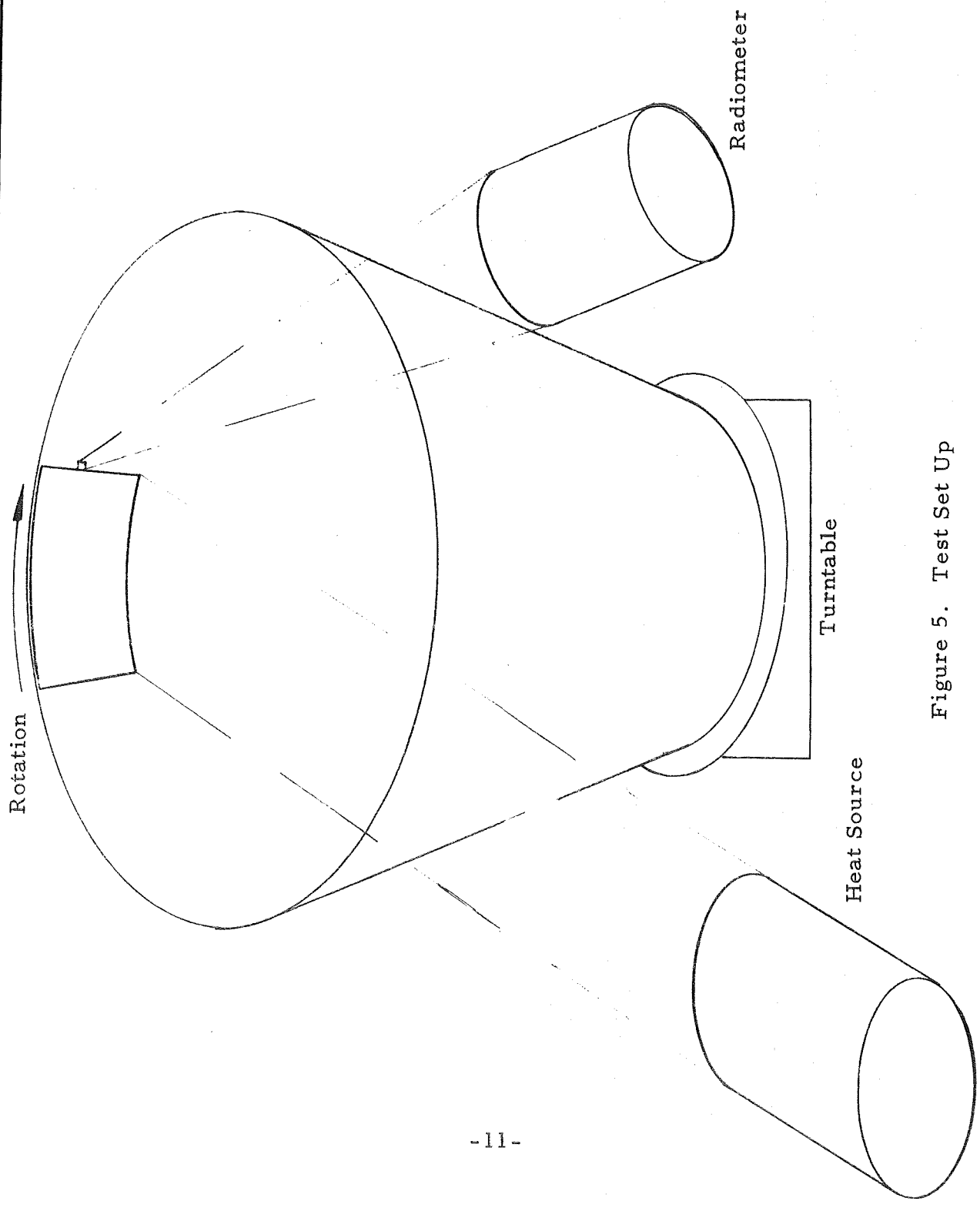

Figure 5. Test Set Up

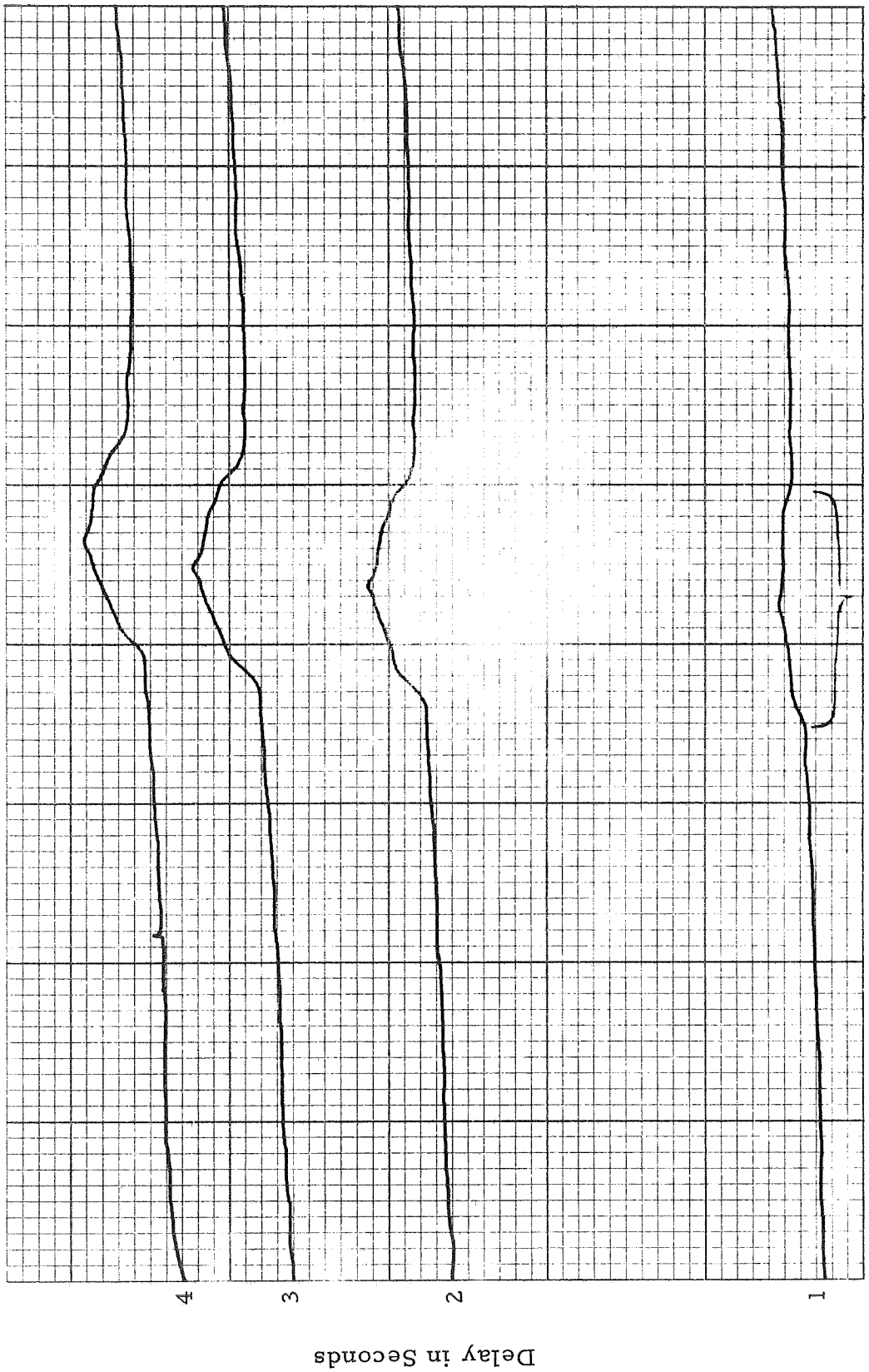

Figure 6. Delays over Delamination

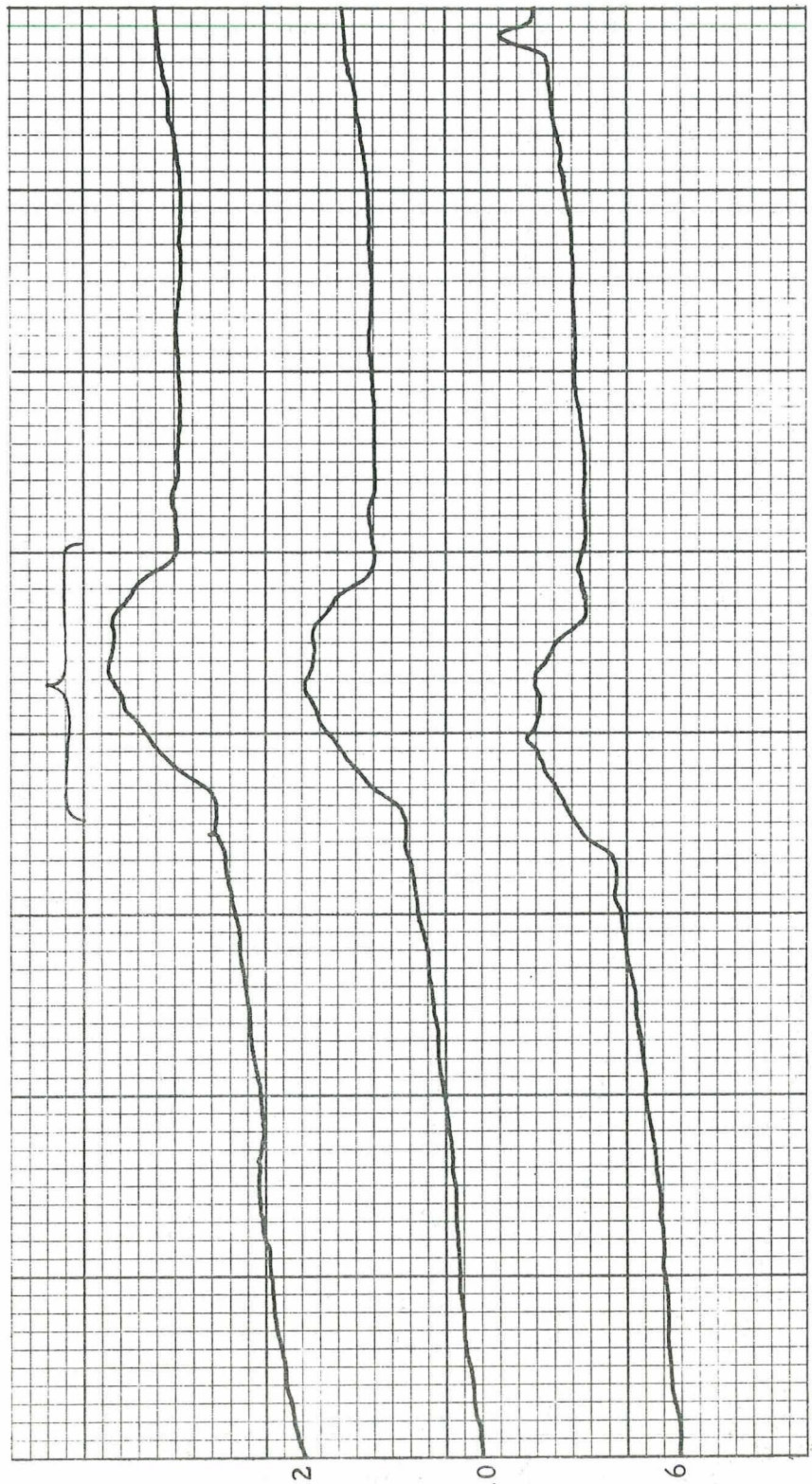

Figure 7. Delays over Delamination

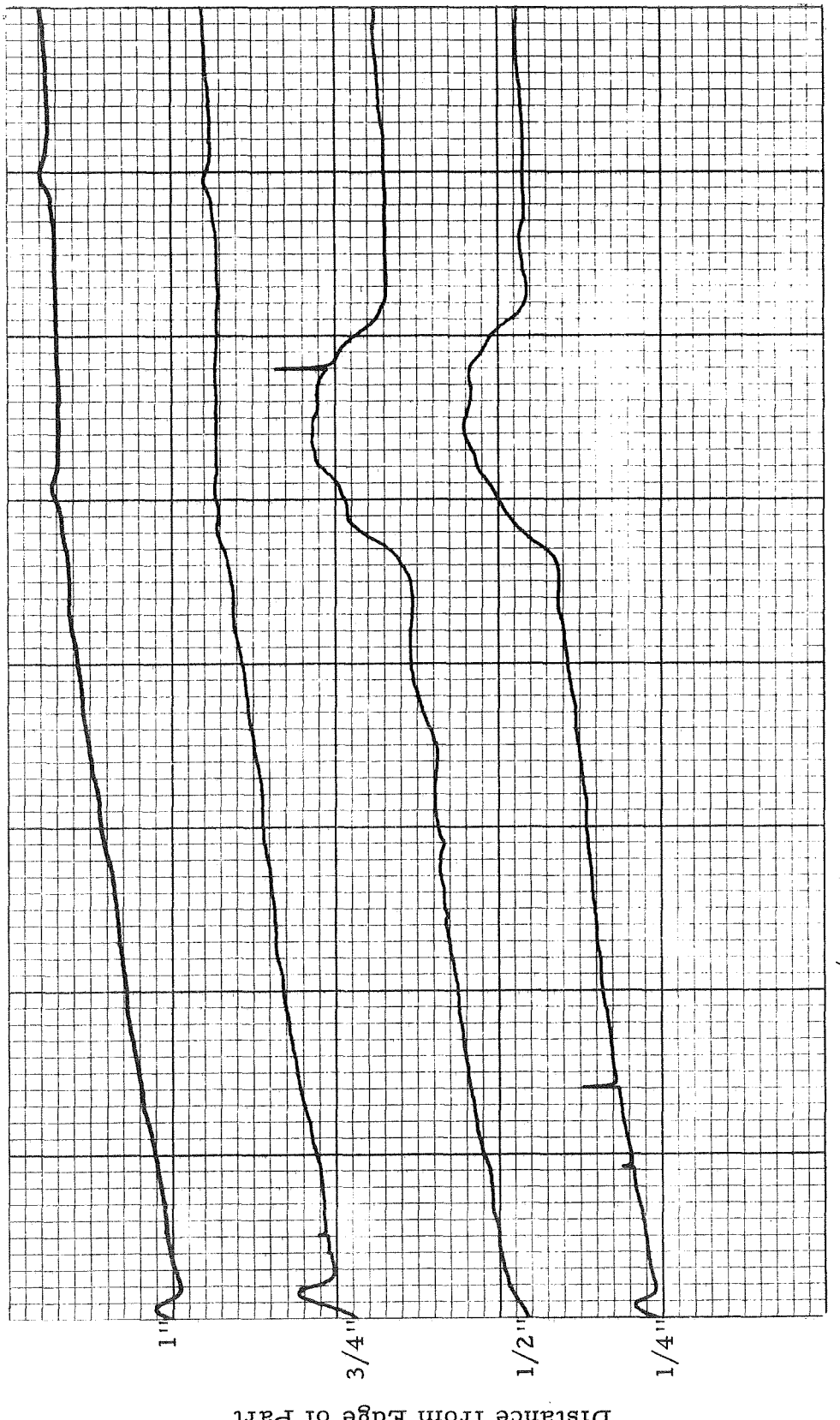

Figure 8. Line Scans over Delamination

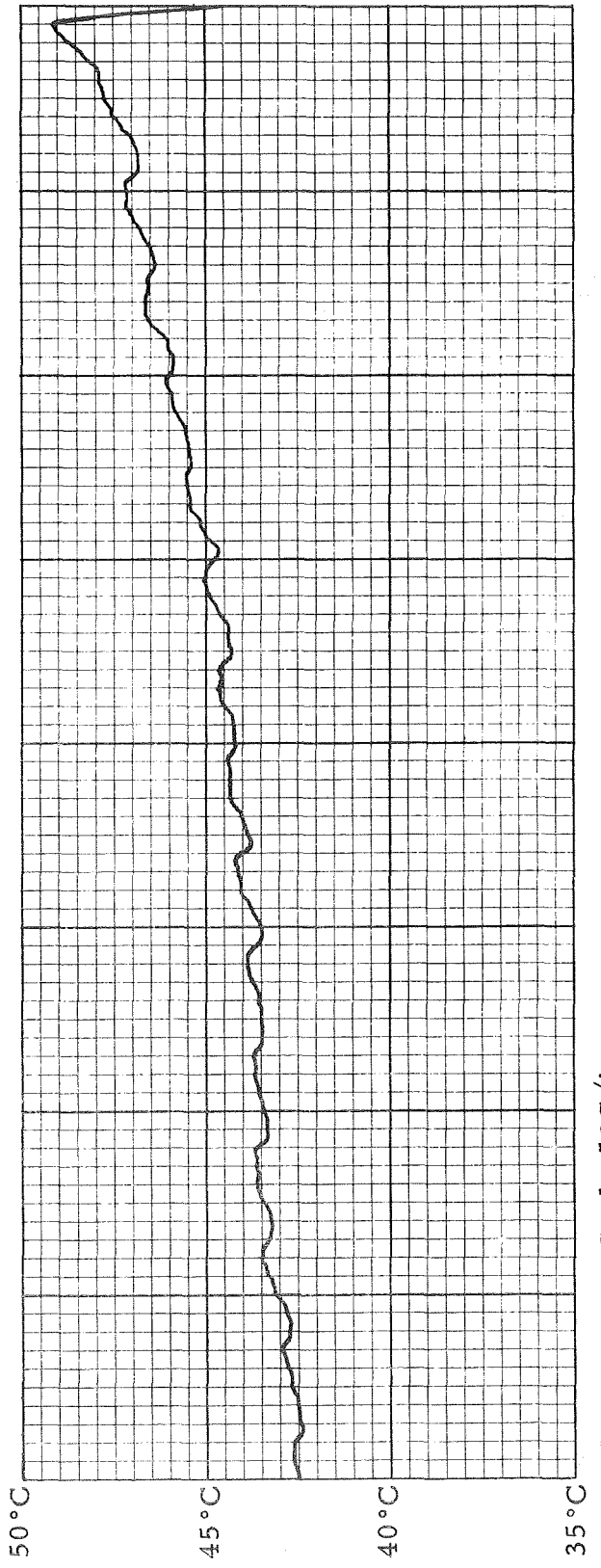

Figure 9. 1 Second Delay

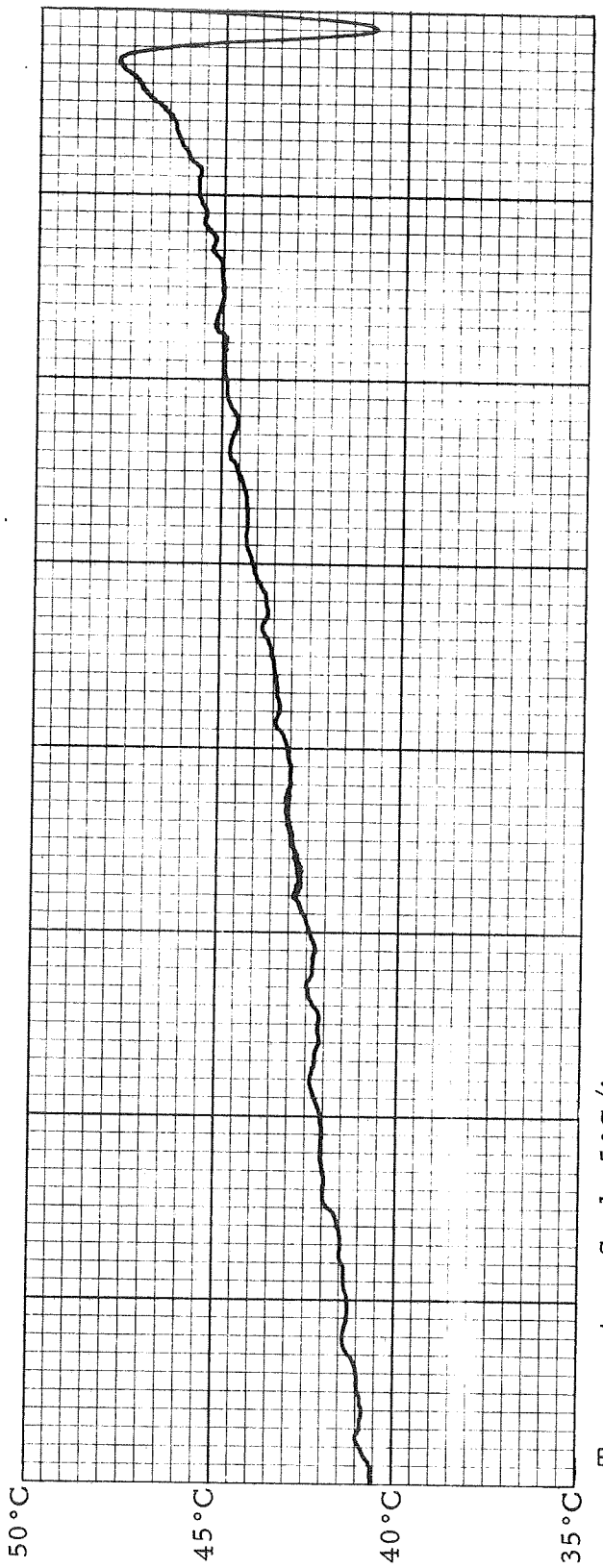

Figure 10. 3 Seconds Delay

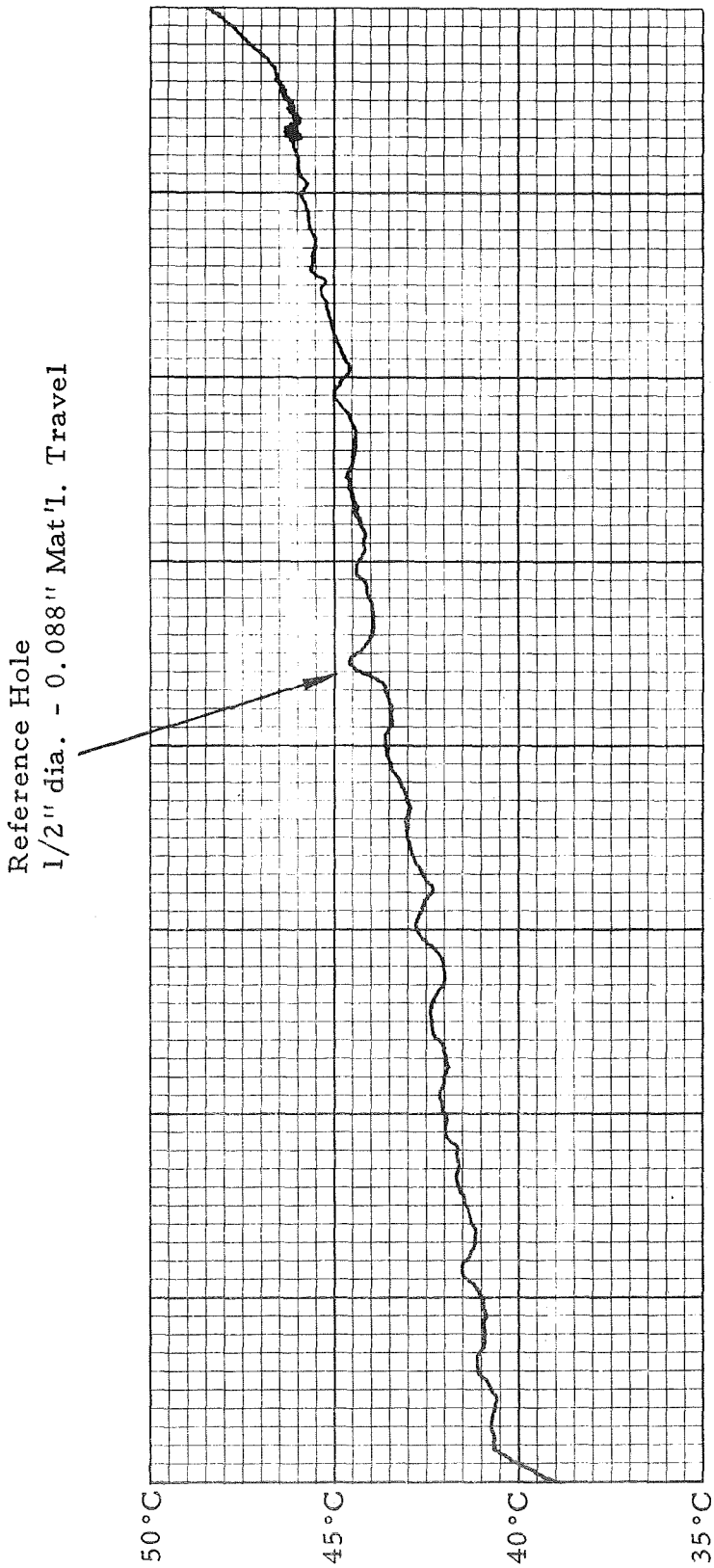

Figure 11. 6 Seconds Delay

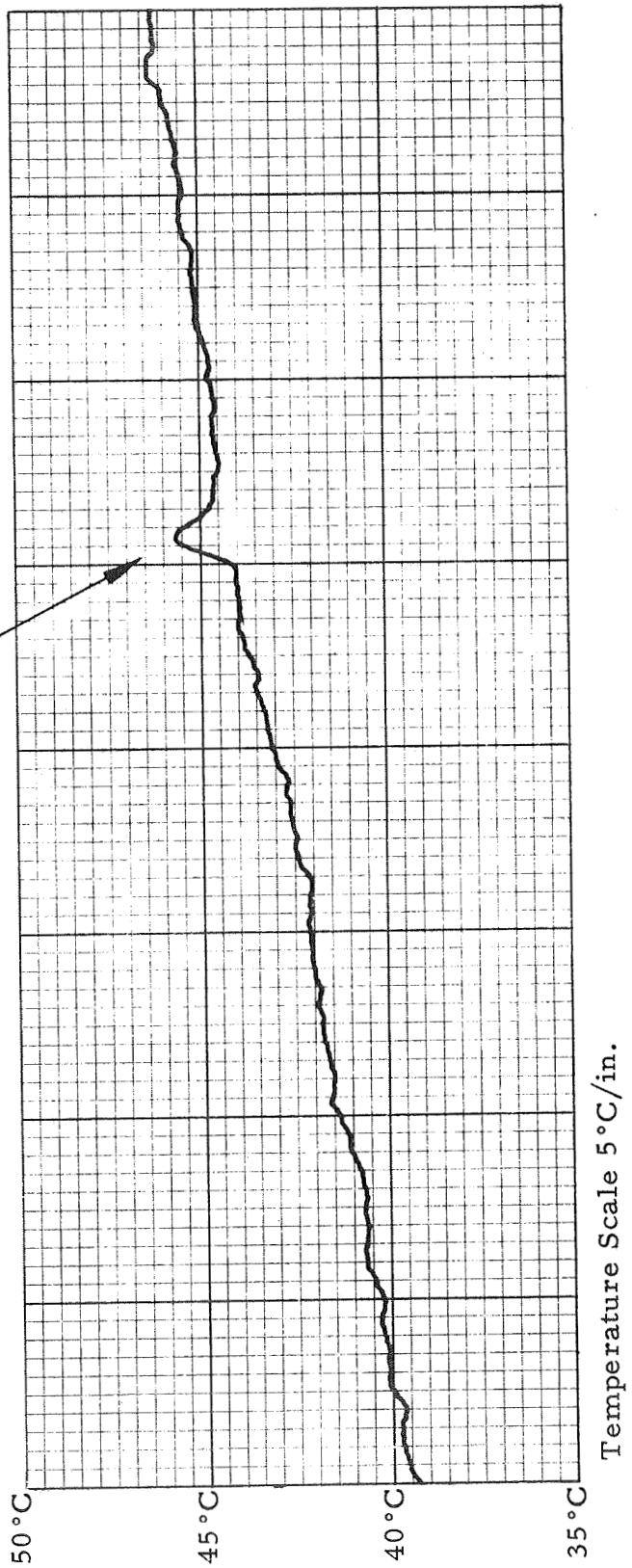

Figure 12. 7 Seconds Delay

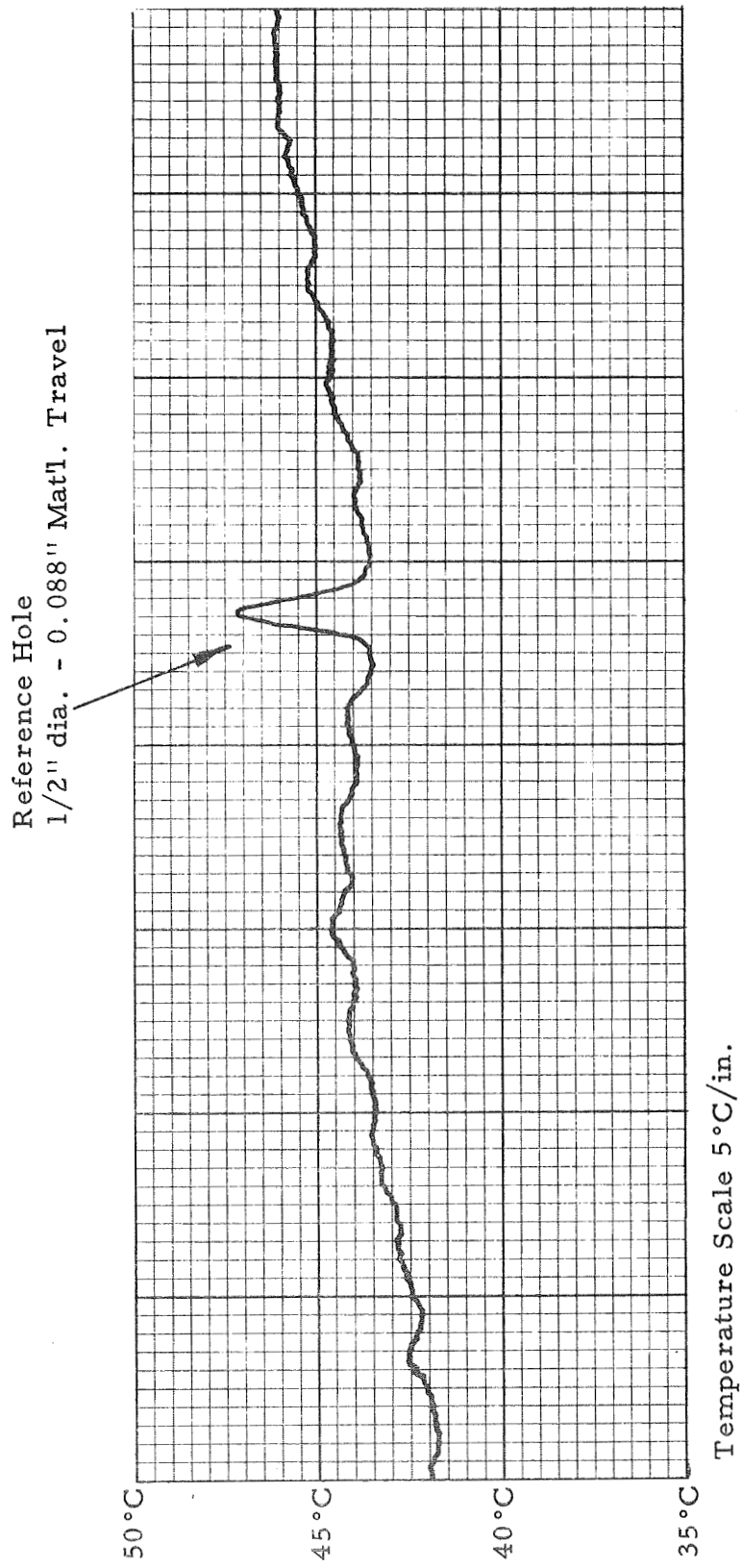

Figure 13. 12 Seconds Delay

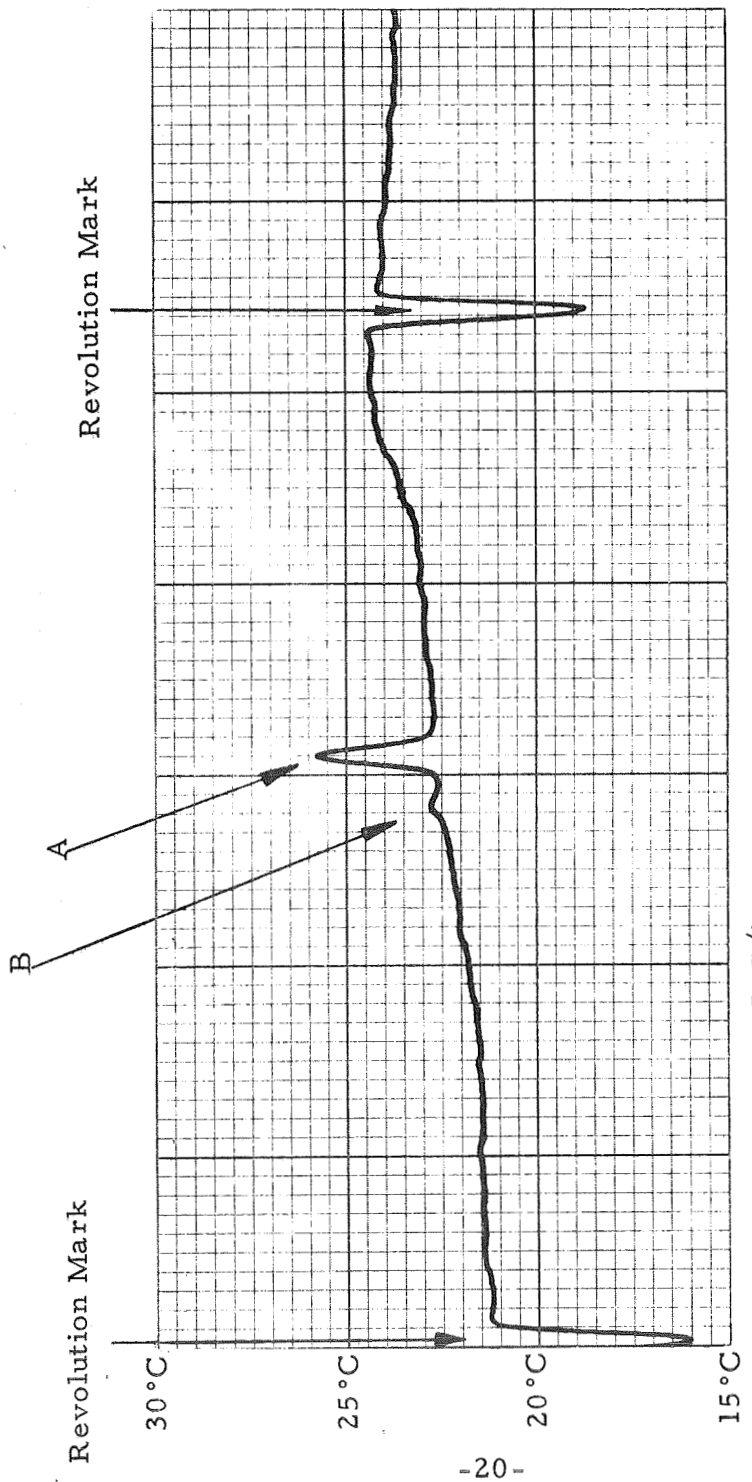

Figure 14. 25 Seconds Delay

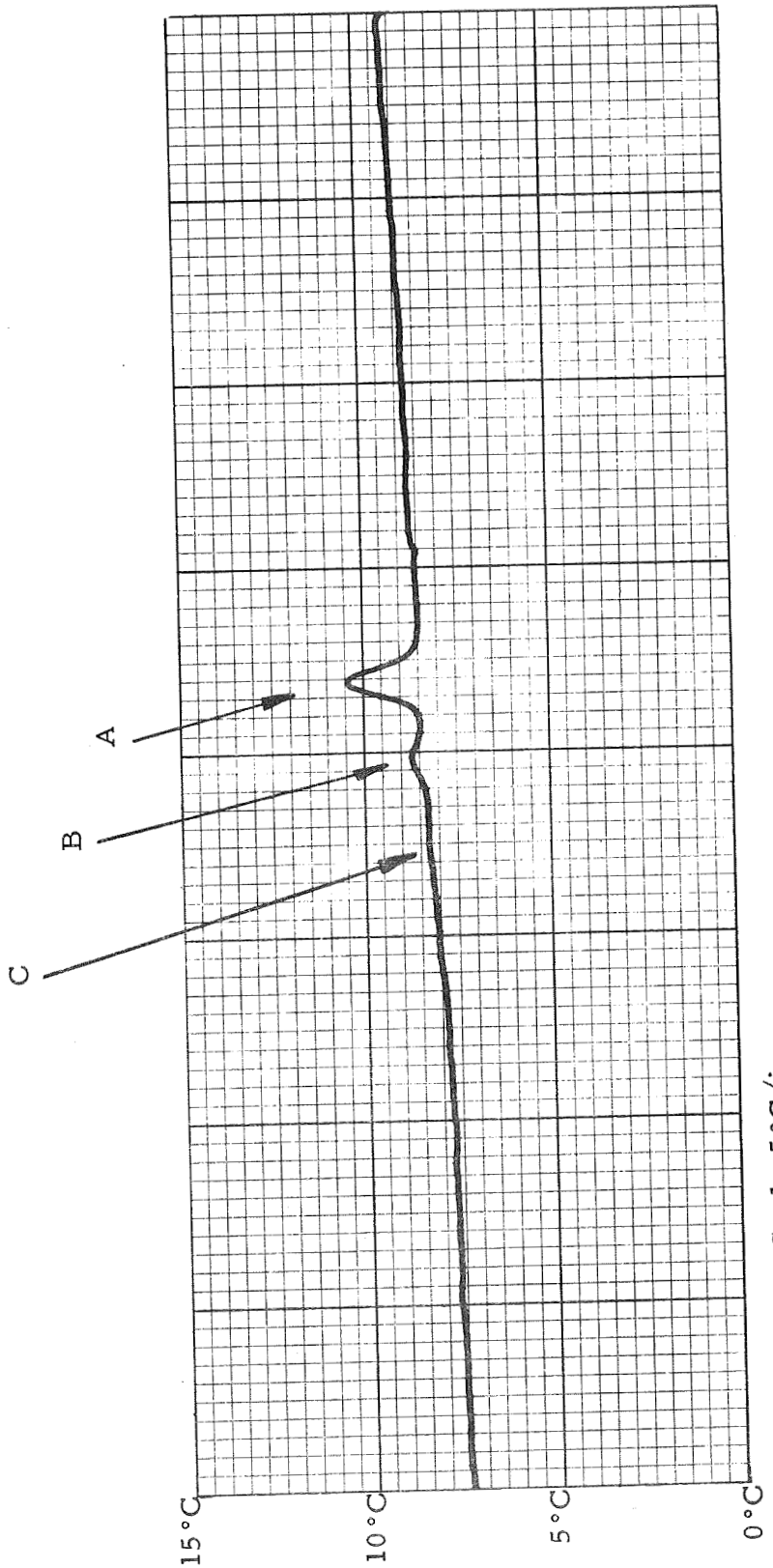

Temperature Scale 5 °C/in.

A = 1/2" dia. - 0.088" Mat'l. Travel
B = 1/2" dia. - 0.176" Mat'l. Travel
C = 1/2" dia. - 0.264" Mat'l. Travel

Figure 15. 50 Seconds Delay

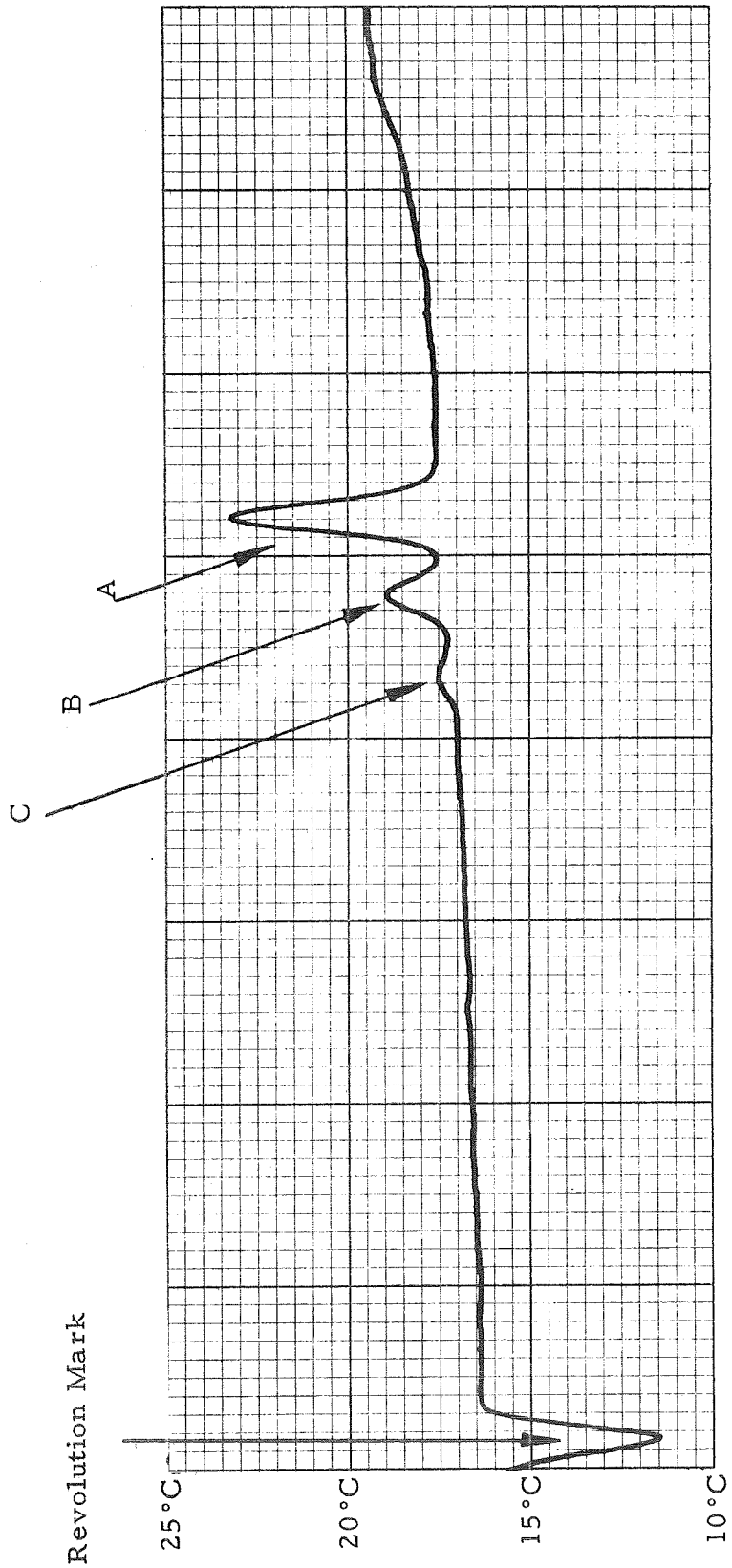

A = 1/2" dia. - 0.088" Mat'l. Travel
B = 1/2" dia. - 0.176" Mat'l. Travel
C = 1/2" dia. - 0.264" Mat'l. Travel

Figure 16. 80 Seconds Delay

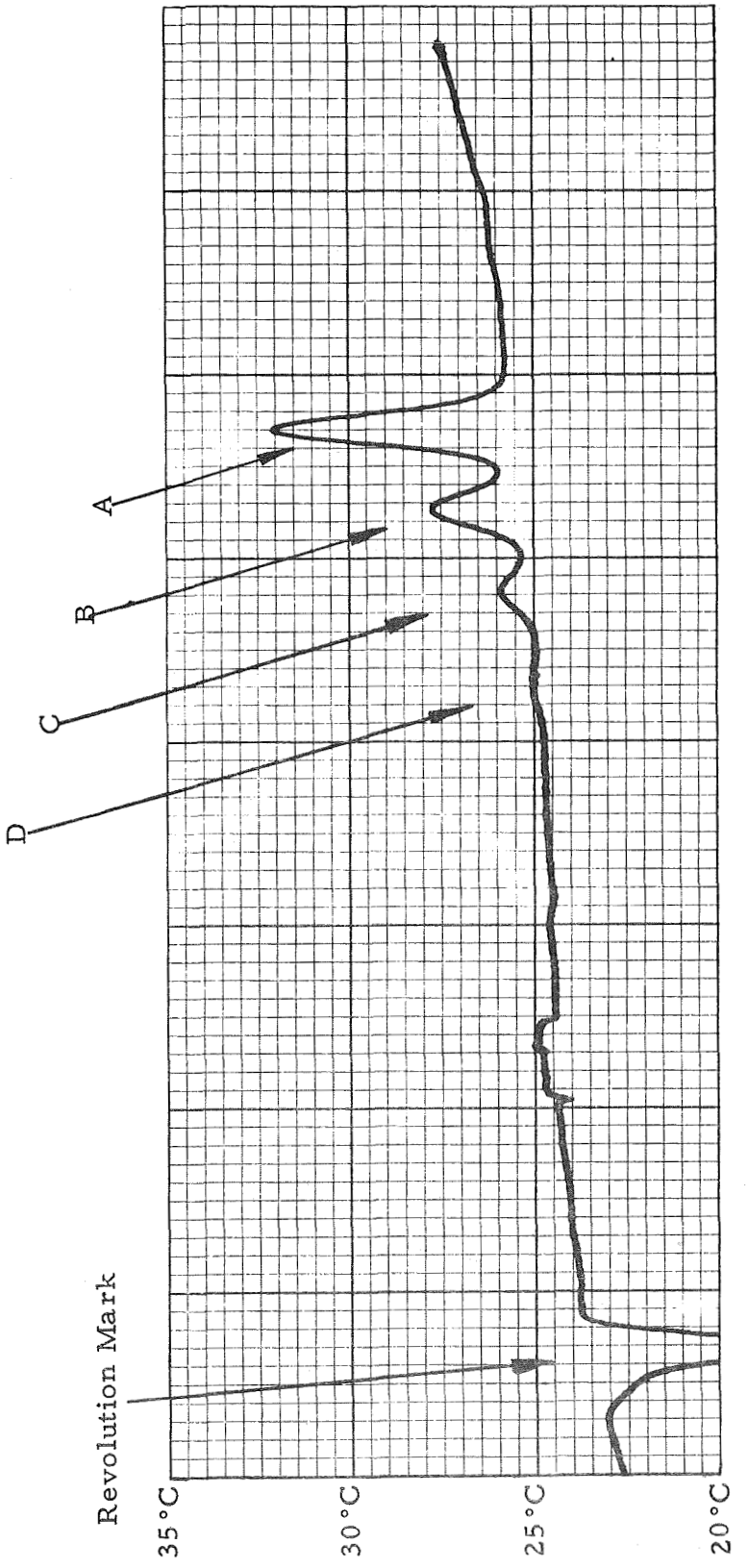

A = 1/2" dia. - 0.088" Mat'l. Travel
B = 1/2" dia. - 0.176" Mat'l. Travel
C = 1/2" dia. - 0.264" Mat'l. Travel
D = 1/2" dia. - 0.353" Mat'l. Travel

Figure 17. 120 Seconds Delay

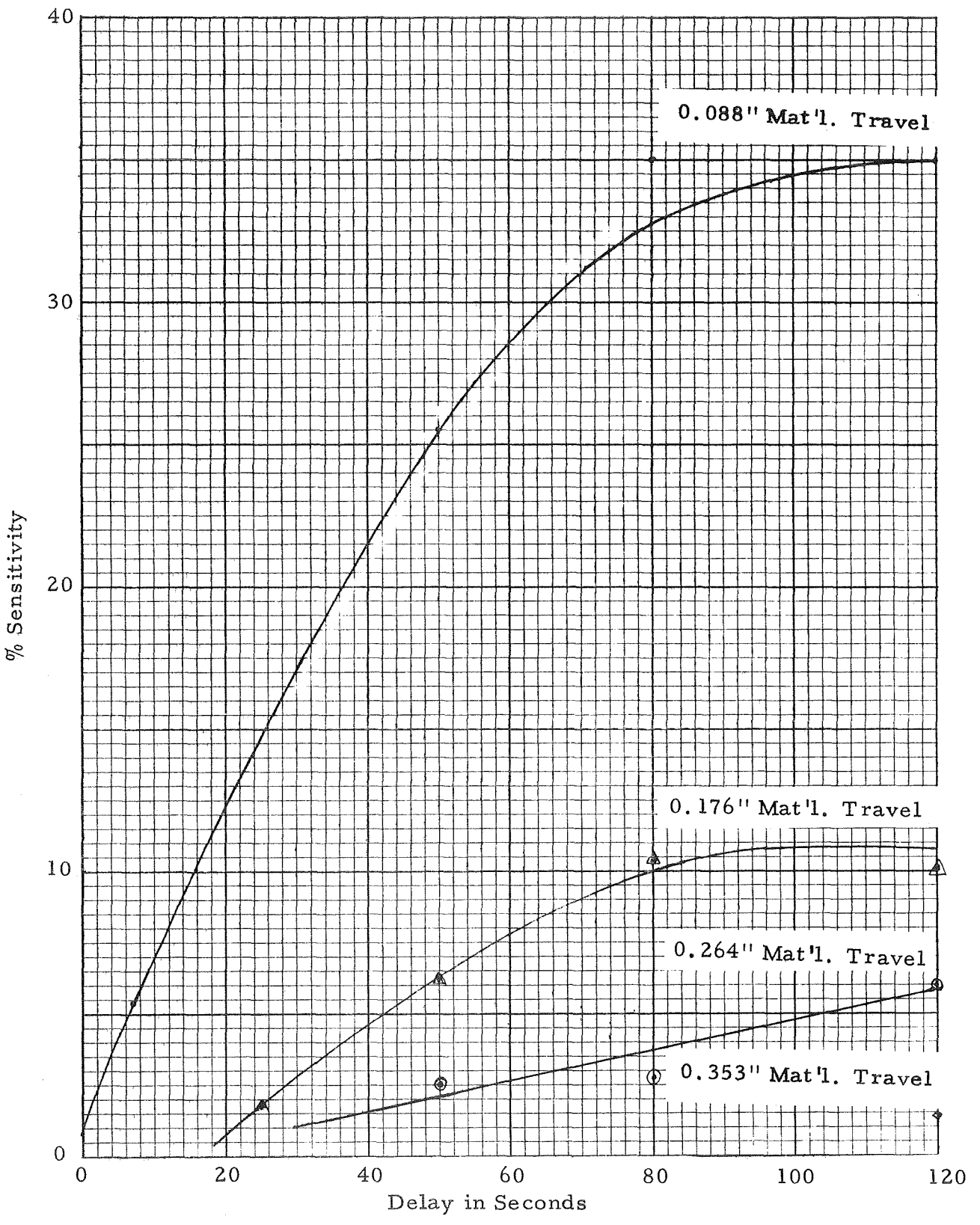

Figure 18. Sensitivity vs Delay

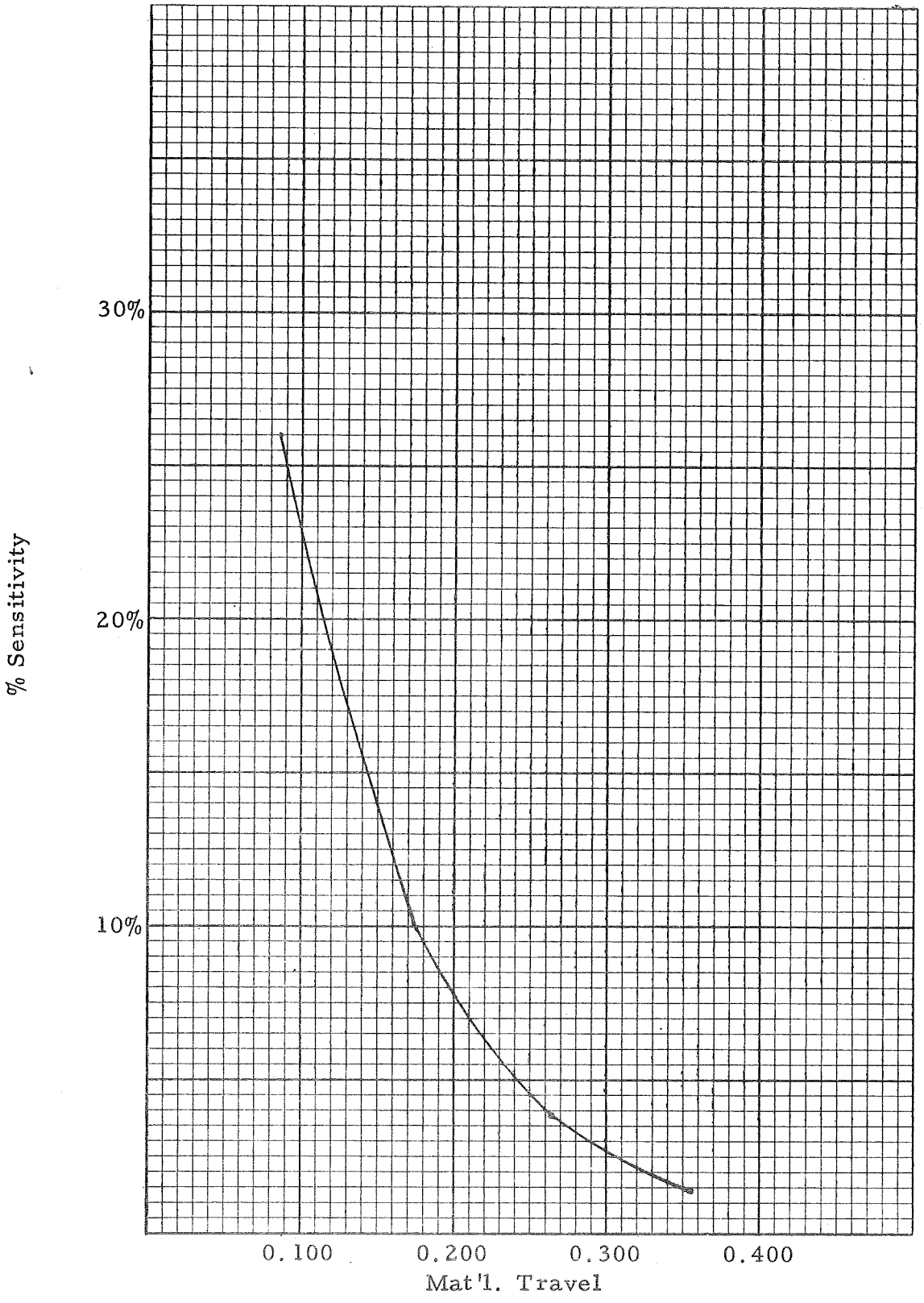

Figure 19. Sensitivity vs Depth

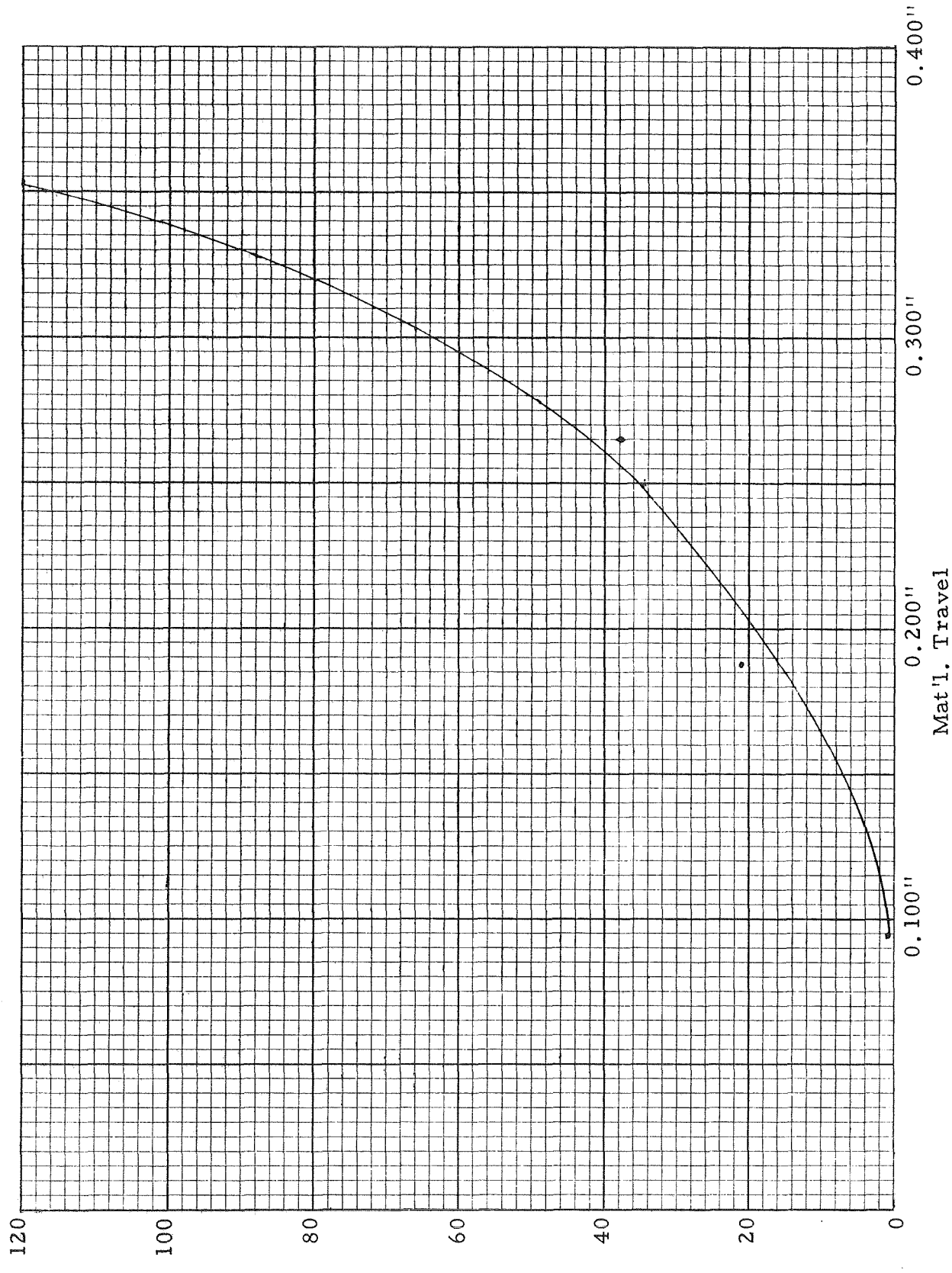

Figure 20. Delay vs Depth at 1-5% Sensitivity

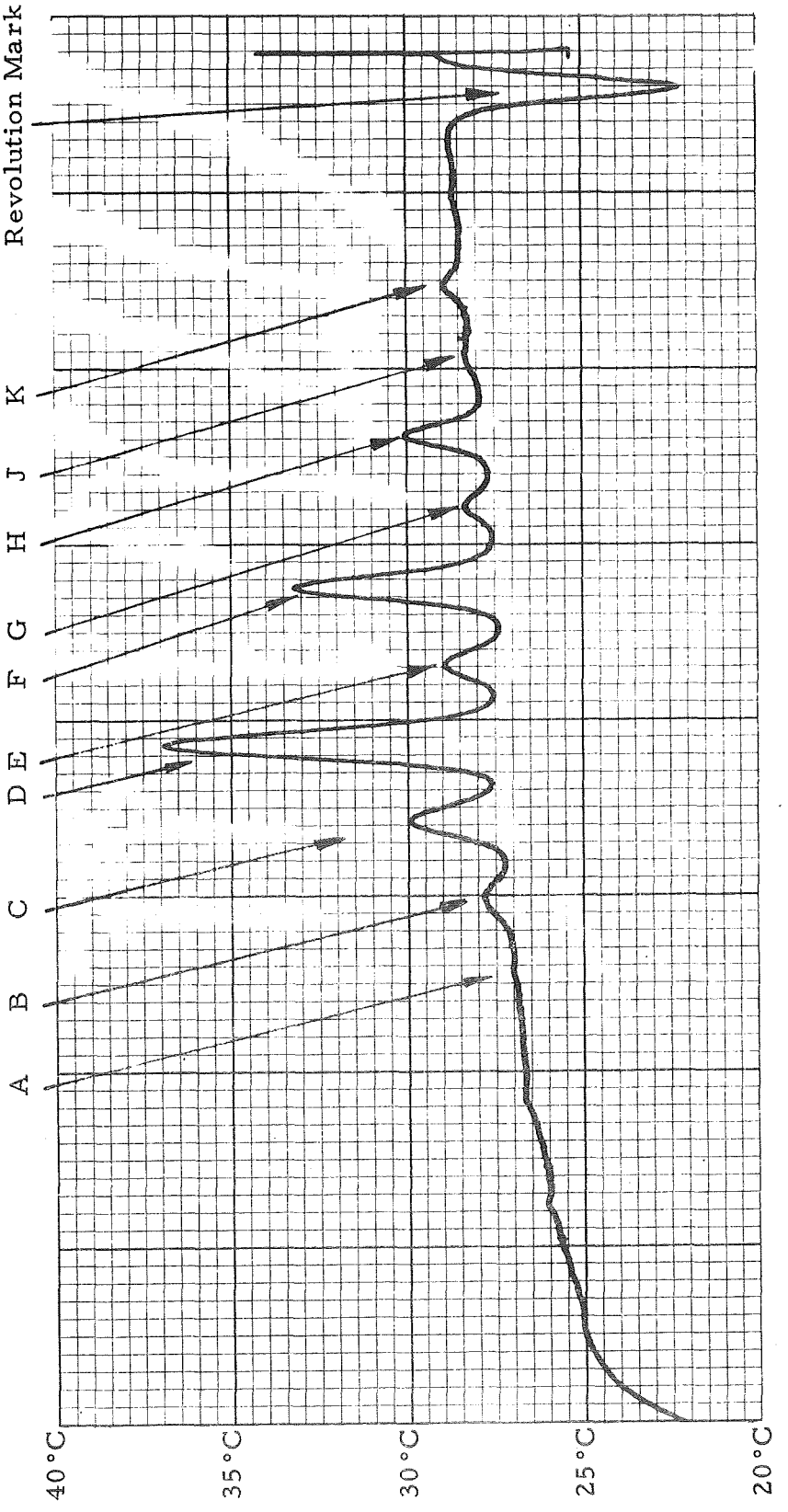

A = 1/2" dia. - 0.353" Mat'l. Travel
B = 1/2" dia. - 0.264" Mat'l. Travel
C = 1/2" dia. - 0.176" Mat'l. Travel
D = 1/2" dia. - 0.088" Mat'l. Travel
E = 3/8" dia. - 0.176" Mat'l. Travel
F = 3/8" dia. - 0.088" Mat'l. Travel
G = 1/4" dia. - 0.176" Mat'l. Travel
H = 1/4" dia. - 0.088" Mat'l. Travel
J = 1/8" dia. - 0.176" Mat'l. Travel
K = 1/8" dia. - 0.088" Mat'l. Travel

Figure 21. Reference Holes, 80 Seconds Delay

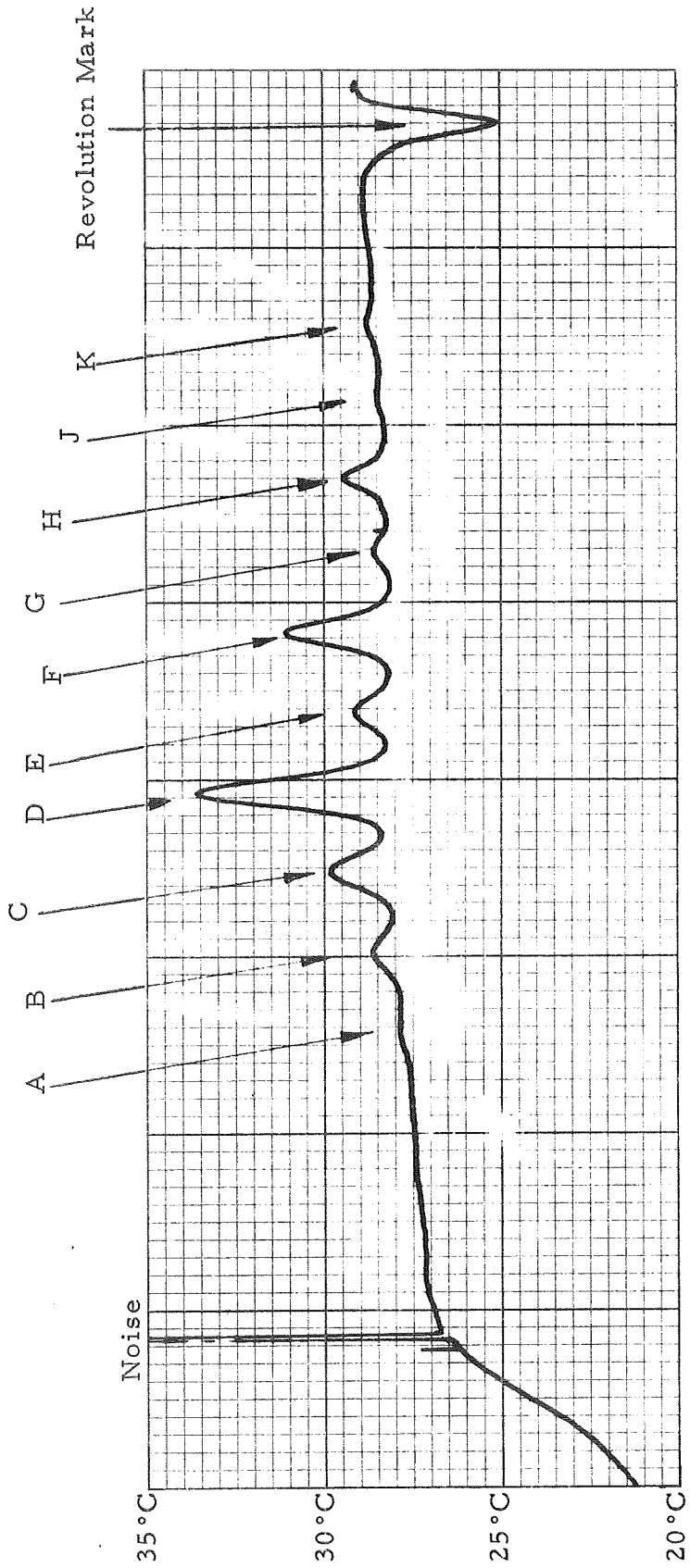

A = 1/2" dia. - 0.353" Mat'l. Travel
B = 1/2" dia. - 0.264" Mat'l. Travel
C = 1/2" dia. - 0.176" Mat'l. Travel
D = 1/2" dia. - 0.088" Mat'l. Travel
E = 3/8" dia. - 0.176" Mat'l. Travel
F = 3/8" dia. - 0.088" Mat'l. Travel
G = 1/4" dia. - 0.176" Mat'l. Travel
H = 1/4" dia. - 0.088" Mat'l. Travel
J = 1/8" dia. - 0.176" Mat'l. Travel
K = 1/8" dia. - 0.088" Mat'l. Travel

Figure 22. Reference Holes, 120 Seconds Delay

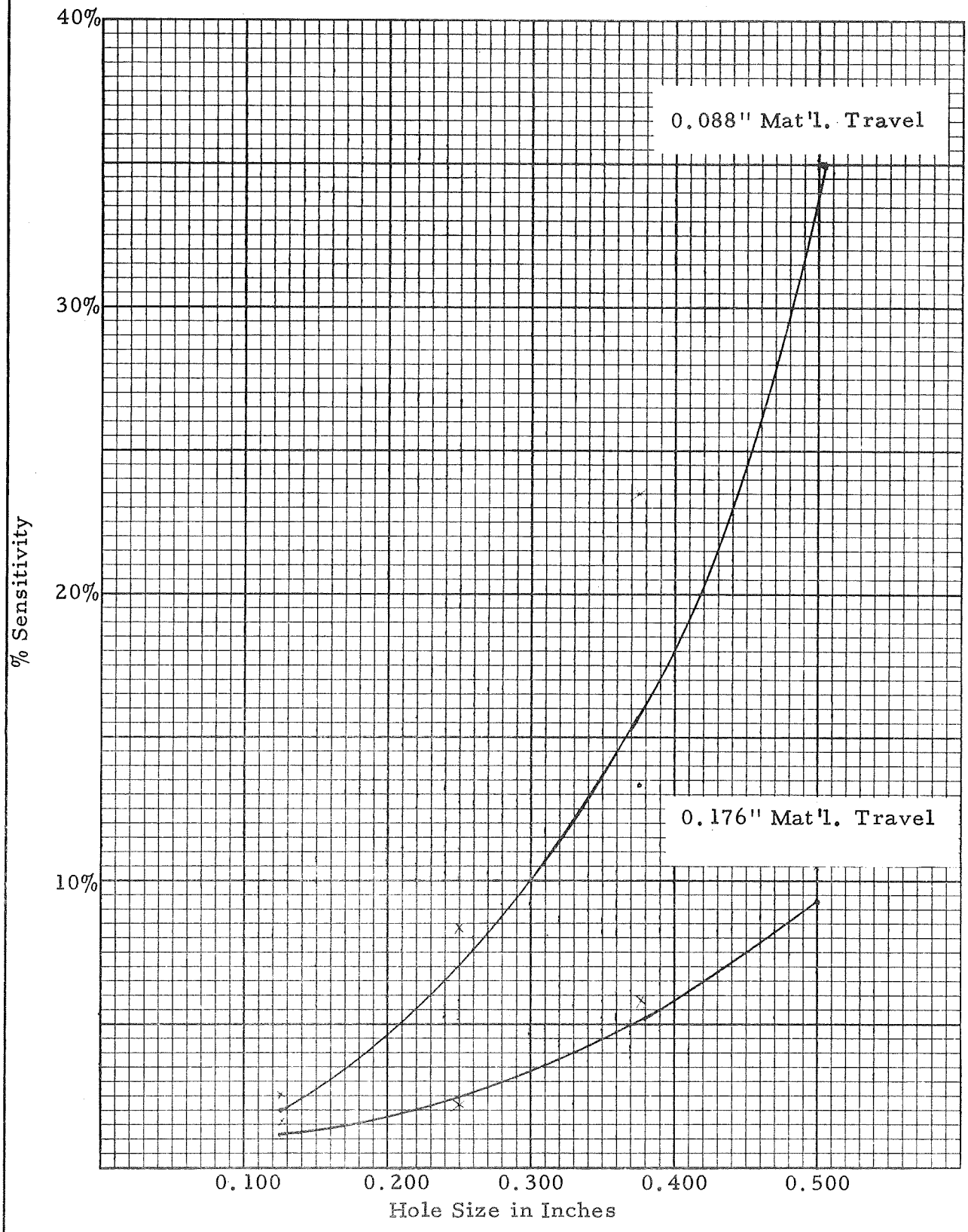

Figure 23. Sensitivity vs Size

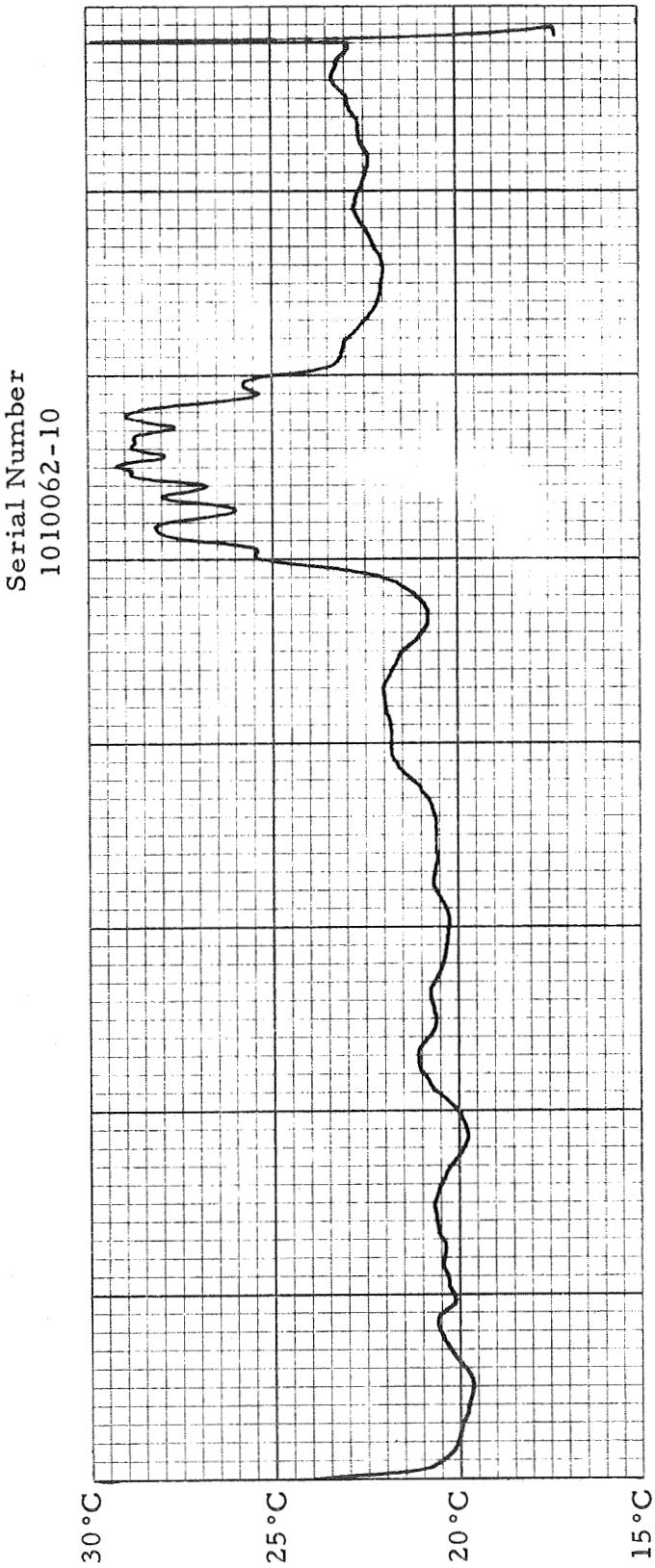

Figure 24. Surface Condition

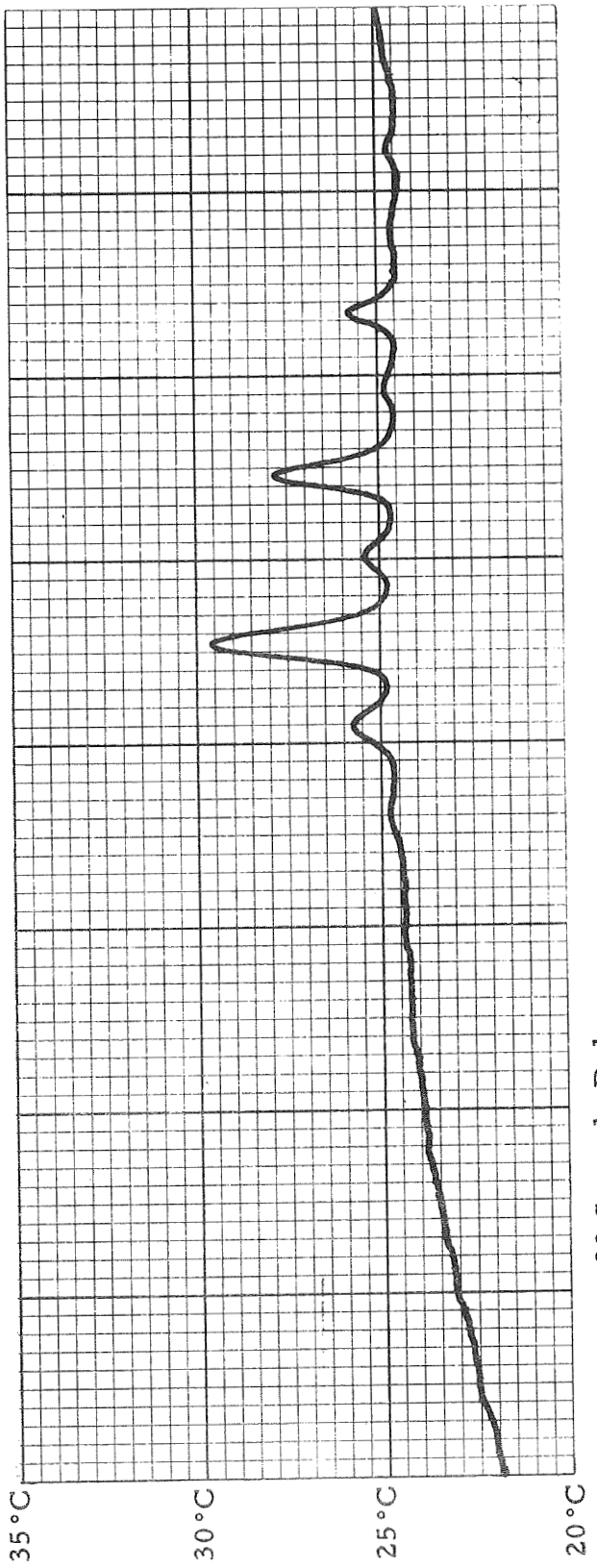

Figure 25. Reference Holes, Surface Painted

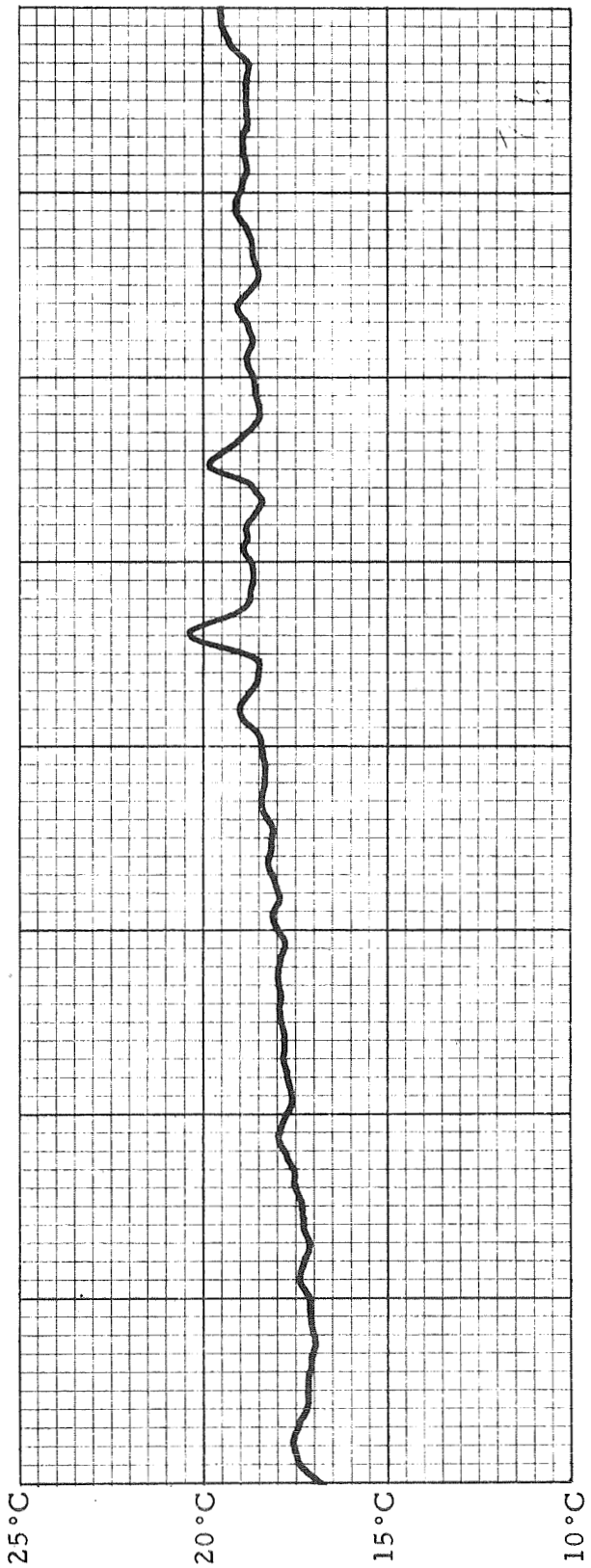

Figure 26. Reference Holes, Surface Unpainted

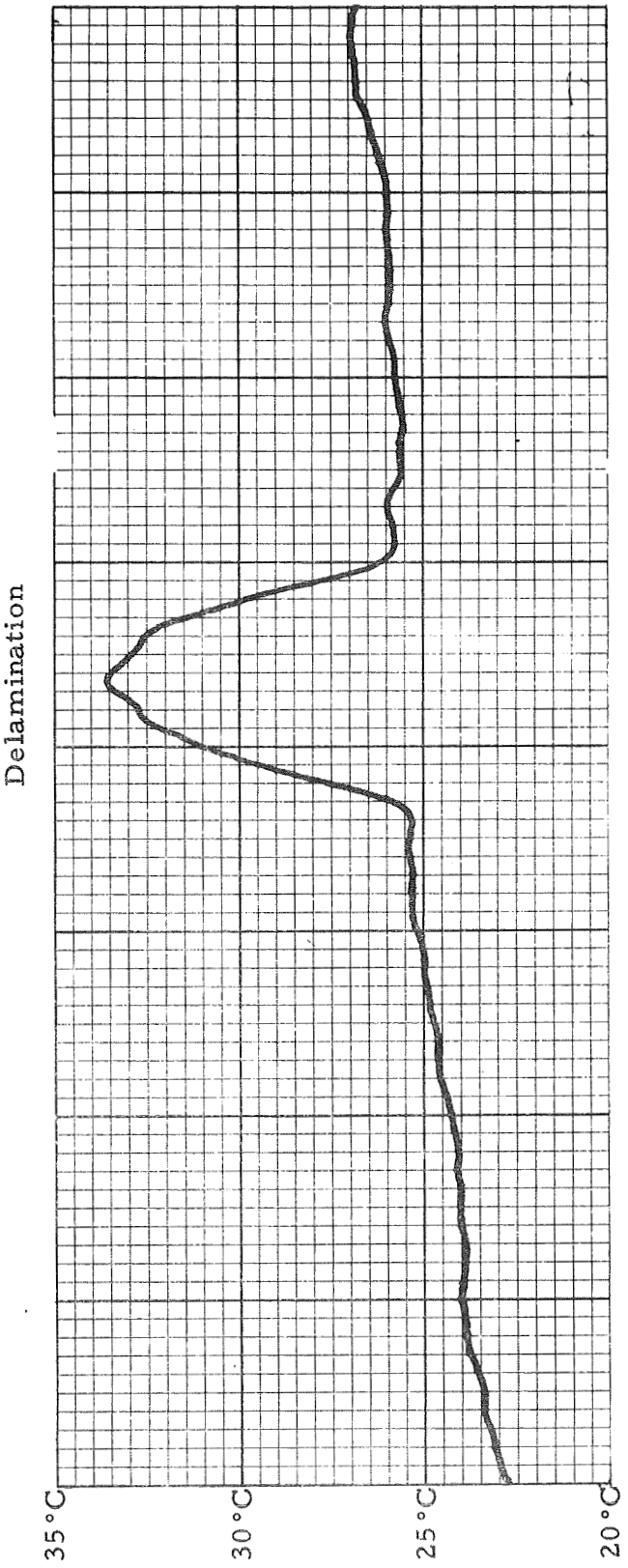

Figure 27. Delamination, Sample #1147245-4

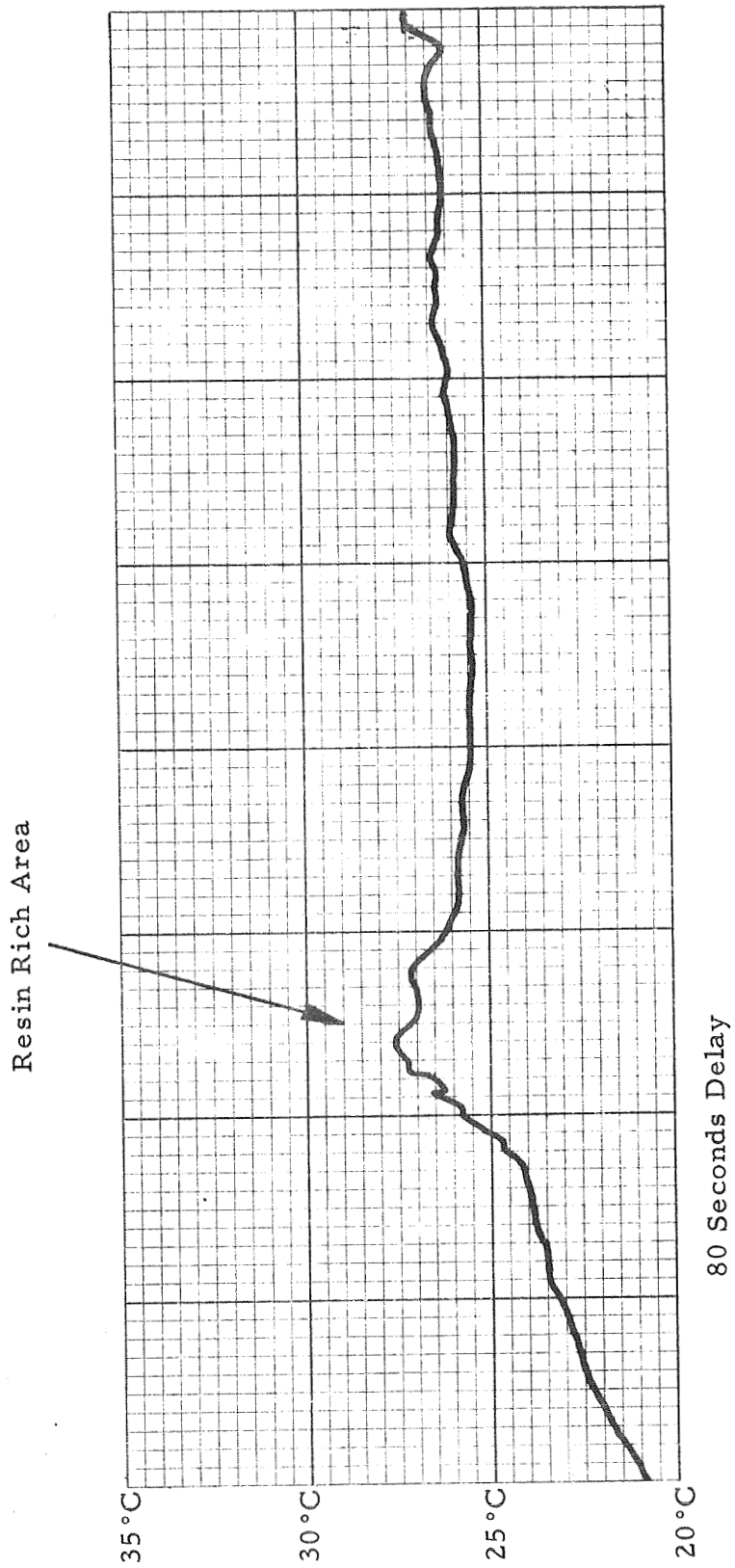

Figure 28. Sample #101006-10 Unpainted

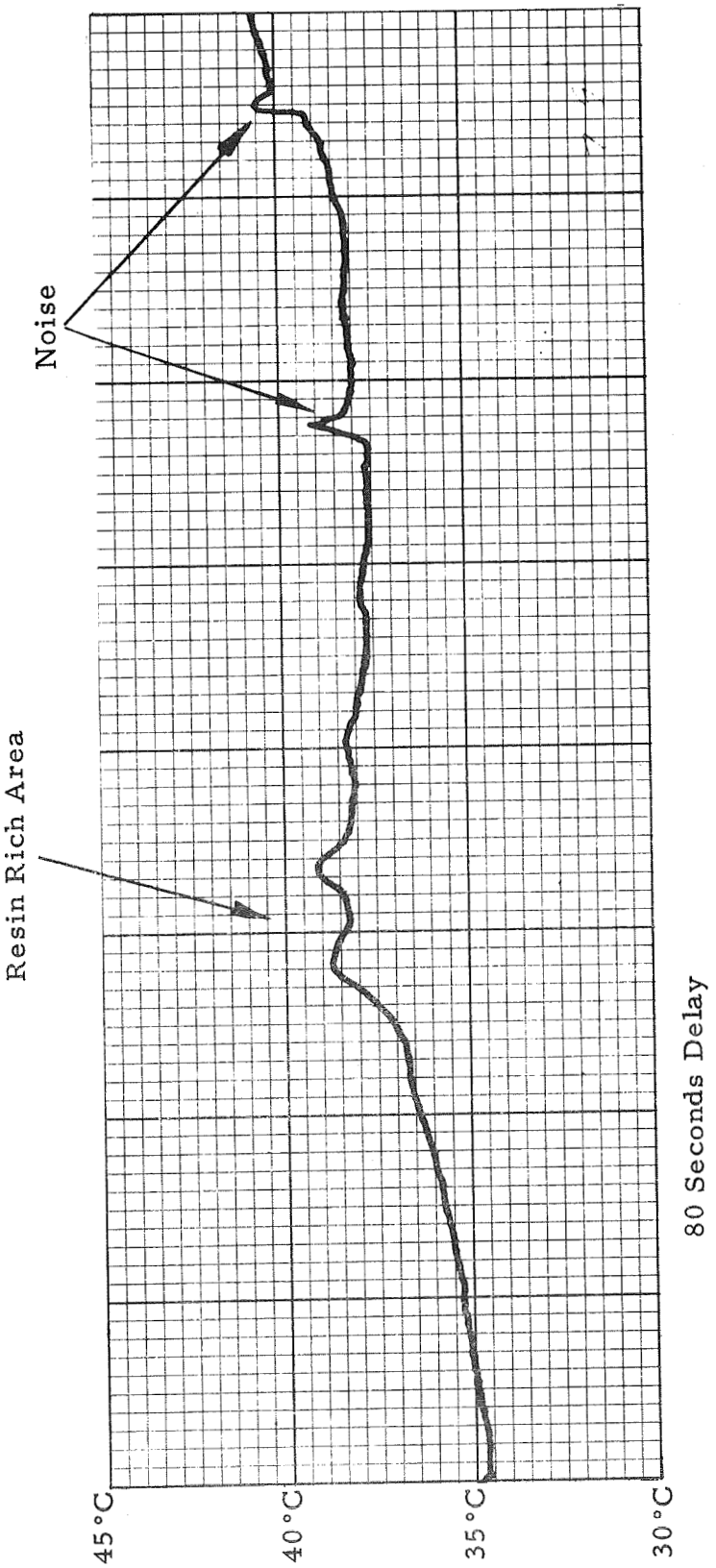

Figure 29. Sample #1010066-10, Painted

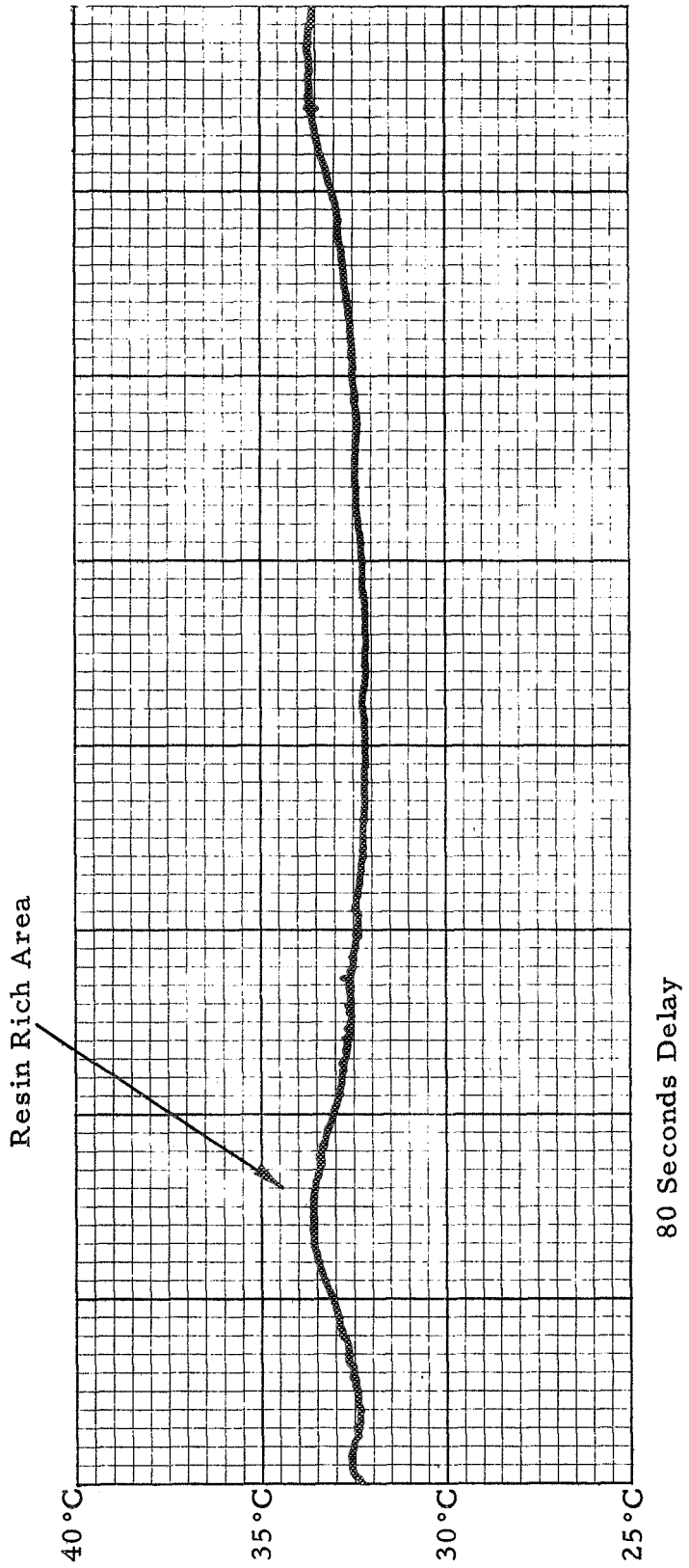

Figure 30. Sample #1010062-10

Distribution List

Recipient	Copies
NASA Lewis Research Center	
21000 Brookpark Road	
Cleveland, Ohio 44135	
Attn: Contracting Officer	
Mail Stop 500-313	(1)
Solid Rocket Technology Branch	
Mail Stop 500-205	(8)
Technical Library	
Mail Stop 60-3	(2)
Tech. Report Control Office	
Mail Stop 5-5	(1)
J. Kennard	
Mail Stop 3-17	(1)
Tech. Utilization Office	
Mail Stop 3-19	(1)
Patent Counsel	
Mail Stop 500-311	(1)
National Aeronautics and Space Administration	
Washington, D.C. 20546	
Attn: RPM/William Cohen	(3)
RPS/Robert W. Ziem	(1)
ATSS-AL/Technical Library	(2)
NASA Ames Research Center	
Moffett Field, California 94035	
Attn: Technical Library	(1)
NASA Langley Research Center	
Langley Station	
Hampton, Virginia 23365	
Attn: Robert L. Swain	(1)
Technical Library	(1)
NASA Goddard Space Flight Center	
Greenbelt, Maryland 20771	
Attn: Technical Library	(1)
NASA Manned Spacecraft Center	
2101 Webster Seabrook Road	
Houston, Texas 77058	
Attn: Technical Library	(1)

Recipient	Copies
NASA George C. Marshall Space Flight Center	
Redstone Arsenal	
Huntsville, Alabama 35812	
Attn: Technical Library	(1)
R-P & VE-PA/K, Chandler	(1)
Jet Propulsion Laboratory	
California Institute of Technology	
4800 Oak Grove Drive	
Pasadena, California 91103	
Attn: Richard Bailey	(1)
Technical Library	(1)
Scientific & Technical Information Facility	
NASA Representative	
P.O. Box 33	
College Park, Maryland 20740	
Attn: CRT	(6)
Government Installations	
AF Space Systems Division	
Air Force Unit Post Office	
Los Angeles, California 90045	
Attn: Col. E. Fink	(1)
AF Research and Technology Division	
Bolling AFB, D.C. 20332	
Attn: Dr. Leon Green, Jr.	(1)
AF Rocket Propulsion Laboratory	
Edwards AFB, California 93523	
Attn: RPM/Mr. C. Cook	(2)
AF Materials Laboratory	
Wright-Patterson AFB, Ohio 45433	
Attn: MANC/D. Schmidt	(1)
MAAE	(1)
P. F. Pirrung	(1)

Distribution List (cont)

Recipient	Copies
AF Ballistic Missile Division P.O. Box 262 San Bernardino, California 92402 Attn: WDSOT	(1)
Structures Division Wright-Patterson AFB, Ohio 45433 Attn: FDT/R. F. Hoener	(1)
Army Missile Command Redstone Scientific Information Center Redstone Arsenal, Alabama 35809 Attn: Chief, Document Section	(1)
Ballistic Research Laboratory Aberdeen Proving Ground, Maryland 21005 Attn: Technical Library	(1)
Picatinny Arsenal Dover, New Jersey 07801 Attn: Technical Library	(1)
Navy Special Projects Office Washington, D.C. 20360 Attn: H. Bernstein	(1)
Naval Air Systems Command Washington, D.C. 20360 Attn: AIR-330/Dr. O. H. Johnson	(1)
Naval Propellant Plant Indian Head, Maryland 20640 Attn: Technical Library	(1)
Naval Ordnance Laboratory White Oak Silver Spring, Maryland 20910 Attn: Technical Library	(1)
Naval Ordnance Test Station China Lak,, California 93557 Attn: Technical Library C. J. Thelen	(1)
Chemical Propulsion Information Agency Applied Physics Laboratory 8621 Georgia Avenue Silver Spring, Maryland 20910	(1)
Defense Documentation Center Cameron Station 5010 Duke Street Alexandria, Virginia 22314	(1)
Defense Materials Information Center Battelle Memorial Institute 505 King Avenue Columbus, Ohio 43201	(1)
Materials Advisory Board National Academy of Science 2101 Constitution Ave., N.W. Washington, D.C. 20418 Attn: Capt. A. M. Blamphin	(1)
Institute for Defense Analysis 1666 Connecticut Ave., N.W. Washington, D.C. 20009 Attn: Technical Library	(1)
Advanced Research Projects Agency Pentagon, Room 3D154 Washington, D.C. 20301 Attn: Technical Information Office	(1)
Naval Research Laboratory Washington, D.C. 20390 Attn: Technical Library	(1)
Industry Contractors	
Aerojet-General Corporation Electronics Division P.O. Box 296 Azusa, California 91702 Attn: Technical Library	(1)

Distribution List (cont)

Recipient	Copies
Hercules Company Bacchus Works P.O. Box 98 Magna, Utah 84044 Attn: Technical Library	(1)
Thiokol Chemical Corporation Elkton Division Elkton, Maryland 21921 Attn: Technical Library	(1)
Thiokol Chemical Corporation Huntsville Division Huntsville, Alabama 35807 Attn: Technical Library	(1)
Minnesota Mining & Mfg Company 2501 Hudson Road St. Paul, Minnesota 55101	(1)
US Polymeric, Inc. 700 E. Dyer Road Santa Ana, California 92707	(1)
Ferro Corporation 3512-20 Helms Avenue Culver City, California 90230	(1)
Fiberite Corporation 645 No. Cypress Street Orange, California 92666	(1)
United Technology Center P.O. Box 358 Sunnyvale, California 94088 Attn: Technical Library	(1)
Aerotherm Corporation Mountain View, California Attn: J. W. Schaefer	(1)
Rohr Corporation Space Products Division 8200 Arlington Boulevard Riverside, California 92503	(1)
Raybestos-Manhattan, Inc. 4651 Pacific Building Los Angeles, California 90053	(1)
Narmco Materials Division Whittaker Corporation 600 Victoria Street Costa Mesa, California 92626	(1)
Hexcel Corporation Coast Division 11711 Dublin Boulevard Dublin, California 94566	(1)
HITCO 1602 West 135 Street Gardena, California 90249	(1)
AVCO Corporation 201 Lowell Street Wilmington, Massachusetts 01887	(1)
TRW, Inc. Structures Division 23444 Euclid Avenue Cleveland, Ohio 44117 Attn: L. Russell	(1)
TRW Systems One Space Park Redondo Beach, California 90278 Attn: M. Lipow	(1)
Thiokol Chemical Corporation Wasatch Division Brigham City, Utah 84302	(1)

Distribution List (cont)

Recipient	Copies
Aerojet Solid Propulsion Company P.O. Box 1168 Sacramento, California 94086	
Attn: Dr. B. Simmons	(1)
Technical Information Center	(1)
Space Booster Department	(8)
Aerospace Corporation 2400 East El Segundo Boulevard El Segundo, California 90245	
Attn: Technical Library	(1)
Solid Motor Dev. Office	(1)
Aerospace Corporation P.O. Box 95085 Los Angeles, California 90045	
Attn: Technical Library	(1)
Atlantic Research Corporation Shirley Highway at Edsall Road Alexandria, Virginia 22314	
Attn: Technical Library	(1)
Battelle Memorial Library 505 King Avenue Columbus, Ohio 43201	
Attn: Edward Unger	(1)
The Boeing Company P.O. Box 3999 Seattle, Washington 98124	
Attn: Technical Library	(1)
Chrysler Corporation Space Division Michoud Operations New Orleans, Louisiana 70150	
Attn: Technical Library	(1)
Hercules, Inc. Allegany Ballistics Laboratory P.O. Box 210 Cumberland, Maryland 21502	
Attn: Technical Library	(1)
Lockheed Missiles & Space Company P.O. Box 504 Sunnyvale, California 94088	
Attn: Technical Library	(1)
Lockheed Propulsion Company P.O. Box 111 Redlands, California 93273	
Attn: Bud White	(1)
Martin Marietta Corporation Baltimore Division Baltimore, Maryland 21203	
Attn: Technical Library	(1)
Mathematical Sciences Corporation 278 Renook Way Arcadia, California 91107	
Attn: M. Fourney	(1)
Philco Corporation Aeronutronics Division Ford Road Newport Beach, California 92660	
Attn: Technical Library	(1)
Rocketdyne Solid Propulsion Operations P.O. Box 548 McGregor, Texas 76657	
Attn: Technical Library	(1)
Rocketdyne 6633 Canoga Avenue Canoga Park, California 91304	
Attn: Technical Library	(1)
Rohm and Haas Redstone Arsenal Research Division Huntsville, Alabama 35807	
Attn: Technical Library	(1)
Douglas Missiles & Space Systems Huntington Beach, California 92647	
Attn: T. J. Gordon	(1)